The role of the serum response factor in the pathogenesis of Huntington's disease

Ali Awada

UNIVERSITÉ DE STRASBOURG

ÉCOLE DOCTORALE des Science de la Vie et de la Santé

Laboratoire de Neurosciences Cognitives et Adaptatives LNCA

UMR 7364 – Université de Strasbourg

THÈSE DE DOCTORAT

Présentée par : **Ali AWADA**

Soutenue le 18 **Mars 2021**

Pour obtenir le grade de : **Docteur de l'université de Strasbourg**

Discipline : Sciences de la Vie et de la Santé

Spécialité : Neurosciences

Rôle du facteur de transcription SRF dans le mécanisme pathogénique de la maladie de Huntington

THÈSE dirigée par :

Mme MERIENNE Karine Directrice de recherche, Université de Strasbourg

RAPPORTEURS :

Mme SOTIROPOULOS Athanassia Directrice de recherche, Institut COCHIN, Paris

M. GARRET Maurice Directeur de recherche, INCIA
UMR 5287- CNRS/Université de Bordeaux

EXAMINATEUR :

M. MENDOZA Jorge Directeur de recherche, INCI
CNRS/Université de Strasbourg

..... Acknowledgement .....

After writing this thesis, I am convinced that it's far from being a solitary task. Indeed, I wouldn't be able to carry out this I work without the support of many people whose generosity, good humor and interest in my research have enabled me to progress in this field.

First of all, I would like to thank the jury members, **Dr. Athanassia SOTIROPOULOS**, **Dr. Maurice GARRET** and **Jorge MENDOZA** for agreeing to evaluate my thesis work and participate in discussing my results.

Thank you, **Prof. Jean-Christophe CASSEL**, the director of the LNCA, for welcoming me i the laboratory and sharing nice discussions.

I would also like to thank **Dr. Anne-Laurence BOUTILLIER**, I appreciate your discussions and kindness during the three years.

Special thanks to my thesis director, **Karine MERIENNE**, for her confidence and numerous advices, for the hours she devoted to direct this research work. Thanks Karine!

Thanks to LNCA teams, especially members of team one for their solidarity. Thanks **Raphael** "le grand", **Isabel** "Bella", **Iris** "the club member", **Baptiste**, **Jonathan**, **Laura**, **Aline**, **Brigitte**, **Laurine**, **Xiao-Lan** and **Charles** and all other Phd and master students.

To my Parents, my sister "jiji", my brother "Aboudi" and Adam, Toula, Larush, Maryoma, Haouraa, Naima, Hanine, Rania, Ghorayeb, Roba, Sima, Amani my family and my friends Thank you all!

We also thank **the Association of Huntington France "AHF"** for funding my Phd during the three years.

…… Table of contents ……

..... List of Figures and Tables .....

Introduction

Materials and Methods

Results

Tables

……. List of Abbreviations ……

ASO	Antisense oligonucleotides
ATF	Activating Transcription Factor
AAV	Adeno-associated viruses
AP	Anteroposterior
AMPA	Amino-Methyl-Phosphoric Acid Alpha
ALS	Amyotrophic Lateral Sclerosis
BG	Basal Ganglia
BiP	Binding immunoglobulin Protein
BBB	Blood-Brain Barrier
BDNF	Brain-derived Neurotropic Factor
BAC	Bacterial Artificial Chromosome
BSA	Bovine Serum Albumin
BER	Base excision repair
Ctx	Cortex
CBP	CREB Binding Protein
CREB	cAMP Response Element
CytC	Cytochrome c
ChIP-seq	Chromatin immunoprecipitation sequencing
CpG	Cytosine-guanine dinucleotide sequences
CSP	Carbon nano sphere
CRISPR	Clustered Regulated Interspaced Short Palindromic Repeat
Cas9	CRISPR associated protein 9
CTGF	Connective Tissue Growth Factor
CNS	Center Nervous System
cDNA	Complementary DNA
CN	Caudate Nucleus
DLS	Dorsolateral striatum
DMS	Dorsomedial striatum
DNMT	DNA methyl transferases
DMPK	Myotonic Dystrophy Protein Kinase
DV	Dorsoventral
DH	Double-H

DAB	3,3'-diaminobenzidine
DNA	Deoxyribonucleic acid
DG	Dentate Gyrus
Drp	Dynamin Related Protein
eARN	enhancer RNA
ER	Endoplasmic Reticulum
ERAD	Endoplasmic Reticulum-Associated Degradation
ERG	Early Response Genes
EBS	Ets Binding Sites
ERK	Extracellular-signal Regulated Kinase
EPSP	Excitatory Postsynaptic Potentials
eRNAs	enhancer RNAs
EHDN	European Huntington's Disease Network
fMRI	functional MRI
FAN1	Fanconi Anemia FANC1 / FANCD2 – associated [endo] nuclease 1
FANS	Fluorescently Activated Nuclei Sorting
FDA	Food and Drug Administration
FANS	Fluorescent-activated nuclei sorting
GWAS	Genome-Wide Association Study
GeM-HD	Genetic Modifiers of Huntington's Disease
GPi	Internal Globus Pallidus
GPe	External Globus Pallidus
GLT1	Transporter Glutamate
GFP	Green Fluorescent Protein
HD	Huntington's Disease
HTT	Huntingtin
HMT	Histone methyl transferase
HAT	Histone Acetyltransferase
HDAC	Histone Deacetylase
HDACi	Histone deacetylase inhibitor
HAP-1	Huntingtin-Associated Protein 1.
Hprt	Hypoxanthine phosphoribosyl transferase
hESC	Human embryonic stem cells
hiPSC	Human induced pluripotent stem cells
Hsp	Heat Shock Proteins
HEAT	Huntingtin, elongation factor 3, protein phosphatise 2A, TOR1.

IT15	Interesting Transcript 15
ITR	Inverted Terminal Repeat
IEGs	Immediate Early Genes
iPSCs	Induced human Pluripotent Stem Cells
JHD	Juvenile Huntington Disease
KI	Knock-in
KO	Knock-out
LCM	laser-capture microdissection
LRGs	late response genes
LSD1	Lysine Specific Demethylase 1
LTP	Long-term synaptic potentiation
LTD	long-term synaptic depression
LXR	Liver X receptors
MSN	Medium-sized Spiny Neurons
MSN-D1	Medium spiny neurons expressing the D1 receptor
MSN-D2	Medium spiny neurons expressing the D2 receptor
mRNA	Messenger RNA
muHTT	mutated HTT
mPTP	transition pore of Mitochondrial permeability
miRNAs	micro RNAs
MSCs	Mesenchymal stem cells
MADS	MCM1-Agamous-Deficiens-SRF
MAPK	Mediate mitogen-activated protein kinase
MEF	Murine embryonic fibroblasts
Mrtfs	Myocardin-related transcription factors
MK2	MAPK-activated protein kinase 2
ML	Mediolateral
miRNA	micro ARN
NaB	sodium butyrate
NSC	Neural stem cells
NGG	Nucleotide-guanine-guanine
NLS	Nuclear localization signal
NW	North West
NE	North East
NMDA	N-Methyl-D-aspartate
3-NP	3-nitropropionic
NES	Nuclear Export Signal

NF-kB	Nuclear factor-kB
PKC	Protein Kinase C
PCR	Polymerization Chain Reaction
PBS	Phosphate-Buffered Saline
PAF	Paraformaldehyde
PPSE	Excitatory postsynaptic potential
PSD95	Postsynaptic Density Protein 95 kDa
PolyQ	Polyglutamine
PTM	Post-Transcriptional Modifications
Put	Putamen
PAM	Protospaser adjacent motif
PRD	Proline rich domain
RNA	Ribonucleic acid
REST/NRSF	Repressor element-1 transcription factor/neuron restrictive silencer factor
RAN	Repeat-associated non ATG
ROS	Reactive Oxygen Species
RNAi	interfering RNAs
RNase H	Ribonuclease H
RIN	RNA Integrity Number
RISC	RNA-induced silencing complex
RNP	Ribonucleoprotein
Rpm	Rotations per minute
RNAi	RNA interfere
RNA PolI	RNA Polymerase II
RNA-seq	RNA-sequencing
S-R	Stimuli- Responses
Sp1	Specific Protein 1
SOD	Superoxide Dismutase
SSRIs	Selective Serotonin Reuptake Inhibitors
SAHA	Suberoxylanilide Hydroxamic Acid
SNPs	Single Nucleotide Polymorphisms
siRNA	short interfering RNA
sgRNA	single guide RNA
Srf	Serum response factor
SRE	Serum Response Element
Str	Stratum
SNP	Single Nucleotide Polymorphism

SNc	Substantia Nigra pars compacta
SNr	Substantia Nigra Pars reticulata
SERE	Simple Error Ratio Estimate
TgHD-CAG51n	Transgenic rat with 51 CAG
TBP	TATA Binding Protein
Tfam	Transcription Factor A
TFEB	Transcription Factor EB
TRAP	Translating Ribosome Affinity purification
TET	Ten-eleven-translocation
TF	Transcription factors
TCAs	Tricyclic antidepressants
TrkB	Tropomyosin kinase receptor
TSA	Trichostatin A
TALENS	Transcription Activator-Like Effector Nucleases
TCFs	Ternary complex factors
TSS	Transcription start site
UBR5	Ubiquitin-Protein ligase E3
UPS	Ubiquitin-Proteasome System
UPR	Unfolded Protein Response
USP	Ubiquitin Specific Protease
VMAT2	Vesicular monoamine transporter type 2
VSCC	Voltage-sensitive calcium channel
YAC	Yeast Artificial Chromosome
ZFN	Zinc Finger Nucleases

“Finally, if you're wondering if it counts and it feels like it counts, it counts.”

— Mary H.K. Choi

..... Introduction .....

Introduction

1. Huntington's Disease

Huntington Disease (HD), along with eight other neurodegenerative disorders are caused by abnormal poly-glutamine (polyQ) expansion(Orr, 2012a). In each of these diseases, the gene carrying the mutation codes for a different protein, although a common mutation affects these proteins. The genes involved in these diseases all have a trinucleotide repeated sequence (CAG)n which codes for a homo-polymer of the glutamines in the concerned proteins. This sequence is polymorphic in healthy populations; however, when the repetition exceeds a certain size, this mutated sequence confers the carrier protein's toxic properties.

HD is a rare genetic disease with autosomal dominant inheritance. It affects about 1 in 10,000 and concerns nearly 18,000 people in France, including 12,000 asymptomatic carriers of the mutated gene and 6,000 reported cases.

In the middle Ages, this disease was known for a long time under the name of "Chorea or dance of Saint Guy" designated by "sacred dances." In the German Rhineland, these dances were strongly associated with a religious rather than a medical setting. Involuntary dancing, singing, and altered mental state like hallucinations and screaming are recorded in people as if demons possessed them. For some, only the practice of exorcism and the reading of passages from the gospel soothed the suffering of these people, while others were arrested and condemned as "sorcerers," possessed by demons (Schechter, 1975)(Hecker, 1862).

1.1. History of Huntington's Disease

George Huntington, a young doctor, was a pioneer in the field as he was the first to distinguish between patients with infectious chorea and those with hereditary disease. In 1872, based on his work and that of his father and grandfather, he drew up an accurate description of this genetic disease. He gave his name to the disease; Huntington's disease. This naming came out, following the presentation of his medical thesis, "On Chorea," which mainly focused on Sydenham's chorea. Here is an excerpt: "The disease exists as far as I know almost exclusively in the far east of Long Island. Hereditary chorea, to be called, is limited to specific families, fortunately rare, and has been transmitted to them, like a legacy of generations going back to a very distant past. It has all the symptoms of common chorea but at higher severity, rarely occurring before adulthood or mid-life, worsening gradually but surely over the years. There are three peculiarities in this affection:

1. Its innate nature: "When one or both the parents have shown manifestations of the disease […], one or more of the offspring almost invariably suffer (Huntington, 2003).
2. Its tendency to madness and suicide, "The tendency to insanity, and sometimes that form of insanity which leads to suicide, is marked. I know of several instances of the suicide of people suffering from this form of chorea, or who belonged to families in which the disease existed (Huntington, 2003).
3. Its seriousness when it occurs in an adult: "I do not know of a single case that has shown any marked signs of chorea before the age of thirty or forty years, while those who pass the fortieth year without symptoms of the disease are seldom attacked (Huntington, 2003).

In 1983, the gene associated with HD was found to be located on chromosome 4 (Gusella et al., 2003). Ten years later, the Huntington's Disease Collaborative Research Group identified this gene, formerly called *IT15* (Interesting Transcript 15) and *HTT* today, and determined the nature of the mutation causing the pathology.

1.2. HD is a genetic Disease

1.2.1. CAG trinucleotides repea

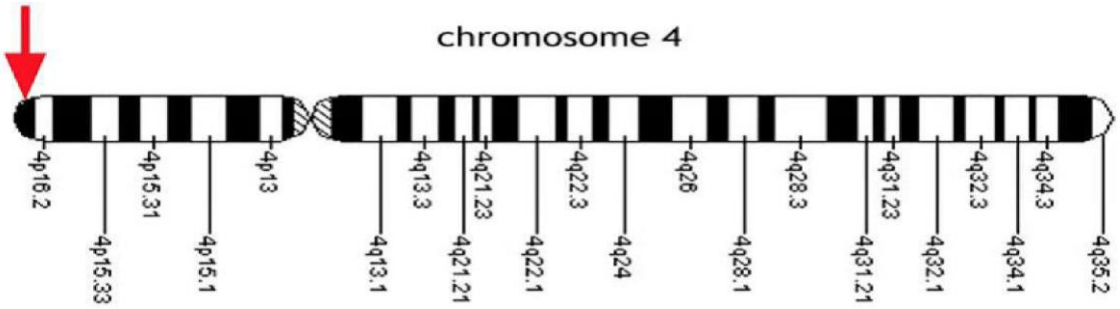

Figure 1: Location of the IT15 associated with HD.
The arrow indicates the location of the gene, on locus 4p16.3, at the end of the short arm of chromosome 4 (Thesis of Najia Toukdaoui).

The *IT-15* gene, responsible for HD, was discovered in 1993 by a collaboration of 58 researchers ("A novel gene containing a trinucleotide repeat that is expanded and unstable on Huntington's disease chromosomes. The Huntington's Disease Collaborative Research Group.," 1993), on the short arm of chromosome 4 (Figure1). Its coding sequence contains a repeat of the CAG trinucleotide (encoding the amino acid glutamine). The mutation causing the disease consists of an abnormal repetition of this trinucleotide encoding a 348kDa protein called huntingtin (HTT) (Huntington's Disease Collaborative Research Group, 1993).

After the gene discovery, a genotype-phenotype correlation was raised according to the size of this polymorphic repetition of CAG triplets in healthy individuals and others affected by HD (Andrew et al., 1993; Duyao et al., 1993; Snell et al., 1993). HD usually starts in adulthood around the age of 40. However, the number of CAG triplets is strongly correlated with the age of onset of first symptoms; so, the higher the number of CAGs, the more the disease is likely to start early (Duyao et al., 1993; Stine et al., 1993) **(Figure 2).** On the other hand, the number of CAGs has no impact on the duration of HD, which lasts an average of 15 years from the onset of the first symptoms until the patient's death (Finkbeiner, 2011).

Contrary to what Dr. Georges Huntington initially thought, HD can also affect children under the form of Juvenile Huntington Disease (JHD) (Milunsky et al., 2003; Nicolas et al., 2011; Telenius

et al., 1993). JHD is characterized by the onset of symptoms before the age of 20, with a 60 to 250 CAG repeats. This form of the disease is rare and represents less than 10% of cases.

Besides, having the number of CAG repeats less than 35 shows no risk of developing HD (Rubinsztein et al., 1996). Conversely, people with more than 41 CAG repeats on one of the two alleles contract this pathology with complete penetrance (MACDONALD, 1993). They showed that penetrance is reduced when the number of CAG repeats varies between 36 and 40 (McNeil et al., 1997), this is due to individual variability, where two people with the same number of CAGs will not necessarily develop the disease at the same age. Several studies show that the age of onset of HD can be advanced or delayed depending on the instability of the repetition, genetic factors, or more environmental factors (The U.S.-Venezuela Collaborative et al., 2004).

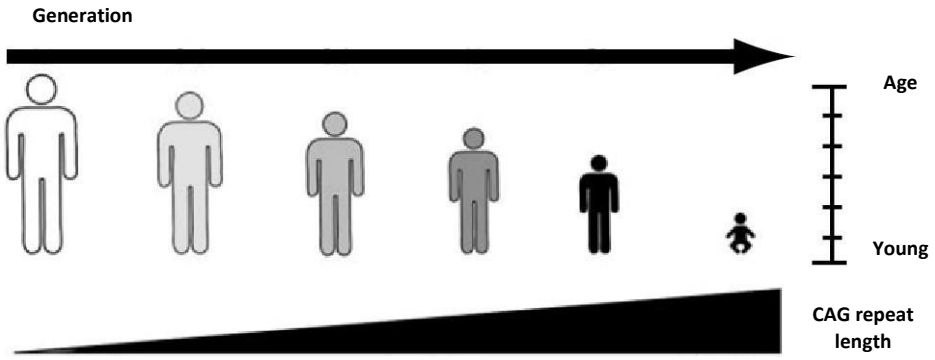

Figure 2: Schematic representation of the correlation between the age of onset of the first symptoms and the length of CAG repeats in HD.
The patient's color indicates the severity of the symptoms (increasing from white to black). The patient's height corresponds to the age at which the first symptoms were declared (scale on the right). Typically, a patient has HD only when he has 35 repeats, the age of the first symptoms being earlier, and the disease severe the higher the expansion of CAG. The size of the CAG expansion increases over generations (Thesis of Aurélien DEVRANCHE).

1.2.2. Germline and somatic instability of CAG expansion

Researchers marked the relative instability in the mutant HTT gene as an effect of CAG trinucleotide repeats. This instability increases in a CAG-length dependent manner (Wheeler et al., 2007). This is usually modified from one to a few triplets with, predominantly, an increase in size.

Moreover, the intergenerational transmission increases the occurrence of such instability, thus speaking of gametic instability. This phenomenon occurs at a higher frequency during

spermatogenesis than during oogenesis, explaining the tendency of parental transmission of the pathology (Wheeler et al., 2007). This is at the origin of the "anticipation" phenomenon observed in Huntington families (Andrew et al., 1993): the expansion of CAG tends to increase in size over the generations. However, since its size is inversely correlated to the age of onset of the disease, HD tends to occur earlier in successive generations.

On the other hand, the supported model provided by the consortium of Genetic Modifiers of Huntington's Disease in 2019 (Genetic Modifiers of Huntington's Disease (GeM-HD) Consortium, 2019), showed that the rate at which HD manifestations emerge, leading to clinical diagnosis, is determined not by length-dependent polyQ toxicity, but by length-dependent somatic expansion of the CAG repeat in critical target cells. It was shown that mouse HD knock-in models display length-dependent somatic expansion of the CAG repeat throughout the brain, but most prominently in the striatum (Str)(Lee et al., 2020; Wheeler, 1999), and this process is modified by DNA maintenance genes (Dragileva et al., 2009; Pinto et al., 2013; Wheeler, 2003). Also, somatic CAG expansion has been demonstrated in HD post-mortem brains (Kennedy, 2003; Swami et al., 2009) with the earliest onset individuals at any inherited CAG repeat length showing the largest somatic expansions, consistent with length-dependent CAG expansion being the rate driver for onset.

1.2.3. Gene modifiers

In an attempt to understand the origin of hereditary variability among individuals, Genome-Wide Association Study (GWAS) was performed on several cohorts of healthy and sick individuals by correlating their genotypes and phenotypes. These studies allow the analysis of genetic variations between healthy people and mutation carriers through their DNA sequencing and regular phenotype monitoring. The goal consists of identifying genetic variants, i.e., nucleotide polymorphisms (Single Nucleotide Polymorphism - SNP) associated with genes involved in pathogenesis.

These genes, also called gene modifiers, could affect the phenotype or expression of other genes and delay or accelerate the onset of HD. In 2015, the GWA study by the GeM-HD

Consortium (Genetic Modifiers of Huntington's Disease) and their collaborators (The Massachusetts HD Center Without Walls -MaHDC-, European Huntington's Disease Network -EHDN-) analyzed the difference between actual age and the predicted age of onset of symptoms in approximately 4,000 Huntington's patients. Three loci significantly associated with a change in the age of onset of HD have been identified (Genetic Modifiers of Huntington's Disease (GeM-HD) Consortium, 2015). Likewise, a locus on chromosome 8 was associated with a 1.6-year acceleration of the onset of the disease's first symptoms. This SNP could correspond to two candidate genes: The ***RRM2B*** (p53-inducible ribonucleotide reductase M2 B); encoding a subunit of an enzyme associated with DNA damage and the ***UBR5*** encoding a domain ubiquitin-protein ligase E3 (Genetic Modifiers of Huntington's Disease (GeM-HD) Consortium, 2015).

Another identified locus, on chromosome 15, with two possible variants, one associated with a 6.1 years' acceleration of the pathology and the other at a delay of 1.4 years. These polymorphisms are found at the level of the ***FAN1*** gene (Fanconi anemia FANC1 / FANCD2-associated [endo] nuclease 1), encoding an enzyme involved in DNA repair mechanisms (Genetic Modifiers of Huntington's Disease (GeM-HD) Consortium, 2015). ***FAN1*** appears to modify the pathogenesis's onset by improving the stability of CAG expansion (Goold et al., 2019). Another SNP was detected on chromosome 3, next to the ***MLH1*** gene (mutL homolog1) (Lee et al., 2017)(Genetic Modifiers of Huntington's Disease (GeM-HD) Consortium, 2015). This gene is known for its involvement in repairing DNA mismatches and in somatic instability of CAG expansion (Pinto et al., 2013). This variant appears to decrease the MLH1 protein activity, leading to a reduced expansion of CAG triplets and a pathology onset time of 0.7 years (Lee et al., 2017). Overall, the mechanisms associated with DNA repair appear to influence the age of onset of the first symptoms of the disease by modifying the stability expansion of CAG triplets of the *HTT* gene.

Furthermore, several new loci have been emerged from genome-wide significant studies in either continuous or dichotomous analysis or both (Genetic Modifiers of Huntington's Disease (GeM-HD) Consortium, 2015). Among the new loci, there exists many genes that are associated with DNA repair mechanisms. These include ***PMS1*** on chromosome 2, ***MSH3/DHFR*** on

chromosome 5, ***PMS2*** on chromosome 7, and ***LIG1*** on chromosome 19). However, other loci like ***TCERG1*** on chr 5 and ***CCDC82*** on chr 11 may not be directly connected to such processes. Nevertheless, two additional loci, ***SYT9*** on chromosome and ***GSG1L*** on chromosome 16, displayed significant signal only from a single very low-frequency SNP allele, suggesting a statistical artifact due to extreme phenotypic outliers. Certainly, a larger sample size and/or functional analysis will be needed to firmly establish these loci as bona fide gene modifiers (Genetic Modifiers of Huntington's Disease (GeM-HD) Consortium, 2015).

Thus, these recent findings along with current investigations would have the potential to highlight specific targets for therapeutic intervention at different disease stages, allowing a stratified approach to treatment over the protracted, complex disease course.

1.3. Neuropathology of HD

Early neuropathological researchers (Alois Alzheimer, /Gerbrandus Jelgersma, Cecile and Oskar Vogt, Ewald Stier) already described that, as the disease progresses, the degeneration and nerve cell loss covers distinct regions of the cerebral cortex of patients with HD. However, the largest and fastest degeneration occurs within the striatum, which is considered the neuropathological hallmark of HD. (Figures 3).

1.3.1. Organization and function of the striatum (basal ganglia)

The striatum is a subcortical nerve structure made up of the caudate nucleus, putamen, and the ventral striatum (Lanciego et al., 2012). The striatum is part of the basal ganglia (BG), organized as shown below in **Figure 3**:

- The dorsal striatum (Caudate Nucleus (CN) and Putamen (Put))
- The ventral striatum (nucleus Accumbens (Acb) and olfactory tubercles)
- The pallidum (internal and external Globus Pallidus ,GPi and GPe)
- Substantia nigra *pars compacta* (SNc) and *pars reticulata* (SNr)
- The Sub-Thalamic nucleus (STN)

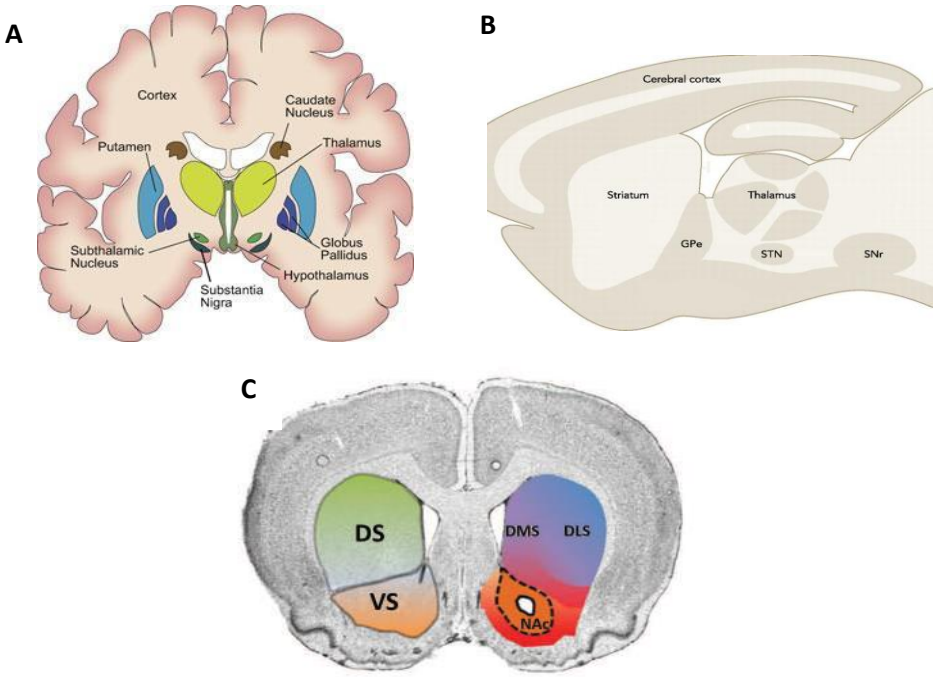

Figure 3: The basal ganglia.
(A) Anatomy of the basal ganglia on a frontal section of the human brain. **(B)** anatomy of the basal ganglia on a sagittal section of a rodent brain. external Globus pallidus par extern (GPe) Subthalamic nucleus (STN) and substantia nigra pars reticulata (SNr). (Carpenter, 1976). **(C)** Structure of the striatum in mice. The striatum is divided into a dorsal part (DS) which itself is made up of the dorsomedial striatum (DMS) and dorsolateral (DLS), and a ventral part (VS) composed of the nucleus accumbens (NAc) (Thesis of Magali CABANAS).

In humans, the striatum is composed of the caudate nucleus (dorsal part), the putamen, and the nucleus accumbens (ventral part) (**Figure 3**). Located in the ventral part of the brain and adjacent to the lateral ventricles, it is the primary entry point for basal ganglia afferents. The striatum receives glutamatergic afferents mainly from the cortex, the thalamus and limbic structures like the amygdala. Dopaminergic afferents supplement these entries from the midbrain, which exert control over the processing of information coming out of the striatum. In rodents, the caudate nucleus and the putamen form one same structure, the striatum.

At the cytoarchitectural level, the striatum is composed mainly of neurons. Striatal neurons are composed of 90 to 95% of medium-sized spiny neurons (MSN) GABAergics, with a soma of 20 at 25µm diameter, recognizable by their numerous dendritic spines and their long axon **(Figure 4A)**(Kawaguchi et al., 1995)**.** On the other hand, 5 to 10% of the striatum cell population is also made up of several categories of interneurons (Kawaguchi et al., 1995): cholinergic large size interneurons (soma 20-40µm diameter) without dendritic spines and GABAergic interneurons

also devoid of dendritic spines, divided into several categories according to their neurochemical properties. Thus, GABAergics interneurons express either parvalbumin, neuropeptide Y and somatostatin, or calretinin.

At the neurochemical level, studies have established the heterogeneous organization of the striatum compartments, including the striosomes (or patches) and the matrix **(Figure 4B, C, D).** It is well known that these compartments differ in the expression of neurochemical markers: striosomes are characterized by a strong expression of μ-opioid receptors and substance P. However, the extra-striosomal matrix is enriched in calbindin, somatostatin, enkephalin and cholinergic markers, such as acetylcholinesterase (Brimblecombe and Cragg, 2017; Crittenden et al., 2016; Gerfen et al., 1987; Graybiel and Ragsdale, 1978; Holt et al., 1997).

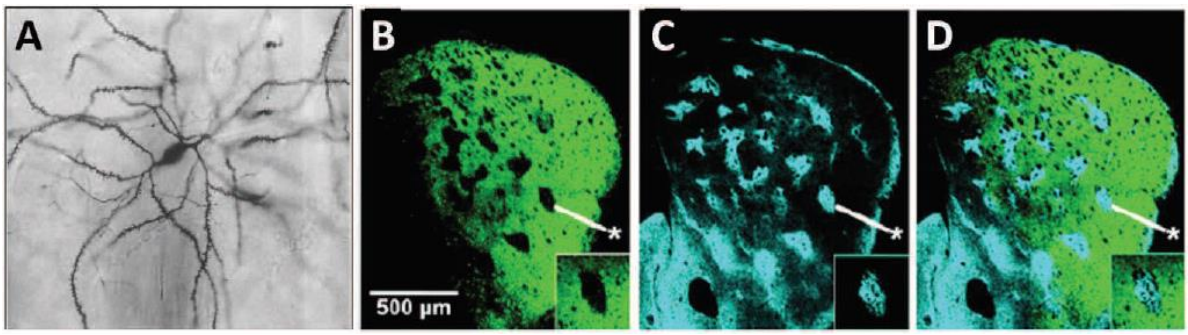

Figure 4: Cytoarchitecture of the striatum in mice.
(A) Median Spiny neuron, dominant cell type in the striatum, revealed by Golgi impregnation (Smith and Bolam, 1990). **(B-D)** Confocal images of a section of striatum from a transgenic mouse expressing fluorescent labeling in the matrix **(B)**, labeled with an antibody recognizing the μ receptors of the striosomes **(C)**, Superposition of markings of the matrix (green) and striosomes (blue) of the striatum **(D)**. Examples of striosomes are indicated by the star white (*) (Crittenden et al., 2016).

The significance of this compartmentalization is still not well understood, but studies have suggested that these two compartments would have also differences in terms of anatomical connectivity. The amygdala and the cortex are connected to striosomes, while the matrix would receive information from the prefrontal cortex mainly from the sensory-motor cortex. In rodents, the neurons of the striosomes project essentially towards the substantia nigra pars compacta (Crittenden et al., 2016; Gerfen, 1992).

The putamen (dorsolateral region) is contacted directly by the motor and sensory cortices. The frontal and parietal associative cortices contact the caudate nucleus (dorsomedial region) **(Figure**

3C). The nucleus accumbens is connected with the limbic structures including the amygdala, hippocampus, and the anterior cingulate and median orbitofrontal cortices.

This topography is believed to confer distinct functions on each striatal region, allowing them to integrate and filter the flow of information and adapt the signals sent to motor control structures. Thus, the dorsal striatum would be more involved in cognitive and sensory-motor functions, while the ventral striatum in limbic functions (Lynd-Balta and Haber, 1994). In HD, the caudate nucleus and the putamen are the most vulnerable structures and are primarily affected by atrophy. The lateral region of the dorsal striatum is necessary for the acquisition of "habits"; it is activated, mainly when performing well-assimilated sequences. On the other hand, the middle part is involved in the learning of behavior directed towards a goal or the extinction of learned behaviors. Thus, it is activated during the learning of new motor sequences or the devaluation of already known sequences (Chevrier et al., 2007; Liljeholm et al., 2011; Yin, 2004; Yin et al., 2005).

1.3.2. The striatal connectivity

The striatum, through its cerebral network; basal ganglia, is crucial for performing motor, associative, cognitive, and mnemonic functions (BOLAM et al., 2000). The principal input to the basal ganglia comes from the cortex (Ctx; glutamatergic) and midbrain (dopaminergic) mainly (Kincaid et al., 1998) through the striatum, although there are also significant cortical projections to the STN (Smith et al., 1994). The GABAergic MSNs are subdivided into two major populations according to their projection region, the pattern of axonal collateralization, and their neurochemical content. One subpopulation project preferentially directly to the output nuclei of the basal ganglia (SNr and GPi), and thus constitute what it is known as the direct pathway. This subpopulation expresses, in addition to GABA, the neuropeptides substance P and dynorphin, and the dopamine D1 and muscarinic M4 subtype of receptors (D1 MSN). The second subpopulation projects, implicated in the indirect pathway, almost exclusively to the GPe, and expresses enkephalin and the D2 subtype of dopamine receptors (D2 MSN) (Figure 5) (Kreitzer, 2009; Llewellyn-Smith et al., 1998; Surmeier and Kitai, 1997). Interneurons play an important role

in controlling the excitability of MSNs; they are quite conserved along with the progression of the disease (Ferrante et al., 1985; VONSATTEL et al., 1985).

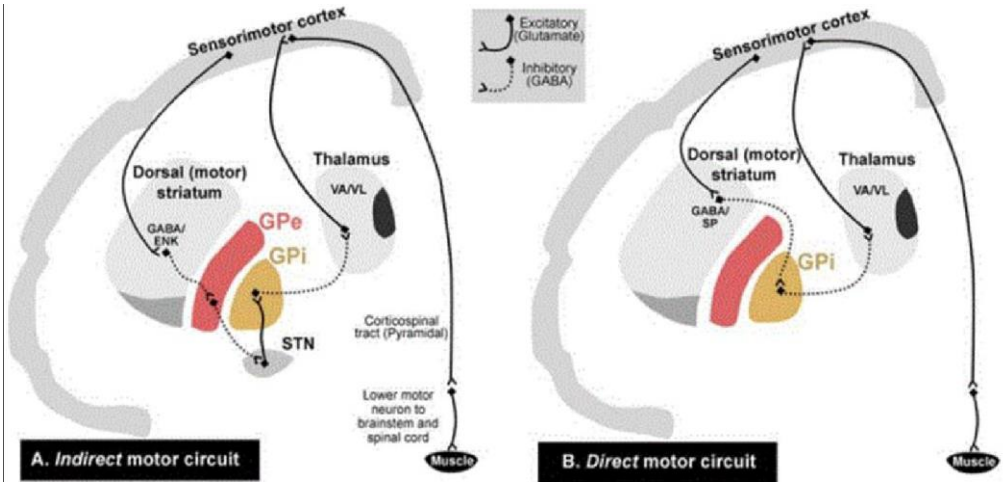

Figure 5: Diagram representing the "direct" and "indirect" connections.
(A) Indirect motor circuit. **(B)** Direct motor circuit. GPe: External Globus Pallidus; GPi: Internal Globus Pallidus internally; STN: Sub-Thalamic nucleus; (Singh-Bains et al., 2016).

Moreover, in HD, MSNs from the direct and indirect pathways differentially degenerate as well (Albin et al., 1992; Sapp et al., 1995). The indirect pathway is impaired at earlier stages of the disease, producing disinhibition of the thalamus, which leads to an over-activation of the cortex, thus producing the hyperkinetic and choreic movements characteristic of the first stages of the disease. At late stages, however, dysfunction of the direct pathway results in the over-inhibition of the thalamus and cortex, producing the hypokinetic and parkinsonian symptomatology appreciable at this stage in HD patients.

1.3.3. The striatum in HD: Striatal atrophy

Brain atrophy in HD patients is complex and occurs before the diagnosis of the first motor symptoms. The neurodegenerative process begins with the early and selective loss of the striatum's spiny afferent neurons (VONSATTEL et al., 1985). Other brain regions such as the cortex, thalamus, sub-thalamic nucleus, and white matter also degenerate with the progression

of the disease (Fennema-Notestine et al., 2004; Rosas et al., 2006). Besides, not all neurons degenerate, but some of them become dysfunctional.

The pathological process of HD leads to striatal atrophy accompanied by an enlargement of the ventricles, and this happens before the symptomatic stage. In 1985, Vonsattel et al. assessed striatal involvement in 163 brains from post-mortem patients. This study was carried out according to macroscopic and microscopic criteria to establish a classification of the pathology in 5 stages (from 0 to 4 in increasing order of severity) (VONSATTEL et al., 1985) (**Figure 6).** Stage 0 corresponds to an absence of macroscopic and microscopic abnormality after histological examination. Stage 1 presents only microscopic abnormalities: 50% neuronal loss in the caudate nucleus' head and tail. In stage 2, astrogliosis (an abnormal increase in the number of astrocytes) is detectable along with neuronal loss. The atrophy of the caudate nucleus at this stage takes on a convex aspect on the ventricular side, which becomes straight in stage 3, then concave in stage 4 **(Figure 6B)**. The latter is the most severe stage, with a 95% loss of striatal neurons (VONSATTEL et al., 1985).

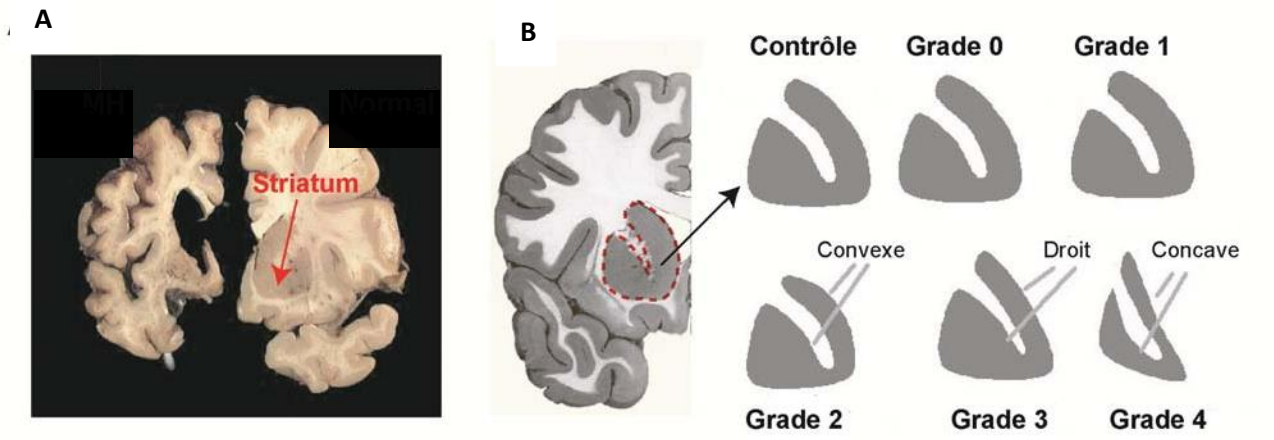

Figure 6: Striatal atrophy.
(A) Frontal sections of post-mortem half-brains of a control individual (right) and an HD patient (left). An overall decrease in the brain's size can be observed with very pronounced atrophy of the striatum and the cerebral cortex. (**B)** Stages of cerebral atrophy. The striatum (in red dotted lines) gradually atrophies during the pathology. At stage 0, the genetic diagnosis is made, but the neuropathological lesions are not apparent; in stage 1, the lesions are only microscopic; in stage 2, atrophy begins, but the head of the caudate nucleus still bulges into the lateral ventricle; in stage 3, the edge of the caudate nucleus is straight; in stage 4 it is concave, and the atrophy is maximal, (according to http://hdroster.iu.edu/AboutHD and http://ist.inserm.fr/basisateliers).

From stage 1 to stage 4 of the disease, the striatum's neuronal loss increases from 50 to 95%. Astrogliosis is also observed in parallel with this degeneration (VONSATTEL et al., 1985). Conversely, the interneurons are spared. The causes of this early and selective degeneration of the striatal spiny neurons are very intriguing and poorly understood. However, some hypotheses have been put forward to try to understand this specificity.

On the other hand, in HD murine models, this progression is not so clear: the work of André et al. (2011) has shown that the frequency of excitatory postsynaptic potentials (EPSP) of MSNs-D1 is increased at an early stage in the pathology of mouse models of HD, then diminished to a stage later, while the EPSP of MSNs-D2 has an unchanged frequency (Andre et al., 2011).

Another electron microscopy study demonstrated that cortico-striatal entries on the dendritic spines of MSNs-D1 are lost in the mouse striatal neuropil models of HD at a late stage of the pathology, while those of MSNs-D2 are spared (Deng et al., 2014). More recently, studies have shown that the electrophysiological properties and structural changes of MSNs-D1 exhibited significantly more robust and extensive than those of MSNs-D2 at the same age in several murine models of HD (Barry et al., 2018; Goodliffe et al., 2018). Finally, the transcriptomic studies suggest that MSNs-D1 and -D2 do not appear differentially altered in HD (Merienne et al., 2019) . The two types of MSNs appear to be differentially affected by mutated HTT in mouse models of HD, but with a different trajectory from that observed in human pathology.

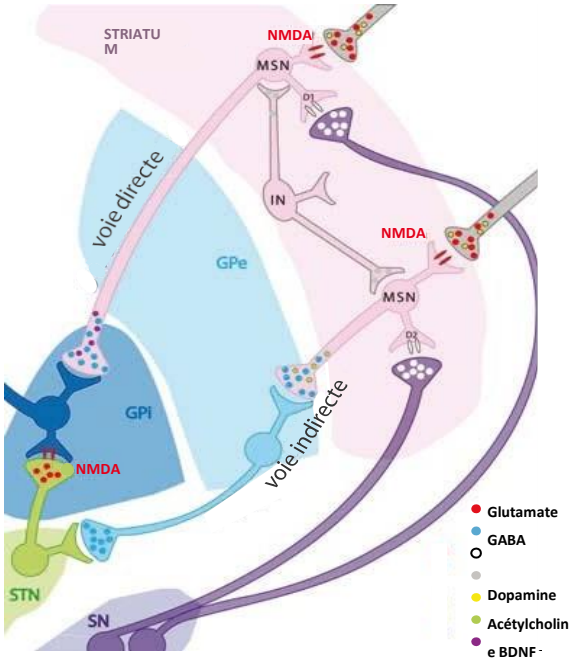

Figure 7: Characteristics of the different cell types affected in HD.
MSNs are GABAergic neurons (GABA: blue circles) that receive large amounts of Brain-Derived Neurotrophic Factor (BDNF; yellow circles) from glutamatergic neurons from the cortex (glutamate: red circles), as well as dopaminergic neurons (dopamine: white circles) of the black substance (SN). Interestingly, the most vulnerable MSNs are those of the "indirect route" which express enkephalin (enkephalin: green circles) and dopaminergic D2 receptors, while the least vulnerable MSNs are those of the "direct route." which secrete substance P (purple circles) and dopamine ergic D1 receptors. IN: interneuron; BDNF: Brain-Derived Neurotrophic Factor; D1: dopaminergic receptor type 1; D2: dopaminergic receptor type 2; NMDAR: NMDA receptor; GPe: globus pallidus, external; GPi: internal globus pallidus; SN, substantia nigra; STN, subthalamic nucleus. According to (Han et al., 2010).

1.2.1. The vulnerability of the striatum in HD

Several studies show that striatal vulnerability could be linked to a lack of neurotrophic factors of cortical origin, in particular, BDNF (Brain-derived neurotrophic factor) (Canals, 2004; ZUCCATO et al., 2005; ZUCCATO and CATTANEO, 2007), which plays an essential role in neuronal survival, synaptic plasticity and maturation of neurons. In HD, the cortico-striatal axis is altered early as shown by imaging studies in pre-symptomatic patients (Poudel et al., 2014; Unschuld et al., 2013) and axonal transport of BDNF is deregulated by mutated HTT (muHTT) (Gauthier et al., 2004). The functional and morphological modifications of the cortex have therefore been proposed as

initial triggers of striatal pathology. They are believed to be involved in the progression of the phenotype in humans and animal models of HD (For review: (Estrada-Sánchez and Rebec, 2013).

On the other hand, an interesting hypothesis is related to excitotoxicity. The striatum, the main target of neurodegeneration, receives abundant glutamatergic innervation from the cortex. Glutamate is the primary excitatory neurotransmitter in the central nervous system of mammals. It activates the ionotropic receptors (ion channels) AMPA (Amino-Methyl-Phosphonic Acid Alpha), NMDA (N-Methyl-D-Aspartate), and kainate, causing neuronal arousal. The excessive abnormal activation of the target cells induces sustained stress, considered to be fatal. This phenomenon is called "excitotoxicity." For a long time, excitotoxicity has been proposed as one of the mechanisms involved in the neurodegenerative process of HD. The origin of this hypothesis dates back to 1976 when Coyle and Schwarcz noticed that injection of kainate, a glutamatergic agonist, into the rat striatum results in lesions showing similarities to certain histological and neurochemical aspects of HD (COYLE and SCHWARCZ, 1976). For example, one of the first mouse models used to study HD were intra-striatal normal mice injected with quinolinic acid, another NMDA receptor agonist. This excitotoxin causes the death of GABAergic neurons, particularly MSNs, while relatively sparing other populations of neurons (Beal et al., 1991).

This pathway of neurodegeneration is still relevant today. Indeed, it has been shown that the 'Riluzole,' an NMDA receptor antagonist and used to treat patients with amyotrophic lateral sclerosis (ALS), reduces gray matter loss in HD patients (Squitieri et al., 2009). However, further studies have shown that riluzole is not effective in treating HD patients (Landwehrmeyer et al., 2007)(Mestre et al., 2009). In fact, in a study carried out on 379 patients followed for three years, there was no significant effect on choreic symptoms following daily treatment with riluzole, compared to placebo treatment (Landwehrmeyer et al., 2007). These results were confirmed in 2009, in a larger cohort of patients (1366 patients) but with a shorter treatment duration (from 30 to 144 weeks) (Mestre et al., 2009).

HTT interacts with the PSD95 protein (95 kDa postsynaptic density protein), regulating the internalization of NMDA receptors present in the plasma membrane. However, when HTT is mutated, its affinity for PSD95 is decreased, resulting in an alteration of internalization of extra-

synaptic NMDA receptors (Sun et al., 2001). The vulnerability of MSNs to excitotoxicity may also be linked to a decrease in the expression of the transporter GLT1 glutamate present on astrocytes, described in the striatum of patients and murine models of HD (Faideau et al., 2010)(Estrada-Sánchez and Rebec, 2012). Therefore, the recapture of glutamate present in the synaptic cleft would be less effective in HD, increasing its excitatory effect.

On the other hand, the pathogenesis of HD involves mitochondrial dysfunction (For review: (Liot et al., 2017)). Mitochondria are stimulated continuously by a primary energy demand linked to glutamatergic synaptic transmission. Alternatively, their ability to manage intracellular calcium is impaired by mutated HTT, which could make MSNs very vulnerable to calcium entry and could thus facilitate excitotoxicity triggered by NMDA receptors in the striatum (Jacquard et al., 2006). Postmortem studies of patient brains revealed dysfunction of the mitochondrial respiratory chain with decreased activity of complexes II, III and IV, specifically in the striatum compared to other brain structures such as the cortex or cerebellum (Aidt et al., 2013; Damiano et al., 2013; Fukui and Moraes, 2007; Gu et al., 1996).

muHTT disrupts the transcription of many genes, particularly in the striatum. So, the expression of genes preferentially expressed in the striatum has been studied in HD patients and mouse models. These genes, also called striatal markers, can have a pro-survival (e.g., *Bcl11*, *FOXP1*, *MSK-1, DCLK3*) or pro-toxic (e.g., example, *RGS2*, *Rhes*). The deregulation of their expression in the striatum of patients and mouse models of HD could play a crucial role in the susceptibility of the striatum to muHTT (For review: (Francelle et al., 2014)).

Finally, as in most diseases linked to an expansion of triplets (CAG or CTG), repeat instability exhibits tissue specificity and is particularly high in the brain, except in the cerebellum. At the cerebral level, the somatic instability of triplet expansions is particularly prominent in the striatum and cortex of models of HD (Kennedy, 2000; Wheeler, 1999) . This phenomenon would involve in particular mechanisms related to oxidative damage to DNA and their repair (Goula and

Merienne, 2013) and would contribute to the vulnerability of striatum facing the mutation of HTT.

- Other regions of degeneration

Even if severely atrophied, the striatum is only one piece of the puzzle. Its degeneration does not fully explain all of the various clinical symptoms observed during disease progression (Rosas et al., 2003). Thus, other regions are also altered in patients, such as the temporal and frontal lobe of the cortex, the entorhinal cortex, the brainstem (Rosas et al., 2003), the cerebellum (Fennema-Notestine et al., 2004), and the hypothalamus (Kassubek et al., 2004). The atrophy or decrease in the volume of these brain tissues is easily identifiable by anatomical observation.

Importantly, there are also neuronal dysfunctions that occur in the absence of cell loss. These dysfunctions are more challenging to identify and require the use of functional imagery. It was thus possible to detect functional changes in the thalamus and the gray and white matter of the cortex (Bonvento et al., 2017; Fennema-Notestine et al., 2004; Rosas et al., 2003). The use of functional MRI (fMRI) has shown reduced blood flow to the prefrontal cortex and the frontotemporal cortex. Dysfunction of these regions may be correlated with memory loss and certain psychiatric symptoms observed in patients (Cabeza and Nyberg, 2000). On the other hand, the reduction in glucose metabolism (measured by PET) in the frontal-parietal and occipital cortex is correlated with cognitive deficits associated with episodic memory, reasoning, attention, and visual-motor skills. The atrophy of the brain in the most severe cases, reveal that the overall weight of a patient's brain may be reduced by more than 40% (Gómez-Tortosa et al., 2001).

1.4. HD: A Triad of Symptoms Pathology

HD is a complex pathology, which results in motor, cognitive, and behavioral disorders. It is important to note that symptoms can vary from patient to patient, even within the same family.

1.4.1. Motor disorders

Patients experience two broad categories of motor disorders: increased involuntary movements, such as chorea, and decreased voluntary movements, such as poor limb coordination (Novak and Tabrizi, 2011). In general, the first symptoms perceived by the patient or his entourage are choreic movements. As the disease progresses, these involuntary movements tend to decrease to give way to dystonia, which is intense and involuntary muscle contraction, as well as muscle stiffness and bradykinesia (slowing down). This development must be taken into account to adapt the treatment, as we will see thereafter. Some patients also suffer from tics and akathisia, which refers to the inability to sit still.

These two successive phases of motor disorders development can be correlated to biphasic degeneration of striatal neurons. Indeed, the D2-MSNs would be more vulnerable to the toxicity of mutated HTT and degenerate earlier, impacting the indirect pathway and inhibition of movement. Thus, an alteration of this path in combination with the direct path's activating role explains the involuntary movements in patients in the early stage of the disease (Figure 8). In the later stages, bradykinesia correlates with the general loss of striatal neurons, including MSNs-D1, resulting in loss of movement control **(Figure 8)** (Plotkin and Surmeier, 2015).

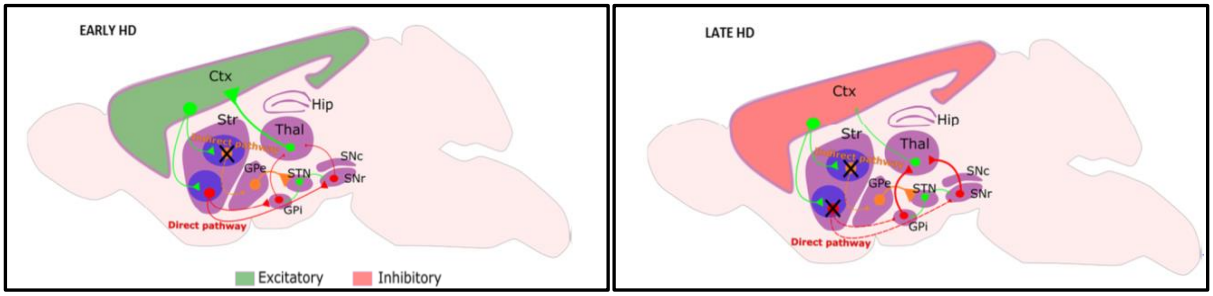

Figure 8: Basal ganglia circuitry alterations in early and late stages of HD.
In early stages of HD, the degeneration of the striatal neurons from the indirect pathway results in the inactivation of STN, leading to the disinhibition of the Thalamus mediated by GPi and the SNr, which over-stimulates the cortex (Ctx), producing the involuntary choreic and hyperkinetic movements characteristic of this stage. At late stages, when striatal neurons from the direct pathway also degenerate, a disinhibition of the GPi and the SNr occurs, producing an over-inhibition of the Thalamus, reducing thus the stimulation of the motor cortex and, consequently, leading to the presence of the parkinsonian and hypokinetic symptomatology appreciable at this stage. (Figure: Thesis of Rafael Alcala vida).

1.4.2. Cognitive impairments

The observed cognitive difficulties in HD can occur years before the diagnosable motor onset of HD (Stout et al., 2011). The declined cognitive functions, like motor deficits, progresses gradually. Notably, in HD patients, they are represented by problems in attention, mental flexibility, planning and emotion recognition, along with cognitive slowing (Stout et al., 2012, 2011). In addition, learning and retrieval of new information is also decreased in the course of HD. Although the speech could be disrupted in HD patients, but language is relatively preserved even at late stages of the disease (Aretouli and Brandt, 2010). Actually, the loss in cognition often intersects with psychiatric domains, where additional problems could be related to HD course like the disability of initiating some actions and the lack of awareness of deficits and disinhibition (Duff et al., 2010). Consequently, HD patients can have social disengagement, decreased participation in conversation and slowed mentation, often associated by lack of awareness of deficits and by impulsivity (Papoutsi et al., 2014).

1.4.2.a. Dorsal striatum and cognition

Old studies, targeting the striatum, have predominantly focused on its implication in different aspects of motor control, which is disturbed in different neurological pathologies. Extensive recent studies of the cortico-striatal loops in the brain have demonstrated other aspects of the striatum's function in decision-making mechanisms, based on affective or reward processes (For review: (Balleine and O'Doherty, 2010; Devan et al., 2011; Grahn et al., 2008). The performance, during these reward-driven actions, reflects the interaction of two different learning processes: one controlling the acquisition of a directed action towards one goal and the other the acquisition of a habit. In the case of "behavior directed towards a goal", the choice of action is governed by an association between the action and its consequence (R-O, responses and outcomes). For learning a habit, the choice of action is controlled by the association between a stimulus and a response (S-R, stimuli and responses). From studies in the Rat (Balleine et al., 1994; Dickinson et al., 1995) and human (Tricomi et al., 2009) have shown that in learning, performance depends primarily on a strategy R-O, but then give way to S-R learning when they become more R-O, but then give way to S-R learning when they become more R-O, more routine.

The investigation of the different neural substrates and their corresponding role in the previously mentioned processed have been studied through lesions-induction of the structures of interest in rodents (Yin et al., 2005) and via imaging experiments in humans (Daw et al., 2006; Gläscher et al., 2009; Tanaka et al., 2008). These studies have evidence that the DMS has a crucial role in learning and expressing behavior, directed towards a goal (R-O) in the rodent. On the other hand, in humans it would be the ventro-median part of the prefrontal cortex and the anterior part of the caudate nucleus which would be involved. Similarly, for the acquisition of habits (S-R), Yin et al. showed that rats with a DLS lesion-maintained R-O behavior even after intensive training, while the control rats used an S-R strategy, demonstrating the crucial role of the DLS in the acquisition of habits (Yin, 2004). By elsewhere, in humans, S-R learning leads to an increase in the activity of the lateral region of the striatum, the caudo-ventral putamen (Tricomi et al., 2009).

Finally, these learning processes have often been considered as competitive and antagonistic processes. However, several arguments suggest that these systems can also cooperate in evaluating and selecting actions. Competition or cooperation of these learning systems would not depend solely on the local interactions of the dorsal striatum but also cortico-striatal, cortico-cortical and cortical interactions and other brain structures that integrate components such as motivational and emotional processes (Balleine and O'Doherty, 2010).

1.4.2.b. Ventral striatum and cognition

The "reward center" represented by the nucleus accumbens has been widely studied for its implication in behaviors associated with appetizers stimuli. However, several studies have shown that many behaviors related to the receipt of rewards are not affected by a disruption in its operation (Castañé et al., 2010; Corbit et al., 2001; Floresco, 2015; Ito et al., 2004). More generally, the accumbens kernel is referred to as a "limbic-motor interface" (MOGENSON et al., 1980) and would play a key role in stock selection, thus facilitating goal-oriented behavior by making it more effective (For review: (Floresco, 2015). The nucleus accumbens receives glutamatergic afferents from the cortex prefrontal and limbic regions (hippocampus, amygdala), which provide different information to promote different behaviors. These glutamatergic inputs

can then be modulated by dopaminergic afferents from ventral tegmental area, to increase the influence of the most protruding entrances and to remove the lowest (Broadbent et al., 2007; Floresco, 2007; O'Donnell, 2003). The nucleus accumbens would therefore be particularly involved in situations where there is an ambiguity, when a set of competing stimuli or actions makes it difficult to identifying the most appropriate way to direct a behavioral approach, or avoidance. The nucleus accumbens could modulate the direction and/or intensity of the behavior to increase the likelihood that certain actions will be committed. This function is probably associated with its afferents to motor regions (Floresco, 2015; GROENEWEGEN et al., 1999; Zahm and Heimer, 1990).

At the anatomical level, the nucleus accumbens consists of two parts, the "core" (nucleus) and the "shell". A dichotomy is observed in the nature of their projections and their cellular and neurochemical diversity, for review: (Castro and Bruchas, 2019), suggesting a different function of the core and the shell in refining the choice of action. Indeed, studies show that the core plays a more important role in establishing a behavioral approach towards a reward signaling stimuli, thus reaching it faster. On the other hand, when the reward is reached or when the behavior is on the way to achieve it, the shell removes irrelevant actions or unrewarded that may hinder the pursuit of the goal, in order to achieve the goal more effectively (Floresco, 2015; Saunders and Robinson, 2012; Stopper and Floresco, 2011).

1.4.3. Psychiatric disorders

In addition to motor and cognitive symptoms, patients very often suffer from depression, sometimes accompanied by thoughts of suicide (Novak and Tabrizi, 2011). Indeed, they are often more anxious, irritable and apathetic. Their behavior and personality change and this usually gets worse during the pathology. These behavioral and psychiatric problems are often the most difficult for patients and their families to bear, triggering hospitalization (van Duijn et al., 2007).

1.4.4. Other symptoms

HD patients suffer from other peripheral problems. For example, they experience significant weight loss, atrophy of the skeletal muscles and testes, and various heart problems and

osteoporosis. These are thought to result either directly from neurodegeneration or the mutated protein's action in skeletal and cardiac muscle cells in particular (van der Burg et al., 2009). The origin of these symptoms is not yet clear. Patients also have communicating and swallowing difficulties which disturb them while eating. Death usually occurs due to cardiac failure or aspiration pneumonia, a condition characterized by gastric reflux into the bronchi (Gil and Rego, 2008).

1.5. HD modeling

The translational potential of an animal model of disease may be determined based on its construct (homology), face (phenotype isomorphism) and predictive validity. These basis help find the best-suited animal model to characterize the molecular mechanisms underlying the pathology and allow the development of therapies of the disease.

The first models of HD appeared long before discovering the genetic mutation, and were therefore based on the neuronal damage observed in patients. Thus, neurodegeneration can be mimicked by injecting neurotoxic products (Ramaswamy et al., 2007), such as posterior kainic acid and quinolinic acid glutamate agonists (Beal et al., 1986; MCGEER and MCGEER, 1976). These "excitotoxic" models have been replaced by models "Energetic", obtained by peripheral administration of mitochondrial toxins, such as malonate or 3-nitropropionic acid (3-NP) which, by causing energetic depletion, resulted in a bilateral preferential spontaneous lesion of MSNs (M. F. Beal et al., 1993; Brouillet et al., 1993; Ferrante et al., 1993). Although these models reproduce the main histological, biochemical and behavioral features of HD, they also have drawbacks, particularly the acute nature of the lesions, which contrasts with the progressive establishment of the striatal degeneration and symptoms of HD.

Then, after identifying the causative gene in HD in 1993, several genetic approaches have been used to generate animal models of this disorder allowing the expression of muHTT and therefore a phenotype closer to that of humans (Pouladi et al., 2013). These approaches can be categorized according to:

- Full length or only fragment of mutated HTT
- The length of the CAG repeat incorporated into the genetic construct
- The expression of the HD mutation from a transgene or knock-in into the endogenous HTT locus
- Use of human HTT or the endogenous gene from the animal
- Use cDNA or genomic DNA containing all the introns and regulatory sequences
- Use of the HTT promoter or another promoter to drive the expression of the mutant protein although transgenic models of Caenorhabditis elegans and Drosophila melanogaster flies, rodents are the most widely used models, which can be categorized according to their genetic modification **(Figure 9).**

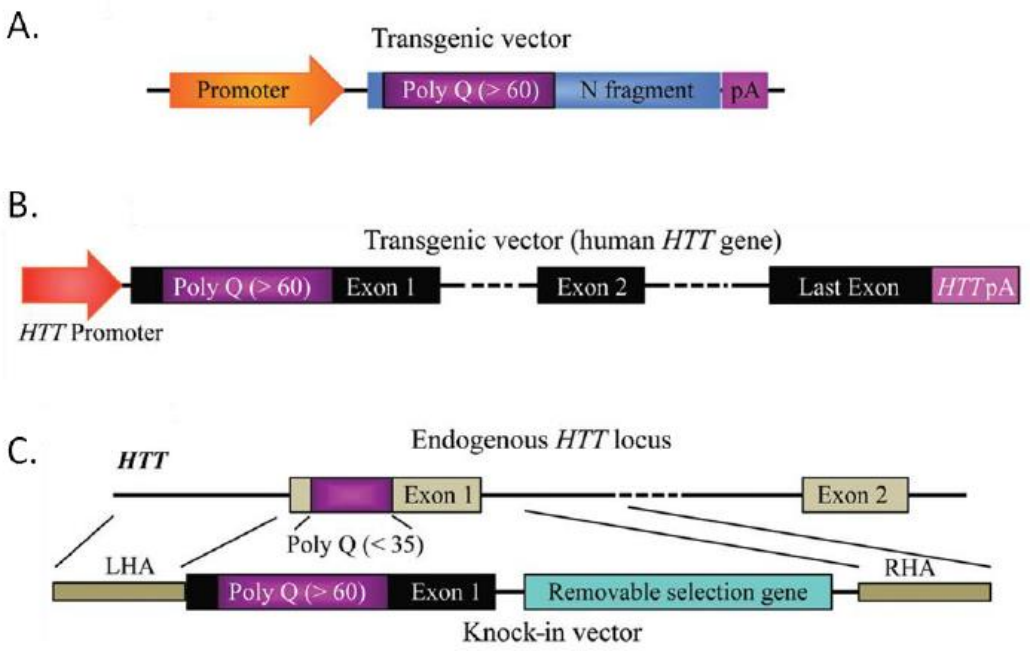

Figure 9: Diagram of the different genetic modification strategies used to generate animal models for HD.
(A) Expression of the N-terminal fragment of HTT with a pathological number of CAG repeats. **(B)** Expression of the entire mutated HTT gene, with its promoter and regulatory regions. **(C)** Targeted replacement of murine exon 1 with mutated human exon 1 generates a knock-in, (adapted from Holm et al., 2016).

Given the diversity of models, mouse models are the most used mammals, by their efficiency, their ease of handling, reproduction and their 99% of shared genes with human.

1.5.1. Transgenic mouse models containing the 5' part of the HTT gene

Due to the size of the *HTT* gene (180 kb) (Ambrose et al., 1994), the first transgenic mouse models contained only a small portion of the gene, including exon 1 with a large number of CAG repeats **(Figure 9A).** Compared to other models, these mice generally exhibit a rapid onset of symptoms, especially the motor and cognitive deficits, weight loss, and premature death (Menalled et al., 2009). This demonstrated that the expression of the N-terminal fragment of HTT support the theory that it is particularly toxic and plays a vital role in pathogenesis. For example, R6/1 and R6/2 mice, the first mouse models of HD, express a 1.9kb fragment containing human HTT promoter and exon-1 under the control of the human HTT promoter (Mangiarini et al., 1996). Originally, this fragment was microinjected into mouse embryos and integrated randomly in 5 regions of the genome of the transgenic mouse. The first generation's analysis revealed that for lines R6/0 and R6/1, the fragment was inserted in one unique copy, unlike the R6/2 line, which integrated three copies. One of the lines (R6/T) has integrated a strongly truncated fragment, and finally, line R6/5 contains four copies of the fragment. Among these lines, R6/1 and R6/2 had the most marked phenotype, associated with the expansion of 116 and 144 CAG, respectively, and 31% transgene expression of the endogenous HTT for the R6/1 mice and 75% for the R6/2 mice (Mangiarini et al., 1996).

The most widely used strain to date is R6/2, with approximately 144 CAG repeats because it exhibits the most robust phenotype. It has been reported that these repeats are unstable and are often larger than initially expected (Menalled and Brunner, 2014). Thus, some R6/2 mouse lines have more than 200 CAG repeats. Surprisingly, the study by Cummings et al. (2012) in R6/2 mice with expansions of 110 to 310 CAG revealed that the number of CAGs and the phenotype show a bell-shaped correlation: an increase in the number of GACs up to 160 is associated with an aggravation of the phenotype of R6/2 mice, while larger expansions, from 200 up to 310 CAG, reduce the severity of the behavioral phenotype and molecular model R6/2 (Cummings et al., 2012; Sawiak et al., 2016). This improvement is correlated with a reduction in the expression of mutated HTT (Dragatsis et al., 2009) and nuclear aggregates (Cummings et al., 2012). However, in R6/2 mice with less than 160 CAG, cognitive and motor deficits are observed respectively from

the age of 3.5 and 5 weeks (Carter et al., 1999; HICKEY et al., 2005; Lione et al., 1999; Mangiarini et al., 1996; Menalled et al., 2009), while cognitive and motor deficits in R6/1 mice were not described before 8 weeks (Hansson et al., 2001). R6/1 and R6/2 mice die early, around 32-40 weeks and 10-13 weeks, respectively, with cerebral atrophy, particularly striatal, and neuropathological changes (Mangiarini et al., 1996; Rattray et al., 2013). However, neuronal losses in the areas affected by the disease are limited, especially in R6/2 mice (Bayram-Weston et al., 2012; Rattray et al., 2013; Turmaine et al., 2000).

Another model expressing only the N-terminal fragment is the N171-82Q mouse, containing 171 AA of huntingtin with 82 glutamines, under the control of a murine prion protein promoter of this transgene mainly in the brain, and more particularly in neurons (Schilling, 1999). This model has fewer CAG repeats, resulting in the pathology's onset later than for the R6/1 and R6/2 mice. Motor and cognitive symptoms appear around the 3rd month. N171-82Q mice also have a reduced lifespan of 5 to 6 months (McBride et al., 2006; Menalled and Brunner, 2014; Ramaswamy et al., 2007).

1.5.2. Transgenic mouse models containing the entire HTT gene

Models containing the entire human *HTT* gene was generated under the control of its human promoter and regulatory elements. For this, different teams have done this either by knock-in of the mutation in the endogenous murine (Wheeler, 1999) Htt gene (Hdh) (For review: (Menalled, 2005), or by insertion of the transgene with the complete human *HTT* gene using an artificial yeast chromosome (YAC - Yeast artificial chromosome) (Hodgson et al., 1999) or an artificial bacterial chromosome (BAC - Bacterial artificial chromosome) (Gray et al., 2008) to produce genetically modified mice expressing mutated human huntingtin (Figure 9B). Knock-in patterns (KI) are generated by homologous recombination on murine embryonic cells (Figure 8C). The most studied mice are the lines HdhQ111 (Wheeler, 1999) , HdhQ150 (Lin, 2001), CAG140KI and zQ175 (Menalled et al., 2012) containing respectively 111, 150, 140 and 190 glutamines. Knock-in models have the advantage of expressing muHTT in the context of the endogenous HTT gene, unlike transgenic mice, where random integration of the transgene can affect its expression. The phenotype of these mice is very light, which explains why most of the studies using these animals

choose homozygous knock-in mice with a more marked phenotype (Menalled et al., 2014)(Menalled and Brunner, 2014). The CAG expansion can then be directly inserted in exon 1 of the murine WT-Hdh gene or a humanized sequence of exon 1. In the first case, the KI lines express mutant murine HTT (Heng et al., 2010; Lin, 2001; Sathasivam et al., 2013), while in the second case, KI mice express a chimeric HTT form with a human part of exon-1 and another murine part (Abd-Elrahman et al., 2017; Menalled et al., 2012, 2003; Stefanko et al., 2017; Wheeler, 2000).

These models have many advantages, including the possibility of obtaining heterozygous animals with one WT-HTT allele and one mutated HTT allele, as in patients. Moreover, their genetic construction is closer to human pathology compared to models expressing a fragment of HTT. Another advantage is the possibility of generating allelic series of KI mice that differ only in the size of their CAG expansion in exon 1, due to the intergenerational instability of the HTT mutation (Neto et al., 2017; Wheeler, 1999). These series show the influence of the size of the CAG expansion on the murine HD phenotype. Thus, several allelic series of KI, from 20 to 365 CAG, were generated by the groups of Wheeler and MacDonald (Wheeler, 1999) and Lin and Detloff (Lin, 2001).

The YAC128 (Slow, 2003) and BACHD (Gray et al., 2008) are mice models containing 128 and 97 glutamines, respectively. Interestingly, the polyQ tail is encoded by CAA-spaced CAGs (also encoding a glutamine) that help to prevent repeat expansion thus stabilizing the mutation (Gray et al., 2008; Menalled and Brunner, 2014; Slow, 2003). Unlike the transgenic models expressing only the N-terminal fragment, the YAC128 and BACHD exhibit a much later phenotype and a relatively average lifespan. Motor problems appear around 6 months in YAC128 mice and are particularly visible on rotarod (Slow, 2003) accompanied by an increase in nuclear HTT. Neurodegeneration of the striatum is evident from 9 months, while the cortex is affected from one year. muHTT aggregates diffuse within neurons, accumulate and are visible in the striatum from 12 months of age. The BACHD mouse presents motor coordination problems from 2 months and the muHTT aggregates are detected in the cortex and very weakly in the striatum (Gray et al., 2008). Surprisingly, while HD patients suffer from weight loss, both transgenic mouse lines

show an increase in body mass. Thus, this should be taken into consideration when interpreting motor tests since weight can also influence mice's activity level (Menalled et al., 2014).

1.5.3. Rat models for HD

In addition to mice, there are also HD rat models, including two models: a transgenic rat (TgHD-CAG51n) with 51 CAG under the control of the promoter of endogenous HTT (von Horsten et al., 2003) and a model created with a BAC containing entire HTT with 97 CAG/CAA and its promoter (BACHD) (Yu-Taeger et al., 2012). TgHD-CAG51n rats exhibit a neuropathological phenotype, motor deficits, and cognitive effects between 6 and 9 months (Kirch et al., 2013; Nguyen et al., 2006; Ortiz et al., 2012). It would be the first model to show movements equivalent to chorea in humans i.e., rapid, irregular, and brief movements in the neck (Cao et al., 2006; von Horsten et al., 2003). Motor deficits have been described in BACHD rats from the age of 1 month, cognitive deficits from 6 months, and molecular alterations, mainly around 12 months (Yu-Taeger et al., 2017, 2012) .

Although the mice models are mainly used to study HD, rats also have many advantages due to their size, ease of manipulation for specific behavioral tasks, and their metabolic characteristics and pharmacologically similar to those of humans. On the other hand, the phenotype of rat models of HD is moderate with variable behavioral outcomes, thus limiting their use.

1.5.4. Large animal models

Different groups have developed larger animal models to assess the effect of mutated huntingtin for long term, on species with a longer lifespan than rodents. On the other hand, it is also interesting to study HD in animals whose brain size approaches humans, particularly for questions of administration and bio-distribution of therapeutic molecules. Thus, in recent years, different models have been generated, such as a rhesus monkey expressing exon 1 of the human HTT gene with 84 CAG repeats. However, these transgenic non-human primates present reproduction and longevity problems (Yang et al., 2008), which complicates their use. A sheep model was also created, by integrating a transgene containing the entire human HTT cDNAs with

69 CAG repeats (Jacobsen et al., 2010). Likewise, teams have developed transgenic dwarf pigs expressing 124 glutamines (Baxa et al., 2013) and a sheep model (Ovis aries) microinjected with a full length human *HTT* cDNA containing 73 polyglutamine repeats under the control of the human promotor (Jacobsen et al., 2010). Overall, these animals do not exhibit a very marked phenotype but may be interesting, particularly in the long-term evaluation of the toxicological profile of therapeutic molecules.

1.5.5. In vitro models: iPSCs

Animal models are widely used to study neurodegenerative diseases and allow many advances in understanding the pathogenic mechanisms underlying neuronal degeneration. However, they have limits and do not represent human pathology in all its aspects. Lack of availability of post-mortem brain tissues from well-characterized patients makes the study of these mechanisms complicated in humans. Recently, the advent of cell differentiation techniques from induced human pluripotent stem cells (iPSCs) has allowed the emergence of new cell models of HD (The HD iPSC Consortium, 2012). These will enable the study of molecular mechanisms, altered by mutated HTT, and the discovery of new therapeutic targets, some of which are tested in animals and show encouraging results.

The first iPSCs were generated from patient's fibroblasts containing 54 and 72 CAG repeats, thanks to a retroviral induction of factors causing pluripotency (Oct3 / 4, Klf- 4, Sox2, c-Myc) (Park et al., 2008; Zhang et al., 2010). They showed that iPSCs from patients could be differentiated into MSNs (Zhang et al., 2010). Many lineages currently exist, most of which were created by the HD iPSCs Consortium, with a varied number of CAG repeats, ranging from 17 to 180 (For review: (Geater et al., 2018; Tousley and Kegel-Gleason, 2016).

Several studies show that these cells exhibit metabolic alteration, transcriptional cell adhesion defect, and increased cell death (An et al., 2012; Ring et al., 2015; The HD iPSC Consortium, 2012). IPSCs lines from juvenile patients (> 70 CAG) present additional molecular alterations, axonal level and altered calcium signaling (Ring et al., 2015; The HD iPSC Consortium, 2012).

The iPSCs and their derived neurons have been used in particular to screen molecules for therapeutic purposes and assess their effects on neuronal survival (Cheng et al., 2013; Dickey et al., 2016; Yao et al., 2015). In other studies, these models are used to study the impact of the HTT mutation on neurodevelopmental processes or to study the mechanisms preceding neuronal death (Molina-Calavita et al., 2014; Nguyen et al., 2013).

Recent advances in genetic modification technologies (Zinc finger nucleases- ZFN, Transcription activator-like effector nucleases - TALENS, clustered regularly-interspaced short palindromic repeats/Cas9-CRISPR/Cas9) also modify iPSCs to study the effect of SNPs (An et al., 2014). Finally, at the epigenetic level, it shows that the epigenetic characteristics of iPSCs originating from their somatic tissue of origin are lost during the of cell line passages(T.-K. Kim et al., 2010a).

One of the advantages that iPSCs could be a good HD model is the possibility of studying human neuropathology, even before the onset of the disease, without depending on the patients' post-mortem tissues. However, at this time, several parameters are not fully understood, such as the genetic variability of iPSCs (genetic anomalies, somatic instability of CAG expansion), validation of the pluripotency of iPSCs and the characteristics of MSNs resulting from their differentiation. Also, the studies' design is sometimes not optimal because the work is generally carried out on one, or even two, iPSCs lines and often lack suitable control lines. In addition, many problems of reproducibility at the level of the differentiation step are also encountered, since protocols and culture conditions are variable between laboratories.

2. Molecular mechanisms and pathogenesis of HD

2.1. The HTT gene

The *HTT* gene, previously known as *IT15* and located on chromosome 4, covers 180 kb and contains 67 exons. At the very N-terminal end, the first exon has been extensively studied since the mutation responsible for HD is located in this part (Ambrose et al., 1994) **(Figure 10).**

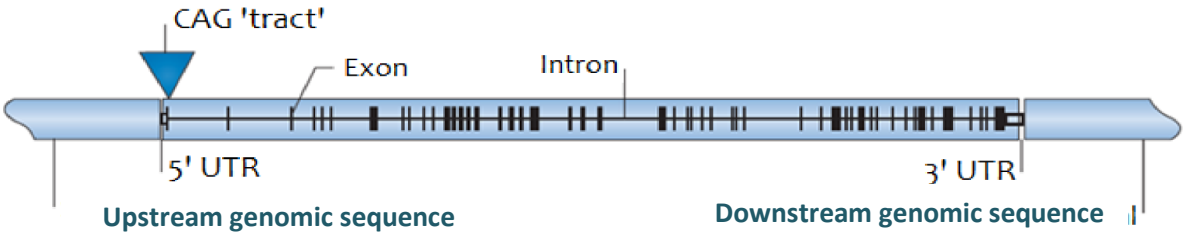

Figure 10: Diagram showing the IT15 or HTT gene encoding Huntingtin.
The vertical rectangles correspond to exons, while the lines symbolize introns. The expansion of CAG, or "CAG tract," is located in exon 1. The upstream and downstream genomic sequences are also shown schematically with the 5 'and 3' UTR (untranslated region) regions (adapted from (Pouladi et al., 2013).

HTT has two major mRNA transcripts: a large 13.7 kb transcript predominantly in the brain and a shorter 10.3 kb transcript found in other tissues such as the heart, muscles, liver, and lungs. Both transcripts vary only by their 3'UTR region (Ambrose et al., 1994; Lin et al., 1993) and therefore code the same 348 kDa protein (MacDonald et al., 1993), Huntingtin. Recently, alternative splicing has been reported for *HTT* with the generation of *HTT* variants that could lack exons 10, 12, 29, and 46 or, alternatively, retain a 57-bp portion of intron 28 or have an additional exon 41b. Although rare, these variants could modify the function of canonical HTT protein-protein interactions, regulation by phosphorylation, and/or susceptibility to cleavage (Hughes et al., 2014; Ruzo et al., 2015).

The HTT protein can also give variants by proteolysis of the whole protein. **Figure 11** thus shows the PEST domains (rich in proline, glutamic, aspartic, serine, and threonine), which are the sites of cleavage by proteases (for review: (Saudou and Humbert, 2016a).

2.1.1. Huntingtin: Biology and Physiology

2.1.1.a. Huntingtin through evolution

HTT protein is ubiquitously expressed with the brain's highest expression level compared to the peripheral nervous system (G. Vonsattel and DiFiglia, 1998; Moffitt et al., 2009). It is present in neurons, glial cells (Ross and Tabrizi, 2011; ZUCCATO and CATTANEO, 2007) and immune cells (Li and DiFiglia, 2012). At the cellular level, HTT Htt is widely expressed, predominantly in the cytoplasm, but can also be found in the nucleus.

Different comparisons among species show that HTT protein is well conserved from flies to mammals. One study focused on the fish Fugu rubripes, the vertebrate with the smallest genome (Baxendale et al., 1995). It shows that, despite a locus homologous to the human *HTT* gene covering only 23 kb in this fish, the 67 exons are still found. On the other hand, it is interesting to note that the beginning of exon 1, which contains the CAG repeats, is remarkably conserved between species. Indeed, the first 17 amino acids (AA) are strictly identical between Fugu, mice, and humans; however, they differ in the number of glutamines with 4, 7, and at least 6 respectively (Barnes et al., 1994; Baxendale et al., 1995). The murine homolog named *Hdh*, located at chromosome 5, is particularly close to the human sequence. It exhibits 86% and 91% identities at nucleotide and protein levels, respectively (Barnes et al., 1994). This high degree of conservation among vertebrates and particularly among mammals, indicates a vital role for Huntingtin.

Figure 11: Schematic representation of the sequence of human HTT protein.

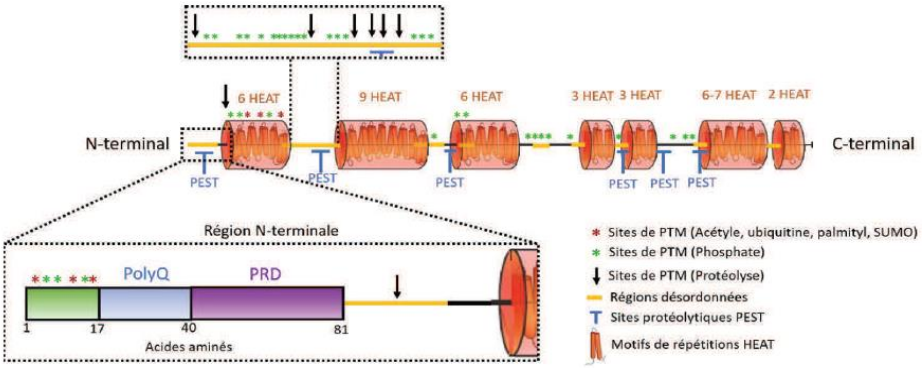

HTT has several HEAT interaction domains and, in its N-terminal part, a PRD interaction domain alongside the polyQ expansion. HTT has many PTM sites: several sites are concentrated in the N-terminal region of 17 amino acids that precede the polyQ expansion, but other sites are also present throughout its protein sequence. PTM: post-translational modifications; HEAT:

Huntingtin, elongation factor 3, protein phosphatase 2A, TOR1; PEST: Proline, glutamate or aspartate, serine, threonine; PRD: proline rich domain; polyQ: polyglutamine. From (Saudou and Humbert, 2016a).

2.1.1.b. The structure of Huntingtin

Unfortunately, there is no significant homology between huntingtin and other known proteins to learn more about its function. The N-terminal end of the protein has been mainly studied since it contains the polyglutamine ((Q)n) expansion, which is located after the first 17 AA and before a proline-rich domain (PRD) (Cattaneo et al., 2005), as shown schematically in **Figure 11**. These 17 amino acid residues function as a nuclear export sequence. They can be subjected to post-translational modifications, which can influence the cell localization and the clearance of HTT (for review, (Saudou and Humbert, 2016a). These also form a helical structure, particularly important for protein retention in the endoplasmic reticulum (Atwal et al., 2007; Rockabrand et al., 2007). The PRD is crucial for protein-protein interactions. Its secondary structure forms a relatively stiff proline-proline helix, which could play a role in stabilizing the polyQ expansion (Southwell et al., 2008). The C-terminal part contains a nuclear export signal (NES) (Xia, 2003).

Including HTT, HEAT tandem repeats of about 40 nucleotides have been found in different proteins. It is named HEAT due to four proteins first identified with this motif: huntingtin (H), elongation factor 3 (E), protein phosphatase 2A (A), and kinase TOR1 (T)(Andrade and Bork, 1995). These repeats are composed of two anti-parallel α helices providing scaffolding for many protein complexes by promoting inter- and intra-protein interactions (Palidwor et al., 2009). Thus, different regions of HTT can interact with each other, sometimes integrating other protein complexes and leading to more than 100 different structural conformations (Seong et al., 2010).

2.1.1.c. Post-translational modifications of Huntingtin

HTT protein is subjected to various Post-translational modifications: acetylation, phosphorylation, SUMOylation, ubiquitination, palmitoylation (**Figure 11).** These processes are important for modulating its interactor affinity, subcellular localization, proteolysis, or degradation (Ehrnhoefer et al., 2011).

These characteristics make HTT indispensable for the proper functioning of cells. Thus, it appears that HTT has crucial roles in cells, potentially via different domains, where the loss of the anti-apoptotic functions of HTT may contribute to HD **(Figures 11 and 12).**

In addition, HTT is subjected to proteolytic cleavage by many proteases (caspases, calpains, cathepsins, and metalloproteases). The proteolytic sites are located in the PEST domains (rich in proline -P- residues, glutamic -E- or aspartic -D-, serine -S-, threonine -T-), mainly present in the disordered regions of HTT (**Figure 11**). This cleavage's physiological role is still poorly understood. Nevertheless, this phenomenon would occur mostly in pathological conditions, often associated with caspases and/or cell death. N-terminal fragments of mutated HTT have been studied for their possible roles in mutation toxicity. However, Wellington et al. (2002) show that HTT cleavage occurs even in wild conditions (Wellington et al., 2002).

2.1.1.d. Huntingtin interactors and physiological roles

Many studies were performed to understand the function of HTT. They showed that HTT and its interacting proteins are involved in the development and neuronal physiology, leading to an essential role of HTT at the cellular level (Saudou and Humbert, 2016a). It is implicated in the regulation of transcription (Nucifora et al., 2001), membrane dynamics (Kegel et al., 2009), mitochondrial efficiency (Aoyama et al., 2006), brain-derived neurotrophic factor (BDNF) transcription (Zuccato, 2001), autophagy (Cortes and La Spada, 2014; Jeong et al., 2009; Kegel et al., 2000; Qin, 2003), and endosomal recycling (Li and DiFiglia, 2012) (Figure 7). More than 350 partners have been identified to bind particularly to the HEAT repeats and to the PRD of HTT (Harjes and Wanker, 2003).

Also, the C-terminal end is considered as a site of interaction with the transcription factor NF-κB p50, suggesting a potential role of HTT as a regulator of specific genes (Takano and Gusella, 2002). HTT is indispensable for embryonic development. Embryonic death at the pre-gastrulation stage reveals the lethal trait of HTT in HTT knockout (Mühlau et al., 2012) and the conditional knockout mice (Cre Lox KO under the CamKII promoter). Even with a 50% expression drop, mice die soon after birth and show malformations of the cortex and striatum (White et al., 1997). Moreover, the late disruption of the gene in adult mice leads to progressive neurodegeneration (Dragatsis

et al., 2000). These results have been supported by studies showing the implication of HTT in neuroblasts differentiation (Reiner et al., 2001) and neuron migration (Barnat et al., 2017; Tong et al., 2011).

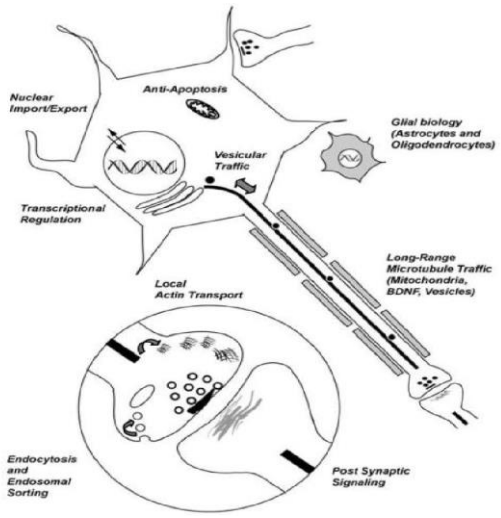

Figure 12: Schematic illustration of WT-HTT biological functions.
A generic neuron with an unsheathed axon (gray boxes represent oligodendrocyte wrapping) and an astrocyte (gray stellate shape). Enlarged circle is a magnified view of a synapse (Schulte and Littleton, 2011).

The subcellular localization of HTT is complex, dynamic and may change conformation depending on its compartmental localization. HTT binds to cytoskeletal proteins such as dynactin and kinesin via its interaction with Huntingtin-associated protein 1 (HAP-1). It controls anterograde and retrograde transport in the axon and neuronal dendrites (Colin et al., 2008; Gauthier et al., 2004; Liot et al., 2013; Twelvetrees et al., 2010; Wong and Holzbaur, 2014). It localizes along microtubules and participates in the transport of a variety of cargo, including mRNAs, proteins, vesicles, and organelles, such as mitochondria (DiFiglia et al., 1995; Kegel et al., 2009, 2000; Schulte and Littleton, 2011) **(Figure 12)**.

At the synapse, HTT has been suggested to have both pre- and postsynaptic roles regulating both neuronal and glial function. It is present in excitatory synapses, where it is associated with synaptic vesicles in the presynaptic terminal, facilitating neurotransmitter release (DiFiglia et al., 1995; Jeong et al., 2009). In the postsynaptic density, HTT is associated with the postsynaptic scaffolding protein PSD95 (Figure 12) (Sun et al., 2001).

It is known that HTT has anti-apoptotic and/or pro-survival properties by modulating apoptosis signaling of caspase-3 and 9 where increased wild type (wt)-HTT expression improves brain cell survival (Rigamonti et al., 2001; Zhang et al., 2006). On the contrary, cells depleted of wt-HTT were more sensitive to apoptotic cell death. They showed an increased caspase-3 activity level compared to control cells (Zhang et al., 2008). Studies in Michael Hayden's group also supported the anti-apoptotic role of Htt. They found that primary striatal neurons from YAC18 transgenic mice overexpressing full-length wild-type human huntingtin were protected from apoptosis compared with cultured striatal neurons from non-transgenic littermates and YAC72 mice expressing mutant human huntingtin (Leavitt et al., 2006).

Another way huntingtin produces anti-apoptotic effects is through regulation of the neurotrophic factor BDNF. Indeed, wt-HTT regulates BDNF gene transcription, downregulated in HD (Rigamonti et al., 2001, 2000; Zuccato, 2001; Zuccato et al., 2003), its transport along the axon, and its vesicular release at the level of cortico-striatal synapses (Gauthier et al., 2004; Saudou and Humbert, 2016b; Zuccato, 2001), using microfluidic arrays, a particularly important mechanism because the striatum does not synthesize this factor neurotrophic (Baquet, 2004). Moreover, HTT levels modulate neurons' sensitivity to apoptotic death elicited by N-Methyl-D-aspartate (NMDA) receptor-mediated excitotoxicity (Leavitt et al., 2006), where Wt-Htt can decrease cellular toxicity of mutant HTT (muHTT) in vivo.

Although HTT is widely present in the cytoplasm, it is also found in the nucleus. It can interact with many transcription factors and/or cofactors (Francelle et al., 2017) such as CBP (cAMP Response Element (CREB) –Binding Protein), NeuroD, Sp1 (Specificity protein 1), NF-kB (Nuclear factor-kB), and p53 (Tumor suppressor protein 53). HTT also interacts with transcriptional activators and repressors, for example, TAFII130 (TATA box–binding protein (TBP) -associated factors (TAFs), REST/NRSF (Repressor element-1 transcription factor/neuron restrictive silencer factor), and NCOR (Nuclear co-repressor). Through its interactions, HTT can promote activation or suppression of transcription of certain genes. As mentioned above, HTT promotes the transcription of the gene encoding the BDNF, the promoter of which contains an

NRSE motif, by sequestering REST/NRSF in the cytoplasm, thus preventing the formation of the RE1/NRSE repressor complex at the BDNF gene (Zuccato, 2001) (Check part 2.3.2. Interaction of mutated huntingtin with transcription regulators, page:54)

2.1.2. Mutated huntingtin

2.1.2.a. From fragmentation to aggregation

HTT, when mutated, shows polyQ expansion in its N-terminal end, which consequently changes its properties and thus its function. Many studies show that HTT cleavage is a critical step in HD pathogenesis.

The processing of muHTT, through proteolysis, produces HTT fragments that could be grouped into two categories: toxic N-terminal fragments containing polyQ expansion, and C-terminal fragments whose role is poorly characterized. El-Daher et al. (2015) have shown that specific cleavages alter intramolecular interactions of HTT. The C-terminal fragments would induce toxicity by triggering the endoplasmic reticulum's stress leading to cell death (El-Daher et al., 2015). On the other hand, the toxic N-terminal fragments, whose corresponding poly-adenylated mRNA is translated into a protein containing only exon 1 of HTT can also be generated by aberrant splicing of mutated HTT intron 1 (Sathasivam et al., 2013). Thus, the translocation of the N-terminal fragments of HTT into the nucleus contributes to the dysfunction and degeneration of neurons (Landles et al., 2010; Ross and Tabrizi, 2011; Saudou et al., 1998; Saudou and Humbert, 2016b). In addition, the three-dimensional structure of the mutated HTT and its fragments being modified through the expansion of polyQ, these have a strong propensity to combine to form oligomers that aggregate in the nucleus and cytoplasm of neurons in patients as in mouse models of HD (Figure 13) (Davies et al., 1997; DiFiglia et al., 1997; Gutekunst et al., 1999; Landles et al., 2010; Lunkes et al., 2002; Ross and Poirier, 2005; Trottier et al., 1995).

Sense and antisense mRNAs with shifting of the reading frame and which are not ATG dependent can be produced. Therefore, expansion proteins homopolymers of the polyAla, polySer, polyLeu and polyCys type called RAN (Repeat- Associated Non ATG), are translated, accumulate and aggregate. Likewise, mutated HTT RNAs can form hairpin structures hair, sCAG RNAs, which

interfere with the transcription of genes and cellular functions (Bañez-Coronel et al., 2015) **(Figure 13)**.

In the cytoplasm, mutated HTT aggregates disrupt proteostasis by affecting protein clearance mechanisms, axonal transport, or mitochondrial metabolism. At the nuclear level, the aggregates cause transcriptional deregulation by sequestering many transcriptional factors and co-factors (Check part 2.3.2. Interaction of mutated huntingtin with transcription regulators, page: 54) (Nucifora et al., 2001; Ross and Tabrizi, 2011; Steffan et al., 2000) **(Figure 13).**

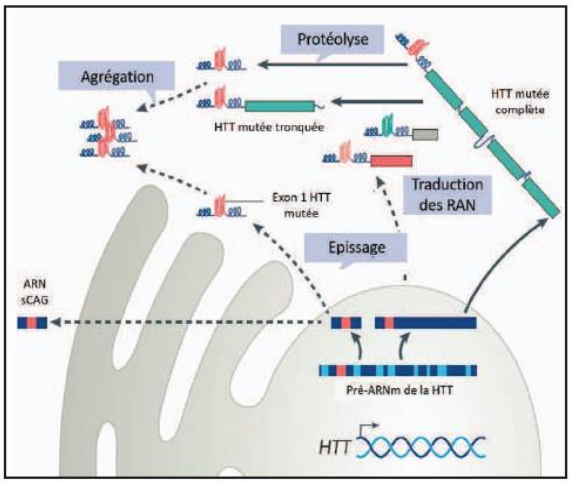

Figure 13: The multiple toxic variants of mutated HTT.
Fragments of mutated HTT, particularly that from exon 1, are toxic and can be generated from several ways: by proteolysis of complete HTT, by aberrant splicing of mutated HTT RNA or again following a shift in the reading frame resulting in the formation of RAN (repeat-associated non ATG). These fragments can then form oligomers and aggregates. Mutated HTT RNA can also form small hairpin RNAs (sCAGs RNAs) (From (Caron et al., 2018).

But, mutated HTT aggregates could have a protective effect by reducing the amount of particularly toxic soluble mutated HTT, highly correlated with neuronal death, Indeed, the amount of soluble mutated HTT correlates with neuronal death. Arrasate and collaborators (2004) show that a large number of neurons degenerate without even contain aggregates of mutated HTT (Arrasate et al., 2004; Kim et al., 1999). In addition, the suppression of aggregate formation increases neuronal death associated with mutated HTT (Saudou et al., 1998). Finally, it has been shown that aggregates of mutated HTT, by reducing the amount of soluble mutated HTT, promote neuronal survival (Arrasate et al., 2004; Miller et al., 2010; Saudou et al., 1998).

2.1.2.b. Mutated Huntingtin: Loss of Function or gain of Function?

In HD, the conventional model of neurodegenerative diseases, two non-exclusive debates were aroused to explain the disturbances observed in the disease's context: loss of function of the wild protein vs gain of function of the mutated protein.

Several data support the hypothesis that HD results from toxic gain of function of the mutated protein. It can be illustrated by the dominant mode of HD transmission where a single mutated allele is sufficient to trigger the disease (Gillian P Bates et al., 2015; Lee et al., 2012; Menalled et al., 2003). Moreover, the abnormal expansion of CAG is itself toxic since its expression, alone or with a fragment of HTT, causes neurological symptoms in mice. A study has also shown that the addition of CAG repeats in the murine Hprt (hypoxanthine phosphoribosyl transferase) gene, which is not originally involved in any disease, leads to intranuclear inclusions and neurological damage leading to the early death of the animals (Ordway et al., 1997). Also, the produced fragments upon HTT cleavage or splicing are also toxic and prone to aggregate. They are detected very early, before the onset of pathogenesis (Jeremy M. Van Raamsdonk et al., 2005; Wellington et al., 2002) (Figure 14).

On the other hand, the pathogenesis would not result only from gain of toxic function of the mutated HTT. Studies show that it may result from progressive loss of normal function of HTT **(Figure 14).** The homozygous KO model for HTT being lethal (Duyao et al., 1995; Nasir et al., 1995; Zeitlin et al., 1995), and the conditional inactivation of the murine *Hdh* gene at E15 and P5 mouse brain leads to progressive neurodegeneration, which would support the hypothesis of loss of function in the pathogenesis of HD (Dragatsis et al., 2000).

In addition, in patients, predominantly heterozygous, wt-HTT is reduced by half. Studies show that many consequences are obtained upon normal HTT lowering strategies, in both healthy and mutant settings: on the one hand, heterozygous KO mice for HTT present cognitive and motor deficits as well as neurodegeneration in STN and globus pallidus, a moderate phenotype comparable to that of KI mice HD models (Nasir et al., 1995; O'Kusky et al., 1999); on the other

hand, Van Raamsdonk and collaborators (2005) generated a mouse model of HD, the YAC128 mouse, only expressing muHTT. These mice exhibit motor deficits and reduced life expectancy compared to normal YAC128 mice (Jeremy M Van Raamsdonk et al., 2005) These results support the hypothesis that part of the pathogenesis of HD is linked to the loss of function of wt-HTT.

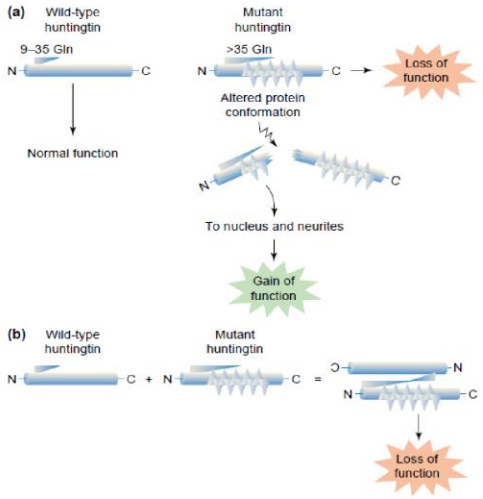

Figure 14: Potential mechanism of cell death in HD.
HD may be viewed as a double disease, it is caused by both a new toxic property of mHtt and by a loss of the neuroprotective activity of wt-Htt (Cattaneo, 2001).

In conclusion, several alterations co-exist, the mutation confers a gain of toxic function to HTT, a characteristic found in all expanding diseases polyQ (cerebellar ataxias, or squamous-bulbar muscular atrophy for example – For review:(Orr, 2012b)), which also explains some phenotypic similarities. But the mutation also alters the normal functions of HTT, and their dysfunction contributes the pathogenic mechanism of HD.

2.2. Cytoplasmic protein toxicity of mutated huntingtin

The combined effects of the mutated HTT alter several cellular processes, such as protein degradation, mitochondrial respiration, and transcription, among many others, leading to neuronal dysfunction and cell death **(Figure 15)**. At the cytoplasmic level, HTT mutation will modify protein clearance, protein interactions, mitochondrial function, endoplasmic reticulum, axonal traffic, and also NMDA receptors activation (For review: (Ross and Tabrizi, 2011).

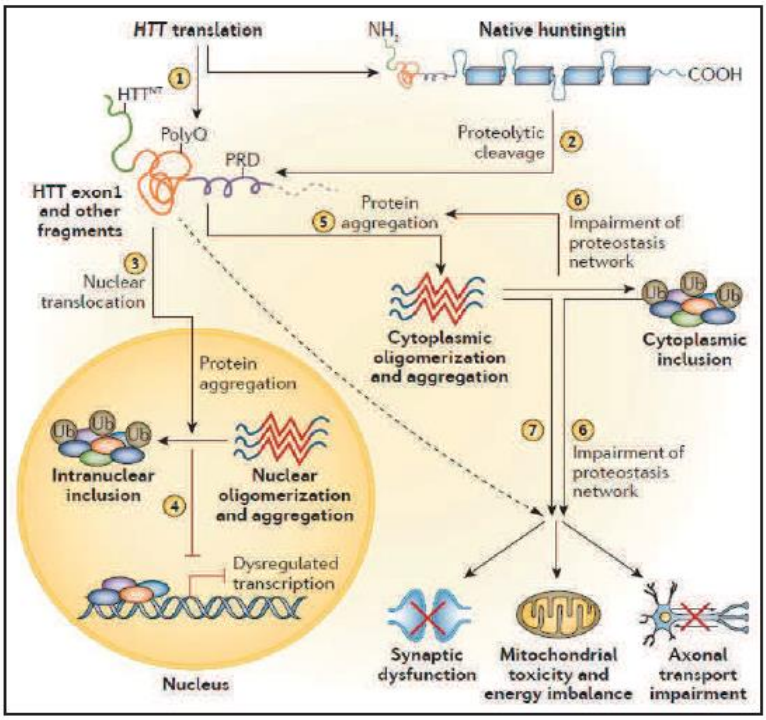

Figure 15: Proteotoxicity of mutated HTT and its fragments.
Fragments of mutated HTT are particularly toxic to neurons and are formed by proteolytic cleavage of HTT (2). Another fragment, called exon 1 of HTT, is generated by abnormal splicing (1). These toxic fragments can enter the nucleus (3), where they will form oligomers and aggregates. By sequestration of many factors, these aggregates disrupt the transcriptional machinery and gene expression (4). Toxic fragments can also aggregate in the cytoplasm of neurons (5) and disrupt overall proteostasis and cellular functions (6, 7). This overall alteration of the cell further exacerbates the aggregation of mutated HTT, which is not more eliminated (6) (Gillian P Bates et al., 2015).

2.2.1. Altered intracellular proteolysis

Protein conformational change, upon mutation, leads to partial unfolding or abnormal folding of HTT. In the cytoplasm, although the cellular homeostasis is disrupted and the proteasomes are less efficient in HD, full-length muHTT is cleaved by proteases. In an attempt to protect against the toxic insults of muHTT proteins and enhance its clearance, the obtained fragments are

subjected to two distinct, but related, pathways of degradation of toxic proteins: autophagy and the ubiquitin-proteasome system (UPS).

2.2.1.a. Autophagy

Autophagy is a process whereby cells remove cytosolic proteins and organelles and, in certain circumstances, degrade themselves from within. Depending on the addressed cargo to lysosomes, it can be decided into three categories: autophagy coordinated by chaperones that address cytosolic proteins directly to lysosomes, micro-autophagy that degrades fragments of the cytosol by lysosomal membrane invagination, and macro-autophagy, more commonly known as autophagy, which sequesters large portions of the cytoplasm in vesicles called autophagosomes, where after maturation, fuse with lysosomes to allow degradation **(Figure 16).**

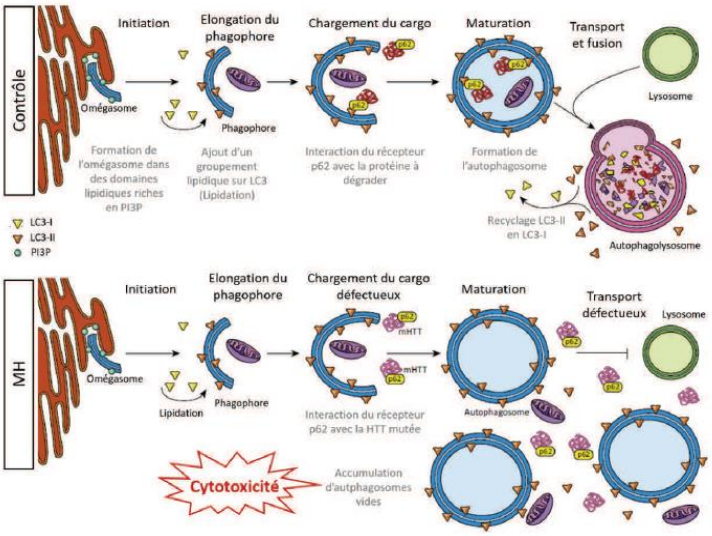

Figure 16: Autophagy dysfunction in HD.
Autophagy involves the formation of a vesicle with a double lipid membrane, the autophagosome, formed from its precursor, the phagophore. The phagophore itself is formed by an elongation of the omegasome, a protusion of the endoplasmic reticulum (ER) enriched with PI3P lipid. Once formed, the autophagosome incorporates organelles and proteins to degrade, sometimes requiring an autophagic receptor like p62. It then fuses with the lysosome to achieve the proteolysis. In the HD (bottom), the cargo loading process is faulty because the mutated HTT would interact with the receiver p62. This defect results in an accumulation of empty autophagosomes and cytotoxicity. (From (Martin et al., 2015).

Selective forms of autophagy exist against the mitochondria or aggregated proteins like mutated HTT. This involves autophagic receptors such as p62 or OPTN. They create a link between the cargo and the proteins anchored in the autophagosomal membrane, such as the LC3-II protein, and allow selective addressing of particles to be degraded to the autophagosome. This has been

recorded in the HD mice model's brains, but the impaired cargo recognition alters its own clearance (Martinez-Vicente et al., 2010). Apoptotic stimuli can induce autophagy in the presence of caspase inhibitors (Merienne et al., 2003). It may contribute to cell death by regulating lysosomal proteases cathepsin B and D (Goula et al., 2012; OHSAWA et al., 1998). Also, the enhancement of autophagy can be obtained by inhibiting Rapamycin's mammalian target (mTOR) by Rapamycin. It improves the survival curve in the R6/2 HD mouse model (Ravikumar et al., 2004), which could be a good trail to develop new therapeutic tools.

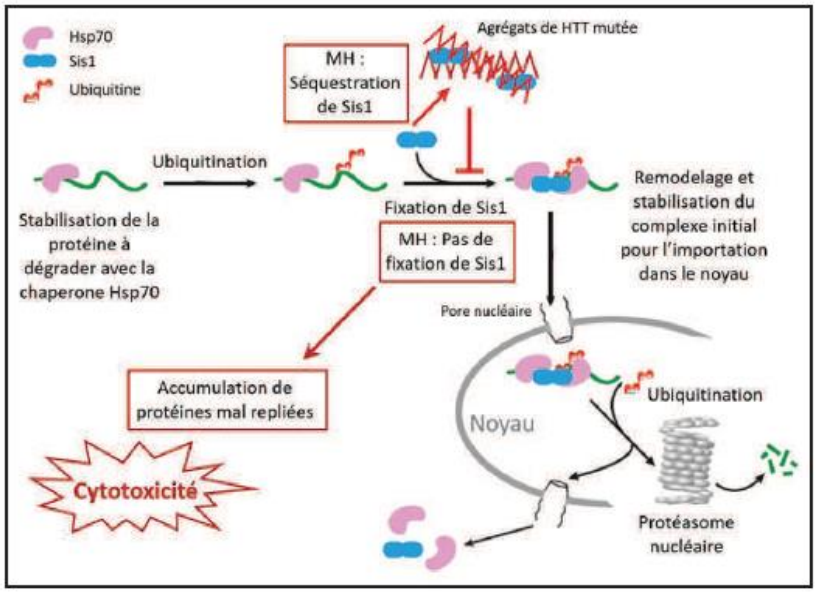

Figure 17: UPS system malfunction in HD.
The UPS system requires the intervention of chaperones to stabilize the proteins to be degraded. The chaperone Sis1 plays a very important role in the proteolytic process since its attachment to the misfolded protein is necessary for its import into the nucleus, where the proteasome will degrade it. But in HD, Sis1 and other chaperones are sequestered in aggregates of mutated HTT, thereby preventing the breakdown of misfolded proteins that accumulate in the cell (From Park et al., 2013).

These data suggest increased autophagic processes in HD; however, this is not correlated by increased protein degradation. Martinez-Vicente et al. (2010) show that autophagosomes are empty content. However, they are increased in HD, which could be due to impaired recognition of the cargo (Martinez-Vicente et al., 2010). Thus, the later could contribute to cytotoxicity due to accumulated HTT aggregates and non-degraded organelle in the cytoplasm even though autophagy initiation is induced. Autophagy induction's failure mechanisms are not well understood, but this could be linked to an aberrant interaction between the autophagic p62 receptor and mutated HTT (Martinez-Vicente et al., 2010). In addition, mutated HTT amplifies

the mechanistic defects of autophagy in HD, by deregulating the transcription of genes associated with these processes and by altering vesicular traffic (For review: (Martin et al., 2015)).

2.2.1.b. UPS system

Substrates labeled by conjugated chains of ubiquitin are of high precision to be recognized and targeted by the Ubiquitin-dependent proteasome system. The polyubiquitinylated molecules are detected by the 26S proteasome, a proteolytic complex. The UPS system usually degrades soluble proteins. Thus it has limited efficiency in the clearance of aggregated protein like HTT (Shaid et al., 2013).

In HD, among many other systems, the UPS system is impaired. This defect would involve accumulating mutated HTT in insoluble aggregates containing ubiquitin (Mitra et al., 2009; Sieradzan et al., 1999; Waelter et al., 2001). This is because muHTT inclusions sequester components of the system, like the Hsp40 chaperones and Sis1p, along with the conformation of polyglutamine expansions which is not optimal for entering the catalytic site of the proteasome, preventing the delivery of misfolded proteins to the proteasome (Figure 17) (Park et al., 2013; Zheng and Diamond, 2012).

Besides, the proteasomes themselves would also be sequestered in the aggregates (Holmberg et al., 2004). Still, it has been shown that this recruitment is reversible and that the sequestered proteasomes remain active and accessible to substrates (Schipper-Krom et al., 2014). A failure of the UPS system could also lead to an increase in autophagy via communication between degradation pathways to maintain normal proteostasis in neurons affected by the toxicity of mutated HTT (Ding and Yin, 2008; Pandey et al., 2007).

2.2.2. Endoplasmic reticulum stress

Protein synthesis and maturation takes place essentially in the endoplasmic reticulum (ER). They are folded and assembled into multiprotein complexes involving chaperone proteins, like the binding immunoglobulin protein (BiP) or GRP94, regulating any errors during the process. This is considered as a critical step to assure the transfer of the correctly folded protein to the

Golgi apparatus; otherwise, the misfolded proteins are either retained in the ER to be corrected by chaperon proteins or directed toward the proteasome after being ubiquitinylated following the Endoplasmic Reticulum-Associated Degradation (ERAD) pathway.

In HD, as in any other pathological condition, proteins with abnormal conformation increases in the ER, leading to chaperones protein and degradation saturation. This chaos triggers an ER stress and thus activates the Unfolded Protein Response (UPR). Once reaching very intense and prolonged stress, it induces the elimination and the refolding of damaged proteins or triggers cell death by apoptosis (Hetz and Papa, 2018). In fact, ER stress was observed very early, even before the formation of mutated HTT aggregates as shown in in-vitro models (Duennwald and Lindquist, 2008; Leitman et al., 2013), murine (Carnemolla et al., 2009; Cho et al., 2009; Noh et al., 2009; Vidal et al., 2012) and in the postmortem brain of patients (Carnemolla et al., 2009). Thus, it is considered as a compelling determinant of cellular toxicity in HD.

The stress of the ER would be triggered by inhibition of the ERAD pathway following the interaction of soluble mutated HTT with its different factors (Duennwald and Lindquist, 2008; Leitman et al., 2013). For example, the ATPase and chaperone p97/VCP proteins involved in ERAD and their cofactors Npl4 and Ufd1, are sequestered by mutated HTT. This interaction results in ER stress, UPR response, and neuronal apoptosis (Leitman et al., 2013). Other cellular factors are sequestered in the aggregates, such as USP14 (Ubiquitin specific protease 14) or ATF5 (Activating transcription factor 5), an element of transcription promoting the expression of anti-apoptotic genes. Both play an essential role in reducing ER stress (Hernández et al., 2017; Hyrskyluoto et al., 2014). One of the consequences of ER stress is the alteration of mitochondrial functions with increased oxidative stress, considered as a key component of mutated HTT cytotoxicity.

2.2.3. Altered energy metabolism

2.2.3.a. Mitochondrial dysfunction

Energy impairment was proposed to play a vital role in HD. Bael (Beal 1992) and Albin (Albin et al. 1992) hypothesized that chronic defects in energy metabolism could cause indirect excitotoxicity. Also, the striatum is particularly sensitive to an alteration in oxidative metabolism, where the latter is more concerned with neurons due to their high energy consumption and thus

are more susceptible to energy failure and oxidative damage (Beal, 1992). These data were supported from the very early studies in mitochondria isolated from HD cortical autoptic tissue showing mitochondrial defects and biochemical abnormalities in HD (Gárdián and Vécsei, 2004; GOEBEL et al., 1978).

Biochemical studies of brain and peripheral tissues from HD patients, as well as studies on HD cells and animal models, revealed decreased activity of several enzymes involved in oxidative phosphorylation such as complex I, II, III, and IV, along with pyruvate dehydrogenase complex, and aconitase (Arenas et al., 1998; Brennan et al., 1985; Brouillet et al., 1995; Butterworth et al., 1985; Damiano et al., 2010; Gu et al., 1996; Mochel and Haller, 2011; Sorbi et al., 1983; Sorolla et al., 2008; Tabrizi et al., 1999). More generally, PET scan studies showed very early brain hypo metabolism, particularly in the striatum (Beal, 1992) (for a review (Brouillet, 1999), as well as an overall alteration of the energy metabolism (For review: (Bonvento et al., 2017). In addition, NMR spectroscopy indicated increased lactate concentrations in HD patients, suggesting defects in oxidative energy metabolism (Jenkins et al., 1998, 1993), possibly at the mitochondria level.

Mitochondria play a central role in cell survival by controlling energy metabolism, apoptotic pathways, and calcium homeostasis. Many dysfunctions have been described in HD (For review: (Liot et al., 2017; Zheng et al., 2018). It has been shown that chronic intoxication with the mitochondrial toxin 3-nitropropionic acid, an inhibitor of mitochondrial complex II (C-II), leads to preferential degeneration in rats (M. Beal et al., 1993) and non-human primates (Brouillet et al., 1995); these pioneering studies led several groups to look closely at the possible effects of muHtt on mitochondria.

Mutant Htt induced an increased production of reactive oxygen species (ROS), possibly through perturbation of oxidative phosphorylation in mitochondria. Although data on post mortem tissues show contrasting results on the presence of oxidative stress products (Browne et al., 1997), different approaches in vitro and in vivo indicated that muHtt produces preferential loss of C-II subunits (Benchoua et al., 2006; Damiano et al., 2013) in HD patients and animal models.

Reduced C-II expression is associated with loss of mitochondrial membrane potential and cell death. Overexpression of these subunits using a lentiviral strategy is neuroprotective against muHTT, indicating that this event is causal in HD.

MuHTT binds directly to mitochondria through Drp1 protein (Dynamin related protein), leading to mitochondrial sequestration in muHTT aggregates, thus slowing their motility (Chang et al., 2006; Shirendeb et al., 2012; Song et al., 2011). Thereby altering their metabolic activity through the decrease in their membrane potential observed in in vitro models (Naia et al., 2015; Panov et al., 2002; Sawa et al., 1999) and by an alteration of mitochondrial fission and fusion (Shirendeb et al., 2011, 2012; Song et al., 2011). Mitochondrial fission and fusion is a mechanism involved in the dynamic recycling of mitochondria and its selective autophagy (mitophagy). This is important to degrade altered mitochondria and maintain its functional network. However, mitophagy is also defective in HD, forming autophagosomes being blocked by mutated HTT (Wong and Holzbaur, 2014).

On the other hand, several transcription factors regulate genes responsible for mitochondrial function and oxidative stress (Cha, 2007). Dimitri Krainc and colleagues' group showed that muHtt also represses transcription of PGC-1α, a gene encoding for a transcriptional co-activator that regulates expression of genes involved in mitochondrial biogenesis and respiration. MuHtt inhibits the activation of PGC-1α's targets and the transcription of antioxidant genes such as *SOD1* and *SOD2* (Superoxide dismutase 1 and 2), and mitochondrial genes such as *Tfam* (Transcription factor A) and *CytC* (Cytochrome c). This inhibition can also be indirect: mutated HTT sequesters the CREB / TAF4 complex, prevents activation of the gene encoding PGC-1, and, therefore, its transcription (Cui et al., 2006). The expression of these genes is severely impaired in the disease. Moreover, PGC-1α knock-out mice exhibit mitochondrial defects accompanied by hyperkinetic movement disorder and striatal degeneration (Cui et al., 2006). Another group has shown that PGC-1α promoted HTT turnover and the elimination of protein aggregates by activating transcription factor EB (TFEB), a master regulator of the autophagy-lysosome pathway (Tsunemi et al., 2012). In addition, an interaction between mutated HTT and the TIM23

mitochondrial protein import complex has been described **(Figure 18).** Most of the mitochondrial proteins being encoded by nuclear DNA; after their translation, they are translocated into the mitochondria. The inhibition of the TIM23 complex by mutated HTT causes a defect in the importation of mitochondrial proteins and induces neuronal death (Yablonska et al., 2019; Yano et al., 2014).

Finally, the mitochondria also control calcium homeostasis since they allow its storage when it is too abundant in the cytosol and its release when its level is too low. However, this "buffer" property of mitochondria is reduced in the brain of HD patients and mouse models (Brustovetsky, 2016; Panov et al., 2002). Thus, maintaining calcium homeostasis is necessary for neuronal survival because overconcentration can lead to the opening of the transition pore of Mitochondrial permeability (mPTP) in the inner membrane. The opening of the mPTP disrupts ATP levels in mitochondria. It leads to cytochrome C's release that may trigger apoptosis **(Figure 18)** (Green and John C. Reed, 1998; Halestrap, 2006; Krieger and Duchen, 2002; Rasola et al., 2010).

In conclusion, the majority of the cellular events compromised during disease progression are highly energy-dependent processes. Hence, impairments of these functions could stem from or be amplified by muHTT-induced mitochondrial and energetic defects.

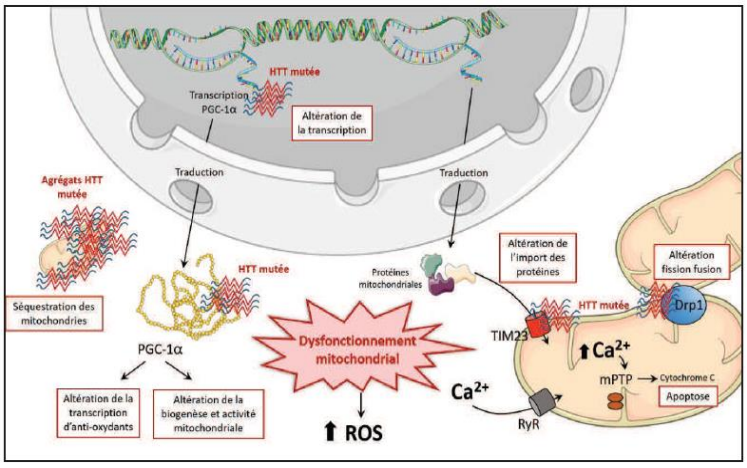

Figure 18: Mitochondrial dysfunction in HD.
Mutated HTT in the nucleus inhibits the transcription of genes important for mitochondria, including the gene encoding the PGC-1 protein, which itself has its functions altered due to its interaction with mutated cytoplasmic HTT. Other mitochondrial processes are disrupted by the mutation such as the import of synthesized mitochondrial proteins in the nucleus, calcium homeostasis and the "buffering" property of mitochondria, which causes the opening of the mPTP pore and apoptosis. In addition, mutated HTT sequesters mitochondria and interacts with Drp1, resulting in mitochondrial fission and fusion. This global mitochondrial dysfunction in HD contributes to increasing the production of reactive oxygen species (ROS), which disrupts all cellular mechanisms (Thesis of Caroline lotz).

2.2.3.b. Oxidative stress

Mitochondrial dysfunctions in HD favor the production of reactive oxygen species (ROS) **(Figure 18).** Endogenous ROS are produced mainly by the synthesis of ATP in the mitochondria. The overrun of cellular anti-oxidant mechanisms leads to oxidative stress through ROS accumulation, which damages proteins, DNA, and lipids contributing to HD pathogenesis. Indeed, it was found that 8-OHdG (8 hydroxydeoxyguanosine) and MDA (Malondialdehyde) are increased in the striatum of HD patients and animal models, which are responsible in the production of oxidized DNA and peroxidized lipids, respectively. (Browne et al., 1997; Tabrizi et al., 2000).

Mitochondrial damage and oxidative stress are closely related and function in synergy, but multiple pathways produce endogenous ROS, such as ER enzymes, cytochrome P450, or even the NADPH oxidases of the plasma membrane (Kumar and Ratan, 2016; Zheng et al., 2018).

2.3. Nuclear proteotoxicity of mutated Huntingtin

2.3.1. Transcriptional deregulations

Over the years, transcriptional dysregulation has been widely studied in HD (reviewed in (Gil and Rego, 2008; Zuccato et al., 2010). Between 1980s and 1990s, selective altered expression of highly identifiable neuronal genes, such as neurotransmitter receptors and neuropeptides, was demonstrated first in patients' brains (through in situ hybridization performed in human post-mortem samples, and later in animal models (Augood et al., 1997; Cha et al., 1998; Emson et al., 1980).

Transcriptional dysregulation in HD is a progressive event particularly affecting brain tissues, notably the striatum (Hervás-Corpión et al., 2018; Hodges et al., 2006; Luthi-Carter et al., 2000). It is an early mechanism that may precede the onset of clinical symptoms of the disease (Hervás-Corpión et al., 2018; Hodges et al., 2006; Langfelder et al., 2016a; Luthi-Carter et al., 2000).

Then, the implementation of the DNA microarray technology, followed by high throughput sequencing techniques, has generated a vast amount of transcriptomic data, allowing the generation of an accurate HD transcriptome profiling in both *in vivo* and *in vitro* disease models

as well as in human post-mortem samples. This demonstrated large changes in the expression of coding and non-coding RNAs, in both directions, most particularly in the striatum (Mayada Achour et al., 2015; Desplats et al., 2006; Hodges et al., 2006; Kuhn et al., 2007; Langfelder et al., 2016a; Lee et al., 2020, 2011; Luthi-Carter, 2002a, 2002b; Luthi-Carter et al., 2000; Martí et al., 2010; Runne et al., 2008; Seredenina and Luthi-Carter, 2012; Valor et al., 2013; Vashishtha et al., 2013).

2.3.1.a. Transcriptional signature of striatal mRNAs

Transcriptomic studies using HD knockin (KI) mice Q allelic series, consisting in different KI mice expressing various length of CAG repeats in endogenous murine Htt, showed that transcriptional dysregulation in response to the HD mutation is a tissue, age and CAG repeat length dependent process **(Figure 19A and B)** (Langfelder et al., 2016a). Among the different brain structures, the striatum is predominantly affected in this these models **(Figure 19C**) (Hodges et al., 2006; Langfelder et al., 2016a; Luthi-Carter, 2002b).

Studies show that down-regulated genes are enriched in markers of striatal neuron identity striatal functions, such as genes encoding dopaminergic spiny projection neurons receptors D1 and D2 (*DRD1* and *DRD2,* respectively) in the striatum of HD patients and mice. For instance, the expression of DARPP32, PDE10a, RGS9 is progressively reduced in HD striatum. In contrast, up-regulated genes in HD striatum are not particularly enriched in neuronal function genes and associate to various biological processes such as cell adhesion, neurodevelopment, neuronal differentiation and metabolic processes (*PGK1*, *SCD2*,…) (Table 1) (Mayada Achour et al., 2015; Francelle et al., 2017; Labadorf et al., 2016; Le Gras et al., 2017; Merienne et al., 2019; Valor, 2015; Vashishtha et al., 2013). Remarkably, these data show that down- and up-regulated genes in HD striatum show specific and distinct signatures.

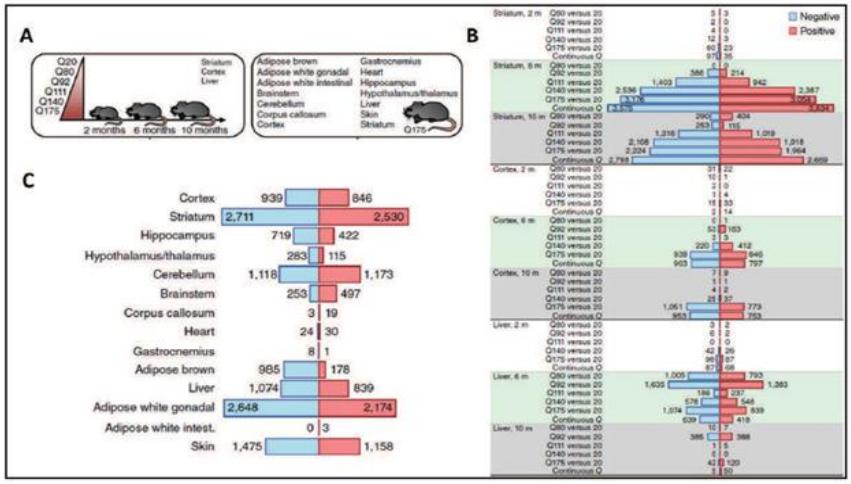

<u>Figure 19:</u> Characteristics of transcriptional deregulation in HD.
(A) Langfelder et al. (2016) used an allelic series of KI models (Q20 to Q175). They assessed the amplitude of transcriptional deregulation in HD by age, size of polyQ expansion, and tissue type. **(B)** The number significantly upregulated (red) and downregulated (blue) (FDR <0.05) genes in KIs compared to WTs, increases with the age of mice and with the number of CAGs, mainly in brain tissue. **(C)** The number of genes significantly upregulated (red) and down-regulated (blue) (FDR <0.05) in several tissues of KI Q175 mice shows that transcriptional deregulation is more important in the striatum (Langfelder et al., 2016a).

To better characterize the role of neurons and glial cells in transcriptional dysregulation in HD striatum, Merienne et al. (2019) profiled different cell populations of the striatum of WT mice, using laser-capture microdissection (LCM) and transgenic mice expressing GFP in specific striatal populations. LCM is a technique that combines the advantages of fluorescent transgenic mouse models and brain sectioning under physiological conditions (cold oxygenated CSF) to avoid fluorescent signal loss and ensure high-quality RNA. Doing so, they generated RNAseq data on D1 and D2 MSNs, striatal astrocytes and striatal microglia. Integrating these data with RNAseq or microarray data generated using the striatum of HD KI mice, HD R6/1 transgenic mice or HD patients, they showed that down-regulated genes in HD striatum were essentially neuronal, being enriched in D1- and D2-MSN specific genes, while up-regulated genes were predominantly glial-specific genes. **(Figure 20)** (Merienne et al., 2019).

Pathway or gene group	Examples of genes with altered expression levels
Neurotransmitter receptors	DRD1A; DRD2; TH; CNR1; ADORA2A*; GABRA5; GABRA4; GABRG2; GABRD; GAD1; GLRB; GRIA1; GRIA3; GRM1; GRM2; GRM3; GRIN2A*; GRIN2B*; SLC1A4; HRH3; OPRM1; OPRK1; OPRD1; HRH3
G-protein receptor signalling	PPP1R1B; ARPP21; GNAL; ADCY5; GNG3; GPR88; GPR6; PDE10A; PDE2A; PDE1B; RGS2; RGS4; RGS9; RASD2; RAS; RAPGEF3; PTPN5; GUCY1A3; GUCY1B3; PRKCB1; NGEF; PAK1
Calcium signalling and homeostasis	RYR1; CALB1; PPP3R1; PCP4/PEP-19; HPCA; RASGRP2; CPNE5, STRN; SCN4B; KCNIP2; KCNA1; SLC24A3; PLCB1; ATP2A2; ITPR1; CAMKK2; CABP1; SYNJ1; TESC
Neurotrophin receptor signalling	BDNF, NTRKB, NTRKA
Synaptic transmission, cytoskeletal and structural proteins	PSD95 (DLG4); ACTN1; NEFL; CPLX1; CPLX2; MARCKS; SYT1; SYNPR; SNAP25; RPH3A; CIT; GSN; SNCA
Neuropeptides	PENK; NPY; PDYN; OXT; AVP; CART; POMC; SST; NTS; CRH
Transcription and chromatin remodelling	POLR2A; PC4; SNF-1 RELATED KINASE; BCL11B; FOXP1; MYT1L; KLF16; PPARGC1A*; NR4A1; ID3
Mitochondrial function; energy metabolism	PPARGC1A; CKMT1; CKB; ATP5C1; PGK1; LDHA; SUCLA2; PCTP; ENO2
Ubiquitin–proteasome system	PSME1; HSPB1; HSPA1B; HSP90AA1
Retinoid signalling	RBP4; RARB; RXRG
Lipid metabolism	SCD 2; LPL; ACADVL; SRD5A1; SLC27A1; STARD4
Transport	VMP; CAMKV; DNC11; VAMP1; SORT1
Inflammation	FKBP4; B2M; C4B; C4A; C3
Misc. signalling	DUSP1; DUSP6; DUSP5; DUSP14; NNAT; PLK2; OLM4; SLC14A1; CD44; AQP1; CSRP2; NDUFB2; PCDH7; DKK3; YWHAZ; ROCK2; nNOS; ARNTL; TMEM90A; FGF13

Table 1: Examples of deregulated genes in Huntington's striatum.
Downregulated genes in the striatum of HD patients and models share a functional signature neuronal (neurotransmission, signaling, neuropeptides, synaptic transmission, calcium homeostasis, transcription). In contrast, genes overexpressed in the striatum are involved in metabolism, the neurodevelopment and cell adhesion. (From (Seredenina and Luthi-Carter, 2012).

Moreover, these transcriptomic signatures are also found in other brain structures like the cortex and the hippocampus, but they are less robust **(Figure 17C)** (Langfelder et al., 2016a; Vashishtha et al., 2013).Taken together, these results show that the molecular processes involved in maintaining neuronal identity, particularly of the striatum, is altered in HD.

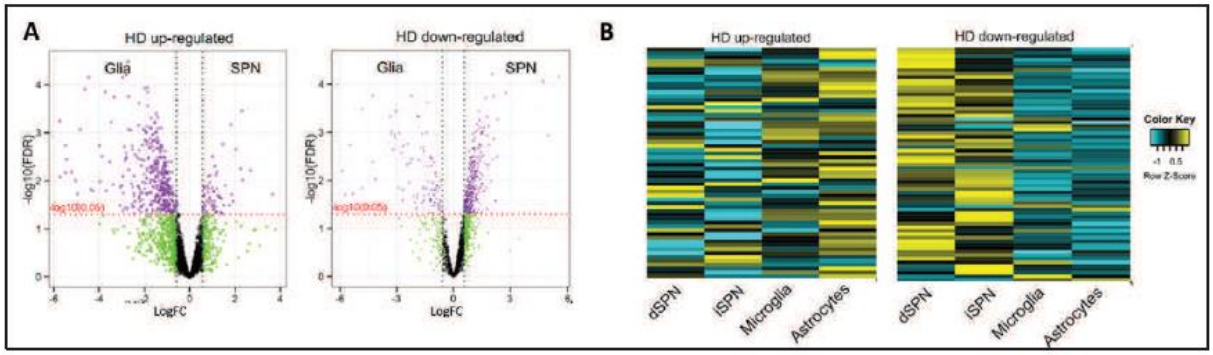

Figure 20: Specific enrichment of deregulated genes in neurons and glial cells of the striatum.
(A) Volcano plots representing the differential enrichment of over-expressed (left) and under-expressed (right) genes in glial cells (Glia) and striatal neurons (SPN) (Merienne et al., 2019). **(B)** Map of densities representing the hierarchical classification of the expression of the 100 most over-expressed (left) and under-expressed (right) genes in different cell types of the Huntington striatum (dSPN: MSN-D1; iSPN: MSN-D2; Microglia; Astrocytes). The color scale corresponds to the z-scores of the genes, with yellow and blue reflecting high and low expression respectively. A proportion large number of overexpressed genes are enriched in microglia and astrocytes compared to neurons, while larger number of under-expressed genes are enriched in MSNs-D1 (dSPN) and MSNs-D2 (iSPN) (Merienne et al., 2019).

Recently, a study conducted by Lee and his colleagues (2020), directly examined HD striatal transcriptome using two different cell-type-specific approaches. They used the translating ribosome affinity purification (TRAP) technology and single nuclei RNA sequencing (snRNA-Seq) to profile different striatal populations of both WT and HD mice and patients. More specifically

they performed their analyses using striatal tissues of R6/2 transgenic mice, HD KI mice and post-mortem tissues of HD patients (Lee et al., 2020). Their unbiased gene expression studies revealed both non-cell-type-specific responses (e.g., synaptic and circadian clock gene dysregulation) and cell type-specific responses (e.g., OXPHOS gene downregulation), along with mitochondrial RNA (mtRNA) release, and innate immune signaling activation as phenomena that may contribute to the enhanced sensitivity of the D2-MSN to muHTT. (Lee et al., 2020). Thus, the HD mutation differentially impacts striatal cell populations.

2.3.1.b. Transcriptional signature of striatal non-coding RNAs

Transcriptional deregulations do not only affect mRNAs but also non-coding RNAs (Francelle et al., 2017; Seredenina and Luthi-Carter, 2012), such as microRNAs (miRNAs) and enhancer RNAs (eRNAs) (Schratt, 2009; Woldemichael and Mansuy, 2016).

miRNAs are post-transcriptional regulatory factors for the expression of genes and have an important role in neuronal development, differentiation and maintenance of mature neurons (Schratt, 2009; Woldemichael and Mansuy, 2016). Expression of miRNAs is deregulated in the striatum of HD patients and animal models (Hoss et al., 2014; Langfelder et al., 2018). Indeed, In the early stages of the disease, several studies in YAC128 mice model highlight an increase in these regulatory miRNAs, while they decrease in later stages (Lee et al., 2011) (For review: (Kerschbamer and Biagioli, 2016; Seredenina and Luthi-Carter, 2012).

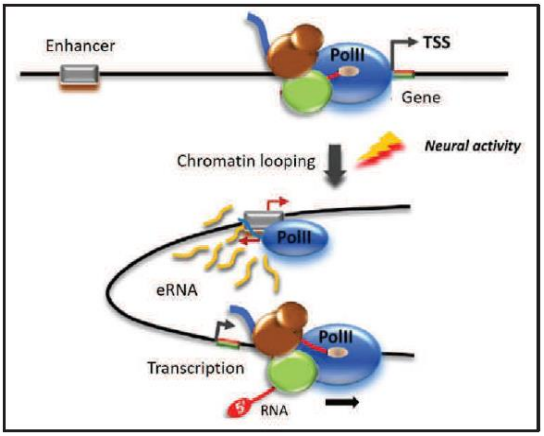

Figure 21: Regulation of gene transcription by enhancers.
RNA polymerase II (RNA Pol II) is recruited in a quiescent form at the gene level. In response to stimulation, the enhancer of the gene is brought close to the promoter by the formation of a chromatin loop, the eRNAs are then transcribed and promote transcription of the gene. (From (Schaukowitch et al., 2014).

Also, enhancer RNAs (eRNAs) are deregulated in the striatum of R6/1 mice. They are a class of long non-coding RNAs, transcribed from active enhancers. They positively regulate the transcription of their target genes from a distance by recruiting, often in a tissue-specific manner, transcription factors and RNA polymerase II (RNA Pol II) **(Figure 21)** (Arner et al., 2015; Plank and Dean, 2014; Schaukowitch et al., 2014). The study by Le Gras et al. (2017) showed that eRNAs regulating striatal marker genes are down-regulated in the striatum of HD R6/1 mice, which associates with decrease in the recruitment of RNA Pol II (Le Gras et al., 2017) (See introduction section 2.3.4.1. Epigenetics and transcriptional dynamics).

2.3.1.c. Functional consequences of transcriptional deregulation

Although it is likely that transcriptional changes contribute pathogenesis, especially down-regulation of striatal marker genes correlating with disease progression, it is also possible that some changes reflect compensatory mechanisms that could reduce cellular stress of affected brain tissues (For review: (Francelle et al., 2014; Seredenina and Luthi-Carter, 2012)). Compensation mechanisms affect several functions and are set up very early in the disease (Francelle et al., 2014). For example, RASD2, which interacts with mutated HTT and increases its toxicity, is downregulated in patients' striatum and mouse models of HD (Seredenina et al., 2011).

Also, the overexpression of proteasome activating subunits is also described in R6/2 mice and would be protective against the toxicity of the HTT mutation (Luthi-Carter et al., 2000; Moumné et al., 2013; Seredenina and Luthi-Carter, 2012; Valor, 2015).

Moreover, studies performed on striatal module hub genes as genetic modifiers, in a Drosophila HD model expressing a muHTT fragment, showed that two independent heterozygous loss-of-function alleles of the Drosophila *Ctcf* gene can significantly, albeit partially, ameliorate climbing deficits in this Drosophila. These modifiers are considered as loss of function suppressors, suggesting that their down-regulation in HD mice may represent compensatory changes to mitigate muHTT toxicity (Langfelder et al., 2016a).

2.3.2. Interaction of mutated huntingtin with transcription regulators

One possible mechanism leading to transcriptional deregulation results from the abnormal interaction of mutated HTT with transcription factors and/or co-factors (For review: (Moumné et al., 2013; Seredenina and Luthi-Carter, 2012; Valor, 2015)). Transcription factors modulate the expression of a gene by either binding to specific sequences in promoter or distant regulatory regions (enhancers) of the genomic DNA, acting both as positive or negative regulators transcription depending on whether they are associated to co-activators or corepressors, respectively (reviewed by (Latchman, 1997)(Brivanlou, 2002; Lan et al., 1999).

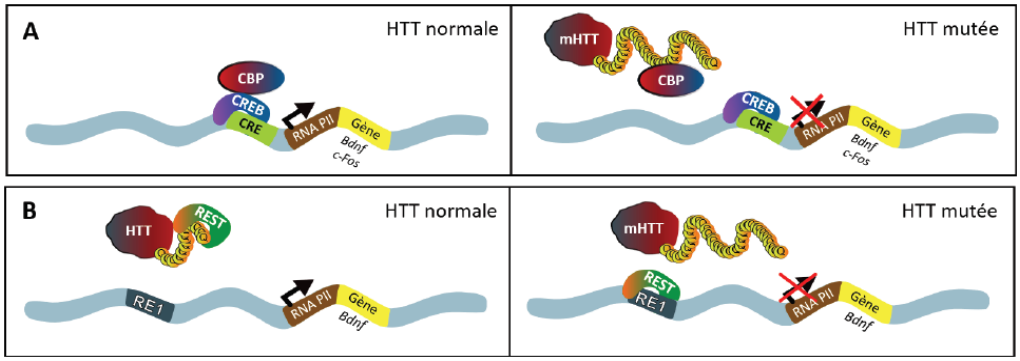

Figure 22: Examples of transcriptional alterations in HD.
(A) The CREB co-activator, CBP, promotes the transcription of CREB target targets such as the Bdnf or Fos genes. In the MH, CBP is sequestered in aggregates of mutated HTT (muHTT) and results in impaired gene transcription associated with the CREB factor. **(B)** Under normal conditions, HTT interacts with the repressor factor REST, preventing its binding on the RE1 sequence and therefore the inhibition of the transcription of genes such as Bdnf. On the other hand, the dysfunction of the mutated HTT accelerates REST binding and selects transcription. (Thesis of Rafael Alcala vida).

Studies show that mutant HTT interacts with CBP, a co-activator with histone acetyltransferase activity. It plays a major role in the regulation of gene expression, and it is predominantly implicated in the development of the nervous system and the maintenance of plasticity and memory process (Alarcón et al., 2004; Barrett et al., 2011; Bousiges et al., 2010; Bridi et al., 2017; Chen et al., 2010; Korzus et al., 2004; Valor et al., 2011; Vieira and Korzus, 2015; Wood et al., 2006). Notably, in response to neuronal stimulation leading to activation of signaling pathways, CBP is recruited to activity-regulated neuronal enhancers and promoters, thus promoting histone acetylation, induction of activity-regulated genes (which are implicated in synaptic plasticity) and adaptive behavior (Yap and Greenberg, 2018). In HD, muHTT interacts with the polyQ domain of

CBP acetyltransferase, where it is sequestered within the mutated HTT aggregates **(Figure:22A)** (Kazantsev et al., 1999; Nucifora Jr., 2001; Steffan et al., 2001)**.** Also, soluble HTT would be able to induce CBP degradation (Cong et al., 2005). Thus altered regulation of CBP may contribute to behavioral and cognitive deficits in the context of HD. As a result, epigenetic strategies using HDAC inhibitors (HDACi) to increase histone acetylation have been early considered for HD when it was found that CBP is recruited into aggregates of muHTT and that HDACi improve phenotypes of different HD models (Kazantsev et al., 2002; Nucifora et al., 2001; Steffan et al., 2001) (See introduction section 3.2.2.a. HDACs inhibitors, p:69).

Moreover, the histone deacetylase complex mSin3a, the tumor suppressor factor p53, and the coactivator CA150 transcription factor are also sequestered within muHtt aggregates (Boutell et al., 1999; Holbert, 2001; Kazantsev et al., 1999; Steffan et al., 2000). The expression of CA150 is greatly increased in the brains of patients, but CA150 is found in the aggregates. Thus, the muHTtt causes CA150 dysfunction in striatal neurons, but overexpression of CA150 would delay toxicity-induced cell death of the muHTT (Arango, 2006). Besides, the soluble form of mutated HTT may inhibit the activity of certain transcriptional regulators such as Sp1, CBP and TBP (Cong et al., 2005; Li et al., 2002).

Dysfunction of transcriptional factors does not only result from toxic gain of function of mutated HTT, but also from loss of function of mutated HTT. For instance, the RE1-silencing transcription factor (REST), a neuronal repressor, is physiologically inhibited by its sequestration in the cytoplasm by normal HTT **(Figure 22B).** PolyQ expansion in mutated HTT decreases its affinity for REST, which is then translocated into the nucleus, where it can bind to RE1/NRSE motif located on several neuronal genes, including the *BDNF* gene (Figure 23B) (Zuccato et al., 2003). In addition, even though HTT is predominantly located in the cytoplasm, it can interact with nuclear receptors like LXRs receptors (Liver X receptors; LXRα and LXRβ) (Futter et al., 2009). These receptors are key regulators of cholesterol metabolism essential for proper brain function. Their transcription is favored through binding to HTT protein, but inhibited by mutant HTT (Futter et al., 2009), resulting in deregulation of cholesterol metabolism (Boussicault et al., 2018, 2016; Kacher et al., 2019; Leoni and Caccia, 2015; Wang et al., 2002).

Finally, studies showed indirect effect of mutated HTT on transcriptional regulators, for instance influencing their degradation by the proteasome (Cong et al., 2005; Godin et al., 2010). Specifically, muHTT increases CBP degradation by the proteasome (Cong et al., 2005). Moreover, the study of Godin et al. (2010) indicates that proteasome degradation of ß-catenin, a transcriptional co-activator, is inhibited by mutated HTT, leading to an abnormal and toxic accumulation of ß-catenin in neurons.

2.3.3. Epigenetic changes in HD

Advances in next-generation sequencing-based techniques, such as massively parallel sequencing coupled with chromatin immunoprecipitation (ChIP-seq), allow assessing epigenetic modifications at genome-wide scale, giving the opportunity to define disease-associated epigenomic landscapes. Many challenges are faced to improve the understanding of epigenetic mechanisms in Neurodegenerative diseases, including HD.

2.3.3.a. Epigenetics and transcriptional dynamics

The current definition of epigenetics relates to "the study of phenomena and mechanisms that cause chromosome-bound, heritable changes to gene expression that is not dependent on the changes of DNA sequence." Many DNA/RNA mediated processes, including transcription, DNA repair, and DNA replication, are regulated by epigenetic mechanisms including various histone post-transcriptional modifications (PTM), DNA methylation and some non-coding RNAs (Allis and Jenuwein, 2016) (**Figure 23**). These processes occur through modulating chromatin structure, a macromolecular complex of DNA, RNA, and proteins notably histones.

In fact, DNA is wrapped around core particles of chromatin, the nucleosomes, which are formed of octamers of histones, including two of each of H2A, H2B, H3, and H4 **(Figure 23)**. Histones are subject to PTM, notably acetylation, methylation, phosphorylation, ubiquitylation. These modifications modulate the degree of compaction of nucleosomes, thereby affecting chromatin accessibility of various factors, particularly transcriptional regulators. (Borrelli et al., 2008; Jenuwein and Allis, 2001; Tsompana and Buck, 2014; Wang and Jin, 2010; Xu et al., 2014). Nucleosomes can be either relaxed, a feature generally associated with transcriptionally active

chromatin (e.g., euchromatin), or compacted (e.g., heterochromatin), usually associated with transcriptional repression (Jenuwein and Allis, 2001).

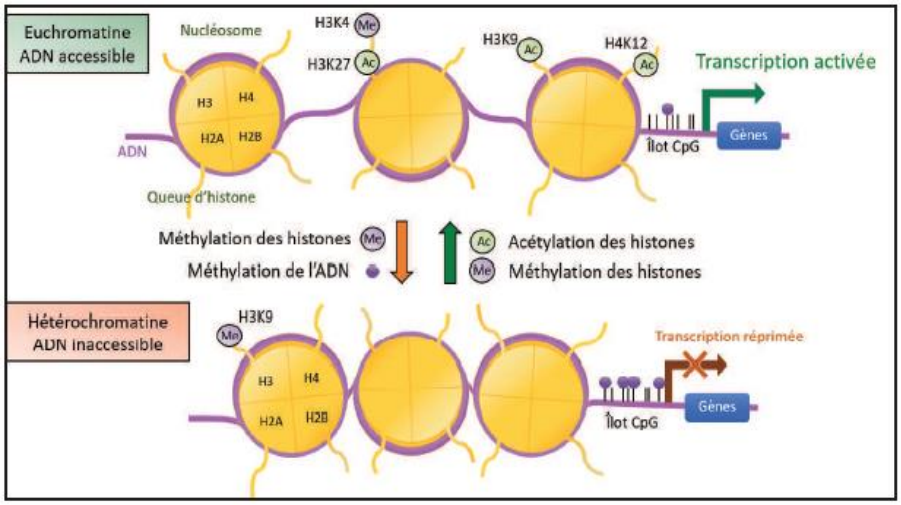

Figure 23: Regulation of transcription by epigenetic modifications of chromatin.
Chromatin is made up of nucleosomes which, by compacting, regulate transcription. Chromatin compacted (heterochromatin) represses transcription, while when it is decompacted (heterochromatin), transcriptional factors may attach to it. This dynamic is regulated by epigenetic processes, such as the acetylation of histone tails which always promotes transcription, histone methylation or evenDNA methylation. (Modified from (Francelle et al., 2017).

Importantly, epigenetic modifications happen in a reversible, combinatorial, and targeted manner by different enzymes that modify histone residues (**Figure 24).** For instance, histone acetylation and deacetylation are caused by histone acetyltransferases (HAT), a family of chromatin-remodeling enzymes, and histone deacetylases (HDAC), respectively **(Figure 24).** Similarly, histone methylases and demethylases regulate the addition and removal of methyl groups on histone residues **(Figure 24).** While histone acetylation always correlates with chromatin relaxation and transcriptional activation, histone methylation is associated with transcriptional repression or activation, depending on the histone residue subject to methylation. For example, H3K27 is acetylated by CBP/p300 acetyltransferases at promoters and enhancers (i.e. distal regulatory regions), which is associated with chromatin loop formation favoring enhancer/promoter interactions, recruitment of transcriptional regulators and active transcription (Kuras et al., 2003; Ren et al., 2017; Rowley and Corces, 2018).

Also, trimethylated H3K4 (H3K4me3) is strongly enriched at transcriptionally active promoters, whereas monomethylated H3K4 (H3K4me1) is specifically enriched at enhancers. Histone methylation can also be associated with a transcriptionally silent heterochromatin state. Well-characterized heterochromatin marks include H3K9 trimethylation (H3K9m3) or H3K27 trimethylation (H3K27me3). Combinatorial nature of so-called histone code allows fine-tune regulation of transcription, through the binding of 'reader' proteins, which convey histone signals into transcriptional response. (Bannister and Kouzarides, 2011; Jenuwein and Allis, 2001; Jones et al., 2016).

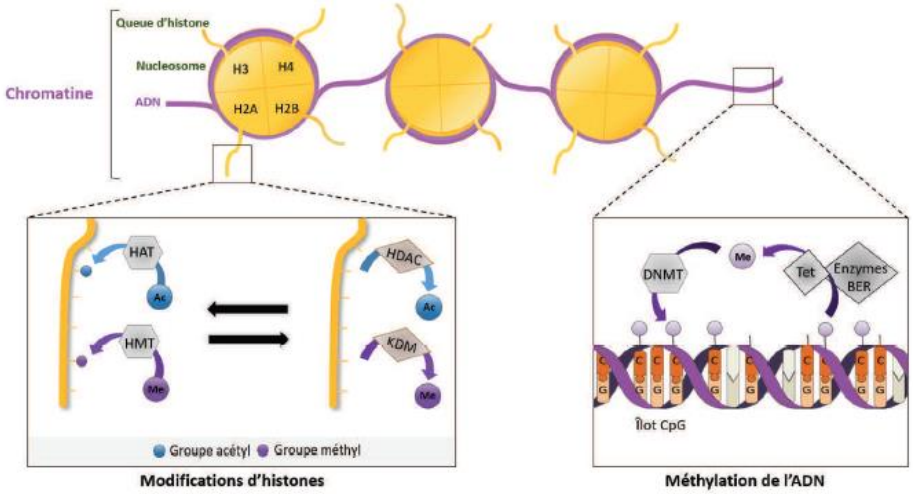

Figure 24: Dynamics of epigenetic modifications of chromatin.
DNA is wrapped around nucleosomes, which are made up of 8 histones and which modulate the compaction of chromatin. Histone tails can undergo post-translational modifications, such as acetylation or methylation of residues. The acetyl and methyl groups are added by histone acetyltransferases (HAT) and methyltransferases (HMT) respectively and removed by histone deacetylases (HDAC) and demethylases (HDM). The chromatin compaction is also regulated by DNA methylation: methyl groups are added by DNA methyl transferases (DNMT) on cytosines from regions of DNA rich in GC, and their removal involves Tet enzymes and DNA repair mechanisms (BER Enzymes). (From (Francelle et al., 2017).

Another important epigenetic mechanism is DNA methylation, consisting in adding a methyl group to cytosines residues. This process often takes place at the C5 position of cytosine, in cytosine-guanine dinucleotide sequences (CpG), the CpG islands, by DNA methyltransferases (DNMT) creating 5-methylcytosine (5-mC). Promoter regions are generally enriched with CpG island. Thus, the methylation of DNA is an important mechanism involved in gene repression **(Figure 23)** (Deaton and Bird, 2011).

Methylation pattern, during DNA replication, is maintained by DNMT1. In contrast, DNMT3a and DNMT3b have been associated with *de novo* DNA methylation (Feng et al., 2010; Jeltsch, 2006). Though DNA methylation was long considered as a stable process, it is now clear that post-mitotic cells can undergo active DNA demethylation through a mechanism implicating TET proteins (Ten-eleven-translocation) (Pastor et al., 2013). TET proteins induce hydroxylation and further involvement in the oxidation of 5-mC. Oxidized 5-hmC are then processed by DNA repair mechanisms and DNA base excision repair (BER) to be converted back to their unmethylated state (Feng et al., 2015; Guo et al., 2011) (Figure 22).

Notably, in mature organisms, and during development, cells respond to any modification in their environment, such as extracellular factors including growth factors, hormones, and neurotransmitters, in a part of change in their gene expression. This change takes place in a way that is temporally and spatially controlled by the coordinated task of trans-acting transcription factors (TFs) that bind to cis-acting DNA regulatory elements including promoters, insulators and enhancers. Usually, conducted studies on such kind of mechanisms focus on promoters, genomic region which lie adjacent to the initiation site of mRNA synthesis. At promoters, the recruitment of the different components of the basal transcription machinery, including RNA-polymerase II, facilitate the assembly of functional transcription complexes that initiate mRNA synthesis (Kee et al., 1996). However, enhancers, which contribute to stimulus-dependent gene expression are distal genomic components which lie away from the transcription start site (Heintzman et al., 2007; Visel et al., 2009).

Enhancers are essential to gene regulation. They are enriched in docking sites for transcription factors (TF) in a sequence-specific manner. The nature and the extent of enhancer-mediated transcription are determined by the different combinatorial binding of the TFs (Inukai et al., 2017). Cell-type-specific differences in TF expression contribute to a cell-type-specific activity of different enhancer elements. However, most sequence-predicted TF binding sites are not occupied, even when cognate TF is expressed (Hombach et al., 2016). This is because enhancer accessibility and ability to interact with promoters is determined by epigenetic mechanisms, thereby also contributing to cell-type-specific regulation of enhancer activity. Chromatin-based

control of enhancer activity includes histone modifications (e.g., H3K27ac) as well as higher-order regulations, which modulate spatial chromatin organization, notably through chromatin loops. More precisely, TF at enhancers recruits chromatin-remodeling enzymes, structural proteins, and additional transcriptional regulators, including RNA polymerase II (RNAPII). Thereby, spatial interaction between enhancers and promoters are enabled by loops formed via TF-dependent recruitment of chromatin-remodeling factors and structural proteins such as the mediator, CTCF, and cohesin (Kuras et al., 2003).

In fact, there are different ways of classifying enhancers, where the distinction of conventional versus super-enhancers is the most likely accepted one. More specifically, cellular identity genes are regulated by, so-called super-enhancers, a category of broad enhancers, containing a complex array of regulatory elements, and highly enriched in cell type-specific master TFs, cofactors, including the mediator, and H3K27ac (Whyte et al., 2013) (**Figure 25).** Chromatin architecture at super-enhancers displays extensive chromatin looping, enabling multiple promoter/enhancer interactions, thereby ensuring the elevated and sustained expression of cellular identity genes, a feature essential to cellular identity acquisition and maintenance (Nord and West, 2020; Yap and Greenberg, 2018).

2.3.3.b. Neuronal plasticity

Dynamic epigenetic regulations are also critical to adjust cellular gene expression programs and cellular activity in response to extrinsic and/or intrinsic signals (Francelle et al., 2017). These regulations seem to be mediated by enhancers and reveal that they are especially critical to neuronal function. For instance, the response to environmental stimuli drives transcriptional reprogramming and consequently promotes synaptic plasticity and adaptive behavior, including learning and memory (Campbell and Wood, 2019; Gräff and Tsai, 2013; Kim et al., 2010; Lopez-Atalaya and Barco, 2014; Yap and Greenberg, 2018). Indeed, this response activates many signaling cascades (e.g., cAMP- and Ras/MAPK-dependent pathways) in neuronal tissues, leading to the recruitment and/or activation of transcription factors and HAT (e.g., CREB and CBP) to enhancers and promoters of early response genes (ERGs), notably the transcription factor *Fos*.

This first, rapid response leads to increased H3K27ac, enhancer RNA (eRNA) transcription, along with the strengthening of enhancer/promoter interaction and thus ERGs up-regulation (e.g., Egr1).

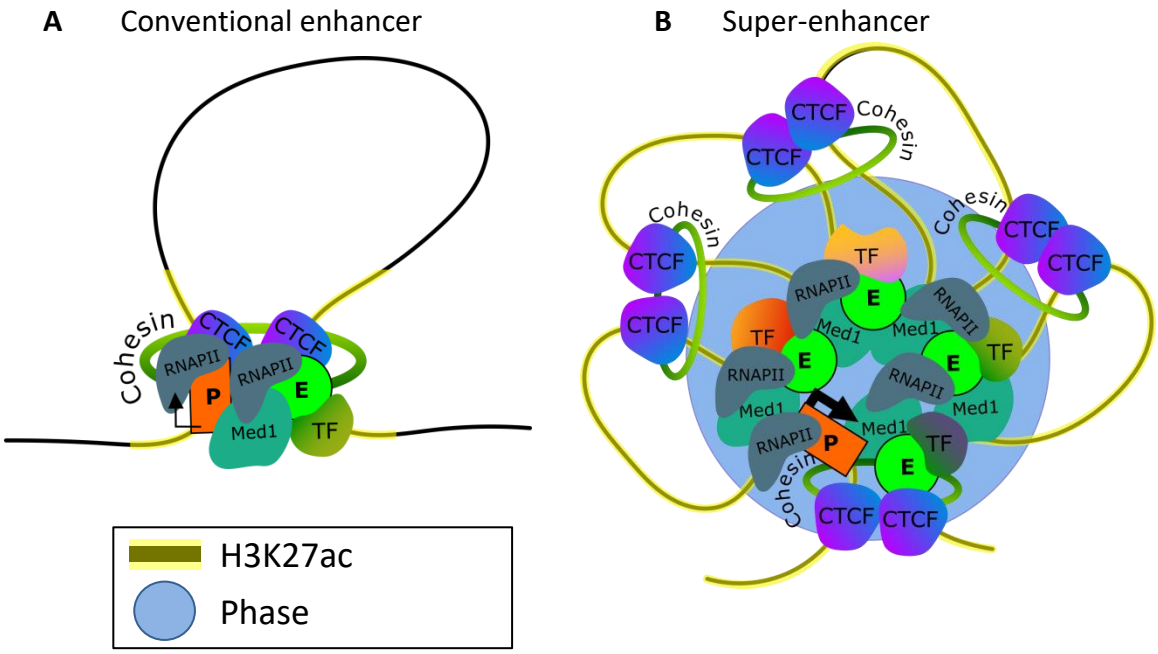

Figure 25: Regulation of brain cell-identity through super-enhancers.
(A) Schematic representations of conventional enhancer-promoter chromatin looping (left) and chromatin looping at super-enhancer-regulated gene (right). Super-enhancers consist of dense clusters of enhancers and are highly enriched in H3K27ac (yellow shadow), RNAPII and transcription factors (TF), including the mediator and cell type-specific TFs, leading to the generation phase-separated condensates (phase-separation, blue circle). Super-enhancers regulate genes that define cell-type specific identity and function, and that are generally highly expressed in their specific tissue/cell type. In contrast, conventional enhancers display more discrete features. **(B)** schematic representation of cell type-specific epigenetic signature of neuronal striatal super enhancers. The striatum comprises different cell types, including neurons (purple) and glial cells (green), expressing cellular identity genes regulated by super-enhancers. Identity genes may be neuronal-specific or glial-specific. The picture is even more complex since different subpopulations of neurons and glial cells are present in the mammalian striatum, expressing each specific subsets of cellular identity genes, controlled by specific super enhancers (for example D1 and D2 MSNs as compared to interneurons, and astrocytes, oligodendrocytes or microglia glial cells) (Review; (Alcalá-Vida et al., 2020).

Thereby, this mechanism induces a second regulatory wave, leading to the activation of cell type-specific late response genes (LRGs) and epigenetic changes, including H3K27ac changes and remodelling of chromatin architecture at enhancers and promoters (Marco et al., 2020) Figure 24). In brain tissue, LRGs are effector genes promoting synaptic plasticity (Vierbuchen et al., 2017). It is noteworthy that, in contrast to activity-regulated enhancers, cellular identity enhancers do not show increased H3K27ac in response to cellular stimulation (Vierbuchen et al., 2017).

2.3.3.c. Characteristics of the epigenome in HD

The transcriptional deregulation associated with HD could be the consequence of altered epigenetic regulations in patients and mouse models of the disease. Studies in the lab showed that downregulated genes in HD mice and patients' striatum are enriched in striatal neuronal identity genes, regulated by super-enhancers (Mayada Achour et al., 2015; Merienne et al., 2019).

The ChIP-seq results of Achour et al. (2015) performed using the striatum of R6/1 mice, show that striatal neuronal super-enhancers have decreased H3K27ac and RNA Pol II levels, correlated with a decrease in the expression of the genes they control, particularly those defining the striatal neuronal identity genes **(Figure 26 & 27).** Similarly, recent results were obtained in the lab from the post-mortem striatum of Huntington patients (Merienne et al., 2019) and the KI CAG 140 mouse model of the disease (Alcalá-Vida et al., 2021). Accordingly, these data suggest a causal role between the decrease in H3K27ac at the level of striatal super-enhancers and the mechanism of striatal identity genes' downregulation.

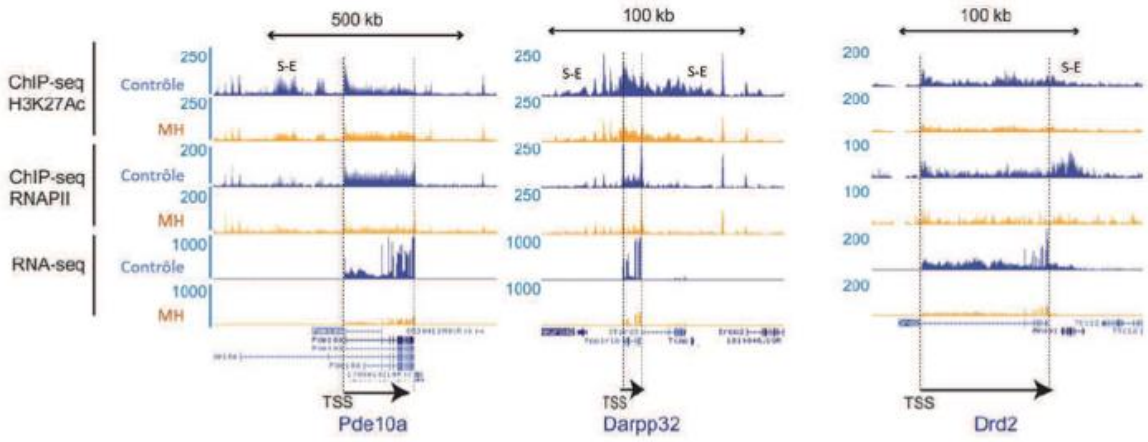

Figure 26: Alteration of the H3K27ac profiles of the super-enhancers of the striatal genes in HD.
The ChIP-seq H3K27ac and RNA Pol II data from the striatum of WT and R6 / 1 mice show that in WT mice, the profile H3K27ac of the striatal identity genes (Pde10a, Darpp32 or Drd2) has H3K27ac enriched regions around of the TSS (Transcription Start Site) of the genes, corresponding to the super-enhancers (S-E). This profile is altered in mice R6 / 1, with a decrease in H3K27ac in S-E and RNA Pol II, correlating with a decrease in the expression of their target genes. (From (Mayada Achour et al., 2015).

On the other hand, studies show that other histone acetylation marks like H3K9ac and H3K14ac could also contribute to these mechanisms (**Figure 27)** (For review: (Francelle et al., 2017).

Decreased levels of H3K9ac and H3K14ac was shown in the striatum of R6/2 and N171-82Q mice, although the link between their variations and transcriptional changes induced by Huntington mutation appear to be poorly correlated (McFarland et al., 2012; Valor et al., 2013).

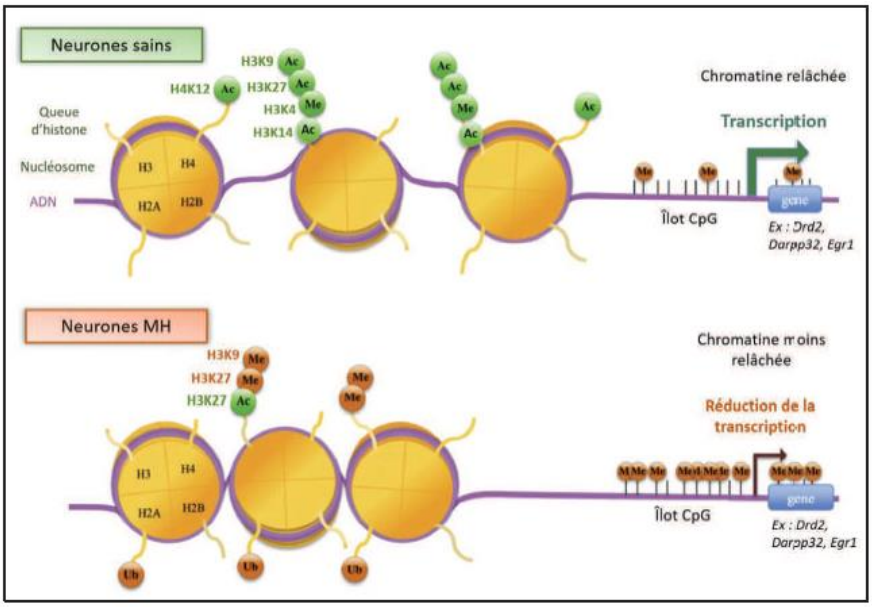

Figure 27: Summary of alteration of histone changes and DNA methylation in neurons affected by mutated HTT. In HD, a decrease in histone changes associated with activation of transcription, including in particular acetylation of histones H3K27, H3K9, H3K14 and H4K12 is observed. At the same time, an increase in modifications histones associated with the repression of transcription (H3K9me2, H3K27me3, H2Aub) are observed in neurons affected by mutated HTT. These epigenetic changes cause chromatin compaction and a decrease in transcription of genes, particularly genes of striatal identity. (From (Francelle et al., 2017)).

In addition, H3K4me3 histone mark, associated with active promoters, was also investigated at the HD promoter (Bai et al., 2015; Dong et al., 2015; Guiretti et al., 2016; Vashishtha et al., 2013). The ChIP-seq data generated using the striatum and the cortex of HD R6/2 transgenic mice revealed that H3K4me3 was widely depleted at neuronal identity gene promoters, which displayed a broad H3K4me3 profile. However, the genes having a developmental signature showed an increase in H3K4me3 level (Vashishtha et al., 2013). Moreover, H3K4me3 was also characterized in the prefrontal cortex of post mortem HD patients showing mild neuropathological involvement of HD (Bai et al., 2015; Dong et al., 2015). This study was carried on using fluorescently activated nuclei sorting (FANS), specifically targeting cortical neurons, where it showed that they are preferentially depleted in H3K4me3 in HD. This depletion of H3K4me could be greatly associated with reduced transcription even though the correlation

between increased H3K4me3 and transcription in the HD brain remains elusive (Dong et al., 2015).

Altogether, the epigenomic data of H3K4me3 and H3K27ac indicate that HD mutation induces the loss of activity of neuronal-specific enhancers and promoters controlling neuronal identity genes. Whether the HD mutation also affects activity-driven epigenetic regulation of neuronal-specific genes implicated in neuronal plasticity is unknown.

In addition, it was shown in patients and mouse models of HD, that DNA methylation is also modified at both the proximal promoter and the distal regulatory regions in response to mutant Htt **(Figure 27)** (Horvath et al., 2016; Thomas et al., 2013; Wang et al., 2013). The 5-hmC and 7-MG were globally reduced in brain tissues of HD mouse models, including YAC128 mice (5-hmC study), R6/2 and CAG140 knock-in mice (7-MG study) (Thomas et al., 2013; Wang et al., 2013). However, minimal evidence of HD-associated DNA methylation was shown by DNA methylation profiling using the post-mortem cortex and liver from HD patients (De Souza et al., 2016). Transcriptional consequences of altered DNA methylation in HD remain elusive. Interestingly, epigenetic age, an epigenetic measure of tissue age, was recently developed that estimate epigenetic age vs chronologic age, analyzing DNA methylation at 353 defined CpG sites (Horvath, 2013). Using brain tissues from HD patients, Horvath and coll. showed accelerated epigenetic aging in HD brain, particularly in cortical tissues. This was not the case for striatal tissues, possibly due to excessive neuronal loss (Horvath et al., 2016). Thus, although the transcriptional significance of accelerated aging in the HD brain is unclear, the data might reveal an age-dependent alteration of epigenetic regulation.

3. Therapeutic strategies for Huntington's disease

3.1. Symptomatic treatments

In the absence of effective disease-modifying therapies for HD, remarkable progress is being made in HD symptomatic treatment, which can significantly impact patients and their families. The first drug approved by the United States Food and Drug Administration (FDA) for an HD-specific indication is the type 2 vesicular monoamine transporter (VMAT2) inhibitor, tetrabenazine. This molecule is used to treat chorea (Zheng et al., 2006) and has the advantage of not causing tardive dyskinesia, unlike the dopaminergic receptors blocking drugs, such as haloperidol, a previously used neuroleptic drug (Bashir and Jankovic, 2018).

Another VMAT2 inhibitor, deutetrabenazine, has recently been approved by the FDA to treat chorea in HD. This compound has a lower risk of side effects (sedation, diarrhea, insomnia) than the treatment with tetrabenazine (Bashir and Jankovic, 2018). Valbenazine, a prodrug of the tetrabenazine, also approved for tardive dyskinesia treatment but is not under current consideration for FDA approval in HD treatment. In addition, other potential therapies for chorea in HD, which show positive results, include the deep brain stimulation trials (Gonzalez et al., 2014). Other motor symptoms, such as stiffness and dystonia, are also improved with tetrabenazine(Geschwind and Paras, 2016), lidocaine, or by performing local injections of botulinum toxins (For review: (Testa and Jankovic, 2019).

On the other hand, most of the psychiatric symptoms in HD, particularly depression, are common with individuals without the disease. Thus the treatment with standard medications is predominantly applicable. For example, psychoses and mood stabilizers are treated with anti-epileptic molecules such as valproate, which also reduces irritability in patients. Also, the use of antidepressants such as selective serotonin reuptake inhibitors (SSRIs) or the tricyclic antidepressants (TCAs) is also used for depression (For review: (Testa and Jankovic, 2019).

However, concerning the cognitive impairments in HD, there is no drug treatment for such a symptom. Although the trial of using Donepezil, a cholinesterase inhibitor used to improve cognitive deficits in Alzheimer's disease, has been tested in people with HD, but no improvement

in motor, cognitive, or quality of life in patients has been observed (Cubo et al., 2006). Thus, non-drug interventions can have a beneficial effect by slowing the disease progression and improve the cognitive disorders of HD patients (Andrews et al., 2015). Indeed, the guidelines and support at different disciplines (speech therapy, physiotherapy, occupational therapy, nutritionist, neurology, psychiatry, psychology) were reported by the European Huntington Disease Network Standards of Care group. Altogether, with the change in patients' lifestyle through better diet and sports, this would positively impact the patients and their families by slowing down HD symptoms, reducing stress, and ameliorating social interactions. (Simpson and Rae, 2012).

3.2. Pharmacological therapies

Since decades, the research community of HD focuses their efforts on the discovery of new pharmacological treatments to improve the cytoplasmic and nuclear proteotoxic alterations caused by mutated HTT **(Figure 28).** Notably, the broad pathogenic paradigm of HD associated with mutated HTT complicates the finding of appropriate pharmacological treatments even though the molecules are found to be simply administered (orally administration) (For review: (Gillian P. Bates et al., 2015; Caron et al., 2018; Ghosh and Tabrizi, 2018).

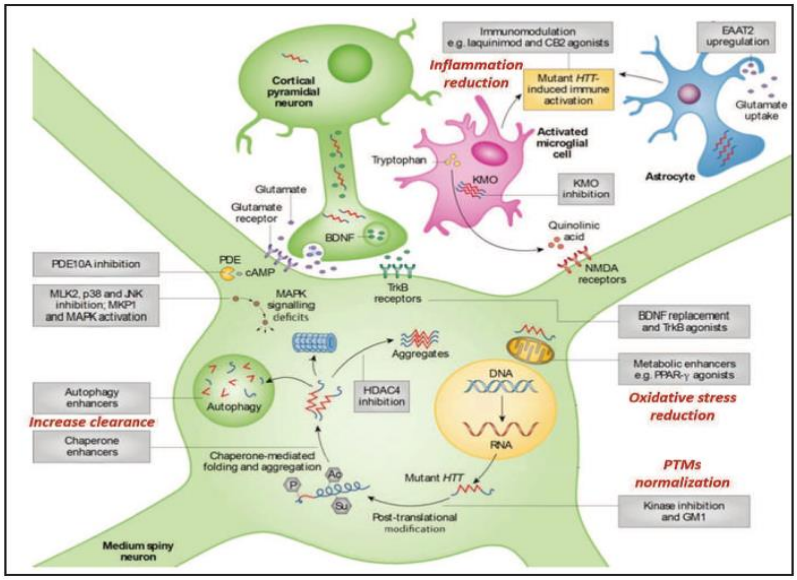

Figure 28: Illustration of cytoplasmic pharmacological targets tested for HD.
The pharmacological molecules used for HD target various pathogenic mechanisms: PTMs of mutated HTT to reduce its toxicity, mitochondrial dysfunction to reduce oxidative stress, impaired processes autophagic to increase the degradation of mutated HTT, dysfunction of BDNF production or even inflammation of the brain caused by an overactive immune system in patients. (Ghosh and Tabrizi, 2018).

3.2.1. Therapies targeting the cytoplasmic proteotoxicity of muHTT

3.2.1.a. PTMs and Kinase activity

The post-translational modifications modulating muHTT toxicity are mediated by several enzymes, which can be good potential targets for HD therapeutics. For example, the phosphorylation of serines 13 and 16 reduces the toxicity of muHTT (Gu et al., 2009) and leads to an increase in its nuclear localization (Atwal et al., 2011). Serine 421 is also an important site of modification since its phosphorylation restores the anterograde and retrograde axonal transport and, in particular, the transport of BDNF (Zala et al., 2008). Thus, kinases or their inhibitors can be potential therapeutic tools, although it seems delicate that their actions do not affect other muHTT sites or other proteins. Various pharmacological agents, such as ganglioside GM1 (Di Pardo et al., 2012) or the synthetic analog of sphingosine (fingolimod), also induce an improvement in motor function and a prolongation of lifespan in R6/2 mice (Di Pardo et al., 2014).

3.2.1.b. Protein Clearance and autophagy Chaperone proteins

The altered mechanisms of protein folding and clearance could also serve as a therapeutic target of HD. (Kaganovich et al., 2008). Hence, the induction of autophagy mechanisms would potentially reduce the level of misfolded mutated HTT and increase its degradation (**Figure 28).** The molecule Selisistat, a Silent information regulator T1 (SIRT1) deacetylase inhibitor, has a neuroprotective effect in cellular and animal models (Smith et al., 2014). It mediates an increase in mutated HTT acetylation, which in role promotes its degradation by autophagic processes. A phase II clinical trial tested this molecule's effect, which is well tolerated in humans, neither cause clinical changes, nor modification of the amount of soluble HTT (Reilmann et al., 2014; Süssmuth et al., 2015). However, autophagy stimulation seems to be effective only at an early stage of the disease, when large, very stable aggregates have not yet formed. The same results are obtained with other types of molecules capable of promoting autophagy, such as lithium, carbamazepine, and trehalose (Renna et al., 2010).

On the other hand, studies show that regulating chaperone proteins could also reduce the neuropathological aspects of HD. For instance, the overexpression of the Heat Shock Proteins, Hsp40 and Hsp70, suppresses neurotoxicity by preventing muHTT aggregation (Muchowski et al., 2000). Besides, pre-clinical studies testing various chaperone molecules showed to have beneficial effects, and they would be promising in reducing the aggregation of HTT (Labbadia et al., 2012; Sontag et al., 2013) and directly increasing macro-autophagy (Renna et al., 2010) (For review: (Gillian P. Bates et al., 2015)).

3.2.1.c. Restoring mitochondrial dysfunctions

The oxidative stress caused by the worsening of mitochondrial functions in HD is also targeted by several clinical approaches **(Figure 28)**. The treatment with coenzyme Q10 and creatine ("Safety and tolerability of high-dosage coenzyme Q 10 in Huntington's disease and healthy subjects," 2010), anti-oxidant molecules, showed no major change in the phenotype (McGarry et al., 2017) (Jiang and Salton, 2013; Todd et al., 2014)while an increase in the ATP amount in cells and slowing brain atrophy (Rosas et al., 2014), respectively. Clinical trials with these two molecules had to be stopped in phase III due to a lack of efficacy (McGarry et al., 2017). Using the same strategy, a new phase I/II clinical trial began in early May 2017 with the SBT-20 molecule. In fact, the use of latter seems promising by its ability to restore the physical and biochemical properties of mitochondria affected in HD (Stealth BioTherapeutics Inc.)

Other approaches, mainly targeting the neurotrophic factor BDNF and its tropomyosin kinase receptor (TrkB), have been tested to improve HD pathology. TrkB agonists' use demonstrates improved motor functions, lifespan, and striatal atrophy in N171-82Q and R6/2 mice models(Jiang and Salton, 2013; Jiang et al., 2013; Simmons et al., 2013; Todd et al., 2014). Other strategies, showing a possible improvement or a slowing down of pathology aim to increase the amount of BDNF in the brain (Reilmann and Schubert, 2017) and reduce brain inflammation associated with glial activation, caused by the overactive immune system of HD patients (Caron et al., 2018).

The abundance of potential therapeutic targets, shown schematically in **Figure 28**, once again demonstrates the very complex pathophysiology of HD which remains partially elucidated for the moment. Likewise, the consequent description of all pharmacological strategies shows the panoply of possible approaches to treat the consequences of the pathology.

3.2.2. Therapies targeting huntingtin nuclear toxicity

3.2.2.a. HDACs inhibitors

Whether epigenetics, mainly involving histone acetylation, is behind the origin of transcription dysregulation in HD has taken important support during the past years (Glajch and Sadri-Vakili, 2015; Jaenisch and Bird, 2003; Lee et al., 2013). This hypothesis was issued after the finding of the sequestration of the HAT CREB-binding protein CBP in muHTT aggregates, and that the treatment with the HDAC inhibitors (HDACi) improve the phenotypes of drosophila and mouse models of HD (Kazantsev et al., 1999; Nucifora Jr., 2001; Steffan et al., 2001) ; Accordingly, HDACi has been early used as an epigenetic strategy to treat HD through increasing histone acetylation. Many HDACi like the suberoxylanilide hydroxamic acid (SAHA), Trichostatin A (TSA), phenylbutyrate, sodium butyrate (NaB) were used in different preclinical studies which non-selectively target HDACs class I and II. Indeed, these studies along with many others that target several HDAC classes are highly varied and show an overall improvement in the phenotype of animal models of HD after treatment (For review: (Francelle et al., 2017; Sharma and Taliyan, 2015; Valor, 2015)).

In an attempt to generate more selective HDACi with less toxic side effects, many compounds have been developed (Herman et al., 2006; E. A. Thomas et al., 2008). For example, the HDACi 4b compound show high potency for inhibiting HDAC1 and HDAC3, and it was reported that it improves the phenotype of HD mice (Jia et al., 2012; E. A. Thomas et al., 2008). Recently, RGFP966, an HDAC3-selective inhibitor, was investigated using HD mice (Jia et al., 2016). This approach suggests that the compound limits glial cell response, diminishing markers of glial cell activation. However, disease-related phenotype were not ameliorated through a heterozygous

inactivation of the *Hdac3* gene in HD mice (Moumné et al., 2012), suggesting that more than 50% knock-down of the Hdac3 gene might be effective to observe beneficial effects in these mice.

Interestingly, HDACi does not induce a decrease in muHTT aggregation; however, they could acetylate the mutated protein itself or genes involved in the UPS system, increasing its clearance (Jia et al., 2012). The neuroprotective effects of HDACi also involve an improvement in the mitochondria's calcium metabolism, which is impacted by HD (Oliveira et al., 2006). On the other hand, inhibition of HDACs increases the acetylation of tubulin, which improves axonal transport and, therefore, the BDNF release (Dompierre et al., 2007).

Overall, HDACi studies reflect heterogeneous functionalities, sometimes beneficial, sometimes without effects, and often seem to target aggregation of mutated HTT while the expression of neuronal identity genes in HD brain tissues remains altered (CoppedÃ¨, 2014; Francelle et al., 2017; Sharma and Taliyan, 2015; Valor, 2015). Moreover, their mode of action is mainly non-specific and non-targeted, leading to long-term cytotoxicity following deacetylation of promoters. (Ganai et al., 2016; Sasakawa et al., 2005).

3.3. Other treatments

During the last twenty years, 99 clinical trials have been carried out on patients with HD with 41 different compounds (McColgan and Tabrizi, 2018). However, the success rate is low, with only 3.5% of trials progressing to the next stage (Travessa et al., 2017). Different strategies have been tested and 23 clinical trials on HD are ongoing (McColgan and Tabrizi, 2018) .

3.3.1. Cell therapy

The progressive neurodegeneration of the striatum, a hallmark of HD disease, favors cell therapy application to replace and compensate for the cell loss in this tissue. However, the ultimate goal is complex since these cells have to replace interrupted neuronal circuits. Thus, limited evidence supports the use of human fetal striatal tissue transplants or autologous stem cell transplants to treat HD patients.

3.3.1.a. Fetal cells

First trials of fetal striatal neuroblasts transplantation have been done in different models of HD, including mice (Deckel et al., 1986), rats (Klein et al., 2013), and non-human primates (Kendall et al., 1998). These grafts yielded successful results as the cells integrated correctly and improved motor capacity in these animals (Kendall et al., 1998).

Although many trials have been performed using fetal cell transplants, the results showed high variabilities between the studies and even within the same research center. The origin of these variabilities is not well defined; indeed, it could be related to many factors, including the biological origin and the limiting supply of the transplanted cells (human fetuses resulting from abortions), the quality control, even though many compatibility tests were performed between the donor and the patient.

In 2000, a French clinical trial highlighted the beneficial effects of a fetal transplant, where 3 out of 5 HD patients showed an increase in the striatum's metabolic activity and an improvement in their motor and cognitive functions (Bachoud-Lévi et al., 2000). However, this is not a lasting treatment since clinical improvements fade 4 to 6 years after surgery (Bachoud-Lévi et al., 2006) where; this could be explained in particular by a lack of vascularization of the graft (Cisbani et al., 2013) or, due to logistical issues, quality control and immunogenicity problems that could complicate the use of these cells (Table I), fostering interest in stem cells (Nicoleau et al., 2011).

3.3.1.b. Pluripotent stem cells

The strong therapeutic potential of the human embryonic stem cells (hESC) and induced pluripotent stem cells (hiPSC) through their abilities to produce and regenerate different cells in the body helped in regenerating GABAergic neurons, where transplanted cells can differentiate into MSNs, which express the striatal marker Darpp32 (Peschanski et al., 1995), and can establish synaptic connections with the target structures of the striatum (Wictorin, 1992). A Pre-clinical rodent study showed neural circuitry reformation inducing an improvement of motor deficits in an HD mouse model using hESC-derived neurons (Ma et al., 2012).

3.3.1.c. Mesenchymal stem cells

Mesenchymal stem cells (MSCs) are also of great interest because they induce little or no immune responses and secrete various cytokines and growth factors. They promote the regeneration of their microenvironment by inhibiting apoptosis, stimulating mitosis and angiogenesis, and reducing inflammation (Caplan and Dennis, 2006). These cells can be isolated from different places, such as adipose tissue and the umbilical cord (Pittenger, 1999). MSCs were transplanted into R6/2 and N171-82Q mice and induced a lengthening of animals' lifespan, decrease in muHTT aggregates and the loss of striatal neurons (Lee et al., 2009). The effect of MSCs is, therefore, very beneficial, although their ability to differentiate into neurons remains controversial. Some teams have also attempted to genetically modify MSCs, overexpressing BDNF. They also improved the phenotype in YAC128 and R6/2 mice (Dey et al., 2010; Pollock et al., 2016). Moreover, since phase II clinical trials using MSCs to treat neurodegenerative diseases have shown no toxicity concerns, this MSC/BDNF approach might be a potential clinical trial for HD (Deng et al., 2016).

Cell therapy is considered to have beneficial effects and improvement in the course of the pathology without determining the precise cause of the neurodegeneration. It doesn't only provide neuroprotection, but it also helps restore the lost functions in HD patients. Although promising, cell therapy is limited by many challenges, such as controlling differentiation to the desired neuronal type, integrating cells into the host tissue, managing their growth so that they do not form tumors, as well as the immune response following surgery (Chen et al., 2014).

To avoid immunological problems, it is now possible to obtain iPSCs from patients' somatic cells, having the same cell identity, thus preventing transplant rejection. However, since these cells still contain the mutated protein, symptoms of the disease may recur (Chen et al., 2014); so that this approach could be mainly used to model the pathology and not to treat it (Jeon et al., 2012).

A combined approach could, however, be considered: the somatic cells would be taken from the patient, reprogrammed in iPSC, differentiated into neural stem cells (NSC), and then corrected before being transplanted into the patient (Chen et al., 2014). An American team carried out this

work; they corrected iPSCs originating from fibroblasts of patients with HD by homologous recombination. This correction makes it possible to reverse the disease phenotype in the NSCs while maintaining the cells' pluripotent characteristics (An et al., 2012).

3.3.2. Gene therapy

3.3.2.a. Gene transfer

Gene transfer involves inserting one or more copies of exogenous genes into a host organism. The DNA insertion could be integrative or non-integrative, depending whether the inserted DNA integrates directly into the host's genome or expressed in an episomal form. Notably, the integrative gene transfer enabled the generation of transgenic animals through micro-injection into the fertilized egg. Usually, gene therapy's transfer is predominantly used for disease treatment, where it aims either to introduce a functional copy of a defective allele into the genome or to overexpress a therapeutic gene. The use of a vector is indispensable in the gene therapy approach to ensure an optimal transfer of the exogenous DNA/RNA into host cells or tissues. For clinical assays, different types of vectors are currently available and used; however, viral vectors remain the most commonly used (Cartier et al., 2009; Cavazzana-Calvo, 2000; Cavazzana-Calvo et al., 2010).

- **3.3.2.a.i. Viral vectors**

Viruses have been used as gene transfer vectors, most often, because they induce higher transfection efficiency. There are many types, briefly mentioning the most used three major families of viruses, namely lentiviruses, adenoviruses, and adeno-associated viruses (AAVs) (whose advantages and disadvantages are listed in **Table 2**.

The major disadvantage to use these viruses is their predominant immunogenicity a few weeks after their injection. Therapeutic viruses are derived from viruses that are infectious for humans. Still, before their use, the pathogenic genetic material is replaced by the therapeutic gene.

However, integrative vectors of the lentivirus type, for example, can insert themselves into oncogenes of the genome, which can lead to deleterious consequences (Hacein-Bey-Abina et al., 2003).

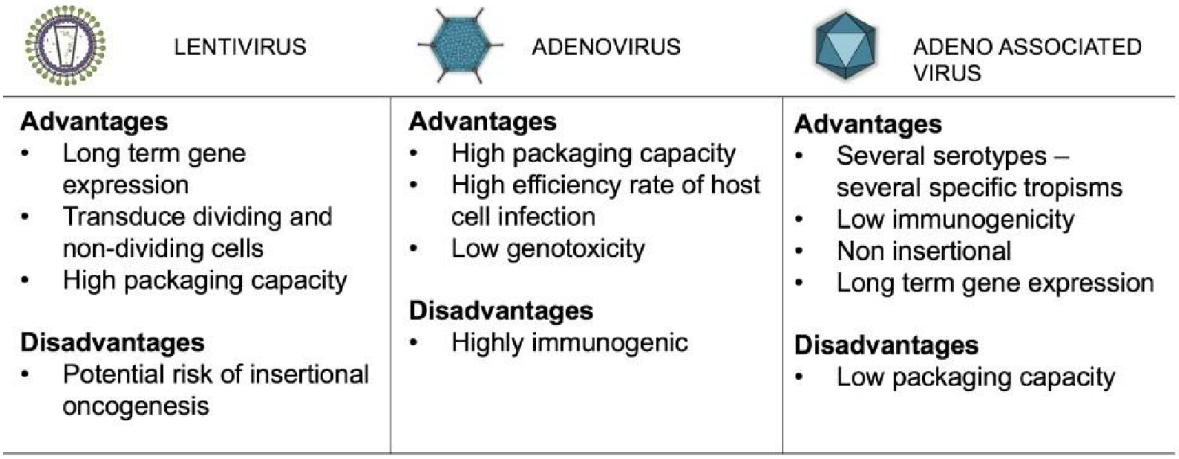

Figure 29: Advantages and Disadvantages of different viruses.
The advantages and disadvantages of lentiviruses, adenoviruses, and adeno-associated viruses (AAVs). (Thesis of Marine Imbert).

These two potentially deleterious consequences (immunogenicity and insertional mutagenesis) are by passed by the use of adeno-associated viruses (AAVs), which still retain their high infection efficiency (Gaj et al., 2016).

3.3.3. Genome editing approaches:

After the failed efficacy of many cell therapies and pharmacological trials, along with the single-gene nature of HD, the research of HD therapeutics shifts toward targeting the causative mutation at the RNA and DNA levels of the HTT gene. The promising strategies aim to lower the expression of muHTT by which it inhibits the pathogenesis in cells and animal models of the disease (For review: (Gillian P Bates et al., 2015; Kordasiewicz et al., 2012; Lu and Yang, 2012; McColgan and Tabrizi, 2018; Miniarikova et al., 2017; Stanek et al., 2013; Tabrizi et al., 2020, 2019; Wild and Tabrizi, 2017).

Several approaches have been used to target mutated HTT mRNAs mainly through antisense oligonucleotides (ASO) and interfering RNAs (RNAi) **(Figure 30).** Unlike DNA, RNAs are not protected by repair mechanisms, thus facilitating the reduction of translation of mutated HTT mRNAs relative to modulation of transcription or the direct alteration of the gene.

3.3.3.a. Therapies targeting mutated huntingtin RNA

- **3.3.3.a.i. Antisense oligonucleotides (ASO)**

Antisense oligonucleotides are synthetic, single-stranded, modified DNA molecules, generally, 12 to 22 bases, which can bind to a complementary sequence of mRNA, modulate its expression, and favor its degradation by the ribonuclease H (RNase H) in the nucleus **(Figure 30)** (Bennett and Swayze, 2010). The binding of the ASO to pre-mRNA, as opposed to mature transcripts, provides more potential binding to intronic and exonic regions (Rinaldi and Wood, 2018). The mechanisms that allow the entrance of the ASO to the cell and the nucleus are still poorly understood (Crooke, 2017). RNase H, an endogenous enzyme, can recognize RNA/DNA hybrids (Larrouy et al., 1992), thus reducing the production of the toxic mRNA of mutated HTT. However, the effect of ASOs on training mRNAs from exon 1 of mutated HTT is still poorly characterized because these fragments would be generated before the formation of the pre-mRNAs recognized by the ASOs.

In mouse models of HD, ASO's repeated intrathecally administration mediates a 50-70%reduction in HTT mRNA (Southwell et al. 2018). A Phase I/IIa clinical treatment using the ASO HTTRx, conducted on adults with early-stage HD by Ionis and Roche, showed a dose-dependent reduction in CSF muHTT concentration compared to the participants receiving the placebo (Tabrizi et al., 2019). Currently, Roche is conducting a phase III trial investigating the clinical efficacy of the **ASO HTTRx** with further recent scales (US National Library of Medicine, 2020). Since ASO HTTRx targets both the mutant and wt-HTT mRNA equally, the Wave Life Science is currently performing a phase Ib/IIa clinical trials against two allele-selective HTT ASOs that target single nucleotide polymorphisms (SNPs) inherited with the mutant allele (Rosas et al., 2006)(Hersch et al. 2017).

Thus, it is still unclear whether the optimal approach is to lower the total HTT or allele-selective muHTT level; however, the results of ongoing clinical trials are still promising. Interestingly, an expression-lowering variant in the *HTT* promoter was associated with a delay in disease onset of 9.3 years when on the expanded CAG allele or 3.9 years when on the normal CAG allele, suggesting that total HTT lowering is beneficial in HD (Bečanović et al., 2015)

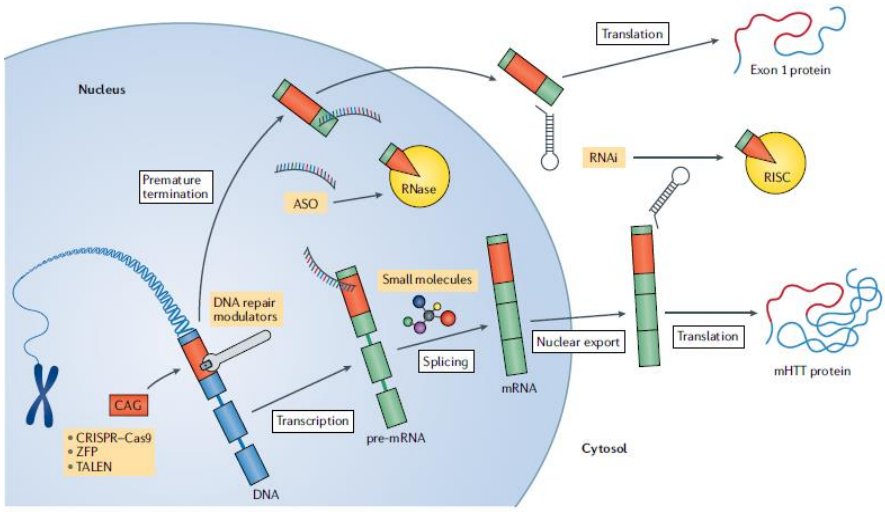

Figure 30: Therapeutic methods for lowering huntingtin expression.
The red sections of DNA, RNA and protein represent the pathogenic expanded CAG tract and its polyglutamine product. The orange boxes are therapeutic approaches. ASO, antisense oligonucleotide; mHTT, mutant huntingtin; RISC, RNA-induced silencing complex; RNAi, RNA interference; RNase, ribonuclease; TALEN, transcription activator-like effector nuclease; ZFP, zinc-finger protein. (Tabrizi et al., 2020).

These findings encourage the continuity with the current total HTT-lowering approaches over allele-specific approaches as they permit to target any HTT region targeted by a single agent that can be used with any HD patient. Moreover, this early partial knockdown, by the total HD-lowering approach, avoids potential effects on development.

- **3.3.3.a.ii. RNAi**

Another therapeutic approach that aims to decrease the expression of a target gene is the RNAi. RNAi is an endogenous cellular process that degrades mature, spliced mRNAs (Setten et al., 2019). This strategy targets the muHTT mRNA by using small RNAs -short interfering RNA (siRNA), microRNAs or even RNAs in hairpin), thus guiding the complementary bound mRNA target to Argonaut 2, the RNase of the RNA-induced silencing complex (RISC) leading to its cleavage and translational repression **(Figure 30)** (Ha and Kim, 2014; Hutvagner and Simard, 2008). Notably,

RNAi can impact the fragments generated from muHTT exon 1, unlike ASO, as they predominantly target the spliced mRNA **(Figure 30).**

The development of this therapeutic strategy is still so challenging. Concretely, the introduction of the synthetic siRNA and/or miRNA directly into the target tissue (striatum) is the limiting step as they cannot cross the blood-brain barrier (Tabrizi et al., 2019). The process requires surgical intervention, mainly stereotaxis and most commonly through viral vector insertion, such as recombinant AAVs. This could carry additional risk to the patient and the tissue distribution might be limited (Lykken et al., 2018). Unlike ASO, and although invasive, a single administration of RNAi tools ensures a permanent reduction of HTT (Wild and Tabrizi, 2017). Current therapeutic strategies are still in the pre-clinical phase (For review: (Wild and Tabrizi, 2017). Many studies showed beneficial effects of the AMT-130 microRNA, an AAV5-delivered, non-allele selective HTT miRNA, produced by the uniQure company, using mini-pigs and rodents HD models (Evers et al., 2018; Miniarikova et al., 2017). Adequately, the released approval from FDA 2019 to uniQure encourages the first clinical trial of HTT-lowering gene therapy in HD patients (Tabrizi et al., 2019).

Although promising, RNAi has a major drawback relatively concerned with reducing mutated HTT and wild-type alleles. Where the reduction in the latter would therefore has harmful effects in mice. That's why it is necessary to adapt this technology and develop mutated allele-specific targeting either against the CAG repeats or the different SNPs associated with HD.

3.3.3.b. Therapies targeting the DNA of muHTT

On the other hand, many DNA-targeting approaches have great therapeutic potential for treating HD. They mainly modify the HTT genetic sequence or its transcription and typically combine a specific DNA-binding element with an effector, such as nucleases. There are three main DNA-targeting approaches; zinc-finger nucleases (ZFNs) (Klug, 2010), Clustered Regulated Interspaced Short Palindromic Repeat/CRISPR associated protein 9 (CRISPR-Cas9) (Adli, 2018), and transcription activator-like effector nucleases (TALENs))**(Figure 30)** (Nemudryi et al., 2014)(For review: (McColgan and Tabrizi, 2018; Wild and Tabrizi, 2017). Each of the mentioned approaches

is based on the use of a viral vector injected intra-cranially that allows transduced cells to produce non-native proteins of ZF proteins, TALENs peptide repeats, or proteins of the CRISPR/Cas9 system.

- **3.3.3.b.i. ZF proteins**

ZFN DNA-binding element consists of an array of zinc finger peptides. Each peptide binds a sequence of 3 to 5 nucleotides, where the association of several domains allows targeting a specific sequence. Once being fused with a gene encoding a nuclease or transcription factor, the ZF protein will eventually cleave and repress the target gene (Klug, 2010). Several studies in HD, in-vitro, and in mice model showed reduced expression of the mutated HTT through selective targeting of the expanded CAG repeats (Garriga-Canut et al., 2012; Zeitler et al., 2019). Regardless of the adverse effects obtained using this approach, the production of non-native proteins thus triggers inflammatory and immune reactions, resulting in neuronal death. This approach leads to an improved phenotype of murine models, associated with reduced expression of the mutated allele (> 95%) while preserving the expression of wt-HTT (80% on average) (Garriga-Canut et al., 2012; Zeitler et al., 2019). Nevertheless, improving the limitation of the immune reactions induced by this approach will raise the long-lasting potential effect in HD treatment (Agustín-Pavón et al., 2016).

- **3.3.3.b.ii. TALENS**

TALENS contain a series of peptide repeats, where each peptide binds to a specific DNA nucleotide(Malankhanova et al., 2017). They seem to be more efficient and specific than ZFNs. They have been used to shorten the expanded CAG repeat(Richard et al., 2014) and suppress *HTT* transcription in vitro (Fink et al., 2016). However, the requirement of a thymine base at the end of the target sequence makes TALENS to have fewer potential targets than ZFNs (Malankhanova et al., 2017).

- **3.3.3.b.iii. CRISPR / Cas9 system**

CRISPR/Cas9 is a naturally occurring bacterial adaptive immune response to viruses (Adli, 2018). The recent discovery of this system has made it possible to edit many genes, including Huntingtin.

This system is not only used for excision, but it can also insert a new DNA fragment into the cleavage site (Savić and Schwank, 2016). The complex's activity requires a single guide RNA (sgRNA) and an RNA-guided DNA endonuclease, the Cas9 (Hsu et al., 2014). The sgRNA is designed to target the DNA of the gene of interest upstream of a Protospacer-Adjacent Motif (PAM) formed by nucleotide-guanine-guanine (NGG) that will allow the recruitment of the Cas9 enzyme and thus induces DNA cleavage (Malankhanova et al., 2017) **(Figure 31).**

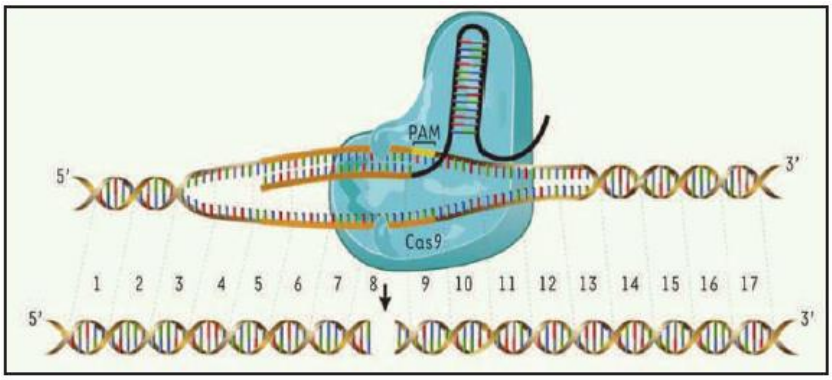

Figure 31: Schematic diagram of the CRISPR / Cas9 system.
The guide RNA (sgRNA) contains a sequence complementary to the target sequence (brown) and a sequence allowing to guide the Cas9 (black). After binding of the sgRNA, Cas9 binds to the PAM sequence (Protospacer adjacent motif) and cleaves the target region. (Tremblay, 2015).

Several trials using CRISPR/Cas9 have been done in the course of HD. Initially, it was used to specifically inactivate the mutant HTT allele by DNA sequence excision in a cell model from patients fibroblasts, leading to the reduction of almost total RNA and mutated protein (Monteys et al., 2017; Shin et al., 2016; Xu et al., 2017).

Kolli and his team have used lentivirus to express the CRISPR/Cas9 system in MSCs from YAC128 mice. They introduced two sgRNAs targeting CAG repeats of the HTT gene on either side, which drastically reduces the expression of muHTT (Kolli et al., 2017).

In parallel, a Chinese group has permanently suppressed the expression of HTT endogenously mutated in the striatum of CAG140 KI mice, using AAVs carrying the CRISPR/Cas9 system, leading to reduced neuropathology and improved motor functions of the mice (Yang and Patel, 2017).

However, this technique is not-specific; it cannot distinguish between the mutated HTT and the wild allele in human cells **(Figure 32).** Hence, several studies have started to work on allele-

specific inactivation of the HTT gene using this system by targeting HD associated SNPs and through altering the NGG of the PAM motif. The sgRNAs will bind to either side of the CAG repeats. The Cas9 will cut the DNA where the PAM motif is correctly established, namely on the chromosome containing the mutated HTT gene (Malkki, 2016; Monteys et al., 2017; Shin et al., 2016).

These results suggest that gene editing via CRISPR / Cas9 could be an interesting therapeutic strategy to eliminate the neuronal toxicity induced by the expansion of polyQ in the HTT gene in patients with HD.

Altogether, a single administration of ZFNs, TALENs, and CRISPR–Cas9 approaches could avert the effect of the mutant HTT, including RNA-mediated toxicity, alternative splicing, and repeat-associated non-AT translation, and provide a long-term treatment for HD. However, the current treatments' administration is still challenging as they require reaching limited brain regions that need the implication of viral vectors. Moreover, the *HTT* mutation correction would eliminate the inter-generational transmission of HD (Ledford, 2019). Also, DNA targeting raises concerns about potential off-target effects elsewhere in the genome, insertional mutagenesis, and immunogenicity (Milone and O'Doherty, 2018).

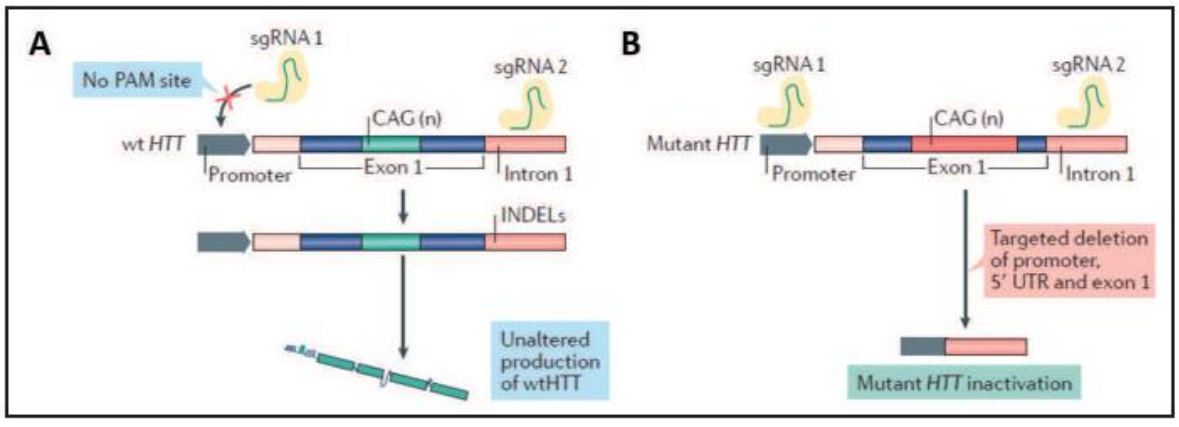

Figure 32: Specific inactivation of the mutated allele mediated by CRISPR / Cas9.
(A) Since the healthy allele does not contain SNPs, shRNAs cannot bind, Cas9 is not recruited and transcription of exon 1 occurs normally. **(B)** To target the mutated HTT allele, two sgRNAs are created to flank exon 1 of the gene. These sgRNAs 1 and 2 target SNPs within PAM sites often associated with the mutated allele. Thus, the excision of exon 1 is carried out specifically in the mutated allele. (From (Caron et al., 2018).

4. Serum Response Factor (SRF)

4.1. Srf expression

The 67-kD serum response factor (Srf) is a **ubiquitous** transcription factor (TF) (Affolter et al., 1994), broadly expressed from flies to humans (Posern and Treisman, 2006). It was first recognized as nuclear protein mediating the transient transcriptional activation of the proto-oncogene (*c-fos*) and the cytoskeletal actin genes after serum induction through binding to a short DNA sequence element, the serum response element (SRE) (Treisman, 1987).

4.1.1. Srf gene

Srf gene is localized on chromosome 17 in mouse and 6 in human. Its mRNA transcript spans 10,607 base pairs, containing seven exons, separated by six introns. Murine Srf mRNA levels were the highest in adult skeletal and cardiac muscle but barely detected in the liver, lung, and spleen tissues (Belaguli et al., 1997).

4.1.2. Srf –MADS box

Srf is the founding member of the MADS (MCM1-Agamous-Deficiens-SRF) box family of transcription factors (Schwarz-Sommer et al., 1990), and it's one of the best understood DNA-binding proteins in the human proteome. The MADS-box transcription factors include the metazoan transcription factors SRF and MEF28, the yeast transcription factors MCM1 and ARG80, and many plant homeotic gene products (Shore and Sharrocks, 1995). It was shown that the DNA-binding domain and a part of the dimerization domain in Srf-like transcription factors are included within the MADS-box motif, which has been highly maintained through evolution **(Figure 33).** The N-terminal half of the MADS-box determines DNA specificity among the different family members. In contrast, the carboxy-terminal half forms part of the dimerization surface. However, an additional 30 residues of the MADS, at the C-terminal end are required to efficiently dimerize and recruit accessory proteins (Treisman, 1995).

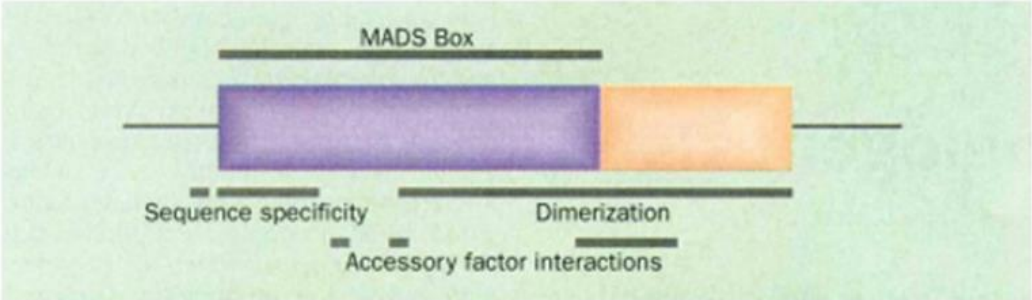

Figure 33: Simplified schematic representation of SRF and MCM1 DNA-binding domains.
The DNA-binding domain is shown as a box, with the MADS-box in purple. Regions of the domain shown biochemically to determine DNA-binding specificity, to mediate dimerization and accessory factor interactions are indicated. Adapted from (Treisman, 1995).

4.1.3. Srf protein

Human SRF protein consists of 508 amino acids (aa) (Norman et al., 1988), while murine Srf contains 504 aa (Belaguli et al., 1997). Srf comprises an N-terminal regulatory domain (aa 1-142), the MADS-box (aa 142-171), and a carboxyl-terminal transactivation domain (aa 266-508). The N-terminal regulatory part is a target of casein kinase II and ribosomal S6 kinase phosphorylation (Johansen and Prywes, 1995). It contains the nuclear localization signal (NLS) (Rech et al., 1994). The MADS domain, which has been highly conserved, as it is identical in humans, chickens, and Xenopus, forms the interaction interface of Srf with its partners (Belaguli et al., 1997; Shore and Sharrocks, 1995). Finally, the transcriptional activation domain is located in the C-terminal region of Srf (Chai and Tarnawski, 2002; Johansen and Prywes, 1993) **(Figure 34).**

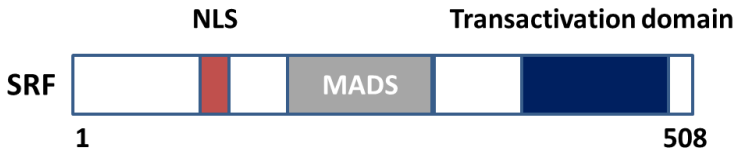

Figure 34: SRF different regions.
(Adapted from (Posern and Treisman, 2006).

4.2. SRF Isoforms

It has been described that Srf is subjected to an alternative splicing mechanism leading to the formation of four isoforms identified in mice as Srf-L, Srf-M, Srf-S, and Srf-I (Kemp and Metcalfe, 2000). These isoforms show a lack of part of the transactivation domain, where exon 5 is deleted in Srf-M, exons 4 and 5 in Srf-S, and exons 3, 4, and 5 in Srf-I **(Figure 35).** The translation of the

Srf-M form, having an intact MADS domain, produces a 57 kDa protein that can bind to DNA, dimerize with Srf-L or Srf-M, and acts as a dominant-negative in vitro (Belaguli et al., 1999). Notably, Gerosa et al. have outlined the expression of Srf-M in mouse and human brain and showed that this spliced form antagonizes SRF function and acts as a potent transcriptional repressor of SRF-dependent promoters (Belaguli et al., 1999; Gerosa et al., 2020). Interestingly, both Srf and Srf-M bind the transcriptional corepressor complex Lysine Specific Demethylase 1 LSD1 and CoREST/HDAC2 via their shared N-terminal repressor domain. Still, relevantly, SRF-M cannot bind ELK1, one of the most characterized positive SRF cofactor (Esnault et al., 2017; Gerosa et al., 2020; Janknecht et al., 1993; Janknecht and Nordheim, 1992).

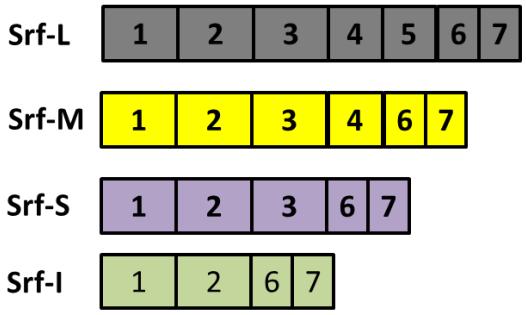

Figure 35: SRF isoforms
(Adapted From (Kemp and Metcalfe, 2000).

4.3. SRF target genes

Srf acts as a homodimer and eventually binds to a CC(A/T)6GG type target sequence called the CArG box (Gustafson and Kedes, 1989; Treisman, 1987). Indeed, known Srf target genes are featured to have one or more CArG boxes in their promoter region, which allow the binding of SRF to its target DNA (Q. Sun et al., 2006). There are two categories of the CArG elements: the consensus CArG element and the CArG-like elements. Effectively, Srf has a higher affinity for the consensus CArG boxes (about 64 possible CArG boxes), represented by the 10 base pair sequences CCW6G, where the Ws are only A or T nucleotides. Note that, Srf has two functional CArG boxes in its promoter, making it its target, facilitating its autoregulation.

In vivo and *silico* studies suggest the presence of different classes of Srf target genes **(Table 4),** with many that promise insight into how SRF exerts its effects on the motility of neurons and brain plasticity (Chai and Tarnawski, 2002; Philippar et al., 2004; Y. Sun et al., 2006) **(Table 5).**

Gene name	Annotated function	Reference
c-fos	Transcriptional regulation, IEG	(Ramanan et al.2005; Etkin et al. 2006 ; Arsenian et al. 1998)
fosB	Transcriptional regulation, IEG	(Ramanan et al.2005; Etkin et al. 2006)
Junb	Transcriptional regulation, IEG	(Ramanan et al.2005 ; Philippar et al. 2004)
Srf	Transcriptional regulation, IEG	(Philippar et al. 2004)
Egr1,Egr2, Egr3	Transcriptional regulation, IEG	(Ramanan et al.2005; Etkin et al. 2006; Philippar et al. 2004))
Nur77	Transcriptional regulation, IEG	(Etkin et al. 2006)
Ldb2	Transcriptional regulation, Lim domain	(Wickramasinghe et al.2008)
Crem	Transcriptional regulation	(Etkin et al. 2006)
Egr4	Transcriptional regulation, IEG	(Cooper et al. 2007)
Npas4	Transcriptional regulation, synapse development	(Cooper et al. 2007)
Cyr61	Extracellular matrix, IEG	(Stritt et al. 2009; Philippar et al. 2004 ; Kalita et al.2006)
Ctgf	Extracellular matrix, IEG	(Stritt et al. 2009; Philippar et al. 2004 ; Sun et al.2006 ; Muehlich et al.2007)
Actb	Actin cytoskeleton	(Ramanan et al.2005 ;Alberti et al. 2005; Knoll et al. 2006 ; Wickramasinghe et al.2008)
Actg1	Actin cytoskeleton	(Wickramasinghe et al.2008)
Gelsolin	Actin cytoskeleton, actin severing	(Alberti et al. 2005)
Arc (Arg3.1)	Actin cytoskeleton, synaptic activity, IEG	(Ramanan et al.2005 ; Etkin et al. 2006 ;Pintchovski et al. 2009; Waltereit et al. 2001; Kawashima et al. 2009)
Filip1L	Actin cytoskeleton, Filamin interacting protein	(Cooper et al. 2007)
Myh2	Actin cytoskeleton, Myosin heavy chain	(Cooper et al. 2007)
Cltc	Clathrin coat, endocytosis	(Etkin et al.2006)
Pmp22	Peripheral myelin protein	(Philippar et al. 2004)
Psd95	Postsynaptic density, synaptic vesicle	(Philippar et al. 2004)
Nestin	Intermediate filament	(Philippar et al. 2004)
App	Amyloid precursor protein, Alzheimer	(Philippar et al. 2004)
Prp	Prion protein	(Philippar et al. 2004)
Sema3a	Axon guidance	(Zhang et al. 2005)
Sema3C	Axon guidance	(Knoll et al. 2006)
Epha4	Axon guidance	(Knoll et al. 2006)
Epha7	Axon guidance	(Knoll et al. 2006)
P35	CDK5 activator	(Etkin et al.2006)
Arhgef5	Rho-GEF	(Knoll et al. 2006)
Bdnf	Neurotrophin	(Etkin et al.2006)
Ngf	Neurotrophin	(Etkin et al.2006)
Cdk5	Cyclin-dependent kinase	(Etkin et al.2006)

Table 2: Srf neuronal target genes.
This table depicts genes bound by SRF (chromatin immuno-precipitation or in silico analysis) or genes affected by SRF deficiency in neurons or embryonic stem cells. This list does not cover all potential neuronal SRF target genes reported, as some genes relevant to nervous system function were identified in non-neuronal cells and await verification of being under SRF control in neurons. Also, direct or indirect regulation of these genes by SRF has not been analyzed in all cases. (Knöll and Nordheim, 2009).

Srf regulates the expression of immediate early genes (IEGs) like *c-fos*, *junB*, and the Egr family (*Egr1*, *Egr2* and *Egr3*). The activation of such genes occurs directly after being stimulated, without requiring the establishment of *de novo* protein synthesis. Notably, these genes are implicated in regulating cell cycle and coding for growth factors.

On the other hand, Srf controls many genes involved in the organization and cytoskeletal dynamics, such as *Actb* and *Actg2* (Chai and Tarnawski, 2002; Y. Sun et al., 2006), in addition to the genes involved in cell-adhesion like integrin subunits 1,5 and 9 or syndecans 2 and 4 (Miano et al., 2007). Moreover, SRF regulates the expression of specific genes of skeletal, smooth, and cardiac muscles, including *MyoD*, which is involved in muscle differentiation. Other genes such as *Acta1*, myosin heavy chain, myosin light chain or troponin, encode proteins of the contractile system, many other genes encoding calcium and energy metabolism (Chai and Tarnawski, 2002; Y. Sun et al., 2006) and others that encode axon guidance (e.g., *Sema3a* and *Epha4*) and synaptic plasticity (e.g., *Arc* and *Psd95*).

4.4. Regulation of Srf activity

Srf acts on gene expression through interaction with other transcription factors, notably ternary complex factors (TCFs), which mediate mitogen-activated protein kinase (MAPK) and Ca2+ signaling (Buchwalter et al., 2004; Shaw et al., 1989), as well as members of the myocardin family of transcriptional cofactors (MRTFA/B; MKL1/2), which mediate actin signaling (Cen et al., 2003; Gineitis and Treisman, 2001; Schröter et al., 1990).

4.4.1. MAPK/TCF pathway

Srf interacts with the Ets domain accessory proteins members, the ternary complex factors (TCF). These factors, including Elk-1, SAP-1, and Net, have a highly conserved Ets domain in the N-terminal region, which enable their binding to conserved DNA regions, GGA (A/T) type, called Ets binding sites (EBS) adjoining the SRF-binding site (Treisman, 1994). They also have a conserved C-terminal activation domain-containing potential MAP kinase consensus sites, favoring their activation by ERK, JNK, or p38 (Price et al., 1995) **(Figure 36)**.

Genomic foot printing studies show that TCF is present at the serum response element (SRE) even in unstimulated cells, suggesting that SRE activation involves regulating transcriptional activation rather than DNA binding (Herrera et al., 1989). In the absence of MAPK signaling, Sap-1 activates transcription, but Net represses it, and Elk-1 is inactive (Giovane et al., 1994).

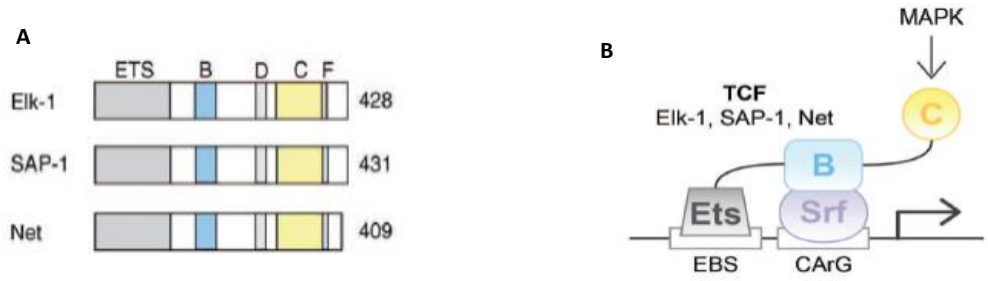

Figure 36: Srf co-factors.
(A) Ternary complex factors. **(B)** MAPK/TCF pathway (From (Posern and Treisman, 2006).

The activation of the MAP kinase pathway, through Ras, Raf, MEK, and ERK, phosphorylates TCFs (Posern and Treisman, 2006), which bind to their own Ets-motif site and Srf in a 'grappling hook' model (Treisman et al., 1992). The formed complex with Srf and a SRE, defined as a promoter region exhibiting an EBS-domain adjacent to a CArG box, leads to activation of the transcription of *c-fos* and other IEGs such as *JunB* and *Egr1* (Buchwalter et al., 2004; Dalton and Treisman, 1992)**(Figure 36 B)**.

Several approaches were performed to investigate the role of TCFs members, leading to different phenotypes depending on the targeted TCF member. For instance, Elk-1 shows strong expression in the central nervous system (Price et al., 1995) and it is restricted to neuronal cells (Sgambato et al., 1998). It is directly activated, phosphorylated by the pro-survival mitogen-activated protein kinases (MAPK)/ extracellular-signal regulated kinase (ERK) signaling pathway (Besnard et al., 2011). Elk-1 was reported to play a role in reducing cell death excitotoxicity in the quinolinic acid-induced model of striatal damage (Ferrer et al., 2001), and more recently, reduction of Elk-1 levels by small-interfering RNAs was shown to promote cell death in the STHdhQ111/Q111 cell line model of HD (Anglada-Huguet et al., 2012).

The deletion of *SAP-1* in mice induces a defect of thymocytes' positive selection in response to the Erk signaling (Costello et al., 2004). Finally, "Net" KO in murine embryonic fibroblasts (MEF) cells causes a migration defect in mutant cells (Buchwalter et al., 2005). Despite their high degree of homology, TCFs do not necessarily have redundant functions within the organism.

4.4.2. RhoA-Actin Signalling

Srf activity is also regulated by the Rho family of small GTPases (Hill et al., 1995) through the recruitment of myocardin-related transcription factors (Mrtfs) at Srf target genes (Olson and Nordheim, 2010). The Mrtfs are SRF's cofactors, which show a high degree of homology with myocardin, including two members: The Mrtf-A (also named MAL, MKL1 or BSAC) and Mrtf-B (MAL16, MKL2) **(Figure 37).**

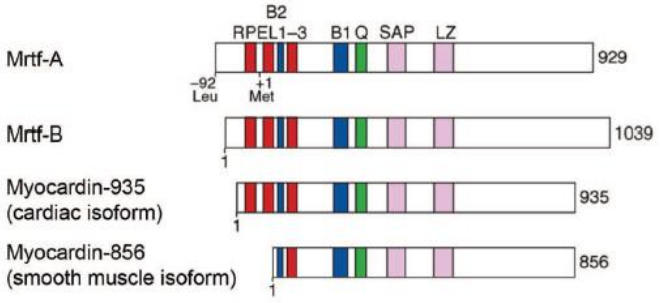

Figure 37: Mrtfs and Myocardin isoforms.
(Posern and Treisman, 2006).

MRTF isoforms are exclusively nuclear and activate constitutively Srf-dependent transcription (Guettler et al., 2008). Mrtf-A and Mrtf-B are expressed ubiquitously, and their localization is regulated by actin dynamics. The cytoplasmic concentration of G-actin is reflected by the concentration of Mrtf retained in the cytoplasm. Eventually, Mrtfs act as "**actin sensors**" in the cytoplasm (Guettler et al., 2008; Miralles et al., 2003; Vartiainen et al., 2007). Nevertheless, following serum stimulation, the release and nuclear translocation of cytoplasmic Mrtfs induce Srf directed target gene activation **(Figure 38).**

Moreover, the alterations in actin dynamics using actin binding drugs, the actin-specific C2 toxin, and actin overexpression demonstrate that G-actin level controls SRF (Sotiropoulos et al., 1999). Moreover, regulation of actin dynamics, the RhoA-actin pathway, is necessary for serum

induction of a subset of SRF target genes, including vinculin, cytoskeletal actin, and *Srf* itself, and also serves for their activation (Posern and Treisman, 2006).

Mrtf-A regulates many Srf target genes which are involved in cytoskeleton regulation. It stimulates both neurite outgrowth and dendritic branches (Knöll et al., 2006; Shiota et al., 2006; Wickramasinghe et al., 2008), and it is targeted by synaptic activity in vitro (Kalita et al., 2006). Moreover, Mrtf-A mutants seem to have no obvious brain phenotype (Li et al., 2006), whereas constitutive Mrtf-B mutants die before birth (Oh et al., 2005). Nevertheless, conditional deletion of both the Mrtf-A and Mrtf-B genes in the mouse brain results in aberrant development of multiple functions including neuronal migration, neurite outgrowth and SRF target genes expression (Mokalled et al., 2010). Thus, the remarkable similarity between neuronal defects associated with SRF (See introduction section 4.5.7; The role of SRF in the nervous system p:94) and Mrtf gene deletion in the brain support the conclusion that SRF and Mrtf function as obligate partners in the control of neuronal development in vivo (Mokalled et al., 2010).

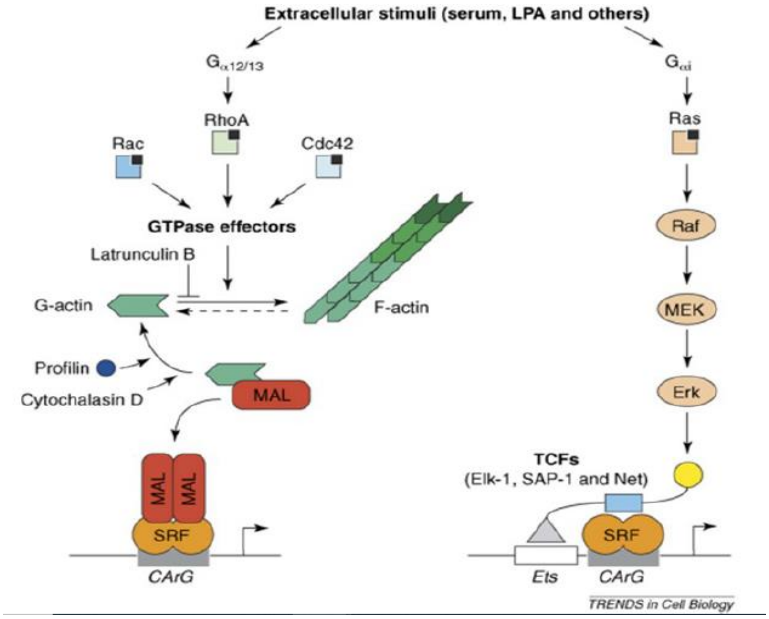

Figure 38: Model of two principal pathways regulating SRF activity in non-muscle cells.
Stimulation activates both Rho-dependent (left) and Ras-dependent (right) signaling. Activation of the MAP kinase pathway through Ras, Raf, MEK and ERK phosphorylates TCFs, which bind to their own Ets DNA recognition site and SRF in the 'grappling hook' model. Signaling through Rho family GTPases (squares, with small black squares indicating GTP) and the actin treadmilling cycle (left) results in the dissociation of MAL from actin, which then binds and activates SRF. From (Posern and Treisman, 2006).

4.4.3. micro RNA Regulation

In addition to the previously mentioned regulatory co-factors, Srf regulates, and it is regulated by several miRNAs. It has been shown that Srf controls certain microRNAs implicated in cardiac and skeletal muscle development. Studies show that microRNAs' expression is altered upon cardiac-specific Srf overexpression (Srf-Tg). The latter leads to downregulation of mir-1 and miR-133a, and upregulation of miR-21 which occurred by 7 days of age in these mice, long before the onset of cardiac hypertrophy, suggesting that SRF overexpression impacted the expression of microRNAs which contribute to cardiac hypertrophy (Zhang et al., 2011). Moreover, a high-level overexpression of Srf leads to the drastic development of fibrosis associated with an increased expression of connective tissue growth factor (CTGF) and a strong downregulation of miR-133a, revealing a crucial role of the SRF/CTGF/miR-133a axis in the regulation of cardiac fibrosis (Angelini et al., 2015).

4.4.4. Other pathways

4.4.4.a. Post translational modification (phosphorylation)

Threonine 159 and serine 162 from the MADS domain of Srf can be phosphorylated by myotonic dystrophy protein kinase (DMPK) and protein kinase C-alpha (PKC), respectively. This event inhibits the binding of Srf to DNA and the formation of complexes with Mrtfs (Iyer et al., 2006, 2003). In fibroblasts, TCF-Mrtf competition at many SRF sites potentially favors Srf-TCF interaction, promoting the activation of cellular proliferation over cytoskeleton and contractility programs (Gualdrini et al., 2016). Thus, the antagonistic TCF-MRTF factors will also be affected by the basal level of Rho-signaling, and factors affecting the degree to which a particular stimulus activates Rho- and ERK-dependent pathways will therefore also influence SRF transcriptional outputs (Gualdrini et al., 2016) **(Figure 39).**

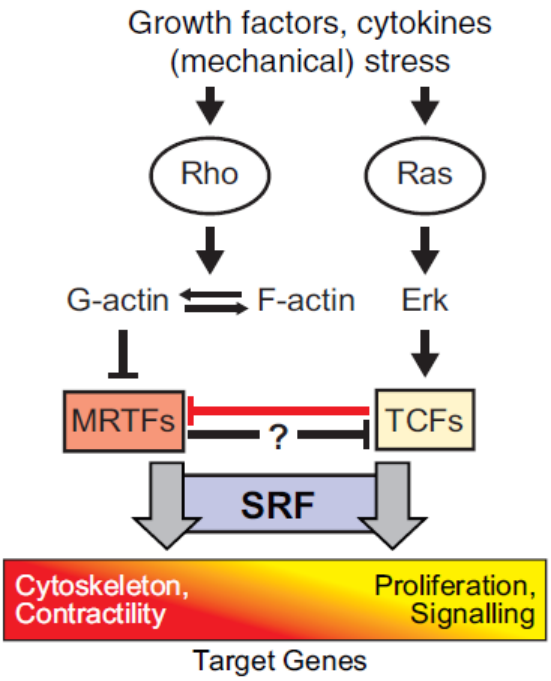

Figure 39: SRF regulation and co-factors.
The TCF and MRTF co-factors. (Gualdrini et al., 2016).

4.4.4.2. Cleavage by caspaces

The two cleavage sites of Srf are targeted by caspases 3 and 7 leading to the generation of two major fragments that are unable of activating c-fos transcription in human BJAB cells (Drewett et al., 2001).

4.5. Role of Srf in pathogenesis

The importance of Srf during mice embryonic development was demonstrated by Nordheim and his colleagues in 1998. They found that Srf knock-out is lethal at E12.5, before the onset of organogenesis, and showed an incomplete gastrulation with an absence of mesoderm (Arsenian et al., 1998). Moreover, the development of many mouse lines expressing the Cre-recombinase under the control of specific promoters have been extensively used to characterize the role of SRF in many tissues, where the different phenotypes resulting from these studies are shown in the table below.

Cre driver	Targeted cell type	Phenotype
Myh7 (βMhc)	Cardiomyocyte	Dilated heart and embryo demise at E10,5-E13,5
Tagln (Sm22α)	Cardiomyocyte / smooth muscle cell	Dilated heart / reduced SMC recruitment and embryo demise at E10,5
Myh6 (αMhc)	Cardiomyocyte	Cardiac insufficiency / reduced myocyte survival
Nkx2.5	Cardiomyocyte	Non-beating heart tube at E8,25
Myh6-MerCreMer	Adult cardiomyocyte	Heart failure and death 10 weeks after KO
Des (Desmin)	Cardiomyocyte	Heart failure and death by 11 months of age
Tie1	Endothelial cell	Aneurysm, hemorrhage, endothelial cell junctional / actin cytoskeletal defects and death at E14,5
Tie2	Endothelial cell	Hemorrhage and endothelial cell junctional / actin cytoskeletal defects, with death at E14,5
Myog-Mef2c	Skeletal muscle cell	Perinatal orthopnea with thinned myofibers
Acta1 (human α-skeletal actin)	Adult skeletal muscle	Muscle hypotrophy and poor regeneration, with 50% mortality by 6 weeks of age / impaired hypertrophy
Tamoxifen-inducible *Acta1*	Adult skeletal muscle	Muscle atrophy (sarcopenia), defective regeneration and accelerated muscle aging
Alb-Afp (Albumin, α-fetoprotein)	Hepatocyte	Reduced body size and chronic liver regeneration
Alb-Afp	Hepatocyte	Impaired hepatic regeneration
Pdx1 (pancreatic / duodenal homeobox-1)	All pancreatic cells	Pancreatitis, loss of exocrine pancreas
Tamoxifen-inducible *Tagln (Sm22α)*	Adult smooth muscle cell	Chronic intestinal pseudo-obstruction and death by 3 weeks after Srf deletion
Camk2a (CamkIIα)	Forebrain neurons	Defective neuronal migration to hippocampus, impaired actin dynamics and axonal guidance
Camk2a or *Syn1 (synapsin-1)*	Forebrain neurons	Attenuated activity-dependent IEG expression and long-term synaptic potentiation
Camk2a	Adult forebrain neurons	Impaired short-term memory and long-term depression
Camk2a	Hippocampal neurons	Defective layering of neurons and dendritic branching
Wnt1	Dorsal root ganglion	Defective extension / branching of axons
Krt5 (keratin-5)	Keratinocytes	Embryonic lethality, skin hemorrhaging / blistering
Krt14 (keratin-14)	Keratinocytes	Thickened epidermis, loss of barrier function and cell-cell contacts due to abnormal cytoskeleton
RU486-inducible *Krt14*	Keratinocytes	Psoriasis-like condition with epidermal hyperproliferation, cytoskeletal and cell-cell contact perturbations
Cd4 (cluster of differentiation-4)	T lymphocytes	Loss in circulating T lymphocytes
Cd19 (cluster of differentiation-19)	B lymphocytes	Decrease in marginal zone B cells, low IgM
Mx1 (Myxovirus resistance 1)	Megakaryocyte	Thrombocytopenia and macrothrombocytopenia
Pf4 (platelet factor 4)	Megakaryocyte	Thrombocytopenia and macrothrombocytopenia ; prolonged bleeding time

Table 3: SRF knock out phenotypes (From (Miano, 2010).

4.5.1. Digestive system

The deletion of *Srf* in hepatocytes causes the death of 35% of postnatal mutant mice males. Moreover, the survived mutant mice looked smaller than normal mice and were characterized by the perpetual liver regeneration showing a constant proliferation and apoptosis of hepatocytes (Sun et al., 2009).

Studies have shown that *Srf* is expressed in the developing and adult pancreas. The deletion of *Srf* leads to pancreatic weaning and pancreatitis in mutant mice at 11 months of age. The exocrine pancreas is destructed and replaced by adipose tissues, while endocrine pancreas structure and function were not affected (Miralles et al., 2006).

Conditional loss of *Srf* in smooth muscle cells leads to chronic pseudo-obstruction of the intestinal tract, represented by chronic intestinal dilation and defective smooth muscle contractility. Moreover, mutant mice develop cachexia and die 2-3 weeks after the loss of Srf (Angstenberger et al., 2007; Mericskay et al., 2007).

4.5.2. Epidermis

The lethality of mouse embryos at E16.5, upon *Srf* deletion in keratinocytes, resulted from the Cre-recombinase expression under the effect of the Krt5 promoter. Mutant embryos showed reduced adhesion and differentiation of keratinocytes and reduced cell-cell and cell-matrix contact within the epidermal layers (Koegel et al., 2009). Moreover, these mutant mice showed inflamed lesions of the epidermis, hyper-proliferation, and abnormal differentiation of the keratinocytes, and disturbed architecture of the cytoskeleton (Koegel et al., 2009).

4.5.3. Hematopoeitic system

At the level of immune cells, *Srf* knock-out leads to maturation defects and an absence of T-cells along with a decreased number of B lymphocytes showing reduced expression of specific surface markers (Fleige et al., 2007).

In addition, the loss of *Srf* in megakaryocytes, cells that produce thrombocytes or blood platelets, leads to an increase in the number of these cells and their accumulation in the bone marrow and spleen. However, mutant mice show a decrease in the number of thrombocytes (macrothrombocytopenia) and an abnormal actin cytoskeleton architecture of both megakaryocytes and thrombocytes, consequently leading to thrombocyte dysfunction with prolonged bleeding time (Halene et al., 2010).

4.5.4. Cardiovascular system

Srf has a vital role in heart formation; its expression is early detected around E7.75 along with the migration of the cardiac progenitor cells to form the cardiac tube. The deletion of *Srf* induces embryonic death at E11.5, having abnormal thin myocardium, dilated heart chambers, and disorganized interventricular septum, after the disruption of the formation of sarcomeres of cardiomyocytes with the development of trabeculations in the ventricles (Miano et al., 2004; Parlakian et al., 2004).

In the adult heart, impaired *Srf* expression causes increased fibrosis and an enlarged heart. Notably, mutant mice die at 11 months due to cardiac arrest mainly due to malorganized sarcomeres which fail to contract (Parlakian et al., 2005).

- **Endothelial cells:** In endothelial cells, studies show that the complexes that build-up the endothelial intercellular junctions are disrupted upon depleted *Srf* expression in endothelial cells (Holtz and Misra, 2008).

4.5.5. Smooth muscle:

Embryonic inactivation of *Srf* in smooth muscle cells provokes a sharp decrease in the number of aortic progenitors at E10.5 (Miano et al., 2004). Moreover, in *in vitro* studies using primary cultures of human cells derived from the coronary artery, the directed inhibition of *Srf* using a siRNA leads to cell cycle arrest at G1, thus stopping the proliferation and causing cell senescence (Werth et al., 2010). In the adulthood stage, decreased arterial contractility and carotid artery stiffness were developed upon the loss of *Srf* in smooth muscle cells (Galmiche et al., 2013).

4.5.6. Skeletal muscles:

Srf deletion in C2C12 myogenic cells revealed that *Srf* is a key regulator of proliferation and differentiation in these cells. Also, the dominant-negative inhibition of Srf to bind the SRE element or the use of specific antibodies against Srf prevents the expression of the myogenic regulatory factor, MyoD (Gauthier-Rouviere et al., 1996).

4.5.7. The nervous system

4.5.7.a. Srf functions in the developing nervous system

Several studies demonstrate that Srf has an important role in different activities during brain development. Srf is evenly expressed in most but not all (e.g., thalamus) brain regions (Herdegen et al., 1997; Knöll et al., 2006; Stringer et al., 2002). This expression starts at the early stages of the embryonic CNS development and the dorsal root ganglia (Wickramasinghe et al., 2008). Notably, abundant expression of SRF is found in neurons, with faint expression in glial cells (Etkin et al., 2006; Herdegen et al., 1997; Ramanan et al., 2005; Stringer et al., 2002; Stritt et al., 2009), thus revealing that SRF controls neuronal functions largely cell-autonomously and not indirectly by glial dependent processes.

4.5.7.a.i. Srf orchestrates neuronal migration and morphological differentiation

Srf actively responds to and, in turn, affects actin microfilament dynamics (Miano et al., 2007; Posern and Treisman, 2006). It controls several neuronal processes requiring motility, including cell migration, neurite outgrowth, and axon guidance. For instance, Srf mutants in the brain show impaired tangential cell migration along the rostral migratory stream, resulting in the ectopic accumulation of progenitor cells in the sub ventricular zone (SVZ) (Alberti et al., 2005). Eventually, disturbed axonal pathfinding of mossy fibers was also found in Srf mutants, resulting in misrouting and aberrant synaptic targeting of axons inside the CA3 pyramidal layer rather than coordinate growth outside in the stratum lucidum (Knöll et al., 2006). Additionally, in Srf mutant hippocampi, genome-wide studies have shown that Srf regulates genes implicated in the development and myelination of oligodendrocytes (Stritt et al., 2009). Surprisingly, the exclusive neuronal deletion of Srf suggested that neuronal Srf affected the development of neighboring glial cells by a paracrine mechanism. This effect has been demonstrated through a transcriptomic-based screen for Srf-dependent paracrine signaling mediators impinging on oligodendrocytes development, where they identified the CTGF (connective tissue growth factor), an Srf target gene outside the brain (Muehlich et al., 2007; Philippar et al., 2004), which contains an IGFBP (insulin growth factor binding protein) domain and showed that CTGF counteracts IGF1-stimulated oligodendrocytes differentiation (Stritt et al., 2009).

4.5.7.b. SRF functions in the adult nervous system

In addition, Srf was also deleted in mature adult brain using CamKIIa-Cre mouse strains (Etkin et al., 2006; Ramanan et al., 2005). Unlike the phenotypic defects obtained in Srf mutants during developmental stages, Srf deletion in the adult brain reveals crucial roles in neuronal-activity-induced gene expression, synaptic plasticity, learning, and memory (Dash et al., 2005; Etkin et al., 2006; Lindecke et al., 2006; Nikitin and Kozyrev, 2007; Ramanan et al., 2005; Tyan et al., 2008). Ginty et al uncovered a strong Srf-dependence of coordinated induction of the IEGs (e.g., *Arc*, *Egr1*, *c-fos*), elicited by the voluntary exploration of a novel environment or forced induction of neuronal activity by electroconvulsive shocks (Ramanan et al., 2005). Moreover, Srf depletion also induces long-term synaptic potentiation (LTP) alteration(Etkin et al., 2006; Ramanan et al., 2005). Besides LTP impairment, Kandel and colleagues reported long-term synaptic depression (LTD) obstruction, preventing the formation of a hippocampus-dependent immediate memory of a novel context, resulting in impaired habituation during exploration of a novel open field environments (Etkin et al., 2006).

Thus SRF-dependent microfilament dynamics is found to be essential for learning and memory-induced transitions converting synaptic efficacy into long-lasting structural rewiring of synaptic connectivity. In this line, the Srf target gene *Arc*, known to be transported to synapses through ribonucleoprotein (RNP), appears to be an important Srf-dependent modulator of synaptic plasticity (Bramham et al., 2008; Messaoudi et al., 2007; Plath et al., 2006; Waltereit et al., 2001). Arc is upregulated by neuronal-activity-stimulated IEG induction. This action is impaired in the absence of Srf (Etkin et al., 2006; Kawashima et al., 2009; Pintchovski et al., 2009; Ramanan et al., 2005).

4.5.7.c. SRF-mediated transcriptional regulation in neurons

To characterize the diverse effects of Srf in neurons, it is apparently important to know under what circumstances SRF-directed transcription is activated. This was identified upon the stimulation eliciting both postsynaptic neuronal activity and SRF-directed transcriptional control. The activation of Srf in neurons is mediated by different growth factors (e.g., NGF, BDNF

activating Trk receptors) in the one hand, and in the other hand through neuronal activity induction, by glutamate or kainate-mediated activation of NMDA receptors or by KCl activation of voltage-sensitive calcium channesl (VSCCs) (Bading et al., 1993; Herdegen et al., 1997; Misra et al., 1994; Xia et al., 1996). The resulting downstream propagation of synaptic activity involves expression by cytosolic Ca2+, a key second messenger activating Srf (Miranti et al., 1995; Misra et al., 1994). Ca2+ activates MAP and Ca2+/calmodulin-dependent (CaM) kinases, resulting either in direct Srf activation or indirect, co-factor mediated Srf stimulation; the TCF or MRTF cofactors of Srf. In addition to Ca2+ regulated signal transduction, Srf can be directly targeted by other kinases such as MSK (Zhang et al., 2008), MAPK-activated protein kinase 2 (MK2) (Heidenreich et al., 1999; T. Thomas et al., 2008) and SGK (Tyan et al., 2008) **(Figure 40).** Besides, G-protein-coupled-receptors (GPCRs), such as Ga12/13 and Ga0/i), which transmit different sensory information to the brain, can target SRF through Rho-GTPases and or MAPK activation (Fromm et al., 1997; Posern and Treisman, 2006; Suzuki et al., 2003). Also, SRF is a downstream target of PI3 kinase-mediated neuronal survival signaling (Chang, 2004). So, better investigation of SRF co-factors would be interesting inorder to understand the different mechanisms and their associated intracellular signaling pathways in response to distinct neuronal stimulation of their target genes.

A crosstalk between SRF and CREB: Overlapping, distinct and concerted functions

As previously mentioned, SRF is a vital element during neuronal development and also display critical functions in the adult brain, including regulation of neuronal-activity-induced gene expression implicated in synaptic plasticity and learning and memory processes. Besides, CREB is also an important transcription factor regulating synaptic plasticity genes, including IEGs (Barco et al., 2003; CARLEZONJR et al., 2005; Lonze and Ginty, 2002). Notably, CREB and SRF cooperate to regulate these genes.

SRF and CREB are mutually implicated in many shared neuronal functions, including cell migration, neurite outgrowth, axonal pathfinding, and neuronal-activity-based gene transcription. They are targeted by neurotrophin signaling and efficiently activated by

postsynaptic Ca2+ signaling (Bonni et al., 1995; Chang, 2004; Finkbeiner et al., 1997; Kalita et al., 2006; Wickramasinghe et al., 2008).

Recent data show that different signaling pathways regulate SRF- and CREB-dependent genes. For instance, the regulation of actin microfilament dynamics is firmly linked to SRF. It has not been reported for CREB or any other neuronal transcription factor. However, CREB is strongly triggered by cAMP/PKA signaling, which, in turn, doesn't appear to directly activate SRF. Moreover, studies done on Creb family mouse mutants revealed massive neuronal degeneration and thus showed that these members are essential regulators to neuron survival, unlike Srf, which didn't regulate neuron proliferation and apoptosis (Lonze and Ginty, 2002; Mantamadiotis et al., 2002; Ramanan et al., 2005; Rudolph et al., 1998).

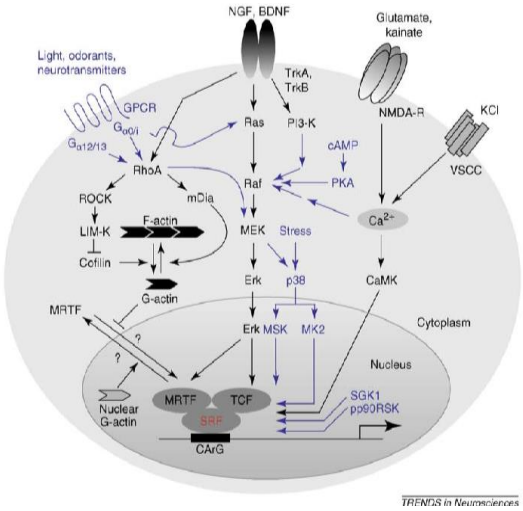

Figure 40: SRF-mediated transcriptional regulation in neurons.
SRF is activated in neurons by growth factors (e.g. NGF, BDNF activating Trk receptors) and neuronal activity via, for example, glutamate and KCl. Downstream signal propagation primarily involves MAPKs, CaM kinases and Rho/actin signaling cascades. These cascades result in direct SRF activation and/or activation of the SRF cofactors MRTF or TCF. Shuttling of MRTFs between the cytoplasm and nucleus as demonstrated for fibroblasts remains to be further analyzed for neurons (indicated by question marks). The major signaling cascades activating SRF, namely signalling by Rho/actin, MAPK and Ca2+, are shown in black. Signaling steps indicated in blue are not demonstrated unambiguously to target SRF in neurons. For references and abbreviations see text. (Knöll and Nordheim, 2009).

Having described both shared and distinct functions of SRF and CREB, it is important to point out that many genes, for example IEGs contain both SRE and CRE control sequence in their promoters, This suggests synergistic functioning of the two factors (Kawashima et al., 2009); Robertson et al. 1995). Indeed, the interdependence of the SRF and CREB binding sites in the c-

fos promoter briefly demonstrated by the first in vivo analysis of the SRF-SRF module in the brain (Curran and Morgan, 1995).

Thus, SRF and CREB can exert an astonishing degree of functional versatility, thereby controlling a wealth of different brain functions. Their common functional characteristics (i.e. responsiveness to Ca2+ signaling), reveal that they act in a complementary manner when eliciting other nervous system activities, for example responses involving actin or cAMP signaling. Nevertheless, the interdependent activity on some target gene promoters show concerted effects of SRF and CREB in enabling some brain functions (e.g. selected IEG responses, synaptic signaling and learning).

4.5.7.d. SRF as a potential pharmacological target in neuropathology

The pivotal role of SRF in the brain provides wide drug targets for the therapeutic modulation in neurological disorders, mainly through targeting SRF, its cofactors, or components of upstream signaling cascades. For instance, in kainate-induced seizures, increased SRF expression and phosphorylation, likely through MK2, might be targeted (Heidenreich et al., 1999; Herdegen et al., 1997; T. Thomas et al., 2008). Targeting SRF activity through enhancing its DNA binding was reported in status epilepticus (Morris et al., 1999). To stimulate the re-growth of lesioned axons, like spinal cord injury, an approach boosting the cytoskeletal dynamics was also reported by modulating SRF activity and stimulating the neurite outgrowth (Knöll et al., 2006; Wickramasinghe et al., 2008).

On the other hand, besides these positive effects of SRF in injured brains, enhancing SRF activity might also aggravate diseases. For example, in Alzheimer's disease, SRF-induced activity provokes the accumulation of the Aß in vessels, thus accelerating the progression of cerebral amyloid angiopathy (Carmeliet, 2005; Medjkane et al., 2009). MRTFs and SRF accelerate experimental tumor metastasis, which is considered a potential finding for glioma etiology (Medjkane et al., 2009).

Collectively, modulation of SRF activity in brain diseases might be a double-edged sword, potentially resulting in either beneficial or detrimental effects.

4.5.7.e. SRF and HD transcription downregulation

Interestingly, it was found that transcription of the serum response factor (SRF) is decreased in HD patients' striatum and HD mice models (Mayada Achour et al., 2015; Hodges et al., 2006; Langfelder et al., 2016b). More specifically, analysis of transcriptomic data generated in HD KI mice expressing mutant Htt with various polyQ length showed that SRF down-regulation appears progressively and selectively in the striatum, and in a Q-length dependent manner (Langfelder et al., 2016b). Thus, down-regulation of SRF in HD mice correlates with pathogenesis. Moreover, genomic enhancers leading to down-regulated eRNAs in the striatum of R6/1 mice were enriched in SRF binding sites (Le Gras et al., 2017), suggesting that SRF decrease might contribute to altered eRNA regulation in HD striatum **(Figure 41).**

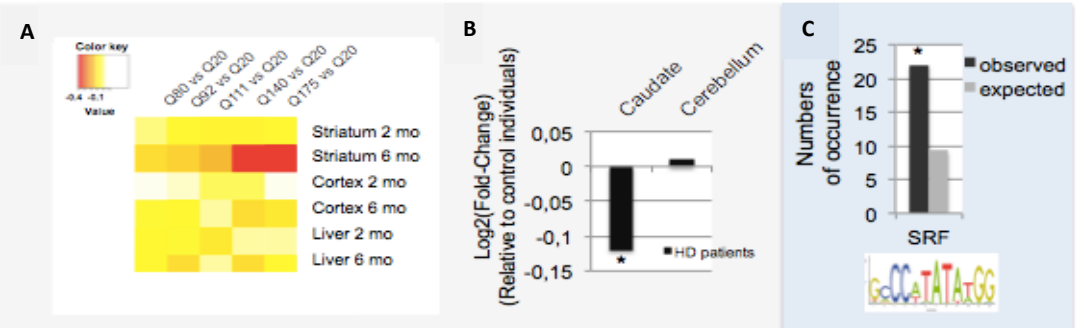

Figure 41: Impaired SRF regulation in HD.
Srf is decreased in **(A)** the striatum of HD knockin (KI) mice, in age and Q-length-dependent manner (RNAseq, Langfelder et al. 2016). KI mice expressing mutant Htt with pathogenic polyQ length (80, 92, 111, 140 and 175Q) were analyzed and compared to control mice (Htt with 20Q). The heat map represents Log2 of fold change between Srf levels in pathogenic and Q20 mice. **(B)** Srf is decreased in HD patients' striatum (Microarrays, Hodges et al. 2006). **(C)** SRF binding sites are enriched at down-regulated RNAs in R6/1 vs WT striatum (Le Gras et al., 2017).

Together, genetic studies showed that SRF has emerged as a prototypical transcriptional regulator with versatile functions in the brain. It is linked to actin dynamics, thereby; it influences morphological neuron differentiation and key processes of neuronal circuit assembly, such as cell migration, axonal outgrowth, guidance and synapse function. Moreover, it was shown that SRF is an essential transcription factor to neuronal plasticity processes required for learning and memory (Etkin et al., 2006; Ramanan et al., 2005), Thus, it would be interesting to better characterize SRF regulatory pathway, understand its molecular and functional role, and investigate the underlying mechanisms of the epigenetic/transcriptional alterations in HD, so that it might be considered as a potential therapeutic target in the pathogenesis.

…… Objectives of the Thesis ……

Objectives of the thesis

The characterized triad of motor, cognitive and psychiatric symptoms in HD is accompanied by transcriptional and epigenetic deregulations which particularly affect the striatum. But, the role of these molecular alterations in the establishment of behavioral deficits, including cognitive alterations, is not well characterized. Defined transcriptional deregulations occur in the striatum of HD, notably a down-regulation of genes regulating neuronal identity and activity, which likely play a role in learning and memory processes. More specifically, down-regulation of Srf mRNA in HD knockin mice correlates with HD pathogenesis (Langfelder et al., 2016b).

SRF is a key regulator of neuro-adaptive processes, including learning and memory, through the regulation of defined gene expression program (Dash et al., 2005; Etkin et al., 2006; Lindecke et al., 2006; Nikitin and Kozyrev, 2007; Ramanan et al., 2005; Tyan et al., 2008). SRF gene targets include neuronal activity-regulated genes (immediate early genes (IEGs) such as *Egr1)* (Ramanan et al., 2005) and genes implicated in actin cytoskeleton such as *Actb*, which are also down-regulated in the striatum of HD knockin mice. Thus, we hypothesized that altered SRF regulation in HD striatum might contribute to striatal dysfunction and behavioral deficits in HD through impaired regulation of SRF-dependent gene program.

The objective of my thesis was to characterize the regulation of SRF in the context of HD and to assess its role in the pathogenesis, particularly in the appearance of behavioral symptoms. To this end, I used HD transgenic R6/1 mouse model which overexpress exon 1 of HTT with 130 CAG repeats. This reference model summarizes the major characteristics of the disease including transcriptional deregulation, aggregation of mutant HTT, striatal atrophy, behavioral symptoms typical of HD and premature death (M. Achour et al., 2015; Desplats et al., 2006; Hodges et al., 2006; Kuhn et al., 2007; Langfelder et al., 2016b; Lee et al., 2020; Luthi-Carter, 2002b; Luthi-Carter et al., 2000; Mangiarini et al., 1996; Martí et al., 2010; Runne et al., 2008; Seredenina and Luthi-Carter, 2012). Srf mRNA and proteins are also early decreased in the striatum of R6/1 mice, and we show correlation with behavioral deficits, including deficit in striatum-dependent memory (procedural memory). Major targets of SRF including *Egr1* and *Actb* are also reduced in

the striatum of HD mice. Then, to modulate SRF expression in HD R6/1 mice, we used viral-mediated gene transfer approach (AAV construct expressing SRF) and stereotaxic injection in the striatum. In a first attempt, we overexpressed full length murine SRF in the striatum of R6/1 mice, which surprisingly worsened motor phenotype of the mice. Second, we overexpressed chimeric construct consisting in SRF DNA binding domain fused to VP16 transactivation domain. Behavioral, histological and molecular (including transcriptomic) analyses helped define the role of SRF in HD pathogenesis.

…….. Materials and Methods ……

Materials and Methods

1. Animals

During my study, R6/1 transgenic mice and their age-matched wild type littermates were used in the experiments. They were from the crossbreeding of female C57/BL6 mice (Charles River) and male R6/1 (C57/BL6 background) (Mangiarini et al., 1996) originally from Jackson Laboratory and maintained in our lab. All animals were genotyped by PCR with DNA extracted from ear specimens. The PCR product size of the expansion of CAG of the R6 / 1 mice was of the order of 150 CAG by the amplification of exon 1 of the mutated HTT with specific primers (Meaning: ATGAAGGCCTTCGAGTCCCTCAAGTCCTTC; Anti-sense: GGCGGCTGAGGAAGCTGAGGA), then the PCR products were deposited on a 1.5% agarose gel and separated by electrophoresis.

The animals were housed in collective cages (up to 5 mice per cage). During surgery and behavioral experiments, the animals were isolated in individual cages. The animals were housed with water and ad libitum food in an animal facility with alternating light 12h/12h, constant temperature conditions (21°C), humidity (55%) and sound environment (radio in the daytime phase). The animal house was continuously monitored. The experimental procedures were carried out in accordance with the European directives concerning animal testing (European Directive 2010/60 / EU French law of rural code R 214-87 131) and with the approval of the Regional Experimental Ethics Committee Animal of the University of Strasbourg (CREMEAS) and the French Ministry of Research (Authorization numbers: APAFIS # 11532-2017092618102093v7).

2. Stereotaxic surgeries and AAV- injections

2.1. Recombinant AAV production and purification

In collaboration with Dr. Emmanuel Brouillet, CEA-MiRCEN-Paris, the plasmid containing the recombinant mouse full length Srf sequence is designed for experiment one and another plasmid

contained the DNA binding domain of Srf and the transactivation domain of the Herpes simplex *virus* protein vp16 for experiment 2. The plasmids were synthesized by Gateway technological (Invitrogen, Life Technologies). Plasmids with DNA sequence encoding green fluorescent protein (GFP) and the Herpes simplex *virus* protein vp16 were designed as a control vectors in experiments 1 and 2 respectively. The promoter and the transgene flanked by attB sequences were produced by PCR. After sequencing, the cassette was transferred into a pDEST vector containing ITR sequences (Inverted Terminal Repeat) and an ampicillin resistance gene by type LR recombination. The plasmid pAAV obtained was transformed, and then the colonies were selected on LB-agar-ampicillin (Invitrogen) type Petri dishes. After amplification on an LB medium containing ampicillin, the plasmid was purified and sequenced. The final pAAV is amplified in LB medium containing ampicillin and purified (Nucleobond Xtra EF Maxiprep kit, # 740424, Macherey-Nagel, Germany) for the production of AAV.

2.2. AAV production

For adeno-associated virus (AAV) production, designed sequences inserted into a single-stranded, rAAV2-based shuttle vector under the control of the mouse PGK promoter, by LR recombination, with Gateway_ technology (Invitrogen, Life Technologies). Constructs were packaged into several AAV serotypes in experiment 1, and in AAVrh10 in experiment 2. AAVrh10 was selected, capsids by the MIRCen viral production platform, as previously described (Berger et al., 2015). Viral particles were produced by the transient co-transfection of HEK-293 cells with an adenovirus helper plasmid (pXX6-80), an AAV packaging plasmid carrying the rep2 and cap10 genes, and the AAV2 transfer vector containing the expression cassettes described above. Virions were purified 72h after transfection and concentrated from the cell lysate and supernatant by ultracentrifugation on an iodixaniol density gradient, followed by dialysis against PBSMK [0.5mM MgCl2 and 1.25mM KCl in phosphate-buffered saline (PBS)]. The concentration of the vector stocks was estimated by quantitative PCR as described by (Aurnhammer et al., 2012) and expressed as the number of viral genomes per ml of concentrated stocks (vg/ml).

2.3. Injection of AAV in the striatum of WT and R6/1 mice

2.3.1. Principle of stereotaxic surgery

Stereotaxic surgery is a neurosurgery technique that allows reproducible targeting of a specific brain region in order to perform various intracerebral procedures (injection, sampling, implantation of a cannula or electrode, etc.). For this, there are stereotaxic atlases which reference the coordinates of different brain structures in 3 axes: anteroposterior (AP), mediolateral (ML) and dorsoventral (DV). First, although we tried several injection coordinates making it possible to target the striatum but it was not difficult as if it's a big structure. Thanks to the stereotaxic atlas "The Mouse Brain" by Franklin and Paxinos (2001).

The coordinates used were taken from the surface of the skull, and from the bregma which is the intersection between the sagittal and frontal sutures. Another landmark is the intersection between the sagittal and lambdoid sutures, the lambda **(Figure 42)**.

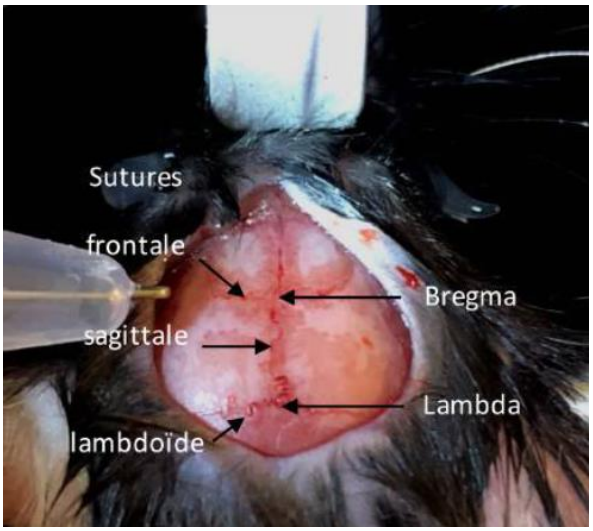

Figure 42: Cranial sutures, bregma and lambda.
The intersection between the frontal and sagittal sutures forms the bregma, and the intersection between the sagittal and lambdoid sutures forms the lambda.

2.3.2. Device

The stereotaxic frame is U-shaped with two ear bars to immobilize the mouse head laterally, and an incisor bar for fixing the muzzle **(Figure 43A**). The bregma and the lambda are located on the same horizontal plane. Once all of these bars are adjusted and the screws tightened, the mouse head cannot move. The frame includes three micromanipulators placed in three orthogonal axes (AP, ML, DV), each equipped with a Vernier allowing precise measurements of the distance of movement of the descender along each axis **(Figure 43 B)**. A syringe adapter is attached to the descender which is moved into three-dimensional space using three micrometer screws. The injection of the AAV vectors is performed using an automated pump system with a 10µl Hamilton® Neuros ™ syringe (7002, P / N 65459-01, Hamilton®) attached to the descender using a 34G 60mm cannulas (phymep, SST34G60/10).

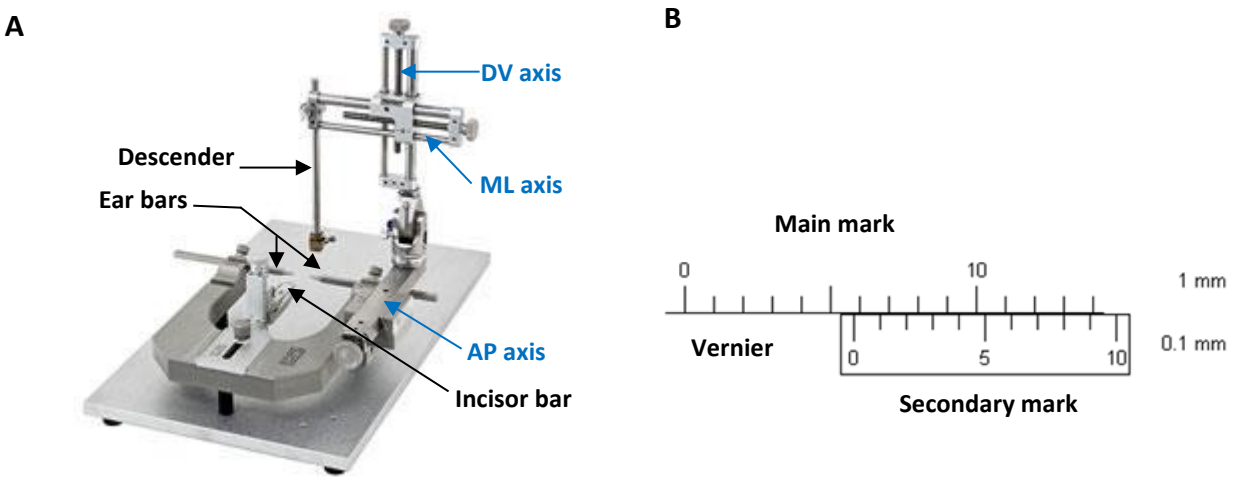

Figure 43: The stereotaxic device.
(A) Photograph of a stereotaxic device. The axes of the three micromanipulators are indicated in blue. **(B)** Operation of the Vernier. We read 5.8 mm (with an accuracy of 0.1mm).

2.3.3. Protocol of stereotaxic injections

The mice were anesthetized by inhalation of isoflurane (4%) in an induction box for 6 mins until the respiration rate stabilizes. The mouse is then placed quickly on the incisor bar around which the anesthesia mask is located within the frame so that the head is completely immobilized. During surgery, isoflurane was reduced between 1% and 1.5%. The body temperature of the animals is controlled using a heating blanket connected to a rectal thermal probe (ATC2000, WPI),

placed under the mouse. The eyes were protected by ophthalmic gel (VITAMIN A DULCIS, Allergan), preventing the drying of the cornea.

Before incision, the animal was injected by Metacam® an anti-inflammatory substance (0.002µl/g, Boehringer Ingelheim) made subcutaneously at the level of the neck of the mouse. The skin of the skull was cleaned and disinfected with 70% ethanol before being incised longitudinally. A second subcutaneous injection, at the level of the skull, with lidocaine (Xylovet®, Ceva Santé Animale) where the field is then immediately flooded favoring a local anesthesia through skin spreading to reveal the skull. The bregma and lambda should be seen upon inscision. Sometimes, to keep the operating field free, retractors are placed on both sides of incised skin. Clean the exposed surface of the skull and use little volume of oxygenated water to visualize the sutures **(Figure 44)**. It is then necessary to measure the DV coordinates of the bregma and the lambda by placing the needle on the skull in order to check if the head of the mouse is in "flat skull" position (with a tolerance of 0.1mm difference). If this is not the case, we loosen the screw which tightens the muzzle on the incisor bar in order to adjust the height of the latter until being in "flat skull". We can then take all the coordinates of the bregma in order to calculate the coordinates of the injection sites. Using a pencil, mark the sites on the skull and puncture it with a dental drill so that the needle can be lowered into the brain parenchyma to the calculated DV coordinates.

Figure 44: Injection into the striatum of a mouse.

The AAV vectors were diluted in a pluronic/PBS solution to obtain a final concentration of **10^{10} vg**. µL-1. A volume of 1.5 µL of AAV suspension was injected in each site in the striatum using a 34 Gauges syringe connected to a 10 µL Hamilton syringe by a catheter polyethylene. Two

injection sites, bilaterally simultaneous, were performed to promote a greater volume of expression in the striatum. The injection speed was set at 0.15 µL.min-1. After injection, the cannulas are left in place for 5 min before removing them. The skull is cleaned, the skin was sutured then the animals were placed in clean individual cages under a heat lamp during their waking phase, and then brought back to their animal house where their general condition is monitored daily during the post-operative period.

The experiments only started 4 weeks after the surgeries to allow the animals to recover and the virus to express the gene.

2.3.4. Stereotaxic coordinates of the striatum

The coordinates of the injection sites were selected using the stereotaxic atlas "The Mouse Brain" by Franklin and Paxinos (2001). Table 7 shows the coordinates used in the stereotaxic injections, relative to the bregma, with a 0.15µl/min speed of injection.

	Site 1	Site 2
AP	+1	-0.2
ML	+2.1	-2.1
DV	-3.2	-3.1

Table 4: Stereotaxic coordinates of striatal injections

2.4. Experimental groups

AAV-Srf-GFP	(April 2019)
8 WT-GFP	3♀ and 5♂
8 R6-GFP	3♀ and 5♂
8 R6-SRF	3♀ and 5♂

AAV-Srf-GFP	(October 2019)
10 WT-SRF	5♀ and 5♂
5 WT-GFP	2♀ and 3♂
4 WT-HC	2♀ and 2♂

AAV-Srf-vp16	(April 2020)
9 WT-vp16	4♀ and 5♂
10 WT-Srfvp16	4♀ and 5♂
9 R6/1-vp16	5♀ and 4♂
8 R6/1-Srfvp16	5♀ and 4♂

Table 5: Experimental groups

3. Evaluation of the spontaneous activity of the mice

3.1. Actography

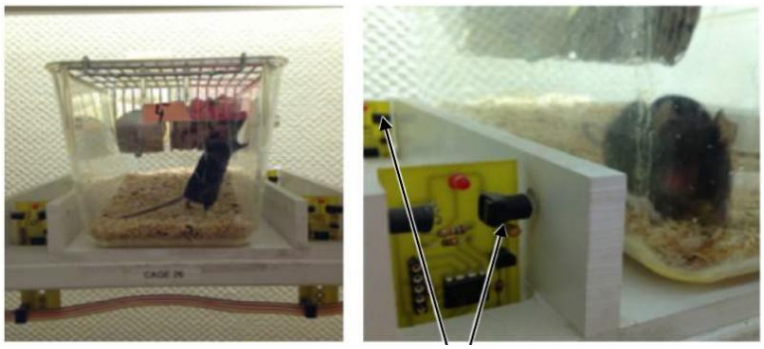

Figure 45: Device of the actography.
Photographs showing the placement of the cage in the actometer rack and the photocells which allow the infrared beams to be detected (Thesis of Estelle SCHUELLER).

The circadian rhythm, the nycthemeral rhythm, which is known by the 24h biological cycle defined by the alternation of a day and a night, is determined by the artificial lights in the animal facility. Mouse spontaneous activity, showing their motor function and/or motivation and the apathy of the mice has been recorded for two nights and two days. A habituation phase of 3 hours preceded the first night. Cages (29.5 x 11.5 x 13 cm) with a clean litter bottom and a handle of their litter of each mouse are placed on a rack provided with photoelectric cells which emit infrared beams at each of their ends **(Figure 45)**. This device is connected to a computer where software accounts for beam crossings by the mice. The successive crossing of the two beams accounts for a horizontal displacement and reflects the locomotor activity of the mice. This spontaneous locomotor activity is recorded at an acquisition frequency of 10 minutes during a habituation period of 3 hours, then during 66 hours. The locomotor activity of the mice during the first night is generally higher than the following two nights. It is therefore possible to exclude this night from the analysis so that the results better reflect the usual locomotor activity of mice.

3.2. Open field test

The Open Field is a widely used test to measure behaviors in animal models like general locomotor ability and anxiety-related emotional behavior. The field maze consists of a wall enclosed area that is of sufficient height to prevent the animal from escaping**.** The mice were

freely put to explore an open field arena for 10 min. The testing apparatus was a classic open field (i.e. a square arena, 50 × 50 cm, with walls 40 cm high), surmounted by a video camera connecting to a computer. Each mouse was placed individually at the arena and the performance was monitored and the time spent in the center and peripheral area and the distance traveled in the arena were automatically recorded by a video tracking system in addition to many other parameters including the number of rears and the number of grooms. (ANY-Maze version 4.5 software, Stoelting Co.) (Chen et al., 2013).

4. Anxiety assessment:

4.1. Light dark test

We assessed the anxiety of mice using the light-dark transition test (Hickey et al., 2008; Pla et al., 2014). The device has 2 boxes separated by a small passage between them, one being completely opaque and dark and another being transparent and enlightened by a lamp (1000 lux) **(Figure 46)**. This test is based on the natural aversion of mice for very bright areas, opposing their spontaneous exploratory behavior in a new environment. So, a mouse with a normal anxiety level visits the illuminated compartment of the box without staying there very long, while an anxious mouse will visit it much less. The protocol we used is to place the mice in the middle of the dark area and measure their activity for 5 minutes. The latency before their first entrance to the illuminated area, as well as the number of visits and the total time spent in the illuminated box are raised.

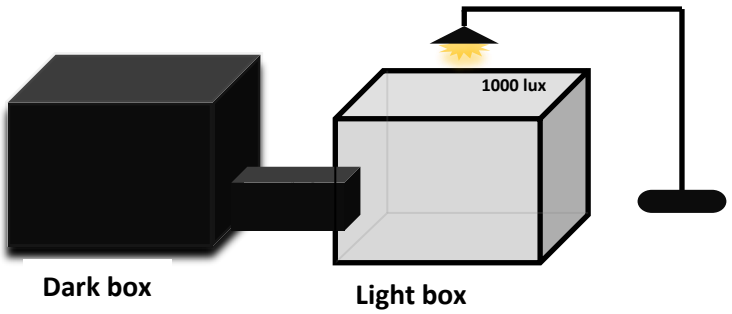

Figure 46: Evaluation of the anxiety of mice with the light/dark transition test.
The box used for this anxiety test has a dark compartment and an aversive compartment lit by a lamp (1000 lux). The mouse is placed in the dark compartment and is free to explore the two compartments for 5 minutes.

5. Evaluation of motor performance

5.1. Mice handling

Animal handling prior to behavioral experimentation is a crucial consideration for all experimental procedures in order to minimize the stress associated with mice handling during behavioral tests. This was done for all the tests except for those assessing anxiety (Light-dark test) and the spontaneous locomotor activity in a home cage. Then mice isolation could be done only after the assessment of their basal anxiety level. The mouse was handled for 1-2 minute(s) per day before 3 days of the start of the behavioral tests.

The mouse is simply held by the base of the tail and placed on the arm, then let it move on until it calms down.

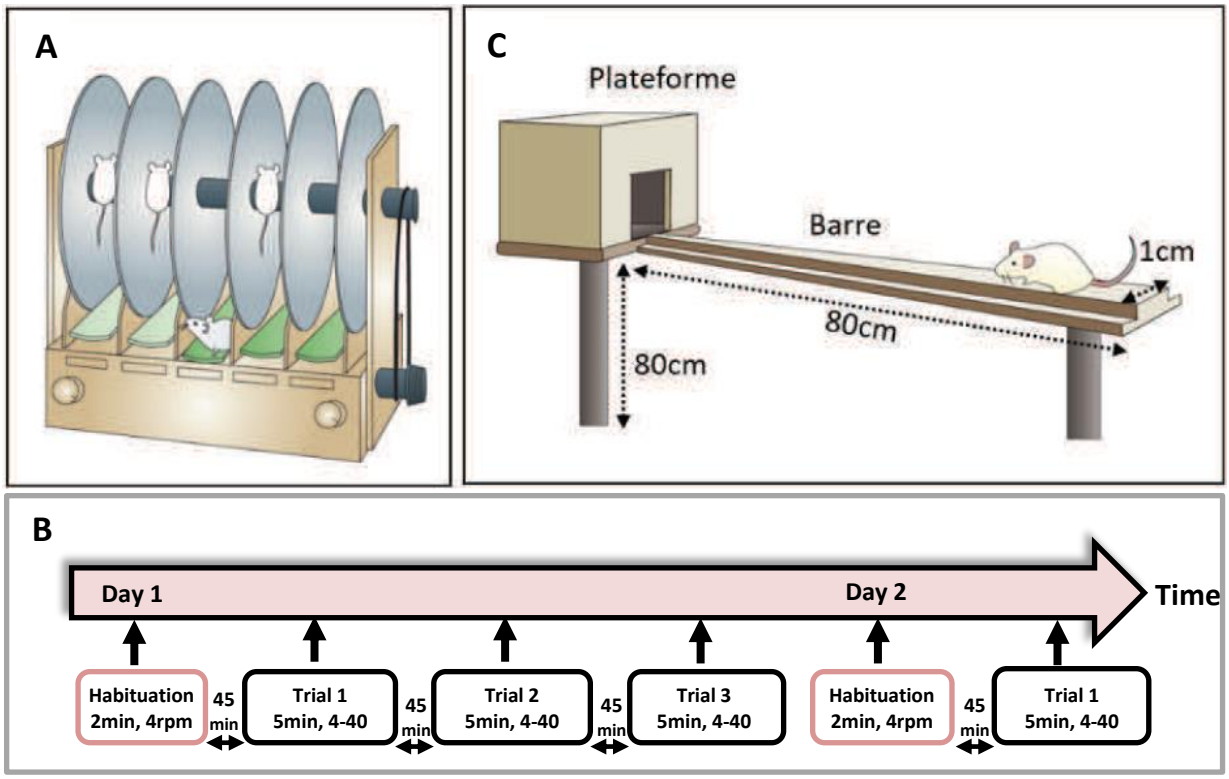

Figure 47: Behavioral tests assessing the motor performance of WT and R6 / 1 mice.
(A) Scheme representing the rotarod (Brooks and Dunnett, 2009). **(B)** The rotarod protocol includes a 2 min habituation during which the cylinder rotates at a speed of 4 rotations per minute (rpm), then 3 tests are carried out with a gradual acceleration of the rotation of 4 to 40rpm over 5 min. The habituation and each test are separated by a delay of 45min. This protocol is repeated over 3 days. **(C)** Diagram representing the crossing of the bar test (Brooks and Dunnett, 2009a).

5.2. Rotarod

For the assessment of the motor coordination and learning skills, we performed the accelerating rotarod test (Brooks and Dunnett, 2009b). The protocol was performed as previously described (Galvan et al., 2018), using a rotating motorized rod of 30mm of diameter which gradually increased the speed of rotation from 4 to 40 rpm along 5 min (Ugo Basile, model 47650).

The test was performed during 3 consecutive days, with 4 trials per day, considering the first trial of the day as habituation. The habituation consists in making the mouse walk on the rotating cylinder with a speed of 4 rotations per minute (rpm) during 2 minutes. The acquisition phase consists of three tests with a maximum duration of 5 minutes, by which the mouse must move on the cylinder whose rotation accelerates gradually from 4 rpm to 40 rpm **(Figure 47A).** The habituation and each test are spaced 45 min apart **(Figure 47B).** The latency to fall was recorded

when the animal was unable to keep up with the increasing speed and fell. The final performance was calculated as the average of the time latency of every day, during the 3 days of the test.

5.3. Bar test

The bar crossing test is used to assess the motor coordination and balance of mice (Brooks and Dunnett, 2009b). The device consists of a wooden board (80x10x1cm) divided into 8 segments of 10 cm, held 80 cm from the ground by a tripod **(Figure 47C**). At its end, there is a rectangular platform (17 x 13.5 cm) which provides access to the mouse's cage. During a training phase, the mice are trained to walk on the bar to reach the platform and join their cage. For this, the mice are placed 10 cm away from the platform where the access to the remaining 70 cm of the bar is blocked. The habituation is stopped only when the mice spontaneously rejoin their breeding cage. The test phase is then made up of 4 discrete tests, with a maximum duration of 1 min. We clean the bar with 35% alcohol and then with water between each mouse. The time required to cross the first 10 cm, as well as the time necessary to cross the remaining 70 cm are raised and respectively reflect the level anxiety and motor coordination of mice.

5.4. Evaluation of mice motivation

5.4.1. Nesting test

Mice are one of the most common models used in behavioral neuroscience research. Nest building is spontaneous and considered as an everyday behavior in laboratory mice where it could regulate their body temperature and decreases the stress level from people. Nesting test is considered as an important test to evaluate the motivation in mice. Where the apathic phenotype should be taken into consideration in HD mice, since this could alter this function.

This test is carried out in rectangular cages (32 x 16 x 14 cm) by which 6 rectangular papers cuts from a cotton sheet are placed on the different edges of the cage, the same material that the mice usually use to build their nest in the laboratory.

Each mouse is placed in a cage with a handle of its litter box and the 6 papers are arranged as illustrated in **(Figure 48A)**. This test is carried out in the mouse animal house. At different times (3h, 5h and 24h), three scores are assigned to each mouse; protocol adapted from (Gaskill et al., 2013) :

1. The score of quality, it can range from 0 to 5 reflecting the number of "empty" areas, where there are no more papers; in this case the score is equal to 4 because 4 zones are empty **(Figure 48B).**
2. The score of motivation, it can range from 0 to 6 reflecting the number of folded and non floded papers after each checkpoint of the test, this could reveal the motivation behavior of the mice while building their nests.
3. The score of complexity adapted from the protocol of Gaskill et al., 2013. This score can take values ranging from 0 to 2 reflecting the quality of the nest (dome form + walls) **(Figure 48C)**
    - 0: the papers are dispersed in the cage (not grouped in one corner)
    - 1: the papers were moved to one corner but they are still folded (the nest have no form: flat).
    - 1.5: the nest is slightly dug, the walls are not very high
    - 2: the nest is closed or almost closed, the walls hide

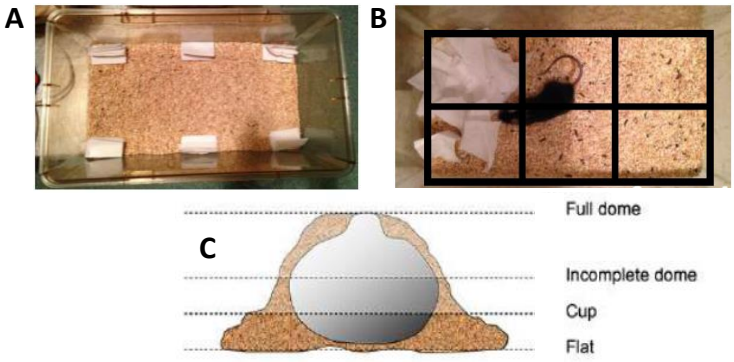

Figure 48: Assignment of nesting scores.
(A) Arrangement of paper rectangles at the start of the test. **(B)** In this photograph, the "zone" score is equal to 4 because 4 zones are empty. **(C)** Diagram representing the quality of the nest, in reality the score is not assigned from the photo because it is difficult to estimate the height of the walls in this way. (Gaskill et al., 2013).

6. Evaluation of cognitive performance: Memory process

6.1. Double-H (DH) water maze

Cognitive performance, a striatum dependent function, of mice was assessed using the double-H maze. This test was initially developed for rats in the laboratory (Cassel et al., 2012; Pol-Bodetto et al., 2011) and then it was adapted to mice. The device consists of 3 parallel arms in plexiglass (55x10x25cm) perpendicular to a central path (100x10x25cm). By convention, the ends of the central arm are designated like the North arm (N) and the South arm (S). The ends of the other two arms are called North West (NW), North East (NE), South West (SW) and South East (SE) (Figure 49A). The double-H is positioned in the Morris pool device, in a room with visual clues. The arms of the double-H are filled with fresh water (21°C), for water coloration 70g of Meudon white is used **(Figure 49 B and C)**.

Figure 49: The double-H maze.
(A) Diagram of the dimensions of the device, consisting of 6 arms (NW, N, NE, SW, S, SE) connected by a central aisle. **(B)** The arms are filled with fresh water, turns cloudy with white Meudon. **(C)** The device is positioned in the basin of the Morris swimming pool in a room containing visual clues (geometric shapes on the wall, water heater).

6.2. Evaluation of procedural memory of mice

The DH maze test consists of a navigation task oriented towards a goal, involving the striatum-dependent procedural memory and the hippocampal-dependent spatial memory. Indeed, during the navigation task, the animals must learn to find a platform immersed in cloudy water, positioned in the NE arm of the device. The platform allows animals to exit the device and escape the aversive situation represented by the aquatic environment.

To find the platform, the mice can follow two navigation strategies: a procedural (egocentric) strategy which consists in learning the sequence of movement allowing reaching the platform or a spatial strategy (allocentric) based on the use of visual cues from the room. During the task, the

starting point of the mice and the position of the platform are constant in order to favor procedural learning. A recall test is then performed to assess the strategy used by the mouse. For this, the start point is shifted into the neighboring arm and the platform is removed.

The protocol was performed as previously described (Cassel et al., 2012; Pol-Bodetto et al., 2011). It includes a habituation phase, an acquisition phase and a recall phase. The Habituation allows mice to learn about the existence of the submerged platform, allowing them to exit the device.

For this, the NW-SW arm is isolated by a removable plexiglass door that closes the access to the rest of the maze **(Figure 50A).** At this phase the water is still clear, the platform is visible, positioned at the end of the NW arm and the mice are released at the end of the SW arm. Four discrete tests with a maximum duration of 1 minute are realized. When the mice reach the platform, a delay of 10 seconds is respected before removing them from the device and replacing them in their home cage under a heat lamp.

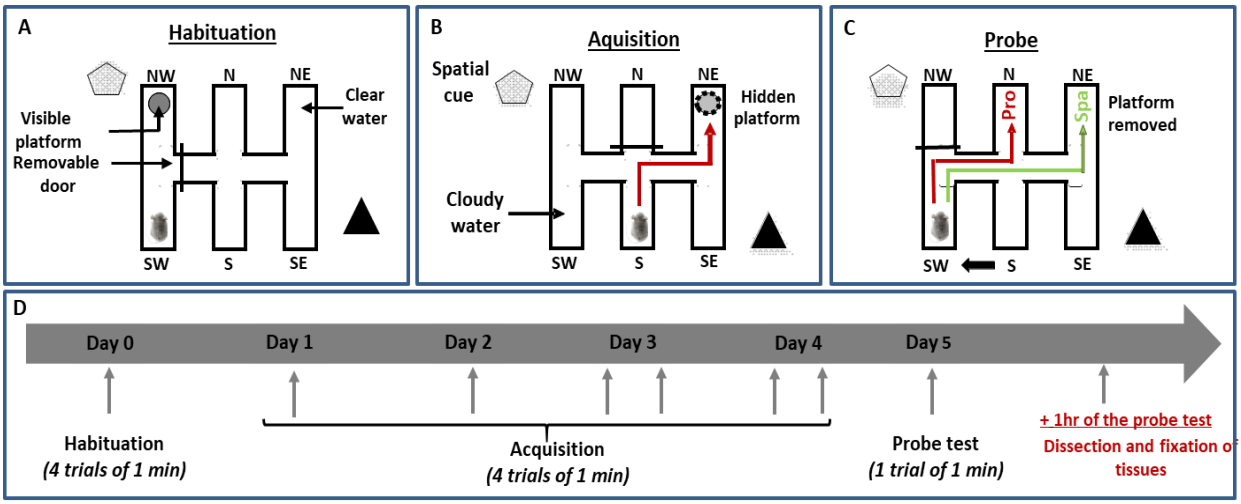

Figure 50: Protocol for evaluating the procedural memory of mice in the double-H maze.
(A) During habituation, the mice must swim in an arm isolated from the device to reach a visible platform. **(B)** During the acquisition phase, the mice are trained to learn a sequence of movements (turn right then left) to reach the submerged platform, hidden in the NE arm, starting from the S arm. **(C)** The mouse learning strategy, procedural vs spatial, is evaluated during the recall test during which the platform is withdrawn and the licking point translated into the SW arm. The mice which mobilize a procedural strategy join the N arm or "procedural" arm (Pro), those which use a spatial strategy reach the S arm or "spatial" arm (Spa). **(D)** The protocol lasts 6 days, with a 4-day acquisition phase comprising 6 training sessions. The following day the recall test is carried out and the mice are put to death 1 hour after the end of it (Lotz et al. in preparation).

During the acquisition phase, the color of water is milky-like (mixed with 70g of Meudon) and the platform is immersed in the target arm (North east arm). The mice are released in the S arm and must learn the sequence of movements (turn right then left) to reach the platform. The

removable plexiglass door closes the N arm **(Figure 50B)**. Six acquisition sessions were carried out over 4 days, where one acquisition per day for the first two days and two acquisitions per day for the last two days **(Figure 50D)**. Each acquisition includes 4 discrete tests, of a duration maximum of 1 minute. When a mouse does not reach the platform before the end of the test, it was guided by the experimenter. As during the habituation, a delay of 10 seconds is respected when the mice reach the platform before removing them from the device and replace them in their home cage under a heat lamp.

After 24 hours of the last day of learning, the recall test is carried out and consists of only 1-minute trial, during which the platform is removed and the mice are released in the SW arm. The NW arm is closed by the plexiglass door to reproduce the conditions of the acquisition phase. Mice using a procedural strategy to find the platform turn right then left and reach the N arm first, also called "Procedural" arm. Mice using a spatial strategy directly join the NE arm, called the “spatial” arm, in which the platform was located during learning phase **(Figure 50C)**.

Thanks to the supplied camera system and to the ANY-maze motion detection software to record mice movement during each trial. Through acquisition, the performance of the animals was assessed by analyzing the distance traveled and the latency to reach the platform. We also calculated the percentage of correct responses by the mice during each trial: a score of 1 was assigned to mice going directly to the platform and a score of 0 for mice committing one or more errors.

During the recall test, the first and second arms visited by the mice are recorded, as well as the latency to reach the target arms (NE and N) and the time spent there. The time spent in each arm is then compared to the “chance” time (8.5 seconds), defined as the test time (60 seconds) divided by the number of arms that can be visited (NE, SE, Central East, N, S, Central West, SW).

7. Tissue collection

7.1. For molecular biology analysis

The mice are killed by cervical dislocation. After decapitation the brain is quickly extracted and the structure of interest (Striatum (Str)) was removed as shown in **Figure 51**. The dissection of mouse brain is done on a platform positioned on ice. The tissues are quickly frozen in liquid nitrogen, to avoid their degradation, and then stored at -80°C until needed.

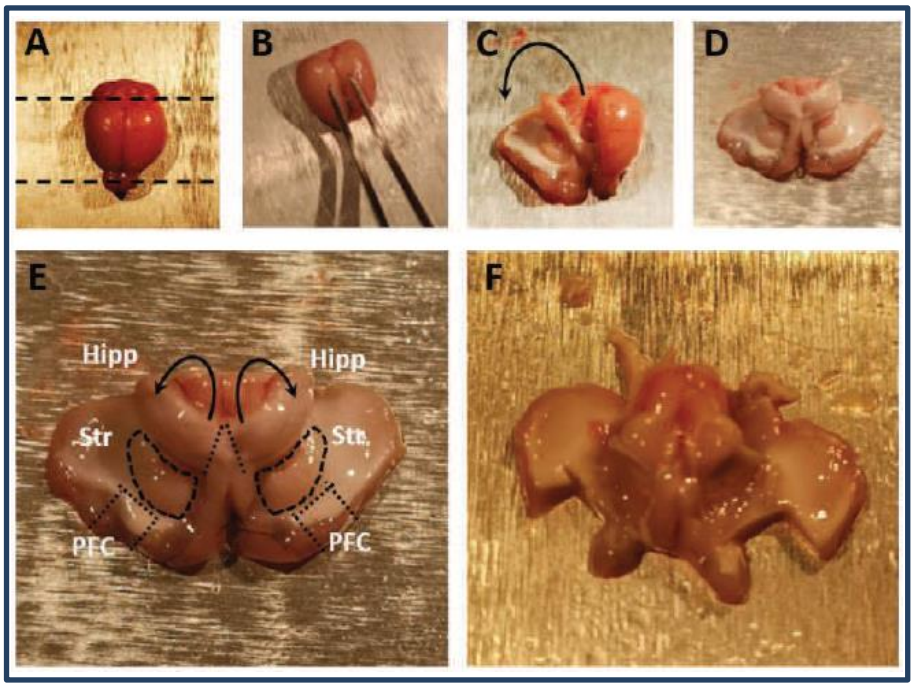

Figure 51: Dissection of the brain structures of mice for molecular analysis.
(A) The mouse brain is positioned on a metal platform cooled by ice. The cerebellum and olfactory bulbs are removed. **(B)** The corpus callosum is exposed by moving the cortex apart with forceps, and then slightly notched. **(C-D)** The cortex of each hemisphere is folded towards the platform with forceps. **(E)** The subcortical structures are then accessible. The striatum (Str), the hippocampus (Hipp) and the prefrontal cortex (PFC) are removed using the scalpel and forceps. **(F)** Illustration of the mouse brain after dissection of the structures of interest. (Thesis of Caroline LOTZ).

7.2. For immunostainings

The mice were killed by intraperitoneal injection of a lethal dose of pentobarbital solution (182.2 mg / kg, Doléthal®, Vetoquinol or 364 mg / kg, Euthasol® Vet, Le Vet. Pharma). An intracardiac perfusion is then performed, first with 0.1% NaCl for 3 min, then with 4% paraformaldehyde (PAF) dissolved in phosphate buffer (0.1M, pH 7.4) at 4°C for about 8 min to fix the tissues. The brain is then extracted and post-fixed in 4% PAF (in 0.1M phosphate buffer; pH 7.4; 4°C) for 6 hours,

then immersed in a 20% sucrose solution (in 0.1M phosphate buffer; pH 7.4; 4°C) for 48 h at 4°C for cryoprotection, and finally frozen in an isopentane solution maintained between -35°C and -40°C, thanks to dry ice. The brains are then stored at -80 ° C.

Using a cryostat (Microm HM560, Thermo Scientific), which maintains the temperature in the enclosure at -20°C ± 2°C, 30µm thick frontal sections are made from frozen brains. The floating sections are placed in a cryoprotection solution (30% glycerol, 30% ethylene glycol, 40% 0.1M phosphate buffer) before being stored at -20°C until being tested.

8. Histological analysis

8.1. Cryostat Brain cuts

The fixed hemispheres **(see section 4.2 Fixation of the brains**, p:X) are cut cryostat (Microm HM560, Thermo Scientific) to make frontal sections of 30µm thick, kept at -20 ° C until being used. In order to respect the principle of the non-biased approach by stereology and allow sampling of brain cuts, blocks containing the structures of interest were defined using stereotaxic coordinates by Paxinos and Watson **(Figure 52A)** (Prefrontal cortex: Bregma 2.34 to 1.34; Striatum: Bregma 1.34 to 0.02; Dorsal hippocampus: Bregma -1.22 to -2.30).

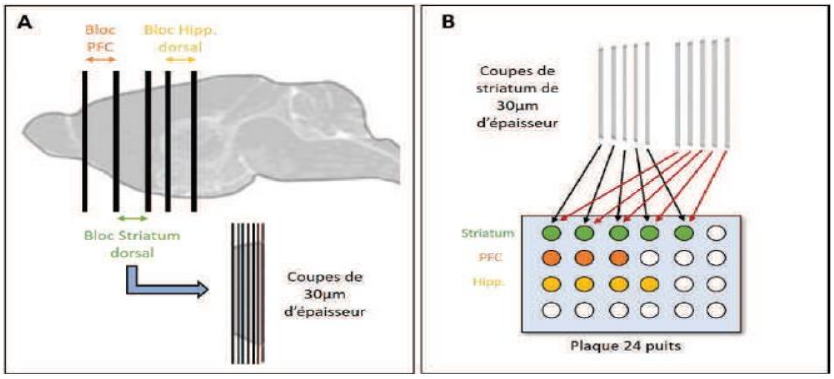

Figure 52: Preparation of mouse brain sections for immunohistochemistry and counting by stereology.
(A) Blocks containing the structures of interest (PFC, striatum, hippocampus) are cut with a cryostat with a thickness of 30µm. **(B)** These sections are then deposited in series in a 24 well plate. PFC: prefrontal cortex, striatum, and Hippocampus.

For each block, sections were collected from a defined number of wells of one 24-well plate containing a cryoprotectant solution (30% glycerol, 30% ethylene glycol, 40% 0.1M phosphate

buffer) **(Figure 52B)**. Thus, the prefrontal cortex, the striatum and the hippocampus were collected in 3, 5 and 4 wells respectively **(Figure 52B)**. For each structure, the sections were placed successively in the wells. Many series of sections are carried out until an average of 7 to 10 sections per well (Figure 52B). Thus, each well contains a representative sample of sections from all of the brain structure.

8.2. Immunohistochemistry on floating sections

Immunostaining was performed on striatal sections. For each animal, the sections were chosen by randomly selecting a single well representative of each structure. The entire immunostaining protocol is carried out at room temperature and under agitation. The sections were first rinsed three times in PBS (Phosphate-Buffered Saline) in order to remove the cryoprotectant solution in which the sections were stored. The endogenous peroxidases were then blocked by a 20-minute incubation in 1% hydrogen peroxide. After three rinses in PBS, the antigenic sites are blocked by incubating the sections for 1 hour in PBS containing 5% horse serum and 0.5% Triton X-100. The sections are then incubated overnight with shaking at room temperature. in a primary antibody solution **(Table 5)**. The next day, after three rinses in PBS, the sections are incubated for 1 hour in a solution of biotinylated antibodies **(Table 5)**. An amplification of the labeling is carried out by exposing the sections to a solution for 45 minutes avidin-biotin-peroxidase diluted to 1/500 (Vectastain Avidin-Biotine Complex Kit, PK6100, Vector Laboratories). After two washes in PBS and washing in TRIS buffer, the labeling is revealed by incubation for 8 to 10 minutes with 3,3'-diaminobenzidine (DAB) (DAB Peroxidase Substrate Kit, SK4100, Vector Laboratories).

	Antibodies	Species	Dilution	Reference
Primary	EM48	Mouse	1/500	MAB5374, Merck Millipore
Secondary	Biotinylated anti-Rabbit	Goat	1/500	ZB1007, Vector laboratories
	Biotinylated anti-Mouse	Horse	1/500	BA2001, Vector laboratories

Table 6: Primary and secondary antibodies for striatum immunostaining.

The reaction is stopped by removing the DAB solution and performing three washes in PBS. The cuts are then mounted on gelatinized slides and dried in an oven at 37 ° C overnight. The the next day, the sections are rinsed in ultra-pure water and then dehydrated in baths successive ethanol in increasing concentrations (70%, 95%, 100%). The cuts are then dives 5 minutes in a solvent (Clearify, Medtronic) and mounted between slide and coverslip with mounting medium (Diamount).

8.3. Stereology

Stereology is a tool based on a set of mathematical methods and statistics allowing extracting quantitative information (volumes, surfaces, lengths, numbers) on elements present in a defined volume. The quantitative estimate within a 3-dimensional structure is made from sections in 2 dimensions and constitutes an unbiased approach. Indeed, the classical techniques of Quantitative measurements in microscopy involve two types of errors: random errors (related for example to the technique and the quality of the material) which can be minimized by multiplying the measures, and the systematic errors (biases) which depend on the methodology and the design of protocol. Stereology helps to reduce systematic errors by limiting the biases at each stage of the protocol during samples preparation. Thus, the estimation of the elements to be counted is made from a systematic sampling, random and representative, in a determined tissue volume and without any initial assumption on the size, shape or spatial distribution of the elements to be measured, so that everyone has the same probability of being counted.

In my studies, using stereological approach, I checked the effect of SRF overexpression on the number of cells expressing EM48, using anti-EM48 antibody reactive against the N-terminal region of human huntingtin, and the length of the nuclei of the EM48 cells in the striatum of R6/1 mice by the quantitative estimation of their numbers. For this, I constituted a non-biased brain structures sampling at two levels of interest:

(1) The level of the selected sections for counting (section sampling) by taking into account the entire interest structure without evaluating the number of immune-labelled neurons over all sections of this structure.

(2) The volume level of each cut in which the counting is carried out (optical dissectors) where the sampling of the cuts begins at the time of brain cutting with the cryostat and the volume of each sampled cut at the time of counting.

8.3.1. Neural counting by stereology

The counts were carried out with an optical microscope (Leica DM5500B), a motorized stage allowing displacement in three dimensions (X, Y, Z) and a digital camera (Optronics Microfire). The software used for quantification by stereology is Mercator (Explora Nova, La Rochelle, France).

8.3.2. Principle of the optical dissector

Sampling the volume of sections in which neurons are counted is performed using optical dissectors (Figure 53A). Dissectors are virtual cubes allowing counting in 3 dimensions using a set of optical sections in the Z plane. Neurons are counted in the X, Y and Z planes, only inside dissectors distributed randomly in the structures of interest, thanks to the software of Mercator counting. The size of the dissectors and their spacing is chosen by the experimenter according to the density of the staining, the size of the elements to count and the targeted brain structure. The reliability of the counting depends on the parameters of the dissectors and is represented by the error coefficient (EC) provided by the Mercator software.

The EC corresponds to the variability of the counts between the sections of an animal and must be less than 0.15 for having reliable results. If the dissectors are too small or too spaced out, too few neurons are counted and the EC will be high. So, a preliminary count of 2 or 3 mice is necessary to obtain a representative ECs and to validate the dissector parameters.
Counting using dissectors requires the determination of the real cuts thickness. Indeed, cuts of 30 µm thick are made in the belief, but in reality, the thickness of the cuts is rather around 15 µm due to their treatment (dehydration, irregularity of the cuts with the cryostat). This requires the removal of 2 µm stain on the lower and upper side of the cut to have a homogeneous block).

The number of stained neurons is then estimated throughout the section and the whole brain structure of each animal. This calculation is carried out by the method of optical fractionator in Mercator software and takes into account the actual thickness of the sections which have been counted, the sampling of the sections and the parameters of the dissectors.

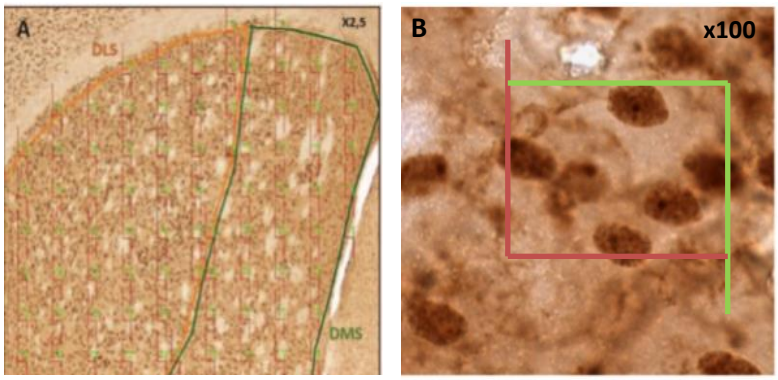

Figure 53: Example of neural counting with optical dissectors.
(A) Random placement of dissectors within regions of interest, here the dorsolateral striatum (DLS) and dorsomedial (DMS), at x2.5 magnifications with Mercator software. **(B)** Example of labeled neurons positively for EM48 protein inside a dissector.

8.3.3. Counting parameters

On each cut, the regions of interest to count are delimited (x2.5) **(Figure 53A).** The counting was carried out with the objective x100 oil immersion, in the striatum subregions, Dorsolateral and Dorsomedial. The parameters of the dissectors used for the counting of of the mutated HTT aggregates marker, EM48, are 25µm apart and 120µm spacing. The actual thickness of the measured cuts was 14µm with a 1/5 sampling for the striatum. For the EM48 counting, the number of nuclei comprising an EM48+ aggregate has been counted and the diameter of the aggregates of mutated HTT was measured using Mercator software (Explora Nova).

9. Molecular analysis of protein expression

9.1. Total protein extraction

The striatum of each animal is used for total protein extraction. It is cut on ice with a scalpel blade then homogenized by pipetting in 150 µL of 1x Laemmli buffer (Laemmli 4x, Bio-Rad,diluted) containing ß- mercaptoethanol (1/40th of the total volume) to promote protein extraction. Then, the lysates are vortexed for 10 seconds and left for 30 minutes on ice, before being sonicated (40% amplitude, 2x 10 s, Bioblock Scientific Vibra Cell 75041). To facilitate cell lysis, the samples are heated 10 mins at 70°C followed by 5 mins at 100°C. After that, they are centrifuged at 14000g for 5 mins, the protein contained in the supernatant is recovered and stored at -20°C. Protein concentrations are measured with the Qubit quantification (Invitrogen) and the Qubit Protein Assay kit (ThermoFisher). Protein stock solutions are kept at -20°C.

9.2. Western blot

For Western blots, the used gels are the pre-cast poly-acrylamide gels gradient (4-20%, Criterion 500; Bio Rad). The gels are placed in a migration tank (Criterion Cell; Bio-Rad) filled with 1X migration buffer (TG-SDS 10X, Euromedex). The quantity of proteins is determined according to the conditions and the antibody used. The volume of each sample is deposited in gel wells as well as the molecular weight scale (PageRuler ™ Plus Prestained Protein, Thermo Scientific), then protein migration is done by electrophoresis (250V for about 30 minutes), until the migration front is almost out of the frost.

The proteins in the gel are then "activated" with the gel visualization device (ChemiDoc ™ Touch Imaging System, Bio-Rad). In Stain Free gels there are alo-alkanes which fix on the deposited proteins and under UV radiation they carboxylate the protein tryptophans, leading to fluorescence emission.

The proteins of the poly-acrylamide gel are then transferred to a membrane of nitrocellulose (Midi-Size Nitrocellulose, TransBlot Turbo; Bio-Rad) thanks to a semi-dry transfer (TransBlot Turbo; Bio-Rad): the nitrocellulose membrane, the Whatman paper and the protein gel are first

moistened with transfer buffer 1X (Trans-Blot Turbo Buffer, Bio-Rad). In the cassette, the successive deposition: a layer of Whatman paper, then the nitrocellulose membrane, the gel and again a layer of Whatman paper also soaked in transfer buffer favor the transfer. The cassette is placed in the transfer device which applies a current from top to bottom of the cassette to migrate the gel proteins onto the membrane.

Following protein transfer, the membrane is then incubated in washing buffer (50mL of Tris pH 7.4, 30mL of 5M NaCl, 500L of Tween 20% in 920mL of distilled water) mixed with powdered milk to block the specific antigenic sites of the membrane proteins. Depending on the used antibodies, the incubation time varies from 30 min to 1h at room temperature and the milk concentration varies from 1% to 5%.

The membrane is then incubated overnight at 4°C, with shaking, with the diluted primary antibody in a washing buffer solution containing 3% milk. The next day, three washes of the membrane are carried out in washing buffer and then the membrane is incubated for 1h at room temperature with the secondary antibody diluted in washing buffer containing 3% milk, with shaking.

Three more washes with washing buffer followed by 2 min incubation with the “ECL” -enhanced chemoluminescence-solution (Clarity Western ECL Substra te; Bio-Rad), the immuno-labelled proteins are revealed and protein bands are visualized by the exposure of the membranes in the ChemiDoc Touch imaging system (Bio-Rad).

The Quantification of protein expression is carried out on the photos of the membranes taken by the ChemiDoc Touch, by measuring the optical density of the protein bands of each sample using ImageLab software (Bio-Rad). Then, the semi-quantification of the revealed proteins is normalized by achieving a ratio either on a housekeeping gene or on the total quantity of the proteins of the membrane (photo taken directly after the transfer; membrane activation step).

10. Molecular analysis of gene expression

In order to evaluate the effect of Srf over expression on striatal transcriptomics, gene expression among different experimental groups was identified through transcriptomic analysis using total RNAs from the striatum of the experimental groups. Total RNAs were analyzed either by qRT-PCR or by RNA-seq. For the first experiment, we carried out a sequencing of the RNAs (RNA-seq) extracted from the striatum of WT and R6/1 mice injected with AAV-GFP and R6/1 mice injected with AAV-SRF. Another RNA-seq was performed on extracted RNAs from the striatum of WT and R6/1 mice injected with the AAV-Srfvp16 and AA-vp16 vectors.

10.1. Total RNA extraction and cDNA synthesis

The entire protocol was carried out at room temperature. The samples have dissociated by the pipette in 350µL of lysis buffer (RNeasy Plus Mini kit, Qiagen) containing ß-mercaptoethanol, until no more tissue fragments are observed. The gDNA eliminator columns from the QIAshredder kit (Qiagen) were used to remove the genomic DNA. The RNAs were then treated with the RNeasy Plus Mini kit columns (Qiagen) according to the protocol provided by the kit. The final solution was made with 30 µl L of water without RNAses supplied by the kit.
The RNA concentrations were measured using the Qubit quantification (Invitrogen) and the RNA BR Assay kit (ThermoFisher). The samples are Stored at -80°C. Thanks to Dr. Caroline LOTZ for her help in total RNA extraction.

cDNA synthesis was performed on 0.5 µg of total RNA (iScript Reverse transcription Supermix for RT-qPCR kit; Bio-Rad). Gene-specific primers are available upon request. qRT-PCR analysis was performed on a Bio-Rad iCycler System (CFX) using SsoAdvanced SYBR Green Supermix (Bio-Rad). qRT-PCR conditions were 2 mins at 50°C, 2 mins at 95 °C, followed by 45 cycles of 3 s at 95 °C and 30 s at 60 °C. RT controls were performed by the omission of RNA template or RT enzyme. A specific standard curve was performed in parallel for each gene, and each sample was quantified in duplicate. Data were analyzed by gene regression using iCycler software and normalized to 18S levels.

11.2. Quantitative PCR (qPCR)

SRF and some of of its known target genes were quantified by qPCR. thanks to the mix of iTaq Universal SYBR Green Supermix (Biorad) according to the manufacturer's protocol having 3.5ng of cDNA per reaction. The amplification was made by a thermocycler (BioRad CFX 96) according to the following program: 3 min at 95°C, denaturation at 95°C for 10 s, hybridization and polymerization at 60 ° C for 30 s, repeated 40 times. The amount of RNA was measured by the ΔΔCt method. Then the amount of SRF was normalized by the normalizing gene (18S and 36B4).

11.3. Sequencing of RNAs and analysis of results

The quality of the RNAs was assessed using their RIN (RNA Integrity Number), which reflects RNA degradation and the presence of contamination. Good quality RNAs has an Upper RIN 8. The RIN of the RNAs was measured by the sequencing platform of the IGBMC (Strasbourg) and the values obtained were between 8 and 10 for all samples. The RNAs have been sequenced at the IGBMC sequencing platform with the Illumina Hiseq 4000 technology. During the preparation of the libraries for sequencing, the RNAs are fragmented and back transcribed into cDNA. The library is of type "stranded
mRNA-seq/standard quantity "and the sequence" Hiseq 4000 1x50 bases ". During sequencing, the cDNAs read sequences are subsequently called "reads" during the bioinformatics analysis. The bioinformatics analysis was carried out by the sequencing platform of the IGBMC (Strasbourg) and by Dr. Jonathan Seguin and Charles Decraene (LNCA, Strasbourg) to obtain the number of genes differentially expressed in the different comparisons.
I performed the functional enrichment analysis together with Dr. Jonathan. After checking the quality of the sequencing, the reads were aligned by the Tophat2 software (Pinto et al., 2013) on the GRCm38 (mm10) version of the mouse genome, provided by the Genomen Reference Consortium (https://www.ncbi.nlm.nih.gov/grc). The reads aligned by sample were then counted using Htseq (Anders et al., 2015) in order to compare the expression of genes under different experimental conditions. The differentially expressed genes are obtained using the R DeSeq2 package (Love et al., 2014) and selected according to the adjusted p-value, less than 5% (based

on the Benjamini-Hochberg test). Functional analysis were carried out with the R Cluster Profiler library (Yu-Taeger et al., 2012) and with DAVID(Huang et al., 2009), from the up-and down-regulated genes lists in the various experimental conditions. The terms of the basics of Gene Ontology (GO) (Ashburner et al., 2000) and KEGG (Kanehisa, 2000; Kanehisa et al., 2019) have been used.

12. Statistical Analysis

All data have been expressed as an average, plus or minus the error standard of the mean (SEM). A Student's t-test was performed for comparisons by pairs between groups. For comparisons of more than 2 groups, an ANOVA was performed: a two-way ANOVA with repeated measurements for behavioral analysis (genotype vs day), multiple comparisons were done using Tukey's and one-way ANOVA for all the others analysis (genotype).

When the criteria of normality and/ or homogeneity of variance were not fulfilled, nonparametric tests were used: The Chi-square test and the binomial test for the comparison of two distributions; the Mann-Whitney and Kruskall-Wallis tests for comparing 2 or more groups, respectively. Multiple comparisons have been done using the Dunn test.

…… Results ……

Results

1. Striatum-dependent memory is early impaired in HD R6/1 transgenic mice

Among the different symptoms of HD, cognitive deficits, particularly striatum-dependent cognitive deficits, are not well characterized. Several studies using the hippocampus and/or the prefrontal cortex have shown that learning and memorization processes imply major transcriptional and epigenetic changes, (Campbell and Wood, 2019; Fernandez-Albert et al., 2019; Jaeger et al., 2018; Yap and Greenberg, 2018). Our team investigates memory-associated epigenetic and transcriptional signatures in the striatum of HD mice models, including the transgenic R6/1 mice. In particular, we generated RNAseq data using brain tissues of R6/1 and control mice during striatum-dependent memory (procedural memory) formation and recall. To this end, we used dedicated navigation task which assesses striatum-dependent memory versus hippocampus-dependent memory (spatial memory) (Cassel et al., 2012; Pol-Bodetto et al., 2011) (Lotz et al., in prep) **(Figure 54A and 54B; see material and methods section p:116)**. The performances of R6/1 and WT mice are presented below (results of Dr. C. Lotz, detailed in the attached manuscript Lotz et al. in prep "Neuronal and non-neuronal memory-associated epigenomic and transcriptomic signatures are impaired in the striatum of Huntington's disease mice").

Procedural memory of R6/1 mice has been assessed at the ages of 11 and 14 weeks, corresponding to early symptomatic stages where the mice do not yet show substantial motor deficits (Brooks et al., 2012; Hansson et al., 2001) and Lotz et al. , in prep). WT and R6/1 mice at 11 and 14 weeks of age were trained for 4 days to find the platform positioned in the NE arm from the S arm **(Figure 54B).** The analysis of the percentage of correct response **(Figure 54C)** shows that performance of R6/1 mice during acquisition is significantly decreased relative to WT mice by 11 weeks of age **(Figure 54C).**

In the probe test, significantly fewer R6/1 mice visited the procedural arm as a first intent compared to WT mice **(Figure 54D)**. Approximately 80% of WT mice, 50% R6/1 mice at 11 weeks, and 30% of R6/1 at 14 weeks visited the procedural arm at first intention. Additionally, WT mice

spent significantly more time in procedural arm than chance, which was not the case of R6/1 mice, whether they were 11 or 14 weeks **(Figure 54E)**. This indicates that WT mice, but not R6/1 mice, use a procedural strategy to find the platform. Moreover, R6/1 mice at 11 and 14 weeks spent significantly more time than chance in the spatial arm **(Figure 54E)**, indicating the preferential use of a spatial strategy by R6/1 mice. Noticeably, the time spent by WT mice in spatial arm was also above chance, this is because, once they realized that the platform was not located in the procedural arm, they shifted to the spatial arm, showing cognitive flexibility **(Figure 54E).**

These results indicate that striatum-dependent memory (procedural memory) is impaired in R6/1 mice, while their hippocampus-dependent memory (spatial memory) appeared preserved.

Since memory process required transcriptional reprograming (Campbell and Wood, 2019; Fernandez-Albert et al., 2019; Jaeger et al., 2018; Yap and Greenberg, 2018), we reasoned that memory-associated transcriptional regulations might be impaired in the striatum of R6/1 mice. We therefore investigated regulatory transcription factors that are known to be implicated in memory, and focused on SRF and CREB, which are two major transcription factors regulating memory process (Buchwalter et al., 2004; Finkbeiner and Greenberg, 1998; Yap and Greenberg, 2018).

2. *Srf* mRNA levels in the striatum of R6/1 HD mice in basal condition

In order to characterize the expression of *Srf i*n the striatum and follow its variation with the disease progression, I re-analyzed RNAseq data that were generated in the lab, using brain tissues of WT and R6/1 mice in basal conditions (e.g. home cage, HC) at 14 weeks and 30 weeks (Mayada Achour et al., 2015); Lotz et al., in prep) **(Figure 55A)**.

The analysis of the data shows that mRNA level of *Srf* is significantly decreased while the mRNA level of *Creb* is significantly increased in the striatum of 14 weeks and 30 weeks R6/1 HC mice (**Figure 55B).** Moreover, the expression of SRF target genes, including the immediate early gene (IEG) *Egr1 and Actb*, identified in previous analyses (Knöll and Nordheim, 2009) are also

decreased in the striatum of R6/1 mice **(Figure 55C).** This indicates that *Srf* and its target genes are decreased while *Creb* is increased in the striatum of R6/1 mice.

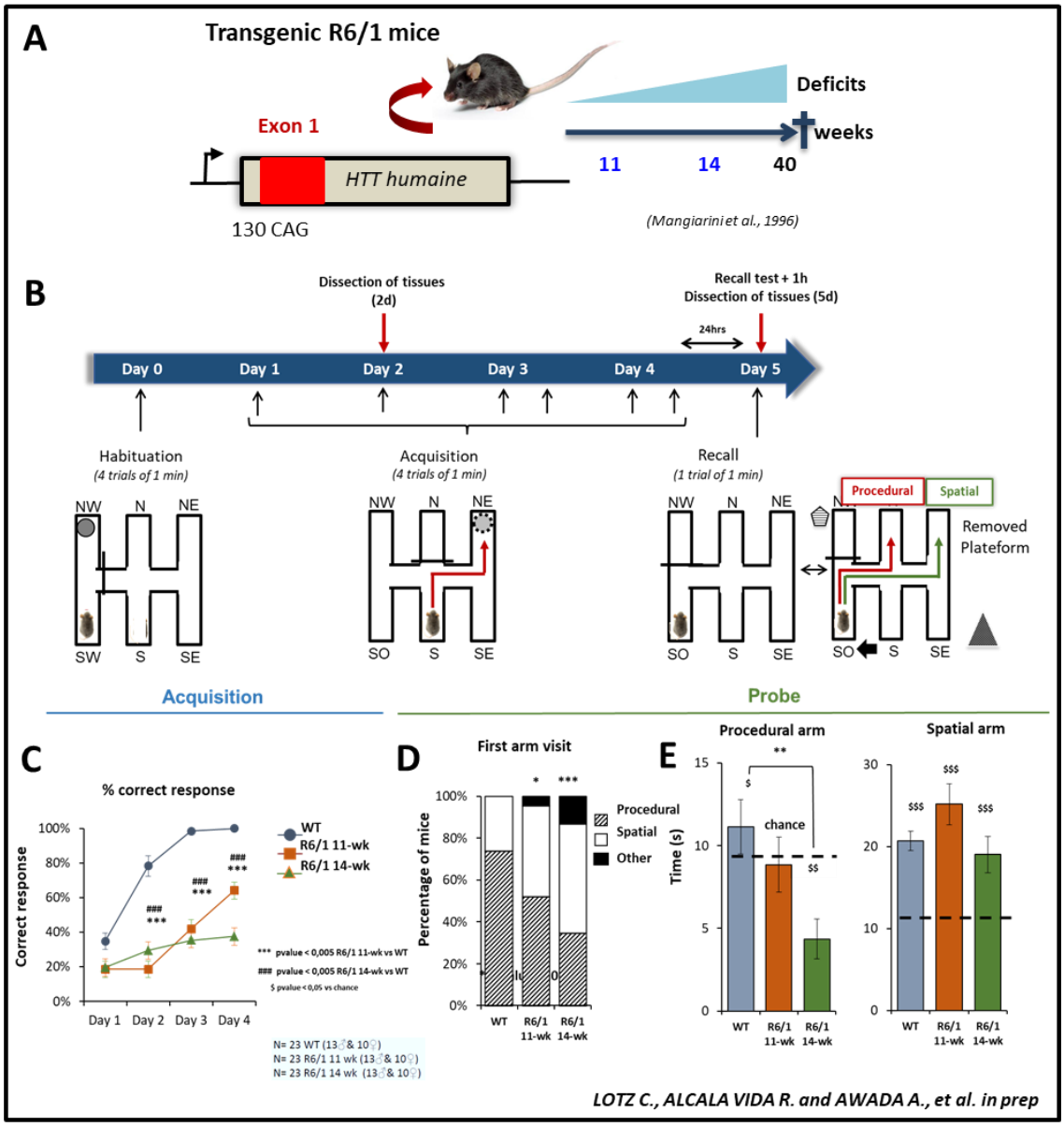

Figure 54: Evaluation of the cognitive phenotype of R6/1 mice in the Double-H maze.
(A)11 and 14 weeks transgenic R6/1 mice. **(B)** Protocol for training mice in the Double-H maze: during habituation, the mice were released from the SW arm, the SW-SE arm is blocked from the other parts of the maze, the platform is exposed. During Acquisition, training phase, the mice are trained to find a hidden platform, submerged in the NE arm, from the S arm. The recall test "probe", the start point is shifted to the SW arm, the NW arm is blocked, the platform is removed and the strategy followed by each mouse to reach the target arm was observed. **(C)** The percentage of correct responses performed by the mice during learning phase (Two-way ANOVA with repeated measurements: p <0.0001). **(D)** First arm visited by each group as a first intention during the probe test. **(E)** The time spent in each of the procedural and spatial arms among the groups and the relative time spent of each group compared to the chance (8.5 seconds) in each of the two arms during the probe test (p-value<0.005).

3. Characterization of the effect of memory on *Srf* mRNA levels in the striatum and the hippocampus of WT and R6/1 mice

In order to evaluate the impact of memory process on the expression of *Srf* and its target genes, we analyzed RNAseq data generated in the lab using the striatum and the hippocampus of WT and R6/1 mice of 14 weeks, during memory process (Lotz et al. in prep). The tissues were collected 1 hour after the last test of the second acquisition in the double-H maze (WT and R6/1 2d), 1 hour after the recall test (WT and R6/1 5d), as well as in basal condition (WT and R6/1 HC) **(Figure 56A).** The 2d and 5d time points correspond to memory formation and memory consolidation/recall, respectively. Of note, only HC and 5d time points were used for transcriptomic analyses using the hippocampus **(Figure 57A)**.

RNAseq data corresponding to these different groups were generated by C. Lotz in the lab, in collaboration with Genomeast platform at the IGBMC. Extracted RNAs were sequenced from the striatum of 3 animals of each group condition (WT HC, WT 2d, WT 5d, R6/1 HC, R6/1 2d and R6/1 5D). Global analysis was performed by Dr. C. Lotz and is not described here. Briefly however, the data show a major effect of the genotype whatever the 'memory' context, particularly in the striatum (Lotz et al. in prep). Notably, down-regulated genes in R6/1 vs WT striatal samples were enriched in striatal identity genes, as we previously found in RNAseq data generated with the striatum of R6/1 mice of 30 weeks (Mayada Achour et al., 2015). Also, the data show that memory-associated transcriptional reprograming is impaired in the striatum of R6/1 mice (Lotz et al. in prep). During my PhD, I focused more specifically on SRF and CREB and their target genes, thereby re-analyzing these RNAseq datasets.

The data show that Srf mRNA level is induced during memory process in the striatum of WT animals. However, this response is altered in the striatum of R6/1 mice. Moreover, the expression of Srf target genes, including the IEGs of the Egr family, is also altered in in R6/1 mice, particularly during early stage of memory formation **(Figure 56B).**

In contrast, *Creb* is significantly upregulated in R6/1 vs WT mice **(Figure 56C)**, suggesting possible compensatory mechanism.

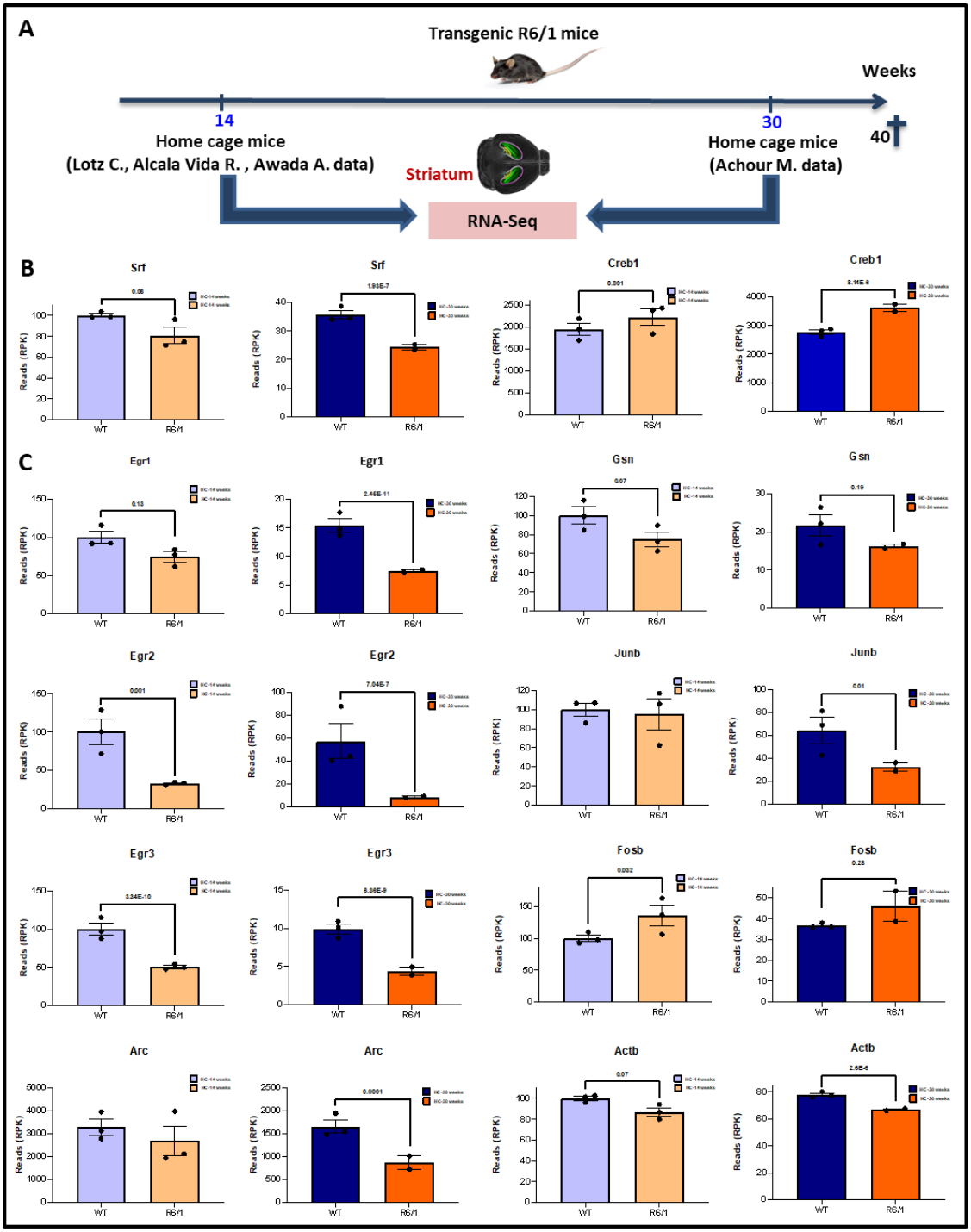

<u>Figure 55:</u> Srf mRNA levels in the striatum of HD mice in basal condition.

(A) Sequencing of RNA from the striatum of WT and R6/1 mice in basal conditions (e.g. home cage, HC) at 14 weeks and 30 weeks. **(B)** The expression of Srf and its selected target genes, the target genes were previously identified by Nordheim et al. (Knöll and Nordheim, 2009) (adjusted p- value<0.05).

We then determined whether SRF and CREB target genes were globally impaired in the striatum of R6/1 mice. We used gene lists from published data where the authors determined SRF and CREB target genes during neuronal activation by using ChIPseq on primary cultures of cortical neurons (T.-K. Kim et al., 2010b).

The intersection of these gene lists with our RNAseq data is represented in **figure 56D**. The boxplots show z-scores computed from RNAseq data generated using the striatum of home cage (HC) animals, animals during memory formation (2d) and during memory consolidation/recall (5d). The data show that SRF target genes are globally reduced in R6/1 vs WT mouse striatum in basal condition (WT-R6/1 HC), and they are not induced in the HD context during memory process, neither at 2 days nor at 5 days. In contrast, CREB target genes are globally increased in R6/1 compared to WT samples, either in basal condition or during memory process. These data further support the notion that dampened down SRF-dependent regulation might be implicated in impaired striatum-dependent procedural memory in R6/1 mice, whereas abnormal activation of CREB-dependent regulation might reflect compensatory mechanism.

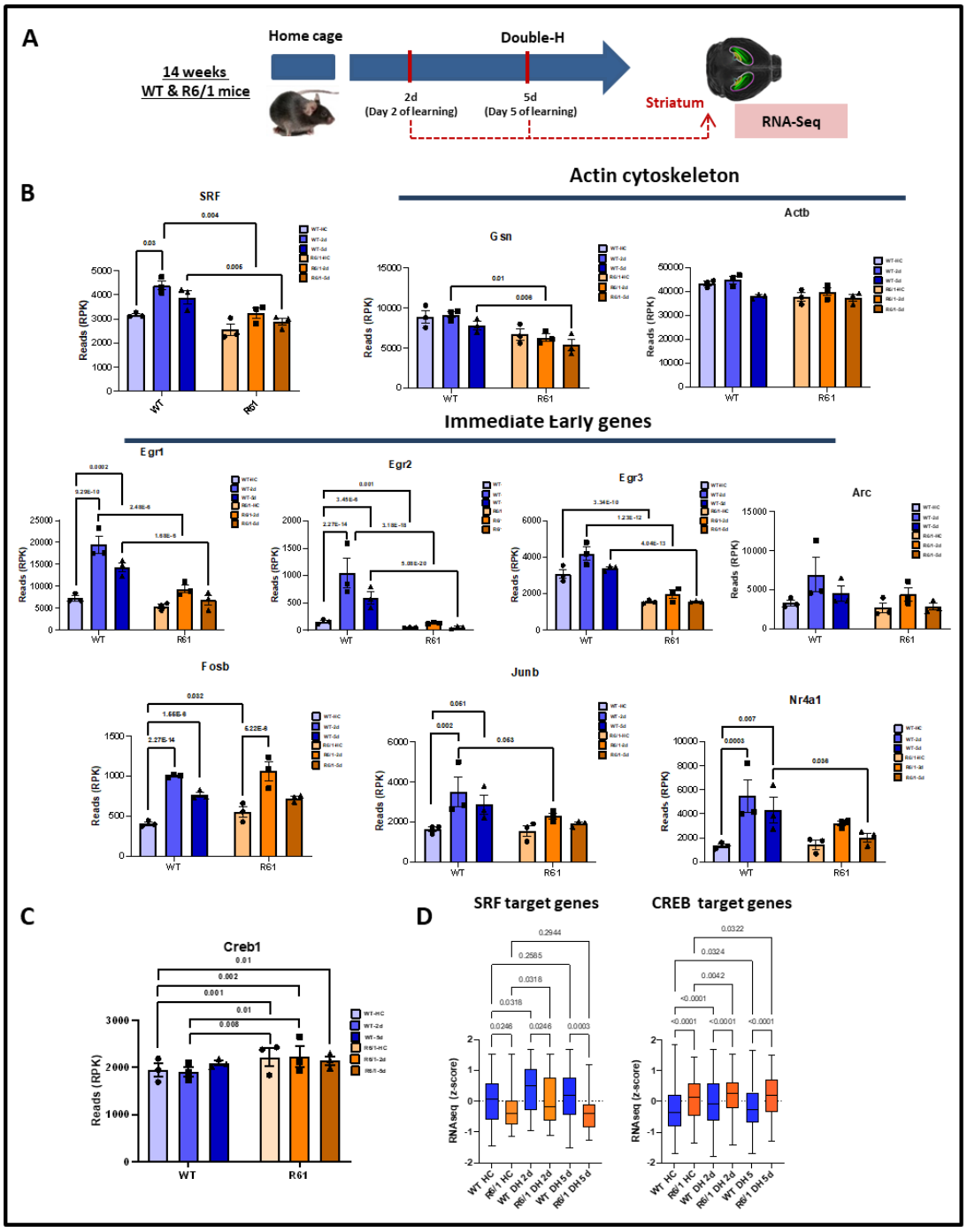

Figure 56: Characterization of the effect of memory on Srf mRNA levels in the striatum of WT and R6/1 mice.
(A) RNAs were extracted and sequenced from collected striata in basal condition (WT and R6/1 HC), 1 hour after the last test of the second acquisition in the Double-H maze (WT and R6/1 2d) and 1 hour after the recall test (WT and R6/1 5d) of double-H learning task. **(B)** The expression of Srf and Srf target genes in the striatum of WT and R6/1 mice. Adjusted p-value <0.05, exact values are shown on the graphs). **(C)** CREB expression level. **(D)** The boxplots show z-scores computed from RNAseq data generated using the striatum of home cage (HC) animals, animals during memory formation (2d) and during memory consolidation/recall (5d). SRF and CREB target genes, retrieved from Greenberg et al. 2010 and intersected with our RNAse data. Data was analysed using Kruskal-Wallis test, adjusting p values for multiple comparisons with Benjamini-Hochberg method. The comparisons of **(B-C)** were done between R6/1 HC vs WT HC, R6/1 2d vs WT 2d, R6/1 5dvs WT 5d, WT HC vs 2d, WT HC vs WT 5d, R6/1 HC vs R6/1 2d and R6/1 HC vs R6/1 5d and the adjusted p-values are represented on the graphs.

Analysis of RNAseq data generated from hippocampal tissues of 14 weeks WT and R6/1 mice in basal conditions (e.g. home cage, HC) and 1 hour after the recall test (WT and R6/1 5d) shows that RNA level of *Srf is* decreased in the hippocampus of R6/1-HC and R6/1-5d mice compared to WT-HC and WT-5d mice, respectively, whereas RNA level of Creb is not different in R6/1 compared to WT **(Figure 57B)**. Globally, Srf and several of its target genes are decreased in the hippocampus of R6/1 mice, less so however as compared to the striatum (**Figure 57C).** Also, Creb expression is not impaired in R6/1 mice.

4. *Srf and Srf* target genes mRNA levels in the striatum of knock-in HD mice

To determine whether *Srf* regulation is impaired in additional HD mouse model, I re-analyzed, with the help of bioinformatician Dr. J. Seguin in the lab, RNAseq data generated using tissues of HD knock-in mice (Langfelder et al., 2016a). The authors generated RNAseq data from different tissues of heterozygous KI mice, including the striatum, cortex, and liver. Moreover, they analyzed the effect of CAG expansion in Htt size on transcriptional dysregulation, using several KI line expressing varying numbers of CAG repeat in Htt, including 20, 80, 92, 111, 140 and 175 CAG repeats. Finally, they investigated the effect of age, generated RNAseq data at 3 time points (2, 6, 10 months) **(Figure 58A)**. **Figure 58B**, representing the results in the form of heatmaps show that Srf and its target genes progressively decrease in the striatum of KI mice, in a CAG-length dependent manner.

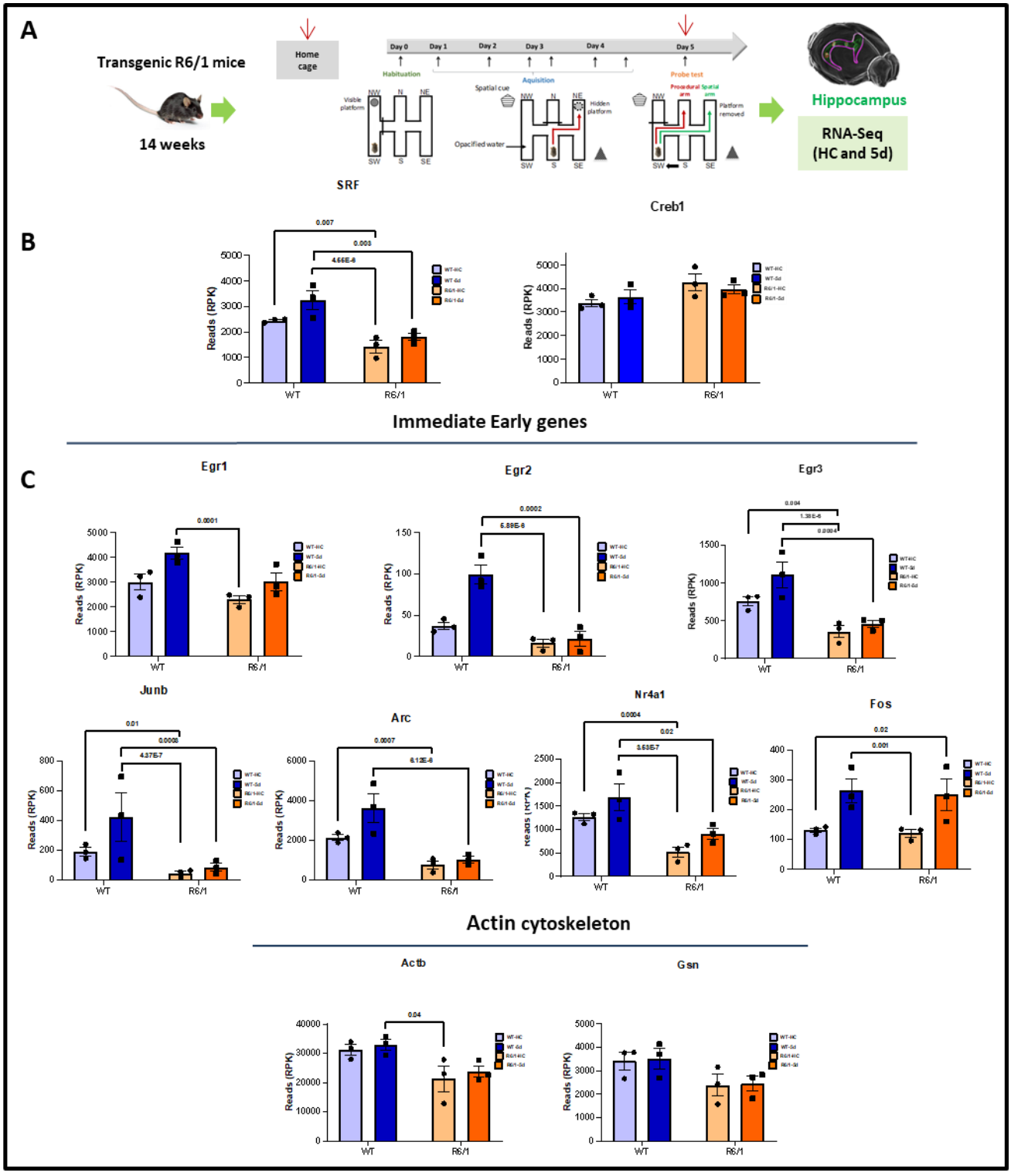

<u>Figure 57:</u> Srf mRNA levels in the hippocampus of R6/1 HD mice.
(A) RNAseq data generated from the hippocampus of 14 weeks WT and R6/1 mice in basal conditions (e.g. home cage, HC) and 1 hour after the recall test (WT and R6/1 5d) **(B)** Srf and Creb mRNA levels. **(C)** SRF target genes expression in the hippocampus of WT and R6/1 mice (comparisons were performed wih an adjusted p-value<0.05 between R6/1 HC vs R6/1 5d, R6/1 HC vs WT HC, R6/1 HC vs WT 5d, R6/1 5d vs WT HC, R6/1 5d vs WT5d and WT HC vs WT 5d; adjusted p-values are represented on the graphs).

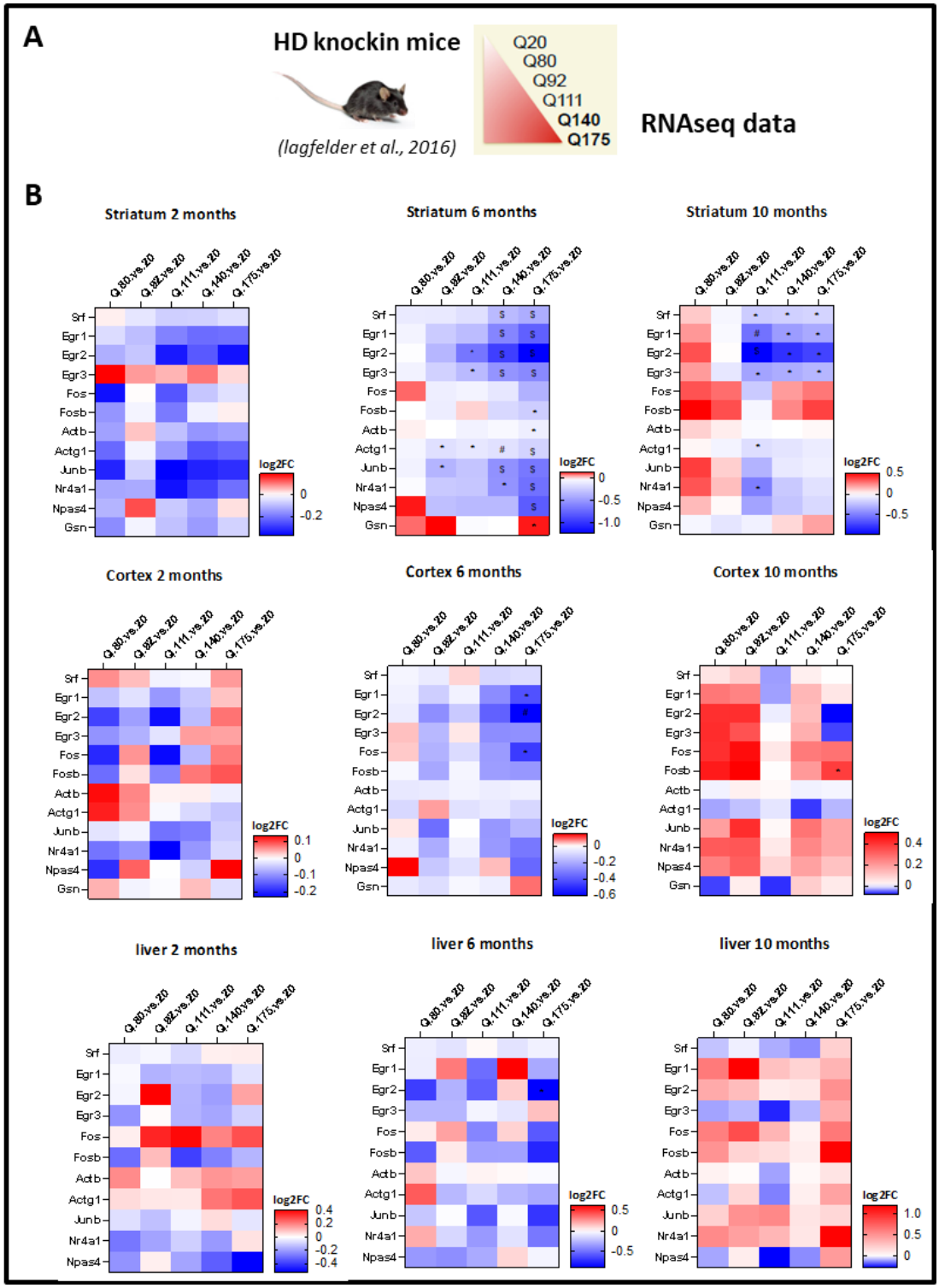

Figure 58: Srf and Srf target genes mRNA levels in the striatum of knock-in HD mice.
(A) RNAseq from published data by Langfelder and his colleagues in 2016 (Langfelder et al. 2016). **(B)** Heat maps representations showing the expression of SRF and its target genes in different tissues, ages and CAG lengths in knock-in HD mouse model. The Log2FC of SRF and its selected target genes in the striatum, cortex and liver is represented in blue-red bars showing the down-up regulation of the genes. Adjusted p-values: (*) <0.05, (#) <0.001 and ($) <0.0001.

5. Srf protein expression in R6/1 and KI HD mice models

We then examined SRF protein levels in the striatum of HD mice by western-blotting **(See materials and methods, p:125).** Protein extracts were prepared from the striatum of 14 weeks WT and R6/1 mice, in HC and DH-5d conditions. Western Blot analysis shows that Srf protein level is significantly decreased in the striatum of R6/1-HC and R6/1-5d mice compared to WT-HC and WT-5d mice, respectively **(Figure 59A).**

In addition to full length SRF (67kDa), we revealed a band at 50 kDa, likely corresponding to the alternatively spliced isoform of Srf (SrfΔ5) recently described (Gerosa et al., 2020). SrfΔ5 is also decreased in R6/1-HC and R6/1-5d mice compared to WT-HC and WT-5d mice. Moreover, it is significantly decreased in WT-5d compared to WT-HC **(Figure 59A).**

We also checked protein levels of Egr1 and Fos in the striatum of 14 weeks R6/1 mice. Western Blot analysis shows that protein level of Egr1 is decreased in the striatum of R6/1-HC and R6/1-5d mice compared to WT-HC and WT-5d mice, respectively. Surprisingly, it is also significantly decreased in WT-5d vs WT-HC samples **(Figure 59C)**. In contrast, Fos didn't change between R6/1 and WT mice in both HC and memory conditions **(Figure 59D)**.

Furthermore, we checked whether Srf protein level is also decreased in the striatum of Q140 KI mice. Protein extracts were prepared from the striatum of 11 months WT and Q140 KI mice, in both HC and DH-5d conditions, and analyzed by Western Blot. Western Blot analysis shows that both Srf and SrfΔ5 protein expression are dropped in KI-HC and KI-5d mice compared to KI-HC and KI-5d mice, respectively **(Figure 59B).**

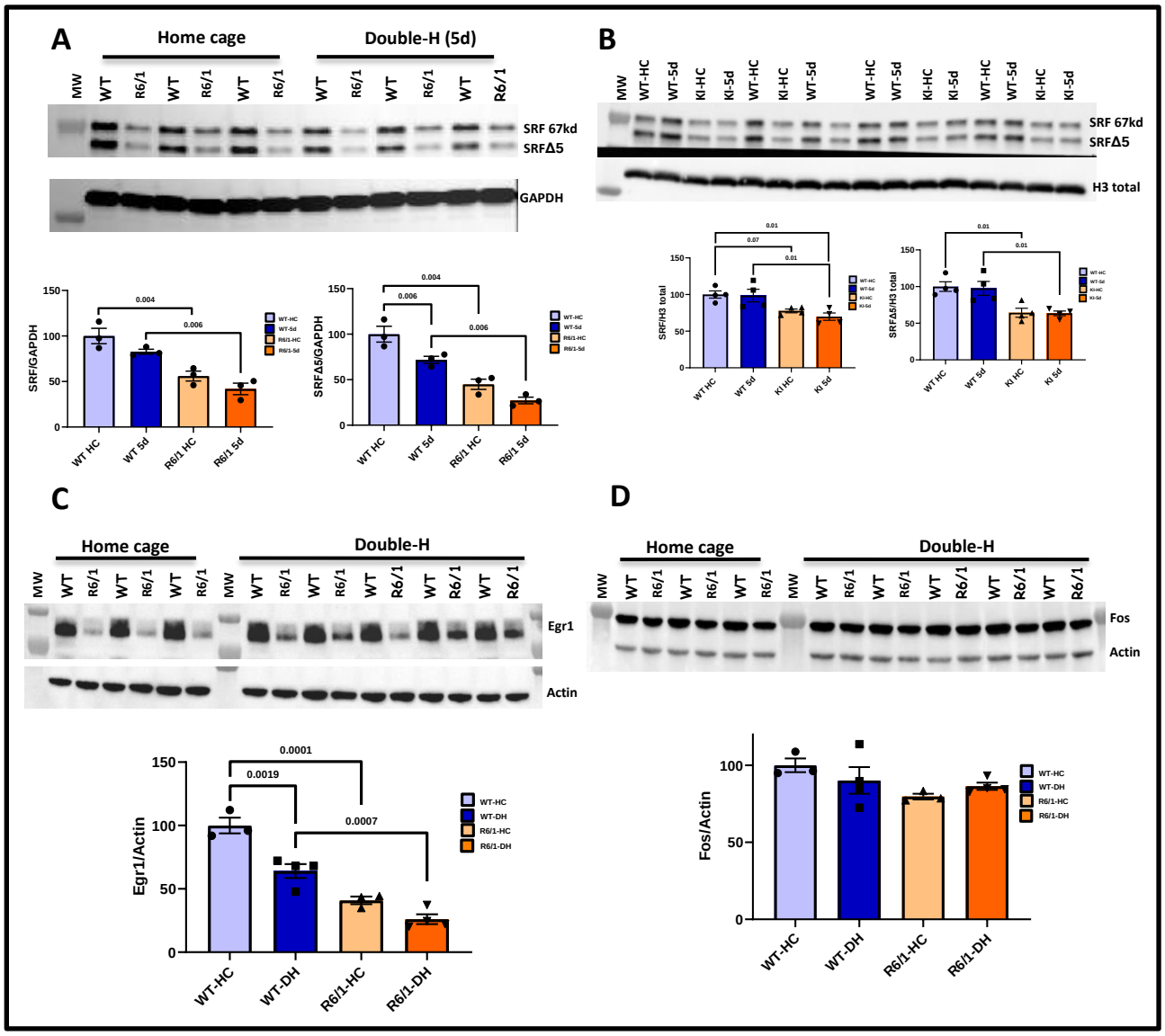

<u>Figure 59:</u> Srf protein expression in R6/1 and KI mice.

Representative immunoblots of SRF, EGr1 and Fos. **(A)** Western blot of SRF and SRFΔ5 (deleted exon 5) and their protein expression levels in the striatum of 14 weeks WT and R6/1 mice (HC and others performed the learning DH), the membrane was also incubated with anti-GAPDH Ab. **(B)** Western Blot of SRF and SRFΔ5 (deleted exon 5) and their protein expression levels in the striatum of 11 months WT and KI mice (HC and DH), the membrane was also incubated with H3-total AB. **(C)** Western Blot of Egr1 protein levels in the striatum of 14 weeks WT and R6/1 mice (HC and DH), the membrane was also incubated with actin Ab. **(D)** Western Blot of Fos protein levels in the striatum of 14 weeks WT and R6/1 mice (HC and DH), the membrane was also incubated with actin Ab. Values are obtained by densitometric analysis of the western blot. The graphs show the ratio of total proteins over a housekeeping gene and compared to 100% of WT HC and represented as mean ±SEM. Data were analyzed by One-way ANOVA, multiple comparisons were done using Tukey's test and the significant adjusted p-values were being represented on the graphs.

In conclusion, consistent with transcriptomic protein analysis in the striatum shows that Srf and Egr1 (but not Fos) protein levels are decreased in HD mice, which supports the hypothesis that altered regulation of SRF-pathway in the HD striatum contributes to disease pathogenesis.

To explore this hypothesis, we have overexpressed SRF in the striatum of HD R6/1 mice in order to rescue SRF-dependent gene program, as well as functional readouts, including behavioral deficits.

6. Murine full length Srf overexpression in R6/1 mice

First, in collaboration with Dr. Emmanuel Brouillet and A. Bemelmans (CEA, MiRCen), we have used adeno-associated viral (AAV) construct overexpressing the full-length sequence of the murine Srf gene. The viral vector was designed, produced, and verified at MiRCen. More specifically, Srf sequence was cloned in an AAV vector under a PGK promotor **(Figure 60A)** in AAV10 vector due to its high efficiency of expression in mouse brain **(Figure 60B) (See materials and methods p:104)**. An AAV-GFP vector was used as a control. The construct validity was done by Western Blotting, where a strong band corresponding to full length Srf was observed in animals subject to stereotaxic injection in the striatum (**Figure 60C).**

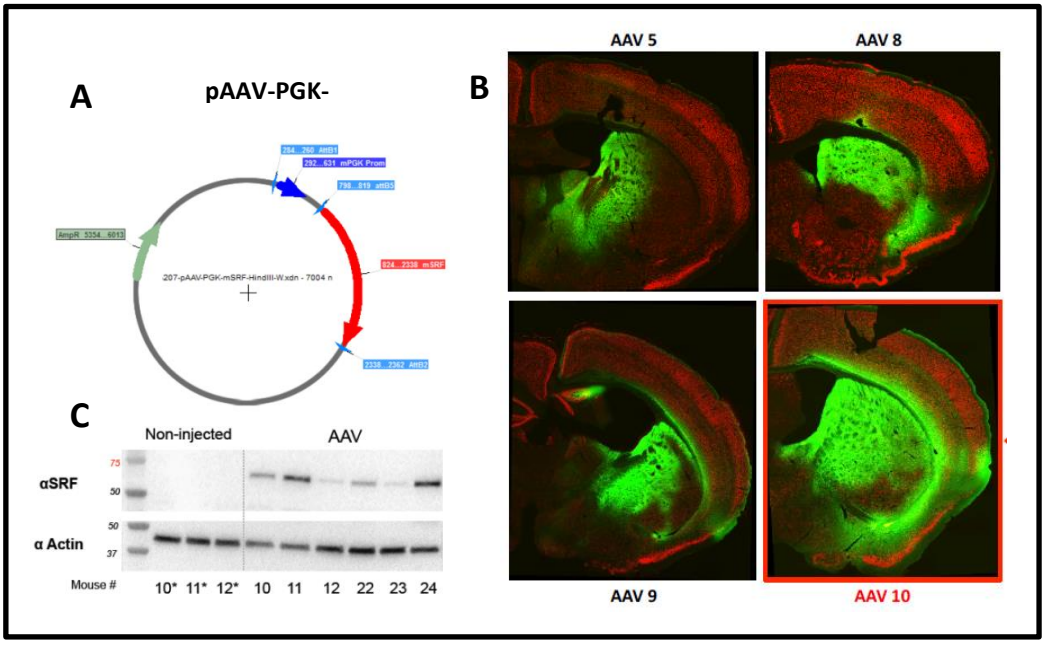

Figure 60: AAV10-Srf design and characterization.
(A) the p-AAV vector design showing inserted sequence of the murine full length Srf gene with the PGK promoter. **(B)** Immunofluorescent striatal sections showing AAV10Srf overexpression in different AAVs serotypes. **(C)** Western Blot of Srf in the injected and non-injected animals, the membrane was also incubated with actin Ab.

The experimental design is shown in **Figure 61.** Three groups (1 WT and 2 R6/1) of 8 mice each (**5 males** & **3 females)** have been stereotaxically injected at pre-symptomatic stage (8 weeks). One group of R6/1 mice has been injected with the AAV-Srf vector (containing the Srf gene) and the other groups were injected with the control AAV-GFP vector **(Figure 61A)**. The injections were done bilaterally in the two hemispheres of the brain at two different sites each, in order to improve striatal targeting **(Figure 61B).**

After four weeks of the injection, the mice were assessed with a battery of behavioral tests, then their memory was tested using the Double-H. The tissues were collected 1 hour after the probe test of the DH and spared for further molecular and histological analysis (**Figure 61B)**.

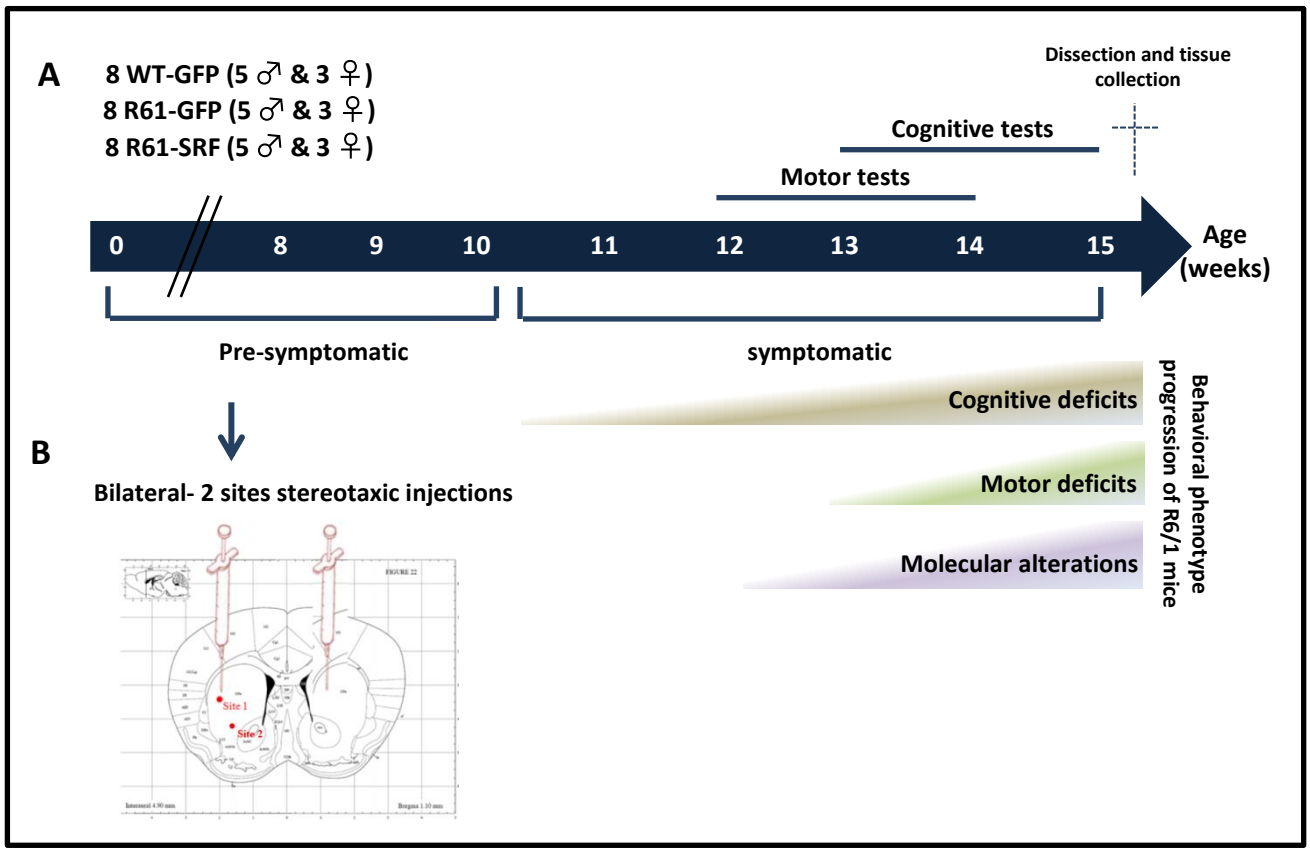

Figure 61: Scheme of the study design to assess the effect of full length murine Srf overexpression in the striatum of R6/1 mice.

(A)The experimental design to evaluate the effect of Srf overexpression in the striatum of R6/1 mice, and the experimental groups and the number of injected animals. The injections were performed during the pre-symptomatic stage, the animals were assessed at 12-14 weeks and the tissues were collected 1hr after the probe test. (B) Bilateral- 2 sites striatal injections of AAV-Srf and AAV-GFP using stereotaxic approach.

6.1. Evaluation of the effect of murine full length SRF overexpression on motor performance of R6/1 mice

First, we assessed the effect of SRF overexpression on spontaneous locomotor activity using actography **(See materials and methods p:110)**. As expected, actography analysis shows an increase of activity in night versus day **(Figure 62A).** The mean of day and night activity is represented by the number of moves per hour of each experimental group. The data shows that night activity is significantly lower in both R6/1-GFP and R6/1-Srf mice compared to WT-GFP mice, and that during the day, R6/1-Srf mice move significantly less than WT-GFP. Also, night activity is significantly reduced in R6/1-Srf compared to R6/1-GFP mice. These results suggest unexpected worsening of motor function in R6/1 mice upon overexpression of Srf in the striatum **(Figure 62A).**

To further explore this possibility, we evaluated the effect of SRF overexpression in R6/1 mice on motor coordination. Using the bar test, latency to cross the bar is significantly increased in R6/1-GFP and R6/1-Srf mice compared to WT-GFP mice, and is even increased in R6/1-Srf compared to R6/1-GFP during the first trial. In the second trial, the latency is significantly higher in R6/1-Srf mice compared to WT-GFP mice, while it is comparable between the different groups in trials 3 and 4. (**Figure 62B).**

We also assessed motor coordination using the accelerating rotarod. Overall, the latency to fall from the rotarod is significantly reduced in R6/1-GFP and R6/1-Srf mice, when compared to WT-GFP mice, and is lower in R6/1-Srf compared to R6/1-GFP mice **(Figure 62C)**. Moreover, SRF overexpression has comparable effect in R6/1 males and females **(Figure 62D)**.

Therefore, these results show that Srf overexpression in the striatum reduces motor function of R6/1 mice.

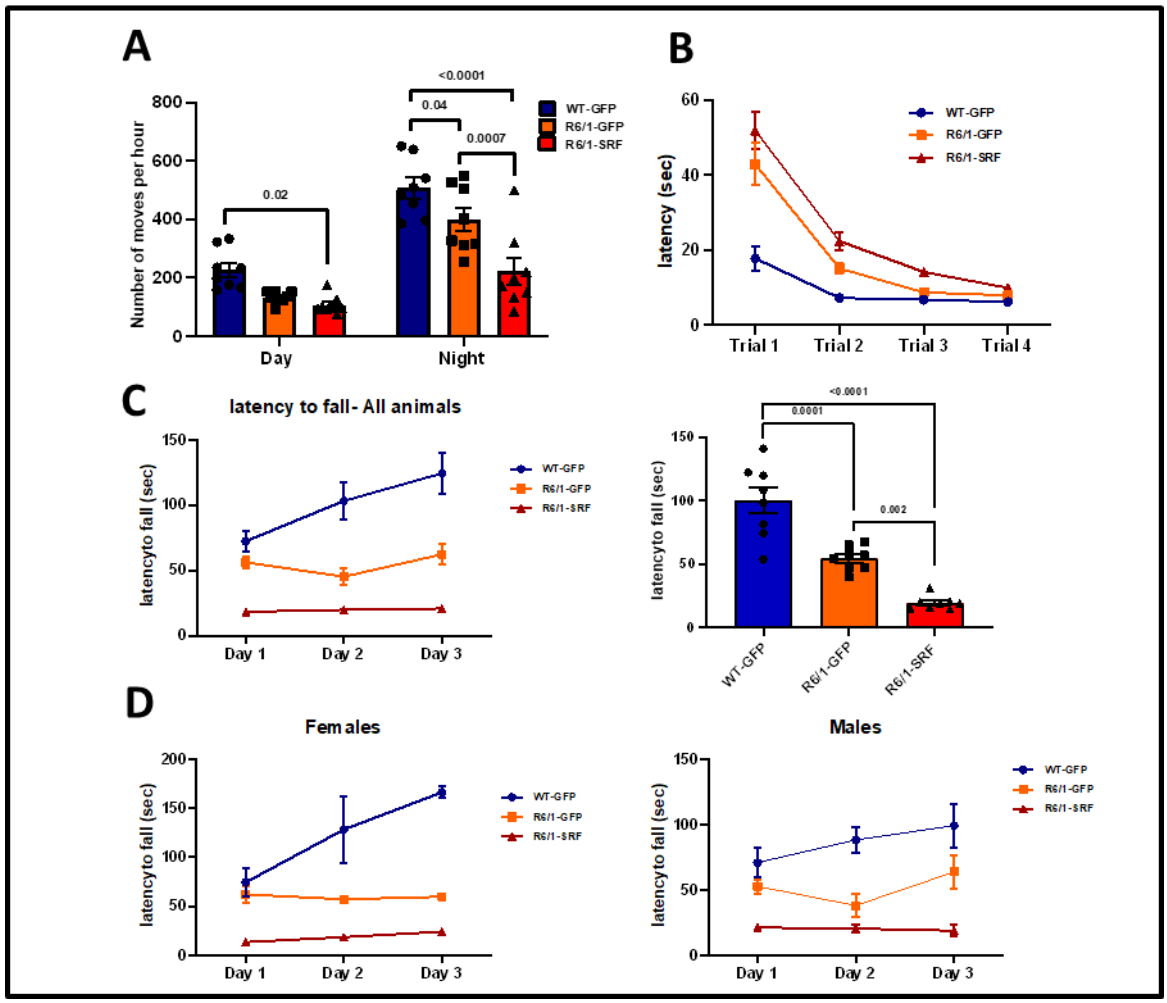

<u>Figure 62</u>: Evaluation of the effect of full length murine SRF overexpression on motor performance of R6/1 mice. **(A)** Evaluation of the effect of SRF overexpression on spontaneous locomotor activity of R6/1 mice in actography. The average number of moves per hour of the mice during the day (8 a.m.-8 p.m.) and night (8 p.m.-8 a.m.), the analysis was performed by Two-way ANOVA; Multiple comparisons with the Tukey's test: Time effect p<0.0001; Genotype effect p=0.37; Interaction Time x Genotype p=0.3). **(B-D)** Evaluation of the effect of SRF overexpression on motor coordination of R6/1 mice with rotarod **(B-C)** and bar test **(D)**. **(B) The** latency required by the mice to cross the bar and join their cage (Two-way ANOVA with multiple repeats; multiple comparisons by Tukey's test: Trial effect P<0.0001; genotype- effect P<0.0001; interaction trials x genotype P<0.0001. Trial 1: WT-GFP vs R6/1 GFP p<0.0001, WT-GFP vs R6/1-Srf p<0.0001, R6/1-GFP vs R6/1-Srf p=0.03. Trial 2: WT-GFP vs R6/1 GFP p=0.08, WT-GFP vs R6/1-Srf p=0.0002. **(C)** **<u>Left:</u>** The latency to fall from the rotarod during the 3 days of learning in the rotarod (Two-way ANOVA with multiple repeats; multiple comparisons by Tukey's test: Day effect P=0.0194; genotype effect P<0.0001; interaction day x genotype P=0.0262. Day 1: R6/1-Srf vs WT-GFP p=0.0001, R6/1-Srf vs R6/1-GFP p=0.0081. Day 2: R6/1-GFP vs WT-GFP p<0.0001, R6/1-Srf vs WT-GFP p<0.0001, R6/1-Srf vs R6/1-GFP p=0.1. Day 3: R6/1-GFP vs WT-GFP p<0.0001, R6/1-Srf vs WT-GFP p<0.0001, R6/1-Srf vs R6/1-GFP p=0.0035. **<u>Right:</u>** Mean latency to fall of the 3 days of training (One-way ANOVA, multiple comparisons with the Tukey's test: significant adjusted p-values are shown on the graphs). **(D)** The latency to fall of both males and females mice (Two-way ANOVA with multiple repeats; multiple comparisons by Tukey's test: Males; Day effect p= 0.21, genotype effect p<0.0001, interaction Day x genotype p=0.3106. Females: Day effect p= 0.01, genotype effect p<0.0001, interaction Day x genotype p=0.0179. The data is represented by the mean ± SEM, n = 8 per group (**5** ♂, **3** ♀) for all tests.

6.2. Evaluation of the effect of murine full length SRF on the anxiety of R6/1 mice

To evaluate the effect of Srf overexpression on the anxiety of R6/1 mice, we used the light-dark transition test **(See materials and methods p:111)**. At the start of the test, mice are placed in the dark compartment. Their anxiety is assessed by recording the number of entries and the time spent in the light compartment.

We observed that the number of entries in the light box is significantly reduced in R6/1-GFP and R6/1-Srf mice when compared to WT-GFP mice **(Figure 63A)**. Also, the latency to enter the light box shows a trend to the increase in R6/1-GFP or R6/1-Srf mice vs WT-GFP mice **(Figure 63B)**. Finally, the time spent in the light compartment does not differ between the three groups **(Figure 63C).** This indicates that R6/1 mice are apathic rather than anxious, and that SRF overexpression does not affect this phenotype.

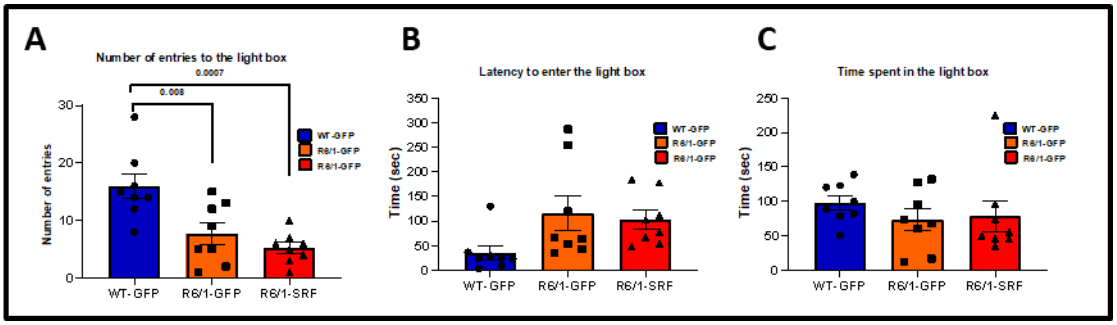

Figure 63: Evaluation of the effect of full length Srf overexpression on the anxiety of R6/1 mice using the light dark test.
(A) The mean number of entries into the light compartment of each of the WT-GFP, R6/1-GFP and the R6/1-Srf. **(B)** Mean latency to enter the light box. **(C)** Time spent in the light box. The analysis was performed using One-way ANOVA; multiples comparisons by Tukey's test and significant adjusted p-values are shown on the graphs. The data is represented by the mean ± SEM. n = 8 per group (5 ♂, 3 ♀) for all tests.

6.3. Evaluation of the effect of murine full length SRF overexpression on procedural memory of R6/1 mice.

We then sought to investigate the effect of Srf overexpression in R6/1 mice on procedural memory, using the DH-maze **(Figure 64A).** R6/1-Srf and R6/1-GFP mice showed poor performances during the acquisition phase, since the percentage of correct responses did not improve over the sessions, in contrast to the performances of WT mice, reaching 100% of correct responses at the end of acquisition (**Figure 64B)**. Also, the distance travelled to reach platform

was decreased in R6/1-SRF compared to R6/1-GFP mice, due to worsening of R6/1 motor function upon SRF overexpression (**Figure 64D**), a result supported by reduced speed of R6/1-SRF vs R6/1-GFP mice **(Figure 64F)**. Comparable results were obtained with both males and females **(Figures 64 C, E and G).** Dramatic alteration of motor function in R6/1-SRF mice prevented proper evaluation of procedural memory in a probe trial.

6.4. Evaluation of the effect of murine full length Srf overexpression on transcriptome

Behavioral analyses showed unexpected worsening of R6/1 motor function upon striatal overexpression of SRF. To get insight into underlying mechanism, we performed q-RT-PCR and RNAseq analyses using striatal tissues.

6.4.1. Expression of SRF and SRF target genes by q-RT-PCR

First, we checked Srf up-regulation after AAV injection in the striatum of R6/1 mice. Using qRT-PCR **(See materials and methods, p: 125)**, we found that *Srf* mRNA level is significantly increased in R6/1-Srf compared to WT-GFP and R6/1-GFP mice **(Figure 65 A, left)**. We further investigated the effect of Srf overexpression on Htt expression, the analysis shows no difference between the three experimental groups **(Figure 65A, left)**. Moreover, we checked mRNA level of Srf taget genes, the expression analysis of *Egr1* and *Fos* genes show no difference between WT and R6/1 mice, however *Arc* is significantly decreased after Srf overexpression compared to WT mice **(Figure 65B).** Nevertheless, we also checked the expression of some neuronal identity genes (Drd2, Darpp32, and Pde10a), their mRNA level is decreased in R6/1-mice and it is more significant in R6/1-Srf compared to WT-GFP **(Figure 65 C)**. These data show that Srf is well up-regulated in the striatum of injected R6/1 mice, however Srf target genes as well as the neuronal identity genes were not induced upon Srf overexpression.

We also investigated the expression of Srf and Srf target genes by RNAseq.

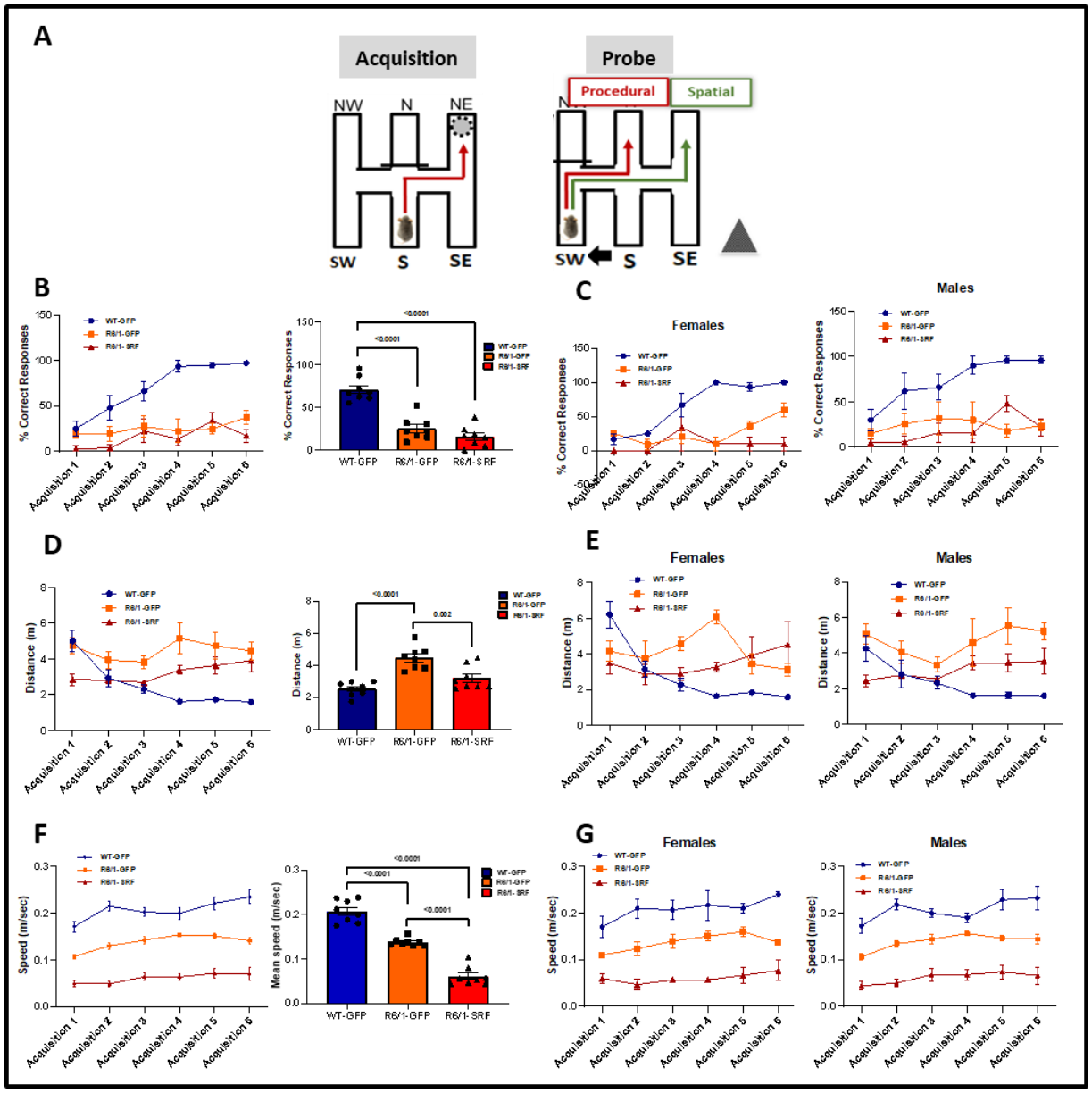

Figure 64: Evaluation of the effect of full length SRF overexpression on memory processing of R6/1 mice.

(A) The procedural memory was assessed by training the mice in the DH to find the hidden platform positioned in the NE arm from S arm (left) and checked for the used learning strategy by shifting the starting point to the SW arm and removing the platform (right). **(B)** Percentage of correct responses by the experimented mice during the acquisitions - on the left - (Two-way ANOVA with multiple repeats; multiple comparisons with Tukey's test: Acquisitions effect P<0.0001; genotype effect P<0.0001; Interaction Acquisitions x genotype P=0.0017. Average percentage of correct answers over all the acquisitions -right- (One-way ANOVA with multiple comparisons: Tukey's test). **(C)** Percentage of correct responses of male and female mice individually (Two-way ANOVA with multiple repeats; multiple comparisons with Tukey's test: Males, Acquisitions effect P=0.0023, genotype effect P<0.0001, interaction Acquisitions x genotype P=0.1090; Females, Acquisitions effect P<0.0001, genotype effect P<0.0001, interaction Acquisitions x genotype P=0.0012. **(D)**Distance traveled by the mice during the acquisitions -left- (Two-way ANOVA with multiple repeats; multiple comparisons with Tukey's test: Acquisition effect P=0.0285; genotype effect P<0.0001; interaction Acquisitions x genotype P<0.0001. Average distance traveled over all the acquisitions -right- (One-way ANOVA : Tukey's test: P<0.0001. **(E)** Distance covered by males and females mice (Two-way ANOVA with multiple repeats; multiple comparisons with Tukey's test: Males; Acquisitions effect P=0.2622, genotype effect P<0.0001, interaction Acquisitions x genotype P=0.0309. Females; Acquisitions effect P=0.0003, genotype effect P<0.0001, interaction Acquisitions x genotype P=0.0001. **(F)** The speed covered by the mice during Acquisitions (Two-way ANOVA with multiple repeats; multiple comparisons with Tukey's test: Males,

Acquisitions effect P=0.0023, genotype effect P<0.0001, interaction Acquisitions x genotype P=0.1090; Females, Acquisitions effect P<0.0001, genotype effect P<0.0001, interaction Acquisitions x genotype P=0.0012. **(G)** The speed of malesand females mice individually (One-way ANOVA; multiple comparisons by Tukey's test: Males, P=0.0002; Females P=0.0038. The data is represented by the mean ± SEM. Numbers: n =8 per group (**5** ♂, **3** ♀) for all tests.

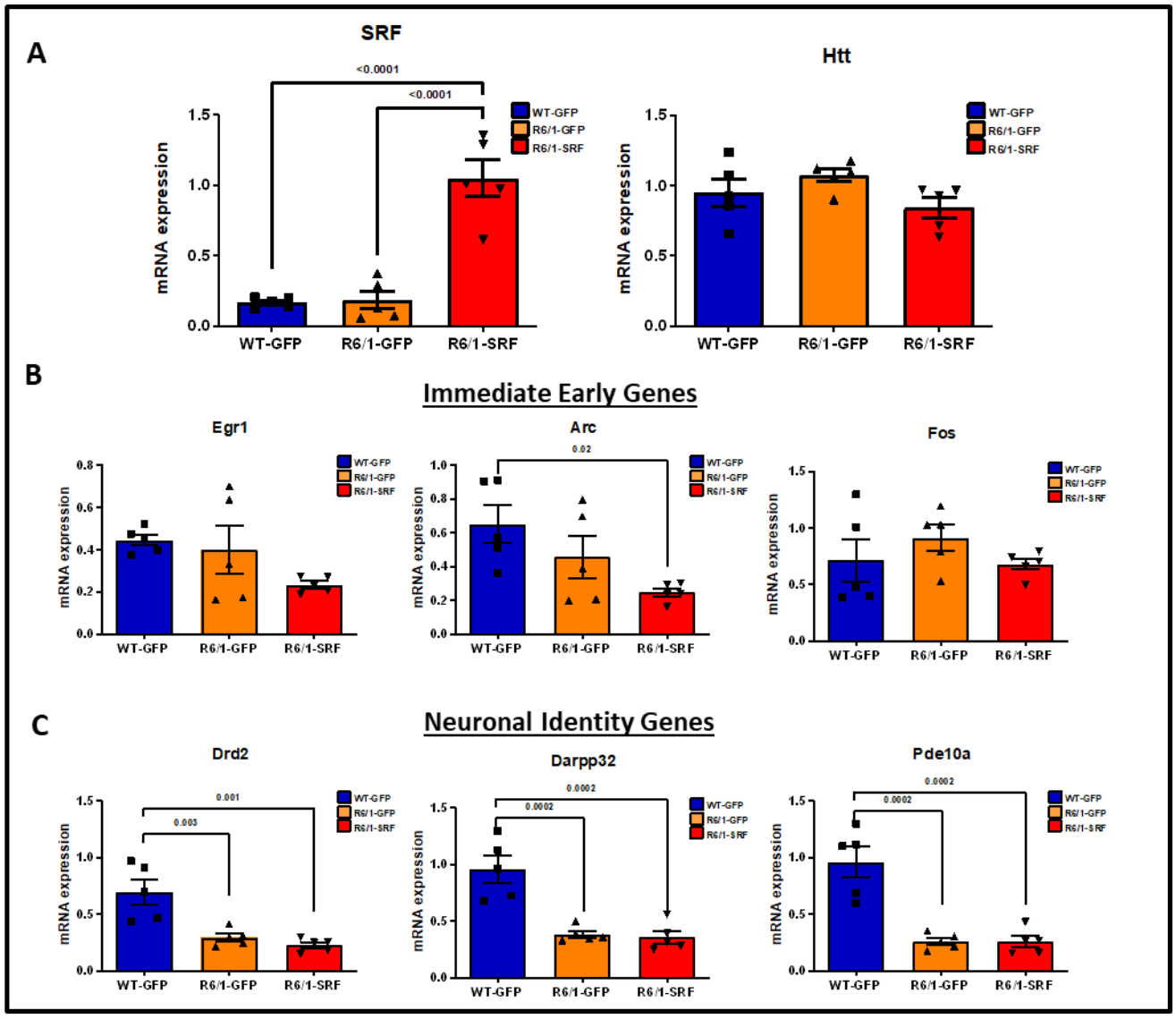

Figure 65: Gene expression analysis by qRT-PCR.

The expression of Srf, Htt, Srf target genes and striatal identity genes of WT and R6/1 mice. **(A)** mRNA levels of Srf and Htt . **(B)** The expression of Srf target genes, the immediate early genes: Egr1, Arc and Fos genes. **(C)** mRNA levels of neuronal identity genes : Drd2, Darpp32 and Pde10a. The analysis was performed by One-way ANOVA, multiple comparisons by Tukey's test and the significant adjusted p-value is shown on the graphs. The data is represented by the mean of the mRNA levels ±SEM (n=5).

6.4.2. RNA-seq: Quality analysis of sequenced samples

Five animals of each experimental group have been used for RNAseq analysis **(Figure 66A)**. Details of sequencing and bioinformatics analysis are shown in **(materials and methods p:x).** Principle component analysis (PCA) shows that genotype (R6/1 vs WT) and treatment (SRF vs GFP) explain both sample variability **(Figure 66B**).

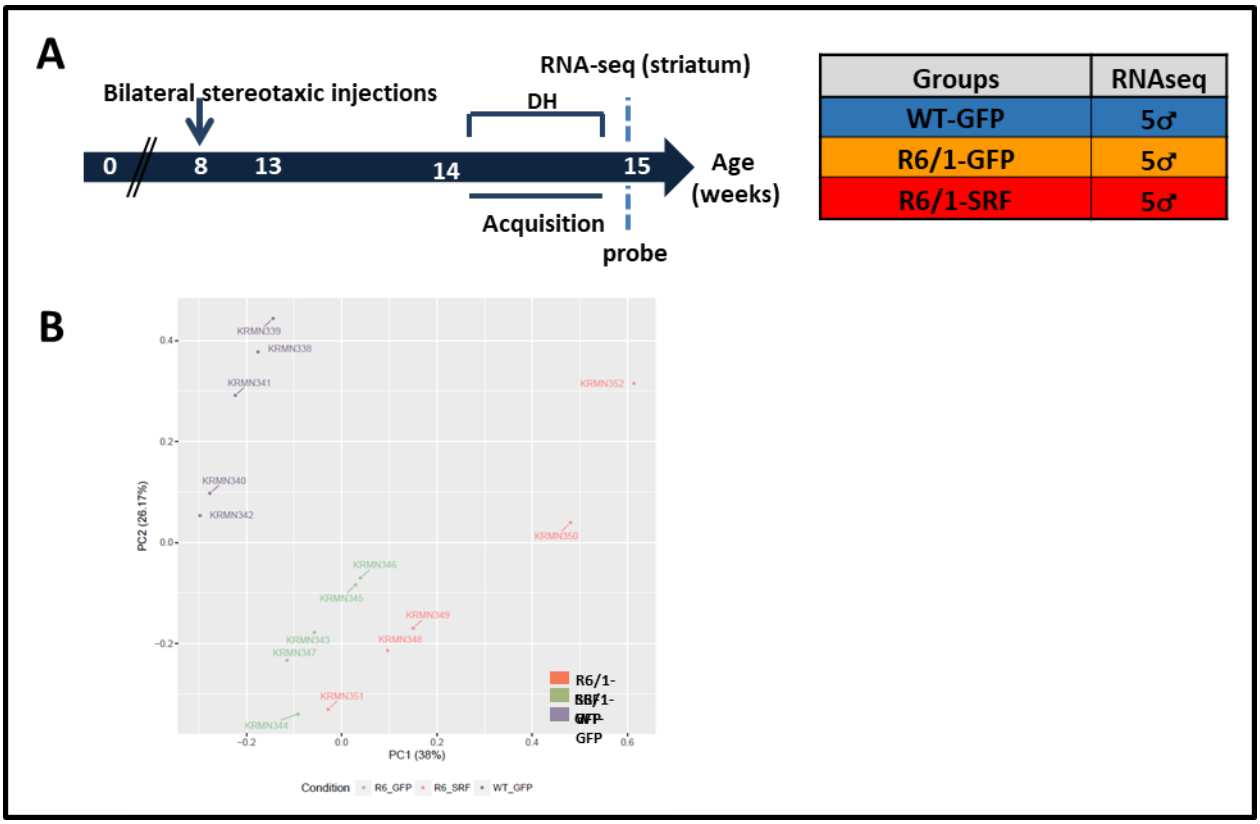

Figure 66: Experimental conditions and quality testing of the sequenced striatal samples.
(A) Schematic representation of study design and tissue collection for sequencing, in order to evaluate the effect of full length Srf overexpression on striatal transcriptome of R6/1 mice. **(B)** Principal component analysis (PCA) of sequenced samples of WT-GFP, R6/1-GFP and R6/1-SRF.

6.4.3. The Effect of murine full length Srf overexpression on R6/1 striatal transcriptomic signature.

As mentioned previously, **(introduction section;2.3.1. Transcriptional deregulations, p:48),** downregulated genes in HD striatum are enriched in neuronal identity genes, such as *Drd1, Drd2, Pde10a, Darpp32…* (Mayada Achour et al., 2015; Le Gras et al., 2017; Merienne et al., 2019). Additionally, our transcriptomic analysis during procedural memory process show that neural activity-regulated genes, including Srf itself and a number of Srf targets are abnormally regulated

in R6/1 mice **(See results section 1.Striatum-dependent memory is early impaired in HD R6/1 transgenic mice, p:131).**

We therefore aimed to determine whether striatal identity genes and/or Srf target genes would be rescued upon overexpression of Srf. First, with the help of bioinformaticians at LNCA, we performed differential expression analysis to assess the number of differentially expressed genes between the different groups **(See section 11.3 Sequencing of RNAs and analysis of the results in materials and methods, p:128).**

The analysis shows that 2422 and 1939 genes are respectively down- and up- regulated in the striatum of R6/1-GFP mice compared to WT-GFP **(Figure 67A)**. Surprisingly, the number of downregulated and upregulated genes (3140 and 3176 genes respectively) in R6/1-Srf mice compared to WT-GFP mice is greater than that of R6/1-GFP mice **(Figure 67A)**. The intersection analysis showed strong overlaps between deregulated genes in R6/1-SRF and R6/1-GFP mice **(Figure 67B)**. We analyzed the expression of Srf and Creb using RNA seq data, Srf is significantly decreased in R6/1-GFP vs WT-GFP, while its expression is significantly increased in R6/1-Srf when compared to both WT-GFP and R6/1-GFP mice. However, Creb expression is increased in both R6/1-GFP and R6/1-Srf (vs WT-GFP) **(Figure 67C)**. Furthermore, Gene ontology analysis show that differentially expressed genes (DEG) in R6/1-SRF vs WT-GFP and R6/1-GFP vs WT-GFP comparisons were comparable. Notably, down-regulated genes were highly significantly enriched in genes implicated in neuronal function **(Figure 67D)**. Finally, typical striatal identity genes, neuronal activity-regulated genes and genes of the actin cytoskeleton system remained significantly decreased in R6/1 striatum, despite SRF overexpression, however AP-1 related genes show no expression difference among the groups **(Figure 67D)**. Together, these data show that overexpression of full length SRF does not rescue HD striatal transcriptome.

Remarkably, SRF overexpression in R6/1 striatum exacerbated cell cycle/DNA replication signature associated with up-regulated genes **(Figure 68).** For example, *Cdk2*, *Cdk6*, *Cdkl3* and *ezh2* involved in cell cycle machinery are overexpressed in R6/1-GFP and R6/1-Srf, more so in R6/1-Srf.

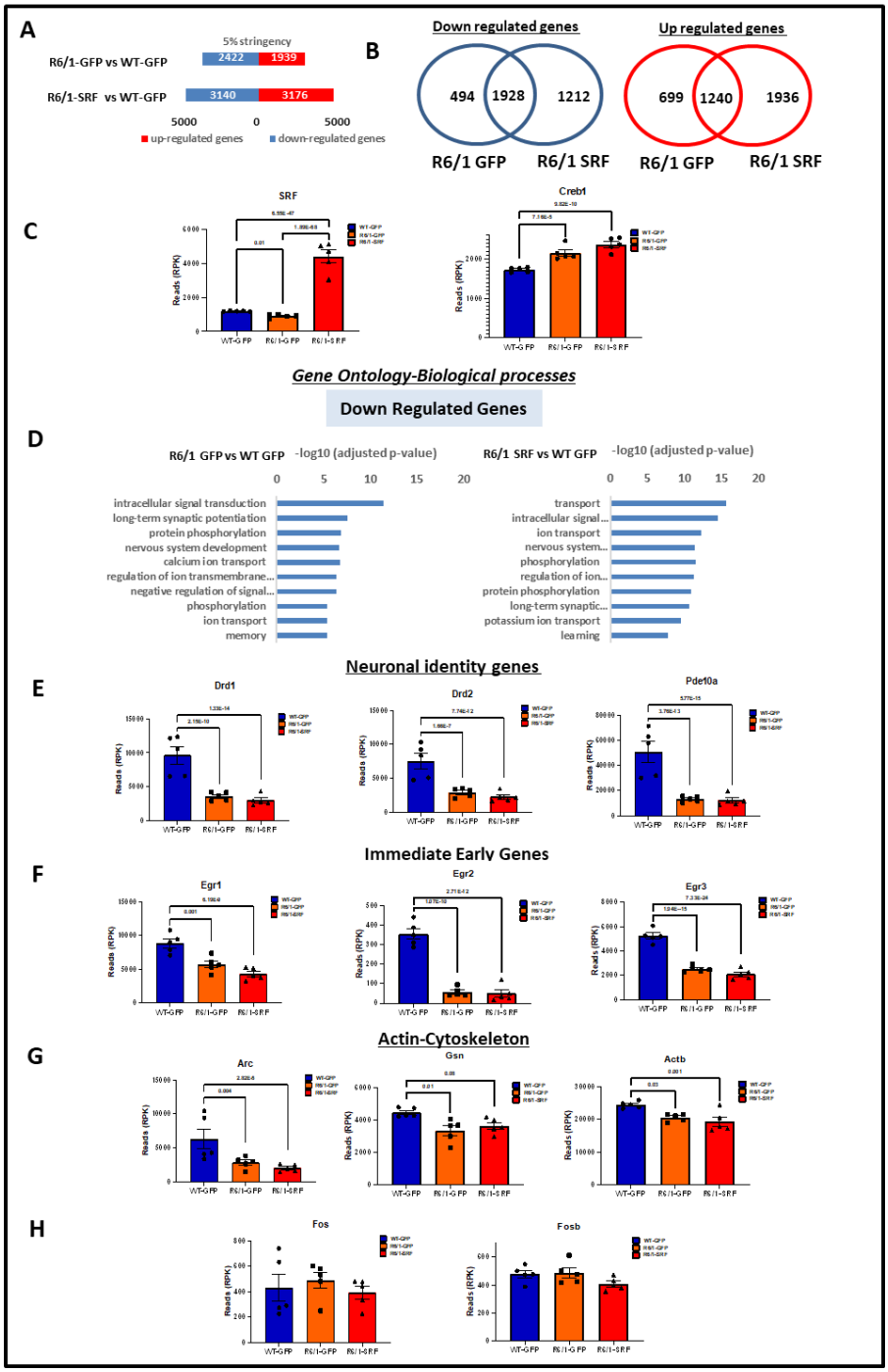

Figure 67: The effect of SRF overexpression on transcriptional signatures of the striatum of R6/1 mice.
Gene lists were selected with log (FC) <0 or log (FC)> 0 and an adjusted p-value <0.05. **(A)** Differentially expressed genes: The number of down-regulated and up-regulated genes in the striatum of R6/1-GFP and R6/1-SRF mice compared to WT-GFP mice (Comparisons: R6/1-GFP vs WT-GFP; R6/1-SRF vs WT-GFP). **(B)** Venn diagrams of the intersection of the up- and down- regulated genes in the striatum of R6/1-GFP and R6/1-SRF mice compared to WT-GFP mice. **(C)** SRF and Creb1 mRNA levels **(D)** Functional enrichment and gene ontology analysis of down-regulated genes in the striatum of R6/1-GFP and R6/1-SRF mice compared to WT-GFP mice. **(E)** Gene expression of striatal identity genes. **(F-G)** Examples of down regulated SRF target genes; **(F)** Immediate early genes. **(G)** Genes of the actin- cytoskeleton system. **(H)** AP-1 (Fos and Fosb) gene expression. Functional analysis was

performed with the R Cluster Profiler library and the terms of the Gene Ontology database have been analyzed by DAVID. The represented gene expression analysis was performed by One-way ANOVA and the multiple comparisons were done using Tukey's test; significant adjusted p-values are shown on the graphs.

To complete the analysis, we then evaluated the direct effect of *Srf* overexpression on the transcriptome of R6/1 mice by comparing striatal transcriptomes of R6/1-Srf mice and R6/1-GFP. Differential expression analysis shows 755 downregulated and 1072 upregulated genes upon *Srf* overexpression in R6/1 mice **(Figure 69A)**. Functional enrichment analysis reveals that downregulated genes are enriched in biological processes related to neuronal function and learning, however, upregulated genes present cell-cycle and DNA replication signature **(Figure 69B).** For example, representative genes of cell cycle machinery, such as Npm1, Hes6 and Ppp2r1b genes, involved in cell cycle machinery are overexpressed in R6/1-GFP and R6/1-Srf, more so in R6/1-Srf are significantly upregulated in R6/1-Srf compared to WT-GFP and R6/1-GFP **(Figure 69C).**

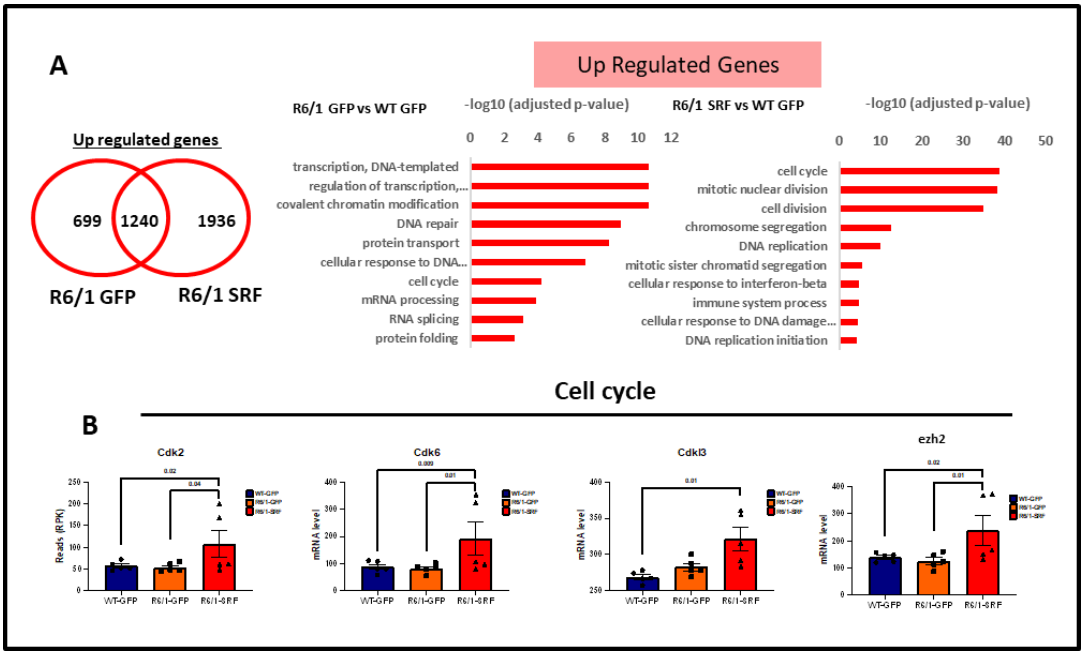

Figure 68: The effect of SRF overexpression on transcriptional signatures of the striatum of R6/1 mice, up-regulated genes.

(A) Functional enrichment and GO analysis of up-regulated genes in the striatum of R6/1-GFP and R6/1-SRF mice compared to WT-GFP mice. **(B)** Examples of up-regulated genes associated with cell cycle. The functional analysis was performed with the R Cluster Profiler library and the terms of the Gene Ontology database were being analyzed by DAVID. The represented gene expression analysis was performed by One-way ANOVA and the multiple comparisons were done using Tukey's test; significant adjusted p-values are shown on the graphs.

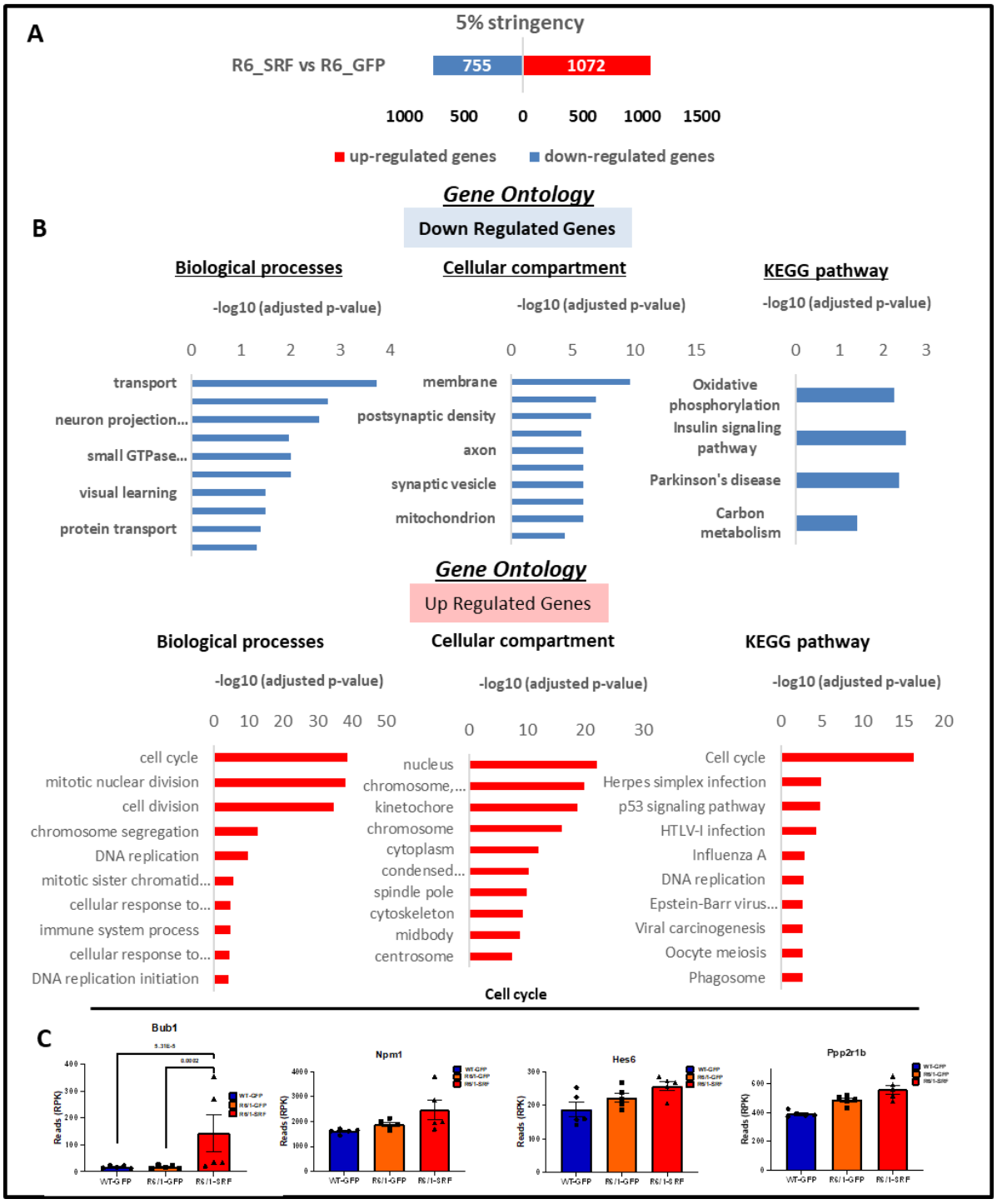

Figure 69: Modulation of striatal transcriptome of R6/1 mice.

Gene lists were selected with log (FC) <0 or log (FC)> 0 and an adjusted p-value <0.05. **(A)** Differentially expressed genes: The number of down- and up- regulated genes in the striatum R6/1-SrF mice vs R6/1-GFP mice. **(B)** Functional enrichment analysis of down- and up- regulated genes in the striatum of R6/1-SRF mice compared to R6/1-GFP mice. **(C)** Examples of cell cycle and DNA replication genes upregulated in R6/1-Srf. The analysis was performed by analyzing the terms of the Gene Ontology databases (Biological Process –BP-; Cellular Component –CC-) and KEGG pathways using DAVID.

These results indicate that *Srf* overexpression didn't rescue the expression of downregulated genes in R6/1 striatum, suggesting that the injected AAV-Srf construct containing the murine full length *Srf* gene, under the effect of the PGK promoter, was not efficient to validate the initial hypothesis of inducing the expression of Srf target genes in this attempt. Moreover, the overexpression of the cell cycle genes might be considered as a compensatory proliferation mechanism versus the HD mutation in R6/1 mice.

We then determined whether SRF and CREB target genes were globally impaired in the striatum of WT and R6/1 mice upon full length Srf overexpression. Also, we checked the regulation of memory genes with sustained expression during memory process (as defined in Lotz et al. in prep). We used again gene lists from published data where the authors determined SRF and CREB target genes during neuronal activation by using ChIPseq on primary cultures of cortical neurons (T.-K. Kim et al., 2010b).

The intersection of these gene lists with the Srf full length-RNAseq data is represented in **Figure 70 A-C**. The boxplots show z-scores computed from RNAseq data generated using the striatum of WT-GFP (represented by WT), R6/1-GFP (represented by R6/1), and R6/1-Srf (represented by R6/1-DRF full) mice. The data shows that SRF target genes are globally reduced in R6/1 vs WT mouse striatum, and they don't change after full length Srf overexpression in R6/1 SRF full mice compared to R6/1 mice **(Figure 70A)**. In contrast, CREB target genes are globally increased in R6/1 compared to WT samples, and they are induced in R6/1 SRF full mice after full length Srf overexpression **(Figure 70B)**. Memory genes tended to be reduced in R6/1 when compared to WT mice and their expression is further decreased in R6/1 SRF compared to WT and R6/1 mice. **(Figure 70C)**. These data support that SRF-dependent regulation is impaired in R61 mice striatum and suggest that full length Srf overexpression worsens transcriptomic signatures of HD R6/1 mice.

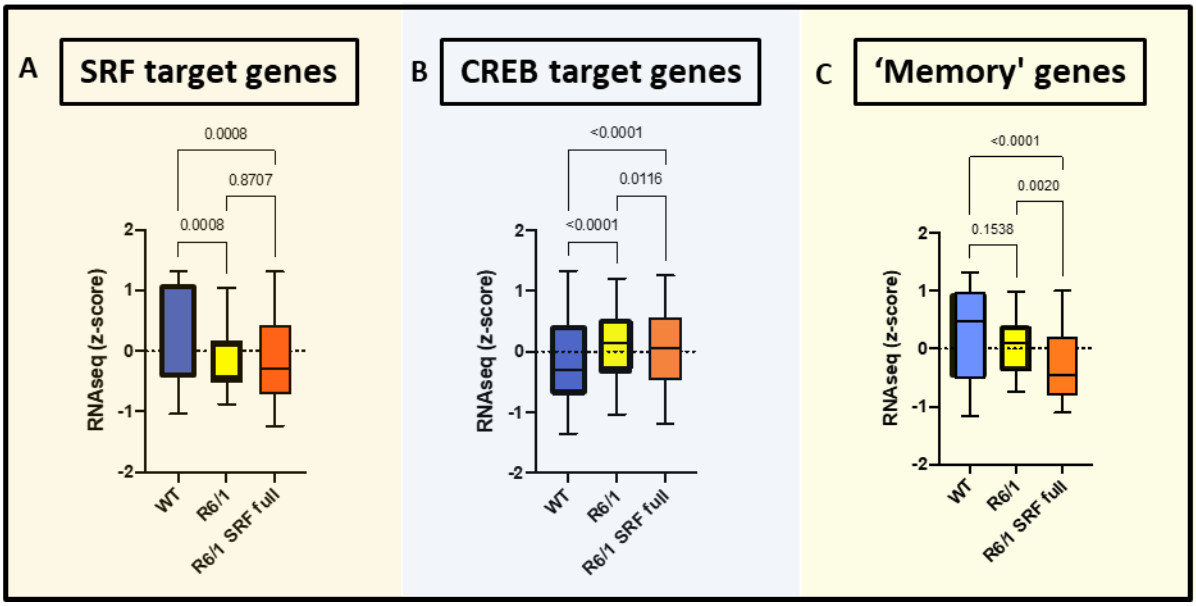

Figure 70: Global gene expression analysis after full length Srf overexpression in the striatum of R6/1 mice.
The boxplots show z-scores computed from RNAseq data generated using the striatum of WT-GFP (WT), R6/1-GFP (R6/1) and R6/1-Srf (R6/1 full). SRF and CREB target genes are retrieved from Greenberg et al. 2010 and intersected with our RNAse data. Global gene expression of: **(A)** SRF target genes. **(B)** CREB target genes. **(C)** Sustained expressed memory genes at 2 and 5 days of learning during the DH. Data was analyzed using Kruskal-Wallis test, adjusted p-values for multiple comparisons were done with Benjamini-Hochberg method.

6.5. Effect of Srf overexpression on mutated HTT aggregates in the striatum of R6/1 mice

We hypothesized that worsening of motor function in R6/1 mice overexpressing SRF might correlate with increased aggregation of mutated HTT. We therefore performed immunohistological analysis of EM48 staining, **using steroeolgy approach (see materials and methods p:X)** to count the number and size of aggregates in R6/1-SRF and R6/1-GFP mice. **(Figure 71A, B)**. The analysis shows that the number of aggregates in the striatum does not changed between R6/1-SRF vs R6/1-GFP mice **(Figure 71C).** Moreover, Srf overexpression has no effect on the length of mutated aggregated as shown in **Figure 71D**).

This indicates that full length Srf overexpression didn't affect the aggregation of mutant HTT.

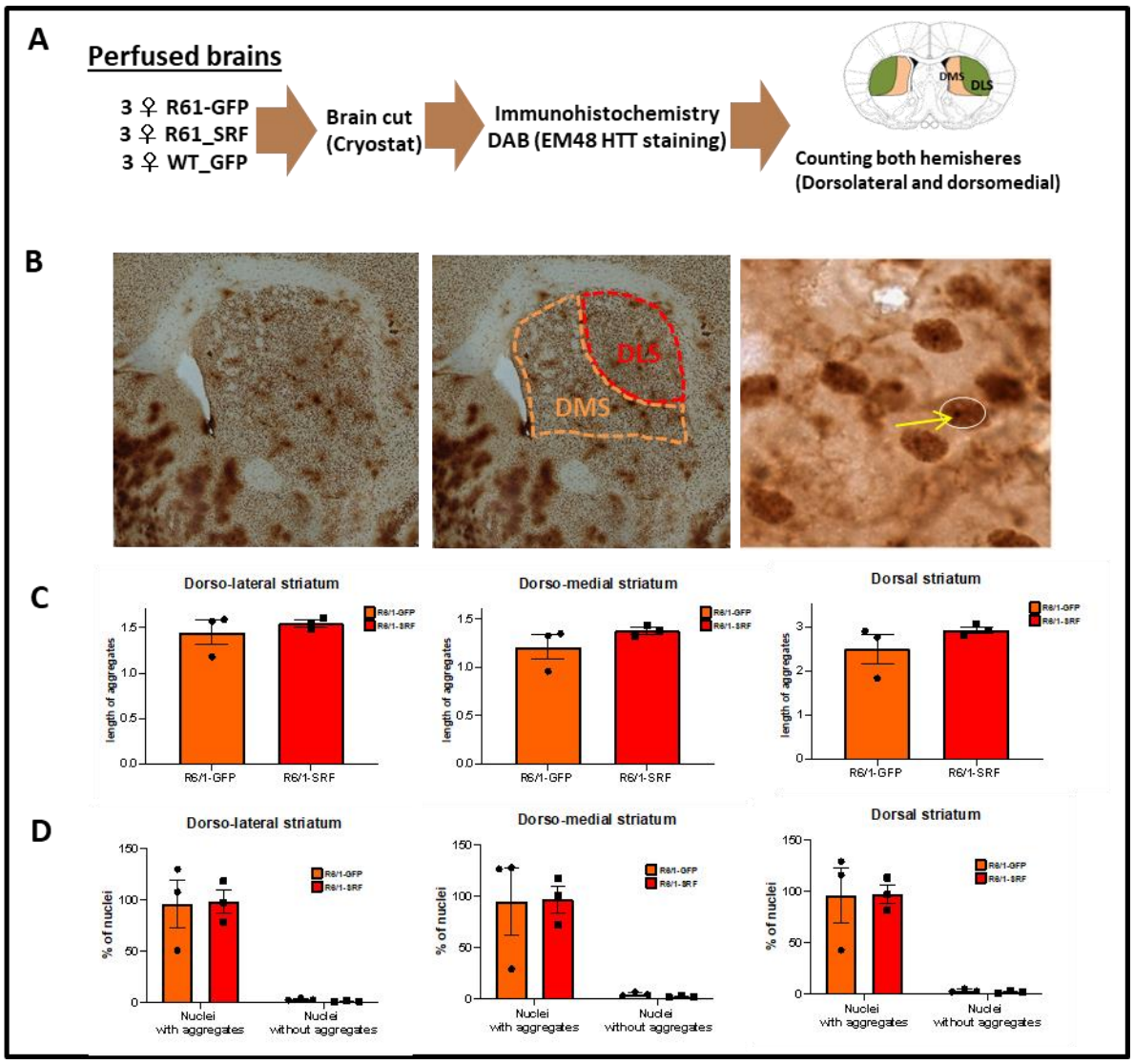

<u>Figure 71:</u> Evaluation of the effect of SRF overexpression on mutated HTT aggregates in the striatum of R6/1 mice. The effect of SRF overexpression on mutated HTT aggregates in the striatum of R6/1 mice was analyzed by stereological counting. **(A)** Scheme of the experimental design and tissue preparations for stereology analysis. **(B)** Example of EM48 protein labeling in the nuclei of striatal cells (Dorsal and medial) of R6/1 mice. The yellow arrow indicates the counted mutated HTT aggregates. Scale: 50µm. **(C)** The Percentage of mutated HTT aggregates counted in dorsolateral and dorsomedial striatum of R6/1-SRF mice compared to that of R6/1-GFP mice. **(D)** The length of aggregates in the dorsolateral, dorsomedial striatum of R6/1-SRF mice compared to that of R6/1-GFP mice. The data shown in dorsal striatum is the sum of both of the dorsolateral and dorsomedial striatum. The % of nuclei with aggregates was analyzed by Two-way ANOVA; interaction Genotype x percentage of aggregates DLS p-value=0.89, DMS p-value=0.88, DS p-value=0.94. The analysis of the length of the aggregates was performed using the student t.test; DLS p-value=0.51, DMS p-value=0.27 and DS p-value=0.27.

7. Murine full length Srf overexpression in WT mice

We asked whether worsening of motor function and lack of up-regulation of SRF target genes upon SRF overexpression in R6/1 striatum were disease-specific. To address this question, the striatum of WT mice has been injected with AAV-SRF and AAV-GFP vectors, 10 (5 males & 5 females) and 4 (3 males & 1 females) WT mice were injected with AAV-SRF and AAV-GFP constructs, respectively. Additional 4 non-injected WT mice (3 males & 1 female) were included in the analysis **(Figure 72A)**.

Locomotor activity and motor coordination were assessed 4 weeks after injection. Procedural memory was then tested using the Double-H maze. Brain tissues were collected 1h after the probe test of the DH. **(Figure 72B).**

To assess the effect of SRF overexpression at protein level, one striatum of each mouse was used to prepare total protein lysates and analyzed by Western Blot. Representative blot shows that all animals, except one, were successfully injected **(Figure 72C).**

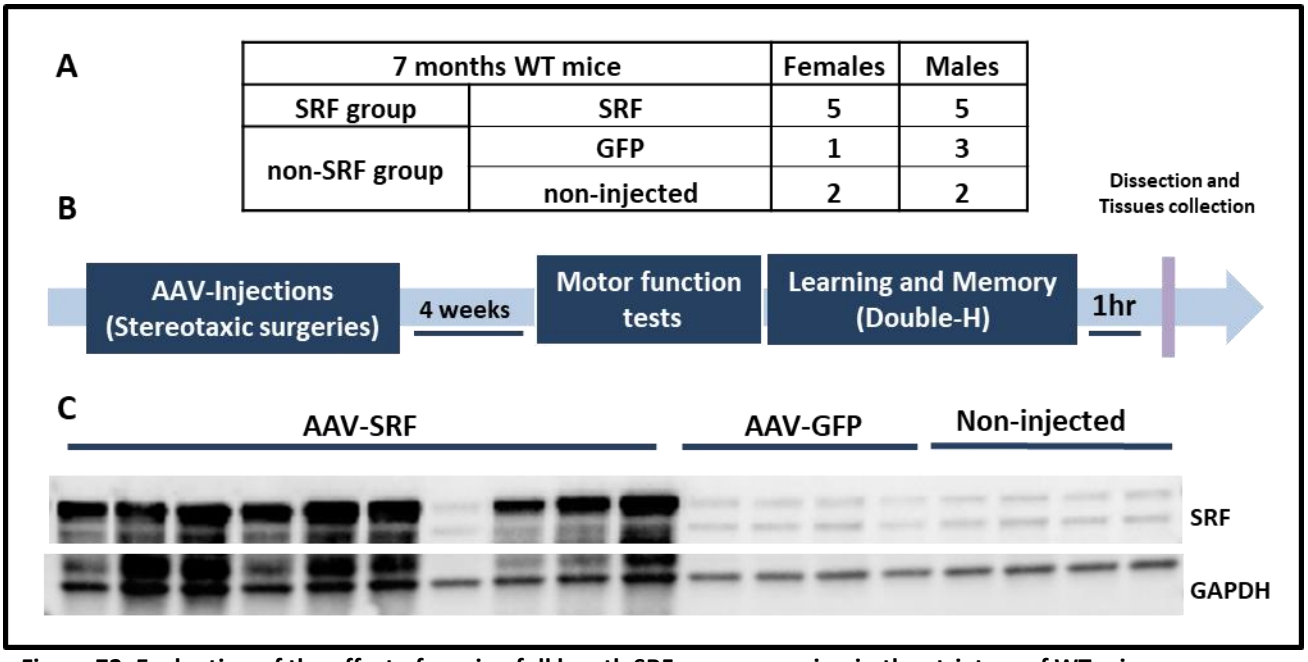

Figure 72: Evaluation of the effect of murine full length SRF overexpression in the striatum of WT mice.
(A) The experimental groups and the number of animals used to assess the effect of Srf overexpression in the striatum of WT mice. **(B)** Scheme of the study design to assess the effect of SRF overexpression in WT mice, **(C)** Representative Western blots of Srf expression to validate the efficiency of Srf injection in the striatum of WT mice. The membrane was also incubated with an anti-GAPDH Anti body.

7.1. Evaluation of the effect of Srf overexpression on motor performance of WT mice

In order to evaluate the effect of Srf overexpression on motor performance of WT mice, we assessed their spontaneous locomotor activity using actography. The activity of the mice was recorded for 24 hours; day (7 a.m.-7 p.m.) and night (7 p.m.-7 a.m.) **(Figure 73A)**.

The actography analysis shows that the activity of the WT mice of both groups is increased during the night (**Figure 73A).** The mean of day and night activity is represented by the number of moves per hour for each experimental group. The data show no significant difference in the activity between WT-Srf mice and control mice during day or night **(Figure 73B).**

Then, we evaluated whether SRF overexpression affects motor coordination of WT mice. Using the bar test, we analyzed the latency to cross the bar. The data shows that there is no significant difference between WT-Srf and control groups **(Figure 73C)**.

We also tested motor coordination using accelerating rotarod. Overall, the analysis shows no significant difference between WT-Srf and control mice, despite a tendency to decreased performance in WT-Srf mice (**Figure 73D-left).**

7.2. Evaluation of the effect Srf overexpression on procedural memory in WT mice

We then investigated the effect of Srf overexpression on procedural memory in WT mice, using the Double-H maze. During acquisition, the distance to reach the platform and % of correct responses were not different between WT-Srf and control mice **(Figure 73E and F)**. However, the latency to reach the platform and the speed of WT-Srf mice were significantly reduced compared to that of control mice (**Figure 73G and H)**.

During the probe test, the distance traveled and the speed of mice were both significantly decreased in WT-Srf compared to control mice **(Figure 73I and J)**.

We also investigated the effect of Srf overexpression on the strategy followed by each group of mice during the probe test. We showed that 75% of the control mice have visited the procedural arm as a first intention, however, WT-Srf mice visited less this arm. Moreover, they visited randomly the other arms of the maze **(Figure 73K).**

These data indicate that overexpression of SRF in the striatum of WT mice also impacts motor function, though to lesser extent than in R6/1 mice, which could possibly affecting their learning strategy. In addition, we cannot exclude that procedural memory is also impaired upon overexpression of full length SRF.

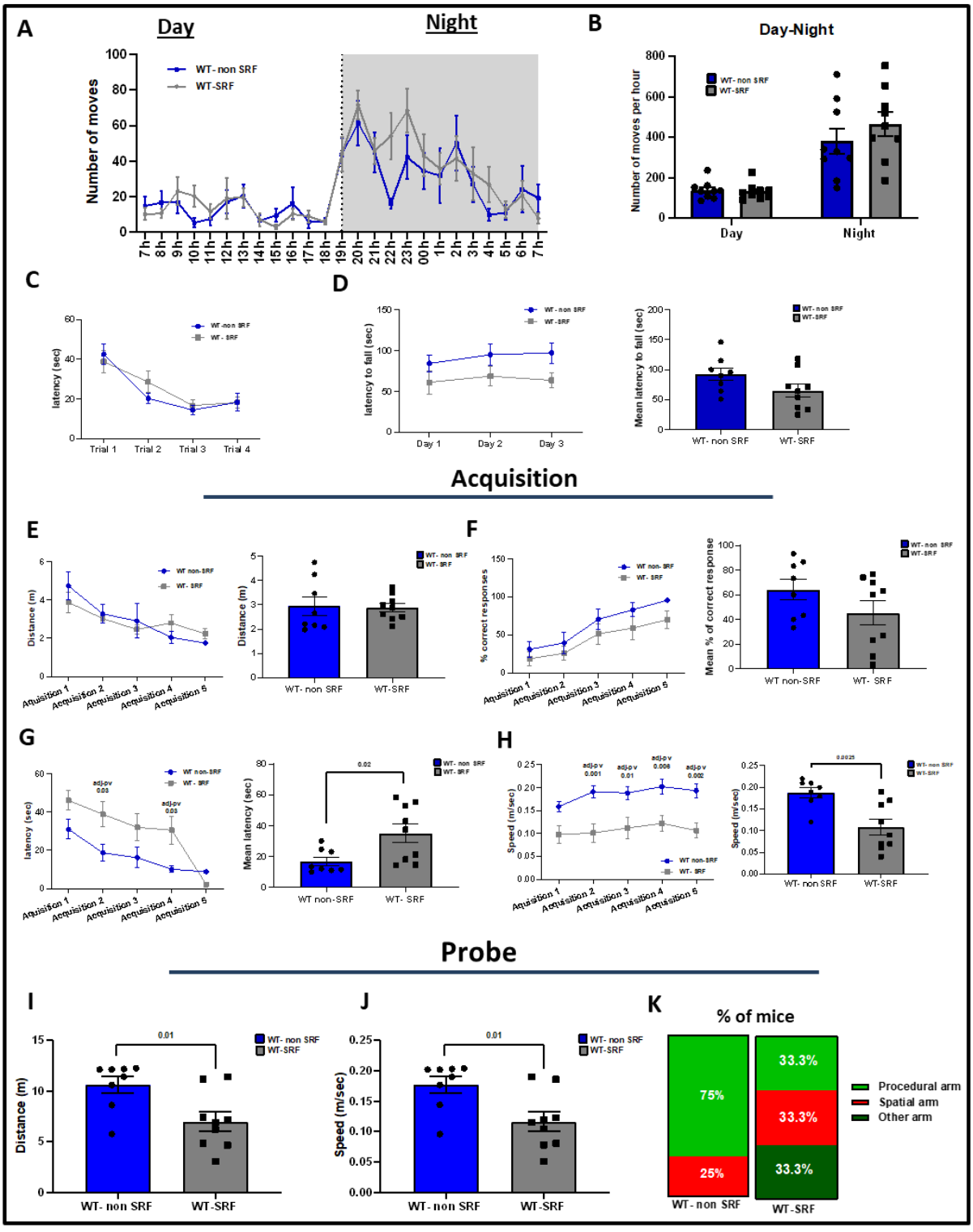

Figure 73: Evaluation of the effect of full length SRF overexpression on motor performance and memory of WT mice.

(A-B) Actography analysis to evaluate the effect of full length Srf overexpression on spontaneous locomotor activity of WT mice. **(A)** Representation of the number of moves of the mice in their cage over 24 hours: Day (7 a.m.-7 p.m.) and night (7 p.m.-7 a.m.)(Two-way ANOVA with multiple repeats: Days effect P<0.0001; Genotype effect P=0.1039; interaction Day x Genotype

P=0.6273. **(B)** Average number of moves of WT-Srf and WT-non Srf mice during the day and night. The analysis was performed using student T.test with p-value=0.7563. (C-D) Evaluation of the effect of SRF overexpression on motor coordination of WT mice with bar test **(C)** and rotarod test **(D-E)**. **(C)** The latency to cross the bar (Two-way ANOVA with multiple repeats: the multiple comparisons were done by Sidak's test: Trial effect P<0.0001, Treatment effect, interaction Trial x Treatment 7 P=0.5494. (D) Left: The latency to fall from the rotarod during the 3 days of learning in the rotarod (Two-way ANOVA with multiple repeats; where multiple comparisons were done by Tukey's test: Day effect p=0.7148, Genotype effect p=0.0064; interaction Day x Genotype p=0.9070. Right: The mean latency to fall of the 3 days of training (student T.test; p-value=0.0865). **(E)** Left: Distance crossed by each group of mice during the Acquisition phase (Two-way ANOVA with multiple repeats; multiple comparisons were done by Sidak's test: Acquisition effect p-value <0.0001, Treatment effect p-value=0.8384, interaction Acquisition x Treatment p-value=0.4280. Right: Mean distance of all the acquisitions crossed by WT-Srf and WT-nonSrf (student T.test; p-value=0.8847). **(F)** The percentage of correct responses of each mice group while looking for the hidden platform during Acquisition phase (Two-way ANOVA with multiple repeats; multiple comparisons were done by Sidak's test: Acquisition effect p-value <0.0001, Treatment effect p-value=0.0123, interaction Acquisition x Treatment p-value=0.9713. **(G)** The latency of each group to reach the hidden platform during the Acquisition phase (Two-way ANOVA with multiple repeats; multiple comparisons were done by Sidak's test: Acquisition effect p-value <0.0001, Treatment effect p-value=0.0002, interaction Acquisition x Treatment p-value=0.0622. **(H)** Left: The speed of each group of mice during the Acquisition phase (Two-way ANOVA with multiple repeats; multiple comparisons were done by Sidak's test: Acquisition effect p-value=0.3878, Treatment effect p-value<0.0001, interaction Acquisition x Treatment p-value=0.9237. Right: The mean speed of Wt-Srf and Wt-nonSrf over all the acquisitions (student T.test with a p-value=0.0025). **(I)** Distance crossed during the probe test (student T.test with a p-value=0.011). (J) The speed of Wt-Srf and Wt-nonSrf mice during the probe test (student T.test with a p-value=0.0109). (K) First arm visited by each group as a first intention during the probe test. The data is represented by the mean ± SEM, n = 9 for WT-SRF and n=8 for the WT-control group.

8. AAV-Srfvp16 overexpression in the striatum of WT and R6/1 mice

Above analyses show that overexpression of full length SRF in mouse striatum, particularly in the striatum of HD R6/1 mice, is detrimental. We reasoned that signaling pathways implicated in SRF regulation might not be properly regulated in this situation, and therefore decided to use another construct, based on previous publications (Beck et al., 2012; Ohrnberger et al., 2015; Sandström et al., 2011; Schratt et al., 2002; Stern et al., 2012) **(Figure 74A**). Specifically, in collaboration with MIRCen (Dr. E. Brouillet and A. Bemelmans, we produced an AAV-based construct allowing expression of SRF DNA binding domain fused to VP16 trans-activator domain (AAV-Srfvp16). As a control, we produced an AAV construct expressing VP16 (AAV-vp16).

However, due to COVID-19 sanitary crisis and the lockdown in March 2020, these vectors could not be verified on time, and due to the difficulty to delay the experiments with R6/1 mice, we decided to inject R6/1 (and WT) mice and perform subsequent behavioral and molecular analyses without prior characterization.

In order to evaluate the effect of the AAV10-Srfvp16 overexpression on motor performance of WT and R6/1 mice, we bilaterally injected AAV10-Srfvp16 and AV10-vp16 viral vectors at 2 different sites using stereotaxic approach; the experimental design is shown in **Figure 74**. For this

purpose, four groups of mice were used, 10 WT mice (5 Females and 5 males) and 9 R6/1 mice (5 Females and 4 males) have been injected with the AAV-SRFvp16 vector representing the WT-SRFvp16 and R6/1-SRFvp16 groups, respectively. Another 9 WT mice (4 Females and 5 males) and 9 R6/1 mice (5 Females and 4 males) corresponding to WT-vp16 and R6/1 vp16 groups, were injected with the control AAVvp16 construct **(Figure 74B)**.

The mice were injected at pre-symptomatic stage (8 weeks), motor coordination functions were assessed starting from 12 weeks (symptomatic stage) using a battery of behavioral experiments followed by memory assessment using the DH. Due to technical issues, locomotor activity was assessed at 15 weeks. After that, the animals were dissected and brain tissues were collected **(Figure 74C)**.

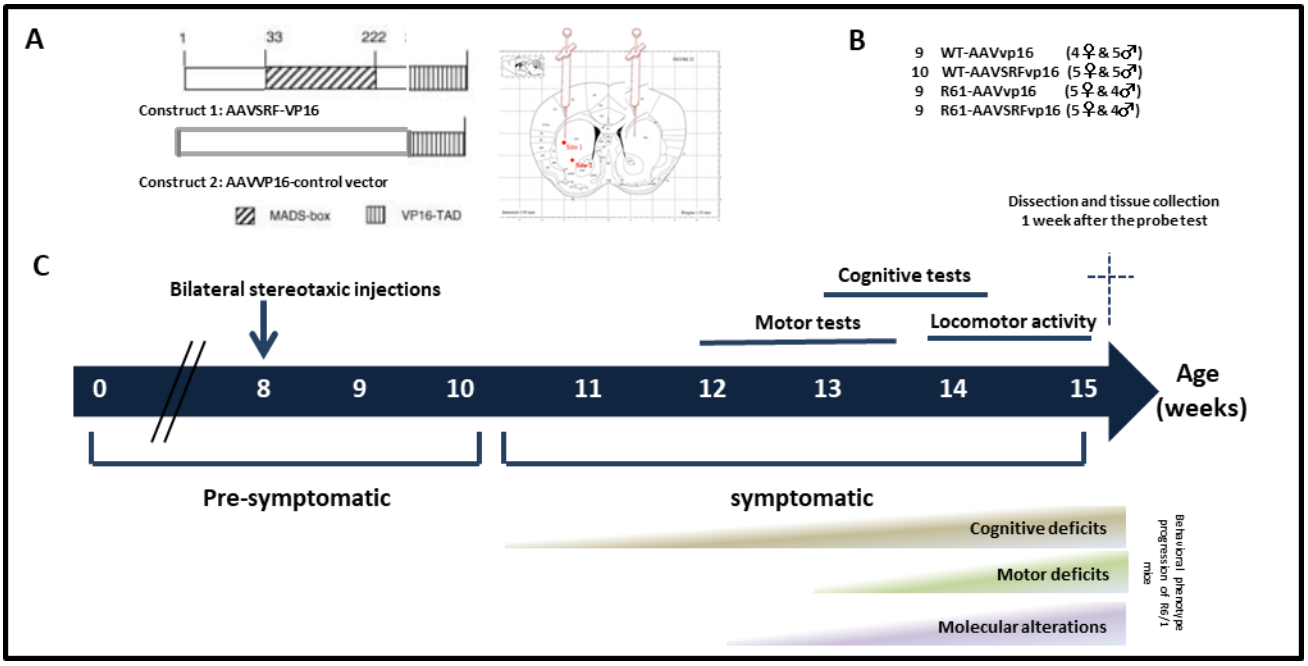

Figure 74: Scheme of the study design to assess the effect of AAVSrfvp16 overexpression in the striatum of WT and R6/1 mice.

(A) Scheme of the AAV construct containing Srf-DNA binding domain and vp16 transactivation domain. **(B)** The experimental groups and the number of animals used for the different injections into the striatum of WT and R6/1 mice. **(C)** Mice were injected at pre-symptomatic stage; motor coordination and function were assessed at 12 weeks (symptomatic stage). The animals were dissected and the tissues were collected after one week of the probe test of the DH.

8.1. Evaluation of the effect of AAV-Srfvp16 overexpression on spontaneous locomotor activity of WT and R6/1 mice using actography.

We Evaluated the effect of SRFvp16 overexpression on spontaneous locomotor activity of WT and R6/1 mice using actography. Actography analysis shows an increase of activity in night versus day **(Figure 75A).** The mean of day and night activity is represented by the number of moves per hour of each experimental group. The data shows no significant difference between the groups except for the nigh activity of R6/1-vp16, which is significantly decreased when compared to WT-Srfvp16, while R6/1-Srfvp16 vs WT-Srfvp16 night activities are not different, suggestion mild effect of Srfvp16 on R6/1 spontaneous activity **(Figure 75B).**

These results suggest that SRFvp16 didn't affect the locomotor activity of both WT and R6/1 mice.

8.2. Evaluation of the effect of AAV-Srfvp16 overexpression on WT and R6/1 mice motivation and spontaneous activity.

In order to investigate the effect of Srfvp16 overexpression on innate behavior and motivation, mice were assessed using the Nesting test **(See section 5.4.1 Nesting test in materials and methods, p:114)**. For each mouse, we measured three different scores at 3 h, 5 h and 24 h after starting the experiment. The mean value of each score over the three time points was represented in **Figures 74 (C-E)**. The results were comparable between WT and R6/1 mice regarding the mean score of quality **(Figure 75C)** and score of motivation, where the latter showed a trend to increase in R6/1-Srfvp16 mice vs R6/1-vp16 **(Figure 75D)**. However, mean score of complexity is significantly reduced in R6/1-vp16 and R6/1-Srfvp16 mice compared to WT-vp16 and WT-Srfvp16 respectively and is not increased in R6/1-SRFvp16 vs R6/1-vp16. (**Figure 75E).**

8.3. Evaluation of the effect of AAV-Srfvp16 overexpression on spontaneous activity of WT and R6/1 mice in the openfield

We also tested the effect of Srfvp16 overexpression on spontaneous activity of WT and R6/1 mice in the open field **(See section 3.2. Open field test in materials and methods, p:110) (Figure 745F-**

J). Overall, the analysis show that the mean time mobile **(Figure 75F)**, the mean speed **(Figure 75G)**, the mean distance **(Figure 75H)** and the mean number of rears **(Figure 75I)** are all significantly lower in R6/1-vp16 and R6/1-

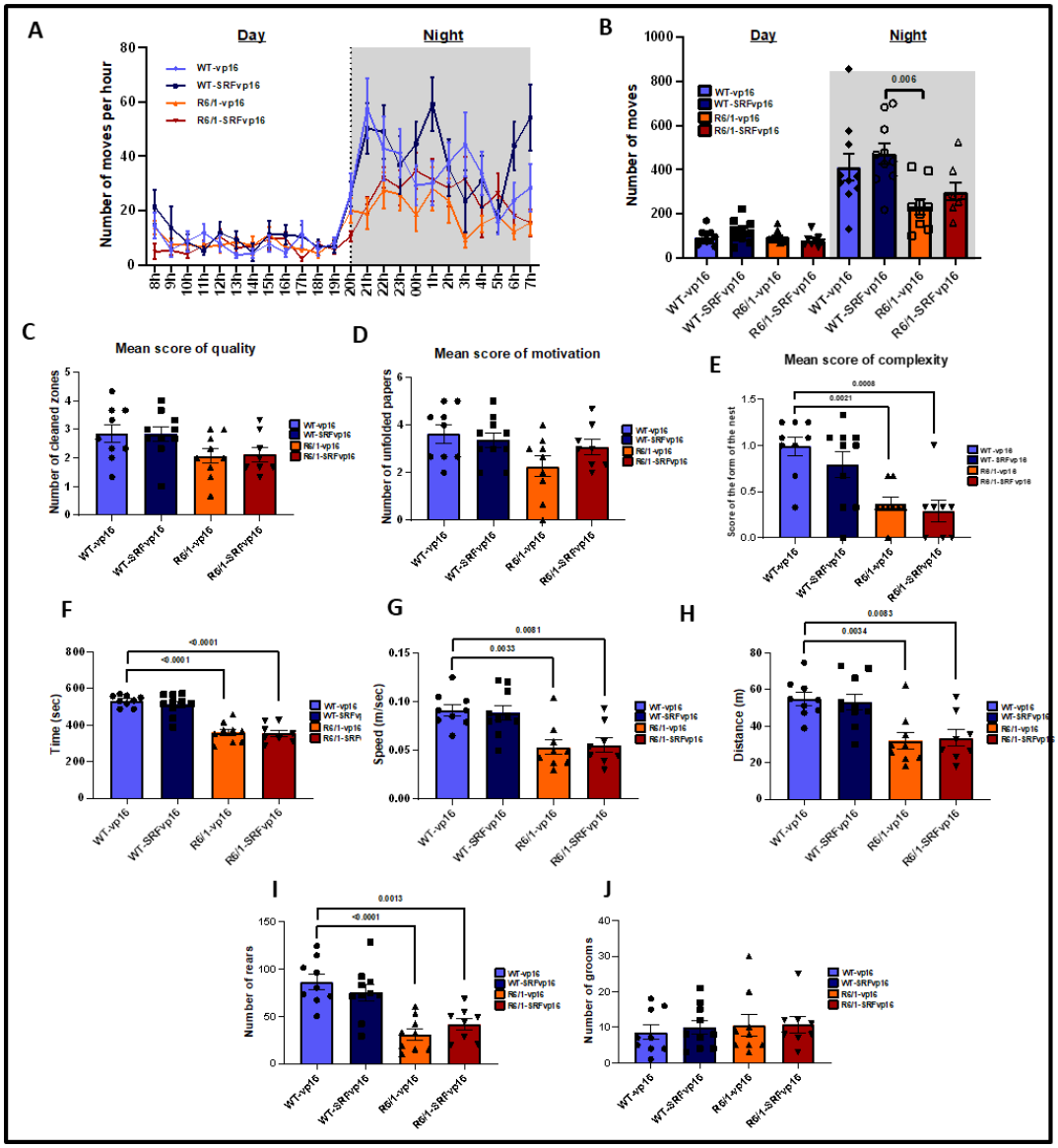

Figure 75: Evaluation of the effect of SRF overexpression (AAV-SRFvp16) on spontaneous locomotor activity and the innate/motivation behavior of WT and R6/1 mice.

(A-B) Evaluation of the effect of SRF overexpression on spontaneous locomotor activity of WT and R6/1 mice in actography. (A) Representation of the number of moves of the mice over 24 hours; 1day (8.am. - 8 p.m.) and 1 night (8.p.m. - 8 a.m.) (Two-way ANOVA with multiple repeats; the multiple comparisons were done using Tukey's test: Hours effect P-value <0.0001; genotype effect P-value <0.0001; interaction Hours x genotype P-value =0.003. **(B)** Average number of moves of the mice during the day and night (One-way ANOVA: Multiple comparisons with the Tukey's test; Day: P=0.1450, Night: P=0.0060). **(C-E)** The mean scores of nesting test to assess the effect of SRF overexpression on the innate behavior of WT and R6/1 mice. The analysis was performed by One-way ANOVA, multiple comparisons were done by Tukey's test and the adjusted p-values are represented on the graphs. **(C)** Mean score of quality (P=0.0828) **(D)** Mean score of motivation (P=0.0618). **(E)** Mean score of complexity (P=0.0002). **(F-J)** Spontaneous activity assessment by openfield test, the analysis was done using One-way ANOVA, multiple comparisons were performed by Tukey's test and the significant adjusted p-values are shown on the graphs. **(F)** Mean time mobile (p<0.0001), **(G)** Mean speed (p=0.0003), **(H)** the mean distance (p=0.0003), **(I)** Mean number of rears (p<0.0001) and **(J)** Mean number of grooms

(p=0.91). The bar graph data represents the mean ± SEM. The number of animals: WT-vp16; n = 9 (4 ♀,5 ♂) , WT-SRFvp16; n=10 (4 ♀,6 ♂), R6/1-vp16; n=9 (5 ♀,4 ♂) and R6/1-SRFvp16; n=8 (5 ♀,3 ♂) for all tests.

Srfvp16 mice compared to WT-vp16 and WT-Srfvp16 mice, respectively. However, no difference was observed in the number of grooms among the groups **(Figure 75J)**.

These results, showing the difference between WT and R6/1 mice together with comparable results between R6/1-vp16 and R6/1-Srf vp16, likely reflect the apathic behavior of R6/1 mice and that Srfvp16 overexpression didn't improve this phenotype.

8.4. Evaluation of the effect of AAV-Srfvp16 overexpression on motor performance of WT and R6/1 mice.

Then, we evaluated whether Srfvp16 overexpression affects motor coordination of WT and R6/1 mice. Using the bar test, we analyzed the latency to cross the bar. The data show that the latency is is not different between the groups **(Figure 76A)**. We also tested motor coordination using accelerating rotarod. Overall, the latency to fall from the rotarod is significantly reduced in R6/1-vp16 and R6/1-Srfvp16 mice when compared to WT-vp16 and WT-Srfvp16 mice, respectively, and not increased in R6/1-Srfvp16 vs R6/1-vp16 **(Figure 76B)**. Moreover, comparable results were observed in males and females **(Figure 76C)**.

Therefore, these results show that Srfvp16 overexpression has no effect on the spontaneous activity and the innate behavior of WT and R6/1 mice. Moreover, it didn't change their motor performance.

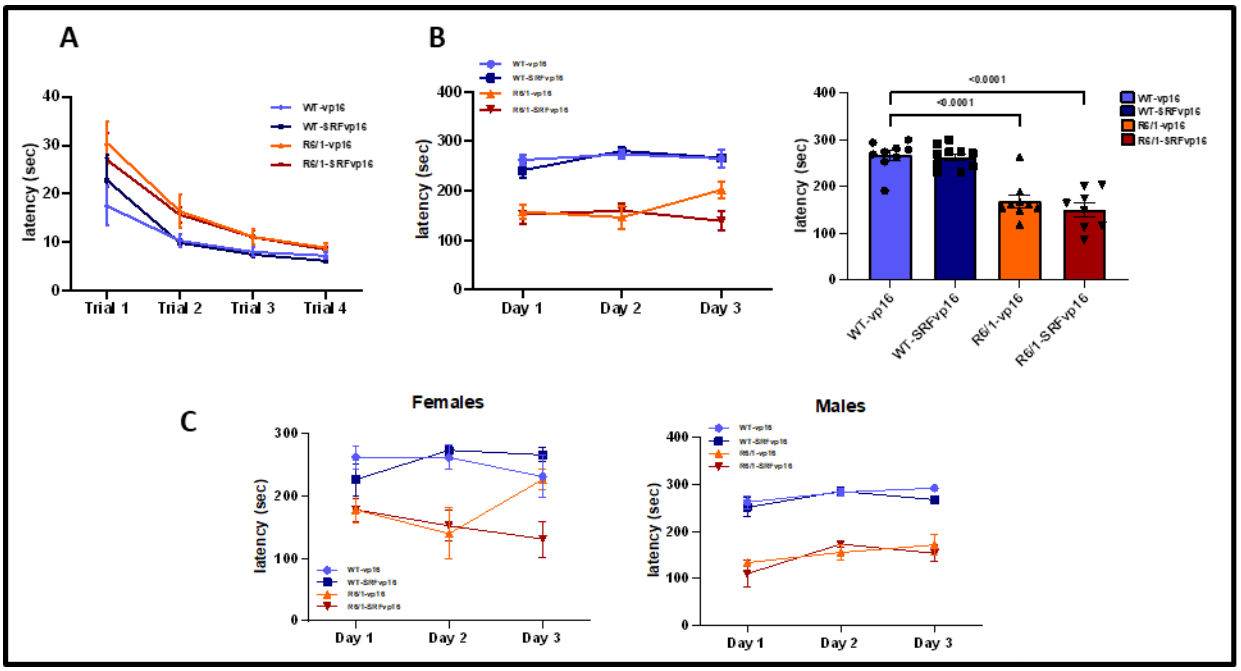

Figure 76: Evaluation of the effect of SRFvp16 overexpression on motor performance of WT and R6/1 mice.
(A-C) Evaluation of the effect of SRFvp16 overexpression on motor coordination of WT and R6/1 mice with bar test (A) and rotarod test **(B-C). (A)** The latency to cross the bar by WT and R6/1 mice and join their cage (Two-way ANOVA with multiple repeats; the multiple comparisons were done using Tukey's test: Trial effect P<0.0001; genotype effect P=0.0040; interaction Trial x genotype P=0.7531). **(B)** Left: The latency to fall from the rotarod during the 3 days of learning in the rotarod (Two-way ANOVA with multiple repeats; the multiple comparisons were done using Tukey's test: Day effect P=0.3349; genotype effect P<0.0001; interaction Day x genotype P=0.1195. Right: The average latency to fall of the 3 days of training (One-way ANOVA, P<0.0001; multiple comparisons were performed with Tukey's test and adjusted p-values are represented on the graphs). **(C)** Rotarod; the latency to fall of males and females' mice (Two-way ANOVA with multiple repeats; multiple comparisons were done using Tukey's test: Males, Day effect P=0.0027, Treatment effect P<0.0001; interaction Day x Treatment P=0.7229; Females, day effect P=0.9243; genotype effect P<0.0001; interaction Day x Treatment P=0.1100. The bar graph data represents the mean ± SEM. The number of animals: WT-vp16; n = 9 (4 ♀,5 ♂), WT-SRFvp16; n=10 (4 ♀,6 ♂), R6/1-vp16; n=9 (5 ♀,4 ♂) and R6/1-SRFvp16; n=8 (5 ♀,3 ♂) for all tests.

8.5. Evaluation of the effect of SRFvp16 overexpression on the anxiety of WT and R6/1 mice

To evaluate the effect of Srfvp16 overexpression on the anxiety of WT and R6/1 mice, we used the light-dark transition test.

We observed that the time spent in the light compartment and the number of entries in the light box does not differ between the four groups **(Figure 77 A-B)**. However, the latency to enter to the light box is significantly higher in R6/1-vp16 and R6/1-Srfvp16 compared to WT-vp16 and WT-Srfvp16 **(Figure 77C).** This suggest that R6/1 mice are apathic rather than anxious, and that SRF overexpression does not affect this phenotype.

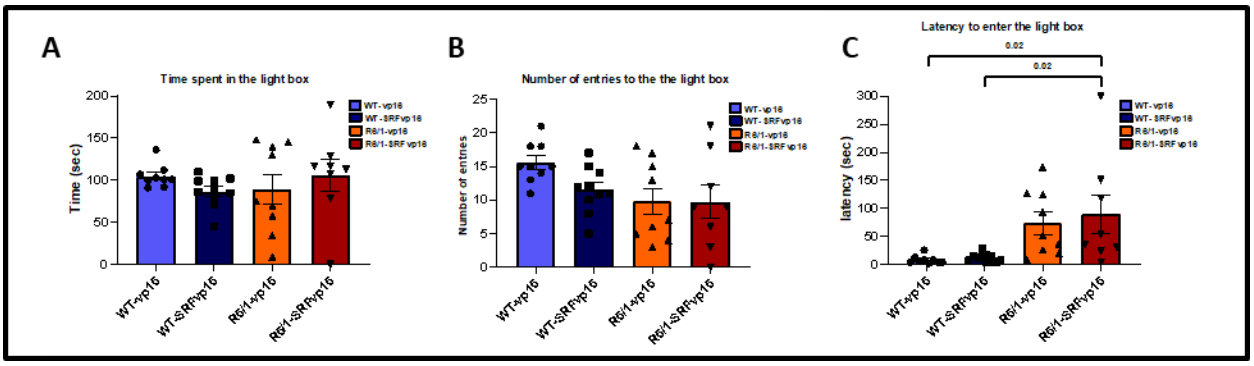

Figure 77: Evaluation of the effect of Srfvp16 overexpression on the anxiety of WT and R6/1 mice using the light dark test.

(A) Mean Time spent in the light box. **(B)** Mean number of entries into the light compartment of WT and R6/1 mice. **(C)** Mean latency to enter the light box. The analysis was performed using One-way ANOVA; multiple comparisons by Tukey's test and significant adjusted p-values are shown on the graphs. The data is represented by the mean ± SEM. n = 8 per group (5 ♂, 3 ♀) for all tests.

8.6. Evaluation of the effect of SRFvp16 overexpression on procedural memory of WT and R6/1 mice in the double-H maze.

We then investigated the effect of Srfvp16 overexpression on memory in WT and R6/1 mice using the DH. During acquisition, the latency to reach the platform is significantly increased in R6/1 when compared to WT mice **(Figure 78A).** Analysis of the speed, % of correct responses and distance to reach the platform are all significantly decreased in R6/1-vp16 and R6/1-Srfvp16 compared to WT-vp16 and WT-Srfvp16 **(Figure 78B-D)**. Mouse performances in the DH are similar in WT-vp16 vs WT-Srfvp16 and R6/1-vp16 vs R6/1-Srfvp16 comparisons **(Figures 78A-D, Figure 78E).** This indicates that the main difference between WT and R6/1 corresponds to HD phenotype and that Srfvp16 overexpression doesn't affect mouse performances.

During the probe test, the distance and speed were significantly decreased in R6/1 compared to WT mice, whether they overexpressed Srfvp16 or not **(Figure 78F)**. Also, surprisingly, latency and time spent in procedural and spatial arms were not different between groups, likely due to the fact that all mice displayed preferential spatial **(Figure 78G-H)**. While discrepancy with results presented in Lotz et al. (in prep) remains unclear, different stress levels between mice of these two experiments might underlie differences in cognitive performances and learning strategies.

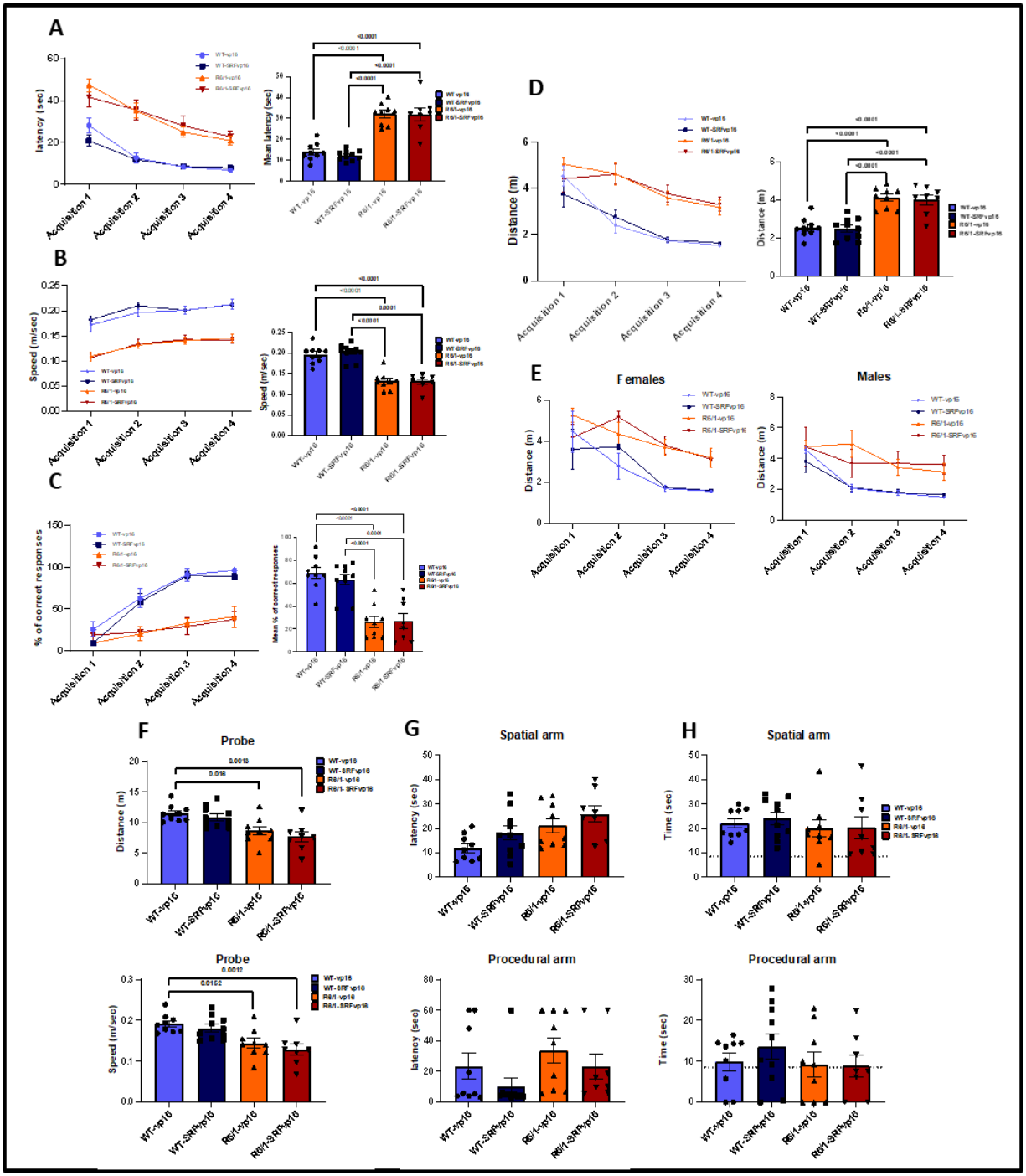

<u>Figure 78:</u> Evaluation of the effect of SRFvp16 overexpression on procedural learning and memory of WT and R6/1 mice in the double-H maze.

(A) The latency to find the hidden platform of each of the WT-vp16, WT-SRFvp16, R6/1-vp16 and R6/1-SRFvp16 during the 4 acquisitions of the DH (Two-way ANOVA with multiple repeats; Acquisition effect P<0.0001; Genotype effect P<0.0001; interaction Acquisition x Genotype P=0.2585. Multiple comparisons were done using Tukey's test. **B)** The speed of the mice during the Acquisitions of the DH (Two-way ANOVA with multiple repeats; Acquisition effect P<0.0001; Genotype effect P<0.0001; interaction Acquisition x Genotype P=0.9802. Multiple comparisons were done using Tukey's test. **(C)** The percentage of correct responses during the acquisitions of the DH (Two-way ANOVA with multiple repeats; Acquisition effect P<0.0001; Genotype effect P<0.0001; interaction Acquisition x Genotype P=0.0007. Multiple comparisons were done using Tukey's test. **(D) <u>Left:</u>** The

distance covered by each mice group during the Acquisition phase while looking for the hidden platform placed in the NE arm (Two-way ANOVA with multiple repeats; Acquisition effect P<0.0001; Genotype effect P<0.0001; interaction Acquisition x Genotype P=0.0963. Multiple comparisons were done using Tukey's test. **Right:** The mean distance traveled by the 4 groups during all the acquisitions (The analysis was performed by One-way ANOVA P<0.0001, the multiple comparisons were done by Tukey's test and adjusted p-values are represented on the graphs). **(E)** The distance covered males and females individually (Two-way ANOVA with multiple repeats; the multiple comparisons were done using Tukey's test: Males; Acquisition effect P<0.0001; Genotype effect P<0.0001; interaction Day x Genotype P<0.0001; interaction Day x Genotype P=0.2932. **(F)** The distance covered (up) and the speed (down) of each experimental group during the probe test (One-way ANOVA: Distance; P=0.0004. Speed; P=0.0004, the multiple comparisons were done by Tukey's test and adjusted p-values are shown on the graphs). **(G)** The latency to reach the spatial arm (up) and the procedural arm (down) during the probe test. (One-way ANOVA: spatial arm; P=0.0143. procedural arm; P=0.1752, the multiple comparisons were done by Tukey's test). **(H)** The time spent in each of the procedural and spatial arms among the groups and the relative time spent of each group compared to the chance (8.5 seconds) in each of the two arms during the probe test (p-value<0.005).

8.7. Evaluation of the effect of Srfvp16 overexpression on the striatal transcriptome of WT and R6 1 mice

Behavioral analysis showed no significant effect of Srfvp16 overexpression on WT and R6/1 motor function and memory. To verify molecular effects of Srfvp16 overexpression, we performed q-RT-PCR and RNAseq analyses using the striatal tissues.

8.7.1. Evaluation of the effect of SRFvp16 overexpression on SRF target genes expression in the striatum of WT and R6/1 mice by qRT-PCR

The mRNA level of *Srf*, Srf target genes and some neuronal identity genes was quantified by qRT-PCR **(Figure 79).** First, we checked the efficiency of striatal injections of AAV-Srfvp16 vector. We targeted a sequence of the AAV-Srfvp16 vector covering a part of both Srf DNA-binding domain and vp16 transactivation domain. The analysis shows that Srfvp16 mRNA level is increased in the striatum of injected WT and R6/1 mice **(Figure 79A).** We also analyzed the expression of endogeneous Srf. The analysis shows no significant difference between the four groups, but its mRNA level has a trend to the increase in both WT-Srfvp16 and R6/1-Srfvp16 **(Figure 79B).**

In addition, the analysis of Srf target genes, neuronal-activity genes, shows that Egr1 mRNA level is significantly induced in WT-Srfvp16 mice vs WT-vp16 mice and shows a trend to the increase in R6/1-Srfvp16 vs R6/1-vp16 mice. The mRNA level of other IEGs, such as *Arc*, *JunB* and *Fosb*

didn't significantly differ among the four groups, however, it shows a tendency to the increase in R6/1-Srfvp16 mice vs R6/1-vp16 mice **(Figure 79C).**

Moreover, we checked the expression of select striatal identity genes. The analysis shows that the mRNA levels of *Drd1* and *Pde10a* are significantly lower in R6/1-vp16 compared to WT-vp16, and there is no significant change in their expression and that of *Darpp32* upon Srfvp16 overexpression **(Figure 79D).**

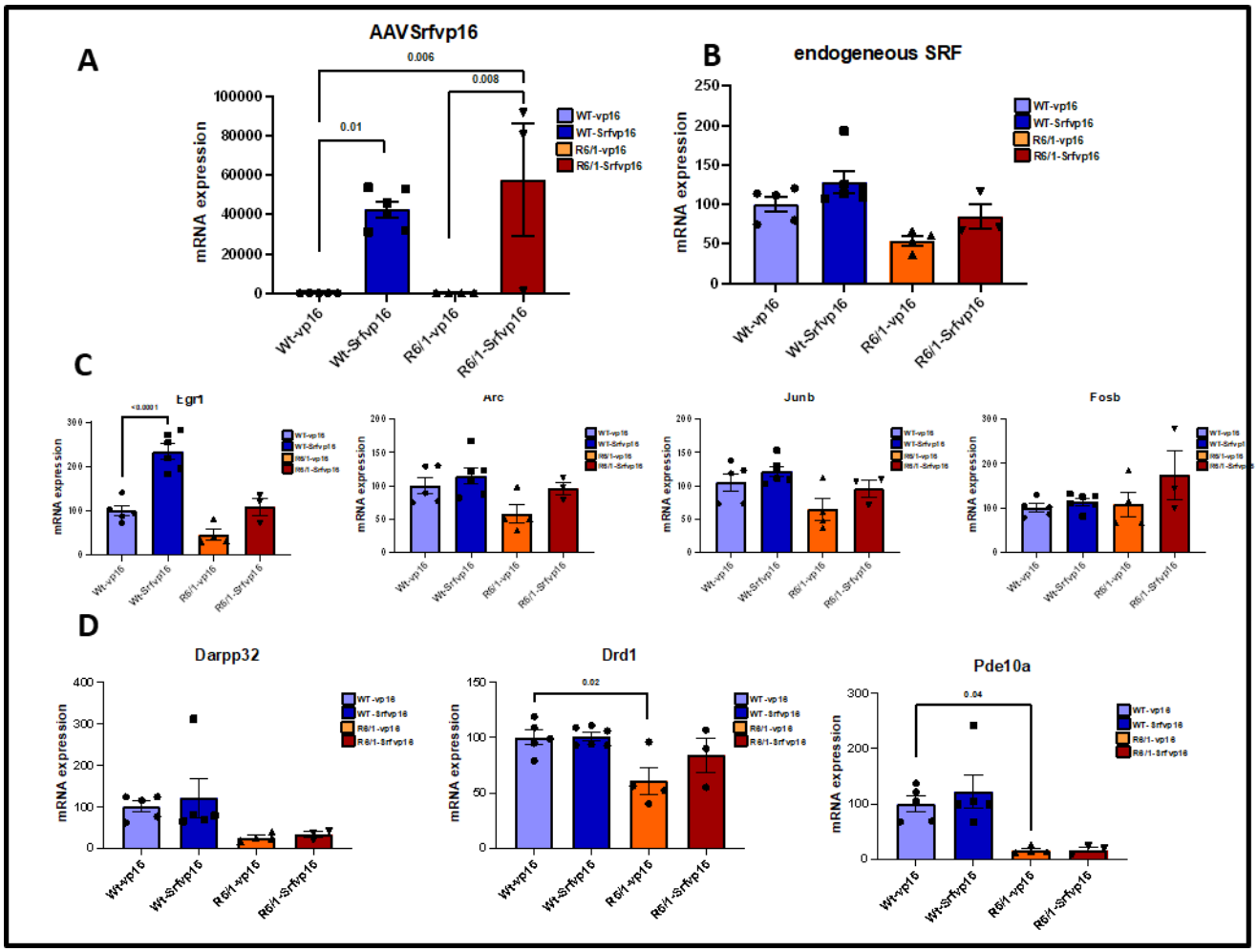

Figure 79: Evaluation of the effect of SRFvp16 overexpression on Srf and Srf target genes by qRT-PCR.
(A) The expression of the injected AAVSrf-vp16. **(B)** Endogenous Srf mRNA level in the striatum of WT and R6/1 mice. **(C)** Expression level of Srf target genes: Egr1, Arc, JunB and Fos. **(D)** mRNA levels of neuronal identity genes: Darpp32, Drd1and Pde10a. The analysis was performed by One-way ANOVA, multiple comparisons by Tukey's test and significant adjusted p-value are shown on the graphs. The data is represented by the mean of the mRNA levels ± SEM. WT-vp16 (n=5), WT-Srfvp16 (n=6), R6/1-vp16 (n=4) and R6/1-Srfvp16 (n=3).

Above data shows that Srfvp16 is upregulated in the striatum of injected WT and R6/1 mice. Using the AAV-Srfvp16 construct, we have a trend to up-regulate the expression of Srf target genes.

We then generated RNAseq data to more precisely characterize transcriptional effects of Srfvp16 in mouse striatum.

8.7.2. RNA-seq: Quality analysis of sequenced samples

Four animals (2 females and 2 males) of each experimental group have been used for RNAseq analysis, except for the R6/1-Srfvp16 group where we used only two female samples due to technical issues **(Figure 80A)**. Principle component analysis (PCA) shows that genotype predominantly explain sample variability, with a high variability between the two R6/1-Srfvp16 samples **(Figure 80B**).

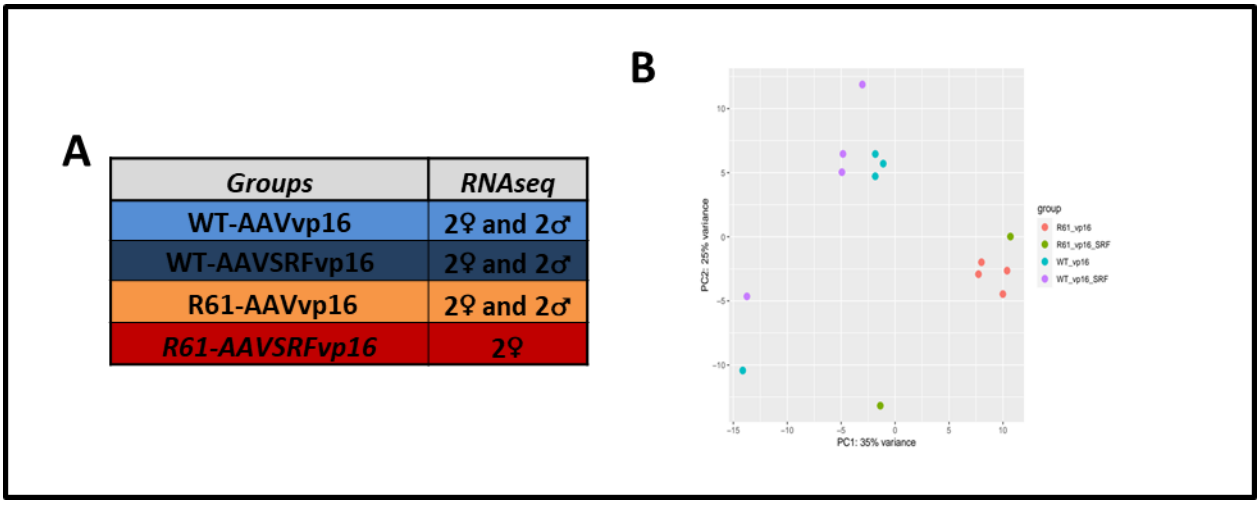

Figure 80: Experimental conditions and quality testing of the sequenced striatal samples.
(A) The experimental groups and the number of animals used for RNA-seq of the striatum of WT and R6/1 mice to evaluate the effect of Srfvp16 overexpression. **(B)** Principal component analysis (PCA) of sequenced samples of WT-vp16, WT-Srfvp16, R6/1-vp16 and R6/1-Srfvp16 mice.

8.7.3. The Effect of murine full length Srf overexpression on WT and R6/1 striatal transcriptomic signature

We aimed to determine whether Srfvp16 overexpression would rescue HD striatal transcriptome. First, with the help of IGBMC bioinformatics platform and Dr. C. Decreane in the lab, we

performed differential expression analysis to assess the number of differentially expressed genes between the different groups**.**

The analysis shows that 2963 and 2281 genes are downregulated while 2691 and 2142 genes are upregulated in the striatum of R6/1-vp16 vs WT-vp16 and R6/1-Srfvp16 vs WT-vp16, respectively **(Figure 81A)**. Intersection analysis showed strong overlaps between deregulated genes in R6/1-vp16 vs WT-vp16 and R6/1-Srfvp16 vs WT-vp16, with 1913 and 1786 common down- and up-regulated respectively **(Figure 81B)**. Gene ontology analysis show that differentially expressed genes (DEG) in R6/1-vp16 vs WT-vp16 and R6/1-Srfvp16 vs WT-vp16 comparisons were comparable. Notably, down-regulated genes were highly significantly enriched in genes implicated in neuronal function (**Figure 81C**). Gene expression analysis show that the expression of Egr1 is significantly upregulated in WT and R6/1 mice upon overexpression of Srfvp16. Besides, other neuronal activity-regulated genes (*Arc* and *Fos*) show a trend to the increase upon overexpression of Srfvp16 (**Figure 82 A-B),** however, typical striatal identity genes (*Drd1*, *Drd2* and *Pde10a*) remained significantly decreased in R6/1 striatum, despite Srfvp16 overexpression (**Figure 82C).** Together, these data show that overexpression of SRFvp16 does not rescue HD striatal identity, however it seems to have an effect on immediate early genes.

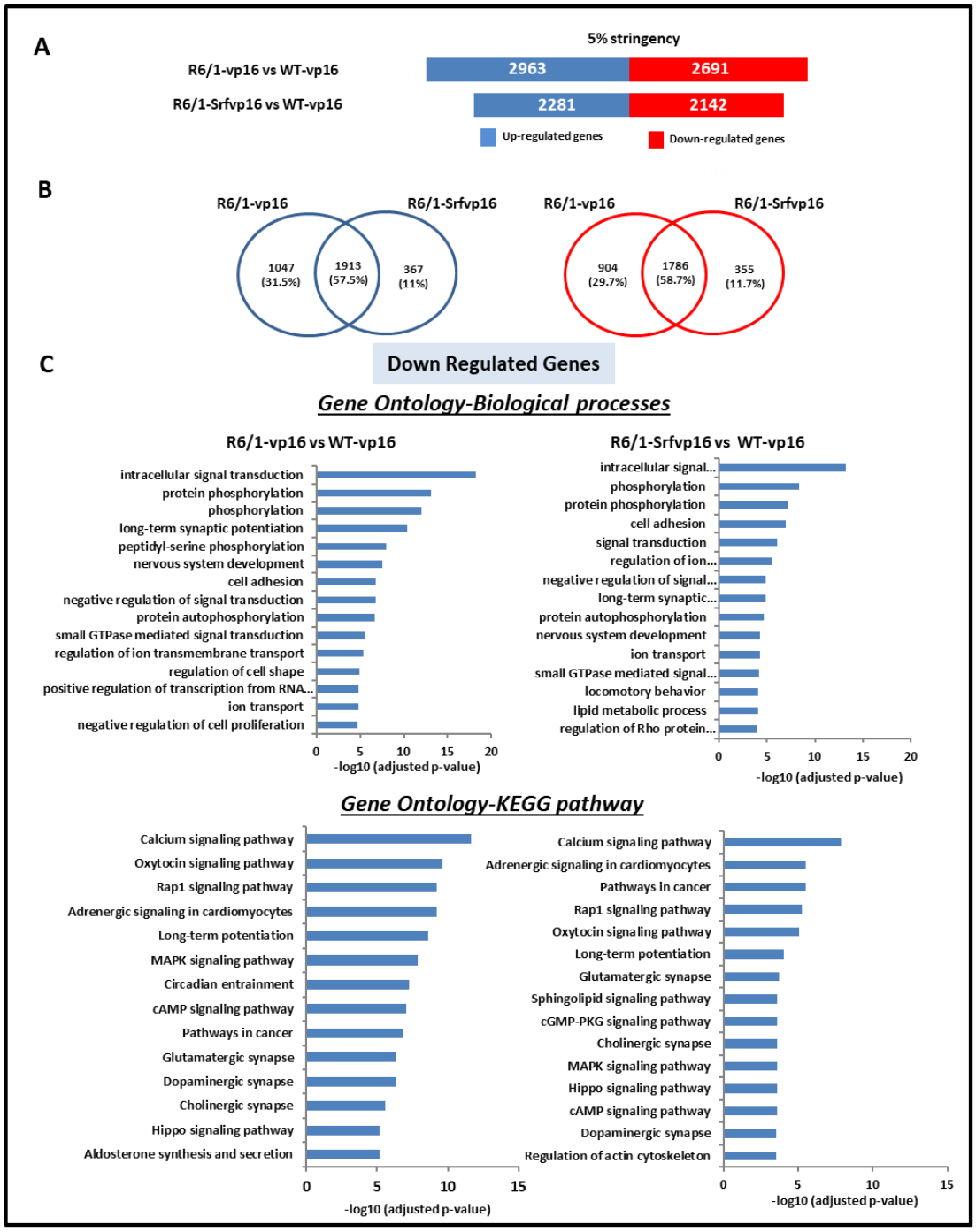

Figure 81: The effect of SRFvp16 overexpression on transcriptional signatures of the striatum of WT and R6/1 mice.

Gene lists were selected with log (FC) <0 or log (FC)> 0 and an adjusted p-value <0.05. **(A)** The number of up-regulated and down-regulated genes in the striatum of R6/1-vp16 and R6/1-Srfvp16 mice compared to WT-vp16 mice (Comparisons: R6/1-vp16 vs WT-vp16; R6/1-Srfvp16 vs WT-vp16). **(B)** Venn diagrams of the intersection of the up- and down- regulated genes in the striatum of R6/1-vp16 and R6/1-Srfvp16 compared to WT-vp16 mice. **(C**) Functional enrichment analysis, Gene ontology analysis: Biological processes and KEGG pathway, of down-regulated genes in the striatum of R6/1-vp16 and R6/1-Srfvp16 compared to WT-vp16 mice.

Moreover, we confirm that Srf is overexpressed upon overexpression of Srfvp16, in both WT and R6/1 mice, while Srfvp16 does not affect Creb expression **(Figure 83C)**.

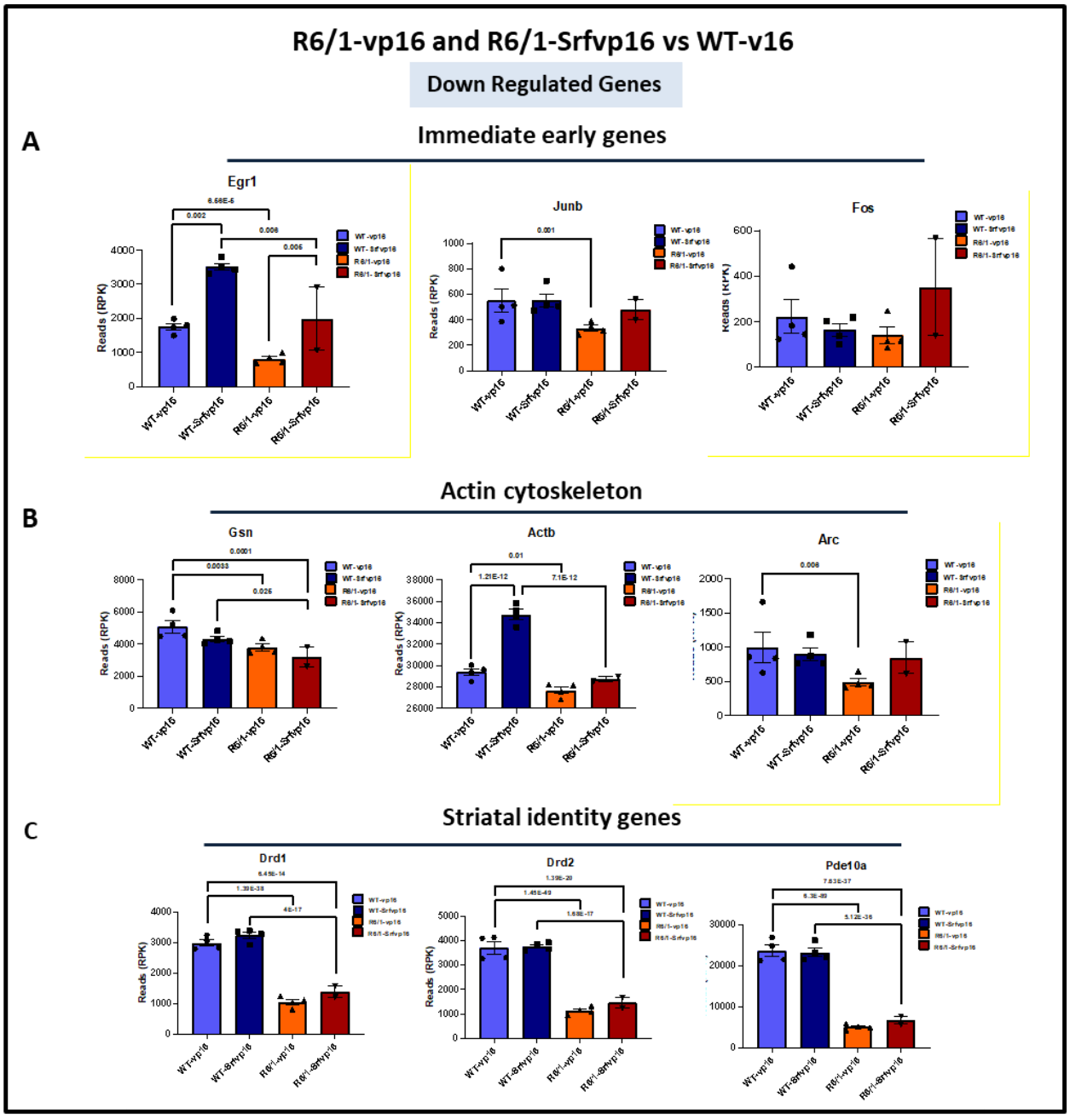

Figure 82: Srf target genes expression in the striatum of R6/1-vp16 and R6/1-Srfvp16 compared to WT-vp16 mice. The expression of Srf target genes after Srfvp16 overexpression in the striatum of WT and R6/1 mice **(A)** Examples of immediate early genes **(B)** striatal identity genes expression. **(C)** Gene expression of actin cytoskeleton system. The represented gene expression analysis was performed by One-way ANOVA and the multiple comparisons were done using Tukey's test; significant adjusted p-values are shown on the graphs).

Also, functional analysis show that up-regulated genes in R6/1-vp16 vs WT-vp16 and R6/1-Srfvp16 vs WT-vp16 display comparable signatures, and are enriched in genes implicated in protein transport, transcription, cell cycle and DNA repair.

To complete the analysis, we then evaluated the direct effect of Srfvp16 overexpression on the transcriptome of WT and R6/1 mice by comparing striatal transcriptomes of R6/1-Srfvp16 vs R6/1-vp16 mice on the one hand, and WT-Srfvp16 vs WT-vp16 on the other hand. Differential expression analysis shows only 4 down-regulated genes and 20 up-regulated genes in R6/1 background, and 253 down- and 435 up- regulated genes in WT background **(Figure 84A)**. Intersection analysis with the genes lists of the down – and up- regulated genes between WT and R6/1 mice are shown in **Figure 84B**.The low number of deregulated genes didn't permit to have significant functional enrichment analysis.

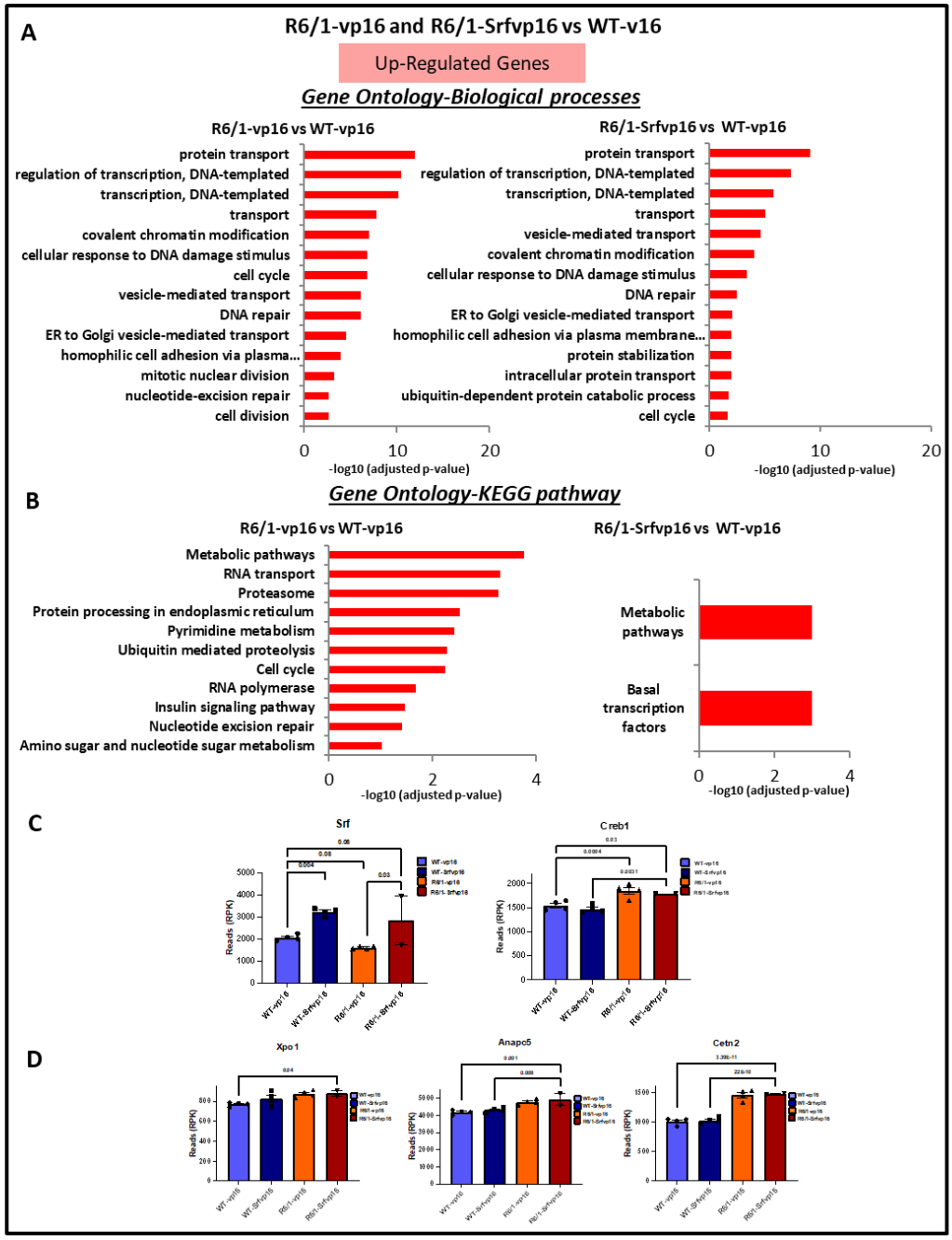

<u>Figure 83:</u> Differential enrichment analysis of up-regulated genes in the striatum of R6/1-vp16 and R6/1-Srfvp16 compared to WT-GFP mice.

(A) Functional enrichment analysis, Gene ontology analysis; Biological processes, of up-regulated genes in the striatum of R6/1-vp16 and R6/1-Srfvp16 compared to WT-vp16 mice. **(B)** Gene ontology analysis of the KEGG pathway of up-regulated genes in the striatum of R6/1-vp16 and R6/1-Srfvp16 compared to WT-vp16 mice. **(C)** Srf and Creb expression in WT-Srfvp16 and R6/1-Srfvp16 mice. **(D)** Examples of up-regulated genes in R6/1-vp16 and R6/1-Srfvp16 mice associated with transcription regulation. Functional analysis was performed with the R Cluster Profiler library and the terms of the Gene Ontology database where been analyzed by DAVID. Gene expression analysis was performed by One-Way ANOVA, adjusted p-values are represented on the graphs., Gene lists were selected with log (FC) <0 or log (FC)> 0 and an adjusted p-value <0.05. **(A)** The Number of down- and up-regulated genes in the striatum of R6/1-Srfvp16 and WT-Srfvp16 mice vs R6/1-vp16 and WT-vp16 mice, respectively. **(B)** Venn diagrams of the intersection of the down- and up- regulated genes in the striatum of R6/1-Srfvp16 and WT-Srfvp16 mice vs R6/1-vp16 and WT-vp16 mice, respectively. Common genes are listed in **Figure 84B**.

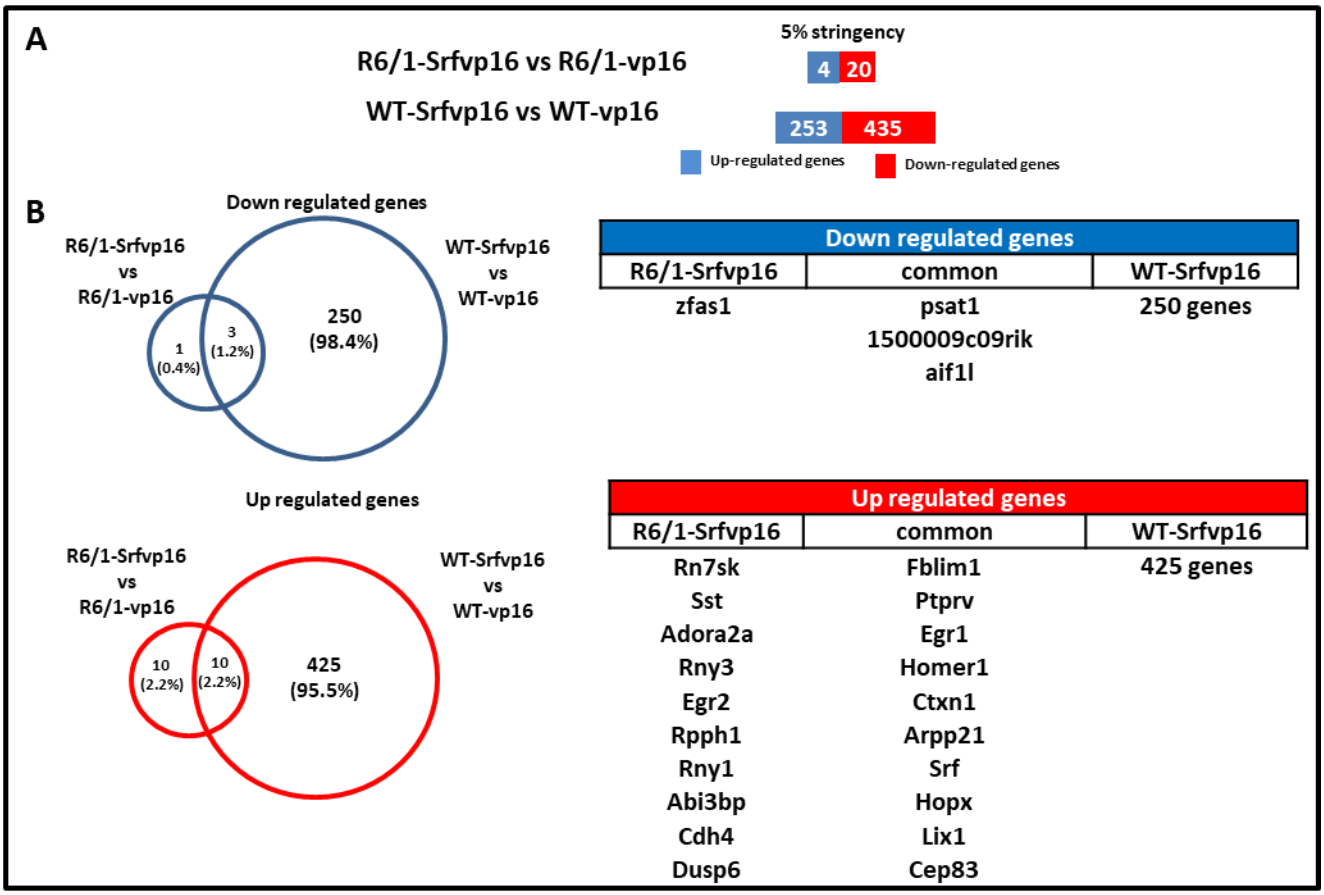

Down regulated genes		
R6/1-Srfvp16	common	WT-Srfvp16
zfas1	psat1	250 genes
	1500009c09rik	
	aif1l	

Up regulated genes		
R6/1-Srfvp16	common	WT-Srfvp16
Rn7sk	Fblim1	425 genes
Sst	Ptprv	
Adora2a	Egr1	
Rny3	Homer1	
Egr2	Ctxn1	
Rpph1	Arpp21	
Rny1	Srf	
Abi3bp	Hopx	
Cdh4	Lix1	
Dusp6	Cep83	

Figure 84: The effect of Srfvp16 overexpression on striatal transcriptome of WT and R6/1 mice.
(A) The number of differentially expressed genes, up-regulated and down-regulated genes in R6/1-Srfvp16 and WT-Srfvp16 vs R6/1-vp16 and WT-vp16 respectively. **(B)** Venn diagram showing the intersection of down- and up- regulated genes between R6/1-Srfvp16 and WT-Srfvp16 compared to R6/1-vp16 and WT-vp16, respectively.

We then determined whether SRF and CREB target genes were globally impaired in the striatum of WT and R6/1 mice upon Srfvp16 overexpression, using same list of genes as previously **(See part 2. in results section, p: 132,** (Kim et al., 2010). Also, we checked the expression of memory genes as defined previously **(see part.3, part 6.4 and part 8.7. in results sections and Lotz et al. in prep).** The intersection of these gene lists with the Srfvp16-RNAseq data is represented in Figure **85 A-C.** The boxplots show z-scores computed from RNAseq data generated using the striatum of WT (vp16 and Srfvp16) and R6/1 (vp16 and Srfvp16) mice. The data shows that SRF target genes are globally reduced in R6/1-vp16 vs WT-vp16 mouse striatum, and they are induced after Srfvp16 overexpression in both WT and R6/1 backgrounds **(Figure 85A).** In contrast, CREB

target genes are globally increased in R6/1-vp16 compared to WT-vp16 samples, and they are neither induced in WT nor in R6/1 backgrounds after Srfvp16 overexpression **(Figure 85B)**. Memory genes show a decrease in R6/1-vp16 compared to WT-vp16. Surprisingly, their expression is decreased in WT-Srfvp16 compared to WT-vp16. However, they are up-regulated in R6/1 Srgvp16 when compared to R6/1-vp16 **(Figure 85C)**. These data support the notion that overexpression of Srfvp16 partially rescues Srf-dependent learning/memory-associated transcriptional program in R6/1 mice.

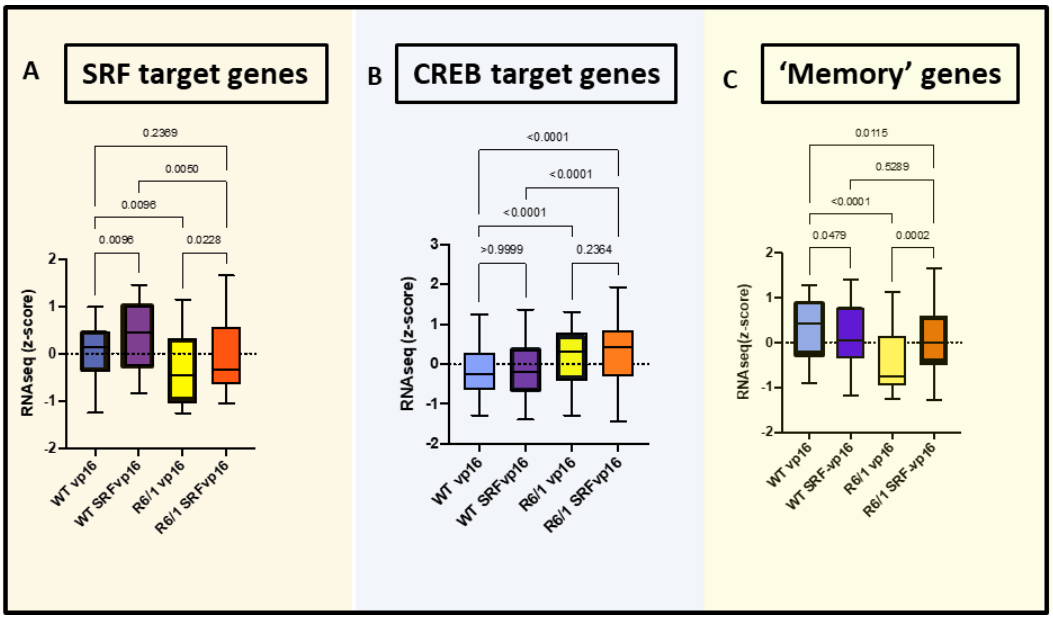

Figure 85: Global gene expression analysis after Srfvp16 overexpression in the striatum of R6/1 mice.
The boxplots show z-scores computed from RNAseq data generated using the striatum of animals of different experimental conditions: WT-vp16, WT-Srfvp16, R6/1-vp16 and R6/1-Srfvp16. SRF and CREB target genes are retrieved from Greenberg et al. 2010 and intersected with our RNAse data. Global gene expression of: **(A)** SRF target genes. **(B)** CREB target genes. **(C)** Sustained expressed memory genes at 2 and 5 days of learning during the DH. Data was analysed using Kruskal-Wallis test, adjusted p-values for multiple comparisons were done with Benjamini-Hochberg method.

All in all, the results indicate that full length *Srf* overexpression didn't rescue HD striatal transcriptome. However, Srfvp16 could improve part of HD striatal transcriptomic signature, particularly Srf-related 'memory' signature. Thus, the AAV-Srfvp16 construct containing the DNA-binding domain of Srf and the vp16 transactivation domain of vp16 was somehow efficient to induce the expression of Srf target genes. It is important to mention that the experimental groups represent a pool of two batches of animals where one batch, received 10x more viral particles that the other group (i.e. 10^{11} vg. µL-1 *instead of* 10^{10} vg. µL-1), which could have affected the reproducibility of our data.

……. Discussion ……

Discussion

In this work, we addressed the role of SRF in Huntington's disease, using HD R6/1 transgenic mice. Using available transcriptomic datasets generated from brain tissues of R6/1 mice and HD Knock-in mice, and from post-mortem tissues of HD patients, we show that Srf and its target genes is progressively decreased in the HD striatum, in contrast to Creb and Creb targets, which are increased. Moreover, we show that Srf and Srf target genes are not properly induced by striatal procedural memory in the striatum of R6/1 mice, correlating with procedural memory deficits. In an attempt to rescue SRF regulation and behavioral deficits in HD, we have overexpressed Srf constructs in the striatum of R6/1 mice using viral-mediated approach based on AAV and stereotaxic injection. First, we have used a construct overexpressing full length murine Srf gene. Using a battery of behavioral tests, we show that overexpression of full length Srf in the striatum of R6/1 mice leads to worsening of their motor function. Moreover, additional histological and molecular analyses, including transcriptomic analyses, show no rescue of targets in R6/1 striatum, despite elevated overexpression of Srf. Second, we have overexpressed in the striatum a construct consisting in Srf DNA binding domain fused to VP16 transactivation domain. While behavioral analyses show an absence of rescue of R6/1 behavioral phenotypes upon overexpression of SRF-VP16 construct in R6/1 striatum, our molecular analyses, including RNAseq data, indicate that Srf target genes and memory/synaptic plasticity-related genes are up-regulated. However, our transcriptomic data indicate that striatal identity genes, which are strongly down-regulated by the HD mutation, are not restored in R6/1 mice. This suggests that restoring Srf level in the HD striatum might not be sufficient to suppress HD pathogenesis, including cognitive phenotypes, due to partial rescue of HD striatal transcriptome.

1.Srf is downregulated in the striatum of HD mice models and HD patients

We used RNAseq and qRT-PCR approaches to define the expression of Srf in HD striatum. We showed that Srf and Srf neuronal targets are downregulated at transcriptional level in the striatum of HD mouse models and HD patients. We also showed that Srf is also decreased at

protein level in HD mouse striatum. Thus, downregulation of Srf in the striatum is a signature of HD.

We provide evidence that SRF impairment is specific, since CREB, another transcription factor essential to synaptic plasticity and memory, and its target genes are not decreased in the striatum of HD mice. On the opposite, they are upregulated, which could suggest a compensatory mechanism.

While the association of CREB with neuronal plasticity has been in the spotlight for decades ((Frank and Greenberg, 1994; Lamprecht, 1999; Shaywitz and Greenberg, 1999; Silva et al., 1998), much less is known regarding SRF. Recently, many studies have shown the critical role of SRF in memory processes, particularly in both long-term potentiation and long-term depression, spine motility and axonal pathfinding (Alberti et al., 2005; Etkin et al., 2006; Knöll et al., 2006; Ramanan et al., 2005) These results are consistent with the view that downregulation of SRF in HD striatum contribute to cognitive deficits in HD.

Along my thesis, we used two strategies to overexpress Srf in the striatum in the striatum of HD mice, with the aim to rescue transcriptome and functional outcome, notably behavioral outcomes.

2.The effect of full length Srf overexpression in the striatum of WT and R6/1 mice

In an attempt to characterize SRF regulation in the striatum of HD mice and its respective role in regulating proliferation/IEGs genes and differentiation/actin-cytoskeleton genes, which are dependent on TCF/ELK and MRTF/MKL signaling pathways, respectively (Buchwalter et al., 2004; Miralles et al., 2003; Olson and Nordheim, 2010; Zaromytidou et al., 2006), we initially aimed to overexpress full length SRF as well as SRF mutants targeting phosphorylation site (e.g. S162A and S162D SRF mutant), regulating the switch between TCF- and MRTF-dependent pathways (Iyer et al., 2006). More specifically, it was shown that phosphorylation of SRF at S162 promotes expression of Fos and proliferation genes, at the expense of actin-cytoskeleton genes (Iyer et al.,

2006). Thus, preventing phosphorylation of S162 with S162A mutant and mimicking this phosphorylation with S162D mutant, we expected to favor TCF- and MRTF-dependent pathways, respectively, and therefore dissect the role of SRF in HD.

However, due to technical issues, only AAV overexpressing WT Srf could be generated and was injected in the striatum of WT and R6/1 mice. Since we could not generate SRF mutants, we were not able to evaluate the effect of Srf overexpression on MRTF- and TCF-dependent pathways. Overexpression of WT Srf in the striatum led to the worsening of motor functions. The effect of the full-length Srf overexpression was particularly dramatic in R6/1 mice, but it also has a tendency to decrease performance in WT mice. Surprisingly, Srf overexpression didn't rescue downregulated genes in R6/1 striatum, including Srf target immediate early genes (Egr1, Arc, etc.…) and striatal identity genes (Drd1, Drd2, etc.…). In addition, Srf overexpression didn't reduce mutant Htt aggregation. Interestingly, studies showed that SRF KO leads to hyperactive phenotype (Förstner and Knöll, 2020; Parkitna et al., 2010a). The study of Rodriguez Parkin et al. show that SRF KO in dopaminoceptive, but not dopaminergic, neurons is responsible for the development of a hyperactivity syndrome, characterized by reduced body weight into adulthood, enhanced motor activity, and deficits in habituation processes (Parkitna et al., 2010b). Whether differential targeting of D1 and D2 MSN by Srf constructs might explain hypoactive behavior in R6/1 mice upon Srf overexpression may be an hypothesis. Moreover, the use of the strong PGK promoter led to high Srf expression levels, which might have caused neurotoxicity. More specifically, high levels of Srf upon overexpression might have altered signaling pathways implicated in SRF regulation, thereby affecting the regulation of Srf target genes. Complementary experiments focusing on these signaling pathways should help addressing this issue.

Also, the dominant negative SRF splicing isoform, SRFΔ5, could possibly explain our results (Belaguli et al., 1997; Croissant et al., 1996; Gauthier-Rouviere et al., 1996; Gauthier-Rouvière et al., 1993). This isoform, which we found expressed at substantial levels in the striatum, as shown by our western-blotting analyses, lacks most part of the transactivation domain, and could therefore inhibit the induction of Srf target genes.

3.The effect of striatal overexpression of Srf-VP16 in WT and R6/1 mice

To further investigate the role of SRF in HD striatal pathogenesis, we tried another strategy using an AAV-based construct allowing expression of SRF DNA binding domain fused to VP16 trans-activator domain, to constitutively induce Srf target genes (Beck et al., 2012; Ohrnberger et al., 2015; Sandström et al., 2011; Schratt et al., 2004, 2002; Stern et al., 2012). However, Srf-vp16 overexpression in the striatum of R6/1 mice did not improve behavior, including motor and cognitive functions.

4.The effect of Srfvp16 overexpression on striatal transcriptome

In contrast, transcriptomic analyses showed that overexpression Srfvp16 in the striatum of R6/1 mice led to partial restoration of genes involved in learning and memory, especially Srf target IEGs (Egr1). However, striatal identity genes were not rescued. Whether TCF/ELK- and/or MRTF-dependent genes are preferentially targeted remains to be determined, but our results showing that IEGs (Egr1) and actin cytoskeleton genes (Actb) are both up-regulated by Srfvp16 suggest that genes in both pathways may be affected by the construct.

We also checked the expression of endogenous Srf levels, we can see that endogenous Srf has the tendency to increase in both WT-Srfvp16 and R6/1-Srfvp16 mice, consistent with the fact that Srf regulates its own expression (Spencer and Misra, 1996).

When analyzing Srf effect on striatal transcriptome in WT and R6/1 mice, we obtained a very few numbers of differentially regulated genes in R6/1-Srfvp16 vs R6/1-vp16 compared to the WT-Srfvp16 vs WT-vp16. Due to genotyping error, we had only 2 samples, with high variability, in the R6/1-Srfvp16 group, while 4 samples were analyzed for the other groups. This might explain the absence of statistical significance power between group comparisons and suggests a weaker differentiation of R6/1 phenotype related to SRF compared to the WT phenotype. Alternatively, SRF may not have as much impact on R6/1 genotype vs WT one, possibly due to impaired signaling pathways in the HD background.

To validate such unexpected results, and considering the limitation of the actual number of replicates for some of the experimental conditions, these experiments should be replicated to achieve a more robust statistical analysis. Moreover, in order to identify Srf targets in the striatum of R6/1 mice, it would be interesting to perform ChIP-seq, so that we can effectively demonstrate a direct effect of Srf modulation in the striatum and particularly in HD context.

Many questions remain about underlying molecular mechanisms leading to altered performance upon Srf overexpression. Cellular toxicity due to non-controlled overexpression of Srf could be resolved by using more precised and commonly used inducible gene expression systems, such as Tet-Off and Tet-On system (Gossen and Bujard, 1992), where transcription is reversibly turned on or off in the presence of the antibiotic tetracycline or one of its derivatives (e.g. doxycycline) (Gossen et al., 1995), in a time specific manner. Moreover, tissue specific Srf overexpression could also be applied by choosing specifc promoters i.e. targeting either neurons (D1 or D2 dopaminergic neurons) or glial cells.

In order to better characterize the upstream Srf signaling pathway, we could complete the analysis with supplementary experiments, such as co-immunoprecipitation. Moreover, it could be also useful to design constructs with protein tagged gene sequences (e.g. HA) to allow specific co-immuno precipitation analysis of over-expressed Srf in order to better understand its cellular effects at molecular level (modulated effector proteins and specific chromatin targeting).

In conclusion, striatal regulation of SRF and its target genes is altered by HTT mutation. We have not been able to show that overexpression of SRF-VP16 can rescue behavioral phenotype of R6/1 mice, although the expression of genes involved in synaptic plasticity was increased. This might suggest that restoring proper level of SRF in HD is not sufficient to significantly delay HD pathogenesis.

..... Publications .....

Publication:1

“Age-related and disease locus-specific mechanisms contribute to early remodelling of chromatin structure in Huntington’s disease mice”

Rafael Alcalá-Vida, Jonathan Seguin, Caroline Lotz, Anne M. Molitor, Ibai Irastorza-Azcarate, Ali Awada, Nezih Karasu, Aurélie Bombardier, Brigitte Cosquer, Jose Luis Gomez Skarmeta, Jean-Christophe Cassel, Anne-Laurence Boutillier, Thomas Sexton & Karine Merienne

nature COMMUNICATIONS

ARTICLE

https://doi.org/10.1038/s41467-020-20605-2 OPEN

Age-related and disease locus-specific mechanisms contribute to early remodelling of chromatin structure in Huntington's disease mice

Rafael Alcalá-Vida[1,2], Jonathan Seguin[1,2], Caroline Lotz[1,2], Anne M. Molitor[3,4,5,6], Ibai Irastorza-Azcarate[7], Ali Awada[1,2], Nezih Karasu[3,4,5,6], Aurélie Bombardier[1,2], Brigitte Cosquer[1,2], Jose Luis Gomez Skarmeta[8], Jean-Christophe Cassel[1,2], Anne-Laurence Boutillier[1,2], Thomas Sexton[3,4,5,6] & Karine Merienne[1,2]✉

Temporal dynamics and mechanisms underlying epigenetic changes in Huntington's disease (HD), a neurodegenerative disease primarily affecting the striatum, remain unclear. Using a slowly progressing knockin mouse model, we profile the HD striatal chromatin landscape at two early disease stages. Data integration with cell type-specific striatal enhancer and transcriptomic databases demonstrates acceleration of age-related epigenetic remodelling and transcriptional changes at neuronal- and glial-specific genes from prodromal stage, before the onset of motor deficits. We also find that 3D chromatin architecture, while generally preserved at neuronal enhancers, is altered at the disease locus. Specifically, we find that the HD mutation, a CAG expansion in the *Htt* gene, locally impairs the spatial chromatin organization and proximal gene regulation. Thus, our data provide evidence for two early and distinct mechanisms underlying chromatin structure changes in the HD striatum, correlating with transcriptional changes: the HD mutation globally accelerates age-dependent epigenetic and transcriptional reprogramming of brain cell identities, and locally affects 3D chromatin organization.

[1] Laboratoire de Neurosciences Cognitives et Adaptatives (LNCA), University of Strasbourg, 67000 Strasbourg, France. [2] CNRS UMR 7364, 67000 Strasbourg, France. [3] Institut de Genetique et de Biologie Moleculaire et Cellulaire (IGBMC), 67404 Illkirch, France. [4] CNRS UMR7104, 67404 Illkirch, France. [5] INSERM U1258, 67404 Illkirch, France. [6] University of Strasbourg, 67000 Strasbourg, France. [7] Berlin Institute of Medical Systems Biology (BIMSB), Max Delbrück Center for Molecular Medicine, Berlin, Germany. [8] Centro Andaluz de Biología del Desarrollo (CABD), CSIC-Universidad Pablo de Olavide-Junta de Andalucía, Seville, Spain. ✉email: karine.merienne@unistra.fr

Huntington's disease (HD) is a progressive inherited neurodegenerative disease caused by abnormal CAG repeat expansion in *HTT* coding region. While HD patients present average onset of motor symptoms at 35 years, subtle changes in behaviour and brain circuitry are observed at prodromal stage. Accordingly, the striatum, which is primarily affected in HD, undergoes early changes, altering brain connectivity[1,2]. As a result, it is believed that HD pathogenesis starts earlier than anticipated, which might have major therapeutic implication. However, we still lack early brain molecular correlates that would specify temporal dynamics of disease progression as well as provide insights into the mechanisms driving pathogenesis.

Epigenetic and transcriptional regulation are altered in HD brain tissues[3–11]. Particularly, in the striatum of HD patients and mice, neuronal identity genes are downregulated and depleted in H3K27 acetylation (H3K27ac), whereas glial-specific genes show an opposite trend[3,10]. However, it is unknown whether HD striatal epigenetic signatures progressively develop from early disease stage. Recent epigenomic and transcriptomic analyses using mouse tissues, including neural tissue, showed that variation in H3K27ac, a tissue-specific mark, is a key predictor of dynamic age-related transcriptional changes[12], which might suggest that H3K27ac changes at striatal identity genes in HD interfere with age-dependent mechanisms.

HD belongs to the family of short tandem repeat-associated diseases[13]. These unstable mutations are frequently located at boundaries of topological associated domains (TADs)[14]. It has been suggested that such chromatin architectural features might be hotspots for epigenetic misregulation, but it is yet unclear whether CAG expansion in the context of HD contributes to local remodelling of chromatin architecture.

Here, we defined temporal dynamics of epigenetic changes induced by the HD mutation, profiling the striatal epigenome of slowly progressing HD knockin (KI) mouse model at two early stages of pathology. Data integration with cell type-specific striatal enhancer and transcriptomic databases demonstrated acceleration of age-related epigenetic remodelling and transcriptional changes at neuronal- and glial-specific genes from the earliest stage, i.e. before the onset of motor deficits. Also, 3D chromatin architecture was generally preserved at neuronal-specific genes, though disrupted at selective loci. Specifically, CAG expansion impaired spatial organization of the chromatin in the region encompassing *Htt*, thereby affecting locally gene regulation. Collectively, we uncovered two early and distinct mechanisms underlying chromatin structure changes in HD striatum, and correlating with transcriptional changes: the HD mutation (1) globally accelerates age-dependent epigenetic and transcriptional reprogramming of brain cell identities, and (2) locally affects spatial organization of TADs adjacent to *Htt*.

Results

Early remodelling of epigenetic landscape in striatal neuron and glial cells of HD Q140 mice. To define temporal dynamics of striatal epigenetic changes caused by the HD mutation, we used the Q140 line. HD Q140 heterozygous (het) mice have normal lifespan, display mild HD-like phenotypes and show limited neuronal death, even at late disease stage[15]. Motor function was preserved up to 6 months in Q140 het mice, though subtle behavioural changes reflecting prodromal stage were observed before 6 months (Supplementary Fig. 1). We used whole striatum of HD Q140 het and WT mice of 2 and 6 months to profile HD striatal epigenome at early disease stage, generating H3K27ac, H3K27me3 and RNA polymerase II (RNAPII) ChIP-seq data (Supplementary Fig. 2). HD is generally described as a sex-independent disease affecting similarly males and females, though recent studies indicate sex-dependent effects influencing disease progression[16,17]. To avoid sex-dependent bias in our analyses, we used striatal tissue from both male and female mice. ChIPseq experiments using Q140 and WT samples of specific age and sex were performed simultaneously. For practical reasons, experiments performed on different sexes and at different ages were conducted at different times (see "Methods"). The data were of high quality, as shown by peak enrichment signal to noise rates, correlation analyses and additional quality analyses (Fig. 1a and Supplementary Figs. 2, 3). Moreover, principal component analysis (PCA) showed that sample variability was essentially explained by age (H3K27ac, RNAPII, H3K27me3), batch/sex (H3K27ac, RNAPII, H3K27me3) and genotype (H3K27ac) (Supplementary Fig. 3). Since sex and batch effects could not be distinguished, we focused our analyses on genotype- and age-dependent changes, analysing together male and female samples to assess epigenetic changes common to both sexes.

Differential enrichment analysis of ChIPseq data between Q140 and WT samples showed changes in H3K27ac from 2 months of age (Supplementary Fig. 4a). Regions depleted in H3K27ac in Q140 vs WT striata were enriched in gene ontology (GO) terms related to neuronal function, while regions showing increased H3K27ac in Q140 vs WT striata were enriched in terms implicated in glial function (Fig. 1b), suggesting distinct epigenetic signatures in neurons and glial cells establish from early disease stage. Regions differentially enriched in RNAPII between Q140 and WT samples displayed similar functional signatures, whereas H3K27me3 ChIPseq showed little changes between Q140 and WT striata (Fig. 1b and Supplementary Fig. 4a). Also, the amplitude of H3K27ac and RNAPII changes between Q140 and WT samples increased over time, demonstrating progressive nature of the mechanism (Supplementary Fig. 4a–c). Independent analysis of male and female ChIPseq samples supported the results of combined analysis of male and female samples (Supplementary Figs. 5, 6). Notably, H3K27ac was early depleted and enriched at neuronal and glial genes, respectively (Supplementary Fig. 5).

To specify temporal dynamics of epigenetic changes in HD neurons and glial cells, we generated H3K27ac and H3K27me3 ChIP-seq data in NeuN+ and NeuN− WT mouse striatal nuclei using the fluorescence activated nuclear sorting (FANS) approach[18] (Fig. 1c and Supplementary Figs. 2, 7a), which allowed the identification of neuronal and non-neuronal (essentially glial) specific enhancers (Supplementary Data 1). Integrated analysis of this cell type-specific striatal enhancer database with ChIPseq data generated on bulk striatum of Q140 and WT mice indicated that neuronal-specific enhancers were depleted in H3K27ac in Q140 vs WT samples, both at 2 and 6 months, whereas regions showing increased H3K27ac in Q140 vs WT samples predominantly originated from glial-specific enhancers (Fig. 1d, e). Remarkably, the effect was more specific at 2 vs 6 months (Fig. 1d, e and Supplementary Fig. 7b) and did not result from neuronal loss and/or astrogliosis, since the relative abundance of neuronal vs non-neuronal populations (including astrocytes) were comparable between the striatum of Q140 and WT mice (Supplementary Fig. 8). Thus, opposite remodelling of epigenetic landscape at neuronal- and glial-specific enhancers in HD mouse striatum is an early mechanism establishing at prodromal stage.

Concomitant epigenetic and transcriptional reprogramming of striatal neuron and glial cell identities in HD Q140 mice. We then investigated whether epigenetic and transcriptional changes were correlated in the striatum of HD Q140 mice, taking

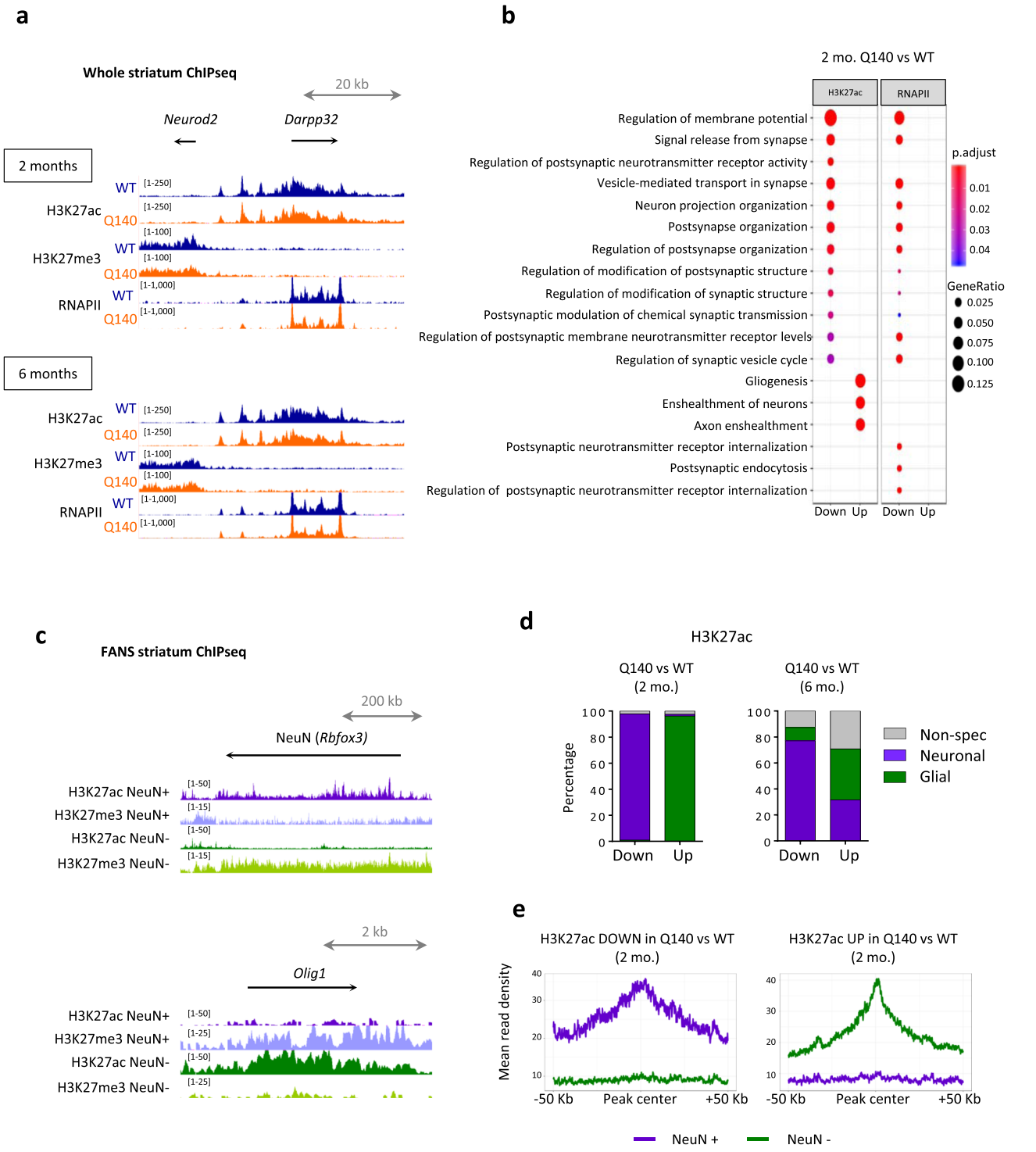

Fig. 1 Striatal epigenetic alterations induced by the HD mutation establish early and in cell-type-dependent manner in HD Q140 mice. a UCSC genome browser capture showing representative H3K27ac, H3K27me3 and RNAPII signals in the striatum of WT and Q140 mouse striatum at 2 and 6 months at selected locus, including active (*Darpp32* (*Ppp1r1b*)) and repressed (*Neurod2*) genes in the adult striatum. 2 mo., 2 months; 6 mo., 6 months **b** Gene Ontology analysis of regions differentially enriched in H3K27ac and RNAPII between Q140 and WT mouse striatal samples at 2 months (FDR < 0.05). Significant biological processes are shown using dot size proportional to gene ratio and heatmap reflecting adjusted *P* value. **c** UCSC genome browser capture showing representative H3K27ac and H3K27me3 signals in striatal NeuN+ and NeuN− populations in WT mice at 6 months at selected neuronal gene (*NeuN* (*Rbfox3*)) and glial gene (*Olig2*). **d** Bargraphs showing cell-type distribution of regions differentially enriched in H3K27ac in Q140 vs WT mouse striatum at 2 and 6 months of age. **e** Metaprofiles showing H3K27ac signal in NeuN+ and NeuN− sorted nuclei, considering differentially enriched peaks in Q140 vs WT striata at 2 months. Source data are provided as a Source Data file.

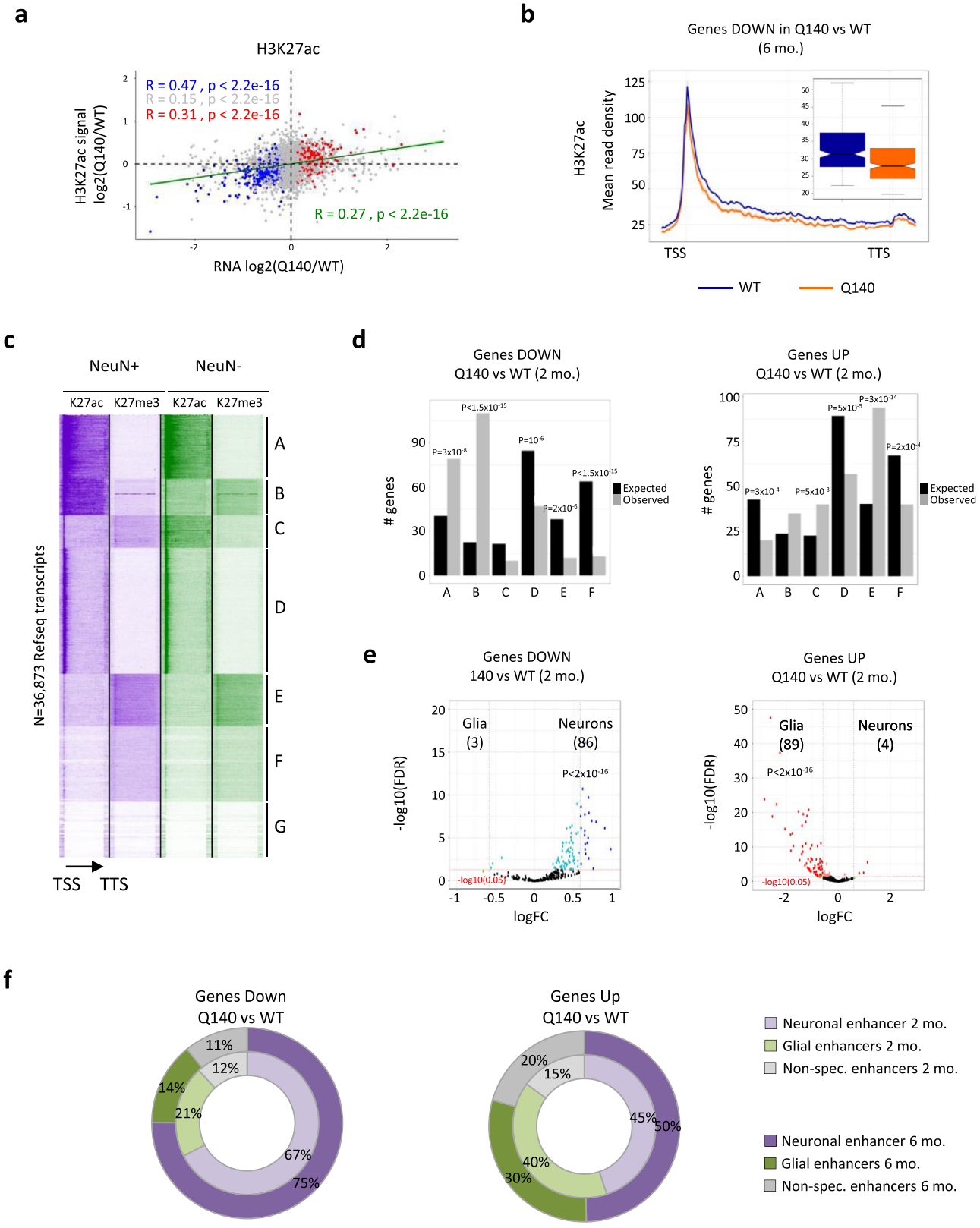

advantage of RNAseq data on HD KI mice[5] (Supplementary Fig. 9a). Integrated analysis was performed between H3K27ac ChIPseq data generated on 2- and 6-month-old striatal tissue of Q140 and WT mice and RNAseq data generated on same mouse line, tissue and ages. Linear regression analysis showed that H3K27ac and mRNA changes between Q140 and WT samples were significantly and positively correlated, with a correlation stronger for down- than up-regulated genes (Fig. 2a). Gene metaprofile analysis supported the conclusion, showing that downregulated genes in Q140 vs WT striatum were specifically depleted in H3K27ac (Fig. 2b and Supplementary Fig. 9b). Similar trends were observed between RNAPII and mRNA changes, but not between H3K27me3 and mRNA changes (Supplementary Fig. 9c, d).

Fig. 2 Concomitant epigenetic and transcriptional reprogramming of neuronal- and glial-specific genes in HD Q140 striatum. a Linear regression analysis between transcriptional and H3K27ac changes in the striatum of Q140 vs WT mice of 6 months. The correlation is shown for all genes (green), genes significantly downregulated (Fold change (FC) <1 and adj. *P* value <0.05; blue), genes significantly upregulated (FC >1 and adj. *P* value <0.05; red) and non-significantly altered genes (grey). Pearson's correlation index and *P* value for fitted linear model are shown. **b** Gene body metaprofiles representing H3K27ac read count distribution for top 300 downregulated genes, ranked according to adj. *P* value, in Q140 mouse striatum at 6 months. TSS transcription start site; TTS transcription termination site. Data from male and female samples were used to generate average profile. Boxplots represent the distribution of mean read density along the profiles and show median, first quartile (Q1), third quartile (Q3) and range (min, Q1−1.5×(Q3−Q1); max, Q3+1.5×(Q3−Q1)). **c** Heatmap of the 36,873 annotated mm10 RefSeq gene transcripts, integrating H3K27ac and H3K27me3 gene profiles from NeuN+ and NeuN− sorted nuclei and showing seven distinct epigenetic profiles generated by *k*-means clustering (clusters A-G). The arrow indicates the orientation of genes; TSS transcription start site; TTS transcription termination site. **d** Histograms showing cluster distribution of genes down- (upper panel) and upregulated (lower panel) in Q140 vs WT striatum at 2 months of age. Three-hundred top dysregulated genes were analysed from RNAseq data[5] and ranked according to *P* value. Observed numbers were compared with expected numbers and a binomial test (two-sided) was used to assess significant differences, with multiple testing correction using the Bonferroni method. **e** Volcano plot representation of differential expression values between glial cells (astrocytes and microglia) and neurons (medium spiny neurons, MSNs, including D1 and D2 MSNs) using top-ranked 300 genes down (top) and 300 genes up (bottom) in Q140 vs WT striatum at 2 months. Genes down in Q140 vs WT striatum and significantly changed in neurons vs glial cells (FC >1 and adj. *P* value <0.05) are shown in blue; genes up in Q140 vs WT striatum and significantly changed in neurons vs glial cells (FC <1 and adj. *P* value <0.05) shown in red. A binomial test (two-sided) was performed to assessed enrichment in neuronal- or glial-specific genes. Adjustment for multiple comparisons was not performed. **f** Pie chart showing the distribution of neuronal-, glial- and non-specific enriched H3K27ac regions (as defined in Supplementary Dataset 1) associated with top 300 genes down (left) and top 300 genes up (right) in Q140 vs WT striatum at 2 and 6 months. Source data are provided as a Source Data file.

Neuronal identity genes, regulated by super enhancers consisting in broad enhancers highly enriched in H3K27ac throughout their target genes[19], are downregulated and depleted in H3K27ac in HD striatum, whereas glial identity genes display an opposite trend[3,10]. To investigate early epigenetic signatures of dysregulated genes in HD mouse striatum at cell type-specific levels, we delineated neuronal and non-neuronal (glial) super enhancer-regulated genes using H3K27ac and H3K27me3 ChIPseq data generated on WT NeuN+ and NeuN− striatal nuclei (Fig. 1c, Supplementary Fig. 2 and Supplementary Data 1). Using *k*-means clustering, we retrieved seven distinct clusters, including clusters enriched in neuronal and non-neuronal super enhancer-regulated genes, respectively (clusters B and C) (Fig. 2c). Specifically, cluster B, which contained neuronal super enhancer-regulated genes, was enriched in H3K27ac and depleted in H3K27me3 in NeuN+ nuclei, but depleted in H3K27ac and enriched in H3K27me3 in NeuN− nuclei (Fig. 2c). Cluster C, comprising non-neuronal super enhancer-regulated genes, showed opposite features (Fig. 2c). Additionally, we identified a cluster enriched in H3K27ac and depleted in H3K27me3 in both NeuN+ and NeuN− nuclei, likely containing super enhancer-regulated genes common to neurons and non-neuronal cells (cluster A, Fig. 2c). Consistently, clusters B and C were enriched in neuronal- and glial-specific genes, respectively, and cluster A contained similar proportion of neuronal- and glial-specific genes (Supplementary Fig. 10a). As expected, genes in clusters B and C were enriched in GO terms reflecting neuronal and glial identities, respectively, while terms associated with cluster A were less homogenous and linked to nucleosome assembly, cell adhesion, and energy metabolism (Supplementary Fig. 10b). Importantly, downregulated genes in the striatum of Q140 vs WT mice at 2 and 6 months were most significantly enriched in the neuronal super enhancer cluster (cluster B, Fig. 2d and Supplementary Fig. 10c), demonstrating that neuronal identity genes are early prone to downregulation in HD mouse striatum. In contrast, upregulated genes in Q140 striatum at 2 months of age were significantly enriched in the glial identity gene cluster (cluster C), as well as in cluster E, containing developmental genes enriched in glial-specific genes (Fig. 2d and Supplementary Fig. 10a, b). Together, these results suggest that maintenance of neuronal and glial identities in the striatum is early challenged by the HD mutation.

Supporting this view, integration of Q140 RNAseq data[5] with cell type-specific striatal transcriptomic database[10] showed that GABAergic medium spiny neurons (MSNs), predominant in the striatum and primarily affected in HD, were highly enriched in downregulated genes in Q140 vs WT striatum, particularly at 2 months, while glial cells were enriched in upregulated genes (Fig. 2e and Supplementary Fig. 10d, e). Finally, integration of Q140 RNAseq data[5] with cell type-specific enhancer database (Supplementary Fig. 2, Supplementary Data 1) showed that downregulated genes in Q140 vs WT striatum were predominantly associated with neuronal-specific enhancers, while substantial glial-specific enhancers were more associated with upregulated genes (Fig. 2f). Together, these results indicate that early remodelling of neuronal- and glial-specific enhancers in HD striatum correlates with transcriptional changes at neuronal and glial identity genes.

Age-related transcriptional changes at striatal identity genes are accelerated in HD Q140 mice. Variation in the amount of H3K27ac at enhancers is a key predictor of age-related transcriptional changes[12], suggesting that age might interact with the HD mutation during epigenetic and transcriptional reprogramming of striatal cell identities. To explore this hypothesis, we first assessed age-dependent transcriptional changes of neuronal- and glial-specific genes in Q140 and WT striatum. Remarkably, neuronal-specific genes were enriched in genes whose expression decreased with age in WT striatum, whereas glial-specific genes showed an opposite trend (Fig. 3a). Importantly, physiological age-dependent transcriptional changes of neuronal- and glial-specific genes were accelerated by the HD mutation: neuronal-specific genes, most particularly genes specific to MSN expressing D1 dopamine receptor (D1 MSN), including *Drd1*, were lower in Q140 than in WT striata at both ages, whereas glial-specific genes (e.g. *Tmem151b*[20]), were increased in Q140 vs WT striatum (Fig. 3b and Supplementary Fig. 11a, b). Integration of transcriptomic databases[5,10] with epigenetic clustering generated in Fig. 2c further supported the conclusions, showing that downregulation of neuronal identity genes (genes in cluster B) and upregulation of glial identity genes (genes in cluster C) were accelerated in Q140 striatum (Supplementary Fig. 12). Thus, neuronal and glial identity genes are regulated in opposite directions with age in mouse, and the HD mutation exacerbates those age-related transcriptional changes.

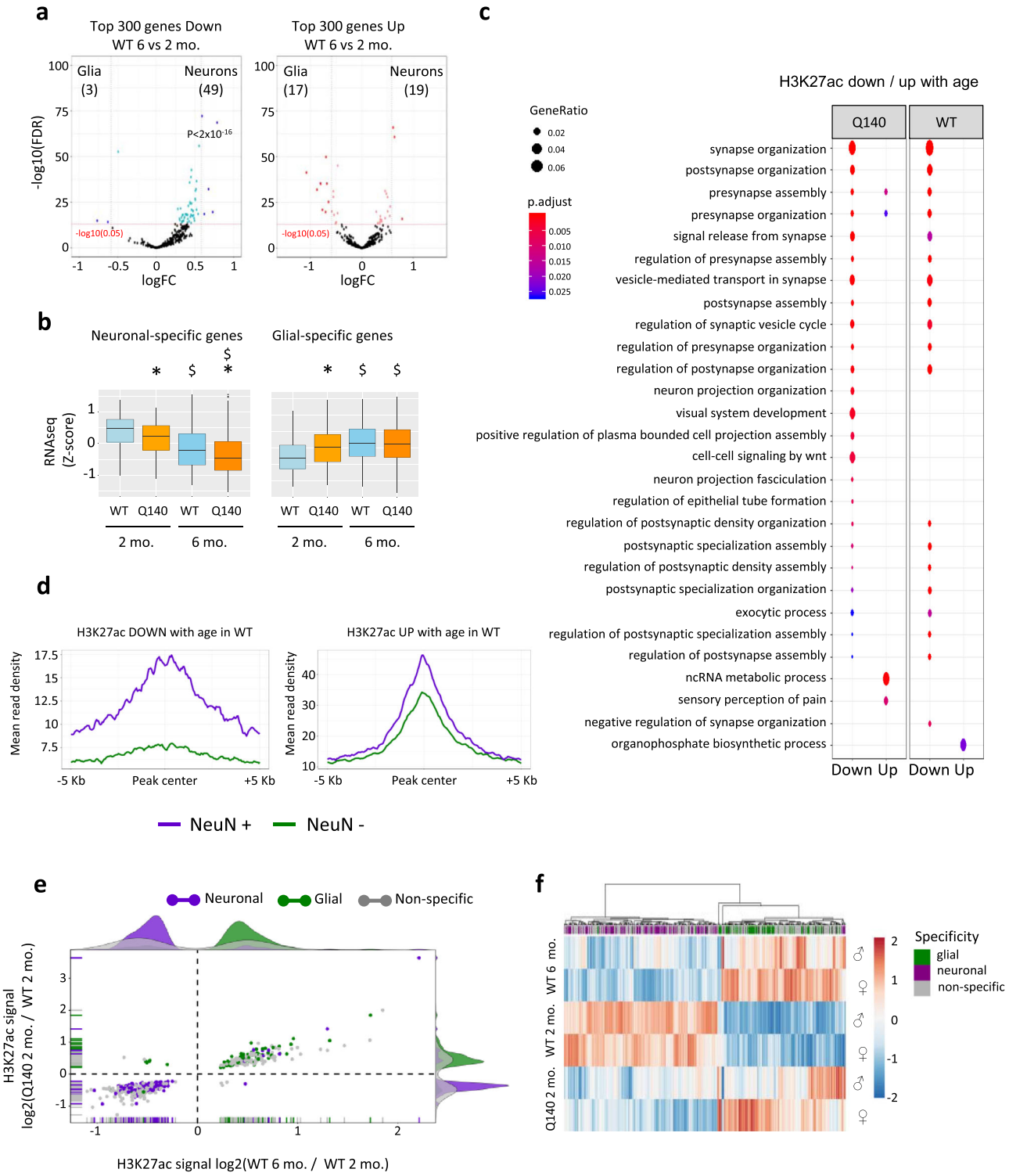

Age-related epigenetic remodelling of neuronal- and glial-specific enhancers is accelerated in HD Q140 mice. We then determined whether acceleration of age-related transcriptional changes in HD mouse striatum would associate with age-related epigenetic mechanisms. Age was the major component of variability of H3K27ac, RNAPII and H3K27me3 ChIPseq data generated on Q140 and WT striata at 2 and 6 months of age (Supplementary Fig. 13a). Moreover, GO analysis indicated that regions depleted in H3K27ac with age associated with neuronal functions in both WT and Q140 samples, whereas functional signatures of regions increased in H3K27ac with age were less consistent (Fig. 3c). Analysis of age-dependent RNAPII changes led to similar signatures, while few GO terms reflecting H3K27me3 changes with age were significantly enriched, whether in WT or Q140 samples (Supplementary Fig. 13b, c). These results suggest that neuronal-specific genes are particularly prone to reduced H3K27ac occupancy and RNAPII recruitment with age. To further explore this possibility, H3K27ac ChIPseq data generated at 2 and 6 months were integrated with cell type-specific enhancer database (Supplementary Fig. 2, Supplementary Data 1). Metaprofile analysis showed alteration of neuronal-specific enhancers over time (Fig. 3d). Specifically, regions

Fig. 3 Age-related epigenetic and transcriptional reprogramming of neuronal and glial identities are accelerated in the striatum of HD Q140 mice. **a** Volcano plot representation of differential expression values between glial cells (astrocytes and microglia) and neurons (medium spiny neurons, MSNs, including D1 and D2 MSNs) using top-ranked (according to adj. *P* val) 300 genes down (left) and top-ranked 300 genes up (right) in WT striatum at 6 months vs 2 months. Genes down at 6 vs 2 months in WT striatum and significantly changed in neurons vs glial cells (FC >1 and adj. *P* value <0.05) are shown in blue; genes up at 6 vs 2 months in WT striatum and significantly changed in neurons vs glial cells (FC <1 and adj. *P* value) are shown in red. A binomial test (two-sided) was performed to assess enrichment in neuronal- or glial-specific genes. Adjustment for multiple comparisons was not performed. **b** Boxplots representing *z*-score values computed from RNAseq data generated in Q140 and WT striatum at 2 months and 6 months, considering genes increased in neurons vs glial cells (neuronal-specific genes, left) and genes increased in glial cells vs neurons (glial-specific genes, right). Boxplots show median, first quartile (Q1), third quartile (Q3) and range (min, Q1−1.5×(Q3-Q1); max, Q3+1.5×(Q3-Q1). Statistical analysis was performed using Kruskal–Wallis test (one-sided), with multiple testing correction using the Benjamini-Hochberg method. Neuronal-specific genes: *, $P < 2 \times 10^{-16}$, Q140 vs WT comparison at 2 months; *, $P < 2 \times 10^{-16}$, Q140 vs WT comparison at 6 months; $, $P < 2 \times 10^{-16}$, 6- vs 2-month comparison in WT; $, $P = 2 \times 10^{-13}$, 6- vs 2-month comparison in R6/1. Glial-specific genes: *, $P < 2 \times 10^{-16}$, Q140 vs WT comparison at 2 months; *; $, $P < 2 \times 10^{-16}$, 6- vs 2-month comparison in WT; $, $P = 9 \times 10^{-10}$, 6- vs 2-month comparison in R6/1. RNAseq data from transcriptomic databases[5,10] were used for these analyses. **c** Gene Ontology analysis of regions differentially enriched in H3K27ac in 6- vs 2-month striatal samples, in Q140 and WT contexts (FDR < 0.05). Significant biological processes are shown using dot size proportional to gene ratio and heatmap reflecting adj. *P* value. **d** Metaprofiles showing H3K27ac signal in NeuN+ and NeuN− sorted nuclei, considering differentially enriched peaks in WT striatal samples of 6 vs 2 months. FC <1 and adj. *P* value <0.05, down, left; FC >1 and adj. *P* value <0.05, up, right. **e** Scatter plot and density population graphs representing log2 of fold-change in H3K27ac at regions significantly changed ($P < 0.05$) both in Q140 vs WT samples at 2 months and in WT samples at 6 vs 2 months. Differentially H3K27ac-enriched regions distribute in three categories: non-specific (Non-specific, grey), neuronal-specific (Neuronal, purple) and glial-specific (Glial, green). **f** Heatmap representing *z*-score values of H3K27ac signal at regions differentially enriched in H3K27ac ($P < 0.05$) both in Q140 vs WT samples at 2 months and in WT samples at 6 vs 2 months. Differentially H3K27ac-enriched regions distribute in three categories: non-specific (Non-specific, grey), neuronal-specific (Neuronal, purple) and glial-specific (Glial, green); hierarchical clustering was performed according to H3K27ac signal. Source data are provided as a Source Data file.

depleted in H3K27ac with age in normal striatum were enriched in neuronal-specific enhancers. In contrast, regions increased in H3K27ac with age originated from both glial- and neuronal-specific enhancers (Fig. 3d).

To investigate possible effect of the HD mutation on age-dependent regulation of neuronal- and glial-specific enhancers, we performed linear regression analysis, comparing the effects of genotype and age on H3K27ac levels: the effects of genotype and age on H3K27ac were significantly and positively correlated, at both neuronal- and glial-specific enhancers (Supplementary Fig. 14a). More specific analysis revealed that regions significantly depleted in H3K27ac with age were also significantly depleted in H3K27ac by the HD mutation, and predominantly originated from neuronal-specific enhancers, whereas glial-specific enhancers contributed to regions showing significant increased H3K27ac with age and in response to the HD mutation (Fig. 3e). Furthermore, hierarchical heatmap representation of regions showing significant H3K27ac variations in both age- and genotype-dependent manners supported this conclusion. Neuronal- and glial-specific enhancers essentially distributed in two distinct clusters, with the cluster of neuronal-specific enhancers containing regions depleted in H3K27ac with age and by the HD mutation, and the cluster of glial-specific enhancers comprising regions with opposite age- and genotype-dependent H3K27ac variations (Fig. 3f).

Moreover, predominant neuronal origin of striatal regions depleted in H3K27ac upon age and in response to the HD mutation was supported by DNA motif analysis, showing enrichment in motifs recognized by DLX/GATA and GCM1/2 (Supplementary Fig. 14b), which are transcription factors essential to the establishment of neuronal fate and striatal identity[21–25]. In contrast, glial origin of striatal regions showing increased H3K27ac due to age and the HD mutation was consistent with enrichment in DNA motif binding THAP12 (Supplementary Fig. 14b), implicated in inflammation and stress response[26]. Finally, neuronal-specific enhancers depleted in H3K27ac in age- and genotype-dependent manners associated with complex network of co-regulated genes, which was significantly enriched in GO terms related to neuronal functions (Supplementary Fig. 14c, d). In contrast, poor complexity characterized the network of co-regulated genes associated with glial-specific enhancers showing age- and HD mutation-dependent increase in H3K27ac (Supplementary Fig. 14c), suggesting a reduced impact of the HD mutation on H3K27ac regulations in glial- than neuronal-specific genes. Together, these results indicate that the HD mutation early accelerates age-dependent remodelling of chromatin landscape at striatal enhancers, precipitating depletion in H3K27ac at neuronal-specific enhancers and, to lesser extent, exacerbating H3K27ac enrichment at glial-specific enhancers, thereby resulting in acceleration of age-related regulation of neuronal and glial identity genes.

3D chromatin architecture is selectively impaired at striatal identity genes in HD mice. To further define the relationship between epigenetic and transcriptional changes in Q140 striatum, we performed 3D chromatin architecture analyses. High levels of H3K27ac at super-enhancers correlate with extensive chromatin looping between promoters and enhancers, which facilitates rapid transcription dynamics[27–29]. We hypothesized that dysregulation of super enhancer-regulated genes in HD striatum may associate with changes in spatial organization of the chromatin, and generated 4C-seq data to explore this possibility. Experiments were performed using the striatum of male and female Q140 and WT mice at 6 months of age, and targeting super enhancer-regulated genes downregulated in HD striatum, including *Pde10a*, *Gpr6* and *Ptpn5*, and non-super enhancer-regulated genes such as *Msh2*, as a control (Fig. 4a, b, Supplementary Figs. 15, 16a–c and Supplementary Data 2). Chromatin looping at *Pde10a* was impaired in male and female Q140 samples (Fig. 4b and Supplementary Fig. 15). Specifically, we identified striatal interactions of the *Pde10a* promoter with four upstream H3K27ac-enriched regions, and three intronic regions of the gene. The upstream interactions were consistently reduced, and intronic interactions were increased, in Q140 vs WT mice. Similar results were obtained from the analysis of 4C-seq data generated on the striatum of another HD mouse, the HD R6/1 transgenic model, over-expressing *HTT* exon-1 with CAG expansion[30] (Fig. 4c). Furthermore, upstream interacting regions were not observed in embryonic stem cells (mESC)[31], suggesting a role in cell type-specific expression of *Pde10a* (Fig. 4c). Finally, H3K9me3

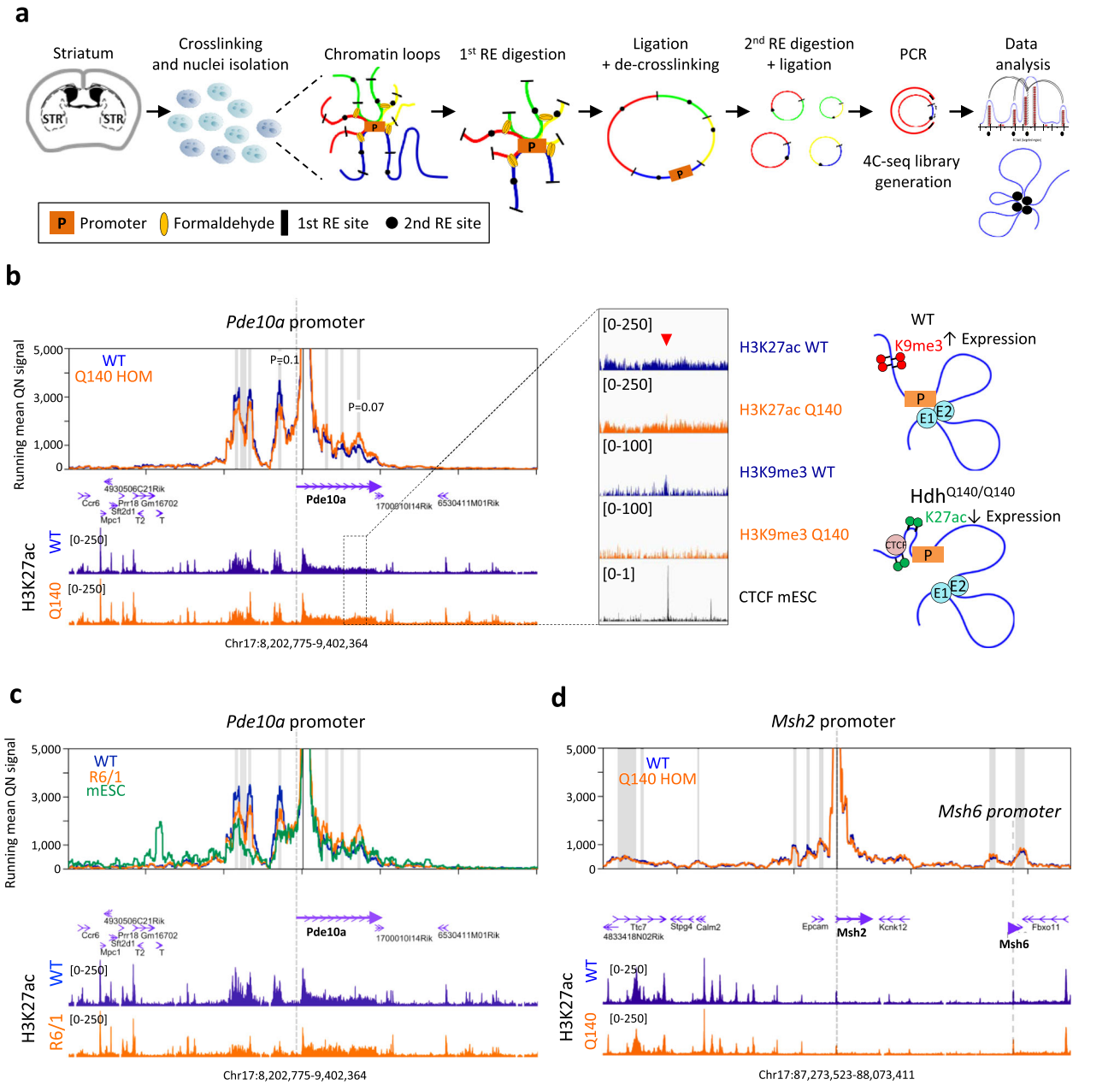

Fig. 4 Chromatin architecture at *Pde10a* is impaired in the striatum of HD Q140 mice. a Scheme showing 4C-seq technique major steps using mouse striatum. PCR primers specific to each bait can be found in the "Methods" section. RE restriction enzyme. **b** On the left, 4C-seq profiles at *Pde10a* locus using HD Q140 (orange) and WT (blue) mouse striatum at 6 months. The mean of male and female 4C-seq quartile normalized read counts is plotted as the main lane for each condition. Statistical analysis of differential interacting peaks in Q140 vs WT was performed using two-paired *t*-test, with multiple testing correction using the Benjamini-Hochberg method. $P = 0.1$ (upstream of *Pde10a* promoter), $P = 0.07$ (downstream of *Pde10a* promoter). Gene annotations are included as well as H3K27ac ChIPseq signals (using ChIPseq data generated in this study on the striatum of Q140 and WT mice at same age). Grey shadows show specific interacting regions. On the middle, zoom into *Pde10a* intronic region, showing H3K27ac and H3K9me3 levels in WT and Q140 mice striatum together with CTCF enrichment (from CTCF ChIP-seq data generated in mESC). On the right, model to explain chromatin conformational changes at *Pde10a* locus in HD mouse striatum. **c** 4C-seq profiles at *Pde10a* locus generated using HD R6/1 (orange) and WT (blue) mouse striatum at 14 weeks of age and using mESC (green). Gene annotations and H3K27ac ChIPseq signals[3] are included. Grey shadows show specific interacting regions. **d** 4C-seq profiles at *Msh2* locus using Q140 (orange) and WT (blue) striatum at 6 months. The mean of male and female 4C-seq quartile normalized read counts is plotted as the main lane for each condition. Gene annotations and H3K27ac ChIPseq signals are included. Grey shadows show specific interacting regions. *Msh6* promoter is annotated to highlight the distal chromatin loop formed with *Msh2* promoter.

ChIPseq data generated on WT mouse striatum showed a specific H3K9me3 peak located at a *Pde10a* intronic region, which interacts with the promoter, coinciding with a CTCF peak (Fig. 4b and Supplementary Fig. 16d, e). Convergent CTCF motifs are a hallmark of many chromatin loops[32], and the *Pde10a* promoter and interacting intronic region comprise such a convergent CTCF pair. Remarkably, this H3K9me3 intronic peak was absent in Q140 striatum (Fig. 4b), suggesting that a repressive intragenic *Pde10a* loop may be stabilized at the expense of upstream activating loops in HD striatum (Fig. 4b), a mechanism reminiscent to the regulation of chromatin architecture at *Grin2b*[33].

Analysis of additional loci indicated that the HD mutation did not substantially affect chromatin looping at the other tested super enhancer-regulated genes or at *Msh2* gene, though specific promoter–enhancer interactions were observed for these genes (Fig. 4d, Supplementary Fig. 16a, b and Supplementary Data 2). For example, we identified a chromatin loop between *Msh6* and *Msh2* promoters (Fig. 4d), which might explain the co-regulation of these two DNA repair proteins forming a heterodimer[34]. Altogether, these results suggest that chromatin topology is largely unchanged by H3K27ac depletion at neuronal super enhancers or transcriptional downregulation of their target genes during HD onset, although locus-specific architectural changes involving additional mechanisms may be observed at subsets of neuronal super enhancers.

CAG expansion locally affects 3D chromatin architecture and transcription in the striatum of HD Q140 mice. Disease-associated short tandem repeats, including CAG expansion in *HTT*, are often located to TAD boundaries[14]. In the case of Fragile X, CGG expansion at *FMR1* was shown to alter proximal chromatin topology. We hypothesized that CAG expansion in the context of HD might similarly impair chromatin architecture of TADs encompassing *HTT*. Consistent with highly conserved TAD organization between mice and humans[35], CAG expansion in human and murine *HTT* is located in the vicinity of a TAD border as depicted by human hippocampal[36] and mouse cortical neuronal[37] Hi-C data (Fig. 5a). We therefore addressed the hypothesis using the striatum of Q140 homozygous (hom) mice (and WT mice as controls), especially since Q140 hom mice, presenting both alleles with CAG expansion in its proper genomic context, embody an ideal experimental model. Striatal tissues of both male and female animals were used in the analysis. Specifically, using striatal tissue of Q140 hom and WT mice, we generated 4C-seq data targeting 5 promoter regions of genes encompassing a two-megabase window of the genome, comprising *Htt* (i.e. *Mxd4*, *Nop14*, *Htt*, *Lrpap1* and *Acox3*) (Fig. 5b). Then, by using the recently developed 4Cin bioinformatics tool[38], we modelled three-dimensional chromatin architecture of this two-megabase region in HD and WT genomic contexts (Fig. 5c and Supplementary Fig. 17a–c).

Overall, generated 3D models showed high levels of similarity across datasets, with correlation coefficients ranging from 0.8 to 0.87 (Supplementary Fig. 17a). Remarkably, superposition between those models and our H3K27ac, H3K27me3 and RNAPII ChIPseq data (Supplementary Fig. 17b and Supplementary Movies 1, 2) indicated that compacted regions of 3D models were enriched in H3K27me3 and depleted in H3K27ac and RNAPII, whereas, on the opposite, open regions were enriched in H3K27ac and RNAPII and depleted in H3K27me3. Moreover, transcriptional activity of genes located in the region was related to spatial proximity of H3K27ac, H3K27me3 and RNAPII ChIPseq peaks (Supplementary Fig. 17c). These analyses showing high degree of coherence across chromatin spatial organization predicted by 3D models, epigenetic features assessed by ChIPseq data analysis, and transcriptional rate measured from RNAseq data, provided strong support to 3D model validity.

To evaluate possible alteration in TAD organization in Q140 mice, we computed an insulation score, quantifying TADs and subTADs boundaries[39]. Regions at TADs/subTADs boundaries associate with low level of compaction and, in consequence, low insulation score. Consistently, *Htt* region in WT striatum was located at TAD boundary, since it associated with low insulation score (Fig. 5c, green arrows). Remarkably, however, corresponding insulation score in Q140 samples was increased, most prominently for female sample. Finally, re-organization of subTAD boundary upstream to *Htt* was consistently observed in Q140 vs WT striata (Fig. 5c, black arrows). In Q140 samples, this boundary was displaced to a downstream region when compared to WT samples. More specifically, the boundary was located <1.5 Mb and >1.5 Mb with respect to distance scale in Q140 and WT samples, respectively (Fig. 6c, black arrows). Together, these results indicate that CAG expansion at *Htt* locally impairs TAD insulation.

Moreover, re-analysing RNAseq data generated in the striatum of Q140 and WT mice, we observed that differentially expressed genes (DEGs) were significantly enriched on chromosome 5, containing *Htt* (Fig. 5d). At 2 months, 16% of DEGs were located in chromosome 5 and they were predominantly in *Htt* close neighbourhood (Fig. 5d). *Htt* itself and juxtaposed gene *Grk4* were decreased and increased in the striatum of HD KI mice, respectively (Supplementary Fig. 17d). As expected, chromosome 5 was not enriched in DEG in the striatum of R6/1 transgenic mice overexpressing CAG-expanded *HTT* exon-1 vs WT mice[30,40], and *Htt* and *Grk4* were unchanged in the striatum of R6/1 mice (Supplementary Fig. 17d–f). Together, this indicates that CAG expansion at *Htt* in striatal tissue locally impairs spatial genome organization, which in turn likely affects transcriptional regulation of the region.

Discussion

Here we have used slowly progressing KI mouse model of HD to investigate HD-associated epigenetic signatures at early disease stages. We have generated H3K27ac, RNAPII and H3K27me3 ChIPseq datasets using striatal tissues of HD mice and WT mice at 2 and 6 months, corresponding to prodromal stages. We have also generated H3K27ac and H3K27me3 ChIPseq datasets in neuronal and non-neuronal striatal cell populations, as well as striatal 4C-seq data at selected genes, including neuronal identity genes (regulated by super-enhancers) and 4C-seq data encompassing *Htt* locus. Those epigenomic datasets were integrated with transcriptomic databases, generated with same mouse model, and with cell-type specific transcriptomic databases[5,10]. We show that in HD mouse striatum, epigenetic and transcriptional reprogramming is an age-related mechanism establishing from prodromal stages: the HD mutation exacerbates age-dependent decreased and increased H3K27ac at neuronal- and glial-specific enhancers, respectively, with RNAPII and gene expression changes following similar dynamics. Thus, we provide evidence that the HD mutation leads to acceleration of age-related transcriptional and epigenetic regulation of neuronal and glial cell identities in the striatum. Moreover, our analyses focused on *Htt* locus reveal local rearrangements of 3D chromatin architecture encompassing CAG expansion, which likely contributes to local dysregulation of transcription. Collectively, these results indicate that epigenetic and transcriptional signatures in HD striatum comprise two distinct components, which are age-related and disease-locus specific.

Epigenetic aging in the brain is an emerging concept that is still poorly defined. The recent studies showing that few hundreds of DNA methylation sites can be used to assess the "epigenetic clock" of a given tissue represent few exceptions[41,42]. Analysing DNA methylation from post-mortem brain tissues of HD patients and control individuals, Horvath and collaborators observed a positive correlation between epigenetic age and HD status, which suggests that the HD mutation leads to acceleration of aging[41]. However, such a correlation was not measured when analysing the striatum, possibly due to major striatal neuronal loss in the samples analysed, collected at rather late disease stage. Our study showing that H3K27ac may be used as a biomarker to assess epigenetic aging extends these results and suggest that the HD

striatum, which is primarily affected in HD, undergoes accelerated epigenetic aging. When precisely acceleration of epigenetic aging may start in HD striatum will remain an open question, but the finding that it might be observed far before motor symptoms arise in HD KI mice indicates that it could be an early biomarker.

Investigating neuronal and non-neuronal (essentially glial) enhancers in mouse striatum using H3K27ac, a cell type-specific histone modification, we provide evidence for age-dependent epigenetic reprogramming of brain cell identities, and show that the mechanism correlates with the transcriptional response. Remarkably, the direction of age-related epigenetic and transcriptional changes at neuronal and glial identity genes was opposite, and consistent with major features of brain aging, i.e. progressive alteration of neuronal activity and activation of glial

Fig. 5 The HD mutation induces disease locus-specific alterations of chromatin architecture and transcription regulation in the striatum of Q140 mice. **a** Hi-C data capture showing 3 and 2.3 megabase genome region from human hippocampus and mouse cortical neurons, respectively. In both cases, *Htt* is in the vicinity of TAD borders (~250 Kb for human *HTT* and ~115 Kb for mouse *Htt*). **b** Genome browser representation of mouse cortical neuron Hi-C data, zooming on the region encompassing *Htt*, and aligned with 4C-seq data generated in this study using striatal tissue of WT (blue) and Q140 (orange) mice. The genomic locations of *Mxd4*, *Nop14*, *Htt*, *Lrpap1* and *Acox3* 4C-seq baits are indicated. **c** Virtual Hi-C heatmap of contact matrices for WT and Q140 striatal data at *Htt* locus (top). Colour scale indicates distance between regions in Angstroms (Å). Colour spheres depicting the location of the original baits are shown. In the bottom, insulation score cumulative heatmaps were computed using bins from 4 (40 Kb) to 30 (300 Kb) adding 1 bin each time[37]. Green arrow shows the location of *Htt* at TAD boundary. Black arrow shows the location of subTAD boundary downstream to *Htt*, displaced in Q140 mice data. **d** Left, Manhattan plot representing the distribution of differentially expressed genes (DEGs) in Q140 vs WT striatum at 2 months across the different chromosomes. Significant DEG (adj. *P* value <0.05) are labelled as red dots and the percentage of DEG within each chromosome is shown in peripheral arc. Right, Histogram showing chromosome distribution of DEGs in Q140 vs WT striatum at 2 months of age. Observed numbers were compared with expected numbers for each chromosome and a binomial test (two-sided) was used to assess significant differences, with multiple testing correction using the Bonferroni correction. Source data are provided as a Source Data file.

cells. While it has been reported that shifts in glial cell identity are transcriptional hallmark of human brain aging[43], it is the first time that integrated epigenetic and transcriptional analysis provides evidence for altered maintenance of neuronal identity with age, and additionally shows that this mechanism is early accelerated in a neurodegenerative disease. Our DNA motif analysis indicating enrichment of a sequence recognized by DLX/GATA transcription factors at neuronal-specific regions depleted in H3K27ac in age- and genotype-dependent manners in mouse striatum further support these results, since these transcription factors are critical to the acquisition and maintenance of GABAergic neurons, including striatal neurons[21,22,24]. Strikingly, *Dlx6*, which remains highly expressed in mature GABAergic neurons[44], was decreased both with age and in Q140 vs WT striatum (Supplementary Fig. 11c). This raises the intriguing hypothesis that the HD mutation precipitates age-related neuronal identity loss through a DLX-dependent mechanism.

Specific H3K27ac changes have also been observed in cortical tissues of Alzheimer disease (AD) patients[45], suggesting H3K27ac might be broadly used to investigate epigenetic landscape of neurodegenerative diseases. Since aging is a strong risk factor in AD, it would therefore be important to determine whether H3K27ac reflects epigenetic aging in AD. Supporting this possibility, increasing evidence indicates that enhancers are critical regions implicated in brain diseases, especially since they are hotspots for genetic variations[45–47]. Additional histone modifications may also be age- and/or disease-associated. For example, H4K16ac, a mark enriched at promoters, increases in senescent cells[48]. In humans, normal aging resulted in increased H4K16ac in the lateral temporal lobe, while in AD patients, the trend was opposite, suggesting dysregulation of epigenetic aging[48]. However, it is unclear whether H4K16ac was differentially regulated in neurons and glial cells upon aging. Nevertheless, these results further support the idea of a role for histone acetylation in epigenetic aging and neurodegenerative diseases.

Cell type-specific identity genes are under the control of super-enhancers[3,19,49]. Through chromatin looping, super-enhancers undergo extensive interactions with promoter regions of target genes[27–29]. We hypothesized that decreased H3K27ac at neuronal super-enhancers of HD striatum might associate with disruption of their chromatin architecture, a mechanism that would contribute to downregulation of neuronal identity genes. Our 4C-seq data using HD mouse striatal tissue indicate that, generally, chromatin architecture at super enhancer-regulated genes is not dramatically altered. However, spatial chromatin organization at *Pde10a*, a neuronal identity gene downregulated from early stage in HD striatum, was impaired[50]. The interaction between *Pde10a* promoter and upstream regulatory enhancers was consistently attenuated in the striatum of two HD mouse models, whereas the interaction between *Pde10a* promoter and downstream intronic region was increased. Our analyses suggest that the HD mutation promotes repressive conformation of chromatin architecture, possibly through a mechanism involving depletion in H3K9me3 and CTCF.

CAG repeat expansion is a dynamic mutation, showing tissue-dependent instability[13]. In HD patients and mouse models, the number of CAG repeats increases over time. Remarkably, somatic CAG repeat expansion is most prominent in the striatum[13,51,52]. Up to 1000 of repeats were measured in post-mortem samples of human patients inheriting <60 repeats[52]. Moreover, recent GWAS studies indicate that gene modifiers of HD onset are enriched in DNA repair genes modulating CAG repeat instability[53,54]. These data strongly support the view that CAG repeat instability contributes to pathogenesis, increasing vulnerability of the striatum[55]. The mechanism may implicate local remodelling of chromatin architecture. In support to this hypothesis, Sun and collaborators recently showed that disease-associated short tandem repeats are located in the vicinity of TAD boundaries. The authors showed that CGG expansion mutation in Fragile X syndrome impairs the insulation between adjacent TADs[14]. Our analyses indicate that CAG expansion in *Htt* gene also lies close to the boundary between two TADs. Using 4C-seq datasets generated across a genomic region encompassing Htt-associated TADs and bioinformatics modelling to build virtual Hi-C maps, we show that CAG expansion mutation in the striatum of HD KI mice affects the insulation of TADs adjacent to disease locus. Moreover, we show that CAG expansion in HD mouse striatum, particularly of young animals, leads to enrichment of genes differentially expressed in chromosome 5, which contains *Htt*. This suggests that CAG expansion locally affects TAD organization and gene regulation. Possible contribution of this mechanism to pathogenesis will remain to be investigated.

In conclusion, we generated high-quality epigenomic datasets to assess the dynamics of epigenetic landscape in neurons and glial cells during early stage of HD progression in mice. Integrating our ChIPseq and 4C-seq datasets with transcriptomic databases, we uncovered that age-related and disease locus-specific mechanisms both contribute to remodelling of chromatin structure in a manner correlating with transcriptional changes. These epigenomic databases, which were generated in a tissue, the striatum, still poorly investigated with omics approaches, represent powerful resource for future studies aimed to decipher brain disease-associated signatures.

Methods

Animals. Heterozygous and homozygous Q140 mice as well as heterozygous R6/1 mice were maintained on C57BL/6J genetic background. All animal studies were conducted in accordance with French regulations (EU Directive 2010/63/UE–French Act Rural Code R 214-87 to 126). The animal facility was approved by veterinary inspectors (authorization no. E6748213) and complies with the Standards for Human Care and Use of Laboratory Animals of the Office of Laboratory

Animal Welfare. All procedures were approved by local ethics committee (CREMEAS) and French Research Ministry (no. APAFIS#4301-2016022912385206v2 and no. APAFIS#504-2015042011568820_v3). Mice were housed in a controlled-temperature room maintained on a 12 h light/dark cycle. Food and water were available ad libitum. For molecular analyses (ChIPseq and 4C-seq), mice were killed by cervical dislocation and their striata were rapidly dissected, snap frozen and stored at −80 °C. For 6 months Q140 mice ChIP-seq experiments, tissues from Jackson Laboratory were used. Genotyping was performed by PCR, using tail DNA obtained from 10–15-day-old Q140 mice with primers amplifying the CAG repeat region within the exon 1 of the Huntingtin gene.

Behavioural tasks. For actography, spontaneous locomotor activity, reflecting motor function and/or motivation/apathy, was measured during 2 consecutive days; 2-, 6- and 12-month-old animals were tested (2 months, WT: $N = 8$ males, $N = 4$ females, Q140 het: $N = 8$ males, $N = 4$ females; 6 months, WT: $N = 10$ males, Q140 het: $N = 10$ males; 12 months, WT: $N = 6$ males, $N = 4$ females, Q140 het: $N = 6$ males, $N = 4$ females). The number of times that mice disrupt infrared laser were scored and averaged across days and nights. For bar test, motor coordination and balance were assessed using the beam walking assay; 6- and 12-month-old male mice (6 months, WT: $N = 10$, Q140 het: $N = 10$; 12 months, WT: $N = 10$, Q140: $N = 8$) were trained on an elevated narrow beam of 80-cm long, to reach a safe platform containing their home cage. Mice were first habituated to the beam, and then tested through four consecutive trials, each lasting 1 min. The time to cross the beam (latency) was assessed. To assess motor coordination and strength, the accelerating rotarod task was performed; 6- and 12-month-old male mice (6 months, WT: $N = 10$, Q140 het: $N = 10$; 12 months, WT: $N = 10$, Q140: $N = 8$) were trained on a rotarod (Bioseb) at 4 r.p.m. for 2 min. Mice were then tested in three consecutive trials with 45 min inter-trial time, in which the speed of the rod increased from 4 to 40 r.p.m. during 5 min. The latency to fall was recorded as a measurement of mouse performance. This sequence was repeated on 3 consecutive days and values were averaged across trials from the same day. Data were expressed as means ± standard error of the mean (SEM).

Fluorescence activated nuclear sorting. Cell-type specific nuclear purification was performed using fluorescent activated nuclear sorting[56,57]. Briefly, frozen striatal tissue was homogenized in ice-cold PBS supplemented with 1× Protease Inhibitors Cocktail (PIC, cOmplete EDTA free, Roche) and cross-linked in 1% formaldehyde for 15 min at room temperature. Cross-linking was stopped by the addition of glycine to final concentration 0.125 M and tissue was washed using ice-cold PBS. Cells were then lysed in Cell Lysis Buffer (10 mM Hepes pH 8; 85 mM KCl; 0.5% NP-40) and nuclei were collected after treatment with Nuclear Extraction Buffer (0.5% SDS, 10 mM EDTA pH 8, 50 mM Tris). Purified nuclei were then resuspended in PBTB (PBS 1×, 5% BSA, 0.5% Tween-20) + 1× PIC, 3% Normal Horse Serum (NHS) and stained using antibody to NeuN (1:1000, Merck Millipore). After washing, nuclei were labelled with Alexa Fluor 488 donkey anti-mouse IgG antibody(1:1500) and washed with ice-cold PBS. Immunostained nuclei were sorted using BD Aria Fusion flow cytometer, recovered in ice-cold 1× PBS, pelleted and stored at −80 °C for posterior ChIP-seq experiments.

NeuN+/− nuclear quantification using FANS. Nuclear extracts using the striatum of WT and Q140 heterozygous mice of 2 and 6 months ($n = 4$ per group) were prepared using non-crosslinking nuclear extraction protocol. Briefly, frozen striata were pulverized using a grinder and pestle settle on dry ice and reconstituted in PBS 1× supplemented with 1× PIC. Cell lysis and nuclear extraction were performed by a 10-min incubation in LB1 buffer (1 M HEPES pH 7.5, 5 M NaCl, 0.5 M EDTA pH 8.0, 50% glycerol, 10% NP-40, 10% Triton X-100, 1× PIC) and mechanical dissociation in a glass douncer. Nuclei were then filtered with a 50-µm pore size cell strainer (Sysmex Partec, Kobe, Japan) and stained using Alexa Fluor 405 (AF405) conjugated NeuN antibody (1:200; Novus Biologicals). Nuclear suspension was then sorted using BD FACS ARIA II flow cytometer with a minimum of 30.000 singlet gated events per sample, and NeuN positive (NeuN+) and negative (NeuN−) nuclear proportions were quantified as a relative value of the total number of events registered in these two categories (i.e. "NeuN+" % = "NeuN+ "/ ("NeuN+" + "NeuN−") × 100 and "NeuN−" % = "NeuN− "/ ("NeuN+" + "NeuN−") × 100).

NeuN and Sox9 immunohistological analysis. WT and Q140 heterozygous mice of 2 months ($n = 4$ per group) were intracardially perfused with 4% paraformaldehyde in 0.1 M phosphate buffer, and brains were recovered and post-fixed for additional 6 h at 4 °C. Brains were then cryoprotected by a 48 h incubation in 20% sucrose 0.2 M phosphate buffer, and frozen by a 1-min submersion in dry-ice chilled isopentane. Frozen brains were cut using Leica Microm HM560 cryostat to generate 30-µm-thick striatal coronal sections inter-spaced 150 µm from each other, throughout the full striatum (8–11 slices per mice were generated). Tissue immunostaining was performed as previously described[58]. Briefly, mice coronal sections were washed twice with PBS during 5 min and incubated with NH4Cl 50 mM during 30 min to block free fixation-remaining aldehyde groups and reduce aldehyde-induced tissue auto-fluorescence. The tissue was then permeated during 20 min with a PBS 1× buffer containing 0.5% Triton X-100 and blocked after it for 1 h at room temperature with PBS 1× plus 0.2%, bovine serum albumin, 0.2% lysine, 0.2% glycine, 0.5% Triton X-100 and 5% normal horse serum. Afterwards, the slices were incubated overnight with neuronal-specific NeuN (1:500, Merck Millipore) and astrocytic-specific Sox9 (refs. [59,60]) (1:200, Cell Signalling) primary antibodies in a buffer containing PBS 1× plus 0.3% Triton X-100, 0.2% bovine serum albumin. Then, brain sections were washed twice in PBS 1x ^{x} during 10 min and incubated for 2 h at room temperature in primary antibody buffer with Alexa Fluor 488 donkey anti-mouse IgG or Alexa Fluor 594 donkey anti-rabbit IgG secondary antibodies (1:1500, Invitrogen). Two additional washes of 10 min each with PBS 1× were done to remove the excess of secondary antibodies and nuclear staining was performed by using Hoechst 33258 (1:1000) at r.t. during 5 min. Before mounting the slices, two additional washes with PBS 1× were performed. Afterwards, slices were mounted in glass slides and Mowiol mounting media was used to incorporate glass coverslip. Hamamatsu Nanozoomer Digital Pathology whole slide imaging system (Hamamatsu Photonics) was used for image acquisition of whole brain sections at 40× magnification. The images were then first processed with NDP View v2 software (Hamamatsu Photonics) to delimit the striatal region within each brain section and corresponding area (mm^2), and image exportation parameters were established for Sox9 and NeuN channels for the whole experimental image set to avoid any possible bias in posterior counting. The number of NeuN+ and Sox9+ nuclei in delimited striatal area of each brain section was automatically counted, using the spot detector module of ICY software (Institut Pasteur, Paris, France) to avoid experimenter bias[61], and normalized by striatal area (mm^2) to compute cell density.

RNAseq analysis. RNAseq datasets generated in the striatum of HD KI mice and control mice (GSE65774, https://www.ncbi.nlm.nih.gov/geo/query/acc.cgi?acc=GSE65774)[5] were re-analysed as previously described[3] starting from fastq files. Datasets were downloaded from GEO website according to the GEO identifier provided by the HDinHD website. Tophat2 (ref. [62]) was used for reads mapping using mm10 genome assembly. Quantification of gene expression was performed using HTSeq v0.6.1p1 (ref. [63]), using gene annotations from Ensembl GRCm38 release 87. Read counts were normalized across libraries with the method proposed by Anders and Huber[64]. The method implemented in the DESeq2 (ref. [65]) Bioconductor package (DESeq2_1.14, R_3.3.2) was used to identify significantly DEGs between different mouse genotypes. Resulting *P*-values were adjusted for multiple testing by using the Benjamini and Hochberg method[66]. Down- and up-regulated genes were defined using adj. *P* val <0.05 and FC < or >1. Top 300-ranked dysregulated genes, based on *P* val or adj *P* val, were used in specific analyses. Manhattan plot for genes differentially expressed at 2 months in Q140 vs WT mice and at 6 months in R6/1 vs WT mice were generated using CMplot R package (https://github.com/YinLiLin/R-CMplot), showing –log10(adjpvalue) for all annotated genes. Volcano plots, boxplots and *z*-score heatmaps were generated using R packages[67]. Cell type-specific striatal RNAseq dataset generated using laser capture microdissected cell populations of WT mouse striatum were analysed as described[10]. Briefly, in this study, the transcriptome of two neuronal populations (i.e. MSNs expressing D1 receptor (D1 MSNs) and MSNs expressing D2 receptor (D2 MSNs), corresponding to neuronal populations affected in HD and predominant in the striatum), and two glial cell populations (astrocytes and microglia), was profiled. To simplify some analyses, D1 and D2 MSNs samples were grouped together and compared to glial samples (i.e. astrocytes and microglia). Down- and upregulated genes in neurons vs glial cells were defined using adj. *P* val <0.05 and FC < or >1, as described[10].

Chromatin Immunoprecipitation and sequencing (ChIPseq). Each ChIP-seq experiment on bulk striatal tissue was performed using the striata of four animals and dividing chromatin extracts in four fractions to allow immunoprecipitating same extract with H3K27ac, H3K27me3 and RNAPII antibodies, and including Input controls. Striata of Q140 heterozygous mice and control wild-type (WT) mice at 2 and 6 months were used in the experiments. ChIPseq data were replicated through four independent experiments (experiment 1, using WT and Q140 striatum at 2 months; experiment 2, using WT and Q140 striatum at 2 months; experiment 3, using WT and Q140 striatum at 6 months; experiment 4, using WT and Q140 striatum at 6 months). Male tissues were used in experiments 1 and 3, and female tissues in experiments 2 and 4. Male and female data of same genotype and age were analysed together to determine differentially enriched regions common to both sexes. Single H3K9me3 ChIPseq experiment was performed using the striatum of Q140 and WT male mice of 6 months. For H3K27ac and H3K27me3 ChIP-seq experiments performed on sorted striatal nuclei of WT mice, 250.000 striatal nuclei were used. The data were replicated through two independent experiments. ChIP-seq was performed as previously described[3] using antibodies to H3K27ac (ab4729,Abcam), H3K27me3 (C15410195, Diagenode), and RNAPII[68]. Briefly, for bulk tissue ChIP-seq experiments, pooled tissues were cut into small fragments, fixed in 1% formaldehyde and incubated for 15 min at room temperature. Cross-linking was stopped by the addition of glycine to final concentration 0.125 M. Tissue fragments were washed with cold PBS supplemented with protease inhibitors. The tissues were then mechanically homogenized in sonication buffer to obtain a homogeneous solution. Tissue homogenates or nuclear suspension (see 'Fluorescence activated cell sorting' in "Methods" section) were sonicated to obtain DNA fragments <500 bp using Covaris Ultrasonicator E220 and centrifuged. The soluble chromatin fraction was pretreated with protein

A Agarose/Salmon Sperm DNA (Millipore) for 45 min at 4 °C. Subsequently, samples were incubated overnight at 4 °C with corresponding primary antibodies. Protein A Agarose/Salmon Sperm DNA was then added and the mixture was incubated for 3 h at 4 °C in a shaker. Agarose beads were washed, protein–DNA complexes were eluted from the beads and de-crosslinked overnight with RNAse A at 65 °C. Proteins were eliminated by 2 h incubation at 45 °C with Proteinase K, and DNA recovered using Qiagen MiniElute PCR Purification Kit.

ChIPseq library preparation. ChIP samples were purified using Agencourt AMPure XP beads (Beckman Coulter) and quantified with Qubit (Invitrogen). ChIP-seq libraries were prepared from 2 ng of double-stranded purified DNA using the MicroPlex Library Preparation kit v2 (C05010014, Diagenode), according to manufacturer's instructions. Illumina compatible indexes were added through PCR amplification (7 cycles). Amplified libraries were purified and size-selected using Agencourt® AMPure® XP beads (Beckman Coulter) to remove unincorporated primers and other reagents. Prior to analyses, DNA libraries were checked for quality and quantified using a 2100 Bioanalyzer (Agilent). Libraries were sequenced on Illumina Hiseq 4000 sequencer as Paired-End 50 base reads following Illumina's instructions (IGBMC Genomeast platform). Image analysis and base calling were performed using RTA 2.7.3 and bcl2fastq 2.17.1.14. All ChIP samples successfully went through QC using fastqc (https://www.bioinformatics.babraham.ac.uk/projects/fastqc/).

ChIPseq analysis: sequence alignment, peak detection and annotation, differential analysis. Reads were mapped onto Mouse reference assembly GRCm38/mm10 using Bowtie 1.0.0. aligner[69]. Peak detection was performed using SICER[70,71] v1.1 with the following parameters: window size: 200; *e* value: 0.003. Gap size parameters were selected according to the score value estimated by statistical method implemented in SICER: selected values of gap size are 1000, 600 and 1400 for H3K27ac, RNAPII and H3K27me3, respectively. Peaks were annotated relative to genomic features using Homer AnnotatePeaks v4.9.1 (ref. [72]) with annotation from Ensembl v87. Male and female data were compared using the Bioconductor package ChIPpeakAnno. Inputs were used as controls. ChIPseq data were normalized based on a method that consists in equalizing background regions. Correlative heatmaps and scatter plots were generated for global comparison of samples and replicate analyses. Clustering analysis were performed using seqMINER v1.2.1 (refs. [73,74]) by using Refseq genes of mouse mm10 genome as reference coordinates. Briefly, the samples were normalized to have 1× genome coverage. Reads counts were then compared across samples. For analysis of genotype effect, differential analysis between WT and Q140 samples was performed using SICER. Increased and decreased H3K27ac, RNAPII or H3K27me3 regions were filtered if their adjusted *P* values $<10^{-5}$, and differential enriched peaks were intersected between replicated experiments and annotated. Independent analyses of male and female samples were also performed using stringent threshold (FDR $<10^{-5}$). Complementary analyses of ChIPseq data were done using the open Galaxy platform GalaxEast (http://www.galaxeast.fr). For analysis of age effect, annotated H3K27Ac, H3K27me3 and RNAPII ChIPseq peaks from independent experiments were intersected to generate a high confidence list of peaks, which was merged across the different biological conditions, for each ChIPseq target. Read coverage was calculated for each sample using bedtools multicov, from BEDTools[75], and differential enrichment analysis was performed using deseq2[65] with default parameters providing as input normalized reads for each peak and biological sample. To generate neuronal and glial-specific striatal enhancer database, differential analysis between NeuN+ and NeuN− H3K27ac ChIPseq data was performed using SICER. Neuronal- vs glial-specific H3K27ac-enriched regions were selected if their *P* values $<10^{-15}$. Neuronal- and glial-specific H3K27ac-enriched regions were intersected with H3K27ac regions differentially enriched in Q140 vs WT mice at 2 and 6 months for cell type-specific genotype and age comparisons.

GO analysis. GO analysis for multiple datasets comparison was performed using ClusterProfiler package from Bioconductor[76]. List of genes for multiple comparisons were provided as input and enriched Biological Processes terms (FDR <0.05) were identified. For graphical simplication, a semantic similarity simplification was applied using GOSemSim function implemented in clusterProfiler, and top 10 more significant enriched terms were plot for each set of genes in the same plot. Significant biological processes were plotted with a dot size proportional to the gene ratio identified for each term and colour scale according to its adj. *P* value. Additionally, GO analysis of seqMiner generated clusters was performed using Panther applying filters previously used[77] to reduce redundancy and generalization of selected terms. Independent GO analysis of male and female samples was performed using GREAT[78], selecting top ten terms significantly enriched (FDR <0.05).

Correlation analysis. Normalized read values of annotated peaks assigned to neuronal- or glial-specific enhancers were used to compute Spearman's correlation coefficient, using ggpubr R package. For cell-type specific analysis of regions changing in age- and genotype-dependent manners, peaks differentially enriched in H3K27ac (*P* <0.05) between Q140 and WT mice at 2 months and between 6 and 2 months in WT mice were filtered and defined as Non-specific, Neuronal-specific or Glial-specific, through intersection with neuronal- and glial-specific enhancer database. Marginal distribution density and scatter plots were simultaneously generated, combining geom density tool from cowplot and ggscatter from ggpubr R packages plotting and using normalized read values obtained from DESeq2. *Z*-score hierarchical heatmap generation was performed using ClustVis[79].

DNA motif analysis. Motif analysis at neuronal- and glial-specific enhancers showing age- and genotype-dependent changes in H3K27ac was performed using RSAT[79,80]. Differentially enriched peaks (*P* <0.05) were categorized as Non-specific, Neuronal-specific or Glial-specific and motif analysis using standard parameters was performed in Neuronal vs Non-specific and Glial vs Non-specific regions. Top discovered motifs (*e*-value $<10^{-4}$) associated to transcription factors found in Hocomoco (version 11) human and mouse PWMs database were selected.

Network analysis. Network analysis of genes linked to neuronal- and glial-specific enhancers showing changes in H3K27ac in age- and genotype-dependent manners was performed using STRING[81,82]. Annotated genes from differentially enriched peaks (*P* <0.05) were selected and categorized in Neuronal- or Glial-specific and protein–protein interaction (PPI) network analysis was conducted using default parameters from STRING. PPI score was used as a measure of co-regulatory network complexity analysis.

Circular chromatin conformation capture (4C-seq). 4C-seq was performed as previously described[83] with slight modifications. 4C-seq data were replicated for each condition, using male tissues in a first replicate and female tissues in the second replicate. Briefly, 5 million nuclei per biological condition were purified using same steps described in the FANS approach[56,57], except that percentage of formaldehyde was increased up to 2%. Purified nuclei were digested O/N with the first restriction enzyme (DpnII, New England Biolabs) and posteriorly subjected to an overnight ligation with T4 DNA Ligase (New England Biolabs). Subsequently, chromatin was de-crosslinked and purified after proteinase K and RNAse A treatment. A second digestion using Csp6I (Thermo Scientific) was performed O/N, followed by final O/N ligation with T4 DNA Ligase and DNA purification using phenol/chloroform extraction after sample volume reduction by using 90% under-saturated phenol (UPT phenol). The resultant 4C DNA template was used to generate 4C-seq libraries by performing a PCR (Long Template PCR system, Roche) with target-specific designed reading and non-reading primers (see table below) containing Illumina sequencer adapters. For primer design, a region surrounding the TSS of the gene of interest (±2 kb) was retrieved and primers were designed using SnapGene (v.1.1.3) for regions that fulfilled the following criteria: distance between DpnII restriction site and the consecutive Csp6I restriction site >350 bp; distance between DpnII restriction site and the following DpnII restriction site after Csp6I >500 bp and <1500 bp (Supplementary Table 1). A primer validation step was included to verify their specificity. Then, generated 4C-seq libraries were purified with SPRI select beads (Beckman) to discard primer dimer DNA products and 4C-seq DNA template were quantified using Bioanalyzer and pooled equimolarly for sequencing using 50 bp single-end Hiseq 4000 sequencer (IGBMC Genomeast platform).

4C-seq data analysis. Reads were mapped to mm10 with Bowtie[69], then processed and visualized with 4See (refs. [53,84]). At the *Pde10a* locus, interactions were called on individual male and female samples with peakC[85] using default parameters, including a window size of 21 fragments. To assess differential interactions at the reproducibly called interacting regions, two-tailed *t* tests were performed on the mean values of the 4See-outputted quantile-normalized scores of the fragments contained within each interacting region. CTCF data from mESC was retrieved from GSE125129 GEO datasets (https://www.ncbi.nlm.nih.gov/geo/query/acc.cgi?acc=GSE125129).

Virtual Hi-C (vHi-C) data generation and analysis. The 3D chromatin models representing the *Htt* region using the different 4C-seq datasets generated on WT and Q140 Homozygous striatal samples were built using 4Cin[38]. The locus modelled is comprised within chromosome 5: 33954729-36029316 of mm10 mouse genome. Default parameters of the program were used except for the number of fragments that each bead represents, which was set to 25. Chromatin painting was performed using H3K27ac, H3K27me3 and RNAPII ChIP-seq data of corresponding biological conditions using paint_model.py script from 4C-in. To identify TAD boundaries using the models, an insulation score was computed as previously described[39].

Statistics. Mice with the same age and sex were randomly allocated to the different experimental groups. Blinding was applied to behavioural experiments. For bar plots, centred regions indicate the mean ± sem; for boxplots, centred regions indicate the median, box limits, upper and lower quartiles and whiskers, 1.5× interquartile range. All measurements were taken from distinct samples. No data were excluded from analyses. For pairwise comparisons of average, data were tested for normality using the Shapiro's test. Statistical analyses included two-tailed, paired or unpaired, Student's *t* test, one-way analysis of variance. In case the

samples were significantly non-normal, non-parametric tests, including Kruskal–Wallis and binomial tests were performed. For multiple comparisons, the Newman-Keuls test or Benjamini-Hochberg method was applied. P values < 0.05 were considered to be statistically significant, except when otherwise indicated. No statistical method was used to predetermine sample size, but our sample sizes are based on similar, previously established, experimental designs.

Reporting summary. Further information on experimental design is available in the Nature Research Reporting Summary linked to this paper.

Data availability

The datasets generated in this study are available at NCBI GEO under the following accession numbers: "GSE144684" and "GSE144699". A reporting summary for this Article is available as a Supplementary Information file. All other relevant data are available within the Article, Supplementary Information, or available from the author upon request. Source data are provided with this paper.

Code availability

Custom codes are available from the corresponding author upon reasonable request.

Received: 11 February 2020; Accepted: 14 December 2020;
Published online: 13 January 2021

References

1. McColgan, P. et al. Selective vulnerability of Rich Club brain regions is an organizational principle of structural connectivity loss in Huntington's disease. *Brain* **138**, 3327–3344 (2015).
2. Bates, G. P. et al. Huntington disease. *Nat. Rev. Dis. Primers* **1**, 15005 (2015).
3. Achour, M. et al. Neuronal identity genes regulated by super-enhancers are preferentially down-regulated in the striatum of Huntington's disease mice. *Hum. Mol. Genet.* **24**, 3481–3496 (2015).
4. Francelle, L., Lotz, C., Outeiro, T., Brouillet, E. & Merienne, K. Contribution of neuroepigenetics to Huntington's disease. *Front. Hum. Neurosci.* **11**, 17 (2017).
5. Langfelder, P. et al. Integrated genomics and proteomics define huntingtin CAG length-dependent networks in mice. *Nat. Neurosci.* **19**, 623–633 (2016).
6. Vashishtha, M. et al. Targeting H3K4 trimethylation in Huntington disease. *Proc. Natl Acad. Sci. USA* **110**, E3027–E3036 (2013).
7. Valor, L. M., Guiretti, D., Lopez-Atalaya, J. P. & Barco, A. Genomic landscape of transcriptional and epigenetic dysregulation in early onset polyglutamine disease. *J. Neurosci.* **33**, 10471–10482 (2013).
8. Biagioli, M. et al. Htt CAG repeat expansion confers pleiotropic gains of mutant huntingtin function in chromatin regulation. *Hum. Mol. Genet.* **24**, 2442–2457 (2015).
9. Bai, G. et al. Epigenetic dysregulation of hairy and enhancer of split 4 (HES4) is associated with striatal degeneration in postmortem Huntington brains. *Hum. Mol. Genet.* **24**, 1441–1456 (2015).
10. Merienne, N. et al. Cell-type-specific gene expression profiling in adult mouse brain reveals normal and disease-state signatures. *Cell Rep.* **26**, 2477–2493.e9 (2019).
11. HD iPSC Consortium. Developmental alterations in Huntington's disease neural cells and pharmacological rescue in cells and mice. *Nat. Neurosci.* **20**, 648–660 (2017).
12. Benayoun, B. A. et al. Remodeling of epigenome and transcriptome landscapes with aging in mice reveals widespread induction of inflammatory responses. *Genome Res.* **29**, 697–709 (2019).
13. Pearson, C. E., Nichol Edamura, K. & Cleary, J. D. Repeat instability: mechanisms of dynamic mutations. *Nat. Rev. Genet.* **6**, 729–742 (2005).
14. Sun, J. H. et al. Disease-associated short tandem repeats co-localize with chromatin domain boundaries. *Cell* **175**, 224–238.e15 (2018).
15. Menalled, L. B., Sison, J. D., Dragatsis, I., Zeitlin, S. & Chesselet, M.-F. Time course of early motor and neuropathological anomalies in a knock-in mouse model of Huntington's disease with 140 CAG repeats. *J. Comp. Neurol.* **465**, 11–26 (2003).
16. Dorner, J. L., Miller, B. R., Barton, S. J., Brock, T. J. & Rebec, G. V. Sex differences in behavior and striatal ascorbate release in the 140 CAG knock-in mouse model of Huntington's disease. *Behav. Brain Res.* **178**, 90–97 (2007).
17. Zielonka, D. & Stawinska-Witoszynska, B. Gender differences in non-sex linked disorders: insights from Huntington's disease. *Front. Neurol.* **11**, 571 (2020).
18. Halder, R. et al. DNA methylation changes in plasticity genes accompany the formation and maintenance of memory. *Nat. Neurosci.* **19**, 102–110 (2016).
19. Whyte, W. A. et al. Master transcription factors and mediator establish super-enhancers at key cell identity genes. *Cell* **153**, 307–319 (2013).
20. Rangaraju, S. et al. Quantitative proteomics of acutely-isolated mouse microglia identifies novel immune Alzheimer's disease-related proteins. *Mol. Neurodegener.* **13**, 34 (2018).
21. Wang, B., Lufkin, T. & Rubenstein, J. L. R. Dlx6 regulates molecular properties of the striatum and central nucleus of the amygdala. *J. Comp. Neurol.* **519**, 2320–2334 (2011).
22. Anderson, S. A. et al. Mutations of the homeobox genes Dlx-1 and Dlx-2 disrupt the striatal subventricular zone and differentiation of late born striatal neurons. *Neuron* **19**, 27–37 (1997).
23. Schreiber, J., Sock, E. & Wegner, M. The regulator of early gliogenesis glial cells missing is a transcription factor with a novel type of DNA-binding domain. *Proc. Natl Acad. Sci. USA* **94**, 4739–4744 (1997).
24. Long, J. E. et al. Dlx1&2 and Mash1 transcription factors control striatal patterning and differentiation through parallel and overlapping pathways. *J. Comp. Neurol.* **512**, 556–572 (2009).
25. Kala, K. et al. Gata2 is a tissue-specific post-mitotic selector gene for midbrain GABAergic neurons. *Development* **136**, 253–262 (2009).
26. Now, H. & Yoo, J.-Y. A protein-kinase, IFN-inducible double-stranded RNA dependent inhibitor and repressor of p58 (PRKRIR) enhances type I IFN-mediated antiviral response through the stability control of RIG-I protein. *Biochem. Biophys. Res. Commun.* **413**, 487–493 (2011).
27. Beagrie, R. A. et al. Complex multi-enhancer contacts captured by genome architecture mapping. *Nature* **543**, 519–524 (2017).
28. Rao, S. S. P. et al. Cohesin loss eliminates all loop domains. *Cell* **171**, 305–320. e24 (2017).
29. Ryu, J., Kim, H., Yang, D., Lee, A. J. & Jung, I. A new class of constitutively active super-enhancers is associated with fast recovery of 3D chromatin loops. *BMC Bioinform.* **20**, 127 (2019).
30. Mangiarini, L. et al. Exon 1 of the HD gene with an expanded CAG repeat is sufficient to cause a progressive neurological phenotype in transgenic mice. *Cell* **87**, 493–506 (1996).
31. Kaaij, L. J. T., Mohn, F., van der Weide, R. H., de Wit, E. & Bühler, M. The ChAHP complex counteracts chromatin looping at CTCF sites that emerged from SINE expansions in mouse. *Cell* **178**, 1437–1451.e14 (2019).
32. Rao, S. S. P. et al. A 3D map of the human genome at kilobase resolution reveals principles of chromatin looping. *Cell* **159**, 1665–1680 (2014).
33. Bharadwaj, R. et al. Conserved higher-order chromatin regulates NMDA receptor gene expression and cognition. *Neuron* **84**, 997–1008 (2014).
34. Edelbrock, M. A., Kaliyaperumal, S. & Williams, K. J. Structural, molecular and cellular functions of MSH2 and MSH6 during DNA mismatch repair, damage signaling and other noncanonical activities. *Mutat. Res.* **743–744**, 53–66 (2013).
35. Dixon, J. R. et al. Topological domains in mammalian genomes identified by analysis of chromatin interactions. *Nature* **485**, 376–380 (2012).
36. Schmitt, A. D. et al. A compendium of chromatin contact maps reveals spatially active regions in the human genome. *Cell Rep.* **17**, 2042–2059 (2016).
37. Jiang, Y. et al. The methyltransferase SETDB1 regulates a large neuron-specific topological chromatin domain. *Nat. Genet.* **49**, 1239–1250 (2017).
38. Irastorza-Azcarate, I. et al. 4Cin: a computational pipeline for 3D genome modeling and virtual Hi-C analyses from 4C data. *PLoS Comput. Biol.* **14**, e1006030 (2018).
39. Crane, E. et al. Condensin-driven remodelling of X chromosome topology during dosage compensation. *Nature* **523**, 240–244 (2015).
40. Chiang, C. et al. Complex reorganization and predominant non-homologous repair following chromosomal breakage in karyotypically balanced germline rearrangements and transgenic integration. *Nat. Genet.* **44**, 390–397 (2012).
41. Horvath, S. et al. Huntington's disease accelerates epigenetic aging of human brain and disrupts DNA methylation levels. *Aging (Albany NY)* **8**, 1485–1512 (2016).
42. Horvath, S. et al. Accelerated epigenetic aging in Down syndrome. *Aging Cell* **14**, 491–495 (2015).
43. Soreq, L. et al. Major shifts in glial regional identity are a transcriptional hallmark of human brain aging. *Cell Rep.* **18**, 557–570 (2017).
44. de Lombares, C. et al. Dlx5 and Dlx6 expression in GABAergic neurons controls behavior, metabolism, healthy aging and lifespan. *Aging (Albany NY)* **11**, 6638–6656 (2019).
45. Marzi, S. J. et al. A histone acetylome-wide association study of Alzheimer's disease identifies disease-associated H3K27ac differences in the entorhinal cortex. *Nat. Neurosci.* **21**, 1618–1627 (2018).
46. Li, P. et al. Epigenetic dysregulation of enhancers in neurons is associated with Alzheimer's disease pathology and cognitive symptoms. *Nat. Commun.* **10**, 2246 (2019).
47. Girdhar, K. et al. Cell-specific histone modification maps in the human frontal lobe link schizophrenia risk to the neuronal epigenome. *Nat. Neurosci.* **21**, 1126–1136 (2018).

48. Dang, W. et al. Histone H4 lysine 16 acetylation regulates cellular lifespan. *Nature* **459**, 802–807 (2009).
49. Heinz, S., Romanoski, C. E., Benner, C. & Glass, C. K. The selection and function of cell type-specific enhancers. *Nat. Rev. Mol. Cell Biol.* **16**, 144–154 (2015).
50. Niccolini, F. et al. Altered PDE10A expression detectable early before symptomatic onset in Huntington's disease. *Brain* **138**, 3016–3029 (2015).
51. Kennedy, L. & Shelbourne, P. F. Dramatic mutation instability in HD mouse striatum: does polyglutamine load contribute to cell-specific vulnerability in Huntington's disease? *Hum. Mol. Genet.* **9**, 2539–2544 (2000).
52. Shelbourne, P. F. et al. Triplet repeat mutation length gains correlate with cell-type specific vulnerability in Huntington disease brain. *Hum. Mol. Genet.* **16**, 1133–1142 (2007).
53. Chao, M. J. et al. Population-specific genetic modification of Huntington's disease in Venezuela. *PLoS Genet.* **14**, e1007274 (2018).
54. Genetic Modifiers of Huntington's Disease (GeM-HD) Consortium. Identification of genetic factors that modify clinical onset of Huntington's disease. *Cell* **162**, 516–526 (2015).
55. Massey, T. H. & Jones, L. The central role of DNA damage and repair in CAG repeat diseases. *Dis. Models Mech.* **11**, dmm031930 (2018).
56. Benito, E. et al. HDAC inhibitor-dependent transcriptome and memory reinstatement in cognitive decline models. *J. Clin. Invest.* **125**, 3572–3584 (2015).
57. Jiang, Y., Matevossian, A., Huang, H.-S., Straubhaar, J. & Akbarian, S. Isolation of neuronal chromatin from brain tissue. *BMC Neurosci.* **9**, 42 (2008).
58. Rué, L. et al. Early down-regulation of PKCδ as a pro-survival mechanism in Huntington's disease. *Neuromolecular Med.* **16**, 25–37 (2014).
59. Burrus, C. J. et al. Striatal projection neurons require Huntingtin for synaptic connectivity and survival. *Cell Rep.* **30**, 642–657.e6 (2020).
60. Sun, W. et al. SOX9 is an astrocyte-specific nuclear marker in the adult brain outside the neurogenic regions. *J. Neurosci.* **37**, 4493–4507 (2017).
61. Besson, M., Forget, B., Correia, C., Blanco, R. & Maskos, U. Profound alteration in reward processing due to a human polymorphism in CHRNA5: a role in alcohol dependence and feeding behavior. *Neuropsychopharmacology* **44**, 1906–1916 (2019).
62. Kim, D. et al. TopHat2: accurate alignment of transcriptomes in the presence of insertions, deletions and gene fusions. *Genome Biol.* **14**, R36 (2013).
63. Anders, S., Pyl, P. T. & Huber, W. HTSeq–a Python framework to work with high-throughput sequencing data. *Bioinformatics* **31**, 166–169 (2015).
64. Anders, S. & Huber, W. Differential expression analysis for sequence count data. *Genome Biol.* **11**, R106 (2010).
65. Love, M. I., Huber, W. & Anders, S. Moderated estimation of fold change and dispersion for RNA-seq data with DESeq2. *Genome Biol.* **15**, 550 (2014).
66. Benjamini, Y. & Hochberg, Y. Controlling the false discovery rate - a practical and powerful approach to multiple testing. *J. R. Stat. Soc. Ser. B Methodol.* **57**, 289–300 (1995).
67. Gu, Z., Eils, R. & Schlesner, M. Complex heatmaps reveal patterns and correlations in multidimensional genomic data. *Bioinformatics* **32**, 2847–2849 (2016).
68. Besse, S., Vigneron, M., Pichard, E. & Puvion-Dutilleul, F. Synthesis and maturation of viral transcripts in herpes simplex virus type 1 infected HeLa cells: the role of interchromatin granules. *Gene Expr.* **4**, 143–161 (1995).
69. Langmead, B., Trapnell, C., Pop, M. & Salzberg, S. L. Ultrafast and memory-efficient alignment of short DNA sequences to the human genome. *Genome Biol.* **10**, R25 (2009).
70. Xu, S., Grullon, S., Ge, K. & Peng, W. Spatial clustering for identification of ChIP-enriched regions (SICER) to map regions of histone methylation patterns in embryonic stem cells. *Methods Mol. Biol.* **1150**, 97–111 (2014).
71. Zang, C. et al. A clustering approach for identification of enriched domains from histone modification ChIP-Seq data. *Bioinformatics* **25**, 1952–1958 (2009).
72. Heinz, S. et al. Simple combinations of lineage-determining transcription factors prime cis-regulatory elements required for macrophage and B cell identities. *Mol. Cell* **38**, 576–589 (2010).
73. Ye, T., Ravens, S., Krebs, A. R. & Tora, L. Interpreting and visualizing ChIP-seq data with the seqMINER software. *Methods Mol. Biol.* **1150**, 141–152 (2014).
74. Ye, T. et al. seqMINER: an integrated ChIP-seq data interpretation platform. *Nucleic Acids Res.* **39**, e35 (2011).
75. Quinlan, A. R. & Hall, I. M. BEDTools: a flexible suite of utilities for comparing genomic features. *Bioinformatics* **26**, 841–842 (2010).
76. Yu, G., Wang, L.-G., Han, Y. & He, Q.-Y. clusterProfiler: an R package for comparing biological themes among gene clusters. *OMICS* **16**, 284–287 (2012).
77. Fernandez-Albert, J. et al. Immediate and deferred epigenomic signatures of in vivo neuronal activation in mouse hippocampus. *Nat. Neurosci.* **22**, 1718–1730 (2019).
78. McLean, C. Y. et al. GREAT improves functional interpretation of cis-regulatory regions. *Nat. Biotechnol.* **28**, 495–501 (2010).
79. Nguyen, N. T. T. et al. RSAT 2018: regulatory sequence analysis tools 20th anniversary. *Nucleic Acids Res.* **46**, W209–W214 (2018).
80. van Helden, J. Regulatory sequence analysis tools. *Nucleic Acids Res.* **31**, 3593–3596 (2003).
81. Szklarczyk, D. et al. The STRING database in 2017: quality-controlled protein-protein association networks, made broadly accessible. *Nucleic Acids Res.* **45**, D362–D368 (2017).
82. von Mering, C. et al. STRING: a database of predicted functional associations between proteins. *Nucleic Acids Res.* **31**, 258–261 (2003).
83. van de Werken, H. J. G. et al. 4C technology: protocols and data analysis. *Methods Enzymol.* **513**, 89–112 (2012).
84. Zouari, Y. B., Platania, A., Molitor, A. M. & Sexton, T. 4See: a flexible browser to explore 4C data. *Front. Genet.* https://doi.org/10.3389/fgene.2019.01372 (2020).
85. Geeven, G., Teunissen, H., de Laat, W. & de Wit, E. peakC: a flexible, non-parametric peak calling package for 4C and Capture-C data. *Nucleic Acids Res.* **46**, e91 (2018).

Acknowledgements

We thank PsychoGenics for providing tissues as part of a contract research agreement with CHDI. We thank O. Bildstein, D. Egesi, G. Edomwonyi and C. Strittmatter (LNCA UMR7364) for assistance in animal care. Sequencing was performed by the GenomEast Platform, a member of the 'France Génomique' consortium (ANR-10-INBS-2009). We thank C3UPO for the high-performance computing (HPC) support at Uni. Pablo de Olavide. This study was supported by CHDI foundation, Inc, the Agence Nationale de la Recherche (ANR-2017-CE12-0027), the Centre National de la Recherche Scientifique (CNRS) and the University of Strasbourg. R.A.V. was supported by post-doctoral fellowship from CHDI. J.S. and A.B. were bioinformatician and technician supported by CHDI. C.L. and A.A. were recipients of doctoral fellowships from the French government and the Association Huntington France (AHF), respectively. Work in the T.S. group is supported by the European Research Council (ERC) under the European Union's Horizon 2020 research and innovation program (Starting Grant 678624 - CHROM-TOPOLOGY), the ATIP-Avenir program, and the grant ANR-10-LABX-0030-INRT, a French State fund managed by the Agence Nationale de la Recherche under the frame program Investissements d'Avenir ANR-10-IDEX-0002-02. A.M.M. was supported by funds from INCA. J.-L.G.-S. was supported by the Spanish government (grant no. BFU2016- 74961-P) and the institutional grant Unidad de Excelencia María de Maeztu (no. MDM-2016-0687). I.I.-A. was supported with a FEBS long-term fellowship.

Author contributions

R.A.V. designed and performed the experiments, analysed the data, and wrote and edited the manuscript. J.S. analysed the data, and wrote and edited the manuscript, C.L. performed the experiments, analysed the data and edited the manuscript, A.M.M. assisted with experiments and data analysis, and edited the manuscript, I.I.A. analysed the data and edited the manuscript, A.A. performed the experiments and edited the manuscript, N.K. assisted with data analysis and edited the manuscript, A.B. performed the experiments and edited the manuscript, B.C. performed the experiments and edited the manuscript, J.L.G.S. interpreted the experiments and edited the manuscript, J.C.C. interpreted the experiments and edited the manuscript, A.L.B. interpreted the experiments and edited the manuscript, T.S. analysed the data, and wrote and edited the manuscript. K.M. designed the experiments, analysed the data, and wrote and edited the manuscript.

Competing interests

The authors declare no competing interests.

Additional information

Supplementary information is available for this paper at https://doi.org/10.1038/s41467-020-20605-2.

Correspondence and requests for materials should be addressed to K.M.

Peer review information *Nature Communications* thanks Angel Barco and the other, anonymous, reviewer(s) for their contribution to the peer review of this work. Peer reviewer reports are available.

Reprints and permission information is available at http://www.nature.com/reprints

Publisher's note Springer Nature remains neutral with regard to jurisdictional claims in published maps and institutional affiliations.

Publication: 2

Review

“Epigenetic mechanisms underlying enhancer modulation of neuronal identity, neuronal activity and neurodegeneration”

Rafael Alcala-Vida, Ali Awada, Anne-Laurence Boutillier, Karine Merienne

Neurobiology of Disease 147 (2021) 105155

Contents lists available at ScienceDirect

Neurobiology of Disease

journal homepage: www.elsevier.com/locate/ynbdi

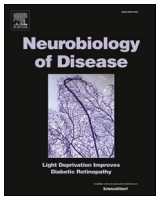

Review

Epigenetic mechanisms underlying enhancer modulation of neuronal identity, neuronal activity and neurodegeneration

Rafael Alcalà-Vida [a,b], Ali Awada [a,b], Anne-Laurence Boutillier [a,b], Karine Merienne [a,b,*]

[a] LNCA, University of Strasbourg, France
[b] CNRS UMR 7364, Strasbourg, France

ARTICLE INFO

Keywords:
Epigenetic regulations
Super enhancer
Neuronal identity
Neuronal activity
Huntington's disease
Alzheimer's disease

ABSTRACT

Neurodegenerative diseases, including Huntington's disease (HD) and Alzheimer's disease (AD), are progressive conditions characterized by selective, disease-dependent loss of neuronal regions and/or subpopulations. Neuronal loss is preceded by a long period of neuronal dysfunction, during which glial cells also undergo major changes, including neuroinflammatory response. Those dramatic changes affecting both neuronal and glial cells associate with epigenetic and transcriptional dysregulations, characterized by defined cell-type-specific signatures. Notably, increasing studies support the view that altered regulation of transcriptional enhancers, which are distal regulatory regions of the genome capable of modulating the activity of promoters through chromatin looping, play a critical role in transcriptional dysregulation in HD and AD. We review current knowledge on enhancers in HD and AD, and highlight challenging issues to better decipher the epigenetic code of neurodegenerative diseases.

1. Neuronal-specific enhancers: neuronal identity vs neuronal activity

1.1. Epigenetic regulations

Epigenetic mechanisms, including DNA methylation, some non-coding RNAs and various histone post-translational modifications acting through combinatory rules defined by the so-called histone code, modulate the chromatin, which can be relaxed, a feature generally associated with transcriptionally active chromatin (e.g. euchromatin), or in a compacted state (e.g. heterochromatin) usually associated with transcriptional repression (Jenuwein and Allis, 2001). While the continuous discovery of new histone post-translational modifications reflects complexity of histone code and epigenetic regulation, unifying rules have been uncovered. Particularly, histone acetylation, through the action of histone acetyltransferases (HAT), a family of chromatin-remodeling enzymes, has always been implicated in chromatin relaxation. Histone acetylation at promoters and distal regulatory regions – enhancers-, is a prerequisite to target gene activation. Particularly, H3K27 acetylation (H3K27ac) by the HAT CBP/P300 is a mark of transcriptionally active enhancers and promoters (Tie et al., 2014). Additional histone post-translational modifications, including methylation on specific histone residues, contribute to histone code of relaxed chromatin. For instance, trimethylated H3K4 (H3K4me3) is strongly enriched at transcriptionally active promoters, whereas monomethylated H3K4 (H3K4me1) is specifically enriched at enhancers. Histone methylation can also be associated with transcriptionally silent heterochromatin state. Well-characterized heterochromatin marks include H3K9 trimethylation (H3K9m3), a mark of constitutive heterochromatin, and H3K27 trimethylation (e.g. H3K27me3), enriched at facultative heterochromatin, which has the potential to convert to euchromatin (Trojer and Reinberg, 2007).

1.2. Transcriptional enhancers

Enhancers are critical regulatory DNA elements enabling cell-type-specific and dynamic regulations of gene expression. They are enriched in docking sites for transcription factors (TF) in sequence-specific manner. Combinatorial binding of TFs determines the nature and extent of enhancer-mediated transcription (Inukai et al., 2017). Thus, cell-type-specific differences in TF expression contribute to cell-type-specific activity of different enhancer elements. However, most sequence-predicted TF binding sites are not occupied, even when cognate TF are expressed (Hombach et al., 2016). This is because

* Corresponding author at: LNCA, University of Strasbourg/ CNRS UMR 7364, 12 rue Goethe, 67000 Strasbourg, France.
E-mail address: karine.merienne@unistra.fr (K. Merienne).

https://doi.org/10.1016/j.nbd.2020.105155
Received 1 April 2020; Received in revised form 23 October 2020; Accepted 26 October 2020
Available online 27 October 2020

enhancer accessibility and ability to interact with promoters are determined by epigenetic mechanisms, which are also regulated in a cell-type-dependent manner. For instance, during cellular differentiation, H3K27ac undergoes massive changes and is deposited at specific gene loci. Lineage-determining TFs, expressed in developmental- and cell type-dependent manners, provide specificity to the mechanism, recruiting chromatin-remodeling enzymes (e.g. HATs) and structural proteins such as the mediator, CTCF and cohesin, in addition to transcriptional cofactors and RNA polymerase II (RNAPII) (Heinz et al., 2015). Chromatin-remodeling enzymes and structural proteins are implicated in chromatin loop formation, facilitating spatial interaction between distal enhancers and promoters, thereby increasing transcriptional activation of RNAPII complex (Kuras et al., 2003; Ren et al., 2017; de Laat and Duboule, 2013) (Fig. 1).

1.3. Super-enhancers and cellular identity genes

Remarkably, enhancers regulating cellular identity genes show specific epigenetic profile, defined as super-enhancer. This category of enhancers correspond to broad genomic regions highly enriched in H3K27ac and cofactors, such as CBP and the mediator, and encompass complex array of regulatory elements containing binding motifs for cell type-specific master TFs (Whyte et al., 2013; Hnisz et al., 2013; Heinz et al., 2015) (Fig. 1). Importantly, chromatin architecture at super-enhancers displays extensive chromatin looping, enabling multiple promoter/enhancer interactions, thereby concentrating transcriptional factors and cofactors and ensuring elevated and sustained expression of cellular identity genes, a feature essential to cellular identity acquisition and maintenance (Nord and West, 2020; Yap and Greenberg, 2018). Recent data indicate that hyper-active regulatory domains defined by super-enhancers induce locally specific biophysics properties, favoring phase-separated condensates of regulatory proteins, including master TFs, coactivators and RNAPII, enabling high-density assembly and elevated expression levels (Sabari et al., 2018; Wang et al., 2019; Zamudio et al., 2019) (Fig. 1).

1.4. Neuronal activity-regulated enhancers

Enhancers also display a highly dynamic regulation since they respond to cellular stimulation, thereby integrating environmental signals and triggering adaptive genomic response. Dynamic regulation of enhancers is especially critical to neuronal function. In response to environmental stimuli, it drives transcriptional reprogramming promoting synaptic plasticity and adaptive behavior, including learning and memory (Campbell and Wood, 2019; Gräff and Tsai, 2013; Kim et al., 2010; Lopez-Atalaya and Barco, 2014; Yap and Greenberg, 2018). In response to stimulation, signaling cascades (e.g. cAMP- and Ras/MAPK-dependent pathways) are activated in neuronal tissues, which leads to the recruitment and/or activation of TFs and HATs (e.g. CREB and CBP) to enhancers and promoters of early response genes (ERGs), notably the transcription factor *Fos*. This first, rapid response leads to increased H3K27ac, enhancer RNA (eRNA) transcription, strengthening of enhancer/promoter interaction and up-regulation of ERGs, thereby inducing a second regulatory wave, leading to activation of cell-type-specific late response genes (LRGs), which depends on the specific function of the cell within a neural circuit (Yap and Greenberg, 2018). In brain tissues, LRGs are effector genes promoting synaptic plasticity. In response to neuronal stimulation, H3K27ac is increased at LRGs enhancers (Fig. 2). LRGs are induced in time and cell-type-specific controlled manners thanks to the cooperation between AP-1 proteins, especially FOS, cell-type-specific pioneer transcription factors and factors regulating nucleosome eviction (Vierbuchen et al., 2017). It is noteworthy that, in contrast to activity-regulated enhancers, cellular identity enhancers did not show increased H3K27ac in response to cellular stimulation (Vierbuchen et al., 2017).

Thus, neuronal enhancers (and H3K27ac regulation) are critical for the acquisition and maintenance of stable neuronal identity, but also for the dynamic regulation of neuronal activity. While genome wide association studies (GWAS) provide increasing evidence that cell-type-specific enhancers, especially super-enhancers, are hotspots for risk variants modulating susceptibility to neurological diseases, fewer epigenomic studies have addressed the role of enhancers in brain diseases (Heinz et al., 2015; Nord and West, 2020; Nott et al., 2019). However, the advent of genome-wide scale approaches to investigate the brain epigenome has made it possible to identify defined epigenetic signatures in neurological diseases, including neurodegenerative diseases such as HD and AD. Whereas genetic mouse models of these diseases have led to pioneered and critical exploratory studies, increasing data are currently being produced using human brain samples. Here we focus on epigenomic data generated using brain tissues from HD and AD mouse models, as well as post-mortem brain samples from patients. Remarkably, the data indicate that, in both HD and AD brains, neuronal- and glial-specific enhancers show distinct epigenetic signatures, which might stimulate the development of common innovative therapeutic strategies.

2. Epigenetic dysregulation and enhancer regulation in HD

2.1. Etiology and neuropathology of HD

HD is a progressive neurodegenerative disease, usually characterized by adult onset, though there are also juvenile forms of the disease, showing severer clinical presentation and faster progression when compared to the adult form. This is a purely genetic disease caused by an unstable CAG triplet repeat expansion in the first exon of the *HTT* gene. The number of CAG repeats at *HTT* is polymorphic in the normal population and does not exceed 36–39 CAGs. Above this threshold, the CAG repeat is pathogenic, resulting in the production of toxic mutated HTT proteins with polyglutamine (polyQ) expansion highly prone to aggregation. Since longer repeats are more toxic, there is an inverse correlation between the number of repeats and age of disease onset (Bates et al., 2015). Moreover, the HD mutation is unstable in the germline and in somatic tissues, which results in increasing numbers of CAG repeats in successive generations and in somatic tissues with age (López Castel et al., 2010). GWAS showed that genetic modifiers in HD, which modulate the age-at-onset, predominantly target DNA repair genes implicated in CAG repeat instability, including *FAN1* and the mismatch repair genes *MLH1* and *MSH3* (Genetic Modifiers of Huntington's Disease (GeM-HD) Consortium, 2019, 2015; Jones et al., 2017). Despite ubiquitous expression of the *HTT* gene, polyQ-HTT is predominantly toxic to specific neurons of the striatum, e.g. *medium* spiny neurons (MSNs). However, as disease progresses, additional brain regions are affected, including cortical regions. Microglia and astrocytes also contribute to the pathogenic process through astrogliosis and inflammatory response, as observed in several neurodegenerative diseases. Neurodegeneration results from a long period of brain cell dysfunction, characterized by multiple cellular defects, resulting from both gain- and loss-of function mechanisms (Bates et al., 2015; Saudou and Humbert, 2016). Particularly, the HD mutation induces large-scale transcriptional and epigenetic dysregulations in the HD brain (Francelle et al., 2017).

2.2. HD transcriptomic signatures

A number of transcriptomic studies were performed using brain tissues of HD mice and post-mortem brain tissues (Francelle et al., 2017; Hodges et al., 2006; Kuhn et al., 2007; Labadorf and Myers, 2015; Luthi-Carter et al., 2000; Seredenina and Luthi-Carter, 2012). Specifically, comprehensive transcriptomic profiling using HD knockin mice expressing mutated *Htt* with different CAG repeat lengths indicated that transcriptional dysregulation in HD is CAG length-, age- and tissue-dependent, being most extensive in the striatum, and thus correlated with disease progression (Langfelder et al., 2016). Dysregulated genes in

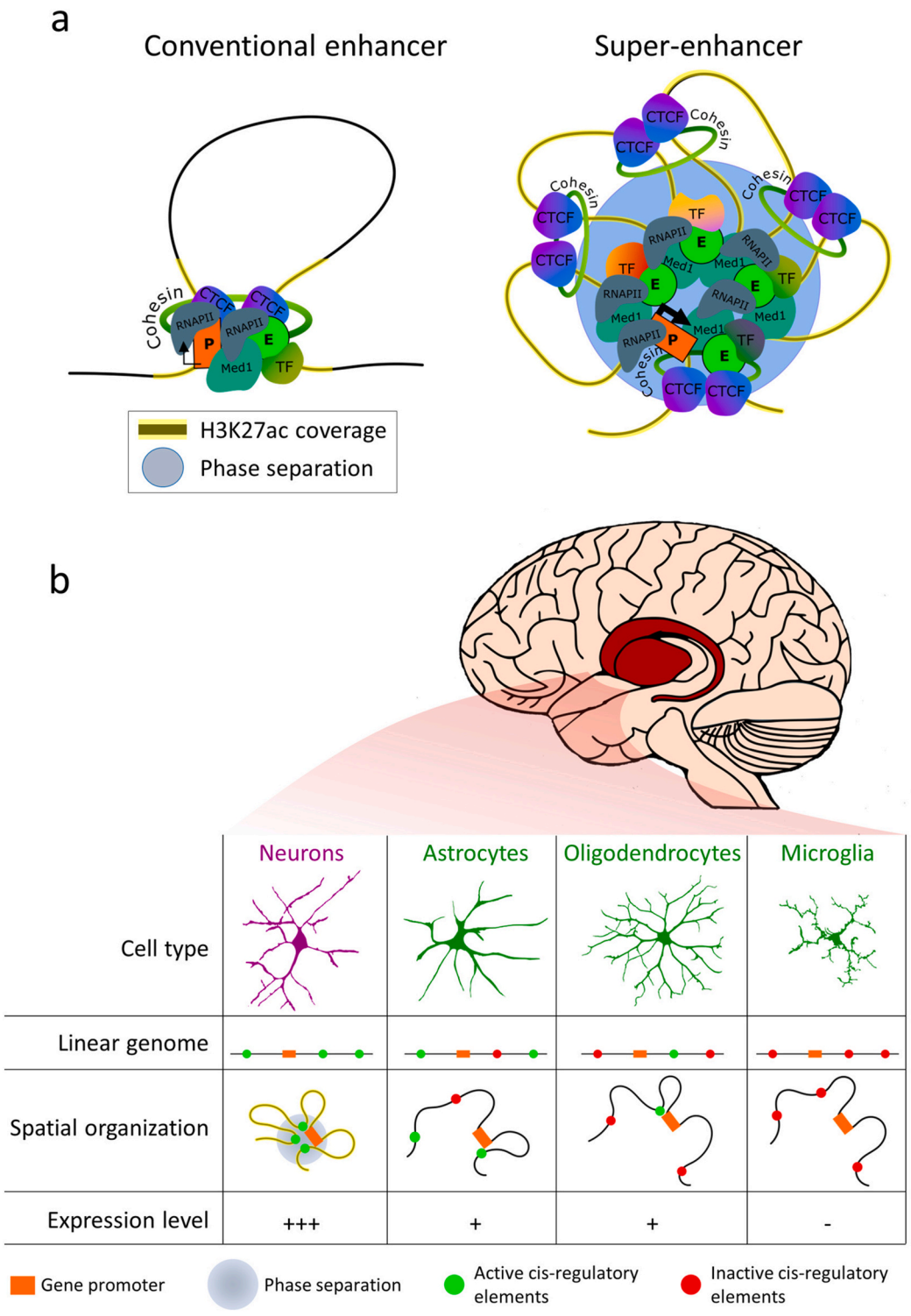

Fig. 1. Regulation of brain cell-identity through super-enhancers. **a**, schematic representations of conventional enhancer-promoter chromatin looping (left) and chromatin looping at a super-enhancer-regulated gene (right). Super-enhancers are highly enriched in H3K27ac (yellow shadow), RNAPII and transcription factors (TF), including the mediator and cell type-specific TFs, leading to the generation of phase-separated condensates (phase-separation, blue circle). Super-enhancers regulate genes that define cell-type-specific identity and function, and that are generally highly expressed in their specific tissue/cell type. In contrast, conventional enhancers display more discrete features. **b**, schematic representation of cell-type-specific epigenetic signature of neuronal striatal super enhancers. The striatum comprises different cell types, including neurons (purple) and glial cells (green), expressing cellular identity genes regulated by super-enhancers. Identity genes may be neuronal-specific or glial-specific. The picture is even more complex since different subpopulations of neurons and glial cells are present in the mammalian striatum, expressing each specific subsets of cellular identity genes, controlled by specific super-enhancers (for example D1 and D2 MSNs as compared to interneurons, and astrocytes, oligodendrocytes or microglia glial cells). (For interpretation of the references to colour in this figure legend, the reader is referred to the web version of this article.)

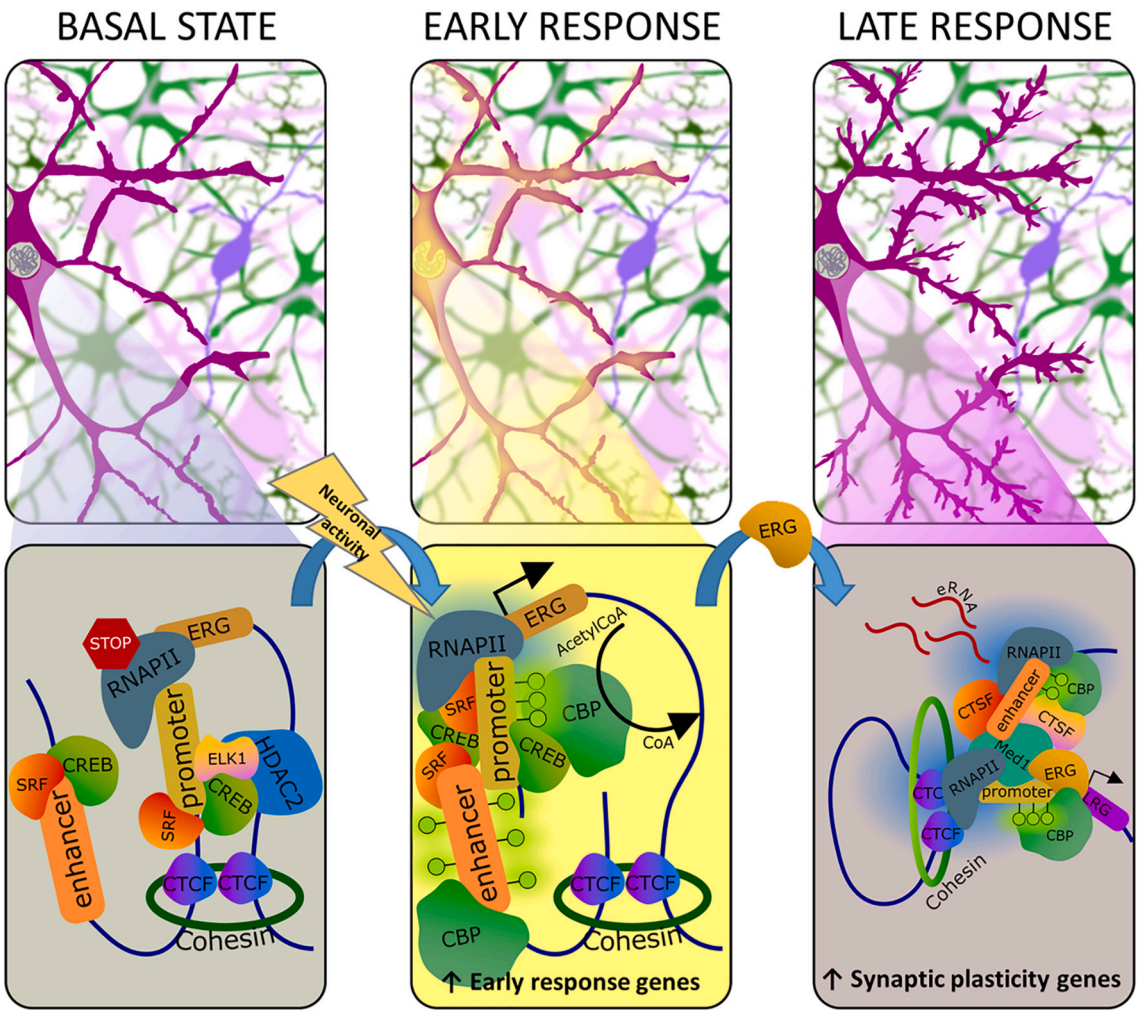

Fig. 2. Neuronal activity modulation of chromatin loops in early and late response genes. Scheme representing the dynamics of chromatin changes at activity-driven genes, including early and late response genes (ERG and LRG, respectively), in response to neural stimulation. In top panels, from the left to the right, the pictures illustrate the physiological neuronal states upon stimulation, starting with basal condition (left), followed by early state of neuronal activation (middle) and ending with late stage of neuronal activation (right), leading to neuronal plasticity. At the molecular level (bottom panels), the induction of ERGs is a crucial event initiating neuronal transcriptional cascades leading to the induction of LRGs implicated in synaptic plasticity. In basal condition (bottom, left panel), ERG promoters already display transcriptionally active features, including the binding of transcription factors (TFs) such as CREB and SRF/ELK1, RNAPII and chromatin loop formation components such as CTCF and cohesin, but also the histone lysine deacetylase 2 (HDAC2), which negatively regulates their expression. Upon neuronal activation, chromatin re-arrangements allow for a proper enhancer-promoter interaction and the histone acetyltransferase CBP is recruited, increasing the levels of H3K27ac (green circles). Altogether, these chromatin changes lead to the transition of RNAPII from a paused state to a transcriptional elongating state, ensuring the induction of ERGs. At late stages of neuronal activation (bottom right), the coordinated activity of ERGs and cell-type specific factors (CTSF) orchestrate the chromatin remodeling of late response gene (LRGs) promoters, triggering their expression and contributing to the final transcriptional wave enriched in synaptic plasticity genes. (For interpretation of the references to colour in this figure legend, the reader is referred to the web version of this article.)

HD striatal tissue display characteristic signature that is conserved across mouse models, including knockin and transgenic mice, and also in post mortem brain tissues from HD patients (Achour et al., 2015; Kuhn et al., 2007; Langfelder et al., 2016; Luthi-Carter et al., 2000; Vashishtha et al., 2013). Specifically, down-regulated genes in HD striatum are enriched in neuronal function genes, particularly in genes that specify striatal identity (Achour et al., 2015; Hervás-Corpión et al., 2018; Langfelder et al., 2016; Vashishtha et al., 2013). These genes include typical markers of mature MSNs, including dopamine D1 receptor (*D1R)*, dopamine D2 receptor (*D2R*), *RGS9, DARPP32*…, and the data indicate that gene down-regulation in HD striatal tissue is not just the consequence of neuronal death (Francelle et al., 2017; Kuhn et al., 2007). Furthermore, mouse data generated at different time points, including pre-symptomatic age, suggest that gene down-regulation in HD is an early process (Langfelder et al., 2016). Remarkably, up-regulated genes in HD brain tissue display a distinct functional signature since they are enriched in immune and developmental genes (Achour et al., 2015; Kuhn et al., 2007; Labadorf and Myers, 2015; Langfelder et al., 2016).

2.3. HD epigenomic signatures

Several epigenomic studies have been generated using brain tissues of HD mice and HD patients (Achour et al., 2015; Bai et al., 2015; Dong et al., 2015; Horvath et al., 2016; McFarland et al., 2012; Merienne et al., 2019; Ng et al., 2013; Valor et al., 2013; Vashishtha et al., 2013) (Table 1). Histone acetylation, including H3K27ac, H3K9,14 ac, H4K12ac and H2Aac, was a major focus in those studies. ChIP-seq analyses indicated that changes in H3K9,14 ac and H4K12ac were limited in the hippocampus and cerebellum of the HD transgenic mouse N171-82Q, and did not particularly correlated with transcriptional changes (Valor et al., 2013). In contrast, extensive changes in H3K27ac were

Table 1
Summary of HD epigenomic studies.

Experimental approach	Biological specimen	Key findings	Bibliographic refference
Co-immunoprecipitation, H3K27m3 and Htt ChIP-PCR	WT, Htt null and HdhQ111 embryoid bodies	Htt involvement in PRC2 complex activity and chromatin binding at heterochromatin domains enriched in H3K27me3	Seong et al., 2010
H3K9/K14ac (H3ac) ChIP-ChIP	R6/2 mice striatum	Genome-wide decrease in H3K9/K14ac but low correlation with differential gene expression	McFarland et al., 2012
Reduced representation bisulfite sequencing (RRBS) and FRA-2, JUND, and SOX2 ChIP-seq	Cells carrying polyglutamine-expanded HTT (STHdhQ111/Q111) and wild-type cells (STHdhQ7/Q7)	DNA methylation changes at genes presenting expanded HTT-mediated transcriptional alterations and AP-1/Sox2 binding sites	Ng et al., 2013
H3K9/14 ac and H4K12ac ChIP-seq	N171-82Q mice hippocampus	Few overlap of H3K9,14 and H4K12 ac and transcriptionally dysregulated genes. Small subset of genes with H3K9,14 and transcriptional dysregulation co-occurrence	Valor et al., 2013
H3K27ac and RNA Polymerase II ChIP-seq	R6/1 HD mice striatum	H3K27ac hipo-acetylation and decreased RNA Polymerase II binding at neuronal super-enhancers associated with genes showing decreased transcriptional levels	Achour et al., 2015
H3K4me3 ChIP-PCR and ChIP-seq	Human cortex from control and HD patients and R6/2 HD mice cortex and striatum	Decreased and increased H3K4me3 at the TSS of genes involved in neuronal function and gene expression regulation, respectively, accompanied by transcriptional dysregulation	Vashishtha et al., 2013
H3K4me3 ChIP-seq	Neuronal (NeuN+) human cortical nuclei	H3K4me3 differentially enriched regions at genes implicated in neuronal development and neurodegeneration	Bai et al., 2015
H3K27me3, H3K4me3 and H3K36me3 ChIP-seq	Isogenic WT, Htt null and heterozygous Htt CAG knock-in ESCs and NPCs	Htt involvement in ESCs for H3K27me3 deposition at "bivalent" loci and in their maintenance and removal in NPCs. CAG size, while slighlty affecting H3K27me3, primarily impact H3K4me3 at "active" loci	Biagioli et al., 2015
H3K4me3 ChIP-seq	Neuronal (NeuN+) human cortical nuclei	Low correlation of H3K4me3 differentially enriched regions and differentially expressed genes in HD human neurons	Dong et al., 2015
Western Blot, Immunohistochemistry, H3ac and H3K4me3 ChIP-PCR	R6/1 and YAC128 HD mice brain, mHtt-electroporated mice brain cells, mHtt-infected neurons and PC12-TetOn-HD23/72Q	Absence of bulk chromatin changes but histone deacetylation at the TSS of particular genes involve in neuronal functions, accompanied in some cases with transcriptional dysregulation and deffective H3K4me3	Guiretti et al., 2016
DNA-methylation by bisulfite sequencing	Human brain tissues from controls and HD patients	HD brain regions present a significant epigenetic age acceleration by an average of 3.2 years in specific brain regions (frontal lobe, parietal lobe, and cingulate gyrus) in a CAG-dependent manner	Horvath et al., 2016
H3K4me3, H3K27ac and H3K36me3 ChIP-seq	Neural cell cultures from differentiated control and HD iPSCs	H3K4me3 and H3K27ac genome-wide alterations affecting genes involved in cell lineage determination	IPSC-HD consortium, 2017

(*continued on next page*)

Table 1 (*continued*)

Experimental approach	Biological specimen	Key findings	Bibliographic refference
		and neuronal fate specification	
H3K9me3 ChIP-on-ChIP	R6/2 mice striatum	H3K9me3 increase in genes involved in cellular protein metabolic processes and intracellular signal transduction and decrease in genes associated with sensory perception and neurological system processes	Lee et al., 2017
eRNA transcriptomic analysis	R6/1 HD mice striatum	Decreased eRNA of striatal neuronal identity genes associated to decreased RNA Polymerase II binding	Le Gras et al., 2017
Transcriptomic meta-analysis	R6/1 and N171-82Q mice striatum, cortex, hippocampus and cerebellum	Significant transcriptional signatures overlap of HD mice models and mouse deficient for epigenetic regulatory genes	Hervás-Corpión et al., 2018
Total H3 and H3K27me3 ChIP-PCR	*Drosophila melanogaster* HD model	H3K27me3 is not altered in flies expressing mutant HTT	Song et al., 2018
H3K27ac ChIP-seq	Human caudate and cerebellum	H3K27ac hipo-acetylation at neuronal super-enhancer regulated genes showing decreased transcriptional levels	Merienne et al., 2019
H3K4me3 ChIP-seq and ATAC-seq	Neuronal cell cultures from differentiated control and HD iPSCs	H3K4me3 alterations near TSS of genes involved in cell-cycle, highly overlapping with transcriptional upregulation for genes with increased H3K4me3 and binding of TFs involved cell-cycle regulation	Smith-Geater et al., 2020
DNA-methylation by bisulfite sequencing	Human blood, lymphoblasts, and fibroblasts tissue from controls and HD patients; Q20 and Q175 HD KI mouse tissue; control and HD sheep blood	Conserved DNA methylation changes in blood samples at 33 CpG sites, including HTT gene associated with motor progression in manifest HD cases at three particular loci (PEX14, GRIK4 and COX412)	Lu et al., 2020

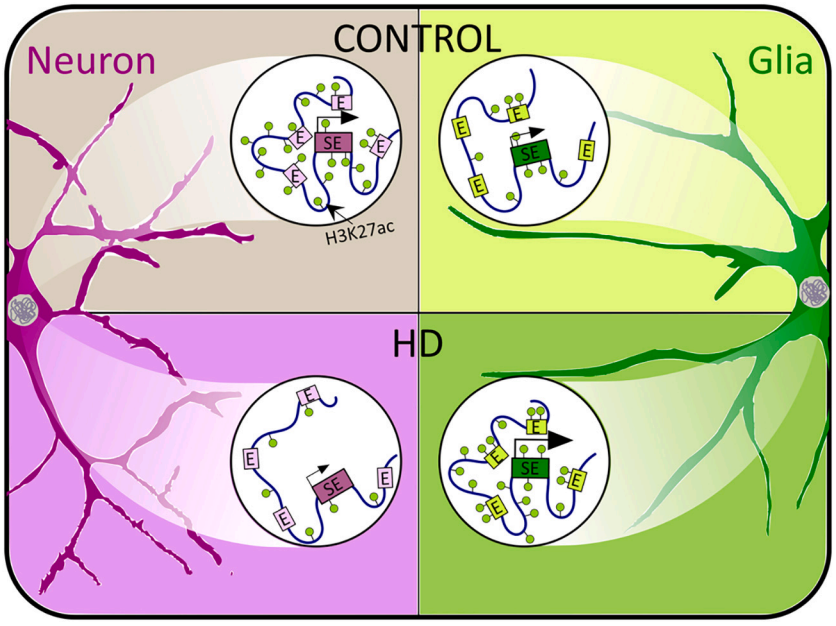

Fig. 3. Cell type-specific dysregulation of super-enhancers in HD. Scheme illustrating epigenetic signatures in the HD striatum. Super-enhancers regulating neuronal identity genes (purple) and glial identity genes (green) are differentially impaired in HD. In control striatum (top panels), both neuronal and glial super-enhancer-regulated genes are highly enriched in H3K27ac (green circles), leading to extensive promoter-enhancer interactions and high transcriptional rates. In the HD striatum (bottom panels), neuronal super-enhancers (bottom left panel) are depleted in H3K27ac, correlating with down-regulation of neuronal identity genes. In contrast, glial super-enhancers in HD (bottom right panel) show increased H3K27ac, associated with increased transcription. (For interpretation of the references to colour in this figure legend, the reader is referred to the web version of this article.)

observed in the striatum of HD R6/1 transgenic mice (Achour et al., 2015; Le Gras et al., 2017). Similar results were found analyzing H3K27ac ChIPseq data generated using post mortem striatal tissue of HD patients at early symptomatic stage (Merienne et al., 2019). Although bulk striatal tissue was used in these studies, integrated analysis with cell type-specific transcriptomic striatal database allowed specifying the contribution of neurons and glial cells to H3K27ac changes. H3K27ac was depleted at neuronal super-enhancers in HD vs controls, which correlated with down-regulation of neuronal super-enhancer-regulated genes (Achour et al., 2015; Merienne et al., 2019)(Fig. 3). Remarkably, this associated with depletion in RNAPII throughout neuronal super-enhancers, and reduced eRNAs (Achour et al., 2015; Le Gras et al., 2017; Sabari et al., 2018). In contrast, H3K27ac and transcription were increased at glial-specific enhancers (Merienne et al., 2019). Whether maintenance or acquisition of striatal cell identity is compromised in HD is an intriguing possibility that could underlie the mechanism.

HD promoter features were also investigated targeting H3K4me3, which is enriched at active promoters (Bai et al., 2015; Dong et al., 2015; Guiretti et al., 2016; Vashishtha et al., 2013) (Table 1). ChIP-seq data generated using the striatum and cortex of HD R6/2 transgenic mice indicated that H3K4me3 was widely depleted at neuronal identity gene promoters, which displayed broad H3K4me3 profiles, while genes showing increased H3K4me3 showed a developmental signature (Vashishtha et al., 2013). H3K4me3 was also investigated using post mortem prefrontal cortex from HD patients, a region however showing mild neuropathological involvement in HD (Bai et al., 2015; Dong et al., 2015). These studies specifically analyzed cortical neurons after nuclei sorting using fluorescently activated nuclei sorting (FANS), and identified hundreds of regions differentially enriched in H3K4me3 in HD vs control samples, which were preferentially depleted in H3K4me3. Although the connection between increased H3K4me3 and transcription in HD brain remains elusive, depleted H3K4me3 in HD vs control samples correlated with reduced transcription (Dong et al., 2015).

Collectively, H3K4me3 and H3K27ac epigenomic data indicate that the HD mutation induces loss of activity of neuronal-specific enhancers and promoters implicated in the control of neuronal identity genes. Whether the HD mutation also affects activity-driven epigenetic regulation of neuronal-specific genes implicated in neuronal plasticity is yet unknown, since none of above epigenomic studies described were performed using behavioral paradigms challenging the brain.

2.4. Abnormal epigenetic aging vs development

On the one hand, HD is an age-related disease that is progressive in nature and generally characterized by adult onset, which might suggest that epigenetic aging is altered in HD. DNA methylation can be used to estimate biological age, which better reflects the aging process than chronological age (Horvath and Raj, 2018). Supporting the concept of epigenetic age (or epigenetic clock), Horvath and collaborators showed that hundreds of defined DNA methylation sites are sufficient to estimate biological age (Horvath, 2013). Using this reference as an epigenetic biomarker of aging, the authors showed significant acceleration of epigenetic age in the frontal lobe, parietal lobe and cingulate gyrus of HD patients (Horvath et al., 2016) (Table 1). Although epigenetic age was not accelerated in striatal tissue of HD patients, likely due to neuronal loss, these data suggest causal relationship between accelerated aging and dysregulation of HD epigenome (Horvath et al., 2016). More recently, using four additional epigenetic biomarkers of aging on blood samples from HD patients, Horvath's lab showed that HD patients display accelerated blood epigenetic aging (Lu et al., 2020). Whether enhancers and/or promoters would be more particularly targeted by such a mechanism is an intriguing hypothesis.

On the other hand, growing evidence indicate that HD comprises a neurodevelopmental component, likely due to partial loss of physiological function of normal HTT (Barnat et al., 2020; Barnat et al., 2017; Mehler et al., 2019; Molero et al., 2016; Molero et al., 2009). More specifically, several studies using human and mouse stem cells differentiated into neurons, including striatal-like cells, showed that mutated HTT leads to defects in neuronal specification and maturation (Conforti et al., 2018; HD iPSC Consortium, 2017; Molero et al., 2009; Ring et al., 2015; Ruzo et al., 2018; Smith-Geater et al., 2020). Induced pluripotent stem cells (iPSC) differentiated in MSN-like neurons showed delayed differentiation in the HD background, which correlated with altered epigenetic and transcriptional reprogramming (HD iPSC Consortium, 2017; Smith-Geater et al., 2020) (Table 1). Specifically, persistent expression of developmental genes, including *OCT4*, was observed during striatal neuron differentiation of HD iPSCs, together with abnormal H3K27ac and H3K4me3 profiles, which reflected more immature neuronal state than that observed in controls (HD iPSC Consortium, 2017; Smith-Geater et al., 2020).

Thus, abnormal epigenetic regulation during neurodevelopment might compromise proper acquisition of cellular identity of HD terminally differentiated neurons. It is possible, however, that HD-mediated epigenetic alterations during development render neurons more vulnerable to environmental stressors, which may be compensated during early life, but not at later stage, due to cellular aging. Thus, HD epigenetic neurodevelopmental and aging-associated components may be related.

2.5. Dysregulation of epigenetic regulators by mutated HTT

A number of studies have provided evidence for dysregulation of specific chromatin regulators in HD, which may contribute to disruption of the HD epigenetic landscape. It was found in early studies that the HAT CBP is recruited in polyQ-HTT aggregates in HD neurons (Nucifora et al., 2001; Seredenina and Luthi-Carter, 2012; Steffan et al., 2001). Since H3K27ac is a *bona-fide* target of CBP (Tie et al., 2014), titration of CBP by polyQ-HTT aggregates could lead to neuronal-specific depletion of H3K27ac. Noticeably however, mutant HTT aggregate formation is a rather late event with respect to HD pathogenesis. Thus, sequestration of CBP in polyQ-HTT aggregates is unlikely to explain epigenetic dysregulation occurring during neuronal differentiation. Nonetheless, a numbers of studies indicate that targeting histone acetylation in HD is beneficial, at least in animal models (Butler and Bates, 2006; Francelle et al., 2017). Specifically, several histone deacetylase inhibitors (HDACi) have been used to treat HD mice and drosophila models, which led to partial recovery of HD-like phenotypes (Ferrante et al., 2003; Gardian et al., 2005; Hockly et al., 2003; Jia et al., 2016; Naia et al., 2017; Siebzehnrübl et al., 2018; Steffan et al., 2001; Suelves et al., 2017; Thomas et al., 2008). Interestingly enough, the HDACi LBH589 improved HD neuronal differentiation (Siebzehnrubl et al., 2007; Siebzehnrübl et al., 2018). However, since no epigenomic data have been generated on HDACi treated animals, it is unclear whether histone acetylation is restored at neuronal super enhancers upon treatment. Moreover, the few transcriptomic data do not support complete rescue of neuronal identity gene transcription, and rather suggest that HDACi modulate metabolic genes (Naia et al., 2017). Yet, in mature neurons, histone acetylation is critical to activity-driven transcription, i.e. to the dynamic regulation of plasticity genes in response to neural stimulation (Malik et al., 2014). Thus, it would be interesting to test whether compounds that target histone acetylation affect activity-driven genes in the context of HD.

Additional pieces of evidence indicate that protein complexes and/or enzymes facilitating a repressive chromatin state are modulated by polyQ-HTT, which could impair the balance between euchromatin and heterochromatin. For example, the activity of polycomb repressive complex 2 (PRC2) was enhanced by mutant HTT, and during neuronal differentiation, HTT was required for proper regulation of H3K27me3, a PRC2 target enriched in facultative heterochromatin (Biagioli et al., 2015; Seong et al., 2010; Song et al., 2018) (Table 1). However, the effect of mutant HTT on H3K27me3 in mature neurons remains elusive. Other studies showed that the histone H3K9 methylase ESET/SETDB1

Table 2
Summary of HD epigenomic studies.

Experimental approach	Biological specimen	Key findings	Bibliographic refference
HDAC1, HDAC2, HDAC3, acetyl H2BK5, acetyl H3K14, acetyl H4K5, acetyl H4K12, phospho-GR1 (S211) and phospho-RNA Pol II ChIP-PCR	Hippocampal tissue from control and CK-p25 mice	HDAC2, but not HDAC1 and HDAC3, is increased at promoter of of genes involved in memory and synaptic plasticity in the AD mice CK-p25, with a concomitant reduction of several histone acetylation marks, RNA Pol II recruitment and gene transcription	Gräff et al., 2012
H3K27ac ChIP-seq and GWAS meta-analysis	Human cell and tissue samples	SNPs associated to AD are over-represented in brain super-enhacers as compared to other tissues	Hnisz et al., 2013
DNA-methylation by bisulfite sequencing	Human prefrontal cortex of control and AD patients	AD associated CpG methylation regions are significantly enriched in weak enhancers	De Jager et al., 2014
H4K12ac ChIP-seq	Hippocampal CA-1 neuronal an non-neuronal cells from control and APP/PS1-21 mice	Global decrease of H4K12ac in both, neuronal and non-neuronal cell populations	Benito et al., 2015
H3K4me1, H3K4me3, H3K9me3, H3K27me3, H3K27ac, H3K36me3 and and H4K20me1 ChIP-seq	Hippocampus from control and CK-p25 AD mice	CK-p25 increased-level enhancer and promoters showed functional enrichment in immune and stimulus-response functions, while decreased-level enhancer and promoters were enriched in synapse and learning-associated functions, matching transcriptional alterations	Gjoneska et al., 2015
H3K4me1 and H3K4me3 ChIP-seq	Hippocampal neuronal nuclei from control, Kmt2a cKO and Kmt2b cKO mice	Significant overlap between H3K4me3 hipo-methylated promoters in the AD mice CK-p25 and the lysine methyltransferase cKO Kmt2a, but not Kmt2b, affecting genes involved in memory- and synaptic-plasticity-related processes	Kerimoglu et al., 2017
H2BK12/K15ac, H2BK5ac and H3K27ac ChIP-seq	Dorsal hippocampus from control and THY-Tau22 transgenic mice	Significant decrease of H2B but not H3K27 acetylation levels in tauopathic mice hippocampus affecting genes involved in neuronal functions	Chatterjee et al., 2018
H3K27ac ChIP-seq	Human entorhinal cortex from control and AD patients	Genome-wide acetylomic alterations at regulatory regions affecting genes involved in the progression of amyloid-β and tau pathology as well as regions containing sporadic late-onset AD variants	Marzi et al., 2018
H4K16ac ChIP-seq	Lateral temporal lobe of young, old cognitively normal, and AD individuals	H4K16ac changes define functionally distinct subsets of age-regulated (changed by aging in physiological and AD conditions), age-dysregulated (changed by aging but not in AD) and disease-specific (only changed in AD)	Nativio et al., 2018
Hi-C	Neuroblastoma cell line SK-N-SH and astrocytoma cell line U-251 MG	High percentage (30%) of non-coding AD SNPs localize at enhancer regions within topologically associated domains shared with their eQTL genes, suggesting a major role of chromatin high-order three-dimensional structures in AD	Kikuchi et al., 2019
H3K9ac ChIP-seq	Aged human prefrontal cortices	Tau protein burden, but not B-amyloid, have major effects on the epigenome in a spatial chromatin organization-dependent manner, partially overlapping with transcriptional alterations	Klein et al., 2019
Bisulfite padlock probe technique for CpG and CpH methylation analysis	Prefrontal cortex neurons of individuals with no/mild, moderate, and severe AD pathology	Predominant hypomethylation of enhancers in AD at intergenic and exonic regions associated with genes involved in neurogenesis and neurodevelopment	Li et al., 2019
Chromatin conformation capture (3C), ChIP-PCR	Immortalized B cells	PM20D1 characterization as an AD-risk associated haplotype via an enhacer-promoter chromatin loop	Sanchez-Mut et al., 2018
ATAC-seq, H3K4me3 and H3k27ac ChIP-seq, PLAC-seq	Neurons, astrocytes, oligodendrocytes and microglia isolated from human brain cortex	Predominant associatiation of sporadic AD variants to microglia specific enhancer regions physically interacting with known and newly characterized gene promoters	Nott et al., 2019

was increased in the striatum of HD transgenic mice, a feature correlating with dysregulation of H3K9me3, a marker of constitutive heterochromatin (Lee et al., 2017; Ryu et al., 2006). Underlying mechanism might involve impaired interaction between mutated HTT and ATF7IP-ESET/SETDB1 complex (Irmak et al., 2018). Finally, using a genetic screen in a drosophila model system indicated that HTT physiological

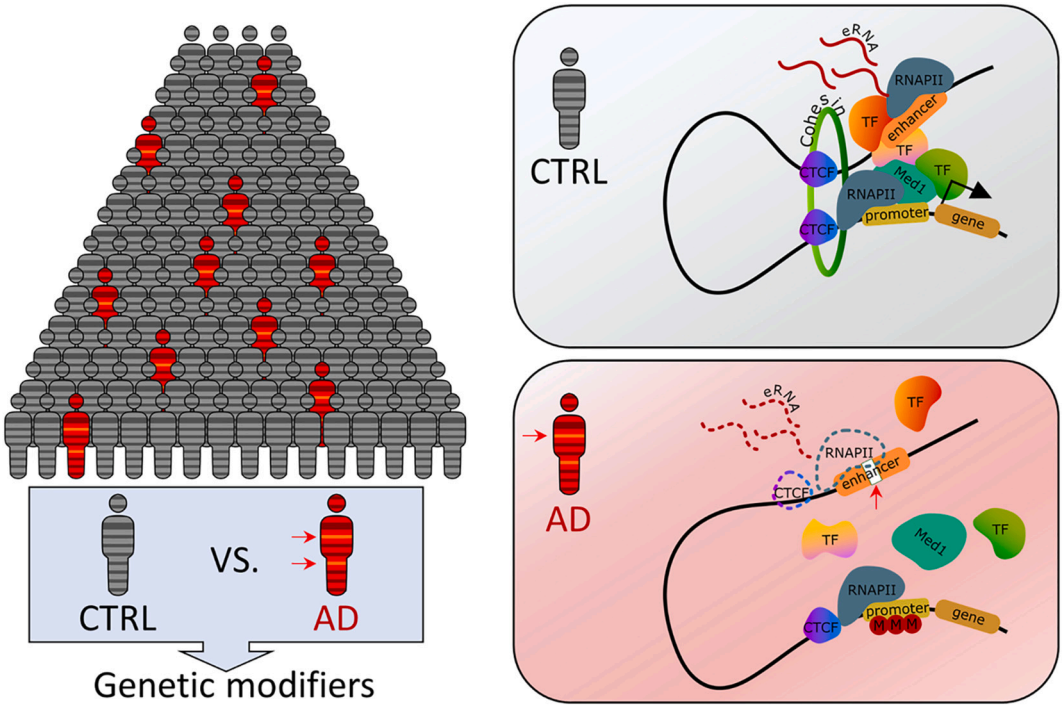

Fig. 4. Disruption of a promoter-enhancer chromatin loop at an AD risk variant. On the left, an illustration of how Genome Wide Association Studies (GWAS), based on the comparison of Single Nucleotide Polymorphisms (SNPs, horizontal stripes) enriched in thousands of individuals corresponding to a healthy reference group (CTRL, grey) or presenting Alzheimer's disease (AD, red) can identify disease-associated risk variants (yellow horizontal stripes). On the right, a scheme illustrating the effect of the AD genetic risk variant rs708727 located in an enhancer-like region interacting with *PM20D1* (Sanchez-Mut et al., 2018). In control individuals (CTRL, right upper panel), *PM20D1* promoter-enhancer interaction results from the recruitment of CTCF at *PM20D1* promoter and enhancer regions, together with additional transcription factors (TF) and Mediator (Med1), establishing the mediator complex, which stimulates enhancer transcription (eRNA) and *PM20D1* mRNA transcription. The presence of the AD associated rs708727 SNP (AD, bottom right panel) in the cis regulatory region of *PM20D1* gene (white mark) impairs promoter chromatin interaction, enhancer CCCTC-binding factor (CTCF) recruitment and leads to *PM20D1* promoter methylation (red M circles) and, as a consequence, a significant impairment of *PM20D1* expression. (For interpretation of the references to colour in this figure legend, the reader is referred to the web version of this article.)

function includes chromatin re-organization through regulation of H3 methylation at heterochromatin-euchromatin boundaries (Dietz et al., 2015). While these studies support the notion that HTT might act as an epigenetic regulator contributing to reprogramming of facultative and/or constitutive heterochromatin during neurodevelopment, the direct effect of mutant HTT on repressive histone marks in mature neurons and their impact on transcriptional regulation remains unclear.

3. Epigenetic dysregulation and enhancer regulation in AD

3.1. Etiology and neuropathology of AD

AD is an aging-related neurodegenerative disease characterized by the accumulation of amyloid beta peptides (Aβ) and neurofibrillary tangles, which are composed of abnormally phosphorylated Tau protein. AD leads to progressive synaptic and neuronal loss, most particularly in the prefrontal cortex and hippocampus, thereby resulting in memory decline (Serrano-Pozo et al., 2011). Neuroinflammatory response is also a major hallmark of AD. A minority of cases, usually characterized by early onset (i.e. <65 years), is caused by mutations in genes implicated in Aβ processing, including APP and presinilins. However, the vast majority of cases are sporadic (>95%) and late onset, and result from more complex etiology implicating both environmental and genetic risk factors. While aging is the strongest environmental risk factor, GWAS studies revealed several genetic risk variants, including variants associated with *APOE* and *BIN1* (Bellenguez et al., 2019; Jansen et al., 2019).

3.2. Brain enhancers, hotspots for AD-risk variants

Consistent with AD pathogenesis, genes associated to AD-risk variants are enriched in 4 major functions, including Aβ formation, tau, lipid metabolism and immune response (Jansen et al., 2019). Thus, it is believed that risk variants play causal role, modulating transcription of associated genes (Grubman et al., 2019; Jansen et al., 2019; Klein et al., 2016; Nott et al., 2019). However, the interpretation of risk variants remains elusive in many instances, since they are often located in non-coding regions of the genome that may be distant to the gene(s) they modulate (Maurano et al., 2012; Nott et al., 2019). Analysis of GWAS catalog database showed that nearly 30% of non-coding AD SNPs are located in enhancers, with 95% of the AD SNPs located in enhancers co-localizing with their expressed quantitative trait locus (eQTL) genes in topologically associated domains (Kikuchi et al., 2019). Epigenome-wide studies using post mortem brain tissues of AD patients further point to a critical role for enhancers in AD-risk variants, since differential DNA methylation patterns between AD and control individuals were enriched at enhancers (De Jager et al., 2014; Li et al., 2019; Lunnon et al., 2014) (Table 2). The role of enhancers and DNA methylation in mediating the effect of risk factors in AD was supported by a study showing that an AD-risk associated haplotype in enhancer-like regulatory region associates to hypermethylation of PM20D1 promoter, which alters the regulation of this stress-responsive gene (Sanchez-Mut et al., 2018) (Table 2). The authors proposed that AD-risk associated haplotype impairs CTCF-mediated chromatin loop implicating PM20D1 promoter and enhancer (Fig. 4).

The heterogeneity of cerebral tissues represents another limitation to the interpretation of risk variants, especially since increasing evidence

indicates that functional consequences of risk variants are cell type-specific (Yeh et al., 2017; Tansey et al., 2018; Nott et al., 2019). Network analysis of bulk AD brain transcriptome indicated gain of microglial gene connectivity and loss of neuronal connectivity, suggesting cell-type-specific effects of AD-risk variants, notably up-regulation of microglial-specific genes and down-regulation of neuronal-specific genes (Zhang et al., 2013). Studies using single-nucleus/cell RNA sequencing on AD and control cortices provided additional insights, showing that *APOE* is upregulated in an AD-specific microglial subpopulation (Grubman et al., 2019; Mathys et al., 2019). To interpret the effects of AD risk variants in a cell-type-specific manner, Nott and collaborators performed epigenomic analysis using human resected cortical brain tissues and found that microglia-specific enhancers were more particularly enriched in AD risk variants (Nott et al., 2019). Using proximity ligation assisted ChIP-seq (PLAC-seq) to establish cell-type-specific enhancer-promoter interactome maps and CRISPR/Cas9 technology, they further showed that risk variant rs6733839, the second highest AD-risk variant, is located in microglia enhancer controlling microglia-specific transcription of *BIN1* (Nott et al., 2019). Thus, increasing evidence indicates that brain-specific enhancers, most particularly microglial-specific enhancers, are hotspots for genetic and/or epigenetic variations in AD, thereby contributing to AD pathogenesis in a cell type-specific manner (De Jager et al., 2014; Jansen et al., 2019; Kikuchi et al., 2019; Nott et al., 2019). Finally, AD-associated risk variants are enriched in super-enhancers, suggesting critical role for super-enhancers in AD etiology (Hnisz et al., 2013; Nott et al., 2019).

3.3. Genome-wide scale enhancer dysregulation in AD

In addition to locus-specific effects on enhancers due to disease-associated genetic variants, several studies indicate more global disruption of transcriptional enhancers in AD brain tissue, correlating with transcriptional alterations (Benito et al., 2015; Chatterjee et al., 2018; Gjoneska et al., 2015; Klein et al., 2016; Li et al., 2019; Marzi et al., 2018) (Table 2). First evidence came from studies using AD mouse models (Benito et al., 2015; Gjoneska et al., 2015). Transcriptomic and epigenomic profiling using the hippocampus of CK-p25 mouse model, showing amyloid and tau pathologies, revealed coordinated down-regulation of synaptic plasticity genes and associated enhancers and promoters and, in contrast, upregulation of immune response genes and regulatory regions, including genes and regulatory regions specifically active in microglia (Gjoneska et al., 2015). H3K27ac and H3K4me3 were reduced at neuronal-specific enhancers and promoters, respectively, which correlated with down-regulation of their target genes, whereas the direction of epigenetic and transcriptional changes at glial-specific regulatory regions/genes was opposite (Gjoneska et al., 2015). Consistently, decreased and increased-level regulatory regions were enriched in distinct DNA motifs, recognized by neuronal- and glial-specific transcriptional regulators, respectively (Gjoneska et al., 2015). H3K27ac profiling of AD post-mortem entorhinal cortex samples supported mouse data, showing that enhancer dysregulation is a major hallmark of AD brain (Marzi et al., 2018). Comparing samples of AD patients vs control individuals, thousands of genes were identified that associated with hyper- or hypo-acetylated peaks, and the direction of change in acetylation positively correlated with some of the transcriptional changes (Marzi et al., 2018). Gene ontology analysis further indicated that genes nearby increased H3K27ac in AD samples were enriched in metabolic functions, possibly including glial response, while neuronal processes associated with regions depleted in H3K27ac (Marzi et al., 2018). This might suggest that AD, similar to HD, leads to opposite H3K27ac changes at neuronal- and glial-specific enhancers. Although super-enhancers and identity genes have not been specifically investigated in AD studies, one cannot exclude that comparable genome-wide scale reprogramming of neuronal and glial cell identities operates in AD and HD brains.

Comprehensive fine-mapping of DNA methylation further suggests a crucial role for enhancer dysregulation in AD neuronal pathogenesis, since thousands of differentially methylated enhancers were identified in neurons isolated from prefrontal cortex of AD patients vs control individuals (Li et al., 2019). Surprisingly however, most of these regions were hypomethylated non-CpG sites (e.g. CpH sites), a result that correlated with increased transcriptional activity of closest genes (Li et al., 2019). Methylation at CpH is a major feature of mature neurons, rising during development and correlating with synaptogenesis (Lister et al., 2013). While the role of these non-canonical methylation sites in AD is yet to be uncovered, the results by Li and collaborators indicate that hypomethylation at CpH sites essentially targets genes linked to neurogenesis, including genes promoting neuronal proliferation and migration (Li et al., 2019). Thus, pathological re-activation of neurodevelopmental genes mediated by loss of CpH methylation in enhancers of neurons might be feature of AD.

Finally, changes in additional histone modifications, particularly histone acetylation, including H3K9ac, H3K14ac, H4K5ac, H4K12ac, H4K16ac and H2Bac were also observed in brain tissues of AD mouse models and/or post mortem AD brain cells. While it is not clear whether those acetylation changes were enriched in specific regulatory regions, these results indicate a degree of complexity of AD epigenetic signature (Benito et al., 2015; Chatterjee et al., 2018; Gräff et al., 2012; Klein et al., 2019; Nativio et al., 2018) (Table 2). Collectively, epigenomic data show that AD leads to significant cell-type-specific epigenetic dysregulation of brain enhancers. While histone acetylation remains a major focus in AD epigenomic studies, H3K4me3 was found dysregulated in AD mice, indicating that epigenetic regulation of promoters is likely impaired in AD (Gjoneska et al., 2015; Kerimoglu et al., 2017).

3.4. Epigenetic control of activity-regulated genes in AD

The dynamic epigenetic control of gene program regulating neuronal plasticity is critical to memory formation and maintenance, and histone acetylation plays a central role in this mechanism (Yap and Greenberg, 2018). Several studies suggest that altered regulation of histone acetylation contributes to memory decline in AD (Fischer, 2014a). Early study revealed that histone deacetylase 2 (HDAC2) was increased at neural plasticity genes, both in brain tissues of AD mice and in post-mortem brains from AD patients (Gräff et al., 2012). Consequently, AD mice were treated with HDAC inhibitors (HDACi), which generally improved memory function and, when tested, also ameliorated synaptic plasticity (Fischer, 2014b; Gräff et al., 2012). More specifically, epigenomic and transcriptomic analyses showed that, in APP/PS1-21 CE mice, treatment with SAHA specifically restored H4K12ac at synaptic plasticity genes in CA1 hippocampal neurons, which correlated with partial transcriptional normalization (Benito et al., 2015). Interestingly enough, memory function and synaptic plasticity were also restored in tauopathic mice treated with an activator of the HAT CBP/P300, the compound CSP-TTK21 (Chatterjee et al., 2018; Chatterjee et al., 2013). Epigenomic and transcriptomic analyses using the dorsal hippocampus of tauopathic mice further showed that the functional amelioration observed (rescue of long-term spatial memory, LTD and learning-induced CA1 dendritic spines) associated with transcriptional rescue of activity-regulated genes and increased H2B acetylation at CBP-regulated enhancers, while H3K27Ac remained unchanged at this age (Chatterjee et al., 2018). In addition, CBP levels were decreased in the hippocampus of tauopathic mice as well as in postmortem prefrontal cortices of AD patients (Bartolotti et al., 2016; Schueller et al., 2020), suggesting a role for CBP in the dysregulation of these genes (Chatterjee et al., 2018), an hypothesis supported by an earlier study showing that gene transfer delivery of CBP in the hippocampus of AD mice improves memory processes (Caccamo et al., 2010).

3.5. Epigenetic aging in AD

Altered epigenetic aging may be another mechanism driving epigenetic defects in the AD brain. Whether epigenetic aging is accelerated and/or dysregulated was recently addressed through epigenomic studies using post mortem brain tissues of AD patients (Li et al., 2019; Nativio et al., 2018). Investigating H4K16ac, a promoter mark linked to DNA damage repair and increased in senescent cells (Dang et al., 2009; Kozak et al., 2010), Nativio and collaborators identified 3 types of changes in the lateral lobe of AD patients (Nativio et al., 2018). A first category of changes corresponded to disease-specific changes and were observed comparing AD patients to age-matched individuals. A second category of age-dysregulated changes defined changes found in aged vs young individuals but not in AD vs young individuals. The last category of changes comprised age-regulated changes, observed in both aged control and AD, vs young individuals. Interestingly, disease-specific changes affected genes were enriched in neuronal functions, while age-dysregulated changes implicated immunity and stress response genes, reflecting glial responses. Age-dysregulated changes were predominantly characterized by age-dependent increase in H4K16ac in control individuals, but age-dependent H4K16ac depletion in AD individuals, suggesting AD leads to dysregulated aging and is not simply accelerated aging (Nativio et al., 2018). However, cell type-specific epigenomic analysis focusing on H4K12ac indicated aging-related acceleration of decreased H4K12ac in hippocampal neurons of AD mice modeling amyloid pathology, and the mechanism correlated with down-regulation of target genes, which were enriched in neuronal plasticity genes (Benito et al., 2015). Also, using the epigenetic clock on enhancer CpG sites from healthy individuals, Li and collaborators found that neurons of advanced AD cases show significant acceleration of epigenetic aging (Li et al., 2019). Thus, current studies provide a rather complex picture of the interplay between AD and epigenetic aging. Undoubtedly, investigating the impact of aging on additional epigenetic marks, including H3K27ac, and at cell type-specific resolution should help refine the conclusions and specify the role of epigenetic aging in AD. It is noteworthy that H3K27ac was found to be a key predictor of age-related transcriptional changes in various mammalian tissues (Benayoun et al., 2019). Finally, recent evidence suggests that tau-related alteration induces widespread reorganization of chromatin architecture, which could contribute to aging-related mechanisms (Klein et al., 2019). Remarkably, neurons appear to be more specifically affected by the mechanism (Klein et al., 2019). Altered maintenance and regulation of heterochromatin due to pathologically phosphorylated tau would be the driving force, through impairment of nuclear lamina organization (Chang et al., 2010; Klein et al., 2019; Mansuroglu et al., 2016).

Several mechanisms might contribute to large-scale dysregulation of epigenetic landscape in AD. Yet, it is unclear whether enhancer dysregulation is a primary defect driving other epigenetic changes or is secondary to earlier mechanisms.

4. Conclusions and perspectives

Epigenomic and transcriptomic data generated on animal models and tissues from HD and AD patients revealed epigenetic changes in affected brain tissues, for both diseases. Remarkably, despite different etiologies between HD and AD, current data indicate that HD and AD pathogenesis associate with large-scale dysregulation of enhancers and promoters, which positively correlates with transcriptional alterations. Although additional studies are required to specify the nature, temporal dynamics, spatial chromatin re-organization and cell type-specificity of changes at HD/AD enhancers and promoters, a picture emerges from current data. Neuronal- and glial-specific regulatory regions and their associated genes show lower and increased activities, respectively, in disease vs control brains, which might contribute to loss of neuronal function and inflammatory responses, two major pathological hallmarks.

More specifically, HD data show that neuronal super-enhancers are particularly vulnerable in the HD striatum, suggesting loss of striatal identity. The role of glial cells in this mechanism needs to be better deciphered, but it is noteworthy that glial-specific genes are increased in the HD striatum, which might support the idea of pathological epigenetic reprogramming. The timing of such defects needs to be investigated, but data generated on stem cell-based models suggest that it could start earlier than anticipated, perhaps during neuronal differentiation. Epigenomic analysis on additional affected brain tissues in HD should also tell whether loss of tissue identity is specific to the striatum, or whether it just develops earlier in this tissue, the primary target of the disease. While the mechanism underlying super-enhancer signature in HD striatum remains unclear, it would be of interest to investigate additional components of enhancers that are particularly enriched in super-enhancers, including CBP, the mediator and master transcriptional factors of tissue-specific identity. Also, it is possible that specific chromatin architecture and/or biophysics properties, promoting phase separation at super-enhancers, are disrupted, thereby contributing to transcriptional effects and cellular reprogramming.

While the role of neuronal super-enhancers in AD remains to be specified, it is noteworthy that glial (particularly microglial) super-enhancers are enriched in AD-associated risk variants, which suggests critical role for super-enhancers in AD etiology. Large-scale remodeling of neuronal and glial epigenetic landscape in AD neuronal tissues might support more global implication of super- enhancers in AD pathology, but this remains to be investigated.

Also remarkably, re-activation and/or persistent activation of neurodevelopmental genes are features observed in both HD and AD models. Whether these events reflect epigenetic reprogramming of HD/AD neural tissues and contribute to loss of tissue identity, is an intriguing possibility. During neuronal differentiation, neurodevelopmental genes undergo PRC-dependent silencing implicating H3K27me3, notably inducing bivalent chromatin state at associated promoters and enhancers, which ensures transcriptional repression while keeping permissive transcriptional state (Rada-Iglesias et al., 2011; Taberlay et al., 2011). In mature neurons, PRC maintains repressive chromatin state at developmental genes, which prevents neurodegeneration as well as down-regulation of mature neuron identity genes (von Schimmelmann et al., 2016). It is tempting to speculate that this mechanism is impaired in HD/AD neurons. If so, would it result from continuous process starting from early neuronal life (e.g. during development and neuronal differentiation) or would it be the consequence of the aging process?

Finally, the regulation of activity-driven regulatory regions and their associated genes is impaired in AD brain tissues, supporting the notion that dynamic regulation of neuronal activity is altered in AD. Whether similar mechanism is at play in HD remains to be investigated.

A unifying mechanism that would underlie epigenetic defects in HD or AD remains to be uncovered. The fact that common chromatin regulators (e.g. CBP) are impaired in both diseases might suggest a degree of overlap. Understanding the mechanism(s) driving epigenetic dysregulation is a current challenge, with potentially major therapeutic implications. Major limitations to take up the challenge include the brain complexity and the difficulty to address causal relationships between epigenetic changes and functional consequences. However, the current development of innovative deep sequencing methods, together with new genome editing tools and behavioral paradigms allowing to characterize and manipulate epigenomic and transcriptomic signatures of particular neural cell populations in specific activation states and at single cell resolution will undoubtedly overcome these issues (Grubman et al., 2019; Liu and Jaenisch, 2019). Also, advanced methods (e.g. Hi-C) to establish 3D maps of enhancer-promoter interactions in vivo at genome-wide and cell-type-specific levels will be critical to decipher causal roles of enhancers in neurodegenerative diseases (Nott et al., 2019). Finally, the generation of multi-omics atlas and databases using diseased brains together with the development of bioinformatics methods will also be

essential to provide comprehensive picture and build accurate models with predictive or instructive values (De Jager et al., 2018; Gosselin et al., 2017). Yet, brain tissue availability from individuals at early disease stages, including pre-symptomatic and prodromal stages, represents a limitation to assess early temporal dynamics of epigenetic and transcriptional changes. In this context, mouse models will remain instrumental.

Declaration of Competing Interest

None.

Acknowledgements

This work was supported by the Agence Nationale de la Recherche (ANR-2017-CE12-0027, ANR-18-CE16-0008, ANR-16-CE92-0031), Association France Alzheimer (SM2017#1664), the Centre National de la Recherche Scientifique (CNRS) and the University of Strasbourg. R.A.V. was supported by post-doctoral IDEX fellowship from University of Strasbourg. A.A. was recipient of doctoral fellowships from the Association Huntington France (AHF).

References

Achour, M., Le Gras, S., Keime, C., Parmentier, F., Lejeune, F.-X., Boutillier, A.-L., Néri, C., Davidson, I., Merienne, K., 2015. Neuronal identity genes regulated by super-enhancers are preferentially down-regulated in the striatum of Huntington's disease mice. Hum. Mol. Genet. 24, 3481–3496. https://doi.org/10.1093/hmg/ddv099.

Bai, G., Cheung, I., Shulha, H.P., Coelho, J.E., Li, P., Dong, X., Jakovcevski, M., Wang, Y., Grigorenko, A., Jiang, Y., Hoss, A., Patel, K., Zheng, M., Rogaev, E., Myers, R.H., Weng, Z., Akbarian, S., Chen, J.-F., 2015. Epigenetic dysregulation of hairy and enhancer of split 4 (HES4) is associated with striatal degeneration in postmortem Huntington brains. Hum. Mol. Genet. 24, 1441–1456. https://doi.org/10.1093/hmg/ddu561.

Barnat, M., Le Friec, J., Benstaali, C., Humbert, S., 2017. Huntingtin-mediated multipolar-bipolar transition of newborn cortical neurons is critical for their postnatal neuronal morphology. Neuron 93, 99–114. https://doi.org/10.1016/j.neuron.2016.11.035.

Barnat, M., Capizzi, M., Aparicio, E., Boluda, S., Wennagel, D., Kacher, R., Kassem, R., Lenoir, S., Agasse, F., Braz, B.Y., Liu, J.-P., Ighil, J., Tessier, A., Zeitlin, S.O., Duyckaerts, C., Dommergues, M., Durr, A., Humbert, S., 2020. Huntington's disease alters human neurodevelopment. Science 369, 787–793. https://doi.org/10.1126/science.aax3338.

Bartolotti, N., Segura, L., Lazarov, O., 2016. Diminished CRE-induced plasticity is linked to memory deficits in familial Alzheimer's disease mice. J. Alzheimers Dis. 50 (2), 477–489. https://doi.org/10.3233/JAD-150650 (PMID: 26682682).

Bates, G.P., Dorsey, R., Gusella, J.F., Hayden, M.R., Kay, C., Leavitt, B.R., Nance, M., Ross, C.A., Scahill, R.I., Wetzel, R., Wild, E.J., Tabrizi, S.J., 2015. Huntington disease. Nat. Rev. Dis. Prim. 1, 15005. https://doi.org/10.1038/nrdp.2015.5.

Bellenguez, C., Grenier-Boley, B., Lambert, J.-C., 2019. Genetics of Alzheimer's disease: where we are, and where we are going. Curr. Opin. Neurobiol. 61, 40–48. https://doi.org/10.1016/j.conb.2019.11.024.

Benayoun, B.A., Pollina, E.A., Singh, P.P., Mahmoudi, S., Harel, I., Casey, K.M., Dulken, B.W., Kundaje, A., Brunet, A., 2019. Remodeling of epigenome and transcriptome landscapes with aging in mice reveals widespread induction of inflammatory responses. Genome Res. 29, 697–709. https://doi.org/10.1101/gr.240093.118.

Benito, E., Urbanke, H., Ramachandran, B., Barth, J., Halder, R., Awasthi, A., Jain, G., Capece, V., Burkhardt, S., Navarro-Sala, M., Nagarajan, S., Schütz, A.-L., Johnsen, S. A., Bonn, S., Lührmann, R., Dean, C., Fischer, A., 2015. HDAC inhibitor-dependent transcriptome and memory reinstatement in cognitive decline models. J. Clin. Invest. 125, 3572–3584. https://doi.org/10.1172/JCI79942.

Biagioli, M., Ferrari, F., Mendenhall, E.M., Zhang, Y., Erdin, S., Vijayvargia, R., Vallabh, S.M., Solomos, N., Manavalan, P., Ragavendran, A., Ozsolak, F., Lee, J.M., Talkowski, M.E., Gusella, J.F., Macdonald, M.E., Park, P.J., Seong, I.S., 2015. Htt CAG repeat expansion confers pleiotropic gains of mutant huntingtin function in chromatin regulation. Hum. Mol. Genet. 24, 2442–2457. https://doi.org/10.1093/hmg/ddv006.

Butler, R., Bates, G.P., 2006. Histone deacetylase inhibitors as therapeutics for polyglutamine disorders. Nat. Rev. Neurosci. 7, 784–796. https://doi.org/10.1038/nrn1989.

Caccamo, A., Maldonado, M.A., Bokov, A.F., Majumder, S., Oddo, S., 2010. CBP gene transfer increases BDNF levels and ameliorates learning and memory deficits in a mouse model of Alzheimer's disease. Proc. Natl. Acad. Sci. U. S. A. 107, 22687–22692. https://doi.org/10.1073/pnas.1012851108.

Campbell, R.R., Wood, M.A., 2019. How the epigenome integrates information and reshapes the synapse. Nat. Rev. Neurosci. 20, 133–147. https://doi.org/10.1038/s41583-019-0121-9.

Chang, K.-H., de Pablo, Y., Lee, Hyun-pil, Lee, Hyoung-gon, Smith, M.A., Shah, K., 2010. Cdk5 is a major regulator of p38 cascade: relevance to neurotoxicity in Alzheimer's disease. J. Neurochem. 113, 1221–1229. https://doi.org/10.1111/j.1471-4159.2010.06687.x.

Chatterjee, S., Mizar, P., Cassel, R., Neidl, R., Selvi, B.R., Mohankrishna, D.V., Vedamurthy, B.M., Schneider, A., Bousiges, O., Mathis, C., Cassel, J.-C., Eswaramoorthy, M., Kundu, T.K., Boutillier, A.-L., 2013. A novel activator of CBP/p300 acetyltransferases promotes neurogenesis and extends memory duration in adult mice. J. Neurosci. 33, 10698–10712. https://doi.org/10.1523/JNEUROSCI.5772-12.2013.

Chatterjee, S., Cassel, R., Schneider-Anthony, A., Merienne, K., Cosquer, B., Tzeplaeff, L., Halder Sinha, S., Kumar, M., Chaturbedy, P., Eswaramoorthy, M., Le Gras, S., Keime, C., Bousiges, O., Dutar, P., Petsophonsakul, P., Rampon, C., Cassel, J.-C., Buée, L., Blum, D., Kundu, T.K., Boutillier, A.-L., 2018. Reinstating plasticity and memory in a tauopathy mouse model with an acetyltransferase activator. EMBO Mol. Med. 10 https://doi.org/10.15252/emmm.201708587.

Conforti, P., Besusso, D., Bocchi, V.D., Faedo, A., Cesana, E., Rossetti, G., Ranzani, V., Svendsen, C.N., Thompson, L.M., Toselli, M., Biella, G., Pagani, M., Cattaneo, E., 2018. Faulty neuronal determination and cell polarization are reverted by modulating HD early phenotypes. Proc. Natl. Acad. Sci. U. S. A. 115, E762–E771. https://doi.org/10.1073/pnas.1715865115.

Dang, W., Steffen, K.K., Perry, R., Dorsey, J.A., Johnson, F.B., Shilatifard, A., Kaeberlein, M., Kennedy, B.K., Berger, S.L., 2009. Histone H4 lysine 16 acetylation regulates cellular lifespan. Nature 459, 802–807. https://doi.org/10.1038/nature08085.

De Jager, P.L., Srivastava, G., Lunnon, K., Burgess, J., Schalkwyk, L.C., Yu, L., Eaton, M. L., Keenan, B.T., Ernst, J., McCabe, C., Tang, A., Raj, T., Replogle, J., Brodeur, W., Gabriel, S., Chai, H.S., Younkin, C., Younkin, S.G., Zou, F., Szyf, M., Epstein, C.B., Schneider, J.A., Bernstein, B.E., Meissner, A., Ertekin-Taner, N., Chibnik, L.B., Kellis, M., Mill, J., Bennett, D.A., 2014. Alzheimer's disease: early alterations in brain DNA methylation at ANK1, BIN1, RHBDF2 and other loci. Nat. Neurosci. 17, 1156–1163. https://doi.org/10.1038/nn.3786.

De Jager, P.L., Ma, Y., McCabe, C., Xu, J., Vardarajan, B.N., Felsky, D., Klein, H.-U., White, C.C., Peters, M.A., Lodgson, B., Nejad, P., Tang, A., Mangravite, L.M., Yu, L., Gaiteri, C., Mostafavi, S., Schneider, J.A., Bennett, D.A., 2018. A multi-omic atlas of the human frontal cortex for aging and Alzheimer's disease research. Sci. Data 5, 180142. https://doi.org/10.1038/sdata.2018.142.

De Laat, W., Duboule, D., 2013. Topology of mammalian developmental enhancers and their regulatory landscapes. Nature. 502, 499–506. https://doi.org/10.1038/nature12753.

Dietz, K.N., Di Stefano, L., Maher, R.C., Zhu, H., Macdonald, M.E., Gusella, J.F., Walker, J.A., 2015. The Drosophila Huntington's disease gene ortholog dhtt influences chromatin regulation during development. Hum. Mol. Genet. 24, 330–345. https://doi.org/10.1093/hmg/ddu446.

Dong, X., Tsuji, J., Labadorf, A., Roussos, P., Chen, J.-F., Myers, R.H., Akbarian, S., Weng, Z., 2015. The role of H3K4me3 in transcriptional regulation is altered in Huntington's disease. PLoS One 10, e0144398. https://doi.org/10.1371/journal.pone.0144398.

Ferrante, R.J., Kubilus, J.K., Lee, J., Ryu, H., Beesen, A., Zucker, B., Smith, K., Kowall, N. W., Ratan, R.R., Luthi-Carter, R., Hersch, S.M., 2003. Histone deacetylase inhibition by sodium butyrate chemotherapy ameliorates the neurodegenerative phenotype in Huntington's disease mice. J. Neurosci. 23, 9418–9427.

Fischer, A., 2014a. Targeting histone-modifications in Alzheimer's disease. What is the evidence that this is a promising therapeutic avenue? Neuropharmacology 80, 95–102. https://doi.org/10.1016/j.neuropharm.2014.01.038.

Fischer, A., 2014b. Epigenetic memory: the Lamarckian brain. EMBO J. 33, 945–967. https://doi.org/10.1002/embj.201387637.

Francelle, L., Lotz, C., Outeiro, T., Brouillet, E., Merienne, K., 2017. Contribution of Neuroepigenetics to Huntington's disease. Front. Hum. Neurosci. 11, 17. https://doi.org/10.3389/fnhum.2017.00017.

Gardian, G., Browne, S.E., Choi, D.-K., Klivenyi, P., Gregorio, J., Kubilus, J.K., Ryu, H., Langley, B., Ratan, R.R., Ferrante, R.J., Beal, M.F., 2005. Neuroprotective effects of phenylbutyrate in the N171-82Q transgenic mouse model of Huntington's disease. J. Biol. Chem. 280, 556–563. https://doi.org/10.1074/jbc.M410210200.

Genetic Modifiers of Huntington''s Disease (GeM-HD) Consortium, 2015. Identification of genetic factors that modify clinical onset of Huntington's disease. Cell 162, 516–526. https://doi.org/10.1016/j.cell.2015.07.003.

Genetic Modifiers of Huntington''s Disease (GeM-HD) Consortium, 2019. CAG Repeat Not polyglutamine length determines timing of huntington's disease onset. Cell 178, 887–900 e14. https://doi.org/10.1016/j.cell.2019.06.036.

Gjoneska, E., Pfenning, A.R., Mathys, H., Quon, G., Kundaje, A., Tsai, L.-H., Kellis, M., 2015. Conserved epigenomic signals in mice and humans reveal immune basis of Alzheimer's disease. Nature 518, 365–369. https://doi.org/10.1038/nature14252.

Gosselin, D., Skola, D., Coufal, N.G., Holtman, I.R., Schlachetzki, J.C.M., Sajti, E., Jaeger, B.N., 2017. An environment-dependent transcriptional network specifies human microglia identity. Science 356 (6344), eaal3222. https://doi.org/10.1126/science.aal3222 (Epub 2017 May 25.PMID: 28546318).

Gräff, J., Tsai, L.-H., 2013. Histone acetylation: molecular mnemonics on the chromatin. Nat. Rev. Neurosci. 14, 97–111. https://doi.org/10.1038/nrn3427.

Gräff, J., Rei, D., Guan, J.-S., Wang, W.-Y., Seo, J., Hennig, K.M., Nieland, T.J.F., Fass, D. M., Kao, P.F., Kahn, M., Su, S.C., Samiei, A., Joseph, N., Haggarty, S.J., Delalle, I., Tsai, L.-H., 2012. An epigenetic blockade of cognitive functions in the neurodegenerating brain. Nature 483, 222–226. https://doi.org/10.1038/nature10849.

Grubman, A., Chew, G., Ouyang, J.F., Sun, G., Choo, X.Y., McLean, C., Simmons, R.K., Buckberry, S., Vargas-Landin, D.B., Poppe, D., Pflueger, J., Lister, R., Rackham, O.J.

L., Petretto, E., Polo, J.M., 2019. A single-cell atlas of entorhinal cortex from individuals with Alzheimer's disease reveals cell-type-specific gene expression regulation. Nat. Neurosci. 22, 2087–2097. https://doi.org/10.1038/s41593-019-0539-4.

Guiretti, D., Sempere, A., Lopez-Atalaya, J.P., Ferrer-Montiel, A., Barco, A., Valor, L.M., 2016. Specific promoter deacetylation of histone H3 is conserved across mouse models of Huntington's disease in the absence of bulk changes. Neurobiol. Dis. 89, 190–201. https://doi.org/10.1016/j.nbd.2016.02.004.

HD iPSC Consortium, 2017. Developmental alterations in Huntington's disease neural cells and pharmacological rescue in cells and mice. Nat. Neurosci. 20, 648–660. https://doi.org/10.1038/nn.4532.

Heinz, S., Romanoski, C.E., Benner, C., Glass, C.K., 2015. The selection and function of cell type-specific enhancers. Nat. Rev. Mol. Cell Biol. 16, 144–154. https://doi.org/10.1038/nrm3949.

Hervás-Corpión, I., Guiretti, D., Alcaraz-Iborra, M., Olivares, R., Campos-Caro, A., Barco, Á., Valor, L.M., 2018. Early alteration of epigenetic-related transcription in Huntington's disease mouse models. Sci. Rep. 8, 9925. https://doi.org/10.1038/s41598-018-28185-4.

Hnisz, D., Abraham, B.J., Lee, T.I., Lau, A., Saint-André, V., Sigova, A.A., Hoke, H.A., Young, R.A., 2013. Super-enhancers in the control of cell identity and disease. Cell 155, 934–947. https://doi.org/10.1016/j.cell.2013.09.053.

Hockly, E., Richon, V.M., Woodman, B., Smith, D.L., Zhou, X., Rosa, E., Sathasivam, K., Ghazi-Noori, S., Mahal, A., Lowden, P.A.S., Steffan, J.S., Marsh, J.L., Thompson, L. M., Lewis, C.M., Marks, P.A., Bates, G.P., 2003. Suberoylanilide hydroxamic acid, a histone deacetylase inhibitor, ameliorates motor deficits in a mouse model of Huntington's disease. Proc. Natl. Acad. Sci. U. S. A. 100, 2041–2046. https://doi.org/10.1073/pnas.0437870100.

Hodges, A., Strand, A.D., Aragaki, A.K., Kuhn, A., Sengstag, T., Hughes, G., Elliston, L.A., Hartog, C., Goldstein, D.R., Thu, D., Hollingsworth, Z.R., Collin, F., Synek, B., Holmans, P.A., Young, A.B., Wexler, N.S., Delorenzi, M., Kooperberg, C., Augood, S. J., Faull, R.L.M., Olson, J.M., Jones, L., Luthi-Carter, R., 2006. Regional and cellular gene expression changes in human Huntington's disease brain. Hum. Mol. Genet. 15, 965–977. https://doi.org/10.1093/hmg/ddl013.

Hombach, D., Schwarz, J.M., Robinson, P.N., Schuelke, M., Seelow, D., 2016. A systematic, large-scale comparison of transcription factor binding site models. BMC Genomics 17, 388. https://doi.org/10.1186/s12864-016-2729-8.

Horvath, S., 2013. DNA methylation age of human tissues and cell types. Genome Biol. 14, R115. https://doi.org/10.1186/gb-2013-14-10-r115.

Horvath, S., Raj, K., 2018. DNA methylation-based biomarkers and the epigenetic clock theory of ageing. Nat. Rev. Genet. 19, 371–384. https://doi.org/10.1038/s41576-018-0004-3.

Horvath, S., Langfelder, P., Kwak, S., Aaronson, J., Rosinski, J., Vogt, T.F., Eszes, M., Faull, R.L.M., Curtis, M.A., Waldvogel, H.J., Choi, O.-W., Tung, S., Vinters, H.V., Coppola, G., Yang, X.W., 2016. Huntington's disease accelerates epigenetic aging of human brain and disrupts DNA methylation levels. Aging (Albany NY) 8, 1485–1512. https://doi.org/10.18632/aging.101005.

Inukai, S., Kock, K.H., Bulyk, M.L., 2017. Transcription factor-DNA binding: beyond binding site motifs. Curr. Opin. Genet. Dev. 43, 110–119. https://doi.org/10.1016/j.gde.2017.02.007.

Irmak, D., Fatima, A., Gutiérrez-Garcia, R., Rinschen, M.M., Wagle, P., Altmüller, J., Arrigoni, L., Hummel, B., Klein, C., Frese, C.K., Sawarkar, R., Rada-Iglesias, A., Vilchez, D., 2018. Mechanism suppressing H3K9 trimethylation in pluripotent stem cells and its demise by polyQ-expanded huntingtin mutations. Hum. Mol. Genet. 27, 4117–4134. https://doi.org/10.1093/hmg/ddy304.

Jansen, I.E., Savage, J.E., Watanabe, K., Bryois, J., Williams, D.M., Steinberg, S., Sealock, J., Karlsson, I.K., Hägg, S., Athanasiu, L., Voyle, N., Proitsi, P., Witoelar, A., Stringer, S., Aarsland, D., Almdahl, I.S., Andersen, F., Bergh, S., Bettella, F., Bjornsson, S., Brækhus, A., Bråthen, G., de Leeuw, C., Desikan, R.S., Djurovic, S., Dumitrescu, L., Fladby, T., Hohman, T.J., Jonsson, P.V., Kiddle, S.J., Rongve, A., Saltvedt, I., Sando, S.B., Selbæk, G., Shoai, M., Skene, N.G., Snaedal, J., Stordal, E., Ulstein, I.D., Wang, Y., White, L.R., Hardy, J., Hjerling-Leffler, J., Sullivan, P.F., van der Flier, W.M., Dobson, R., Davis, L.K., Stefansson, H., Stefansson, K., Pedersen, N. L., Ripke, S., Andreassen, O.A., Posthuma, D., 2019. Genome-wide meta-analysis identifies new loci and functional pathways influencing Alzheimer's disease risk. Nat. Genet. 51, 404–413. https://doi.org/10.1038/s41588-018-0311-9.

Jenuwein, T., Allis, C.D., 2001. Translating the histone code. Science 293, 1074–1080. https://doi.org/10.1126/science.1063127.

Jia, H., Wang, Y., Morris, C.D., Jacques, V., Gottesfeld, J.M., Rusche, J.R., Thomas, E.A., 2016. The effects of pharmacological inhibition of histone deacetylase 3 (HDAC3) in Huntington's disease mice. PLoS One 11, e0152498. https://doi.org/10.1371/journal.pone.0152498.

Jones, L., Houlden, H., Tabrizi, S.J., 2017. DNA repair in the trinucleotide repeat disorders. Lancet Neurol. 16, 88–96. https://doi.org/10.1016/S1474-4422(16)30350-7.

Kerimoglu, C., Sakib, M.S., Jain, G., Benito, E., Burkhardt, S., Capece, V., Kaurani, L., Halder, R., Agís-Balboa, R.C., Stilling, R., Urbanke, H., Kranz, A., Stewart, A.F., Fischer, A., 2017. KMT2A and KMT2B mediate memory function by affecting distinct genomic regions. Cell Rep. 20, 538–548. https://doi.org/10.1016/j.celrep.2017.06.072.

Kikuchi, M., Hara, N., Hasegawa, M., Miyashita, A., Kuwano, R., Ikeuchi, T., Nakaya, A., 2019. Enhancer variants associated with Alzheimer's disease affect gene expression via chromatin looping. BMC Med. Genet. 12, 128. https://doi.org/10.1186/s12920-019-0574-8.

Kim, T.-K., Hemberg, M., Gray, J.M., Costa, A.M., Bear, D.M., Wu, J., Harmin, D.A., Laptewicz, M., Barbara-Haley, K., Kuersten, S., Markenscoff-Papadimitriou, E., Kuhl, D., Bito, H., Worley, P.F., Kreiman, G., Greenberg, M.E., 2010. Widespread transcription at neuronal activity-regulated enhancers. Nature 465, 182–187. https://doi.org/10.1038/nature09033.

Klein, H.-U., Bennett, D.A., De Jager, P.L., 2016. The epigenome in Alzheimer's disease: current state and approaches for a new path to gene discovery and understanding disease mechanism. Acta Neuropathol. 132, 503–514. https://doi.org/10.1007/s00401-016-1612-7.

Klein, H.-U., McCabe, C., Gjoneska, E., Sullivan, S.E., Kaskow, B.J., Tang, A., Smith, R.V., Xu, J., Pfenning, A.R., Bernstein, B.E., Meissner, A., Schneider, J.A., Mostafavi, S., Tsai, L.-H., Young-Pearse, T.L., Bennett, D.A., De Jager, P.L., 2019. Epigenome-wide study uncovers large-scale changes in histone acetylation driven by tau pathology in aging and Alzheimer's human brains. Nat. Neurosci. 22, 37–46. https://doi.org/10.1038/s41593-018-0291-1.

Kozak, M.L., Chavez, A., Dang, W., Berger, S.L., Ashok, A., Guo, X., Johnson, F.B., 2010. Inactivation of the Sas2 histone acetyltransferase delays senescence driven by telomere dysfunction. EMBO J. 29, 158–170. https://doi.org/10.1038/emboj.2009.314.

Kuhn, A., Goldstein, D.R., Hodges, A., Strand, A.D., Sengstag, T., Kooperberg, C., Becanovic, K., Pouladi, M.A., Sathasivam, K., Cha, J.-H.J., Hannan, A.J., Hayden, M. R., Leavitt, B.R., Dunnett, S.B., Ferrante, R.J., Albin, R., Shelbourne, P., Delorenzi, M., Augood, S.J., Faull, R.L.M., Olson, J.M., Bates, G.P., Jones, L., Luthi-Carter, R., 2007. Mutant huntingtin's effects on striatal gene expression in mice recapitulate changes observed in human Huntington's disease brain and do not differ with mutant huntingtin length or wild-type huntingtin dosage. Hum. Mol. Genet. 16, 1845–1861. https://doi.org/10.1093/hmg/ddm133.

Kuras, L., Borggrefe, T., Kornberg, R.D., 2003. Association of the Mediator complex with enhancers of active genes. Proc. Natl. Acad. Sci. U. S. A. 100, 13887–13891. https://doi.org/10.1073/pnas.2036346100.

Labadorf, A.T., Myers, R.H., 2015. Evidence of extensive alternative splicing in post mortem human brain HTT transcription by mRNA sequencing. PLoS One 10, e0141298. https://doi.org/10.1371/journal.pone.0141298.

Langfelder, P., Cantle, J.P., Chatzopoulou, D., Wang, N., Gao, F., Al-Ramahi, I., Lu, X.-H., Ramos, E.M., El-Zein, K., Zhao, Y., Deverasetty, S., Tebbe, A., Schaab, C., Lavery, D. J., Howland, D., Kwak, S., Botas, J., Aaronson, J.S., Rosinski, J., Coppola, G., Horvath, S., Yang, X.W., 2016. Integrated genomics and proteomics define huntingtin CAG length-dependent networks in mice. Nat. Neurosci. 19, 623–633. https://doi.org/10.1038/nn.4256.

Le Gras, S., Keime, C., Anthony, A., Lotz, C., De Longprez, L., Brouillet, E., Cassel, J.-C., Boutillier, A.-L., Merienne, K., 2017. Altered enhancer transcription underlies Huntington's disease striatal transcriptional signature. Sci. Rep. 7, 42875. https://doi.org/10.1038/srep42875.

Lee, J., Hwang, Y.J., Kim, Y., Lee, M.Y., Hyeon, S.J., Lee, S., Kim, D.H., Jang, S.J., Im, H., Min, S.-J., Choo, H., Pae, A.N., Kim, D.J., Cho, K.S., Kowall, N.W., Ryu, H., 2017. Remodeling of heterochromatin structure slows neuropathological progression and prolongs survival in an animal model of Huntington's disease. Acta Neuropathol. 134, 729–748. https://doi.org/10.1007/s00401-017-1732-8.

Li, P., Marshall, L., Oh, G., Jakubowski, J.L., Groot, D., He, Y., Wang, T., Petronis, A., Labrie, V., 2019. Epigenetic dysregulation of enhancers in neurons is associated with Alzheimer's disease pathology and cognitive symptoms. Nat. Commun. 10, 2246. https://doi.org/10.1038/s41467-019-10101-7.

Lister, R., Mukamel, E.A., Nery, J.R., Urich, M., Puddifoot, C.A., Johnson, N.D., Lucero, J., Huang, Y., Dwork, A.J., Schultz, M.D., Yu, M., Tonti-Filippini, J., Heyn, H., Hu, S., Wu, J.C., Rao, A., Esteller, M., He, C., Haghighi, F.G., Sejnowski, T. J., Behrens, M.M., Ecker, J.R., 2013. Global epigenomic reconfiguration during mammalian brain development. Science 341, 1237905. https://doi.org/10.1126/science.1237905.

Liu, X.S., Jaenisch, R., 2019. Editing the epigenome to tackle brain disorders. Trends Neurosci. 42, 861–870. https://doi.org/10.1016/j.tins.2019.10.003.

López Castel, A., Cleary, J.D., Pearson, C.E., 2010. Repeat instability as the basis for human diseases and as a potential target for therapy. Nat. Rev. Mol. Cell Biol. 11, 165–170. https://doi.org/10.1038/nrm2854.

Lopez-Atalaya, J.P., Barco, A., 2014. Can changes in histone acetylation contribute to memory formation? Trends Genet. 30, 529–539. https://doi.org/10.1016/j.tig.2014.09.003.

Lu, A.T., Narayan, P., Grant, M.J., Langfelder, P., Wang, N., Kwak, S., Wilkinson, H., Chen, R.Z., Chen, J., Simon Bawden, C., Rudiger, S.R., Ciosi, M., Chatzi, A., Maxwell, A., Hore, T.A., Aaronson, J., Rosinski, J., Preiss, A., Vogt, T.F., Coppola, G., Monckton, D., Snell, R.G., William Yang, X., Horvath, S., 2020. DNA methylation study of Huntington's disease and motor progression in patients and in animal models. Nat. Commun. 11, 4529. https://doi.org/10.1038/s41467-020-18255-5.

Lunnon, K., Smith, R., Hannon, E., De Jager, P.L., Srivastava, G., Volta, M., Troakes, C., Al-Sarraj, S., Burrage, J., Macdonald, R., Condliffe, D., Harries, L.W., Katsel, P., Haroutunian, V., Kaminsky, Z., Joachim, C., Powell, J., Lovestone, S., Bennett, D.A., Schalkwyk, L.C., Mill, J., 2014. Methylomic profiling implicates cortical deregulation of ANK1 in Alzheimer's disease. Nat. Neurosci. 17, 1164–1170. https://doi.org/10.1038/nn.3782.

Luthi-Carter, R., Strand, A., Peters, N.L., Solano, S.M., Hollingsworth, Z.R., Menon, A.S., Frey, A.S., Spektor, B.S., Penney, E.B., Schilling, G., Ross, C.A., Borchelt, D.R., Tapscott, S.J., Young, A.B., Cha, J.H., Olson, J.M., 2000. Decreased expression of striatal signaling genes in a mouse model of Huntington's disease. Hum. Mol. Genet. 9, 1259–1271. https://doi.org/10.1093/hmg/9.9.1259.

Malik, A.N., Vierbuche, T., Hember, M., Rubin, A.A., Ling, E., Couch, C.H., Stroud, H., Spiegel, I., Farh, K.K.-H., Harmin, D.A., Greenberg, M.E., 2014. Genome-wide identification and characterization of functional neuronal activity-dependent enhancers. Nat. Neurosci. 17, 1330–1339. https://doi.org/10.1038/nn.3808.

Mansuroglu, Z., Benhelli-Mokrani, H., Marcato, V., Sultan, A., Violet, M., Chauderlier, A., Delattre, L., Loyens, A., Talahari, S., Bégard, S., Nesslany, F., Colin, M., Souès, S.,

Lefebvre, B., Buée, L., Galas, M.-C., Bonnefoy, E., 2016. Loss of tau protein affects the structure, transcription and repair of neuronal pericentromeric heterochromatin. Sci. Rep. 6, 33047. https://doi.org/10.1038/srep33047.

Marzi, S.J., Leung, S.K., Ribarska, T., Hannon, E., Smith, A.R., Pishva, E., Poschmann, J., Moore, K., Troakes, C., Al-Sarraj, S., Beck, S., Newman, S., Lunnon, K., Schalkwyk, L. C., Mill, J., 2018. A histone acetylome-wide association study of Alzheimer's disease identifies disease-associated H3K27ac differences in the entorhinal cortex. Nat. Neurosci. 21, 1618–1627. https://doi.org/10.1038/s41593-018-0253-7.

Mathys, H., Davila-Velderrain, J., Peng, Z., Gao, F., Mohammadi, S., Young, J.Z., Menon, M., He, L., Abdurrob, F., Jiang, X., Martorell, A.J., Ransohoff, R.M., Hafler, B.P., Bennett, D.A., Kellis, M., Tsai, L.-H., 2019. Author correction: single-cell transcriptomic analysis of Alzheimer's disease. Nature 571, E1. https://doi.org/10.1038/s41586-019-1329-6.

Maurano, M.T., Humbert, R., Rynes, E., Thurman, R.E., Haugen, E., Wang, H., Reynolds, A.P., Sandstrom, R., Qu, H., Brody, J., Shafer, A., Neri, F., Lee, K., Kutyavin, T., Stehling-Sun, S., Johnson, A.K., Canfield, T.K., Giste, E., Diegel, M., Bates, D., Hansen, R.S., Neph, S., Sabo, P.J., Heimfeld, S., Raubitschek, A., Ziegler, S., Cotsapas, C., Sotoodehnia, N., Glass, I., Sunyaev, S.R., Kaul, R., Stamatoyannopoulos, J.A., 2012. Systematic localization of common disease-associated variation in regulatory DNA. Science 337, 1190–1195. https://doi.org/10.1126/science.1222794.

McFarland, K.N., Das, S., Sun, T.T., Leyfer, D., Xia, E., Sangrey, G.R., Kuhn, A., Luthi-Carter, R., Clark, T.W., Sadri-Vakili, G., Cha, J.-H.J., 2012. Genome-wide histone acetylation is altered in a transgenic mouse model of Huntington's disease. PLoS One 7, e41423. https://doi.org/10.1371/journal.pone.0041423.

Mehler, M.F., Petronglo, J.R., Arteaga-Bracho, E.E., Gulinello, M.E., Winchester, M.L., Pichamoorthy, N., Young, S.K., DeJesus, C.D., Ishtiaq, H., Gokhan, S., Molero, A.E., 2019. Loss-of-huntingtin in medial and lateral ganglionic lineages differentially disrupts regional interneuron and projection neuron subtypes and promotes Huntington's disease-associated behavioral, cellular, and pathological hallmarks. J. Neurosci. 39, 1892–1909. https://doi.org/10.1523/JNEUROSCI.2443-18.2018.

Merienne, N., Meunier, C., Schneider, A., Seguin, J., Nair, S.S., Rocher, A.B., Le Gras, S., Keime, C., Faull, R., Pellerin, L., Chatton, J.-Y., Neri, C., Merienne, K., Déglon, N., 2019. Cell-type-specific gene expression profiling in adult mouse brain reveals Normal and disease-state signatures. Cell Rep. 26, 2477–2493 e9. https://doi.org/10.1016/j.celrep.2019.02.003.

Molero, A.E., Gokhan, S., Gonzalez, S., Feig, J.L., Alexandre, L.C., Mehler, M.F., 2009. Impairment of developmental stem cell-mediated striatal neurogenesis and pluripotency genes in a knock-in model of Huntington's disease. Proc. Natl. Acad. Sci. U. S. A. 106, 21900–21905. https://doi.org/10.1073/pnas.0912171106.

Molero, A.E., Arteaga-Bracho, E.E., Chen, C.H., Gulinello, M., Winchester, M.L., Pichamoorthy, N., Gokhan, S., Khodakhah, K., Mehler, M.F., 2016. Selective expression of mutant huntingtin during development recapitulates characteristic features of Huntington's disease. Proc. Natl. Acad. Sci. U. S. A. 113, 5736–5741. https://doi.org/10.1073/pnas.1603871113.

Naia, L., Cunha-Oliveira, T., Rodrigues, J., Rosenstock, T.R., Oliveira, A., Ribeiro, M., Carmo, C., Oliveira-Sousa, S.I., Duarte, A.I., Hayden, M.R., Rego, A.C., 2017. Histone deacetylase inhibitors protect against pyruvate dehydrogenase dysfunction in Huntington's disease. J. Neurosci. 37, 2776–2794. https://doi.org/10.1523/JNEUROSCI.2006-14.2016.

Nativio, R., Donahue, G., Berson, A., Lan, Y., Amlie-Wolf, A., Tuzer, F., Toledo, J.B., Gosai, S.J., Gregory, B.D., Torres, C., Trojanowski, J.Q., Wang, L.-S., Johnson, F.B., Bonini, N.M., Berger, S.L., 2018. Publisher correction: dysregulation of the epigenetic landscape of normal aging in Alzheimer's disease. Nat. Neurosci. 21, 1018. https://doi.org/10.1038/s41593-018-0124-2.

Ng, C.W., Yildirim, F., Yap, Y.S., Dalin, S., Matthews, B.J., Velez, P.J., Labadorf, A., Housman, D.E., Fraenkel, E., 2013. Extensive changes in DNA methylation are associated with expression of mutant huntingtin. Proc. Natl. Acad. Sci. U. S. A. 110, 2354–2359. https://doi.org/10.1073/pnas.1221292110.

Nord, A.S., West, A.E., 2020. Neurobiological functions of transcriptional enhancers. Nat. Neurosci. 23, 5–14. https://doi.org/10.1038/s41593-019-0538-5.

Nott, A., Holtman, I.R., Coufal, N.G., Schlachetzki, J.C.M., Yu, M., Hu, R., Han, C.Z., Pena, M., Xiao, J., Wu, Y., Keulen, Z., Pasillas, M.P., O'Connor, C., Nickl, C.K., Schafer, S.T., Shen, Z., Rissman, R.A., Brewer, J.B., Gosselin, D., Gonda, D.D., Levy, M.L., Rosenfeld, M.G., McVicker, G., Gage, F.H., Ren, B., Glass, C.K., 2019. Brain cell type-specific enhancer-promoter interactome maps and disease-risk association. Science 366, 1134–1139. https://doi.org/10.1126/science.aay0793.

Nucifora, F.C., Sasaki, M., Peters, M.F., Huang, H., Cooper, J.K., Yamada, M., Takahashi, H., Tsuji, S., Troncoso, J., Dawson, V.L., Dawson, T.M., Ross, C.A., 2001. Interference by huntingtin and atrophin-1 with cbp-mediated transcription leading to cellular toxicity. Science 291, 2423–2428. https://doi.org/10.1126/science.1056784.

Rada-Iglesias, A., Bajpai, R., Swigut, T., Brugmann, S.A., Flynn, R.A., Wysocka, J., 2011. A unique chromatin signature uncovers early developmental enhancers in humans. Nature 470, 279–283. https://doi.org/10.1038/nature09692.

Ren, G., Jin, W., Cui, K., Rodrigez, J., Hu, G., Zhang, Z., Larson, D.R., Zhao, K., 2017. CTCF-mediated enhancer-promoter interaction is a critical regulator of cell-to-cell variation of gene expression. Mol. Cell 67, 1049–1058 e6. https://doi.org/10.1016/j.molcel.2017.08.026.

Ring, K.L., An, M.C., Zhang, N., O'Brien, R.N., Ramos, E.M., Gao, F., Atwood, R., Bailus, B.J., Melov, S., Mooney, S.D., Coppola, G., Ellerby, L.M., 2015. Genomic analysis reveals disruption of striatal neuronal development and therapeutic targets in human Huntington's disease neural stem cells. Stem Cell Rep. 5, 1023–1038. https://doi.org/10.1016/j.stemcr.2015.11.005.

Ruzo, A., Croft, G.F., Metzger, J.J., Galgoczi, S., Gerber, L.J., Pellegrini, C., Wang, H., Fenner, M., Tse, S., Marks, A., Nchako, C., Brivanlou, A.H., 2018. Chromosomal instability during neurogenesis in Huntington's disease. Development 145. https://doi.org/10.1242/dev.156844.

Ryu, H., Lee, J., Hagerty, S.W., Soh, B.Y., McAlpin, S.E., Cormier, K.A., Smith, K.M., Ferrante, R.J., 2006. ESET/SETDB1 gene expression and histone H3 (K9) trimethylation in Huntington's disease. Proc. Natl. Acad. Sci. U. S. A. 103, 19176–19181. https://doi.org/10.1073/pnas.0606373103.

Sabari, B.R., Dall'Agnese, A., Boija, A., Klein, I.A., Coffey, E.L., Shrinivas, K., Abraham, B. J., Hannett, N.M., Zamudio, A.V., Manteiga, J.C., Li, C.H., Guo, Y.E., Day, D.S., Schuijers, J., Vasile, E., Malik, S., Hnisz, D., Lee, T.I., Cisse, I.I., Roeder, R.G., Sharp, P.A., Chakraborty, A.K., Young, R.A., 2018. Coactivator condensation at super-enhancers links phase separation and gene control. Science 361. https://doi.org/10.1126/science.aar3958.

Sanchez-Mut, J.V., Heyn, H., Silva, B.A., Dixsaut, L., Garcia-Esparcia, P., Vidal, E., Sayols, S., Glauser, L., Monteagudo-Sánchez, A., Perez-Tur, J., Ferrer, I., Monk, D., Schneider, B., Esteller, M., Gräff, J., 2018. PM20D1 is a quantitative trait locus associated with Alzheimer's disease. Nat. Med. 24, 598–603. https://doi.org/10.1038/s41591-018-0013-y.

Saudou, F., Humbert, S., 2016. The biology of huntingtin. Neuron 89, 910–926. https://doi.org/10.1016/j.neuron.2016.02.003.

Seong, I.S., Woda, J.M., Song, J.-J., Lloret, A., Abeyrathne, P.D., Woo, C.J., Gregory, G., Lee, J.-M., Wheeler, V.C., Walz, T., Kingston, R.E., Gusella, J.F., Conlon, R.A., MacDonald, M.E., 2010. Huntingtin facilitates polycomb repressive complex 2. Hum. Mol. Genet. 19, 573–583. https://doi.org/10.1093/hmg/ddp524.

Schueller, E., Paiva, I., Blanc, F., Wang, X.L., Cassel, J.C., Boutillier, A.L., Bousiges, O., 2020. Dysregulation of histone acetylation pathways in hippocampus and frontal cortex of Alzheimer's disease patients. Eur. Neuropsychopharmacol. 33, 101–116. https://doi.org/10.1016/j.euroneuro.2020.01.015 (Epub 2020 Feb 11.PMID: 32057591).

Seredenina, T., Luthi-Carter, R., 2012. What have we learned from gene expression profiles in Huntington's disease? Neurobiol. Dis. 45, 83–98. https://doi.org/10.1016/j.nbd.2011.07.001.

Serrano-Pozo, A., Frosch, M.P., Masliah, E., Hyman, B.T., 2011. Neuropathological alterations in Alzheimer disease. Cold Spring Harb. Perspect. Med. 1 https://doi.org/10.1101/cshperspect.a006189 a006189.

Siebzehnrubl, F.A., Buslei, R., Eyupoglu, I.Y., Seufert, S., Hahnen, E., Blumcke, I., 2007. Histone deacetylase inhibitors increase neuronal differentiation in adult forebrain precursor cells. Exp. Brain Res. 176, 672–678. https://doi.org/10.1007/s00221-006-0831-x.

Siebzehnrübl, F.A., Raber, K.A., Urbach, Y.K., Schulze-Krebs, A., Canneva, F., Moceri, S., Habermeyer, J., Achoui, D., Gupta, B., Steindler, D.A., Stephan, M., Nguyen, H.P., Bonin, M., Riess, O., Bauer, A., Aigner, L., Couillard-Despres, S., Paucar, M.A., Svenningsson, P., Osmand, A., Andreew, A., Zabel, C., Weiss, A., Kuhn, R., Moussaoui, S., Blockx, I., Van der Linden, A., Cheong, R.Y., Roybon, L., Petersén, Å., von Hörsten, S., 2018. Early postnatal behavioral, cellular, and molecular changes in models of Huntington disease are reversible by HDAC inhibition. Proc. Natl. Acad. Sci. U. S. A. 115, E8765–E8774. https://doi.org/10.1073/pnas.1807962115.

Smith-Geater, C., Hernandez, S.J., Lim, R.G., Adam, M., Wu, J., Stocksdale, J.T., Wassie, B.T., Gold, M.P., Wang, K.Q., Miramontes, R., Kopan, L., Orellana, I., Joy, S., Kemp, P.J., Allen, N.D., Fraenkel, E., Thompson, L.M., 2020. Aberrant development corrected in adult-onset Huntington's disease iPSC-derived neuronal cultures via WNT signaling modulation. Stem Cell Rep. 14, 406–419. https://doi.org/10.1016/j.stemcr.2020.01.015.

Song, W., Zsindely, N., Faragó, A., Marsh, J.L., Bodai, L., 2018. Systematic genetic interaction studies identify histone demethylase Utx as potential target for ameliorating Huntington's disease. Hum. Mol. Genet. 27, 759. https://doi.org/10.1093/hmg/ddy020.

Steffan, J.S., Bodai, L., Pallos, J., Poelman, M., McCampbell, A., Apostol, B.L., Kazantsev, A., Schmidt, E., Zhu, Y.Z., Greenwald, M., Kurokawa, R., Housman, D.E., Jackson, G.R., Marsh, J.L., Thompson, L.M., 2001. Histone deacetylase inhibitors arrest polyglutamine-dependent neurodegeneration in Drosophila. Nature 413, 739–743. https://doi.org/10.1038/35099568.

Suelves, N., Kirkham-McCarthy, L., Lahue, R.S., Ginés, S., 2017. A selective inhibitor of histone deacetylase 3 prevents cognitive deficits and suppresses striatal CAG repeat expansions in Huntington's disease mice. Sci. Rep. 7, 6082. https://doi.org/10.1038/s41598-017-05125-2.

Taberlay, P.C., Kelly, T.K., Liu, C.-C., You, J.S., De Carvalho, D.D., Miranda, T.B., Zhou, X.J., Liang, G., Jones, P.A., 2011. Polycomb-repressed genes have permissive enhancers that initiate reprogramming. Cell 147, 1283–1294. https://doi.org/10.1016/j.cell.2011.10.040.

Tansey, K.E., Cameron, D., Hill, MJ., 2018. Genetic risk for Alzheimer's disease is concentrated in specific macrophage and microglial transcriptional networks. Genome Med. 10 (1), 14. https://doi.org/10.1186/s13073-018-0523-8 (PMID: 29482603).

Thomas, E.A., Coppola, G., Desplats, P.A., Tang, B., Soragni, E., Burnett, R., Gao, F., Fitzgerald, K.M., Borok, J.F., Herman, D., Geschwind, D.H., Gottesfeld, J.M., 2008. The HDAC inhibitor 4b ameliorates the disease phenotype and transcriptional abnormalities in Huntington's disease transgenic mice. Proc. Natl. Acad. Sci. U. S. A. 105, 15564–15569. https://doi.org/10.1073/pnas.0804249105.

Tie, F., Banerjee, R., Saiakhova, A.R., Howard, B., Monteith, K.E., Scacheri, P.C., Cosgrove, M.S., Harte, P.J., 2014. Trithorax monomethylates histone H3K4 and interacts directly with CBP to promote H3K27 acetylation and antagonize Polycomb silencing. Development 141, 1129–1139. https://doi.org/10.1242/dev.102392.

Trojer, P., Reinberg, D., 2007. Facultative heterochromatin: is there a distinctive molecular signature? Mol. Cell 28, 1–13. https://doi.org/10.1016/j.molcel.2007.09.011.

Valor, L.M., Guiretti, D., Lopez-Atalaya, J.P., Barco, A., 2013. Genomic landscape of transcriptional and epigenetic dysregulation in early onset polyglutamine disease. J. Neurosci. 33, 10471–10482. https://doi.org/10.1523/JNEUROSCI.0670-13.2013.

Vashishtha, M., Ng, C.W., Yildirim, F., Gipson, T.A., Kratter, I.H., Bodai, L., Song, W., Lau, A., Labadorf, A., Vogel-Ciernia, A., Troncosco, J., Ross, C.A., Bates, G.P., Krainc, D., Sadri-Vakili, G., Finkbeiner, S., Marsh, J.L., Housman, D.E., Fraenkel, E., Thompson, L.M., 2013. Targeting H3K4 trimethylation in Huntington disease. Proc. Natl. Acad. Sci. U. S. A. 110, E3027–E3036. https://doi.org/10.1073/pnas.1311323110.

Vierbuchen, T., Ling, E., Cowley, C.J., Couch, C.H., Wang, X., Harmin, D.A., Roberts, C. W.M., Greenberg, M.E., 2017. AP-1 transcription factors and the BAF complex mediate signal-dependent enhancer selection. Mol. Cell 68, 1067–1082 e12. https://doi.org/10.1016/j.molcel.2017.11.026.

von Schimmelmann, M., Feinberg, P.A., Sullivan, J.M., Ku, S.M., Badimon, A., Duff, M.K., Wang, Z., Lachmann, A., Dewell, S., Ma'ayan, A., Han, M.-H., Tarakhovsky, A., Schaefer, A., 2016. Polycomb repressive complex 2 (PRC2) silences genes responsible for neurodegeneration. Nat. Neurosci. 19, 1321–1330. https://doi.org/10.1038/nn.4360.

Wang, X., Cairns, M.J., Yan, J., 2019. Super-enhancers in transcriptional regulation and genome organization. Nucleic Acids Res. 47, 11481–11496. https://doi.org/10.1093/nar/gkz1038.

Whyte, W.A., Orlando, D.A., Hnisz, D., Abraham, B.J., Lin, C.Y., Kagey, M.H., Rahl, P.B., Lee, T.I., Young, R.A., 2013. Master transcription factors and mediator establish super-enhancers at key cell identity genes. Cell 153, 307–319. https://doi.org/10.1016/j.cell.2013.03.035.

Yeh, F.L., Hansen, D.V., Sheng, M., 2017. TREM2, microglia, and neurodegenerative diseases. Trends Mol. Med. 23 (6), 512–533. https://doi.org/10.1016/j.molmed.2017.03.008 (Epub 2017 Apr 22.PMID: 28442216 Review).

Yap, E.-L., Greenberg, M.E., 2018. Activity-regulated transcription: bridging the gap between neural activity and behavior. Neuron 100, 330–348. https://doi.org/10.1016/j.neuron.2018.10.013.

Zamudio, A.V., Dall'Agnese, A., Henninger, J.E., Manteiga, J.C., Afeyan, L.K., Hannett, N.M., Coffey, E.L., Li, C.H., Oksuz, O., Sabari, B.R., Boija, A., Klein, I.A., Hawken, S.W., Spille, J.-H., Decker, T.-M., Cisse, I.I., Abraham, B.J., Lee, T.I., Taatjes, D.J., Schuijers, J., Young, R.A., 2019. Mediator condensates localize signaling factors to key cell identity genes. Mol. Cell 76, 753–766 e6. https://doi.org/10.1016/j.molcel.2019.08.016.

Zhang, B., Gaiteri, C., Bodea, L.-G., Wang, Z., McElwee, J., Podtelezhnikov, A.A., Zhang, C., Xie, T., Tran, L., Dobrin, R., Fluder, E., Clurman, B., Melquist, S., Narayanan, M., Suver, C., Shah, H., Mahajan, M., Gillis, T., Mysore, J., MacDonald, M.E., Lamb, J.R., Bennett, D.A., Molony, C., Stone, D.J., Gudnason, V., Myers, A.J., Schadt, E.E., Neumann, H., Zhu, J., Emilsson, V., 2013. Integrated systems approach identifies genetic nodes and networks in late-onset Alzheimer's disease. Cell 153, 707–720. https://doi.org/10.1016/j.cell.2013.03.030.

Publication: 3

“Neuronal and non-neuronal memory-associated epigenomic and transcriptomic signatures are impaired in the striatum of Huntington’s disease mice”

Caroline Lotz, Rafael Alcalá-Vida , Jonathan Seguin, Baptiste Brulé, Ali Awada, Aurélie Bombardier, Brigitte Cosquer, Anne Pereira de Vasconcelos, Anne-Laurence Boutillier, Jean-Christophe Cassel and Karine Merienne

Neuronal and non-neuronal memory-associated epigenomic and transcriptomic signatures are impaired in the striatum of Huntington's disease mice

Caroline Lotz [1,2#], Rafael Alcalá-Vida [1,2#], Jonathan Seguin[1,2], Baptiste Brulé [1,2], Ali Awada [1,2], Aurélie Bombardier [1,2], Brigitte Cosquer [1,2], Anne Pereira de Vasconcelos [1,2], Anne-Laurence Boutillier [1,2], Jean-Christophe Cassel [1,2], Karine Merienne[1,2*]

[1] Laboratoire de Neurosciences Cognitives et Adaptatives (LNCA), University of Strasbourg, Strasbourg 67000, France

[2] CNRS UMR 7364, Strasbourg 67000, France

First co-authors

* Corresponding author

karine.merienne@unistra.fr

LNCA, University of Strasbourg/ CNRS UMR 7364, 12 rue Goethe, 67000 Strasbourg, France

Summary

The relationship between altered epigenetic gene regulation and behavioral deficits in Huntington's disease (HD), a striatal neurodegenerative disease, is unclear. Here, we have developed a new cognitive test to investigate epigenomic and transcriptomic signatures during striatal procedural memory in HD mice. Behavioral, histological, RNAseq and ChIPseq analyses indicate that altered procedural memory in HD mice results from defective neural-activity driven epigenomic and transcriptomic regulations in the striatum, implicating both neuronal and non-neuronal cells. Specifically, transcriptomic changes associated with memory formation and consolidation/recall were impaired in HD mouse striatum, due to reduced induction of synaptic plasticity and extracellular matrix genes. Moreover, we show that H3K9 acetylation is a striatal mnemonic substrate implicated in epigenetic priming of myelin genes during memory consolidation/recall, and this mechanism is impaired in HD mouse striatum. Collectively, our data connecting histone acetylation, transcription and cognition provide insights into the mechanism underlying cognitive deficits in HD.

Introduction

Huntington's disease (HD) is a progressive genetic neurodegenerative disease, which primarily affects the striatum and leads to a triad of motor, cognitive and psychiatric symptoms. Cognitive deficits, which can precede by several years the onset of motor impairments, dramatically affect the quality of life of patients[1–3]. However, since studies historically focused on motor symptoms, the mechanism underlying cognitive alterations in HD remains unclear, and no treatment, whether symptomatic or curative, improves cognition in HD[4,5].

Brain tissues of HD patients and mice display specific transcriptomic and epigenomic signatures[6–15]. Notably, down-regulated genes are enriched in striatal identity genes in the HD striatum, likely due to depletion in RNA polymerase II (RNAPII) and H3K27 acetylation (H3K27ac)[13,16–18]. HD transcriptomic and epigenomic signatures establish early -before the onset of motor symptoms in mice-, are age-dependent and correlate with striatal pathology, suggesting a role for epigenetic and transcriptional regulations in HD pathogenesis, including cognitive deficits[9,13,16].

In support to this hypothesis, dynamic reprogramming of neuronal transcriptome and epigenome, in response to environmental stimuli/experience, drives neuronal plasticity and instructs behavioral changes, including memory processes[19–22]. Moreover, impairment of those regulations was implicated in cognitive deficits in Alzheimer disease[22–26]. In response to neuronal stimulation during memory, calcium-dependent signaling pathways are activated, leading to rapid induction of immediate early genes (IEGs), notably *FOS* and *EGR1*[27,28]. This first response leads to secondary transcriptional waves, targeting cell-type-specific effector genes, promoting neuronal plasticity and memory, though precise temporal dynamics of those transcriptional waves are not fully understood[19,20,29]. Changes in histone acetylation accompany memory-associated transcriptional regulations, creating a permissive transcriptional state for memory-related genes[21,22,25,26,29–33]. However, the nature, timescale and genomic targets of histone acetylation marks involved in memory remain elusive[20,22,29]. Moreover, so far, epigenetic and transcriptional regulations associated with memory were essentially addressed in hippocampal neurons[19,20,27,34]. It remains to be demonstrated whether similar rules govern memory-related epigenetic and transcriptional changes in the striatum. Finally, the contribution of non-neuronal cells to these mechanisms was not investigated.

Here, we have addressed the role of histone acetylation and transcription in HD cognitive deficits, profiling the striatum of HD R6/1 mice by using ChIPseq/RNAseq and IEGs imaging, during striatum-dependent procedural memory. ChIPseq and RNAseq data integration with cell type-specific striatal databases assessed the contribution of neuronal and non-neuronal cells to neural activity-driven epigenomic and transcriptomic signatures in both physiological and HD contexts. Our RNAseq and ChIPseq data generated in resting animals, during early memory formation and during consolidation/recall demonstrate that memory-associated transcriptome and epigenome are impaired

in the striatum of HD R6/1 mice, in both neuronal and non-neuronal cells, which correlates with procedural memory deficits and altered striatal plasticity, as shown by Egr1 imaging. Most remarkably, our data indicate that H3K9ac is a striatal mnemonic substrate implicated in cognitive epigenetic priming of oligodendrocyte myelin genes during memory consolidation/recall, which is impaired in HD R6/1 mice, indicating non-neuronal cells contribute to cognitive deficits in HD.

Results

Striatal procedural memory is early impaired in HD R6/1 mice using the double-H maze task

Deficits in striatum-dependent procedural learning and memory were observed from early stage in HD, while hippocampus-dependent spatial memory remained preserved until late disease stage[35–43]. Thus, to investigate transcriptional and epigenetic regulations during memory process in HD mice, we used cognitive task assessing procedural memory. We developed a new test, using the double-H (DH) maze, an aquatic navigation test initially set up in rats, which allows assessing the interaction between striatum- and hippocampus-dependent memories[44,45]. Early symptomatic HD R6/1 mice of 11 and 14 weeks were trained in this maze, together with control littermates (WT) (supplementary Fig. 1a,b). During an acquisition phase of 4 days, mice were released from the 'south' (S) arm of the maze and had to swim to the 'north-east' (NE) arm to find a hidden platform and escape water (Fig. 1a). Through these successive repetitive trials, mice were expected to shift from early spatial (hippocampal) to late procedural (striatal) searching strategy[44,46]. By the end of training, WT mice (males and females) perfectly learnt the defined motor sequence allowing reaching most efficiently the hidden platform (e.g. turn right then turn left) (Fig. 1b,c and supplementary Fig. 1c,d,e). In contrast, R6/1 mice showed reduced performances, most particularly at 14 weeks, indicating that progressive impairment of memory formation (Fig. 1b,c and supplementary Fig. 1c,d,e,f).

A probe test was performed the 5th day to assess whether procedural and/or spatial memory was retrieved during memory recall. The platform was removed and mice released from the 'South-West' (SW) arm instead of the S arm used during training (Fig. 1a). 80% of WT mice visited first the N arm (e.g. 'procedural' arm), and the time spent in this arm was higher than chance level, indicating that WT mice predominantly initiated procedural strategy during recall (Fig. 1d). The second arm visited by 70% of WT mice (> 80% of mice first visiting the N arm) was the NE arm (e.g. 'spatial' arm), and the time spent in this arm was also higher than chance level, suggesting cognitive flexibility resulting from shifting of procedural to spatial strategy (Fig. 1d). In contrast, R6/1 mice at 11 and 14 weeks predominantly visited the 'spatial' NE arm in first instance (Fig. 1d). As a result, the time spent in the 'procedural' N arm was not different from chance level, indicating that striatal procedural memory was impaired in R6/1 mice (Fig. 1e,f and supplementary Fig. 1g). The time spent in the NE arm

was higher than chance level, suggesting that hippocampal spatial memory remained functional in R6/1 mice (Fig. 1f and supplementary Fig. 1h). These results were comparable between female and male animals (supplementary Fig. 1). The object location and Morris water maze tasks supported that hippocampus-dependent memory was relatively preserved in early symptomatic R6/1 mice (supplementary Fig. 2a,b). Also, motor coordination, as assessed using the bar test, was preserved in 14-week-old R6/1 mice (supplementary Fig. 2c). Thus, DH maze task is a robust and rapid cognitive test showing early impairment of striatal procedural memory in HD R6/1 mice.

Egr1 and Fos neuronal plasticity markers are differently affected in the striatum of HD R6/1 mice

To investigate molecular mechanism underlying impaired procedural memory in R6/1 mice, we assessed striatal and hippocampal protein levels of the IEGs Egr1 and Fos, two major markers of neuronal plasticity and memory. Western-blotting analysis showed that Egr1, which was more abundant in the striatum compared to the hippocampus, was significantly reduced in R6/1 vs WT striatum in basal state, while Fos was expressed at similar levels between both genotypes (Fig. 2a).

Stereological counting was then performed on dorso-median striatum (DMS) and dorso-lateral striatum (DLS) to specify spatio-temporal regulation of Egr1 and Fos in R6/1 mice during procedural memory process. Egr1 and Fos positive cells were counted during memory formation (at day 2 of DH task, DH-2d), during memory consolidation/recall (at day 5 of DH task, DH-5d) and in home-cage controls (HC) (Fig. 2b and supplementary Fig. 3). As expected, Egr1, but not Fos, positive cells were decreased in R6/1 vs WT animals, whatever memory stage (Fig. 2c). Moreover, in WT mice, Egr1 was increased in DMS and DLS at DH-2d and DH-5d, respectively (Fig. 2c), consistent with the implication of DMS in memory formation and DLS in consolidation/recall (Yin HH Costa RM Nat Neuro 2009; Kupferschmidt DA Lovinger DM Neuron 2017). In contrast, Fos was normal in the DMS of R6/1 mice, but was abnormally increased in their DLS, notably during memory formation (Fig. 2c). These alterations were specific to the striatum, since Egr1 and Fos regulations were similar between R6/1 and WT dorsal hippocampus (Fig. 2d). Together, these data indicate that neuronal plasticity during procedural memory is altered in R6/1 striatum, and Egr1 and Fos contribute differentially to the mechanism.

Common and memory-specific signatures characterize striatal transcriptome of HD R6/1 mice in basal and memory conditions

To get further insights into the regulation of plasticity genes, we assessed striatal transcriptome of R6/1 mice during procedural memory, generating RNAseq datasets through memory process (Fig. 3a, supplementary Fig. 4 and supplementary dataset 1). Genotype had a major effect since differentially expressed genes (DEG) in R6/1 vs WT striatum exceeded 2500, in the 3 contexts (HC, dH-2d and DH-

5d) (Fig. 3b). However, increased numbers of DEG were observed in 'memory' vs HC conditions and memory process affected clustering of DEG in WT but not R6/1 samples, which suggested an interaction between genotype and memory factors (Fig. 3b,c). Additionally, DEG between R6/1 and WT samples in HC, DH-2d and DH-5d strongly overlapped, with down- and up-regulated genes showing 64 % and 50% overlap across the 3 conditions, respectively (Fig. 3b). Common DEG genes in HD vs WT contexts displayed signatures that were consistent with previous studies[6,8,9,18,47] (supplementary Fig. 4b). Specifically, genes down in R6/1 vs WT striatum were enriched in gene ontology (GO) terms linked to neuronal function, and included striatal identity genes such as *Drd1, Drd2* and *Darpp32*, while up-regulated genes in R6/1 vs WT samples were enriched in GO terms related to cell adhesion, metabolism and chromatin (Fig. 3d and supplementary Fig. 4b). Specific GO terms were also enriched in each of the 3 conditions. Down-regulated genes in R6/1 vs WT striatum were enriched in biological processes linked to neurotransmission, cell projection and cell adhesion in HC, DH-2d and DH-5d, respectively, while up-regulated genes in R6/1 vs WT mice in memory conditions were more specifically linked to metabolism (Fig. 3e,f). We also generated RNAseq data using the hippocampus of R6/1 and WT mice in HC and DH-5d conditions (supplementary Fig. 5 and supplementary dataset 1). As expected, fewer genes were dysregulated in the hippocampus of R6/1 mice, compared to the striatum, indicating that R6/1 hippocampus was less affected by the HD mutation than the striatum (supplementary Fig. 5a), a result consistent with our behavioral and histological data and with transcriptomic data generated on HD knockin mice[9]. Consistent with neuronal identity signature[9,12,18], striatal and hippocampal down-regulated genes in R6/1 vs WT samples were poorly correlated despite comparable functional signatures (Fig. 3e and supplementary 5c,d). In contrast, up-regulated genes in R6/1 striatum and hippocampus showed greater correlation, supporting common unspecific stress response (Fig. 3e and supplementary Fig. 5c,d). Together, this indicates that the mechanism underlying transcriptional dysregulation in HD striatum and hippocampus is similar in nature but different in amplitude.

Neural-activity driven transcriptomes is impaired in the striatum of HD R6/1 mice

To specify the effect of the HD mutation on the regulation of memory-related genes, we compared DEG in memory vs HC conditions in WT and R6/1 animals (Fig. 4). DEG in WT striatum progressively increased during mnemonic process (Fig. 4a and supplementary dataset 1). Specifically, 152 and 397 genes were up-regulated in DH-2d vs HC samples and in DH-5d vs HC samples, respectively (Fig. 4a). Fewer genes were down-regulated upon memory, since 74 and 102 genes were diminished between DH-2d and HC WT samples and between DH-5d and HC WT samples, respectively (Fig. 4a). DEG in DH-2d vs HC and in DH-5d vs HC comparisons partially overlapped, which allowed defining early, sustained and late memory-associated genes (Fig. 4b,c). We reasoned that these 3 categories might reflect the transition from memory formation to consolidation/recall. Supporting this hypothesis, early and

sustained up-regulated genes were enriched in GO terms linked to cell signaling (e.g. MAPK signaling) and gene regulation, consistent with predominant nuclear response during memory formation. Sustained genes comprised IEGs, including members of Egr and Fos/AP-1 families (Fig. 4c,d and supplementary Fig. 4c,d). Strikingly, late up-regulated genes were enriched in terms related to extracellular matrix (ECM) and included notably several collagen genes, suggesting a role of ECM in memory consolidation (Fig. 4c,d and supplementary Fig. 4c). Transcriptional regulation during procedural memory was dramatically impaired in R6/1 mice (Fig. 4a-c). Noticeably, only 25 and 40 genes were changed in DH-2d vs HC and in DH-5d vs HC R6/1 striatal samples (Fig. 4a). This effect was specific to the striatum, since 24 and 43 genes were differentially expressed in DH-5d vs HC conditions in the hippocampus of WT and R6/1 mice, respectively (supplementary Fig. 5e). Supporting our histological analyses, the induction of *Egr1* during memory formation and consolidation/recall was significantly attenuated in the striatum of R6/1 mice, while that of *Fos* was comparable between R6/1 and WT samples (Fig. 4e). Moreover, promoters of early and sustained up-regulated genes in WT striatum were enriched in Egr1 and AP-1 DNA motifs, whereas promoters of late up-regulated genes were more specifically enriched in motifs recognized by NF-Y, which is implicated in MAPK/JNK-dependent nuclear response promoting axon formation and dendritic growth[48] (Fig. 4f). In R6/1 striatum, the few up-regulated genes were enriched in AP-1 but not Egr1 or NF-Y motifs (Fig. 4f). Together, this suggests that altered induction of memory-related genes in R6/1 mice results from *Egr1* down-regulation. Also, the proportion of late genes vs early and sustained genes was reduced in R6/1 samples compared to WT samples, indicating that transcriptional dysregulation in R6/1 mice in memory formation affects gene regulation in memory consolidation/recall (Fig. 4g). Additionally, integrated analysis of our striatal RNAseq data with cell type-specific striatal database[16] showed that early transcriptional changes in WT samples predominantly involved neuronal-specific genes, while late up-regulated genes comprised both neuronal- and glial-specific genes, suggesting neuronal and non-neuronal cells contribute with different temporal dynamics to striatal plasticity and procedural memory (Fig. 4h). Together, our data show that transcriptional dynamics of neuronal and glial activity-regulated genes during procedural memory formation and consolidation/recall is altered in the striatum of HD R6/1 mice.

H3K9ac, a new histone acetylation mark impaired in HD mouse striatum

We then asked whether altered reprograming of striatal transcriptome during procedural memory in R6/1 mice could correlate with dysregulation of histone acetylation, and therefore generated ChIPseq data using the striatum of 14-week-old R6/1 and WT mice in HC and DH-5d conditions. We targeted H3K27ac and RNAPII, since these marks were found impaired in basal state in HD models[13,16,18,49], as well as H3K9ac, which was not investigated in the context of HD but had been implicated in memory,

though supportive epigenomic data were lacking[20,25]. Our data were of high quality as shown by peak enrichment signal to noise rates, correlation analyses and additional quality analyses (Fig.5a,b, supplementary Fig. 6,7). Regarding H3K27ac, > 7000 genomic regions were differentially enriched in R6/1 vs WT striatal tissues, whatever behavioral context, with depleted regions more prominent than increased regions (supplementary Fig. 8a and supplementary dataset 2). We identified hundreds of differentially enriched regions (DER) comparing R6/1 and WT RNAPII samples, which were essentially depleted, both in HC and DH-5d conditions (supplementary Fig. 8a and supplementary dataset 2). Finally, thousands of regions were differentially enriched in H3K9ac in R6/1 vs WT striata, and they were also predominantly depleted (Fig. 5c and supplementary dataset 2). Remarkably however, in contrast to H3K27ac and RNAPII marks, H3K9ac DER were 3-fold reduced in DH-5d vs HC conditions (Fig. 5c).

H3K9ac, H3K27ac, RNAPII and transcriptional changes in R6/1 vs WT samples were significantly correlated, suggesting causal relationship (Fig.5d and supplementary Fig. 8b,c and 9a,b). However, correlations were greater in HC vs memory contexts (Fig. 5d and supplementary Fig. 8b,9b). Further integration with cell-type-specific enhancer striatal database[13] showed that H3K9ac and H3K27ac deacetylated regions were enriched in neuronal-specific regions in HC and DH-5d mice, whereas hyperacetylated regions were enriched in neuronal- and non-neuronal specific regions (Fig. 5e, supplementary Fig. 10a,b and supplementary dataset 3). Remarkably however, relative contribution of neurons and non-neuronal cells to H3K9ac-increased regions in R6/1 vs WT striatum was modulated by memory: H3K9ac-increased regions in R6/1 striatum were predominantly glial-specific in HC animals and predominantly neuronal-specific in DH-5d animals (Fig. 5e and supplementary Fig. 10a,b). GO analysis supported neuronal origin of depleted regions in H3K9ac, H3K27ac and RNAPII in R6/1 vs WT samples, which displayed strong neuronal signatures, and mixed origin of H3K9ac- and H3K27ac-increased regions, which were enriched in developmental- (e.g. glial) and neuronal-related terms (Fig. 5f and supplementary Fig. 10c). GO analysis also confirmed specific effect of memory on H3K9ac-enriched regions in R6/1 vs WT striatum, which were enriched in distinct terms between HC and DH-5d conditions (Fig. 5f). Notably, H3K9ac-increased regions in R6/1 striatum displayed strong developmental and chromatin-related signatures in HC and DH-5D conditions, respectively (Fig. 5f). Together, our epigenomic data demonstrate that H3K9ac is dysregulated in the striatum of R6/1 mice, and that H3K9ac changes caused by the HD mutation globally correlate with H3K27ac, RNAPII and transcriptional changes, suggesting general alteration of histone acetylome in HD. Also, memory had little effect on H3K27ac regulation in R6/1 striatum, but significant quantitative and qualitative impact on HD H3K9ac signatures, suggesting specific role of H3K9ac during striatal memory.

H3K9ac is a striatal mnemonic substrate whose regulation is impaired in HD R6/1 mouse striatum

To specifically investigate the role of H3K9ac in striatal memory, we compared H3K9ac-enriched regions between HC and DH-5d conditions in WT and R6/1 striatum (Fig. 6a and supplementary dataset2). Same analyses were also performed using H3K27ac and RNAPII ChIPseq datasets (supplementary dataset2). In WT animals, 5022 regions were differentially enriched in H3K9ac in memory vs HC contexts, with 2646 and 2376 regions showing increased and decreased H3K9ac, respectively (Fig. 6a). In contrast, in R6/1 mice, 201 H3K9ac DER were found comparing memory vs HC contexts, with 141 and 60 regions increased and decreased in H3K9ac, respectively (Fig. 6a). Thus, dynamic regulation of H3K9ac during procedural memory was dramatically altered in R6/1 striatum. The effect was specific to H3K9ac, since H3K27ac and RNAPII were not significantly changed between memory and HC contexts, in both genotypes (supplementary dataset2). Remarkably, regions increased in H3K9ac by memory in WT animals showed abnormally elevated basal H3K9ac levels in R6/1 mice and, conversely, regions depleted in H3K9ac during memory process displayed lower basal H3K9ac levels in R6/1 vs WT mice (Fig. 6b). In agreement, H3K9ac changes caused by memory and the HD mutation highly overlapped and were significantly positively correlated (Fig. 6c,d). Collectively, our data indicate that H3K9ac is a striatal mnemonic substrate whose regulation during memory consolidation/recall is altered in R6/1 striatum, likely due to abnormal basal H3K9ac levels at memory-regulated genomic regions.

Epigenetic priming of myelin genes by H3K9ac is impaired in HD R6/1 mouse striatum

GO analysis was then performed to characterize H3K9ac DER during memory. Remarkably, H3K9ac-increased regions by memory in WT samples were most significantly enriched in genes implicated in myelination (Fig. 7a,b). Specifically, oligodendrocyte genes including *Sox10, Olig2, Myrf* and their targets showed increased H3K9ac upon memory (supplementary Fig. 11a and supplementary dataset 2). Those signatures were less significant in R6/1 mice (Fig. 7a and supplementary dataset 2). Moreover, and counter-intuitively, H3K9ac-depleted regions by memory in WT animals displayed neuronal signature, including glutamate receptor and calcium-regulated genes (e.g. *Grin2b, Gria2, Camk2b*…), which was suppressed in R6/1 mice (Fig. 7a, supplementary Fig. 11b and supplementary dataset 2). Furthermore, integrated analysis using cell-type-specific enhancer striatal database[13] showed that, in WT samples, H3K9ac -depleted and -increased regions in DH-5d vs HC contexts were enriched in neuronal- and glial-specific enhancers, respectively (Fig. 7c and supplementary dataset 3). Additional integration using single-cell ATACseq data generated on mouse striatum[50] further showed that memory-associated H3K9ac deacetylation and hyperacetylation affected more specifically accessible chromatin of striatal neurons (e.g. medium spiny neurons, MSN) and oligodendrocytes (Oligos), respectively (Fig. 7d and supplementary dataset 4). Additionally, MSN- and oligodendrocyte-specific H3K9ac-decreased and –increased peaks by memory were enriched in DNA motifs recognized

by ER stress-induced transcription factor Ddit3/CHOP, implicated in neuronal death, and oligodendrocyte lineage master gene Sox10, respectively[51–54] (Fig. 7b). However, genes associated with enriched and depleted H3K9ac upon memory were not impacted at transcriptional level (supplementary Fig. 11c). More generally, Pearson correlation analysis showed that H3K9ac and transcriptomic changes during memory poorly correlated, consistent with previous studies indicating that neural-activity driven epigenetic and transcriptional regulations operate at different timescales[27,34] (Fig. 7e). Collectively, our results indicate that H3K9ac contributes to neuronal and non-neuronal mechanisms during memory consolidation/recall, through epigenetic inhibition of neuronal genes (e.g. glutamate-/calcium-dependent genes implicated in excitotoxicity) and epigenetic priming of glial genes (e.g. myelin genes), respectively. In support to these results, excitotoxicity and myelination were implicated in memory loss and memory consolidation/recall, respectively, though epigenetic-driven mechanisms were not hypothesized[55–61].

Since memory-associated H3K9ac changes at myelin genes were reduced in R6/1 striatum, this suggested a role for oligodendrocytes in memory deficits. To investigate this hypothesis, we assessed oligodendrocyte precursors (OPC) proliferation, treating WT and R6/1 mice with the thymidine analogue 5-Ethylnyl-2'-deoxyuridine (EdU), and traced actively dividing cells during memory process using the DH maze (Fig. 8a,b,c and supplementary Fig. 12). Co-labeling of EdU and Pgdfrα, an OPC-specific marker, showed that memory consolidation/recall led to significant reduction in OPC proliferation in R6/1 vs WT striatum, a result consistent with impaired activity-dependent oligodendrogenesis in R6/1 mice (Fig. 8d and supplementary Fig. 12). Moreover, cells positive for ASPA, a marker of mature oligodendrocytes, were not increased in the striatum of WT mice after memory consolidation/recall (supplementary Fig. 12), indicating that increased H3K9ac at oligodendroctyte myelin genes precedes oligodendrocyte differentiation and myelin production. Thus, this result is consistent with studies showing that those two mechanisms are required for long-term memory consolidation and develop weeks after memory formation[57,59,62]. Collectively, our results highlight a role for H3K9ac in epigenetic priming of myelin genes during procedural memory consolidation/recall, and show that this role is defective in R6/1 striatum. Thus, impairment of epigenetically-driven non-neuronal striatal plasticity likely contributes to HD memory deficit.

Discussion

In this study, we investigated memory-associated epigenomic and transcriptomic signatures in the striatum of HD and control mice. We developed a new cognitive task, using the double-H maze, which showed that striatal procedural memory was early impaired in HD mice, while hippocampal memory remained preserved. Memory deficit in HD mice correlated with altered striatal regulation of neuronal

plasticity markers, notably Egr1, which suggested dysregulation of transcriptional and epigenetic mechanisms induced by memory process. Through generation of RNAseq and ChIPseq data, we established first transcriptomic and epigenomic maps of physiological striatal memory, and showed that these maps were dramatically impaired in HD mice. Remarkably, cell-type-specific analyses revealed that both neuronal and glial cells of the striatum underwent specific histone acetylation and transcriptional changes upon memory, and those changes were strongly attenuated in the two types of cells of the HD mouse striatum. Our data further suggest different temporal dynamics for neuronal and glial regulations during memory, since glial responses were more specifically implicated in late phase of memory process, e.g. consolidation and/or recall. Strikingly, we found that H3K9ac is a striatal mnemonic substrate, playing a specific role in this mechanism through epigenetic priming of myelin genes, which was impaired in HD mouse striatum. Collectively, our data indicate that dysregulation of neural activity-driven epigenomic and transcriptomic signatures is involved in striatal memory deficit in HD mice, through complex interplay between neuronal and glial responses.

Previous transcriptomic and epigenomic studies using brain tissues of HD patients and mice in basal state defined temporal dynamics and cell-type specificity of HD transcriptomic and epigenomic signatures[9,13,14,16,63,64]. Our RNAseq and ChIPseq datasets generated in behaving animals go a step further. Our transcriptomic data generated during memory process in the striatum of WT mice revealed first wave of transcriptional activation enriched in neuronal plasticity genes, including IEGs regulated by transcription factors of the AP-1 and EGR families. This signature was highly similar to that described in hippocampal neurons, following behavioral paradigms such as contextual fear conditioning, novel context exploration or spatial navigation[19,27,28,34]. This suggests that common rules govern transcriptomic regulations during memory formation in the striatum and hippocampus. Transcriptional regulation associated with late phase of physiological striatal memory process revealed a glial signature reflecting ECM-mediated mechanism. Although increasing evidence indicates critical role for non-neuronal plasticity, including a role for ECM and perineuronal nets in fine-tuning neuronal plasticity during memory consolidation[65–67], to the best of our knowledge, this is the first time that transcriptomic data support such a mechanism. To which extent this glial signature is specific to the striatum and/or type of behavior will remain to be investigated in future studies. Importantly, we found that both early and late transcriptional regulations associated with striatal memory process were impaired in the striatum of HD mice, indicating that plasticity mechanisms mediated by neurons and glial cells were both affected.

Earlier studies suggested a major role for histone acetylation in HD. Notably, CBP was found recruited in the aggregates formed by mutant HTT, and H3K27ac, a bona-fide target of CBP, was depleted at neuronal identity genes in HD striatum, suggesting causal relationship between altered CBP activity and decreased H3K27ac in the HD striatum[13,16,18,68–70] Our epigenomic data identified a

new histone acetylation mark -H3K9ac- contributing to impaired acetylome of HD striatum. H3K9ac and H3K27ac were depleted at common genes in HD vs WT striatum, which were enriched in neuronal-specific genes and were transcriptionally down-regulated in the HD background. This suggests that convergent mechanisms leading to histone deacetylation underlie down-regulation of neuronal-specific genes in HD striatum. In contrast, H3K9ac and H3K27ac were increased at more distinct genes, including glial-specific genes, in HD vs WT striatum, suggesting divergent mechanisms modulate H3K9ac and H3K27ac in HD glial cells.

H3K9ac was regulated by memory, in contrast to H3K27ac. However, it remains possible that H3K27ac is implicated in early response associated with memory formation, whereas H3K9ac rather drives late response involved in memory consolidation/recall. Additionally, we cannot exclude that variability between H3K27ac biological replicates masks memory-associated H3K27ac changes. Nonetheless, our results showing reduced H3K9ac changes in HD mouse striatum during memory support a role for H3K9ac in HD cognitive deficits. Additionally, since regions with increased and decreased H3K9ac in memory vs HC samples in WT animals showed increased and decreased H3K9ac in HD vs WT samples in resting animals, respectively, this suggests that memory-related epigenetic program is already induced in basal state in the HD striatum. The significance of this intriguing result is yet unclear and might reflect compensatory or/and aberrant hyper excitability response. Collectively, our results indicate that HD striatal histone acetylome is more broadly affected than anticipated, and it is tempting to speculate that KAT2B/PCAF, which targets H3K9ac[71], is implicated in the mechanism. Addressing this question might open new therapeutic strategies, representing an alternative to HDAC inhibitors, showing partial beneficial effects in HD[68,72–78].

Increasing studies show that activity-dependent oligodendrocyte myelination plays a major role in memory consolidation/recall, facilitating the re-organization and/or stabilization of neuronal networks shaped during memory formation[57–61,79–82]. Our epigenomic data showing that H3K9ac was increased at myelin genes during physiological memory consolidation suggest that these mechanisms are epigenetically driven, at least in the striatum.

ATACseq and HiC analyses were used in previous studies to show changes in chromatin accessibility and spatial organization in stimulated hippocampal neurons following contextual fear conditioning (CFC) or novel context exploration[27,34]. These chromatin-associated changes preceded transcriptional response, hence epigenomic and transcriptomic regulations poorly correlated, which is in line with our observations. In fact, different timescales between epigenetic and transcriptional regulations support the concept of epigenetic priming earlier theorized [20,22,25]. However, ATACseq and HiC experiments did not allow identifying the nature of mnemonic substrates underlying such a mechanism. Our data showing that H3K9ac is enriched at myelin genes during memory consolidation/recall, at a time where these genes are not induced and oligodendrogenesis is not

increased, indicate that H3K9ac is a critical mnemonic substrate of oligodendrocyte response. Finally, given that oligodendrocytes can produce ECM and oligodendrogenesis is regulated by ECM-mediated microenvironment stiffness[83,84], it is likely that the transcriptomic and epigenomic signatures we observed during physiological striatal memory consolidation/recall reflect coordinated response.

Since increased H3K9ac at myelin genes during memory was strongly attenuated in HD mouse striatum, activity-dependent myelination might be impaired in HD. This hypothesis is consistent with recent studies, showing early structural impairment of myelin in HD patients and mouse models, resulting from reduced expression of myelin-related genes, including Myrf and Myrf-dependent genes, which is in agreement with our transcriptomic data[85–88]. Moreover, specific expression of mutant Htt in mouse oligodendrocytes was sufficient to induce progressive neurological symptoms, age-dependent demyelination and reduced expression of myelin genes, further supporting specific role of oligodendrocytes in HD pathogenesis[86]. Thus, we propose that H3K9ac plays a critical role in altered neural plasticity, myelination and cognition in HD.

Materials and Methods

Animals. Heterozygous R6/1 mice were maintained on C57BL/6J genetic background. All animal studies were conducted in accordance with French regulations (EU Directive 2010/63/UE –French Act Rural Code R 214-87 to 126). The animal facility was approved by veterinary inspectors (authorization no. E6748213) and complies with the Standards for Human Care and Use of Laboratory Animals of the Office of Laboratory Animal Welfare. All procedures were approved by local ethics committee (CREMEAS) and French Research Ministry (no. APAFIS#504-2015042011568820v5 and APAFIS#10529-2017070614283086). Mice were housed in a controlled-temperature room maintained on a 12h light/dark cycle. Food and water were available *ad libitum*. For molecular analyses (RNAseq, ChIPseq, 4Cseq), mice were killed by cervical dislocation and their striata were rapidly dissected, snap frozen and stored at -80°C. Genotyping was performed by PCR, using tail DNA obtained from 10-15 day-old R6/1 mice with primers amplifying the CAG repeat region within the exon 1 of the human Huntingtin gene.

Behavioral tests. R6/1 and WT mice were subject to a battery of behavioral tests using the following sequence: the bar test was performed first, then the accelerating rotarod and the double-H maze test, using a protocol that assesses procedural vs spatial memories. Generally, behavioral experiments were performed using at least 8-10 animals per group, and both male and female animals were tested when possible. Also, behavioral tests were performed during the light phase.

Double-H maze. The double-H maze is a navigation test comprising 6 arms linked through a central corridor (north N, south S, north-east NE, south-east SE, north-west NW, south-west SW) filled with

opacified water (21°C). The test was initially developed for rats[44,45]. We adapted the test to mice to assess procedural memory of R6/1 mice. Here, we used WT and R6/1 mice of 11 and 14 weeks (11 weeks: WT n= 27 (17 males, 10 females); R6/1 n= 23 (13 males, 10 females); 14 weeks: WT n= 28 (17 males, 11 females); R6/1 n= 23 (13 males, 10 females)). Mice were first habituated to the task (i.e. to escape water, reaching a platform). To this end, they were trained to reach a visible platform in the NW arm, a guillotine door blocking the access to the other arms (1 session of 4 trials of 1 min were performed). Second, during an acquisition phase lasting 4 consecutive days (1 to 2 sessions of 4 trials of 1 min each day were performed), mice, always released from the S arm, had to find a hidden platform located in the NE arm. The N arm was closed by a transparent guillotine door. To learn how to locate the platform, mice had the possibility to develop a procedural strategy (involving the striatum), using across trials an invariable motor sequence (to turn right, then to turn left). They also had the possibility to develop a spatial strategy (involving the hippocampus) to locate the platform, using spatial cues that were present in the test room. The distance to reach the platform and the number of correct response (when mice turn right then left to reach directly the platform) were recorded to assess performance during task acquisition (reflecting learning). The actual learning strategy developed by the mice (procedural or spatial) was then evaluated with a probe test (of 1 min), the day after the last acquisition. To this purpose, the platform was removed, and the starting point was translated in the SW arm. Mice that used a procedural strategy turned right then left and first reached the N arm ("Procedural arm"). Those using a spatial strategy went first to the NE arm ("Spatial arm") (Fig. 1A). The first and second arms visited was recorded, as well as the time spent in "procedural" and "spatial" arms.

Spatial object location task. The spatial object location task was used to assess spatial memory based on the spatial configuration of objects in an environment. These tasks were performed in a square plexiglas open field (52 cm × 52 cm) with black walls (40 cm high) and a white floor divided into 25 equal squares by black lines. A striped card was fixed against a wall. The device was illuminated by an indirect halogen light (open field center, 50 lux), and a radio played a background noise (open field center, 45 ± 5 dB). Object exploration time was recorded and defined as the nose pointing toward the object within 1 cm. Before testing, all mice received a habituation trial of 10 min with two objects placed in the center of the open field, returned to their home cage for 3 hours, and then received another 10 min habituation trial with the same objects. 11 and 14 weeks-old mice (11 weeks: WT n= 11 males, R6/1 n= 11 males; 14 weeks: WT n= 11 males, R6/1 n= 11 males) were tested with a 10 min exploration trial (acquisition) of 3 objects placed in 3 corners of the open field. Mice returned in their home cage for 3 hours and then received a 10 min exploration trial (retention) with a new spatial configuration resulting from the shift of on object from on corner to the opposite corner of the open field. The performance of mice was evaluated with the percentage of exploration of the moved object,

corresponding to the exploration time of the moved object divided by the total exploration time of the 3 objects, and their performances were compared to chance level (33%).

Morris Water maze. Spatial learning and memory were assessed in a Morris water maze, a circular water tank of 120 cm in diameter and filled by opacified fresh water (21°C). Four positions around the edge of the device were arbitrarily designated north (N), south (S), east (E), and west (W); this defined the division of the water maze into 4 quadrants: NE, SE, SW, and NW. An escape platform was submerged 0,5 cm below the water surface and placed at the midpoint of one of the quadrants. Here, we used WT and R6/1 mice of 11 and 14 weeks (11 weeks: WT n= 10 males; R6/1 n= 10 males; 14 weeks: WT n= 9 females; R6/1 n= 9 females). Mice were first habituated to the task (i.e. to escape water, reaching a platform). To this end, they were trained to reach a visible platform in the NW quadrant from the middle of the maze (1 session of 4 trials of 1 min were performed). Second, during an acquisition phase lasting 5 consecutive days (1 to 2 sessions of 4 trials of 1 min each day were performed), mice, randomly released from the N, S, E or W, had to find a hidden platform located in the SW quadrant. The distance to reach the platform was recorded to assess performance during task acquisition (reflecting learning). Spatial memory of mice was then evaluated with a probe test the day after the last acquisition, with a single 1 min trial without platform. The time spent in each quadrant was recorded and compared to chance level (20 s).

Bar test. Motor coordination and balance were assessed using the beam walking assay. 11 weeks-old mice were trained on an elevated narrow beam of 80 cm-long, to reach a safe platform containing their cage (WT n= 10 males; R6/1 n= 13 males). They were first habituated to the beam, and then tested through 4 consecutive trials, each lasting 1 min. The time to cross beam (latency) was assessed.

Accelerating rotarod. The rotarod test was used to assess procedural motor learning. 11 and 14-week-old mice were trained on a rotarod (Bioseb) at 4 rpm for 2 min (11 weeks: WT n= 10 males; R6/1 n= 11 males; 14 weeks: WT n= 11 males; R6/1 n= 11 males). Mice were then tested in 3 consecutive trials with 45 min inter-trial time, in which the speed of the rod increased from 4 to 40 rpm during 5 min. The latency to fall was recorded as a measurement of mice performance. This sequence was repeated on 3 consecutive days and values were averaged across trials from the same day and across all days of training (fall latency).

Immunohistological tissue preparation. Mice were killed by cervical dislocation in basal condition (HC), 1h after the last trial of the second day of training (DH-2d) or 1h after the probe test in the double-H maze (DH-5d). Brains were removed and cut between the two hemispheres. The right hemisphere was fixed in 4% paraformaldehyde during 6h at 4°C and then stored in 20% sucrose in phosphate buffer during 48h before freezing them in isopentane. Floating coronal sections (30 µm) were cut using a cryostat (Microm HM560, Thermo Scientific) in serial sections within a block of tissue extending from

+1.34 to +0.02 from Bregma for the dorsal striatum, and from -1.22 to -2.30 from Bregma for the dorsal hippocampus. Sections were stored at -20°C in tissue cryoprotective solution (30% glycerol, 30% ethyleneglycol, 40% phosphate buffer 0.1M).

Fos and Egr1 immunohistological analysis. Sections were washed in PBS prior to incubation for 20 min in 1% H_2O_2 in PBS to quench endogenous peroxidase activity. Non-specific binding was blocked with a 1h incubation in 5% normal serum with 0.5% Triton X-100 in PBS. Sections were then incubated overnight at RT in primary antibodies against Egr1 (1:500, sc-110, Santa-Cruz Biotechnology) or Fos (1:4000, 226003/3, Synaptic System). Incubation in appropriate biotinylated secondary antibody (IgG Goat anti-Rabbit, 1:500, ZB1007, Vector Laboratories) is then performed for 1h at RT and followed by 45 min incubation in an avidin-biotinylated-peroxyde complex (1:500, Vectastain Avidine-Biotine Complex Kit, PK6100, Vector Laboratories). 3,3'-diaminobenzidine (DAB Peroxydase Substrate Kit, SK4100, Vector Laboratories) was used as the chromagen. The quantitative analyses of Fos- and Egr1-positive nuclei were performed in the dorsal striatum (dorsomedian striatum -DMS-, dorsolateral striatum -DLS-) and dorsal hippocampus (CA1, CA3, dentate gyrus -DG-). Unbiased stereological estimates of volume and neuronal number were obtained using Mercator software (Explora Nova, La Rochelle, France) and a Leica DM5500B light microscope coupled with a MicroFire CDD color camera (Optronics) equipped with a motorized x-y stage control. All stereological measurements were performed with observer being blind to the animals' condition. To obtain unbiased estimates of neuronal numbers, the optical fractionator technique was employed (coefficient of error <0.1). Areas of interest in stained section were first outlined using a 2.5x objective and Egr1- and Fos-positive cells were counted using a 100x (numerical aperture of 1.40) oil-immersion objective. Counting grids were applied appropriate to the structure measured (dorsal striatum: 120 µm x 120 µm; dorsal hippocampus: 30 µm x 30 µm) with optical dissectors (40 µm x 40 µm) and a mean thickness of 14 µm. Guard zones of 1 µm were applied at the top and the bottom of each dissector, with a mean dissector height of 12 µm. The total number of Egr1- and Fos-positive nuclei/mm^3 of cerebral tissue was estimated from 7 or 8 sections per animal (section sampling fraction (ssf) = 1/5 for dorsal striatum and 1/4 for dorsal hippocampus, from the total number of nuclei counted in all optical dissectors).

EdU cell proliferation immunohistological analysis. Tissue immunostaining was performed as previously described[89]. Briefly, mice coronal sections were washed twice with PBS during 5 min and incubated with NH4Cl 50 mM during 30 min to block free fixation-remaining aldehyde groups and reduce aldehyde-induced tissue auto-fluorescence. Brain slices were then permeated during 20 min with a PBS 1× buffer containing 0.5% Triton X-100 and blocked after it for 1 h at room temperature with PBS 1× plus 0.2%, bovine serum albumin, 0.2% lysine, 0.2% glycine, 0.5% Triton X-100 and 5%

normal horse serum. Afterwards, slices were incubated overnight with primary antibodies against neuronal-specific NeuN protein (1:500, Merck Millipore), oligodendrocyte precursor cells' (OPCs) marker PDGFRα[60] and mature myelinating oligodendrocyte's marker aspartoacylase[58] (ASPA) (Merck Millipore) in a buffer containing PBS 1× plus 0.3% Triton X-100 and 0.2% bovine serum albumin. Then, brain sections were washed twice in PBS 1x during 10 min and incubated for 2 h at room temperature in primary antibody buffer with Alexa Fluor 350 donkey anti- guinea pig (1:500), Alexa Fluor 488 donkey anti-mouse IgG or Alexa Fluor 594 donkey anti-rabbit IgG (1:1500, Invitrogen) secondary antibodies. Two additional washes of 10 min each with PBS 1× were done to remove the excess of secondary antibodies. For EdU staining, samples were additionally incubated in PBS 1x plus 0.3% Triton X-100 during 15 minutes and with the AlexaFluor-947 Click-iT detection kit (C10340, Invitrogen) solution for 30 minutes. Before mounting the slices, two additional washes with PBS 1× were performed to remove the excess of Click-iT reaction mix. Afterwards, slices were mounted in glass slides and Mowiol mounting media was used to incorporate glass coverslip. Hamamatsu Nanozoomer Digital Pathology whole slide imaging system (Hamamatsu Photonics) was used for image acquisition of whole brain sections at 40× magnification. For EdU counting, images were first processed with NDP View v2 software (Hamamatsu Photonics) to delimit the striatal region within each brain section and corresponding area (mm^2), and the number of Edu+ nuclei co-stained or not with other cell-type specific markers were manually counted blindly to the experimenter. For total NeuN+, PDGFRα+ or ASPA+ cell counting, images were first processed with Qupath software[90] to delimit the striatal region within each brain section and corresponding area (mm^2) and counted following two different methodologies according to the possible automatization of the process. Nuclear NeuN positive cells were counted using automated approach combining Qupath for striatal region delimitation and ImageJ Stardist[91] plugin for automated cell detection. Due to the impossibility of equally automatize their counting, PDGFRα+ and ASPA+ cells were manually counted blindly by two different experimenters bilaterally in four striatal sections distributed in different anteroposterior coordinates.

Protein expression analyses. Mice were killed by cervical dislocation in basal condition (HC) and their striata were rapidly dissected, snap frozen and stored at -80°C. One striatum per mice was lysed and homogenized in Laemmli buffer (BioRad), containing β-mercaptoethanol (1/40 of the total volume), using a Potter homogenizer followed by a 30 min incubation on ice. Samples were sonicated for 15 sec (Bioblock Scientific Vibra Cell 75041, power 30%), heated 5 min at 100°C, centrifuged (13 000 rpm, 5 min), and supernatant frozen at -20°C. Protein concentration was measured using the Qubit Protein Assay Kit (ThermoFisher). Protein samples were diluted and separated using 4-20% polyacrylamide gels (Criterion 500, BioRad) in TG-SDS buffer (Euromedex). Proteins were blotted onto nitrocellulose

(Midi-Size Nitrocellulose, TransBlot Turbo, BioRad) using the TransBlot Turbo Transfer System (BioRad). Blots were blocked in 5% milk powder and polyclonal antibodies against Egr1 (1:500, sc-110, Santa-Cruz Biotechnology) and Fos (1:2000, 226003/3 Synaptic System) were incubated overnight at 4°C with 3% milk powder in washing buffer (Tris pH 7,4, NaCl 5M, Tween 20%, distillated water). Blots were washed 3 times in washing buffer before secondary antibodies were added (horseradish peroxidase-conjugated whole-goat anti-rabbit IgG, 111035003, Jackson Laboratories). After 1h incubation at room temperature and 3 washing, blots were revealed with ECL (Clarity Western ECL Substrate, BioRad) and exposed with ChemiDoc Touch Imaging System (BioRad). Results were quantified using the ImageLab software (BioRad).

Generation of RNAseq data. For RNA-seq data generation, total RNA was extracted from a single striatum or hippocampus of R6/1 or WT mouse using the RNeasy Plus Kit (Qiagen, #74136) according to manufacturer's instructions. Quality assessment was performed using Bioanalyser eukaryotic total RNA nano series II chip (Agilent, #5067-1511), and all samples achieved RNA integration number (RIN) between 8 and 10. RNAseq libraries were generated from 600 ng of total RNA using TruSeq Stranded mRNA LT Sample Preparation Kit (Illumina), according to manufacturer's instructions. Briefly, following purification with poly-T oligo attached magnetic beads, the mRNA was fragmented using divalent cations at 94°C for 2 minutes. The cleaved RNA fragments were copied into first strand cDNA using reverse transcriptase and random primers. Strand specificity was achieved by replacing dTTP with dUTP during second strand cDNA synthesis using DNA Polymerase I and RNase H. Following addition of a single 'A' base and subsequent ligation of the adapter on double stranded cDNA fragments, the products were purified and enriched with PCR (30 s at 980C; [10 s at 98°C, 30 s at 60°C, 30 s at 72°C] x 12 cycles; 5 min at 72°C) to create the cDNA library. Surplus PCR primers were further removed by purification using AMPure XP beads (Beckman-Coulter) and the final cDNA libraries were checked for quality and quantified using capillary electrophoresis. Libraries were sequenced on Hiseq 4000 sequencer (Illumina) as single-end 50 base reads following Illumina's instructions (IGBMC, Genomeast platform).

RNAseq analysis. RNAseq datasets generated in the striatum and hippocampus of R6/1 mice and WT mice were analyzed as previously described starting from fastq files (Alcala Vida et al. 2021). Tophat2 v2.1.1 associated with bowtie2 was used for reads mapping using mm10 genome assembly[92]. Quantification of gene expression was performed using HTSeq v0.6.1p1, using gene annotations from Ensembl GRCm38 release 87[93]. Read counts were normalized across libraries with the method proposed by Anders and Huber[94]. The method implemented in the DESeq2 Bioconductor package (DESeq2_1.14, R_3.3.2) was used to identify significantly differentially expressed genes between

different mouse genotypes[95]. Resulting p-values were adjusted for multiple testing by using the Benjamini and Hochberg method[96]. Down- and up-regulated genes were defined using adj. p val<0.05 or adj. p val<0.1 and FC< or >1. Top 300-ranked dysregulated genes, based on adj p val, were used in specific analyses. Volcanoplots, z-score heatmaps and GO Clusterprofiler[97] representations were generated using R packages. Motif analysis was performed using RSAT (see motif analysis section below for more details)[98,99]. Cell type-specific striatal RNAseq dataset generated using laser capture microdissected cell populations of WT mouse striatum were analyzed as described[16]. Briefly, the transcriptome of two neuronal populations (i.e. medium spiny neurons (MSNs) expressing D1 receptor (D1 MSNs) and medium spiny neurons expressing D2 receptor (D2 MSNs), corresponding to neuronal populations affected in HD and predominant in the striatum), and two glial cell populations (astrocytes and microglia), was profiled. To simplify the analyses, D1 and D2 MSNs samples were grouped together and compared to glial samples (i.e. astrocytes and microglia). Down- and up-regulated genes in neurons vs glial cells were defined using adj. p val<0.05 and FC< or >1, as described[13,16].

Chromatin Immunoprecipitation and sequencing (ChIPseq). For each ChIP-eq experiment, bulk striatal tissue from four R6/1 or WT animals in basal (home-cage) or learning/memory consolidation (double-H 5 days, DH-5d) conditions was used. Chromatin extracts were divided in four fractions to allow immunoprecipitation of same extract with H3K27ac, H3K9ac and RNAPII antibodies, including Input controls. ChIPseq data were replicated through two independent experiments. Male tissues were used in experiment and female tissues in experiments 2 and. Male and female data of same genotype and age were analysed together to determine differentially enriched regions common to both sexes. ChIPseq was performed as previously described[13] using antibodies to H3K27ac (ab4729, Abcam), H3K29ac (ab4441, Abcam), and RNAPII[100]. Briefly, pooled tissues were cut into small fragments, fixed in 1% formaldehyde and incubated for 15 min at room temperature. Cross-linking was stopped by the addition of glycine to final concentration 0.125 M. Tissue fragments were washed with cold PBS supplemented with protease inhibitors. The tissues were then mechanically homogenized in sonication buffer to obtain a homogeneous solution. Tissue homogenates were sonicated to obtain DNA fragments <500 bp using Covaris Ultrasonicator E220 and centrifuged. The soluble chromatin fraction was pretreated with protein A Agarose/Salmon Sperm DNA (Millipore) for 45 min at 4 °C. Subsequently, samples were incubated overnight at 4 °C with corresponding primary antibodies. Protein A Agarose/Salmon Sperm DNA was then added and the mixture was incubated for 3h at 4 °C in a shaker. Agarose beads were washed, protein–DNA complexes were eluted from the beads and de-crosslinked overnight with RNAse A at 65 °C. Proteins were eliminated by 2 h incubation at 45 °C with Proteinase K, and DNA recovered using Qiagen MiniElute PCR Purification Kit.

ChIPseq library preparation. ChIP samples were purified using Agencourt AMPure XP beads (Beckman Coulter) and quantified with Qubit (Invitrogen). ChIP-seq libraries were prepared from 2 ng of double-stranded purified DNA using the MicroPlex Library Preparation kit v2 (C05010014, Diagenode), according to manufacturer's instructions. Illumina compatible indexes were added through PCR amplification (7 cycles). Amplified libraries were purified and size-selected using Agencourt® AMPure® XP beads (Beckman Coulter) to remove unincorporated primers and other reagents. Prior to analyses, DNA libraries were checked for quality and quantified using a 2100 Bioanalyzer (Agilent). Libraries were sequenced on Illumina Hiseq 4000 sequencer as paired-end or single-end 50 base reads following Illumina's instructions (IGBMC Genomeast platform). Image analysis and base calling were performed using RTA 2.7.3 and bcl2fastq 2.17.1.14. All ChIP samples successfully went through QC using fastqc (https://www.bioinformatics.babraham.ac.uk/projects/fastqc/).

ChIPseq analysis: sequence alignment, peak detection and annotation, differential analysis. Reads were mapped onto Mouse reference assembly GRCm38/mm10 using Bowtie 1.0.0. aligner[101]. Peak detection of H3K27ac, H3K9ac and RNAPII was performed using SICER v1.1[102,103] with the following parameters: window size: 200; e-value: 0.003. Gap size parameters were determined according to the score value estimated by SICER: selected values of gap size are 1000, 600 and 400 and 1400 for H3K27ac, H3K9ac and RNAPII, respectively. Peaks were annotated relative to genomic features using Homer AnnotatePeaks v4.9.1 [104] with annotation from Ensembl v87. Global comparison of samples and clustering analysis were performed using seqMINER v1.2.1[105,106]. As reference coordinates, Refseq genes for Mouse mm10 genome or differentially enriched peaks were used for the genes or peaks analysis, respectively. For the differential enrichment analysis, one reference bed file containing all peaks for a particular marker was created by selecting common region of peaks between replicates and then merging all peaks between different groups of comparison (e.g WT HC, WT DH-5d, R6/1 HC and R6/1 DH-5d). Mapped reads per sample are counted along all peaks within the reference bed file. The intersect, merge and multicov tools available within the BEDtools suite v 2.26[107] were used to select the common region of peaks, to merge them and count the mapped reads. The resulting count table was used for the differential enrichment analysis. The method implemented in the DESeq2 Bioconductor package[95], DESeq2_1.14, R_3.3.2) was used to identify significantly differentially enriched peaks between different mouse genotypes and learning comparisons. This method is based on the statistics described in Anders and Huber[94]. Resulting p-values were adjusted for multiple testing by using the Benjamini and Hochberg method[96]. Enriched and depleted peaks were defined using adjpval<0.05 and FC< or >1, respectively. Striatal neuronal- and glial-specific H3K27ac-enriched regions from previously generated database[13] or top cell-type specific chromatin accessible regions from striatal single-nuclei ATAC-seq database[50] were intersected with H3K9ac regions differentially enriched

in the different experimental conditions for cell type-specific genotype and learning/memory comparisons using bedsect[108]. For statistical analysis of the intersections, we made use of the SuperExacttest R package[109], which calculates Jaccard statistics according to the total number of overlapping regions between datasets

Gene ontology analysis. GO analysis for multiple datasets comparison was performed using ClusterProfiler package from Bioconductor[97]. List of genes for multiple comparisons were provided as input and enriched Biological Processes terms (FDR <0.05) were identified. For graphical simplication, a semantic similarity simplification was applied using GOSemSim function implemented in clusterProfiler, and top 10 more significant enriched terms were plot for each set of genes in the same plot. Significant biological processes were plotted with a dot size proportional to the gene ratio identified for each term and colour scale according to its adj. *P* value. Additionally, GO analysis of individual experimental comparisons was performed using GREAT[110] (FDR<0.05) combined with the semantic simplification of GO terms REVIGO[111].

Correlation analysis. Normalized read values of H3K9ac, H3K27ac or RNAPII peaks annotated to their closer gene were summarize to obtain single value per gene and resulting values were newly normalized using deseq2 as described in ChIP-seq analysis methods section. The log_2(Fold change) values between different sets of data corresponding to the same annotated gene were used to compute Spearman's correlation coefficient using ggpubr R package. Different categories of genes (down-regulated, up-regulated or non-significant) were defined according to the differentially expressed genes (adj. P value < 0.05) list obtained for the concrete comparison in the RNA-seq data generated in this study. Additionally, H3K9ac normalized read values of annotated peaks were used to compute Spearman's correlation coefficient between log_2(Fold change) values of genotype in basal state (R6/1 HC vs WT HC) and physiological learning (WT DH-5d vs WT HC). Different categories of peaks (down, up or non-significant) were defined in this case according to the differentially enriched regions (adj. P value < 0.05) obtained when comparing WT DH-5d with WT HC H3K9ac data.

DNA motif analysis. For RNA-seq data, motif analysis using promoter +/- 150 bp of up-regulated genes corresponding to early, sustained or late categories previously defined in RNA-seq analysis methods section was performed using RSAT[98,99]. Heatmaps showing e-value of over-represented motifs were generated for comparison across different categories. For ChIP-seq data, H3K9ac differentially enriched regions between WT DH-5d and WT HC conditions intersecting with top oligodendrocyte- or MSN-specific regions from striatal ATAC-seq data (ref) were used as inputs for RSAT over-representation motif analysis, and top identify motif found in Hocomoco (version 11) human and mouse PWMs database was shown for each category. Network analysis. Network analysis of genes participating in myelination biological process associated to increased H3K9ac regions (adj P value <0.05) between WT DH-5d and WT HC was generated using STRING[112,113].

Statistics. Mice with the same age and sex were randomly allocated to the different experimental groups. Blinding was applied to behavioral experiments. For bar plots, centered regions indicate the mean +/-sem, for boxplots, centered regions indicate the median, box limits, upper and lower quartiles and whiskers, 1.5x interquartile range. All measurements were taken from distinct samples. No data were excluded from analyses. For pairwise comparisons of average, data were tested for normality using the Shapiro's test. Statistical analyses included one-sample or two-tailed unpaired Student's *t* test, one-way analysis of variance and two-ways analysis of variance with repeated measures. In case the samples were significantly non-normal, non-parametric tests, including Kruskal-Wallis, one-sample Wilcoxon and binomial tests were performed. For multiple comparisons, the Tukey test or Dunn test was applied. *P* values <0.05 were considered to be statistically significant, except when otherwise indicated. No statistical method was used to predetermine sample size, but our sample sizes are based on similar, previously established, experimental designs.

References

1. Bates, G. P. *et al.* Huntington disease. *Nat. Rev. Dis. Prim.* **1**, 15005 (2015).
2. Harrington, D. L. *et al.* Cross-sectional and longitudinal multimodal structural imaging in prodromal Huntington's disease. *Mov. Disord.* **31**, 1664–1675 (2016).
3. Lawrence, A. D. *et al.* The relationship between striatal dopamine receptor binding and cognitive performance in Huntington's disease. *Brain* **121 (Pt 7**, 1343–55 (1998).
4. Harris, K. L., Kuan, W.-L., Mason, S. L. & Barker, R. A. Antidopaminergic treatment is

associated with reduced chorea and irritability but impaired cognition in Huntington's disease (Enroll-HD). *J. Neurol. Neurosurg. Psychiatry* **91**, 622–630 (2020).

5. McColgan, P. & Tabrizi, S. J. Huntington's disease: a clinical review. *Eur. J. Neurol.* **25**, 24–34 (2018).

6. Hodges, A. *et al.* Regional and cellular gene expression changes in human Huntington's disease brain. *Hum. Mol. Genet.* **15**, 965–77 (2006).

7. Kuhn, A. *et al.* Mutant huntingtin's effects on striatal gene expression in mice recapitulate changes observed in human Huntington's disease brain and do not differ with mutant huntingtin length or wild-type huntingtin dosage. *Hum. Mol. Genet.* **16**, 1845–61 (2007).

8. Vashishtha, M. *et al.* Targeting H3K4 trimethylation in Huntington disease. *Proc. Natl. Acad. Sci. U. S. A.* **110**, E3027-36 (2013).

9. Langfelder, P. *et al.* Integrated genomics and proteomics define huntingtin CAG length-dependent networks in mice. *Nat. Neurosci.* **19**, 623–33 (2016).

10. Valor, L. M., Guiretti, D., Lopez-Atalaya, J. P. & Barco, A. Genomic landscape of transcriptional and epigenetic dysregulation in early onset polyglutamine disease. *J. Neurosci.* **33**, 10471–82 (2013).

11. Bai, G. *et al.* Epigenetic dysregulation of hairy and enhancer of split 4 (HES4) is associated with striatal degeneration in postmortem Huntington brains. *Hum. Mol. Genet.* **24**, 1441–56 (2015).

12. Alcalá-Vida, R. *et al.* Neuron type-specific increase in lamin B1 contributes to nuclear dysfunction in Huntington's disease. *EMBO Mol. Med.* e12105 (2020) doi:10.15252/emmm.202012105.

13. Alcalá-Vida, R. *et al.* Age-related and disease locus-specific mechanisms contribute to early remodelling of chromatin structure in Huntington's disease mice. *Nat. Commun.* **12**, 364 (2021).

14. Lee, H. *et al.* Cell Type-Specific Transcriptomics Reveals that Mutant Huntingtin Leads to Mitochondrial RNA Release and Neuronal Innate Immune Activation. *Neuron* **107**, 891–908.e8 (2020).

15. Horvath, S. *et al.* Huntington's disease accelerates epigenetic aging of human brain and disrupts DNA methylation levels. *Aging (Albany. NY).* **8**, 1485–512 (2016).

16. Merienne, N. *et al.* Cell-Type-Specific Gene Expression Profiling in Adult Mouse Brain Reveals Normal and Disease-State Signatures. *Cell Rep.* **26**, 2477–2493.e9 (2019).

17. Le Gras, S. *et al.* Altered enhancer transcription underlies Huntington's disease striatal transcriptional signature. *Sci. Rep.* **7**, 42875 (2017).

18. Achour, M. *et al.* Neuronal identity genes regulated by super-enhancers are preferentially down-regulated in the striatum of Huntington's disease mice. *Hum. Mol. Genet.* **24**, 3481–96 (2015).

19. Yap, E.-L. & Greenberg, M. E. Activity-Regulated Transcription: Bridging the Gap between Neural Activity and Behavior. *Neuron* **100**, 330–348 (2018).

20. Mews, P. *et al.* From Circuits to Chromatin: The Emerging Role of Epigenetics in Mental Health. *J. Neurosci.* **41**, 873–882 (2021).

21. Lopez-Atalaya, J. P. & Barco, A. Can changes in histone acetylation contribute to memory formation? *Trends Genet.* **30**, 529–39 (2014).

22. Burns, A. M. & Gräff, J. Cognitive epigenetic priming: leveraging histone acetylation for memory amelioration. *Curr. Opin. Neurobiol.* **67**, 75–84 (2020).

23. Benito, E. *et al.* HDAC inhibitor-dependent transcriptome and memory reinstatement in cognitive decline models. *J. Clin. Invest.* **125**, 3572–84 (2015).

24. Fischer, A., Sananbenesi, F., Wang, X., Dobbin, M. & Tsai, L.-H. Recovery of learning and memory is associated with chromatin remodelling. *Nature* **447**, 178–82 (2007).

25. Gräff, J. *et al.* Epigenetic priming of memory updating during reconsolidation to attenuate remote fear memories. *Cell* **156**, 261–76 (2014).

26. Chatterjee, S. *et al.* Reinstating plasticity and memory in a tauopathy mouse model with an acetyltransferase activator. *EMBO Mol. Med.* **10**, (2018).

27. Fernandez-Albert, J. *et al.* Immediate and deferred epigenomic signatures of in vivo neuronal activation in mouse hippocampus. *Nat. Neurosci.* **22**, 1718–1730 (2019).

28. Vierbuchen, T. *et al.* AP-1 Transcription Factors and the BAF Complex Mediate Signal-Dependent Enhancer Selection. *Mol. Cell* **68**, 1067–1082.e12 (2017).

29. Campbell, R. R. & Wood, M. A. How the epigenome integrates information and reshapes the synapse. *Nat. Rev. Neurosci.* **20**, 133–147 (2019).

30. Levenson, J. M. *et al.* Regulation of histone acetylation during memory formation in the hippocampus. *J. Biol. Chem.* **279**, 40545–59 (2004).

31. Villain, H., Florian, C. & Roullet, P. HDAC inhibition promotes both initial consolidation and reconsolidation of spatial memory in mice. *Sci. Rep.* **6**, 27015 (2016).

32. Takuma, K. *et al.* Chronic treatment with valproic acid or sodium butyrate attenuates novel object recognition deficits and hippocampal dendritic spine loss in a mouse model of autism. *Pharmacol. Biochem. Behav.* **126**, 43–9 (2014).

33. Halder, R. *et al.* DNA methylation changes in plasticity genes accompany the formation and maintenance of memory. *Nat. Neurosci.* **19**, 102–10 (2016).

34. Marco, A. *et al.* Mapping the epigenomic and transcriptomic interplay during memory formation and recall in the hippocampal engram ensemble. *Nat. Neurosci.* **23**, 1606–1617 (2020).

35. Lawrence, A. D. *et al.* Executive and mnemonic functions in early Huntington's disease. *Brain* **119 (Pt 5**, 1633–45 (1996).

36. Lawrence, A. D. *et al.* Evidence for specific cognitive deficits in preclinical Huntington's disease. *Brain* **121 (Pt 7**, 1329–41 (1998).

37. Heindel, W. C., Butters, N. & Salmon, D. P. Impaired learning of a motor skill in patients with Huntington's disease. *Behav. Neurosci.* **102**, 141–7 (1988).

38. Schmidtke, K., Manner, H., Kaufmann, R. & Schmolck, H. Cognitive procedural learning in patients with fronto-striatal lesions. *Learn. Mem.* **9**, 419–29.

39. Gabrieli, J. D., Stebbins, G. T., Singh, J., Willingham, D. B. & Goetz, C. G. Intact mirror-tracing and impaired rotary-pursuit skill learning in patients with Huntington's disease: evidence for dissociable memory systems in skill learning. *Neuropsychology* **11**, 272–81 (1997).

40. Ciamei, A. & Morton, A. J. Progressive imbalance in the interaction between spatial and procedural memory systems in the R6/2 mouse model of Huntington's disease. *Neurobiol. Learn. Mem.* **92**, 417–28 (2009).

41. Puigdellívol, M. *et al.* A role for Kalirin-7 in corticostriatal synaptic dysfunction in Huntington's disease. *Hum. Mol. Genet.* **24**, 7265–85 (2015).

42. Lione, L. A. *et al.* Selective discrimination learning impairments in mice expressing the human Huntington's disease mutation. *J. Neurosci.* **19**, 10428–37 (1999).

43. Voermans, N. C. *et al.* Interaction between the human hippocampus and the caudate nucleus during route recognition. *Neuron* **43**, 427–35 (2004).

44. Cassel, R., Kelche, C., Lecourtier, L. & Cassel, J.-C. The match/mismatch of visuo-spatial cues between acquisition and retrieval contexts influences the expression of response vs. place memory in rats. *Behav. Brain Res.* **230**, 333–42 (2012).

45. Pol-Bodetto, S. *et al.* The double-H maze test, a novel, simple, water-escape memory task: acquisition, recall of recent and remote memory, and effects of systemic muscarinic or NMDA receptor blockade during training. *Behav. Brain Res.* **218**, 138–51 (2011).

46. Packard, M. G. & McGaugh, J. L. Inactivation of hippocampus or caudate nucleus with lidocaine differentially affects expression of place and response learning. *Neurobiol. Learn. Mem.* **65**, 65–72 (1996).

47. Luthi-Carter, R. *et al.* Dysregulation of gene expression in the R6/2 model of polyglutamine disease: parallel changes in muscle and brain. *Hum. Mol. Genet.* **11**, 1911–26 (2002).

48. Tiwari, V. K. *et al.* A chromatin-modifying function of JNK during stem cell differentiation. *Nat. Genet.* **44**, 94–100 (2011).

49. HD iPSC Consortium. Developmental alterations in Huntington's disease neural cells and pharmacological rescue in cells and mice. *Nat. Neurosci.* **20**, 648–660 (2017).

50. Zhong, J. *et al.* Integrated profiling of single cell epigenomic and transcriptomic landscape of Parkinson's disease mouse brain. *bioRxiv* 2020.02.04.933259 (2020) doi:10.1101/2020.02.04.933259.

51. Silva, R. M. *et al.* CHOP/GADD153 is a mediator of apoptotic death in substantia nigra dopamine neurons in an in vivo neurotoxin model of parkinsonism. *J. Neurochem.* **95**, 974–86 (2005).

52. Aimé, P. *et al.* The drug adaptaquin blocks ATF4/CHOP-dependent pro-death Trib3 induction and protects in cellular and mouse models of Parkinson's disease. *Neurobiol. Dis.* **136**, 104725 (2020).

53. Hu, H., Tian, M., Ding, C. & Yu, S. The C/EBP Homologous Protein (CHOP) Transcription Factor Functions in Endoplasmic Reticulum Stress-Induced Apoptosis and Microbial Infection. *Front. Immunol.* **9**, 3083 (2018).

54. Santos, A. K. *et al.* Decoding cell signalling and regulation of oligodendrocyte differentiation. *Semin. Cell Dev. Biol.* **95**, 54–73 (2019).

55. Mehta, A., Prabhakar, M., Kumar, P., Deshmukh, R. & Sharma, P. L. Excitotoxicity: bridge to various triggers in neurodegenerative disorders. *Eur. J. Pharmacol.* **698**, 6–18 (2013).

56. Armada-Moreira, A. *et al.* Going the Extra (Synaptic) Mile: Excitotoxicity as the Road Toward Neurodegenerative Diseases. *Front. Cell. Neurosci.* **14**, 90 (2020).

57. Xin, W. & Chan, J. R. Myelin plasticity: sculpting circuits in learning and memory. *Nat. Rev. Neurosci.* **21**, 682–694 (2020).

58. Pan, S., Mayoral, S. R., Choi, H. S., Chan, J. R. & Kheirbek, M. A. Preservation of a remote fear memory requires new myelin formation. *Nat. Neurosci.* **23**, 487–499 (2020).

59. Bacmeister, C. M. *et al.* Motor learning promotes remyelination via new and surviving oligodendrocytes. *Nat. Neurosci.* **23**, 819–831 (2020).

60. Steadman, P. E. *et al.* Disruption of Oligodendrogenesis Impairs Memory Consolidation in Adult Mice. *Neuron* **105**, 150–164.e6 (2020).

61. McKenzie, I. A. *et al.* Motor skill learning requires active central myelination. *Science* **346**, 318–22 (2014).

62. Li, W., Ma, L., Yang, G. & Gan, W.-B. REM sleep selectively prunes and maintains new synapses in development and learning. *Nat. Neurosci.* **20**, 427–437 (2017).

63. Bigan, E. *et al.* Genetic cooperativity in multi-layer networks implicates cell survival and senescence in the striatum of Huntington's disease mice synchronous to symptoms. *Bioinformatics* **36**, 186–196 (2020).

64. Miyazaki, H. *et al.* FACS-array-based cell purification yields a specific transcriptome of striatal medium spiny neurons in a murine Huntington disease model. *J. Biol. Chem.* **295**, 9768–9785 (2020).

65. Tsien, R. Y. Very long-term memories may be stored in the pattern of holes in the perineuronal net. *Proc. Natl. Acad. Sci. U. S. A.* **110**, 12456–61 (2013).

66. Nguyen, P. T. *et al.* Microglial Remodeling of the Extracellular Matrix Promotes Synapse Plasticity. *Cell* **182**, 388–403.e15 (2020).

67. Fawcett, J. W., Oohashi, T. & Pizzorusso, T. The roles of perineuronal nets and the perinodal extracellular matrix in neuronal function. *Nat. Rev. Neurosci.* **20**, 451–465 (2019).

68. Butler, R. & Bates, G. P. Histone deacetylase inhibitors as therapeutics for polyglutamine disorders. *Nat. Rev. Neurosci.* **7**, 784–96 (2006).

69. Steffan, J. S. *et al.* Histone deacetylase inhibitors arrest polyglutamine-dependent neurodegeneration in Drosophila. *Nature* **413**, 739–43 (2001).

70. Nucifora, F. C. *et al.* Interference by huntingtin and atrophin-1 with cbp-mediated transcription leading to cellular toxicity. *Science* **291**, 2423–8 (2001).

71. Jin, Q. *et al.* Distinct roles of GCN5/PCAF-mediated H3K9ac and CBP/p300-mediated H3K18/27ac in nuclear receptor transactivation. *EMBO J.* **30**, 249–62 (2011).

72. Hockly, E. *et al.* Suberoylanilide hydroxamic acid, a histone deacetylase inhibitor, ameliorates motor deficits in a mouse model of Huntington's disease. *Proc. Natl. Acad. Sci. U. S. A.* **100**, 2041–6 (2003).

73. Ferrante, R. J. *et al.* Histone deacetylase inhibition by sodium butyrate chemotherapy ameliorates the neurodegenerative phenotype in Huntington's disease mice. *J. Neurosci.* **23**, 9418–27 (2003).

74. Gardian, G. *et al.* Neuroprotective effects of phenylbutyrate in the N171-82Q transgenic mouse model of Huntington's disease. *J. Biol. Chem.* **280**, 556–63 (2005).

75. Thomas, E. A. *et al.* The HDAC inhibitor 4b ameliorates the disease phenotype and transcriptional abnormalities in Huntington's disease transgenic mice. *Proc. Natl. Acad. Sci. U. S. A.* **105**, 15564–9 (2008).

76. Suelves, N., Kirkham-McCarthy, L., Lahue, R. S. & Ginés, S. A selective inhibitor of histone deacetylase 3 prevents cognitive deficits and suppresses striatal CAG repeat expansions in Huntington's disease mice. *Sci. Rep.* **7**, 6082 (2017).

77. Naia, L. *et al.* Histone Deacetylase Inhibitors Protect Against Pyruvate Dehydrogenase Dysfunction in Huntington's Disease. *J. Neurosci.* **37**, 2776–2794 (2017).

78. Siebzehnrübl, F. A. *et al.* Early postnatal behavioral, cellular, and molecular changes in models of Huntington disease are reversible by HDAC inhibition. *Proc. Natl. Acad. Sci. U. S. A.* **115**, E8765–E8774 (2018).

79. Mensch, S. *et al.* Synaptic vesicle release regulates myelin sheath number of individual oligodendrocytes in vivo. *Nat. Neurosci.* **18**, 628–30 (2015).

80. Hines, J. H., Ravanelli, A. M., Schwindt, R., Scott, E. K. & Appel, B. Neuronal activity biases axon selection for myelination in vivo. *Nat. Neurosci.* **18**, 683–9 (2015).

81. Mitew, S. *et al.* Pharmacogenetic stimulation of neuronal activity increases myelination in an axon-specific manner. *Nat. Commun.* **9**, 306 (2018).

82. Xiao, L. *et al.* Rapid production of new oligodendrocytes is required in the earliest stages of motor-skill learning. *Nat. Neurosci.* **19**, 1210–1217 (2016).

83. Segel, M. *et al.* Niche stiffness underlies the ageing of central nervous system progenitor cells. *Nature* **573**, 130–134 (2019).

84. Susuki, K. *et al.* Three mechanisms assemble central nervous system nodes of Ranvier. *Neuron* **78**, 469–82 (2013).

85. Teo, R. T. Y. *et al.* Structural and molecular myelination deficits occur prior to neuronal loss in the YAC128 and BACHD models of Huntington disease. *Hum. Mol. Genet.* **25**, 2621–2632 (2016).

86. Huang, B. *et al.* Mutant huntingtin downregulates myelin regulatory factor-mediated myelin gene expression and affects mature oligodendrocytes. *Neuron* **85**, 1212–26 (2015).

87. Tabrizi, S. J. *et al.* Predictors of phenotypic progression and disease onset in premanifest and early-stage Huntington's disease in the TRACK-HD study: analysis of 36-month observational data. *Lancet. Neurol.* **12**, 637–49 (2013).

88. Wilton, D. K. & Stevens, B. The contribution of glial cells to Huntington's disease pathogenesis. *Neurobiol. Dis.* **143**, 104963 (2020).

89. Rué, L. *et al.* Early down-regulation of PKCδ as a pro-survival mechanism in Huntington's disease. *Neuromolecular Med.* **16**, 25–37 (2014).

90. Bankhead, P. *et al.* QuPath: Open source software for digital pathology image analysis. *Sci. Rep.* **7**, 16878 (2017).

91. Schmidt, U., Weigert, M., Broaddus, C. & Myers, G. Cell Detection with Star-convex Polygons. (2018) doi:10.1007/978-3-030-00934-2_30.

92. Kim, D. *et al.* TopHat2: accurate alignment of transcriptomes in the presence of insertions, deletions and gene fusions. *Genome Biol.* **14**, R36 (2013).

93. Anders, S., Pyl, P. T. & Huber, W. HTSeq--a Python framework to work with high-throughput sequencing data. *Bioinformatics* **31**, 166–9 (2015).

94. Anders, S. & Huber, W. Differential expression analysis for sequence count data. *Genome Biol.* **11**, R106 (2010).

95. Love, M. I., Huber, W. & Anders, S. Moderated estimation of fold change and dispersion for RNA-seq data with DESeq2. *Genome Biol.* **15**, 550 (2014).

96. Benjamini, Y. & Hochberg, Y. Controlling the False Discovery Rate: A Practical and Powerful Approach to Multiple Testing. *J. R. Stat. Soc. Ser. B* **57**, 289–300 (1995).

97. Yu, G., Wang, L.-G., Han, Y. & He, Q.-Y. clusterProfiler: an R package for comparing biological themes among gene clusters. *OMICS* **16**, 284–7 (2012).

98. Nguyen, N. T. T. *et al.* RSAT 2018: regulatory sequence analysis tools 20th anniversary. *Nucleic Acids Res.* **46**, W209–W214 (2018).

99. van Helden, J. Regulatory sequence analysis tools. *Nucleic Acids Res.* **31**, 3593–6 (2003).

100. Besse, S., Vigneron, M., Pichard, E. & Puvion-Dutilleul, F. Synthesis and maturation of viral transcripts in herpes simplex virus type 1 infected HeLa cells: the role of interchromatin granules. *Gene Expr.* **4**, 143–61 (1995).

101. Langmead, B., Trapnell, C., Pop, M. & Salzberg, S. L. Ultrafast and memory-efficient alignment of short DNA sequences to the human genome. *Genome Biol.* **10**, R25

(2009).

102. Zang, C. *et al.* A clustering approach for identification of enriched domains from histone modification ChIP-Seq data. *Bioinformatics* **25**, 1952–8 (2009).

103. Xu, S., Grullon, S., Ge, K. & Peng, W. Spatial clustering for identification of ChIP-enriched regions (SICER) to map regions of histone methylation patterns in embryonic stem cells. *Methods Mol. Biol.* **1150**, 97–111 (2014).

104. Heinz, S. *et al.* Simple combinations of lineage-determining transcription factors prime cis-regulatory elements required for macrophage and B cell identities. *Mol. Cell* **38**, 576–89 (2010).

105. Ye, T., Ravens, S., Krebs, A. R. & Tora, L. Interpreting and visualizing ChIP-seq data with the seqMINER software. *Methods Mol. Biol.* **1150**, 141–52 (2014).

106. Ye, T. *et al.* seqMINER: an integrated ChIP-seq data interpretation platform. *Nucleic Acids Res.* **39**, e35 (2011).

107. Quinlan, A. R. & Hall, I. M. BEDTools: a flexible suite of utilities for comparing genomic features. *Bioinformatics* **26**, 841–2 (2010).

108. Mishra, G. P., Ghosh, A., Jha, A. & Raghav, S. K. BedSect: An Integrated Web Server Application to Perform Intersection, Visualization, and Functional Annotation of Genomic Regions From Multiple Datasets. *Front. Genet.* **11**, 3 (2020).

109. Wang, M., Zhao, Y. & Zhang, B. Efficient Test and Visualization of Multi-Set Intersections. *Sci. Rep.* **5**, 16923 (2015).

110. McLean, C. Y. *et al.* GREAT improves functional interpretation of cis-regulatory regions. *Nat. Biotechnol.* **28**, 495–501 (2010).

111. Supek, F., Bošnjak, M., Škunca, N. & Šmuc, T. REVIGO summarizes and visualizes long lists of gene ontology terms. *PLoS One* **6**, e21800–e21800 (2011).

112. Szklarczyk, D. *et al.* The STRING database in 2017: quality-controlled protein-protein association networks, made broadly accessible. *Nucleic Acids Res.* **45**, D362–D368 (2017).

113. von Mering, C. *et al.* STRING: a database of predicted functional associations between proteins. *Nucleic Acids Res.* **31**, 258–61 (2003).

Figure Legends

Fig. 1. Procedural memory is early impaired in HD R6/1 mice. (a) Scheme representing procedural memory task using the double-H maze. **(b)** left panel, graph showing the curves of tendency of the distance travelled to reach the platform (mean ± sem) in 11 and 14 wk-old WT and R6/1 mice. Two-ways ANOVA with repeated measures, with Tukey post-hoc test. Right panel, Bar graph showing mean distance across the 4 days of training (+/- sem). Kruskal-Wallis test with Dunn post-hoc test, ***p<0,005, R6/1 vs WT. **(c)** left panel, graph showing the curves of tendency of the percentage of correct response (mean ± sem) in 11 and 14 wk-old WT and R6/1 mice. Two-ways ANOVA with repeated measures, with Tukey post-hoc test. Right panel, bar graph showing mean percentage of correct response across the 4 days of training (+/- sem). Kruskal-Wallis test, with Dunn post-hoc test, ***p<0,005, R6/1 vs WT. **(d)** Heatmap showing the mean trajectories of 11 and 14 weeks-old WT and R6/1 mice in the double-H maze during the probe test. **(e)** Bar graphs showing first and second arms visited during the probe test for 11 and 14 wk-old WT and R6/1 mice. Binomial test (Percentage of mice visiting procedural arm vs other arms; Percentage of mice visiting spatial arm vs other arms), *p<0,05, ***p<0,005, R6/1 vs WT. **(f)** Bar graphs showing time spent in the target arms (Procedural –N- and Spatial –NE- arms) (mean ± sem) in 11 and 14 wk-old WT and R6/1 mice during the probe test. Kruskal-Wallis test, with Dunn post-hoc test, *p<0,05, ***p<0,005, R6/1 vs WT. Time spent in the targets arms was compared to chance level (8,5 seconds) using one-sample Wilcoxon test, $$$ p<0,005, WT and R6/1 vs chance level.

Fig. 2. Basal and memory-driven regulations of Egr1 are impaired in HD R6/1 mouse striatum. (a) upper panel, Western-blotting analysis showing Egr1 and Fos proteins in the striatum and hippocampus of 14-wk-old R6/1 and WT mice. Actin was used as a control. Lower panels, bar graphs showing quantifications of Egr1 and Fos proteins (mean ± sem) in the striatum and hippocampus of R6/1 and WT mice. Unpaired t-test, *p<0,05 R6/1 vs WT. **(b)** Scheme showing the different experimental groups selected for histological analyses with respect to memory process. HC, DH-2d and DH-5d correspond to basal, memory formation and memory consolidation/recall stages, respectively. **(c)** graphs showing the curves of tendency of the percentage of Egr1- and Fos-positive cells (mean ± sem) in the DMS and DLS of 14-wk-old WT and R6/1 mice. One-way ANOVA with Tukey post-hoc test. Egr1: *p<0,05 R6/1 DH-2d vs WT DH-2d, **p<0,01 and ***p<0,005 R6/1 DH-5d vs WT DH-5d, $ p<0,05 WT DH-2d vs WT DH-5d, # p<0,05 WT DH-5d vs WT HC. Fos: ***p<0,005 R6/1 DH-2d vs WT DH-2d, ## p<0,01 WT DH-5d vs WT HC, ### p<0,005 WT DH-2d vs WT HC and R6/1 DH-2d vs R6/1 HC, $ p<0,05 WT DH-5d vs WT DH-2d and R6/1 DH-5d vs R6/1 DH-2d. **(d)** graphs showing the curves of tendency of

the percentage of Egr1- and Fos- positive cells (mean ± sem) in the dorsal hippocampus of 14-wk-old R6/1 and WT mice. One-way ANOVA with Tukey post-hoc test, ### p<0,005 WT DH-2d vs WT HC and R6/1 DH-2d vs R6/1 HC, $ p<0,05 R6/1 DH-5d vs R6/1 DH-2d, $$$ p<0,005 WT DH-5d vs WT DH-2d.

Fig. 3. HD transcriptional signatures establish from early symptomatic stage in HD R6/1 mouse striatum. (a) scheme representing the design of transcriptomic experiment. **(b)** upper panel, bar graphs showing the numbers of differentially expressed genes in the striatum of R6/1 vs WT mice, in HC and DH conditions (DH-2d and DH-5d). Fold change (*FC*)<1 and adj. *p* val <0.05. Lower panel, Venn diagrams showing overlapping down- (blue) and up (red) -regulated genes in R6/1 vs WT mice in HC, DH-2d and DH-5d conditions. **(c)** Heatmap of z-score values representing top down- and up-regulated genes in R6/1 HC vs WT HC. **(d)** Bargraphs representing mRNA levels (mean ± sem) of select down- and up-regulated genes in R6/1 vs WT striatal samples. Expression values were computed from RNAseq data. RPK, reads per kilobases. The Benjamini and Hochberg method was used for multiple testing correction. Drd1: *, adj. *p* val = $4x10^{-5}$ R6/1 HC vs WT HC; *, adj. *p* val = $2x10^{-10}$ R6/1 DH-2d vs WT DH-2d; *, adj. *p* val = $3x10^{-10}$ R6/1 DH-5d vs WT DH-5d; Drd2; *, adj. *p* val = $3x10^{-6}$ R6/1 HC vs WT HC; *, adj. *p* val = 10^{-11} R6/1 DH-2d vs WT DH-2d; *, adj. *p* val = $7x10^{-9}$ R6/1 DH-5d vs WT DH-5d; Darpp32: *, adj. *p* val = $4x10^{-6}$ R6/1 HC vs WT HC; *, adj. *p* val = 10^{-11} ; R6/1 DH-2d vs WT DH-2d; *, adj. *p* val = 10^{-5} R6/1 DH-5d vs WT DH-5d; Atp6v1a: *, adj. *p* val = $7x10^{-3}$ R6/1 HC vs WT HC; *, adj. *p* val = $8x10^{-5}$; R6/1 DH-2d vs WT DH-2d; *, adj. *p* val = $2x10^{-2}$ R6/1 DH-5d vs WT DH-5d; Pdchb9: *, adj. *p* val = 10^{-11} R6/1 HC vs WT HC; *, adj. *p* val = $2x10^{-8}$; R6/1 DH-2d vs WT DH-2d; *, adj. *p* val = $2x10^{-9}$ R6/1 DH-5d vs WT DH-5d; Suv39h1: *, adj. *p* val = $2x10^{-3}$ R6/1 HC vs WT HC; *, adj. *p* val = 10^{-4} ; R6/1 DH-2d vs WT DH-2d; *, adj. *p* val = $2x10^{-7}$ R6/1 DH-5d vs WT DH-5d . **(e,f)** gene ontology analysis of genes differentially expressed in R6/1 vs WT striatal samples (adj. *p* val <0.05), in HC, DH-2d and DH-5d conditions. Top significant biological processes are shown using dot size proportional to gene ratio and heatmap reflecting adj. *p* value.

Fig. 4. Memory-regulated transcriptome is impaired in HD R6/1 mouse striatum. **(a)** Bargraph showing the numbers of differentially expressed genes (FDR < 0.1) in DH-2d vs HC and DH-5d vs HC comparisons, in WT and R6/1 striatal samples. **(b)** Venn diagrams showing overlapping down-and up-regulated genes in DH-2d vs HC and DH-5d vs HC comparisons for WT and R6/1 striatal samples. Early, sustained and late genes correspond to genes only changed after 2 days of memory process, genes changed after 2 days and 5 days of memory process and genes changed only after 5 days of memory process, respectively. **(c)** Heatmaps of z-score values representing early-, sustained- and late-dysregulated genes in WT samples. **(d)** Gene ontology analysis of early, sustained and late WT up-regulated genes. Significant biological processes are shown using dot size proportional to gene ratio

and heatmap reflecting adj. pvalue. **(e)** Bargraphs representing mRNA levels (mean ± sem) of Egr1 and Fos in striatal samples. Expression values were computed from RNAseq data. RPK, reads per kilobases. The Benjamini and Hochberg method was used for multiple testing correction. Egr1: adj. p val = 10^{-1} R6/1 HC vs WT HC; *, adj. p val = $2x10^{-6}$ R6/1 DH-2d vs WT DH-2d; *, adj. p val = $2x10^{-6}$ R6/1 DH-5d vs WT DH-5d; $, adj. p val = $9x10^{-10}$ WT DH-2d vs WT HC; $, adj. p val = $2x10^{-4}$ WT DH-5d vs WT HC; *, adj. p val = $8x10^{-2}$ R6/1 DH-2d vs R6/1 HC. **(f)** Heatmap of evalues representing DNA motifs enriched at promoters of early, sustained and late up-regulated genes in WT and R6/1 striatal samples. **(g)** Bargraphs representing the proportion of early, sustained and late up-regulated genes in WT and R6/1 striatal samples. **(h)** Volcano plot representations of differential expression values between glial cells and neurons (Medium Spiny Neurons, MSN) using early and late up-regulated genes in WT striatum. Genes significantly increased and decreased in neurons vs glial cells (FC>1 and adj. p val <0,05) are shown in purple and green, respectively. A binomial test (two-sided) was performed to assess enrichment of memory-related genes in glial-specific genes in early vs late stage, p=10^{-3}.

Fig 5. H3K9ac striatal epigenetic alterations establish early in a cell-type specific manner in HD R6/1 mice. (a) Scheme showing the different ChIP-seq datasets generated using whole striatal tissue from WT and R6/1 mice in basal (home-cage, HC) or in learning (double-H 5 days, DH-5d) conditions. **(b)** UCSC genome browser capture showing representative H3K27ac, H3K9ac and RNAPII signals in the striatum of WT and R6/1 mouse striatum at basal (home-cage, HC) 2 or in learning (double-H 5 days, DH-5d) conditions at *Pde10a* gene locus in the adult striatum. **(c)** Volcano plots representation of H3K9ac differential enriched regions between WT and R6/1 mice striatum at basal (home-cage, HC, left) and learning (double-H 5 days, DH-5d, right) conditions (N=2). Regions with decreased, increased or unchanged H3K9ac levels (adj P value <0.05) in R6/1 mice compared to WT mice are displayed in blue, red and black, respectively. **(d)** Linear regression analysis between transcriptional and H3K9ac changes in the striatum of R6/1 vs WT mice at 14 weeks of age at basal (home-cage, HC, left) and learning (double-H 5 days, DH-5d, right) conditions (N=2). The correlation is shown for all genes (green), genes significantly downregulated (Fold change (FC) <1 and adj. *P* value <0.05; blue), genes significantly upregulated (FC >1 and adj. *P* value <0.05; red) and non-significantly altered genes (grey). Pearson's correlation index and *P* value for fitted linear model are shown. **(e)** Horizontal bargraphs showing cell-type distribution of H3K9ac regions differentially enriched in R6/1 vs WT mouse striatum at basal (home-cage, HC) and learning (double-H 5 days, DH-5d) conditions. Bars corresponding to regions with decreased or increased H3K9ac levels in R6/1 mice compared to WT mice are displayed with blue and red borders, respectively. Non-specific- (non-spec), neuronal- and glial-enriched regions are depicted in grey, purple and green, respectively. **(f)** Gene Ontology analysis of H3K9ac regions differentially enriched (adj. P value <0.05) between R6/1 and WT mouse striatal samples at basal

(home-cage, HC) and learning (double-H 5 days, DH-5d) conditions (*FDR* <0.05). Significant biological processes are shown using dot size proportional to gene ratio and heatmap reflecting adjusted *P* value.

Fig. 6. H3K9ac striatal memory-associated physiological changes correlate with basal alterations in HD R6/1 mice. (a) Volcano plots representation of H3K9ac differential enriched regions in WT (left) and R6/1 (right) mouse striatum between basal (home-cage, HC) and learning (double-H 5 days, DH-5d) conditions (N=2). Regions with decreased, increased or unchanged H3K9ac levels (adj P value <0.05) in DH-5d compared to HC mice are displayed in blue, red and black, respectively. **(b)** Metaprofiles showing H3K9ac signal in WT and R6/1 mouse striatum at basal (home-cage, HC) and learning (double-H 5 days, DH-5d) conditions (N=2), considering differentially enriched peaks between HC and DH-5d WT mice ChIP-seq data. **(c)** Venn Diagram showing the overlap between H3K9ac decreased (left) and increased (right) regions changing between R6/1 HC vs. WT HC (yellow), R6/1 DH-5d vs. WT DH-5d (orange) and WT DH-5d vs. WT HC (blue). **(d)** Linear regression analysis of H3K9ac changes in the striatum of R6/1 vs WT mice at basal (home-cage, HC) conditions and in WT DH-5d vs. WT HC conditions (N=2). The correlation is shown for all identified regions (green), regions with significantly decreased H3K9ac levels (Fold change (FC) <1 and adj. *P* value <0.05; blue), regions with significantly increased H3K9ac levels (Fold change (FC) <1 and adj. *P* value <0.05; blue) and non-significantly altered genes (grey) when comparing WT DH-5d vs. WT HC ChIP-seq data. Pearson's correlation index and *P* value for fitted linear model are shown.

Fig.7. H3K9ac is a mnemonic substrate of striatal memory which is early impaired in HD R6/1 mice. (a) Gene Ontology analysis of regions showing decreased (down, left) or increased (up, right) H3K9ac levels between basal (home-cage, HC) and learning/memory (double-H 5d, DH-5d) conditions (FDR<0.05) for WT (grey) or R6/1 (white) mouse striatum ChIP-seq data. **(b)** UCSC genome browser capture showing representative H3K27ac, H3K9ac and RNAPII signals in the striatum of WT and R6/1 mouse striatum at basal (home-cage, HC) or in learning (double-H 5 days, DH-5d) conditions at neuronal-specific *Grin2b* and myelination-related *Myrf* gene locus in the adult striatum. **(c)** Circular plot illustrating all possible intersections between different sets of genomic regions and the corresponding statistics. The five tracks in the middle represent the five genomic regions sets (H3K9ac WT-modified, H3K9ac R6/1-modified, H3K27ac glial-specific, H3K27ac neuronal-specific and H3K27ac non-specific regions), with individual blocks for each colour indicating the presence or absence of the genomic regions sets in the particular intersection. The height of the bars in the external layer is proportional to the intersection sizes (number of intersecting regions indicated by the numbers on the top of the bars) and the color intensity of the bars represents the P value significance of the intersections. **(d)** Radar plot showing the cell-type specific distribution of H3K9ac regions significantly

(adj. P value <0.05) decreased (DOWN, blue) or increased (UP, red) in WT mice striatum between basal basal (home-cage, HC) and learning/memory (double-H 5d, DH-5d) conditions when intersected with top cell-specific striatal chromatin accessible regions from single nuclei ATAC-seq data (ref biorxiv). Values represent the percentage from total number of intersecting regions per category (DOWN or UP). **(e)** Linear regression analysis between transcriptional and H3K9ac changes in the striatum of WT mice between basal (home-cage, HC, left) and learning (double-H 5 days, DH-5d, right) conditions (N=2). The correlation is shown for all genes (green), genes significantly downregulated (Fold change (FC) <1 and adj. *P* value <0.05; blue), genes significantly upregulated (FC >1 and adj. *P* value <0.05; red) and non-significantly altered genes (grey) between WT DH-5d and WT HC mice striatum. Pearson's correlation index and *P* value for fitted linear model are shown.

Fig. 8. Oligodendrocyte precursor cells (OPCs) proliferation is impaired in HD R6/1 mice during procedural memory. (a) Schematic representation of the protocol used to assess OPCs proliferation in response to procedural memory in the double-H maze. **(b)** Representative striatal images showing the staining patterns of the OPC marker PDGFRα (red), the mature myelinating oligodendrocyte marker aspartoacylase (ASPA, green), the neuronal nuclear marker NeuN (blue) and the proliferating cells labelled by EdU (grey). Images were acquired at 10x (left) or 40x (right) magnifications. Yellow arrows indicate EdU positive cells co-immunostained with the OPC marker PDGFRα. Scale bars of 200 and 50 µm are shown for low and high magnification, respectively. **(c)** Representative striatal images showing the staining patterns of the OPC marker PDGFRα (red) and the proliferating cells labelled by EdU (grey) in WT and R6/1 mice at basal (home-cage, HC) or in learning (double-H 5 days, DH-5d) conditions. Images were acquired at 10x or 40x (internal images) magnifications. Scale bars of 250 and 100 µm are shown for low and high magnification, respectively. **(d)** Bargraphs showing the number of Edu+/ PDGFRα cells per mm^2 as a mean ± sem in WT (blue) and R6/1 (orange) mice striatum at basal (home-cage, HC) or in learning (double-H 5 days, DH-5d) conditions (WT HC N=4, WT DH-5d N=4, R6/1 HC N=3, R6/1 DH-5d N=4). Individual values are depicted as circles. Data were analysed using two-way Anova; multiple comparisons used the Bonferroni's post-hoc test: $ *P*<0.05, R6/1 DH-5d vs R6/1 HC comparison.

Fig. 1

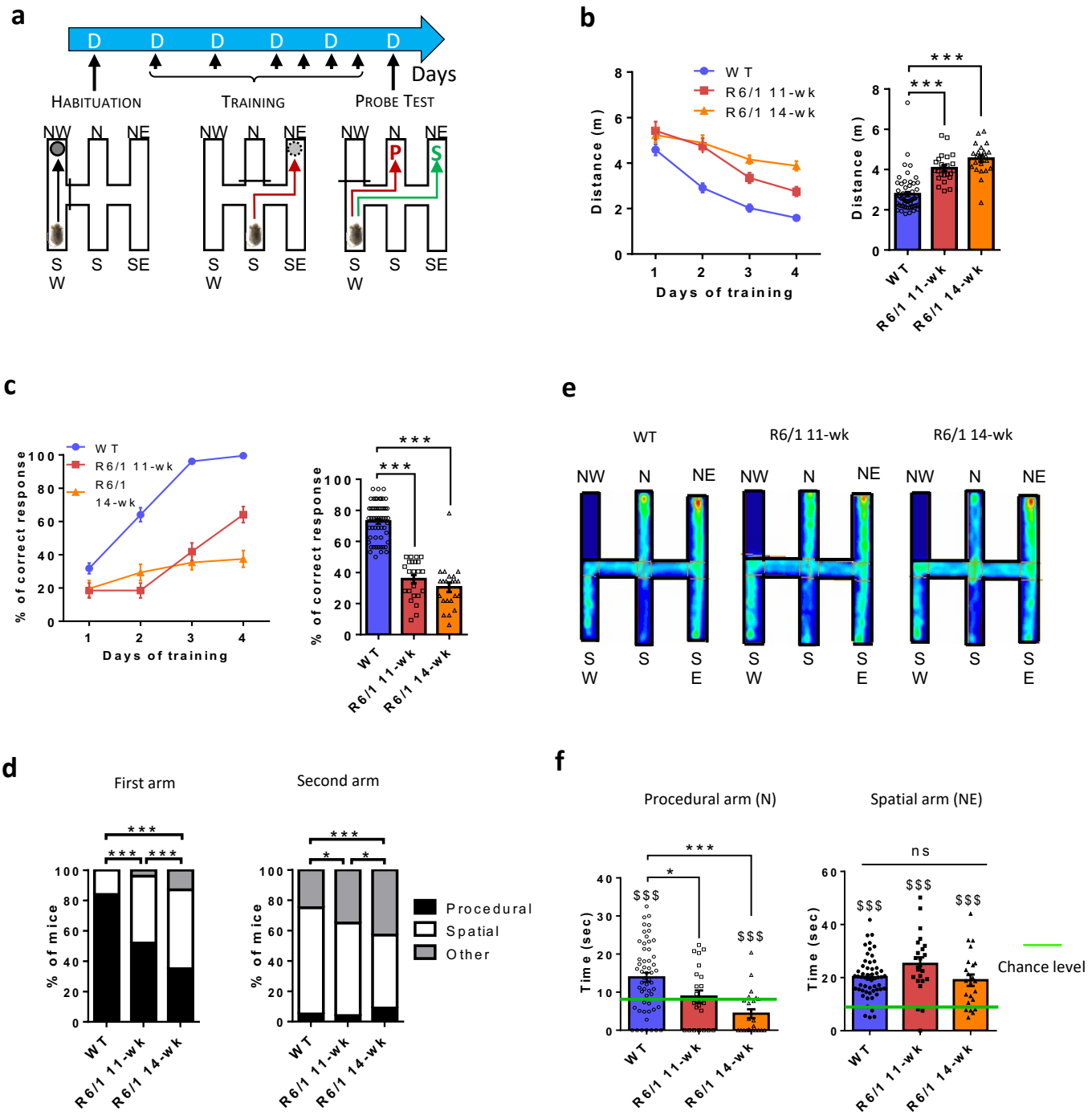
a
D
Days
HABITUATION
TRAINING
PROBE TEST
NW N NE
S W
S
SE
P
S
b
WT
R6/1 11-wk
R6/1 14-wk
Distance (m)
Days of training
***
c
% of correct response
Days of training
d
First arm
Second arm
% of mice
Procedural
Spatial
Other
e
WT
R6/1 11-wk
R6/1 14-wk
f
Procedural arm (N)
Spatial arm (NE)
Time (sec)
ns
$$$
Chance level

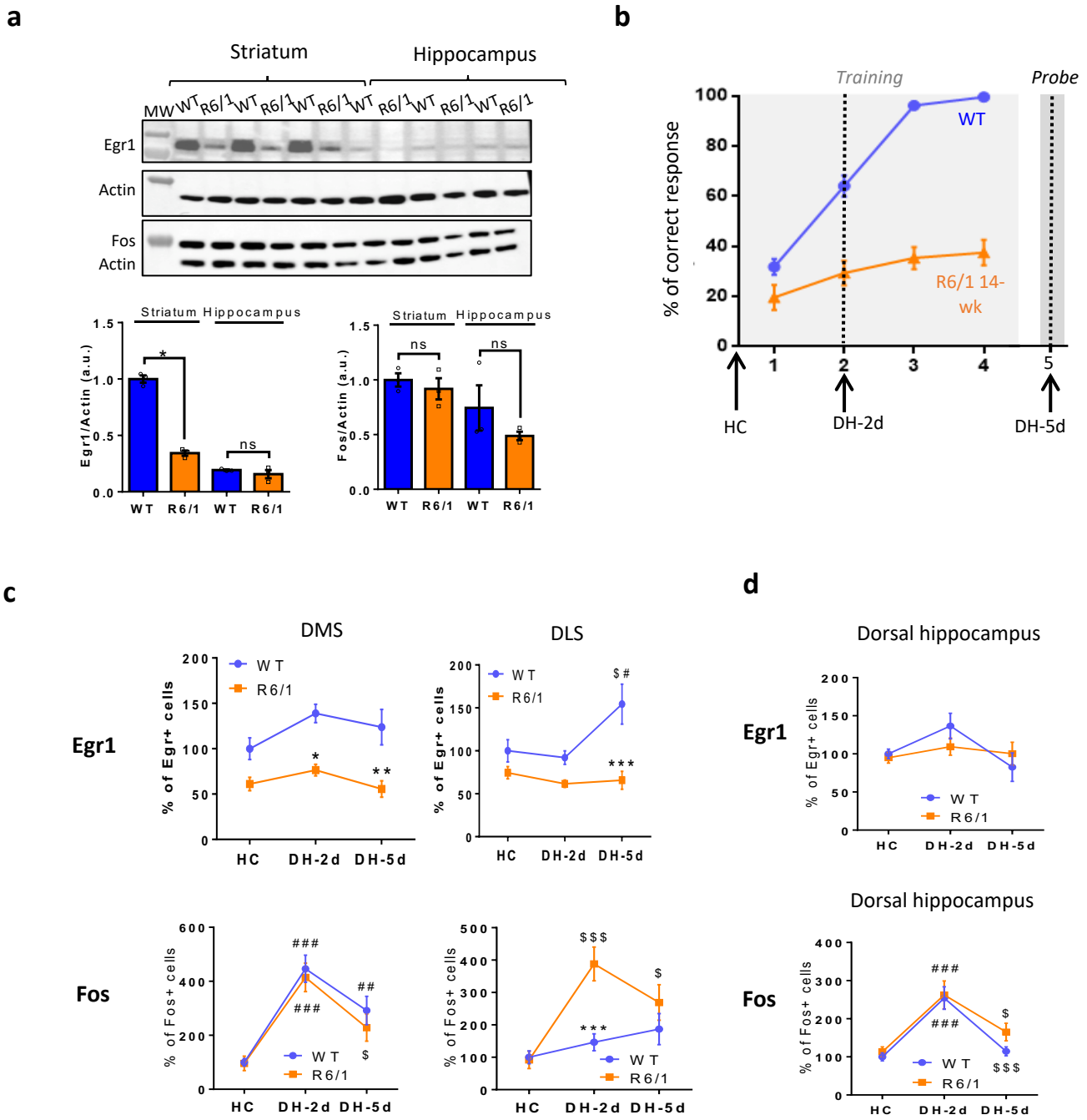
a
Striatum
Hippocampus
MW WT R6/1 WT R6/1 WT R6/1 WT R6/1 WT R6/1 WT R6/1
Egr1
Actin
Fos
Actin
Striatum Hippocampus
Egr1/Actin (a.u.)
Fos/Actin (a.u.)
WT R6/1 WT R6/1
b
Training
Probe
% of correct response
WT
R6/1 14-wk
HC
DH-2d
DH-5d
c
DMS
DLS
Egr1
Fos
% of Egr+ cells
% of Fos+ cells
WT
R6/1
HC DH-2d DH-5d
d
Dorsal hippocampus
Egr1
Fos

Fig. 3

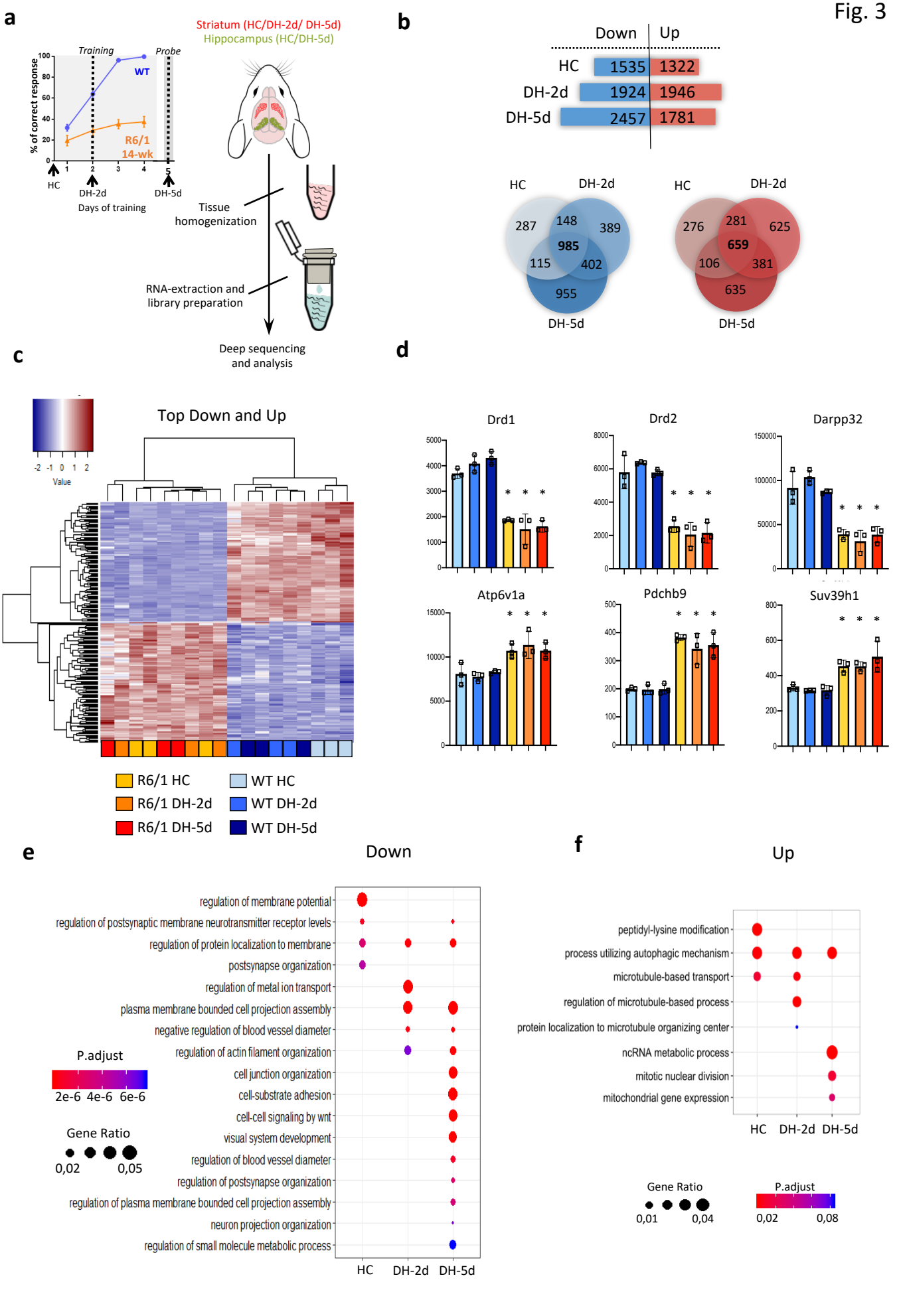
a
Striatum (HC/DH-2d/ DH-5d)
Hippocampus (HC/DH-5d)
Training
Probe
% of correct response
WT
R6/1
14-wk
HC
DH-2d
DH-5d
Days of training
Tissue homogenization
RNA-extraction and library preparation
Deep sequencing and analysis
b
Down
Up
HC 1535 1322
DH-2d 1924 1946
DH-5d 2457 1781
HC
DH-2d
DH-5d
287
148
389
985
115
402
955
276
281
625
659
106
381
635
c
Top Down and Up
Value
R6/1 HC
R6/1 DH-2d
R6/1 DH-5d
WT HC
WT DH-2d
WT DH-5d
d
Drd1
Drd2
Darpp32
Atp6v1a
Pdchb9
Suv39h1
e
Down
regulation of membrane potential
regulation of postsynaptic membrane neurotransmitter receptor levels
regulation of protein localization to membrane
postsynapse organization
regulation of metal ion transport
plasma membrane bounded cell projection assembly
negative regulation of blood vessel diameter
regulation of actin filament organization
cell junction organization
cell-substrate adhesion
cell-cell signaling by wnt
visual system development
regulation of blood vessel diameter
regulation of postsynapse organization
regulation of plasma membrane bounded cell projection assembly
neuron projection organization
regulation of small molecule metabolic process
P.adjust
2e-6 4e-6 6e-6
Gene Ratio
0,02 0,05
HC DH-2d DH-5d
f
Up
peptidyl-lysine modification
process utilizing autophagic mechanism
microtubule-based transport
regulation of microtubule-based process
protein localization to microtubule organizing center
ncRNA metabolic process
mitotic nuclear division
mitochondrial gene expression
HC DH-2d DH-5d
Gene Ratio
0,01 0,04
P.adjust
0,02 0,08

Fig. 4

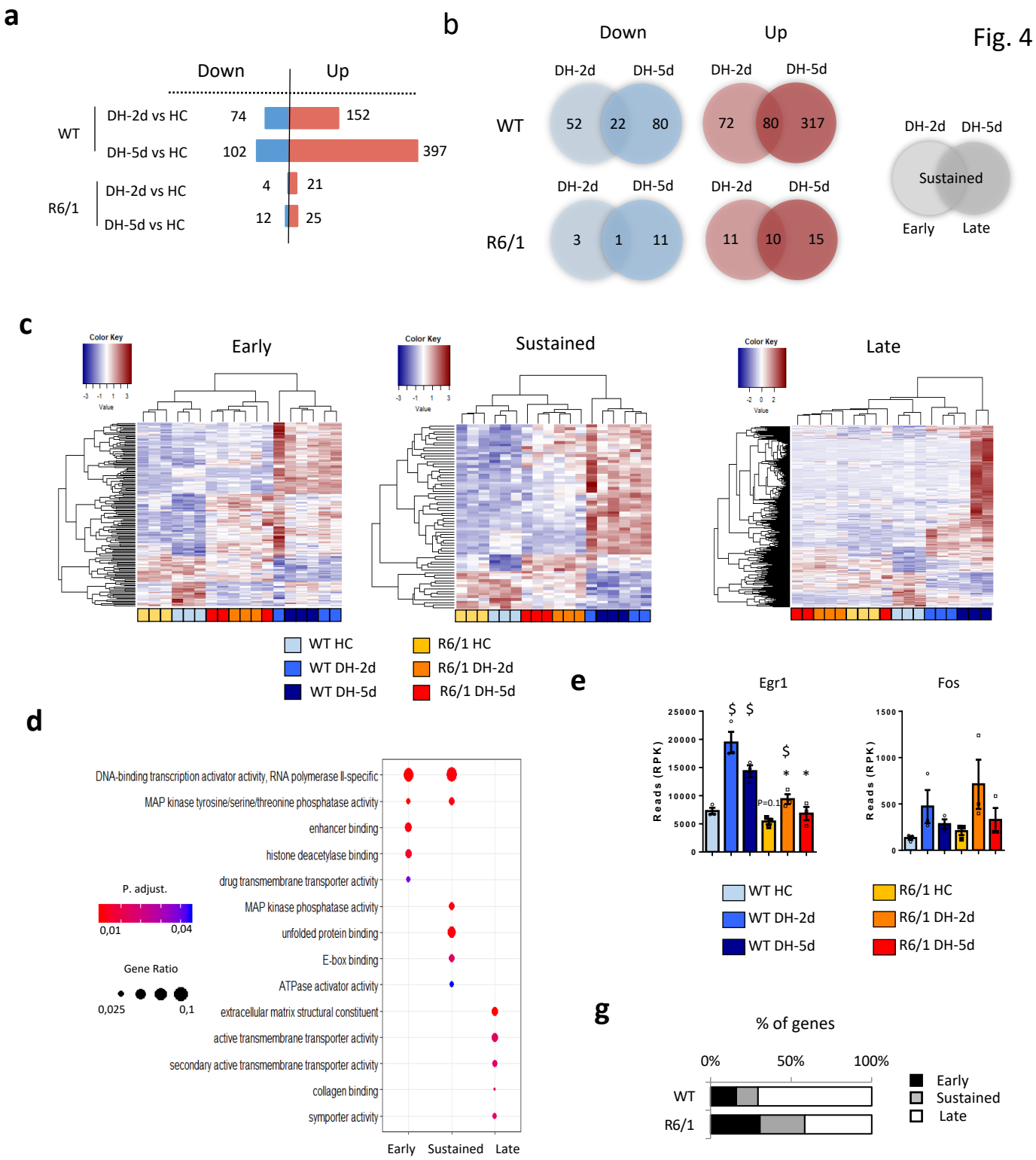
a
Down
Up
WT
DH-2d vs HC
74
152
DH-5d vs HC
102
397
R6/1
DH-2d vs HC
4
21
DH-5d vs HC
12
25
b
Down
Up
DH-2d
DH-5d
WT
52
22
80
72
80
317
R6/1
3
1
11
11
10
15
Sustained
Early
Late
c
Color Key
Value
Early
Sustained
Late
WT HC
WT DH-2d
WT DH-5d
R6/1 HC
R6/1 DH-2d
R6/1 DH-5d
d
DNA-binding transcription activator activity, RNA polymerase II-specific
MAP kinase tyrosine/serine/threonine phosphatase activity
enhancer binding
histone deacetylase binding
drug transmembrane transporter activity
MAP kinase phosphatase activity
unfolded protein binding
E-box binding
ATPase activator activity
extracellular matrix structural constituent
active transmembrane transporter activity
secondary active transmembrane transporter activity
collagen binding
symporter activity
P. adjust.
0,01
0,04
Gene Ratio
0,025
0,1
Early
Sustained
Late
e
Egr1
Fos
Reads (RPK)
P=0.1
WT HC
WT DH-2d
WT DH-5d
R6/1 HC
R6/1 DH-2d
R6/1 DH-5d
f
Motifs promoters
WT
Early
Sustained
Late
AP1
EGR1
NFY
Early
WT
R6/1
AP1
EGR1
eval
g
% of genes
0%
50%
100%
WT
R6/1
Early
Sustained
Late
h
UP - Early
UP- Late
Glia
MSN
-log10(adj pval)
log2(FC)

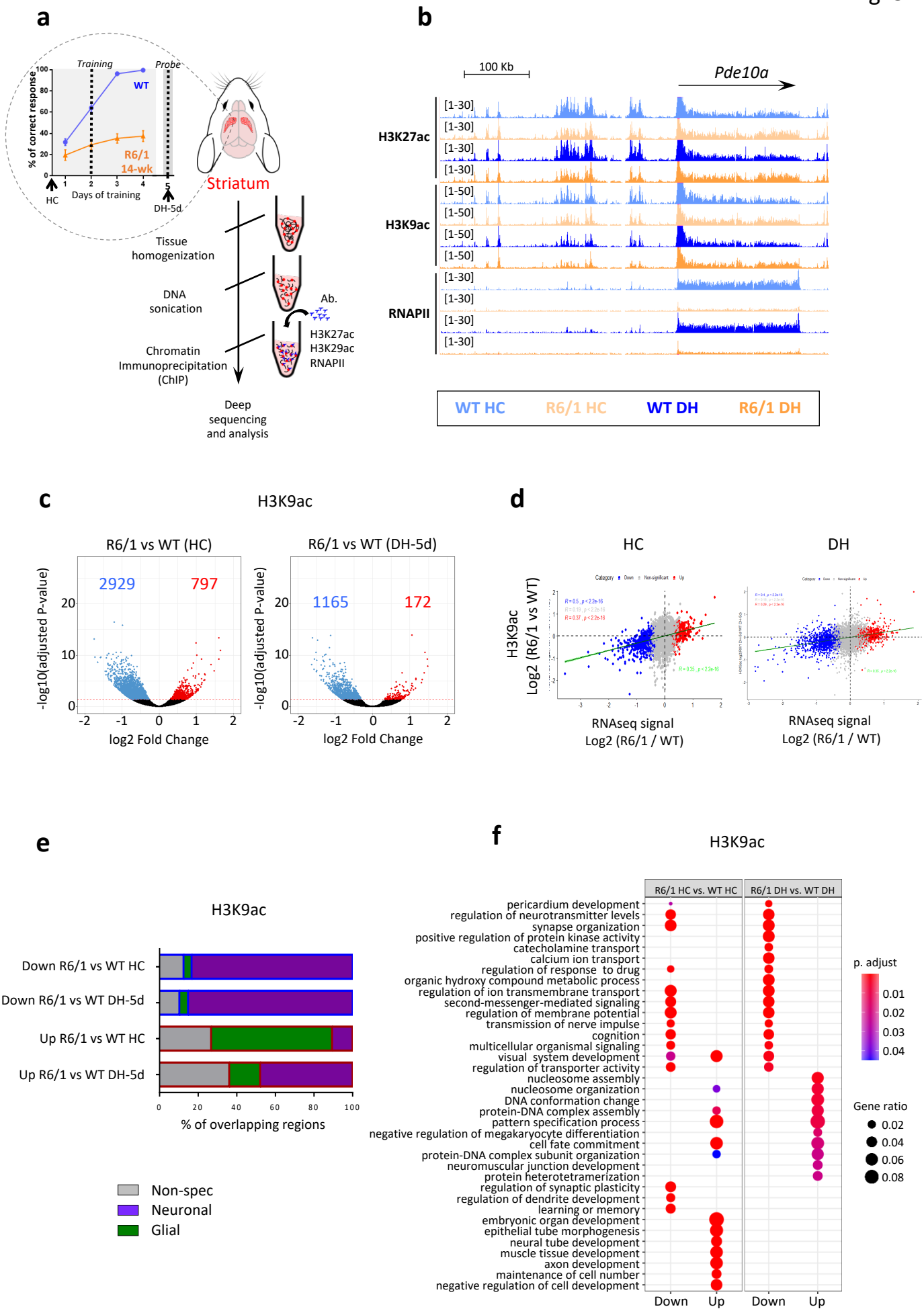
a
Training
Probe
WT
R6/1
14-wk
% of correct response
Days of training
HC
DH-5d
Striatum
Tissue
homogenization
DNA
sonication
Ab.
H3K27ac
H3K29ac
RNAPII
Chromatin
Immunoprecipitation
(ChIP)
Deep
sequencing
and analysis
b
100 Kb
Pde10a
H3K27ac
H3K9ac
RNAPII
WT HC
R6/1 HC
WT DH
R6/1 DH
c
H3K9ac
R6/1 vs WT (HC)
R6/1 vs WT (DH-5d)
2929
797
1165
172
-log10(adjusted P-value)
log2 Fold Change
d
HC
DH
H3K9ac
Log2 (R6/1 vs WT)
RNAseq signal
Log2 (R6/1 / WT)
e
H3K9ac
Down R6/1 vs WT HC
Down R6/1 vs WT DH-5d
Up R6/1 vs WT HC
Up R6/1 vs WT DH-5d
% of overlapping regions
Non-spec
Neuronal
Glial
f
H3K9ac
R6/1 HC vs. WT HC
R6/1 DH vs. WT DH
pericardium development
regulation of neurotransmitter levels
synapse organization
positive regulation of protein kinase activity
catecholamine transport
calcium ion transport
regulation of response to drug
organic hydroxy compound metabolic process
regulation of ion transmembrane transport
second-messenger-mediated signaling
regulation of membrane potential
transmission of nerve impulse
cognition
multicellular organismal signaling
visual system development
regulation of transporter activity
nucleosome assembly
nucleosome organization
DNA conformation change
protein-DNA complex assembly
pattern specification process
negative regulation of megakaryocyte differentiation
cell fate commitment
protein-DNA complex subunit organization
neuromuscular junction development
protein heterotetramerization
regulation of synaptic plasticity
regulation of dendrite development
learning or memory
embryonic organ development
epithelial tube morphogenesis
neural tube development
muscle tissue development
axon development
maintenance of cell number
negative regulation of cell development
Down
Up
p. adjust
Gene ratio

a

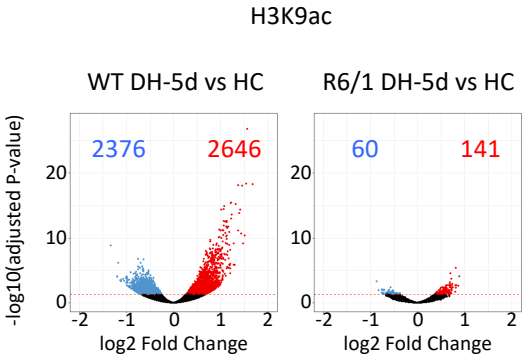
H3K9ac
WT DH-5d vs HC
R6/1 DH-5d vs HC
2376
2646
60
141
-log10(adjusted P-value)
log2 Fold Change
log2 Fold Change

b

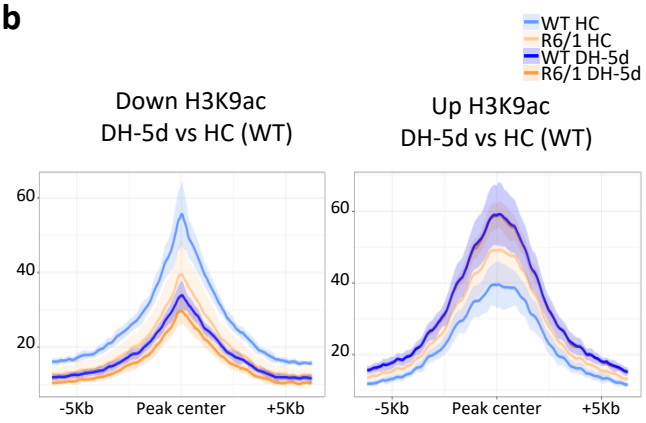
WT HC
R6/1 HC
WT DH-5d
R6/1 DH-5d
Down H3K9ac
DH-5d vs HC (WT)
Up H3K9ac
DH-5d vs HC (WT)
-5Kb
Peak center
+5Kb
-5Kb
Peak center
+5Kb

c

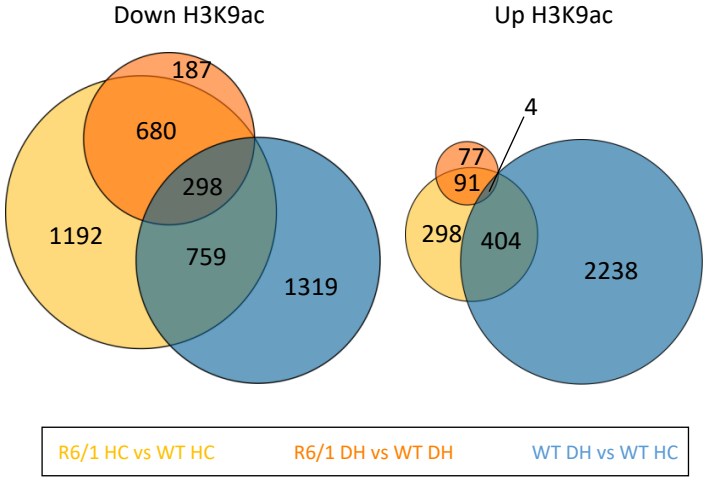
Down H3K9ac
Up H3K9ac
187
680
298
1192
759
1319
4
77
91
298
404
2238
R6/1 HC vs WT HC
R6/1 DH vs WT DH
WT DH vs WT HC

d

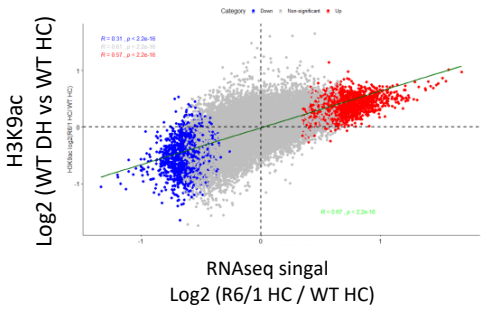
H3K9ac
Log2 (WT DH vs WT HC)
RNAseq singal
Log2 (R6/1 HC / WT HC)

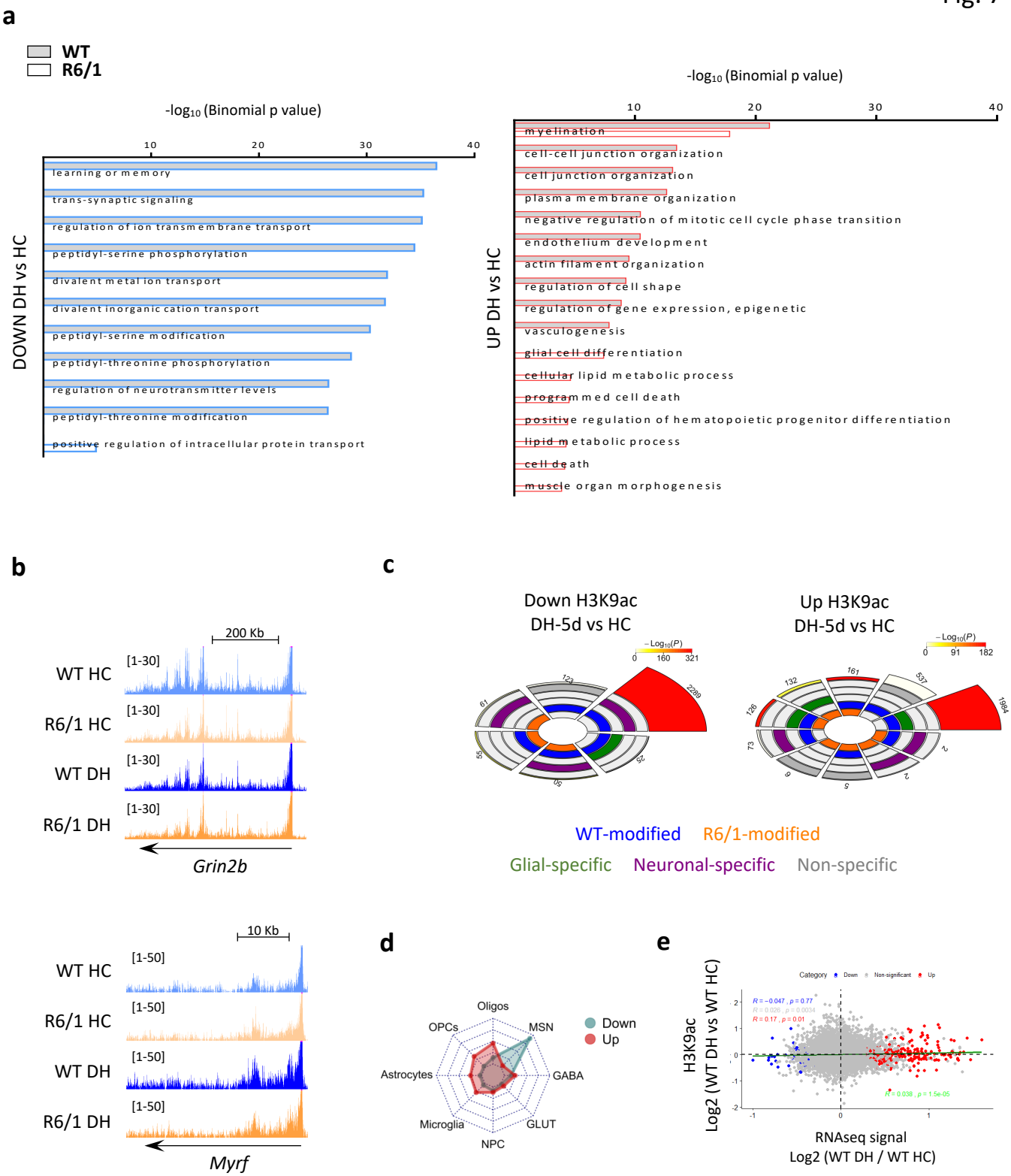
a
WT
R6/1
-log10 (Binomial p value)
10
20
30
40
DOWN DH vs HC
learning or memory
trans-synaptic signaling
regulation of ion transmembrane transport
peptidyl-serine phosphorylation
divalent metal ion transport
divalent inorganic cation transport
peptidyl-serine modification
peptidyl-threonine phosphorylation
regulation of neurotransmitter levels
peptidyl-threonine modification
positive regulation of intracellular protein transport
-log10 (Binomial p value)
10
20
30
40
UP DH vs HC
myelination
cell-cell junction organization
cell junction organization
plasma membrane organization
negative regulation of mitotic cell cycle phase transition
endothelium development
actin filament organization
regulation of cell shape
regulation of gene expression, epigenetic
vasculogenesis
glial cell differentiation
cellular lipid metabolic process
programmed cell death
positive regulation of hematopoietic progenitor differentiation
lipid metabolic process
cell death
muscle organ morphogenesis
b
200 Kb
WT HC
R6/1 HC
WT DH
R6/1 DH
[1-30]
Grin2b
10 Kb
[1-50]
Myrf
c
Down H3K9ac
DH-5d vs HC
Up H3K9ac
DH-5d vs HC
WT-modified
R6/1-modified
Glial-specific
Neuronal-specific
Non-specific
d
Oligos
MSN
GABA
GLUT
NPC
Microglia
Astrocytes
OPCs
Down
Up
e
H3K9ac
Log2 (WT DH vs WT HC)
RNAseq signal
Log2 (WT DH / WT HC)
Category
Down
Non-significant
Up

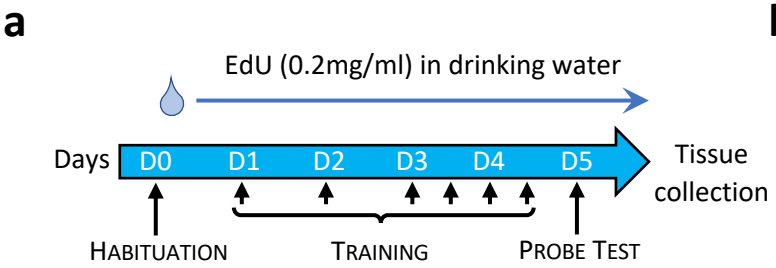
a
EdU (0.2mg/ml) in drinking water
Days
D0
D1
D2
D3
D4
D5
Tissue collection
HABITUATION
TRAINING
PROBE TEST

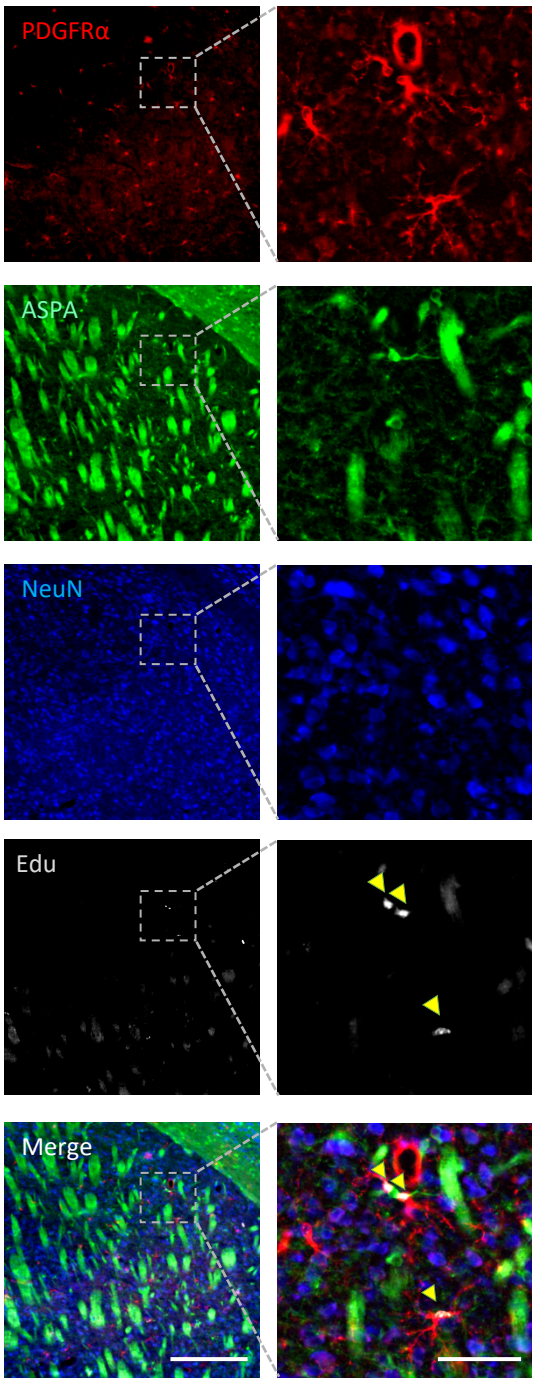
b
PDGFRα
ASPA
NeuN
Edu
Merge

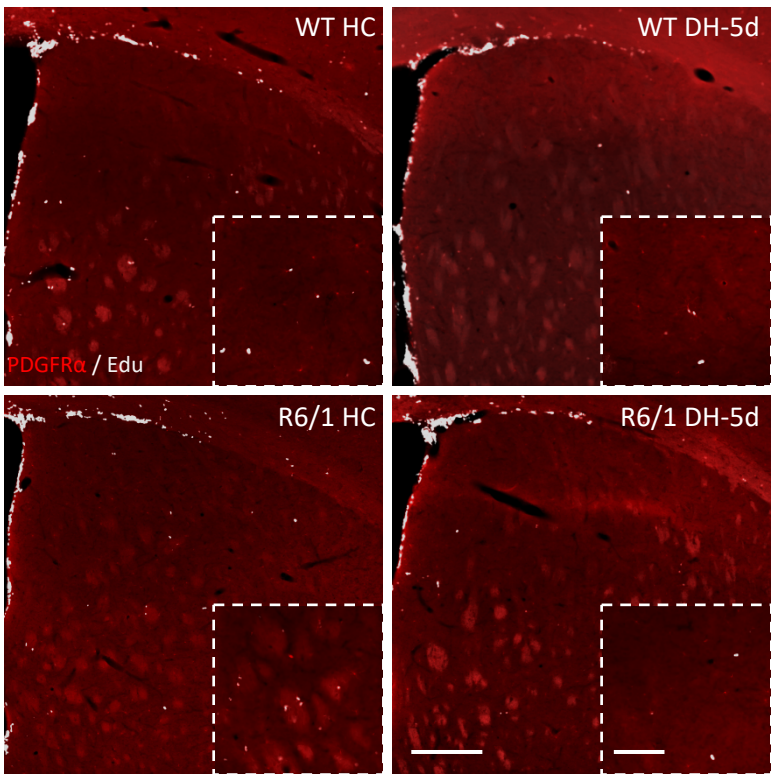
c
WT HC
WT DH-5d
PDGFRα / Edu
R6/1 HC
R6/1 DH-5d

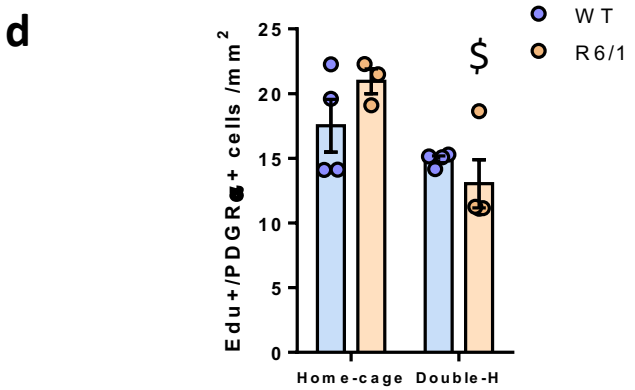
d
WT
R6/1
Edu+/PDGFRα+ cells /mm2
25
20
15
10
5
0
$
Home-cage
Double-H

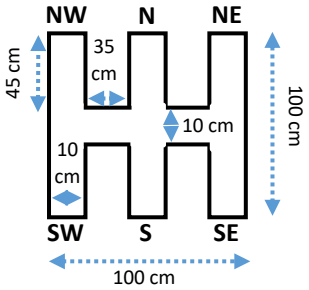
a
NW
N
NE
35 cm
45 cm
10 cm
100 cm
10 cm
SW
S
SE
100 cm

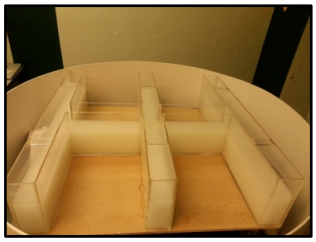
b

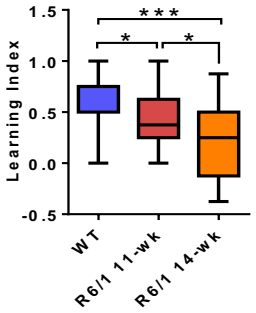
e
Learning Index
1.5
1.0
0.5
0.0
-0.5
***
*
*
WT
R6/1 11-wk
R6/1 14-wk

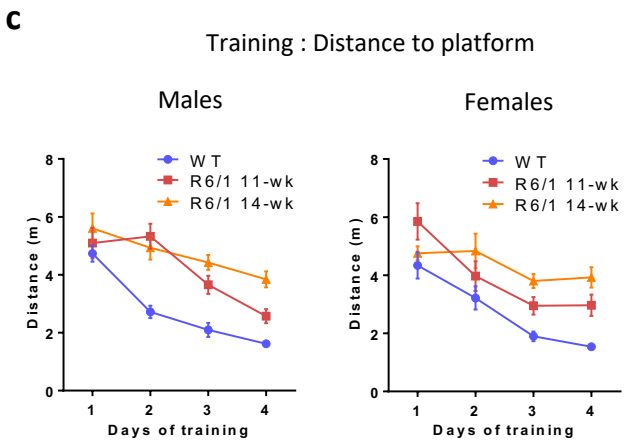
c
Training : Distance to platform
Males
Females
WT
R6/1 11-wk
R6/1 14-wk
Distance (m)
Days of training

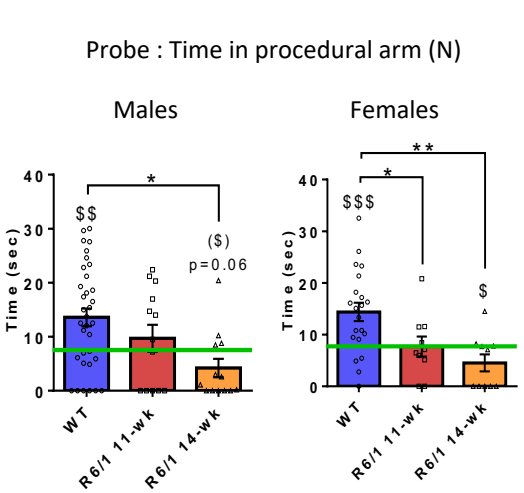
f
Probe : Time in procedural arm (N)
Males
Females
Time (sec)
$$
($)
p=0.06
$$$
$
*
**
WT
R6/1 11-wk
R6/1 14-wk

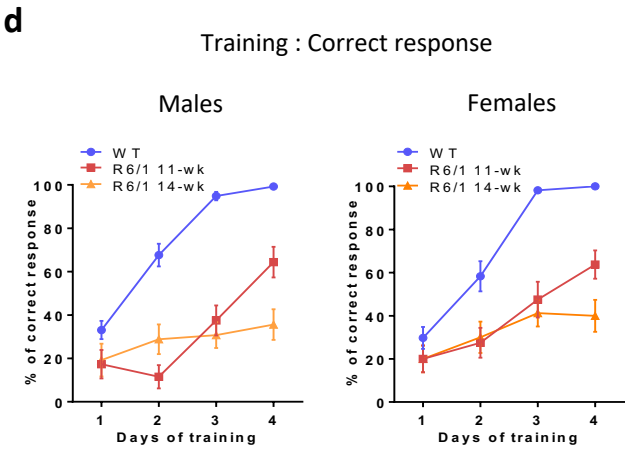
d
Training : Correct response
Males
Females
WT
R6/1 11-wk
R6/1 14-wk
% of correct response
Days of training

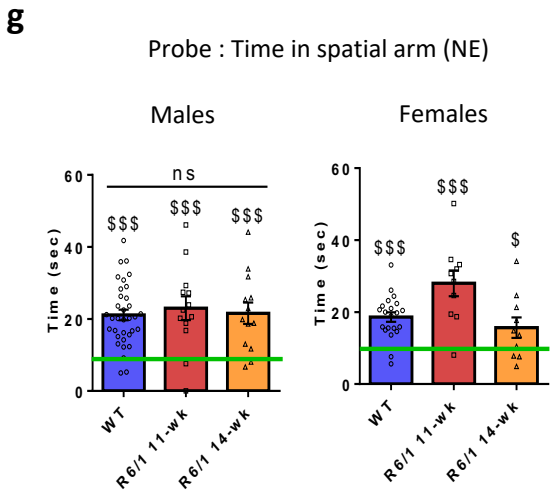
g
Probe : Time in spatial arm (NE)
Males
Females
Time (sec)
ns
$$$
$
WT
R6/1 11-wk
R6/1 14-wk

Supplementary Fig.1. Procedural memory is early impaired in HD R6/1 mice. (a), Scheme of the double-H maze. The device, holding in a square of 100cm x 100cm, is composed of 3 parallel arms connected by a central arm. The ends of the arms are named NW, SW, N, S, NE and SE by convention. **(b)** Photograph showing the general aspect of the maze, filled with opacified water. **(c)** Graphs showing the curves of tendency of the distance travelled to reach the platform (mean ± sem) in 11- and 14-wk-old WT and R6/1 male (left) and female (right) mice. Two-ways ANOVA with repeated measures, with Tukey post-hoc test. **(d)** Graphs showing the curves of tendency of the percentage of correct response (mean ± sem) in 11- and 14-wk-old WT and R6/1 male (left) and female (right) mice. Two-ways ANOVA with repeated measures, with Tukey post-hoc test. **(e)** Boxplot showing learning index (mean ± sem) computed as follows: (% of correct responses at day 4 – day 1)/divided by % of correct response at day 4. Kruskal-Wallis test with Dunn post-hoc test, *p<0,05, ***p<0,005. **(f)** Bargraphs showing time spent in the procedural arm -N- (mean ± sem) in 11- and 14-wk-old WT and R6/1 male (left) and female (right) mice during the probe test. Kruskal-Wallis test, with Dunn post-hoc test, *p<0,05, **p<0,01. The time spent in the procedural arm was compared to chance level (8,5 seconds) using one-sample Wilcoxon test, $ p<0,05, $$ p<0,01, $$$ p<0,005, WT and R6/1 vs chance level. **(h)** Bargraphs showing time spent in the Spatial arm -NE- (mean ± sem) for 11- and 14-wk-old WT and R6/1 male (left) and female (right) mice during the probe test. Kruskal-Wallis test with Dunn post-hoc test. The time spent in the spatial arm was compared to chance level (8,5 seconds) using one-sample Wilcoxon test, $ p<0,05, $$$ p<0,005, WT and R6/1 vs chance level.

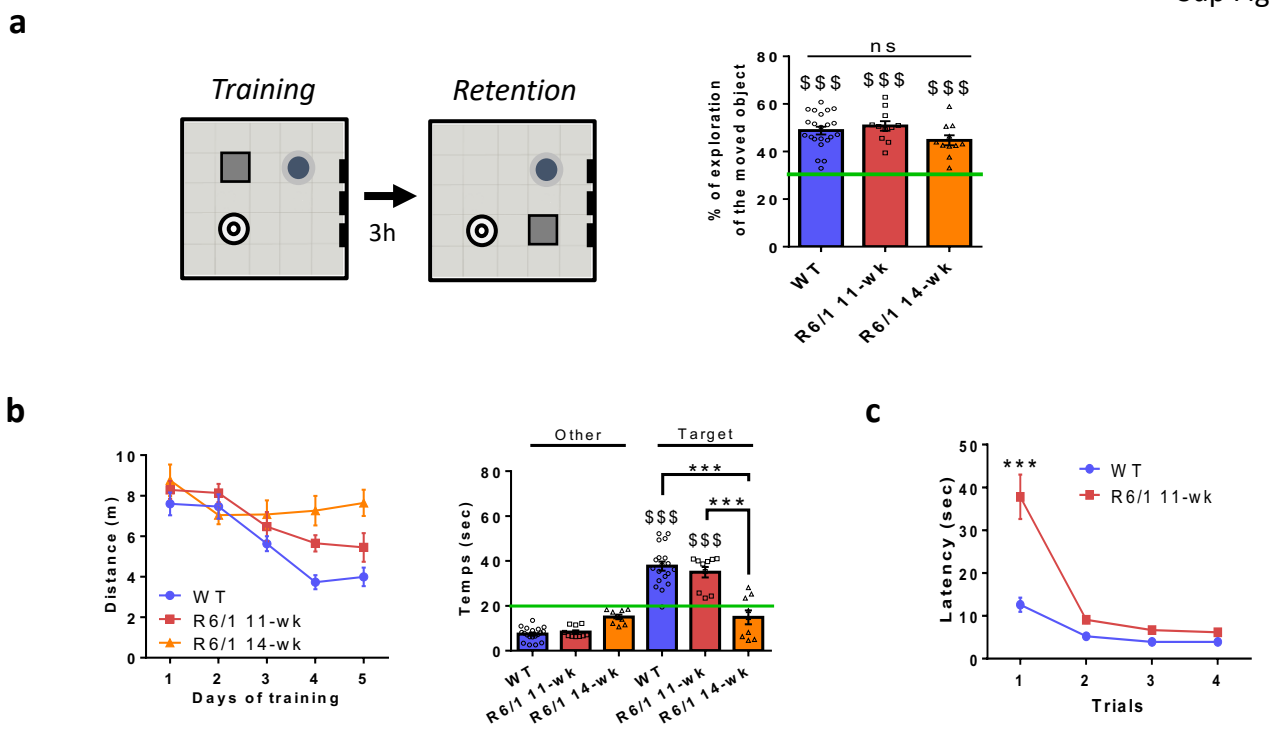

Supplementary Fig.2. Spatial memory and motor functions are preserved at early disease stage in HD R6/1 mice. (a) Left panel, scheme showing protocol of object location task. Right panel, bargraph showing the percentage of exploration of moved vs unmoved objects (mean ± sem) in 11- and 14- wk-old WT and R6/1 mice. One-way ANOVA, with Tukey post-hoc test. The percentage of exploration of moved object was compared to chance level (33%) using one-sample T-test, $$$ p<0,005, WT and R6/1 vs chance level. **(b)** Left panel, graph showing the curves of tendency of distance travelled to reach the platform in the Morris water maze (mean ± sem) in 11- and 14- wk-old WT and R6/1 mice. Two-ways ANOVA with repeated measures, with Tukey post-hoc test. Right panel, bargaph showing the time spent in target quadrant vs other quadrants (mean ± sem) in 11- and 14-wk-old WT and R6/1 mice during the probe test. One-way ANOVA with Tukey post-hoc test, *** p<0,005. Time spent in quadrants was compared to chance level (20 s) using one-sample T-test, $$$ p<0,005 WT and R6/1 vs chance level. **(c)** Graph showing the curves of tendency of the latency to reach the platform (mean ± sem) in the bar test in 11- and 14-wk-old WT and R6/1 mice. Two-ways ANOVA with repeated measures, with Tukey post-hoc test, *** p<0,005 R6/1 11-wk vs WT.

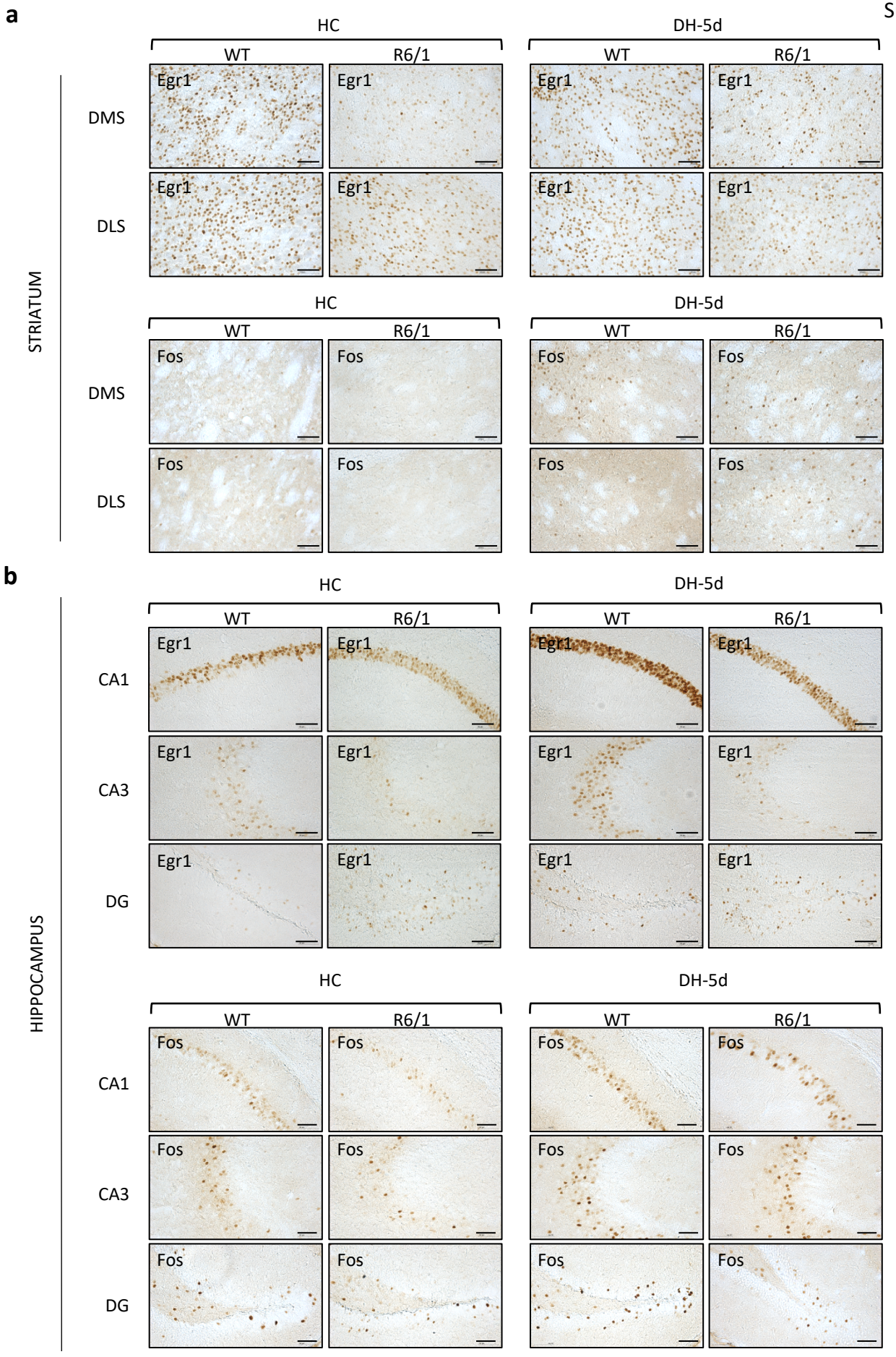
a
HC
DH-5d
WT
R6/1
STRIATUM
DMS
DLS
Egr1
Fos
b
HIPPOCAMPUS
CA1
CA3
DG

Supplementary Fig.3. Egr1 and Fos immunostaining in the striatum and hippocampus of WT and HD R6/1 mice. (a) Representative photographs of Egr1 (upper panels) and Fos (lower panels) immunostaining in R6/1 and WT dorsal striatum, including DMS and DLS, in basal condition (HC) and after 5 days in the double-H maze (DH-5d). Scale, 10 µm. **(b)** Representative photographs of Egr1 (upper panels) and Fos (lower panesl) immunostaining in R6/1 and WT dorsal hippocampus subregions, including CA1, CA3 and Dentate gyrus (DG), in basal condition (HC) and after 5 days in the double-H maze (DH-5d). Scale, 10 µm.

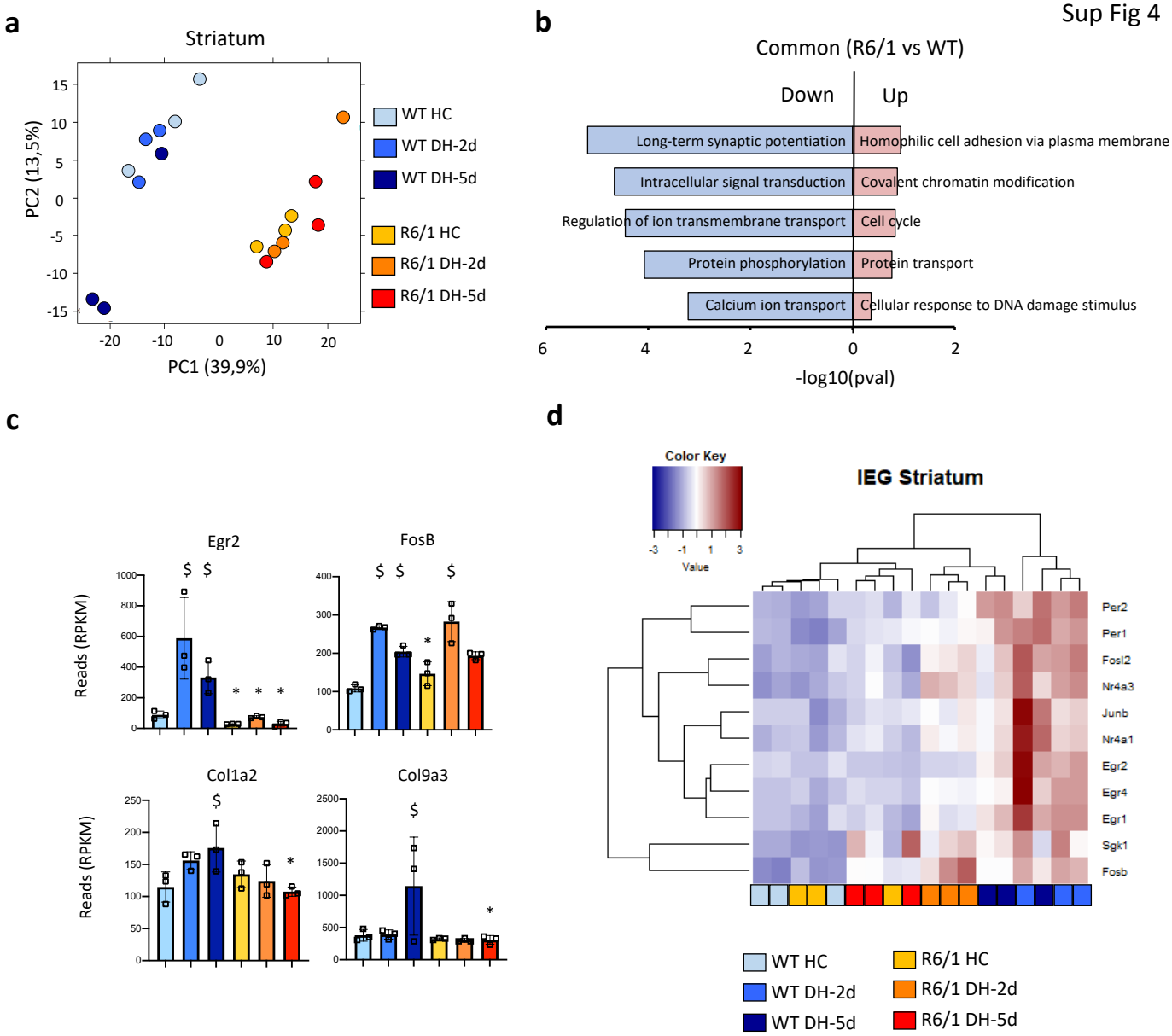

Supplementary Fig.4. Early striatal transcriptomic signature in HD R6/1 mice. (a) Principal component analysis (PCA) computed from striatal RNAseq datasets generated in WT and R6/1 mice in HC, DH-2d and DH-5d conditions. **(b)** Gene ontology analysis of common down- and up-regulated genes in R6/1 vs WT between the 3 conditions (e.g. HC, DH-2d and DH-5d). **(c)** Bargraphs representing mRNA levels (mean ± sem) of select up-regulated genes by memory in WT striatal samples. Expression values were computed from RNAseq data. RPK, reads per kilobases. The Benjamini and Hochberg method was used for multiple testing correction. Egr2: *, adj. *p* val = 10^{-3} R6/1 HC vs WT HC; *, adj. *p* val = $3x10^{-18}$ R6/1 DH-2d vs WT DH-2d; *, adj. *p* val = $5x10^{-20}$ R6/1 DH-5d vs WT DH-5d; $, adj. *p* val = $2x10^{-14}$ WT DH-2d vs WT HC; $, adj. *p* val = $3x10^{-6}$ WT DH-5d vs WT HC. FosB: *, adj. *p* val = $3x10^{-2}$ R6/1 HC vs WT HC; $, adj. *p* val = $2x10^{-14}$ WT DH-2d vs WT HC; $, adj. *p* val = 10^{6} WT DH-5d vs WT HC; $, adj. *p* val = $5x10^{-6}$ R6/1 DH-2d vs R6/1 HC. Col1a2: *, adj. *p* val = $2x10^{-3}$ R6/1 DH-5d vs WT DH-5d; $, adj. *p* val = $6x10^{-2}$ WT DH-5d vs WT HC; Col9a3: *, adj. *p* val = $2x10^{-3}$ R6/1 DH-5d vs WT DH-5d; $, adj. *p* val = 10^{-2} WT DH-5d vs WT HC.**(d)** Heatmap of z-score values representing mRNA levels of sustained up-regulated IEGs by memory in WT striatal samples.

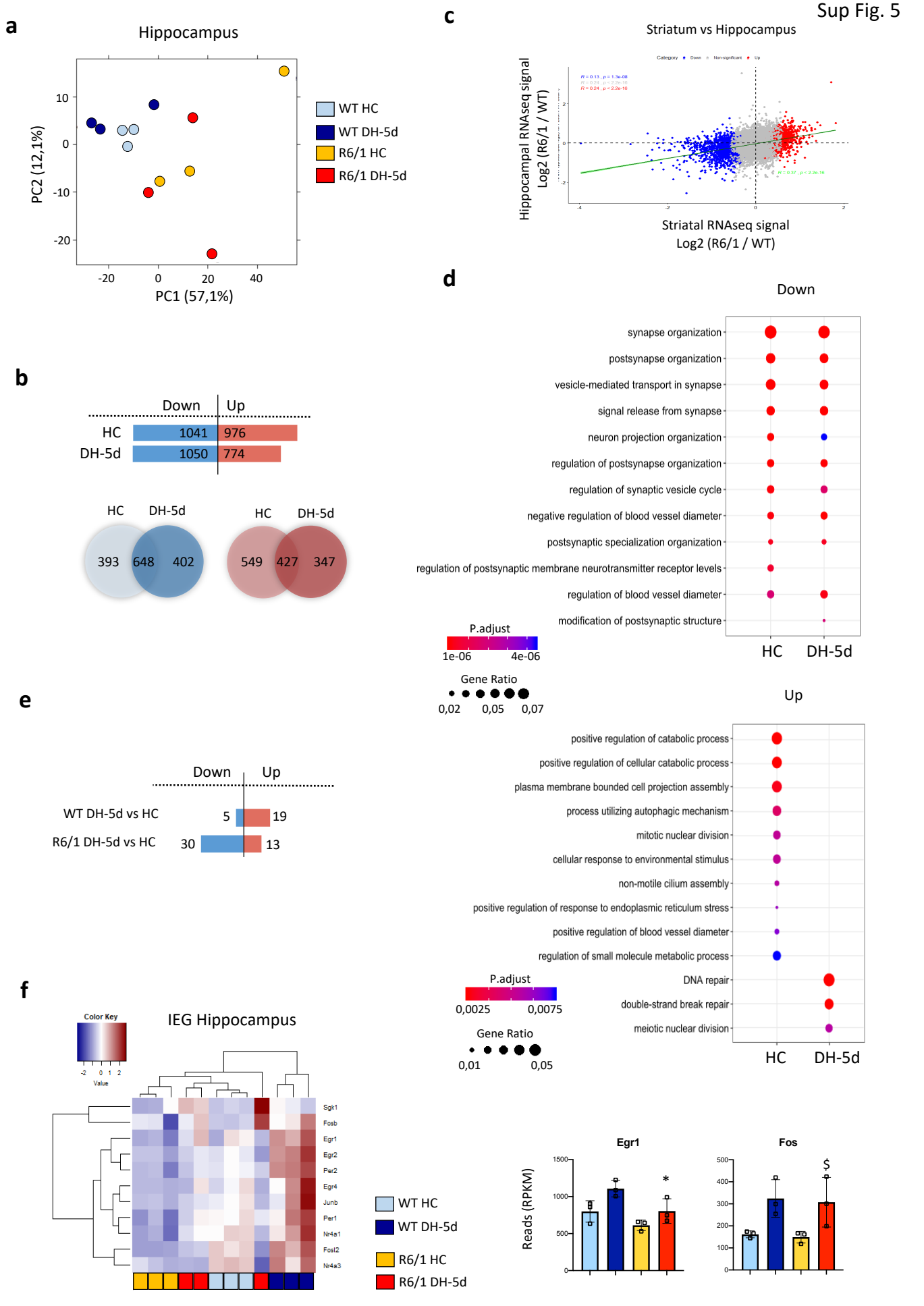
a
Hippocampus
PC2 (12,1%)
PC1 (57,1%)
WT HC
WT DH-5d
R6/1 HC
R6/1 DH-5d
b
Down
Up
HC 1041 976
DH-5d 1050 774
HC DH-5d
393 648 402
HC DH-5d
549 427 347
c
Striatum vs Hippocampus
Hippocampal RNAseq signal
Log2 (R6/1 / WT)
Striatal RNAseq signal
Log2 (R6/1 / WT)
d
Down
synapse organization
postsynapse organization
vesicle-mediated transport in synapse
signal release from synapse
neuron projection organization
regulation of postsynapse organization
regulation of synaptic vesicle cycle
negative regulation of blood vessel diameter
postsynaptic specialization organization
regulation of postsynaptic membrane neurotransmitter receptor levels
regulation of blood vessel diameter
modification of postsynaptic structure
P.adjust
1e-06 4e-06
Gene Ratio
0,02 0,05 0,07
HC DH-5d
e
Down Up
WT DH-5d vs HC 5 19
R6/1 DH-5d vs HC 30 13
Up
positive regulation of catabolic process
positive regulation of cellular catabolic process
plasma membrane bounded cell projection assembly
process utilizing autophagic mechanism
mitotic nuclear division
cellular response to environmental stimulus
non-motile cilium assembly
positive regulation of response to endoplasmic reticulum stress
positive regulation of blood vessel diameter
regulation of small molecule metabolic process
DNA repair
double-strand break repair
meiotic nuclear division
P.adjust
0,0025 0,0075
Gene Ratio
0,01 0,05
HC DH-5d
f
Color Key
Value
IEG Hippocampus
Sgk1
Fosb
Egr1
Egr2
Per2
Egr4
Junb
Per1
Nr4a1
Fosl2
Nr4a3
WT HC
WT DH-5d
R6/1 HC
R6/1 DH-5d
Egr1
Fos
Reads (RPKM)
*
$

Supplementary Fig.5. Early hippocampal transcriptomic signature in HD R6/1 mice. (a) Upper panel, Principal component analysis (PCA) computed from striatal RNAseq datasets generated in WT and R6/1 mice in HC and DH-5d conditions.**(b)** Bargraph showing the number of differentially expressed genes in the hippocampus of R6/1 vs WT mice in HC and DH-5d conditions. Fold change (*FC*)<1 and adj. *p* value <0.05. Lower panel, Venn diagrams showing overlapping down- and up-regulated genes in R6/1 vs WT hippocampal samples in HC and DH-5d conditions **(c)** Linear regression analysis between transcriptional striatal and hippocampal changes in R6/1 vs WT samples. The correlation is shown for all genes (green), genes significantly down-regulated in R6/1 HC vs WT HC striatum (FC<1 and adj. *p* value <0.05; blue), genes significantly up-regulated in R6/1 HC vs WT HC striatum (FC>1 and adj. *p* value <0.05; red) and non-significantly altered genes in R6/1 HC vs WT HC striatum (Grey). Pearson's correlation index and *P* value for fitted linear model are shown. **(d)** Gene ontology analysis of genes differentially expressed in R6/1 vs WT hippocampal samples (FDR<0.05), in HC and DH conditions. Top significant biological processes are shown using dot size proportional to gene ratio and heatmap reflecting adj. pvalue. (**e**) Bargraph showing the numbers of differentially expressed genes (adj. *P* value < 0.1) in DH-5d vs HC comparison, in WT and R6/1 hippocampal samples. **(f)** Heatmap of z-score values representing IEGs. (**g)** Bargraphs representing mRNA levels (mean $\pm$ sem) of Egr1 and Fos in hippocampal samples. Expression values were computed from RNAseq data. RPK, reads per kilobases. The Benjamini and Hochberg method was used for multiple testing correction. Egr1: *, adj. *p* val = 10^{-1} R6/1 DH-5d vs WT DH-5d; Fos: $, adj. *p* val = 10^{-1} R6/1 DH-5d vs R6/1 HC

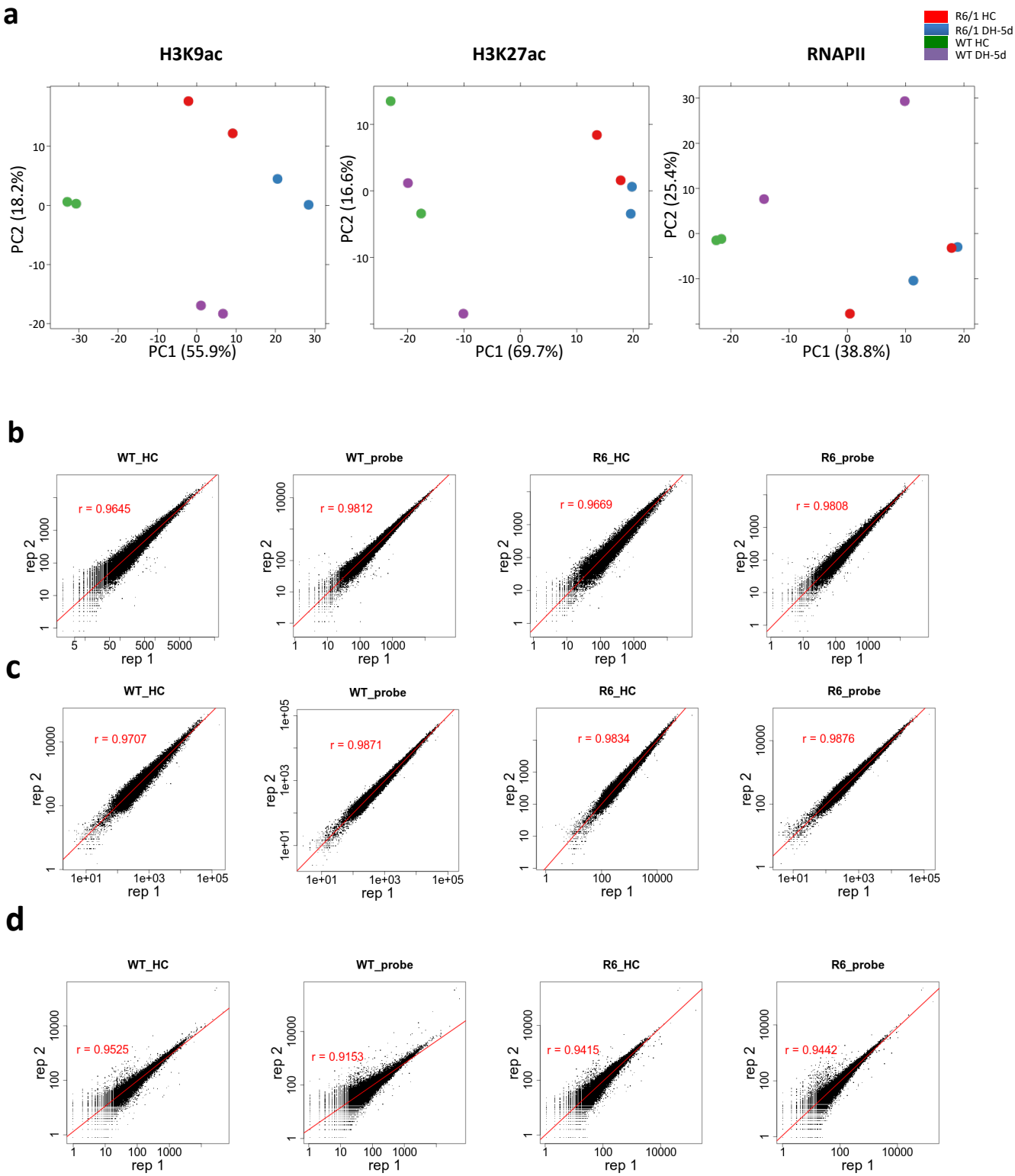

Supplementary Fig. 6. Quality of H3K9ac, H3K27ac and RNAPII ChIPseq data generated on bulk striatal tissue in WT and R6/1 mice at basal and learning conditions: complementary information and analyses **(a)** Variance observation between H3K9ac (left), H3K27ac (middle) and RNAPII (right) ChIPseq datasets generated on the striatum of WT and R6/1 mice at basal (home-cage, HC) or learning (double-H 5 days, DH-5d) conditions. Principal component analysis (PCA) was computed on variance stabilized data using the method proposed by Anders and Huber (REF). Sample colours indicate groups (R6/1 HC, red; R6/1 DH-5d, blue; WT HC, green; WT DH-5d, purple). First factorial plans are represented. The first axis explains the major variability between the samples, predominantly separating them according to genotype. **(b-d)** Scatterplots showing the comparison of ChIPseq read count per peak between replicates for H3K9ac (**b**), H3K27ac (**c**) and RNAPII (**d**) and for each condition (WT-HC, WT-DH-5d, R6/1-HC and R6/1-DH-5d).

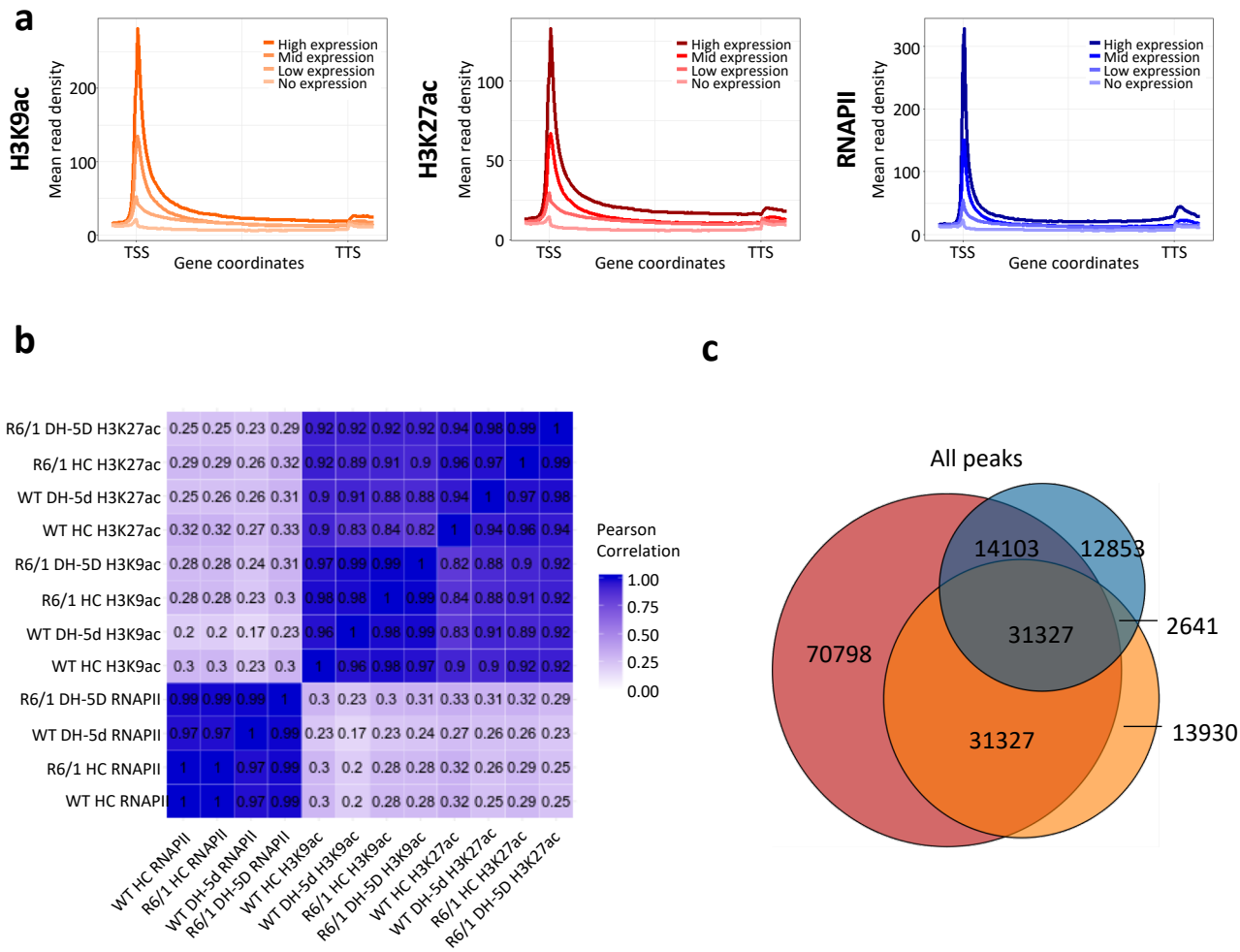

Supplementary Fig. 7. Quality of H3K9ac, H3K27ac and RNAPII ChIPseq data generated on bulk striatal tissue in WT and R6/1 mice at basal and learning conditions: expression and correlation analysis. (a) Representative gene metaprofiles for H3K9ac (left), H3K27ac (middle) and RNAPII (right) at no, low-, mid- and high-expressed genes in the striatum. No-, low-, mid- and high-expressed genes were delineated according to quartile distribution of normalized striatal RNAseq values (i.e. no-expressed < 1st, 1st <low-expressed < 2nd, 2nd<mid-expressed<3rd, high-expressed>4th quartiles). H3K9ac, H3K27ac and RNAPII ChIPseq data and RNAseq data generated on WT striatum at basal state (home-cage, HC) were used in the analysis. TSS, Transcription Start Site; TTS, Transcription Termination Site. As expected, H3K9ac, H3K27ac and RNAPII signals are proportional to gene expression levels. **(b)** Correlation heatmap for H3K9ac, H3K27ac and RNAPII in WT and R6/1 striatum at basal (home-cage, HC) and learning (double-H 5 days, DH-5d) conditions. This example heatmap was generated using one biological replicate of ChIPseq data generated on this study, and computing read enrichment every 5Kb bins across the entire genome. Spearman correlation coefficients are provided for each regression. As expected, H3K27ac and H3K9ac signals are higher correlated as compared to RNAPII. **(c)** Venn Diagram showing the overlap between all H3K27ac (red), H3K9ac (orange) and RNAPII (blue) identified peaks found in all generated ChIP-seq datasets.

a

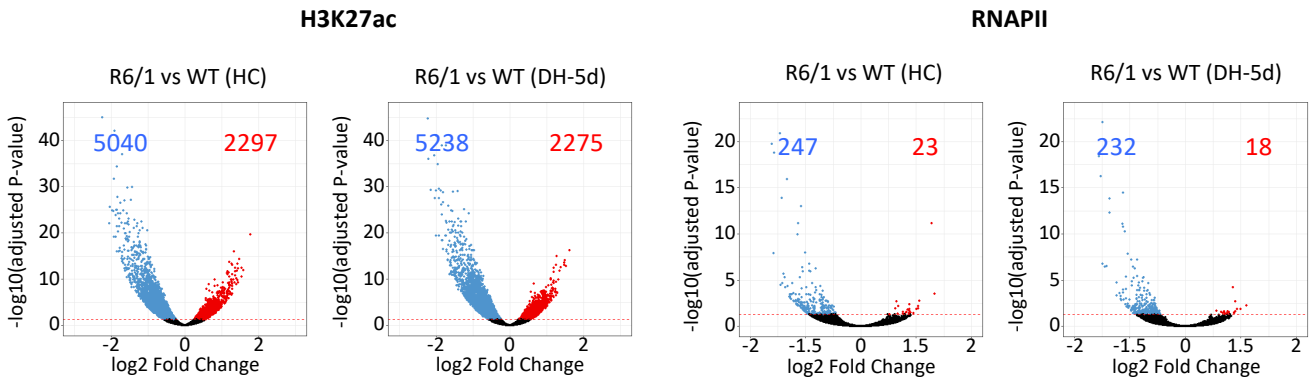
H3K27ac
RNAPII
R6/1 vs WT (HC)
R6/1 vs WT (DH-5d)
R6/1 vs WT (HC)
R6/1 vs WT (DH-5d)
5040
2297
5238
2275
247
23
232
18
-log10(adjusted P-value)
log2 Fold Change

b

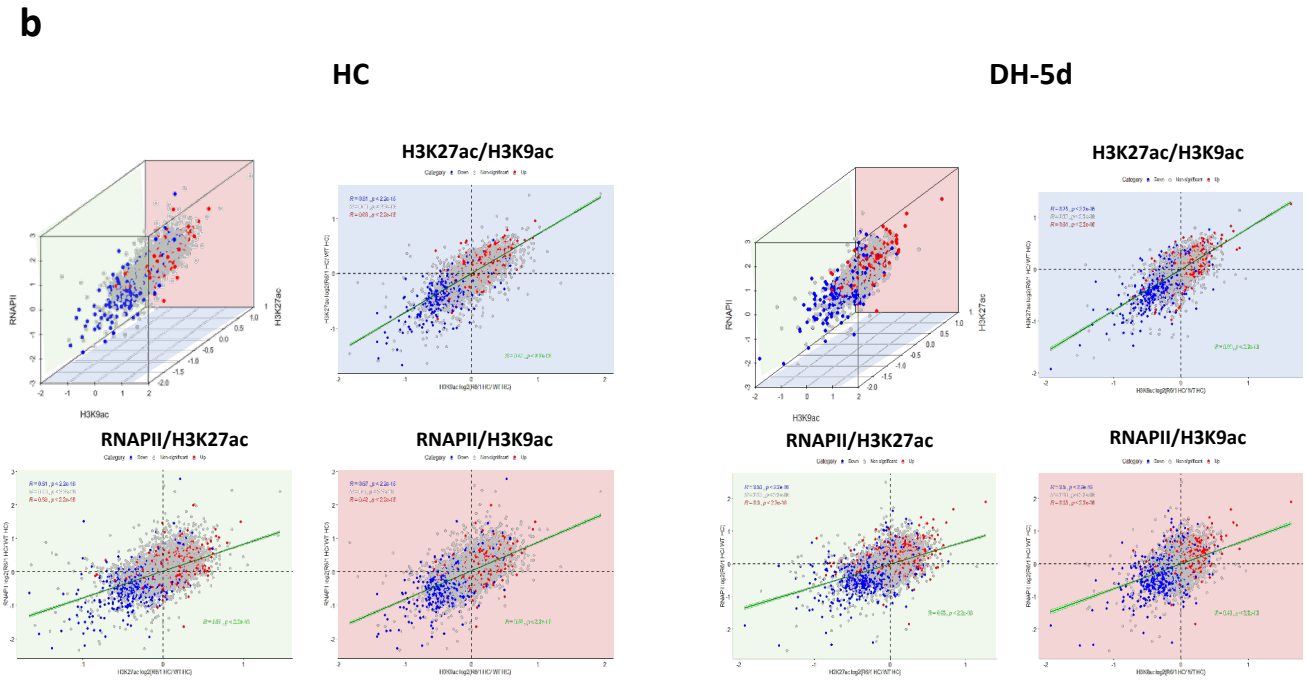
HC
DH-5d
H3K27ac/H3K9ac
RNAPII/H3K27ac
RNAPII/H3K9ac
RNAPII
H3K27ac
H3K9ac

c

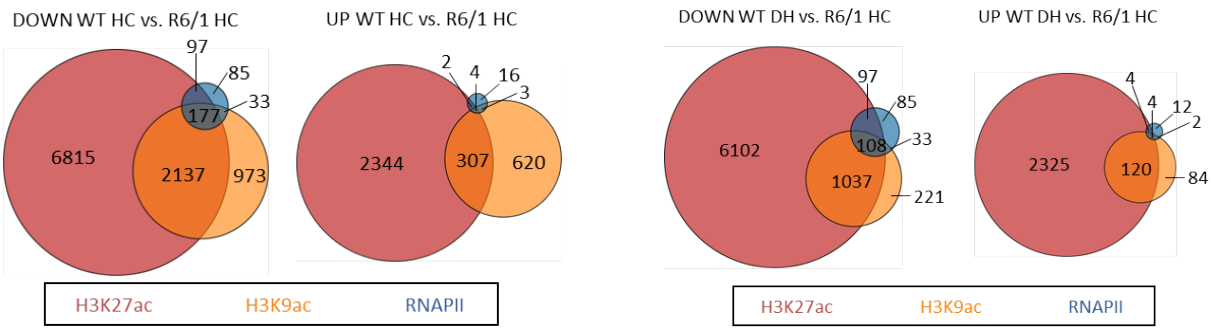
DOWN WT HC vs. R6/1 HC
UP WT HC vs. R6/1 HC
DOWN WT DH vs. R6/1 HC
UP WT DH vs. R6/1 HC
6815
97
85
177
33
2137
973
2344
2
4
16
3
307
620
6102
97
85
108
33
1037
221
2325
4
4
12
2
120
84
H3K27ac
H3K9ac
RNAPII

Supplementary Fig. 8. H3K9ac, H3K27ac and RNAPII R6/1 mice striatum alterations are highly correlated. **(a)** Volcano plots representation of H3K27ac (left) and RNAPII (right) differential enriched regions between WT and R6/1 mice striatum at basal (home-cage, HC) and learning (double-H 5 days, DH-5d) conditions (N=2). Regions with decreased, increased or unchanged H3K9ac levels (adj P value <0.05) in R6/1 mice compared to WT mice are displayed in blue, red and black, respectively. **(b)** 3D scatterplot and 2D orthogonal projections graphs showing the correlation between H3K9ac, H3K27ac and RNAPII at differentially expressed genes between WT and R6/1 mice striatum at basal (home-cage, HC, left) and learning (double-H 5 days, DH-5d, right) conditions. Linear regression analysis between the three sets of ChIP-seq data paired according to the different orthogonal projections is shown for all genes (green), genes significantly downregulated (Fold change (FC) <1 and adj. *P* value <0.05; blue), genes significantly upregulated (FC >1 and adj. *P* value <0.05; red) and non-significantly altered genes (grey). Pearson's correlation index and *P* value for fitted linear model are shown. **(c-d)** Venn Diagrams showing the overlap between regions significantly (adj. P value <0.05) depleted (DOWN, left) or enriched (UP,right) in H3K27ac (red), H3K9ac (orange) and RNAPII (blue) between WT and R6/1 mice striatum at basal (home-cage, HC, **c**) and learning (double-H 5 days, DH-5d, **d**) conditions.

a

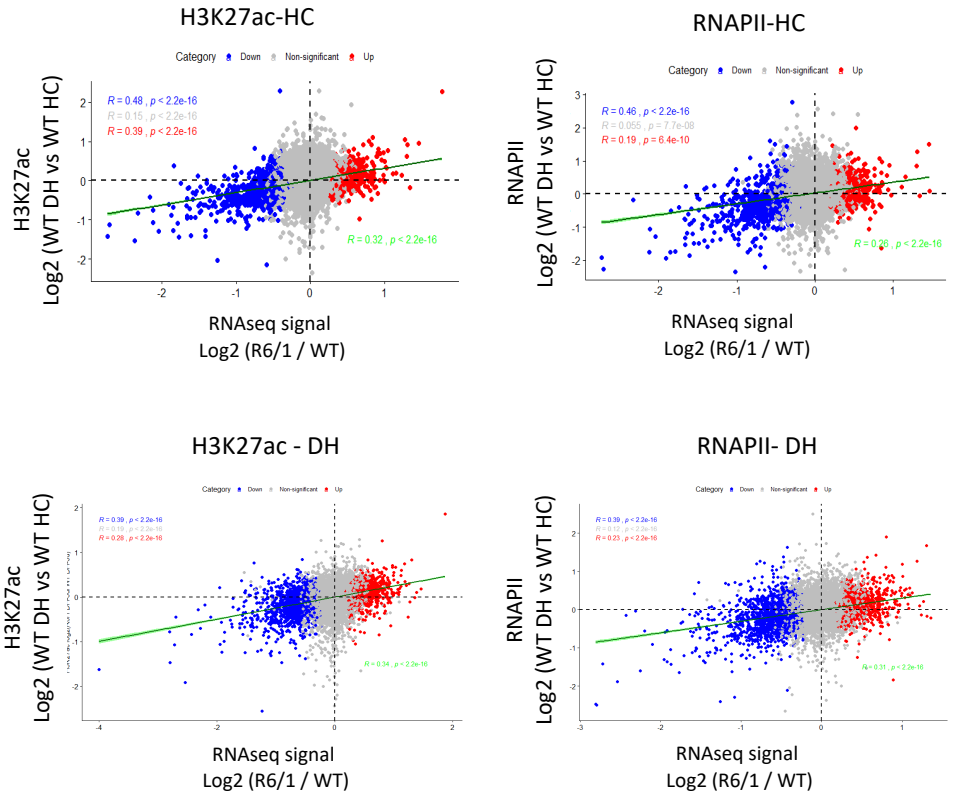
H3K27ac-HC
RNAPII-HC
H3K27ac - DH
RNAPII- DH
Category Down Non-significant Up
H3K27ac Log2 (WT DH vs WT HC)
RNAPII Log2 (WT DH vs WT HC)
RNAseq signal Log2 (R6/1 / WT)

b

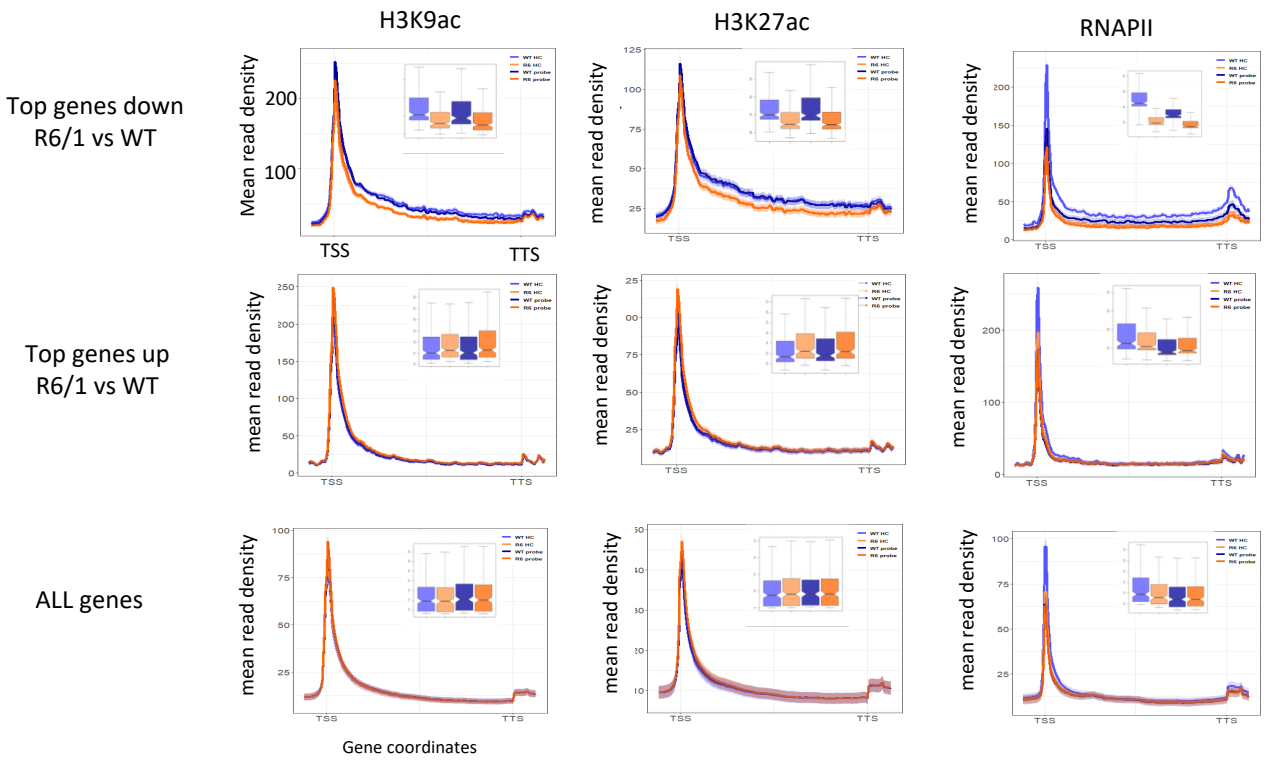
H3K9ac
H3K27ac
RNAPII
Top genes down R6/1 vs WT
Top genes up R6/1 vs WT
ALL genes
Mean read density
mean read density
TSS
TTS
Gene coordinates

Supplementary Fig. 9. Alterations in H3K9ac, H3K27ac and RNAPII R6/1 mice striatum highly correlate with transcriptional dysregulation. (a) Linear regression analysis between transcriptional and H3K27ac (left) or RNAPII (right) changes in the striatum of R6/1 vs WT mice at 14 weeks of age at basal (home-cage, HC, upper panels) and learning (double-H 5 days, DH-5d, bottom panels) conditions (N=2). The correlation is shown for all genes (green), genes significantly downregulated (Fold change (FC) <1 and adj. *P* value <0.05; blue), genes significantly upregulated (FC >1 and adj. *P* value <0.05; red) and non-significantly altered genes (grey). Pearson's correlation index and *P* value for fitted linear model are shown. **(b)** Gene body metaprofiles representing H3K9ac (left panels), H3K27ac (central panels) and RNAPII (right panels) read count distribution for top 300 down-regulated genes (upper panels), top 300 up-regulated genes (middle panels) or all genes ranked according to adj. *P* value, in R6/1 vs WT mouse striatum at basal stage (home-cage, HC). TSS, Transcription Start Site; TTS, Transcription Termination Site. Data from two biological replicates were used to generate average profile. Boxplots represent the distribution of mean read density along the profiles and show median, first quartile (Q1), third quartile (Q3) and range (min, Q1-1.5x(Q3-Q1); max, Q3+1.5x(Q3-Q1)).

a

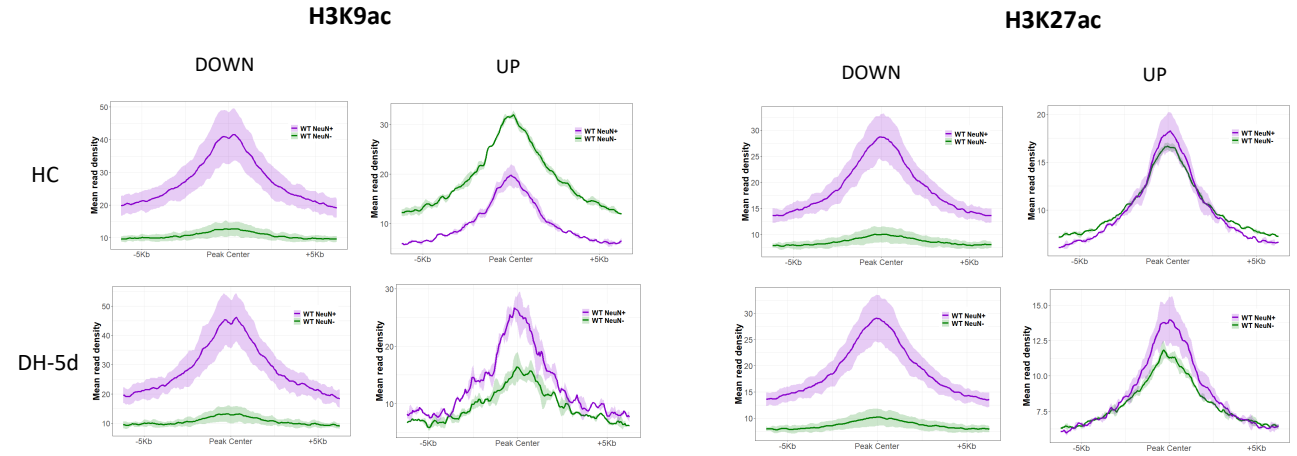
H3K9ac
H3K27ac
DOWN
UP
DOWN
UP
HC
DH-5d
Mean read density
WT NeuN+
WT NeuN-
-5Kb
Peak Center
+5Kb

b

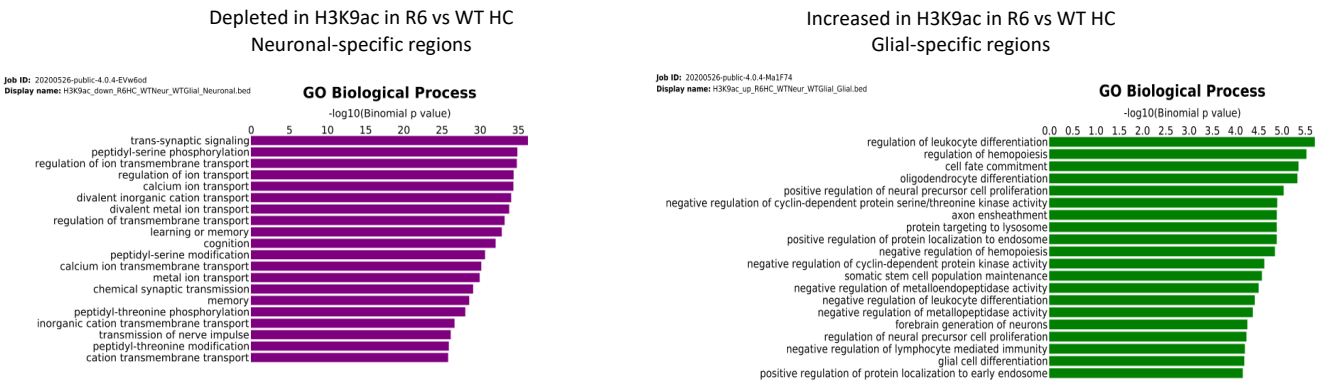
Depleted in H3K9ac in R6 vs WT HC
Neuronal-specific regions
Increased in H3K9ac in R6 vs WT HC
Glial-specific regions
GO Biological Process
-log10(Binomial p value)
trans-synaptic signaling
peptidyl-serine phosphorylation
regulation of ion transmembrane transport
regulation of ion transport
calcium ion transport
divalent inorganic cation transport
divalent metal ion transport
regulation of transmembrane transport
learning or memory
cognition
peptidyl-serine modification
calcium ion transmembrane transport
metal ion transport
chemical synaptic transmission
memory
peptidyl-threonine phosphorylation
inorganic cation transmembrane transport
transmission of nerve impulse
peptidyl-threonine modification
cation transmembrane transport
regulation of leukocyte differentiation
regulation of hemopoiesis
cell fate commitment
oligodendrocyte differentiation
positive regulation of neural precursor cell proliferation
negative regulation of cyclin-dependent protein serine/threonine kinase activity
axon ensheathment
protein targeting to lysosome
positive regulation of protein localization to endosome
negative regulation of hemopoiesis
negative regulation of cyclin-dependent protein kinase activity
somatic stem cell population maintenance
negative regulation of metalloendopeptidase activity
negative regulation of leukocyte differentiation
negative regulation of metallopeptidase activity
forebrain generation of neurons
regulation of neural precursor cell proliferation
negative regulation of lymphocyte mediated immunity
glial cell differentiation
positive regulation of protein localization to early endosome

c

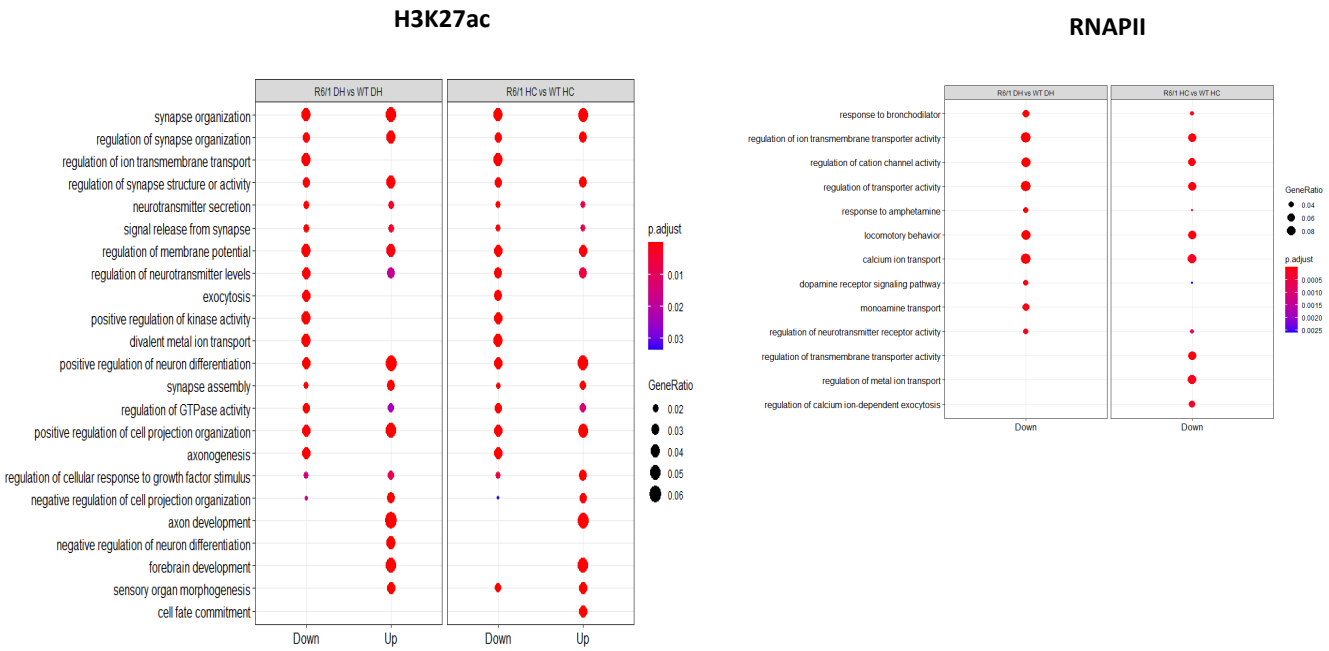
H3K27ac
RNAPII
R6/1 DH vs WT DH
R6/1 HC vs WT HC
synapse organization
regulation of synapse organization
regulation of ion transmembrane transport
regulation of synapse structure or activity
neurotransmitter secretion
signal release from synapse
regulation of membrane potential
regulation of neurotransmitter levels
exocytosis
positive regulation of kinase activity
divalent metal ion transport
positive regulation of neuron differentiation
synapse assembly
regulation of GTPase activity
positive regulation of cell projection organization
axonogenesis
regulation of cellular response to growth factor stimulus
negative regulation of cell projection organization
axon development
negative regulation of neuron differentiation
forebrain development
sensory organ morphogenesis
cell fate commitment
Down
Up
p.adjust
GeneRatio
response to bronchodilator
regulation of ion transmembrane transporter activity
regulation of cation channel activity
regulation of transporter activity
response to amphetamine
locomotory behavior
calcium ion transport
dopamine receptor signaling pathway
monoamine transport
regulation of neurotransmitter receptor activity
regulation of transmembrane transporter activity
regulation of metal ion transport
regulation of calcium ion-dependent exocytosis

Supplementary Fig. 10. Alterations in H3K9ac, H3K27ac and RNAPII R6/1 mice striatum differently affect neuronal- and glial-associated enhancer regions. (a) Metaprofiles showing H3K27ac signal in WT NeuN+ (purple) and NeuN- (green) sorted nuclei ChIP-seq data previously generated in WT mice striatum (Alcala Vida et al. 2021) for regions changing in H3K9ac (left) or in H3K27ac (right) between WT and R6/1 mice striatum in basal (home-cage, HC, upper panels) or in learning/memory (double-H 5 days, DH-5d, lower panels). **(b)** Gene Ontology analysis of regions showing decreased (left) or increased (right) H3K9ac levels and intersecting with neuronal- or glial-specific enhancers, respectively, in reference to Figure 5e. **(c)** Gene Ontology analysis of H3K27ac (left) and RNAPII (right) regions differentially enriched (adj. P value <0.05) between R6/1 and WT mouse striatal samples at basal (home-cage, HC) and learning (double-H 5 days, DH-5d) conditions (*FDR* <0.05). Significant biological processes are shown using dot size proportional to gene ratio and heatmap reflecting adjusted *P* value.

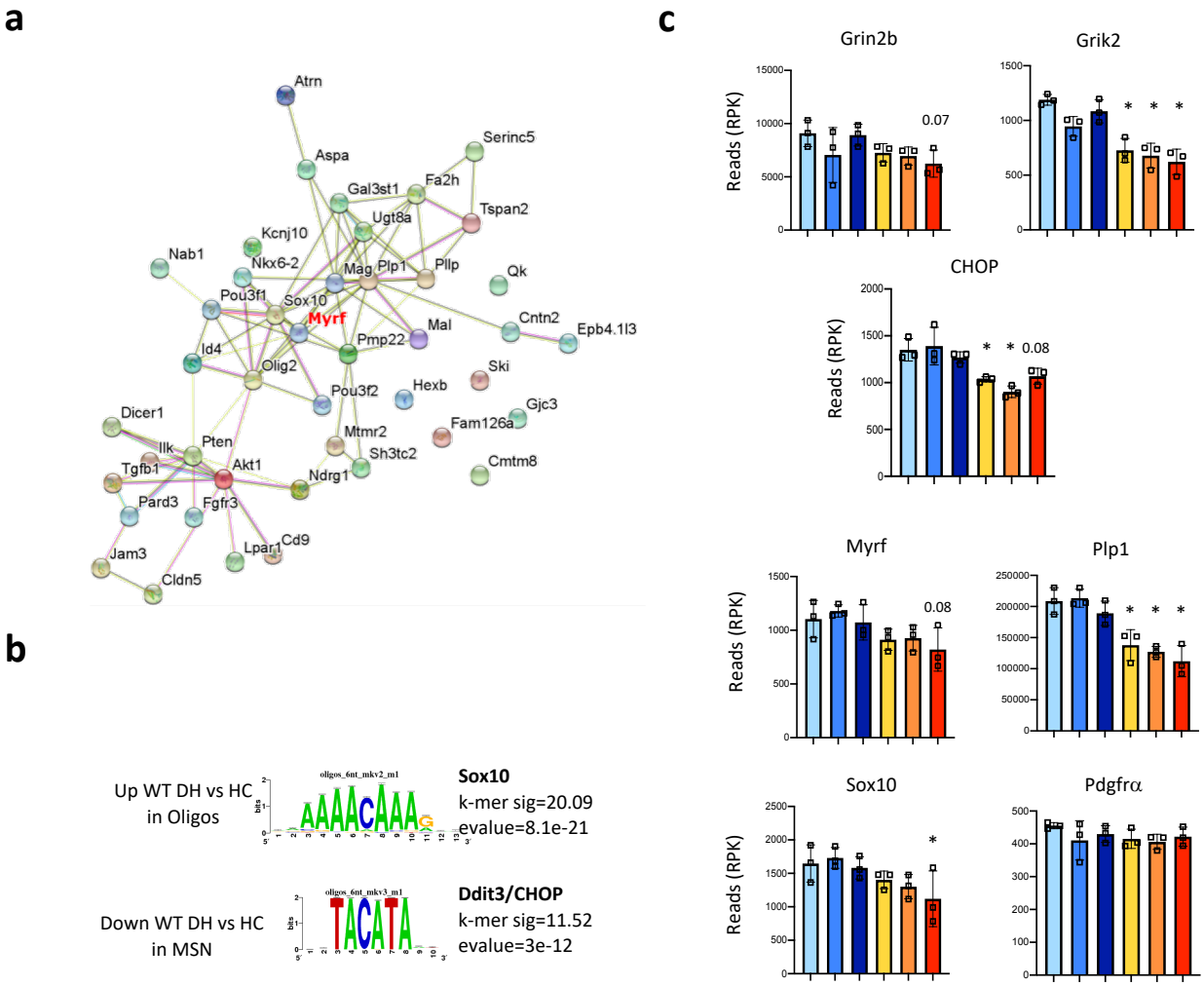

Supplementary Fig. 11. Myelin- and neuronal-related genes associated with H3K9ac changes in physiological striatal procedural learning are differently affected in R6/1 mouse striatum. (a) STRING network representation of proteins encoded by genes close to differentially enriched H3K9ac regions (adj P value <0.05) between WT animals in basal (home-cage, HC) and learning/memory (double-H 5 days, DH-5d) and participating in "myelin formation" biological processes. **(b)** Results of DNA motif analysis, using significantly increased (top) or decreased (bottom) H3K9ac regions between WT DH-5d and WT HC and intersecting with top oligodendrocyte- or MSN-specific ATAC-seq peaks, respectively. Significantly enriched motifs are shown with corresponding statistics. **(c)** Bargraphs representing mRNA levels (mean ± sem) of select down- and up-regulated genes in R6/1 vs WT striatal samples. Expression values were computed from RNAseq data. RPK, reads per kilobases. The Benjamini and Hochberg method was used for multiple testing correction. Grin2b: adj. *p* val = $7x10^{2}$ R6/1 DH-5d vs WT DH-5d; Grik2: *, adj. *p* val = 10^{-4} R6/1 HC vs WT HC; *, adj. *p* val = $2x10^{-1}$ R6/1 DH-2d vs WT DH-2d; *, adj. *p* val = $4x10^{-6}$ R6/1 DH-5d vs WT DH-5d; CHOP: *, adj. *p* val = $6x10^{-3}$ R6/1 HC vs WT HC; *, adj. *p* val = $6x10^{-7}$ R6/1 DH-2d vs WT DH-2d; adj. *p* val = $8x10^{-2}$ R6/1 DH-5d vs WT DH-5d. Myrf: adj. *p* val = $8x10^{-2}$ R6/1 DH-5d vs WT DH-5d. Plp1: *, adj. *p* val = 10^{-3} R6/1 HC vs WT HC; *, adj. *p* val = $3x10^{-5}$ R6/1 DH-2d vs WT DH-2d; *, adj. *p* val = $2x10^{-5}$ R6/1 DH-5d vs WT DH-5d. Sox10: *, adj. *p* val = $5x10^{-2}$ R6/1 DH-5d vs WT DH-5d.

a

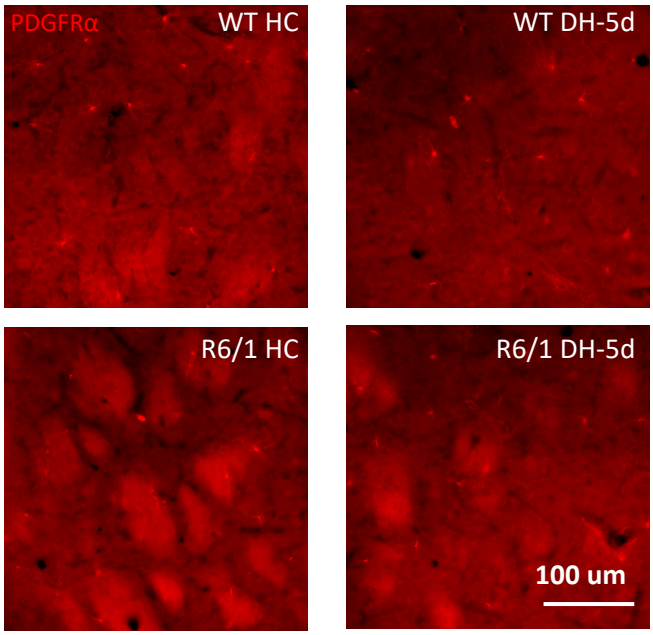
PDGFRα
WT HC
WT DH-5d
R6/1 HC
R6/1 DH-5d
100 um

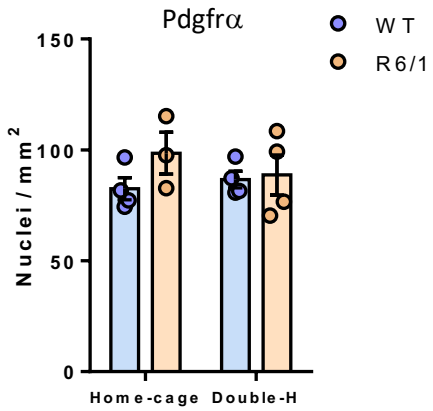
Pdgfrα
WT
R6/1
Nuclei / mm2
150
100
50
0
Home-cage
Double-H

b

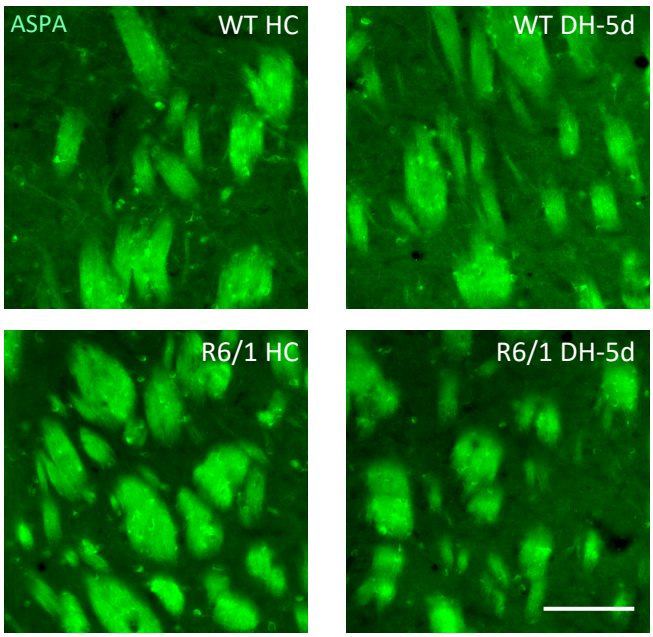
ASPA
WT HC
WT DH-5d
R6/1 HC
R6/1 DH-5d

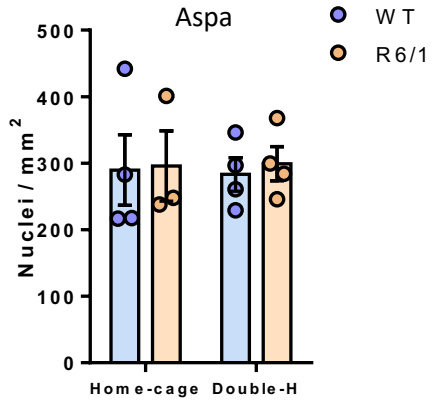
Aspa
WT
R6/1
Nuclei / mm2
500
400
300
200
100
0
Home-cage
Double-H

c

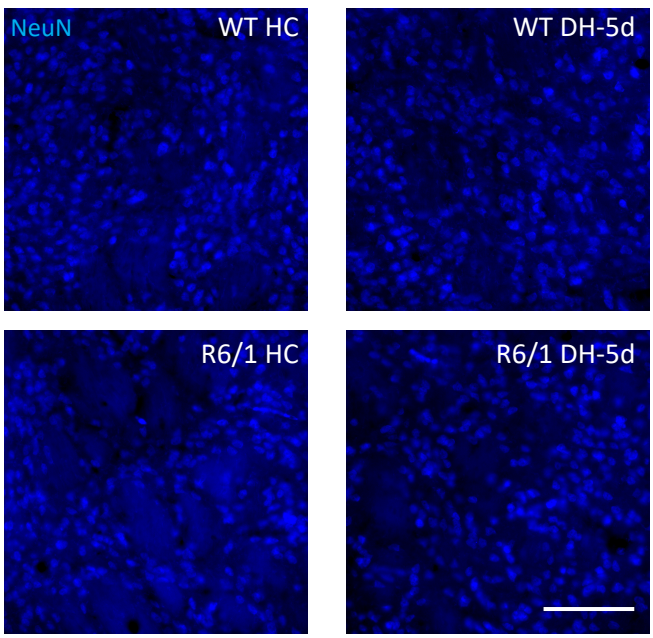
NeuN
WT HC
WT DH-5d
R6/1 HC
R6/1 DH-5d

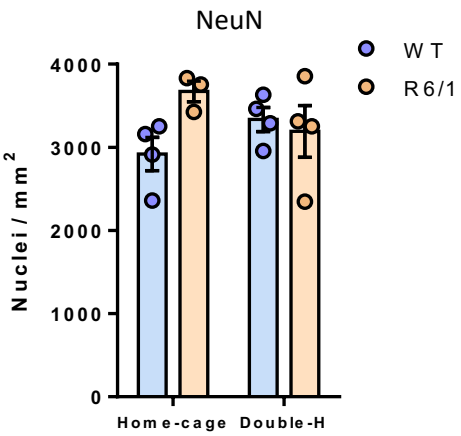
NeuN
WT
R6/1
Nuclei / mm2
4000
3000
2000
1000
0
Home-cage
Double-H

Supplementary Fig. 12. PDGDRα, ASPA and NeuN positive cell numbers in WT and R6/1 mice striatum do not differ between genotypes or after striatal procedural learning task performance. (a-c) Immunohistological counting results of PDGFRα (**a**), ASPA (**b**) and NeuN (**c**) positive cells in WT and R6/1 mice striatum at basal (home-cage, HC) and learning/memory (double-H 5 days, DH-5d) conditions. On the left, representative images are shown for PDGFRα (red, **a**), ASPA (green, **b**) and NeuN (blue, **c**). On the right, , bargraphs showing the total number of PDGFRα (**a**), ASPA (**b**) and NeuN (**c**) positive cells per mm^2 as a mean ± sem in WT (blue) and R6/1 (orange) mice striatum at basal (home-cage, HC) or in learning (double-H 5 days, DH-5d) conditions (WT HC N=4, WT DH-5d N=4, R6/1 HC N=3, R6/1 DH-5d N=4). Individual values are depicted as circles. Data were analysed using two-way Anova and multiple comparisons used the Bonferroni's post-hoc test.

…… Bibliography ……

Bibliography

A novel gene containing a trinucleotide repeat that is expanded and unstable on Huntington's disease chromosomes. The Huntington's Disease Collaborative Research Group., 1993. . Cell 72, 971–83. https://doi.org/10.1016/0092-8674(93)90585-e

Abd-Elrahman, K.S., Hamilton, A., Hutchinson, S.R., Liu, F., Russell, R.C., Ferguson, S.S.G., 2017. mGluR5 antagonism increases autophagy and prevents disease progression in the zQ175 mouse model of Huntington's disease. Sci. Signal. 10, eaan6387. https://doi.org/10.1126/scisignal.aan6387

Achour, M., Le Gras, S., Keime, C., Parmentier, F., Lejeune, F.-X., Boutillier, A.-L., Neri, C., Davidson, I., Merienne, K., 2015. Neuronal identity genes regulated by super-enhancers are preferentially down-regulated in the striatum of Huntington's disease mice. Hum. Mol. Genet. 24, 3481–3496. https://doi.org/10.1093/hmg/ddv099

Achour, Mayada, Le Gras, S., Keime, C., Parmentier, F., Lejeune, F.-X., Boutillier, A.-L., Néri, C., Davidson, I., Merienne, K., 2015. Neuronal identity genes regulated by super-enhancers are preferentially down-regulated in the striatum of Huntington's disease mice. Hum. Mol. Genet. 24, 3481–96. https://doi.org/10.1093/hmg/ddv099

Adli, M., 2018. The CRISPR tool kit for genome editing and beyond. Nat. Commun. 9, 1911. https://doi.org/10.1038/s41467-018-04252-2

Affolter, M., Montagne, J., Walldorf, U., Groppe, J., Kloter, U., LaRosa, M., Gehring, W.J., 1994. The Drosophila SRF homolog is expressed in a subset of tracheal cells and maps within a genomic region required for tracheal development. Development 120, 743–53.

Agustín-Pavón, C., Mielcarek, M., Garriga-Canut, M., Isalan, M., 2016. Deimmunization for gene therapy: host matching of synthetic zinc finger constructs enables long-term mutant Huntingtin repression in mice. Mol. Neurodegener. 11, 64. https://doi.org/10.1186/s13024-016-0128-x

Aidt, F.H., Nielsen, S.M.B., Kanters, J., Pesta, D., Nielsen, T.T., Nørremølle, A., Hasholt, L., Christiansen, M., Hagen, C.M., 2013. Dysfunctional mitochondrial respiration in the striatum of the Huntington's disease transgenic R6/2 mouse model. PLoS Curr. https://doi.org/10.1371/currents.hd.d8917b4862929772c5a2f2a34ef1c201

Alarcón, J.M., Malleret, G., Touzani, K., Vronskaya, S., Ishii, S., Kandel, E.R., Barco, A., 2004. Chromatin Acetylation, Memory, and LTP Are Impaired in CBP+/− Mice. Neuron 42, 947–959. https://doi.org/10.1016/j.neuron.2004.05.021

Alberti, S., Krause, S.M., Kretz, O., Philippar, U., Lemberger, T., Casanova, E., Wiebel, F.F., Schwarz, H., Frotscher, M., Schutz, G., Nordheim, A., 2005. Neuronal migration in the murine rostral migratory stream requires serum response factor. Proc. Natl. Acad. Sci. 102, 6148–6153. https://doi.org/10.1073/pnas.0501191102

Albin, R.L., Reiner, A., Anderson, K.D., Dure, L.S., Handelin, B., Balfour, R., Whetsell, W.O., Penney, J.B., Young, A.B., 1992. Preferential loss of striato-external pallidal projection neurons in presymptomatic Huntington's disease. Ann. Neurol. 31, 425–430. https://doi.org/10.1002/ana.410310412

Alcalá-Vida, R., Seguin, J., Lotz, C., Molitor, A.M., Irastorza-Azcarate, I., Awada, A., Karasu, N.,

Bombardier, A., Cosquer, B., Skarmeta, J.L.G., Cassel, J.-C., Boutillier, A.-L., Sexton, T., Merienne, K., 2021. Age-related and disease locus-specific mechanisms contribute to early remodelling of chromatin structure in Huntington's disease mice. Nat. Commun. 12, 364. https://doi.org/10.1038/s41467-020-20605-2

Alcalá-Vida, R., Garcia-Forn, M., Castany-Pladevall, C., Creus-Muncunill, J., Ito, Y., Blanco, E., Golbano, A., Crespí-Vázquez, K., Parry, A., Slater, G., Samarajiwa, S., Peiró, S., Di Croce, L., Narita, M., Pérez-Navarro, E., 2020. Neuron type-specific increase in lamin B1 contributes to nuclear dysfunction in Huntington's disease. EMBO Mol. Med. https://doi.org/10.15252/emmm.202012105

Allis, C.D., Jenuwein, T., 2016. The molecular hallmarks of epigenetic control. Nat. Rev. Genet. 17, 487–500. https://doi.org/10.1038/nrg.2016.59

Ambrose, C.M., Duyao, M.P., Barnes, G., Bates, G.P., Lin, C.S., Srinidhi, J., Baxendale, S., Hummerich, H., Lehrach, H., Altherr, M., Wasmuth, J., Buckler, A., Church, D., Housman, D., Berks, M., Micklem, G., Durbin, R., Dodge, A., Read, A., Gusella, J., MacDonald, M.E., 1994. Structure and expression of the Huntington's disease gene: Evidence against simple inactivation due to an expanded CAG repeat. Somat. Cell Mol. Genet. 20, 27–38. https://doi.org/10.1007/BF02257483

An, M.C., O'Brien, R.N., Zhang, N., Patra, B.N., De La Cruz, M., Ray, A., Ellerby, L.M., 2014. Polyglutamine Disease Modeling: Epitope Based Screen for Homologous Recombination using CRISPR/Cas9 System. PLoS Curr. https://doi.org/10.1371/currents.hd.0242d2e7ad72225efa72f6964589369a

An, M.C., Zhang, N., Scott, G., Montoro, D., Wittkop, T., Mooney, S., Melov, S., Ellerby, L.M., 2012. Genetic Correction of Huntington's Disease Phenotypes in Induced Pluripotent Stem Cells. Cell Stem Cell 11, 253–263. https://doi.org/10.1016/j.stem.2012.04.026

Anders, S., Pyl, P.T., Huber, W., 2015. HTSeq--a Python framework to work with high-throughput sequencing data. Bioinformatics 31, 166–169. https://doi.org/10.1093/bioinformatics/btu638

Andrade, M.A., Bork, P., 1995. HEAT repeats in the Huntington's disease protein. Nat. Genet. 11, 115–116. https://doi.org/10.1038/ng1095-115

Andre, V.M., Cepeda, C., Fisher, Y.E., Huynh, M., Bardakjian, N., Singh, S., Yang, X.W., Levine, M.S., 2011. Differential Electrophysiological Changes in Striatal Output Neurons in Huntington's Disease. J. Neurosci. 31, 1170–1182. https://doi.org/10.1523/JNEUROSCI.3539-10.2011

Andrew, S.E., Paul Goldberg, Y., Kremer, B., Telenius, H., Theilmann, J., Adam, S., Starr, E., Squitieri, F., Lin, B., Kalchman, M.A., Graham, R.K., Hayden, M.R., 1993. The relationship between trinucleotide (CAG) repeat length and clinical features of Huntington's disease. Nat. Genet. 4, 398–403. https://doi.org/10.1038/ng0893-398

Andrews, S.C., Domínguez, J.F., Mercieca, E.-C., Georgiou-Karistianis, N., Stout, J.C., 2015. Cognitive interventions to enhance neural compensation in Huntington's disease. Neurodegener. Dis. Manag. 5, 155–164. https://doi.org/10.2217/nmt.14.58

Angelini, A., Li, Z., Mericskay, M., Decaux, J.-F., 2015. Regulation of Connective Tissue Growth Factor and Cardiac Fibrosis by an SRF/MicroRNA-133a Axis. PLoS One 10, e0139858. https://doi.org/10.1371/journal.pone.0139858

Anglada-Huguet, M., Giralt, A., Perez-Navarro, E., Alberch, J., Xifró, X., 2012. Activation of Elk-1

participates as a neuroprotective compensatory mechanism in models of Huntington's disease. J. Neurochem. 121, 639–648. https://doi.org/10.1111/j.1471-4159.2012.07711.x

Angstenberger, M., Wegener, J.W., Pichler, B.J., Judenhofer, M.S., Feil, S., Alberti, S., Feil, R., Nordheim, A., 2007. Severe Intestinal Obstruction on Induced Smooth Muscle–Specific Ablation of the Transcription Factor SRF in Adult Mice. Gastroenterology 133, 1948–1959. https://doi.org/10.1053/j.gastro.2007.08.078

Aoyama, K., Suh, S.W., Hamby, A.M., Liu, J., Chan, W.Y., Chen, Y., Swanson, R.A., 2006. Neuronal glutathione deficiency and age-dependent neurodegeneration in the EAAC1 deficient mouse. Nat. Neurosci. 9, 119–126. https://doi.org/10.1038/nn1609

Arango, M., 2006. CA150 Expression Delays Striatal Cell Death in Overexpression and Knock-In Conditions for Mutant Huntingtin Neurotoxicity. J. Neurosci. 26, 4649–4659. https://doi.org/10.1523/JNEUROSCI.5409-05.2006

Arenas, J., Campos, Y., Ribacoba, R., Martín, M.A., Rubio, J.C., Ablanedo, P., Cabello, A., 1998. Complex I Defect in muscle from patients with Huntington's disease. Ann. Neurol. 43, 397–400. https://doi.org/10.1002/ana.410430321

Aretouli, E., Brandt, J., 2010. Episodic Memory in Dementia: Characteristics of New Learning that Differentiate Alzheimer's, Huntington's, and Parkinson's Diseases. Arch. Clin. Neuropsychol. 25, 396–409. https://doi.org/10.1093/arclin/acq038

Arner, E., Daub, C.O., Vitting-Seerup, K., Andersson, R., Lilje, B., Drabløs, F., Lennartsson, A., Rönnerblad, M., Hrydziuszko, O., Vitezic, M., Freeman, T.C., M. N. Alhendi, A., Arner, P., Axton, R., Baillie, J.K., Beckhouse, A., Bodega, B., Briggs, J., Brombacher, F., Davis, M., Detmar, M., Ehrlund, A., Endoh, M., Eslami, A., Fagiolini, M., Fairbairn, L., Faulkner, G.J., Ferrai, C., Fisher, M.E., Forrester, L., Goldowitz, D., Guler, R., Ha, T., Hara, M., Herlyn, M., Ikawa, T., Kai, C., Kawamoto, H., M. Khachigian, L., Klinken, S.P., Kojima, S., Koseki, H., Klein, S., Mejhert, N., Miyaguchi, K., Mizuno, Y., Morimoto, M., Morris, K.J., Mummery, C., Nakachi, Y., Ogishima, S., Okada-Hatakeyama, M., Okazaki, Y., Orlando, V., Ovchinnikov, D., Passier, R., Patrikakis, M., Pombo, A., Qin, X.-Y., Roy, S., Sato, H., Savvi, S., Saxena, A., Schwegmann, A., Sugiyama, D., Swoboda, R., Tanaka, H., Tomoiu, A., Winteringham, L.N., Wolvetang, E., Yanagi-Mizuochi, C., Yoneda, M., Zabierowski, S., Zhang, P., Abugessaisa, I., Bertin, N., Diehl, A.D., Fukuda, S., Furuno, M., Harshbarger, J., Hasegawa, A., Hori, F., Ishikawa-Kato, S., Ishizu, Y., Itoh, M., Kawashima, T., Kojima, M., Kondo, N., Lizio, M., Meehan, T.F., Mungall, C.J., Murata, M., Nishiyori-Sueki, H., Sahin, S., Nagao-Sato, S., Severin, J., de Hoon, M.J.L., Kawai, J., Kasukawa, T., Lassmann, T., Suzuki, H., Kawaji, H., Summers, K.M., Wells, C., Hume, D.A., Forrest, A.R.R., Sandelin, A., Carninci, P., Hayashizaki, Y., 2015. Transcribed enhancers lead waves of coordinated transcription in transitioning mammalian cells. Science (80-.). 347, 1010–1014. https://doi.org/10.1126/science.1259418

Arrasate, M., Mitra, S., Schweitzer, E.S., Segal, M.R., Finkbeiner, S., 2004. Inclusion body formation reduces levels of mutant huntingtin and the risk of neuronal death. Nature 431, 805–810. https://doi.org/10.1038/nature02998

Arsenian, S., Weinhold, B., Oelgeschläger, M., Rüther, U., Nordheim, A., 1998. Serum response factor is essential for mesoderm formation during mouse embryogenesis. EMBO J. 17, 6289–6299. https://doi.org/10.1093/emboj/17.21.6289

Ashburner, M., Ball, C.A., Blake, J.A., Botstein, D., Butler, H., Cherry, J.M., Davis, A.P., Dolinski, K., Dwight, S.S., Eppig, J.T., Harris, M.A., Hill, D.P., Issel-Tarver, L., Kasarskis, A., Lewis, S., Matese, J.C., Richardson, J.E., Ringwald, M., Rubin, G.M., Sherlock, G., 2000. Gene Ontology: tool for the unification of biology. Nat. Genet. 25, 25–29. https://doi.org/10.1038/75556

Atwal, R.S., Desmond, C.R., Caron, N., Maiuri, T., Xia, J., Sipione, S., Truant, R., 2011. Kinase inhibitors modulate huntingtin cell localization and toxicity. Nat. Chem. Biol. 7, 453–460. https://doi.org/10.1038/nchembio.582

Atwal, R.S., Xia, J., Pinchev, D., Taylor, J., Epand, R.M., Truant, R., 2007. Huntingtin has a membrane association signal that can modulate huntingtin aggregation, nuclear entry and toxicity. Hum. Mol. Genet. 16, 2600–2615. https://doi.org/10.1093/hmg/ddm217

Augood, S.J., Faull, R.L.M., Emson, P.C., 1997. Dopamine D1 and D2 receptor gene expression in the striatum in Huntington's disease. Ann. Neurol. 42, 215–221. https://doi.org/10.1002/ana.410420213

Aurnhammer, C., Haase, M., Muether, N., Hausl, M., Rauschhuber, C., Huber, I., Nitschko, H., Busch, U., Sing, A., Ehrhardt, A., Baiker, A., 2012. Universal Real-Time PCR for the Detection and Quantification of Adeno-Associated Virus Serotype 2-Derived Inverted Terminal Repeat Sequences. Hum. Gene Ther. Methods 23, 18–28. https://doi.org/10.1089/hgtb.2011.034

Bachoud-Lévi, A.-C., Gaura, V., Brugières, P., Lefaucheur, J.-P., Boissé, M.-F., Maison, P., Baudic, S., Ribeiro, M.-J., Bourdet, C., Remy, P., Cesaro, P., Hantraye, P., Peschanski, M., 2006. Effect of fetal neural transplants in patients with Huntington's disease 6 years after surgery: a long-term follow-up study. Lancet Neurol. 5, 303–309. https://doi.org/10.1016/S1474-4422(06)70381-7

Bachoud-Lévi, A.-C., Rémy, P., Nguyen, J.-P., Brugières, P., Lefaucheur, J.-P., Bourdet, C., Baudic, S., Gaura, V., Maison, P., Haddad, B., Boissé, M.-F., Grandmougin, T., Jény, R., Bartolomeo, P., Barba, G.D., Degos, J.-D., Lisovoski, F., Ergis, A.-M., Pailhous, E., Cesaro, P., Hantraye, P., Peschanski, M., 2000. Motor and cognitive improvements in patients with Huntington's disease after neural transplantation. Lancet 356, 1975–1979. https://doi.org/10.1016/S0140-6736(00)03310-9

Bading, H., Ginty, D., Greenberg, M., 1993. Regulation of gene expression in hippocampal neurons by distinct calcium signaling pathways. Science (80-.). 260, 181–186. https://doi.org/10.1126/science.8097060

Bai, G., Cheung, I., Shulha, H.P., Coelho, J.E., Li, P., Dong, X., Jakovcevski, M., Wang, Y., Grigorenko, A., Jiang, Y., Hoss, A., Patel, K., Zheng, M., Rogaev, E., Myers, R.H., Weng, Z., Akbarian, S., Chen, J.-F., 2015. Epigenetic dysregulation of hairy and enhancer of split 4 (HES4) is associated with striatal degeneration in postmortem Huntington brains. Hum. Mol. Genet. 24, 1441–1456. https://doi.org/10.1093/hmg/ddu561

Balleine, B., Ball, J., Dickinson, A., 1994. Benzodiazepine-induced outcome revaluation and the motivational control of instrumental action in rats. Behav. Neurosci. 108, 573–589. https://doi.org/10.1037/0735-7044.108.3.573

Balleine, B.W., O'Doherty, J.P., 2010. Human and Rodent Homologies in Action Control: Corticostriatal Determinants of Goal-Directed and Habitual Action. Neuropsychopharmacology 35, 48–69. https://doi.org/10.1038/npp.2009.131

Bañez-Coronel, M., Ayhan, F., Tarabochia, A.D., Zu, T., Perez, B.A., Tusi, S.K., Pletnikova, O., Borchelt, D.R., Ross, C.A., Margolis, R.L., Yachnis, A.T., Troncoso, J.C., Ranum, L.P.W., 2015. RAN Translation in Huntington Disease. Neuron 88, 667–677. https://doi.org/10.1016/j.neuron.2015.10.038

Bannister, A.J., Kouzarides, T., 2011. Regulation of chromatin by histone modifications. Cell Res. 21, 381–395. https://doi.org/10.1038/cr.2011.22

Baquet, Z.C., 2004. Early Striatal Dendrite Deficits followed by Neuron Loss with Advanced Age in the Absence of Anterograde Cortical Brain-Derived Neurotrophic Factor. J. Neurosci. 24, 4250–4258. https://doi.org/10.1523/JNEUROSCI.3920-03.2004

Barco, A., Pittenger, C., Kandel, E.R., 2003. CREB, memory enhancement and the treatment of memory disorders: promises, pitfalls and prospects. Expert Opin. Ther. Targets 7, 101–114. https://doi.org/10.1517/14728222.7.1.101

Barnat, M., Le Friec, J., Benstaali, C., Humbert, S., 2017. Huntingtin-Mediated Multipolar-Bipolar Transition of Newborn Cortical Neurons Is Critical for Their Postnatal Neuronal Morphology. Neuron 93, 99–114. https://doi.org/10.1016/j.neuron.2016.11.035

Barnes, G.T., Duyao, M.P., Ambrose, C.M., McNeil, S., Persichetti, F., Srinidhi, J., Gusella, J.F., MacDonald, M.E., 1994. Mouse Huntington's disease gene homolog (Hdh). Somat. Cell Mol. Genet. 20, 87–97. https://doi.org/10.1007/BF02290678

Barrett, R.M., Malvaez, M., Kramar, E., Matheos, D.P., Arrizon, A., Cabrera, S.M., Lynch, G., Greene, R.W., Wood, M.A., 2011. Hippocampal Focal Knockout of CBP Affects Specific Histone Modifications, Long-Term Potentiation, and Long-Term Memory. Neuropsychopharmacology 36, 1545–1556. https://doi.org/10.1038/npp.2011.61

Barry, J., Akopian, G., Cepeda, C., Levine, M.S., 2018. Striatal Direct and Indirect Pathway Output Structures Are Differentially Altered in Mouse Models of Huntington's Disease. J. Neurosci. 38, 4678–4694. https://doi.org/10.1523/JNEUROSCI.0434-18.2018

Bashir, H., Jankovic, J., 2018. Deutetrabenazine for the treatment of Huntington's chorea. Expert Rev. Neurother. 18, 625–631. https://doi.org/10.1080/14737175.2018.1500178

Bates, Gillian P, Dorsey, R., Gusella, J.F., Hayden, M.R., Kay, C., Leavitt, B.R., Nance, M., Ross, C.A., Scahill, R.I., Wetzel, R., Wild, E.J., Tabrizi, S.J., 2015. Huntington disease. Nat. Rev. Dis. Prim. 1, 15005. https://doi.org/10.1038/nrdp.2015.5

Bates, Gillian P., Dorsey, R., Gusella, J.F., Hayden, M.R., Kay, C., Leavitt, B.R., Nance, M., Ross, C.A., Scahill, R.I., Wetzel, R., Wild, E.J., Tabrizi, S.J., 2015. Huntington disease. Nat. Rev. Dis. Prim. 1, 15005. https://doi.org/10.1038/nrdp.2015.5

Baxa, M., Hruska-Plochan, M., Juhas, S., Vodicka, P., Pavlok, A., Juhasova, J., Miyanohara, A., Nejime, T., Klima, J., Macakova, M., Marsala, S., Weiss, A., Kubickova, S., Musilova, P., Vrtel, R., Sontag, E.M., Thompson, L.M., Schier, J., Hansikova, H., Howland, D.S., Cattaneo, E., DiFiglia, M., Marsala, M., Motlik, J., 2013. A Transgenic Minipig Model of Huntington's Disease. J. Huntingtons. Dis. 2, 47–68. https://doi.org/10.3233/JHD-130001

Baxendale, S., Abdulla, S., Elgar, G., Buck, D., Berks, M., Micklem, G., Durbin, R., Bates, G., Brenner, S., Beck, S., Lehrach, H., 1995. Comparative sequence analysis of the human and pufferfish

Huntington's disease genes. Nat. Genet. 10, 67–76. https://doi.org/10.1038/ng0595-67

Bayram-Weston, Z., Jones, L., Dunnett, S.B., Brooks, S.P., 2012. Light and electron microscopic characterization of the evolution of cellular pathology in YAC128 Huntington's disease transgenic mice. Brain Res. Bull. 88, 137–147. https://doi.org/10.1016/j.brainresbull.2011.05.005

Beal, M., Brouillet, E., Jenkins, B., Ferrante, R., Kowall, N., Miller, J., Storey, E., Srivastava, R., Rosen, B., Hyman, B., 1993. Neurochemical and histologic characterization of striatal excitotoxic lesions produced by the mitochondrial toxin 3-nitropropionic acid. J. Neurosci. 13, 4181–4192. https://doi.org/10.1523/JNEUROSCI.13-10-04181.1993

Beal, M., Ferrante, R., Swartz, K., Kowall, N., 1991. Chronic quinolinic acid lesions in rats closely resemble Huntington's disease. J. Neurosci. 11, 1649–1659. https://doi.org/10.1523/JNEUROSCI.11-06-01649.1991

Beal, M.F., 1992. Does impairment of energy metabolism result in excitotoxic neuronal death in neurodegenerative illnesses? Ann. Neurol. 31, 119–130. https://doi.org/10.1002/ana.410310202

Beal, M.F., Hyman, B.T., Koroshetz, W., 1993. Do defecs in mitochondrial energy metabolism underlie the pathology of neurodegenerative diseases? Trends Neurosci. 16, 125–131. https://doi.org/10.1016/0166-2236(93)90117-5

Beal, M.F., Kowall, N.W., Ellison, D.W., Mazurek, M.F., Swartz, K.J., Martin, J.B., 1986. Replication of the neurochemical characteristics of Huntington's disease by quinolinic acid. Nature 321, 168–171. https://doi.org/10.1038/321168a0

Bečanović, K., Nørremølle, A., Neal, S.J., Kay, C., Collins, J.A., Arenillas, D., Lilja, T., Gaudenzi, G., Manoharan, S., Doty, C.N., Beck, J., Lahiri, N., Portales-Casamar, E., Warby, S.C., Connolly, C., De Souza, R.A.G., Tabrizi, S.J., Hermanson, O., Langbehn, D.R., Hayden, M.R., Wasserman, W.W., Leavitt, B.R., 2015. A SNP in the HTT promoter alters NF-κB binding and is a bidirectional genetic modifier of Huntington disease. Nat. Neurosci. 18, 807–816. https://doi.org/10.1038/nn.4014

Beck, H., Flynn, K., Lindenberg, K.S., Schwarz, H., Bradke, F., Di Giovanni, S., Knöll, B., 2012. Serum Response Factor (SRF)-cofilin-actin signaling axis modulates mitochondrial dynamics. Proc. Natl. Acad. Sci. 109, E2523–E2532. https://doi.org/10.1073/pnas.1208141109

Belaguli, N.S., Schildmeyer, L.A., Schwartz, R.J., 1997. Organization and Myogenic Restricted Expression of the Murine Serum Response Factor Gene. J. Biol. Chem. 272, 18222–18231. https://doi.org/10.1074/jbc.272.29.18222

Belaguli, N.S., Zhou, W., Trinh, T.-H.T., Majesky, M.W., Schwartz, R.J., 1999. Dominant Negative Murine Serum Response Factor: Alternative Splicing within the Activation Domain Inhibits Transactivation of Serum Response Factor Binding Targets. Mol. Cell. Biol. 19, 4582–4591. https://doi.org/10.1128/MCB.19.7.4582

Benchoua, A., Trioulier, Y., Zala, D., Gaillard, M.-C., Lefort, N., Dufour, N., Saudou, F., Elalouf, J.-M., Hirsch, E., Hantraye, P., Déglon, N., Brouillet, E., 2006. Involvement of Mitochondrial Complex II Defects in Neuronal Death Produced by N-Terminus Fragment of Mutated Huntingtin. Mol. Biol. Cell 17, 1652–1663. https://doi.org/10.1091/mbc.e05-07-0607

Bennett, C.F., Swayze, E.E., 2010. RNA Targeting Therapeutics: Molecular Mechanisms of Antisense

Oligonucleotides as a Therapeutic Platform. Annu. Rev. Pharmacol. Toxicol. 50, 259–293. https://doi.org/10.1146/annurev.pharmtox.010909.105654

Berger, A., Lorain, S., Joséphine, C., Desrosiers, M., Peccate, C., Voit, T., Garcia, L., Sahel, J.-A., Bemelmans, A.-P., 2015. Repair of Rhodopsin mRNA by Spliceosome-Mediated RNA Trans -Splicing: A New Approach for Autosomal Dominant Retinitis Pigmentosa. Mol. Ther. 23, 918–930. https://doi.org/10.1038/mt.2015.11

Besnard, A., Galan-Rodriguez, B., Vanhoutte, P., Caboche, J., 2011. Elk-1 a Transcription Factor with Multiple Facets in the Brain. Front. Neurosci. 5. https://doi.org/10.3389/fnins.2011.00035

BOLAM, J.P., HANLEY, J.J., BOOTH, P.A.C., BEVAN, M.D., 2000. Synaptic organisation of the basal ganglia. J. Anat. 196, 527–542. https://doi.org/10.1046/j.1469-7580.2000.19640527.x

Bonni, A., Ginty, D.D., Dudek, H., Greenberg, M.E., 1995. Serine 133-Phosphorylated CREB Induces Transcription via a Cooperative Mechanism That May Confer Specificity to Neurotrophin Signals. Mol. Cell. Neurosci. 6, 168–183. https://doi.org/10.1006/mcne.1995.1015

Bonvento, G., Valette, J., Flament, J., Mochel, F., Brouillet, E., 2017. Imaging and spectroscopic approaches to probe brain energy metabolism dysregulation in neurodegenerative diseases. J. Cereb. Blood Flow Metab. 37, 1927–1943. https://doi.org/10.1177/0271678X17697989

Borrelli, E., Nestler, E.J., Allis, C.D., Sassone-Corsi, P., 2008. Decoding the Epigenetic Language of Neuronal Plasticity. Neuron 60, 961–974. https://doi.org/10.1016/j.neuron.2008.10.012

Bousiges, O., Vasconcelos, A.P. de, Neidl, R., Cosquer, B., Herbeaux, K., Panteleeva, I., Loeffler, J.-P., Cassel, J.-C., Boutillier, A.-L., 2010. Spatial Memory Consolidation is Associated with Induction of Several Lysine-Acetyltransferase (Histone Acetyltransferase) Expression Levels and H2B/H4 Acetylation-Dependent Transcriptional Events in the Rat Hippocampus. Neuropsychopharmacology 35, 2521–2537. https://doi.org/10.1038/npp.2010.117

Boussicault, L., Alves, S., Lamazière, A., Planques, A., Heck, N., Moumné, L., Despres, G., Bolte, S., Hu, A., Pagès, C., Galvan, L., Piguet, F., Aubourg, P., Cartier, N., Caboche, J., Betuing, S., 2016. CYP46A1, the rate-limiting enzyme for cholesterol degradation, is neuroprotective in Huntington's disease. Brain 139, 953–970. https://doi.org/10.1093/brain/awv384

Boussicault, L., Kacher, R., Lamazière, A., Vanhoutte, P., Caboche, J., Betuing, S., Potier, M.-C., 2018. CYP46A1 protects against NMDA-mediated excitotoxicity in Huntington's disease: Analysis of lipid raft content. Biochimie 153, 70–79. https://doi.org/10.1016/j.biochi.2018.07.019

Boutell, J.M., Thomas, P., Neal, J.W., Weston, V.J., Duce, J., Harper, P.S., Lesley Jones, A., 1999. Aberrant Interactions of Transcriptional Repressor Proteins with the Huntington's Disease Gene Product, Huntingtin. Hum. Mol. Genet. 8, 1647–1655. https://doi.org/10.1093/hmg/8.9.1647

Bramham, C.R., Worley, P.F., Moore, M.J., Guzowski, J.F., 2008. The Immediate Early Gene Arc/Arg3.1: Regulation, Mechanisms, and Function. J. Neurosci. 28, 11760–11767. https://doi.org/10.1523/JNEUROSCI.3864-08.2008

Brennan, W.A., Bird, E.D., Aprille, J.R., 1985. Regional Mitochondrial Respiratory Activity in Huntington's Disease Brain. J. Neurochem. 44, 1948–1950. https://doi.org/10.1111/j.1471-4159.1985.tb07192.x

Bridi, M.S., Hawk, J.D., Chatterjee, S., Safe, S., Abel, T., 2017. Pharmacological Activators of the NR4A Nuclear Receptors Enhance LTP in a CREB/CBP-Dependent Manner. Neuropsychopharmacology 42, 1243–1253. https://doi.org/10.1038/npp.2016.253

Brimblecombe, K.R., Cragg, S.J., 2017. The Striosome and Matrix Compartments of the Striatum: A Path through the Labyrinth from Neurochemistry toward Function. ACS Chem. Neurosci. 8, 235–242. https://doi.org/10.1021/acschemneuro.6b00333

Brivanlou, A.H., 2002. Signal Transduction and the Control of Gene Expression. Science (80-.). 295, 813–818. https://doi.org/10.1126/science.1066355

Broadbent, N.J., Squire, L.R., Clark, R.E., 2007. Rats depend on habit memory for discrimination learning and retention. Learn. Mem. 14, 145–151. https://doi.org/10.1101/lm.455607

Brooks, S.P., Dunnett, S.B., 2009a. Tests to assess motor phenotype in mice: a user's guide. Nat. Rev. Neurosci. 10, 519–529. https://doi.org/10.1038/nrn2652

Brooks, S.P., Dunnett, S.B., 2009b. Tests to assess motor phenotype in mice: a user's guide. Nat. Rev. Neurosci. 10, 519–529. https://doi.org/10.1038/nrn2652

Brooks, S.P., Janghra, N., Workman, V.L., Bayram-Weston, Z., Jones, L., Dunnett, S.B., 2012. Longitudinal analysis of the behavioural phenotype in R6/1 (C57BL/6J) Huntington's disease transgenic mice. Brain Res. Bull. 88, 94–103. https://doi.org/10.1016/j.brainresbull.2011.01.010

Brouillet, E., 1999. Replicating Huntington's disease phenotype in experimental animals. Prog. Neurobiol. 59, 427–468. https://doi.org/10.1016/S0301-0082(99)00005-2

Brouillet, E., Hantraye, P., Ferrante, R.J., Dolan, R., Leroy-Willig, A., Kowall, N.W., Beal, M.F., 1995. Chronic mitochondrial energy impairment produces selective striatal degeneration and abnormal choreiform movements in primates. Proc. Natl. Acad. Sci. 92, 7105–7109. https://doi.org/10.1073/pnas.92.15.7105

Brouillet, E., Jenkins, B.G., Hyman, B.T., Ferrante, R.J., Kowall, N.W., Srivastava, R., Roy, D.S., Rosen, B.R., Beal, M.F., 1993. Age-Dependent Vulnerability of the Striatum to the Mitochondrial Toxin 3-Nitropropionic Acid. J. Neurochem. 60, 356–359. https://doi.org/10.1111/j.1471-4159.1993.tb05859.x

Browne, S.E., Bowling, A.C., Macgarvey, U., Baik, M.J., Berger, S.C., Muquit, M.M.K., Bird, E.D., Beal, M.F., 1997. Oxidative damage and metabolic dysfunction in Huntington's disease: Selective vulnerability of the basal ganglia. Ann. Neurol. 41, 646–653. https://doi.org/10.1002/ana.410410514

Brustovetsky, N., 2016. Mutant Huntingtin and Elusive Defects in Oxidative Metabolism and Mitochondrial Calcium Handling. Mol. Neurobiol. 53, 2944–2953. https://doi.org/10.1007/s12035-015-9188-0

Buchwalter, G., Gross, C., Wasylyk, B., 2005. The Ternary Complex Factor Net Regulates Cell Migration through Inhibition of PAI-1 Expression. Mol. Cell. Biol. 25, 10853–10862. https://doi.org/10.1128/MCB.25.24.10853-10862.2005

Buchwalter, G., Gross, C., Wasylyk, B., 2004. Ets ternary complex transcription factors. Gene 324, 1–14.

https://doi.org/10.1016/j.gene.2003.09.028

Butterworth, J., Yates, C.M., Reynolds, G.P., 1985. Distribution of phosphate-activated glutaminase, succinic dehydrogenase, pyruvate dehydrogenase and γ-glutamyl transpeptidase in post-mortem brain from Huntington's disease and agonal cases. J. Neurol. Sci. 67, 161–171. https://doi.org/10.1016/0022-510X(85)90112-1

Cabeza, R., Nyberg, L., 2000. Neural bases of learning and memory: functional neuroimaging evidence. Curr. Opin. Neurol. 13, 415–421. https://doi.org/10.1097/00019052-200008000-00008

Campbell, R.R., Wood, M.A., 2019. How the epigenome integrates information and reshapes the synapse. Nat. Rev. Neurosci. 20, 133–147. https://doi.org/10.1038/s41583-019-0121-9

Canals, J.M., 2004. Brain-Derived Neurotrophic Factor Regulates the Onset and Severity of Motor Dysfunction Associated with Enkephalinergic Neuronal Degeneration in Huntington's Disease. J. Neurosci. 24, 7727–7739. https://doi.org/10.1523/JNEUROSCI.1197-04.2004

Cao, C., Temel, Y., Blokland, A., Ozen, H., Steinbusch, H.W.M., Vlamings, R., Nguyen, H.P., von Hörsten, S., Schmitz, C., Visser-Vandewalle, V., 2006. Progressive deterioration of reaction time performance and choreiform symptoms in a new Huntington's disease transgenic ratmodel. Behav. Brain Res. 170, 257–261. https://doi.org/10.1016/j.bbr.2006.02.028

Caplan, A.I., Dennis, J.E., 2006. Mesenchymal stem cells as trophic mediators. J. Cell. Biochem. 98, 1076–1084. https://doi.org/10.1002/jcb.20886

CARLEZONJR, W., DUMAN, R., NESTLER, E., 2005. The many faces of CREB. Trends Neurosci. 28, 436–445. https://doi.org/10.1016/j.tins.2005.06.005

Carmeliet, P., 2005. Angiogenesis in life, disease and medicine. Nature 438, 932–936. https://doi.org/10.1038/nature04478

Carnemolla, A., Fossale, E., Agostoni, E., Michelazzi, S., Calligaris, R., De Maso, L., Del Sal, G., MacDonald, M.E., Persichetti, F., 2009. Rrs1 Is Involved in Endoplasmic Reticulum Stress Response in Huntington Disease. J. Biol. Chem. 284, 18167–18173. https://doi.org/10.1074/jbc.M109.018325

Caron, N.S., Dorsey, E.R., Hayden, M.R., 2018. Therapeutic approaches to Huntington disease: from the bench to the clinic. Nat. Rev. Drug Discov. 17, 729–750. https://doi.org/10.1038/nrd.2018.133

Carpenter, M.B., 1976. Anatomy of the basal ganglia and related nuclei: a review. Adv. Neurol. 14, 7–48.

Carter, R.J., Lione, L.A., Humby, T., Mangiarini, L., Mahal, A., Bates, G.P., Dunnett, S.B., Morton, A.J., 1999. Characterization of Progressive Motor Deficits in Mice Transgenic for the Human Huntington's Disease Mutation. J. Neurosci. 19, 3248–3257. https://doi.org/10.1523/JNEUROSCI.19-08-03248.1999

Cartier, N., Hacein-Bey-Abina, S., Bartholomae, C.C., Veres, G., Schmidt, M., Kutschera, I., Vidaud, M., Abel, U., Dal-Cortivo, L., Caccavelli, L., Mahlaoui, N., Kiermer, V., Mittelstaedt, D., Bellesme, C., Lahlou, N., Lefrere, F., Blanche, S., Audit, M., Payen, E., Leboulch, P., L'Homme, B., Bougneres, P., Von Kalle, C., Fischer, A., Cavazzana-Calvo, M., Aubourg, P., 2009. Hematopoietic Stem Cell Gene Therapy with a Lentiviral Vector in X-Linked Adrenoleukodystrophy. Science (80-.). 326, 818–823. https://doi.org/10.1126/science.1171242

Cassel, R., Kelche, C., Lecourtier, L., Cassel, J.-C., 2012. The match/mismatch of visuo-spatial cues between acquisition and retrieval contexts influences the expression of response vs. place memory in rats. Behav. Brain Res. 230, 333–342. https://doi.org/10.1016/j.bbr.2012.02.021

Castañé, A., Theobald, D.E.H., Robbins, T.W., 2010. Selective lesions of the dorsomedial striatum impair serial spatial reversal learning in rats. Behav. Brain Res. 210, 74–83. https://doi.org/10.1016/j.bbr.2010.02.017

Castro, D.C., Bruchas, M.R., 2019. A Motivational and Neuropeptidergic Hub: Anatomical and Functional Diversity within the Nucleus Accumbens Shell. Neuron 102, 529–552. https://doi.org/10.1016/j.neuron.2019.03.003

Cattaneo, E., 2001. Loss of normal huntingtin function: new developments in Huntington's disease research. Trends Neurosci. 24, 182–188. https://doi.org/10.1016/S0166-2236(00)01721-5

Cattaneo, E., Zuccato, C., Tartari, M., 2005. Normal huntingtin function: an alternative approach to Huntington's disease. Nat. Rev. Neurosci. 6, 919–930. https://doi.org/10.1038/nrn1806

Cavazzana-Calvo, M., 2000. Gene Therapy of Human Severe Combined Immunodeficiency (SCID)-X1 Disease. Science (80-.). 288, 669–672. https://doi.org/10.1126/science.288.5466.669

Cavazzana-Calvo, M., Payen, E., Negre, O., Wang, G., Hehir, K., Fusil, F., Down, J., Denaro, M., Brady, T., Westerman, K., Cavallesco, R., Gillet-Legrand, B., Caccavelli, L., Sgarra, R., Maouche-Chrétien, L., Bernaudin, F., Girot, R., Dorazio, R., Mulder, G.-J., Polack, A., Bank, A., Soulier, J., Larghero, J., Kabbara, N., Dalle, B., Gourmel, B., Socie, G., Chrétien, S., Cartier, N., Aubourg, P., Fischer, A., Cornetta, K., Galacteros, F., Beuzard, Y., Gluckman, E., Bushman, F., Hacein-Bey-Abina, S., Leboulch, P., 2010. Cavazzana-Calvo, Payen, et al. al. 2010. Nature 467, 318–322. https://doi.org/10.1038/nature09328

Cen, B., Selvaraj, A., Burgess, R.C., Hitzler, J.K., Ma, Z., Morris, S.W., Prywes, R., 2003. Megakaryoblastic Leukemia 1, a Potent Transcriptional Coactivator for Serum Response Factor (SRF), Is Required for Serum Induction of SRF Target Genes. Mol. Cell. Biol. 23, 6597–6608. https://doi.org/10.1128/MCB.23.18.6597-6608.2003

Cha, J.-H.J., 2007. Transcriptional signatures in Huntington's disease. Prog. Neurobiol. 83, 228–248. https://doi.org/10.1016/j.pneurobio.2007.03.004

Cha, J.-H.J., Kosinski, C.M., Kerner, J.A., Alsdorf, S.A., Mangiarini, L., Davies, S.W., Penney, J.B., Bates, G.P., Young, A.B., 1998. Altered brain neurotransmitter receptors in transgenic mice expressing a portion of an abnormal human Huntington disease gene. Proc. Natl. Acad. Sci. 95, 6480–6485. https://doi.org/10.1073/pnas.95.11.6480

Chai, J., Tarnawski, A.S., 2002. Serum response factor: discovery, biochemistry, biological roles and implications for tissue injury healing. J. Physiol. Pharmacol. 53, 147–57.

Chang, D.T.W., Rintoul, G.L., Pandipati, S., Reynolds, I.J., 2006. Mutant huntingtin aggregates impair mitochondrial movement and trafficking in cortical neurons. Neurobiol. Dis. 22, 388–400. https://doi.org/10.1016/j.nbd.2005.12.007

Chang, S.H., 2004. A Novel Role For Serum Response Factor in Neuronal Survival. J. Neurosci. 24, 2277–2285. https://doi.org/10.1523/JNEUROSCI.4868-03.2004

Chen, G., Zou, X., Watanabe, H., van Deursen, J.M., Shen, J., 2010. CREB Binding Protein Is Required for Both Short-Term and Long-Term Memory Formation. J. Neurosci. 30, 13066–13077. https://doi.org/10.1523/JNEUROSCI.2378-10.2010

Chen, Y., Carter, R.L., Cho, I.K., Chan, A.W.S., 2014. Cell-based therapies for Huntington's disease. Drug Discov. Today 19, 980–984. https://doi.org/10.1016/j.drudis.2014.02.012

Chen, Y., Liang, Z., Blanchard, J., Dai, C.-L., Sun, S., Lee, M.H., Grundke-Iqbal, I., Iqbal, K., Liu, F., Gong, C.-X., 2013. A Non-transgenic Mouse Model (icv-STZ Mouse) of Alzheimer's Disease: Similarities to and Differences from the Transgenic Model (3xTg-AD Mouse). Mol. Neurobiol. 47, 711–725. https://doi.org/10.1007/s12035-012-8375-5

Cheng, P.-H., Li, C.-L., Chang, Y.-F., Tsai, S.-J., Lai, Y.-Y., Chan, A.W.S., Chen, C.-M., Yang, S.-H., 2013. miR-196a Ameliorates Phenotypes of Huntington Disease in Cell, Transgenic Mouse, and Induced Pluripotent Stem Cell Models. Am. J. Hum. Genet. 93, 306–312. https://doi.org/10.1016/j.ajhg.2013.05.025

Chevrier, A.D., Noseworthy, M.D., Schachar, R., 2007. Dissociation of response inhibition and performance monitoring in the stop signal task using event-related fMRI. Hum. Brain Mapp. 28, 1347–1358. https://doi.org/10.1002/hbm.20355

Cho, K.J., Lee, B.I., Cheon, S.Y., Kim, H.W., Kim, H.J., Kim, G.W., 2009. Inhibition of apoptosis signal-regulating kinase 1 reduces endoplasmic reticulum stress and nuclear huntingtin fragments in a mouse model of Huntington disease. Neuroscience 163, 1128–34. https://doi.org/10.1016/j.neuroscience.2009.07.048

Cisbani, G., Freeman, T.B., Soulet, D., Saint-Pierre, M., Gagnon, D., Parent, M., Hauser, R.A., Barker, R.A., Cicchetti, F., 2013. Striatal allografts in patients with Huntington's disease: impact of diminished astrocytes and vascularization on graft viability. Brain 136, 433–443. https://doi.org/10.1093/brain/aws359

Colin, E., Zala, D., Liot, G., Rangone, H., Borrell-Pagès, M., Li, X.-J., Saudou, F., Humbert, S., 2008. Huntingtin phosphorylation acts as a molecular switch for anterograde/retrograde transport in neurons. EMBO J. 27, 2124–2134. https://doi.org/10.1038/emboj.2008.133

Cong, S.-Y., Pepers, B.A., Evert, B.O., Rubinsztein, D.C., Roos, R.A.C., van Ommen, G.-J.B., Dorsman, J.C., 2005. Mutant huntingtin represses CBP, but not p300, by binding and protein degradation. Mol. Cell. Neurosci. 30, 12–23. https://doi.org/10.1016/j.mcn.2005.05.003

CoppedÃ¨, F., 2014. The potential of epigenetic therapies in neurodegenerative diseases. Front. Genet. 5. https://doi.org/10.3389/fgene.2014.00220

Corbit, L.H., Muir, J.L., Balleine, B.W., 2001. The Role of the Nucleus Accumbens in Instrumental Conditioning: Evidence of a Functional Dissociation between Accumbens Core and Shell. J. Neurosci. 21, 3251–3260. https://doi.org/10.1523/JNEUROSCI.21-09-03251.2001

Cortes, C.J., La Spada, A.R., 2014. The many faces of autophagy dysfunction in Huntington's disease: from mechanism to therapy. Drug Discov. Today 19, 963–971. https://doi.org/10.1016/j.drudis.2014.02.014

Costello, P.S., Nicolas, R.H., Watanabe, Y., Rosewell, I., Treisman, R., 2004. Ternary complex factor SAP-1

is required for Erk-mediated thymocyte positive selection. Nat. Immunol. 5, 289–298. https://doi.org/10.1038/ni1038

COYLE, J.T., SCHWARCZ, R., 1976. Lesion of striatal neurons with kainic acid provides a model for Huntington's chorea. Nature 263, 244–246. https://doi.org/10.1038/263244a0

Crittenden, J.R., Tillberg, P.W., Riad, M.H., Shima, Y., Gerfen, C.R., Curry, J., Housman, D.E., Nelson, S.B., Boyden, E.S., Graybiel, A.M., 2016. Striosome–dendron bouquets highlight a unique striatonigral circuit targeting dopamine-containing neurons. Proc. Natl. Acad. Sci. 113, 11318–11323. https://doi.org/10.1073/pnas.1613337113

Croissant, J.D., Kim, J.-H., Eichele, G., Goering, L., Lough, J., Prywes, R., Schwartz, R.J., 1996. Avian Serum Response Factor Expression Restricted Primarily to Muscle Cell Lineages Is Required for α-Actin Gene Transcription. Dev. Biol. 177, 250–264. https://doi.org/10.1006/dbio.1996.0160

Crooke, S.T., 2017. Molecular Mechanisms of Antisense Oligonucleotides. Nucleic Acid Ther. 27, 70–77. https://doi.org/10.1089/nat.2016.0656

Cubo, E., Shannon, K.M., Tracy, D., Jaglin, J.A., Bernard, B.A., Wuu, J., Leurgans, S.E., 2006. Effect of donepezil on motor and cognitive function in Huntington disease. Neurology 67, 1268–1271. https://doi.org/10.1212/01.wnl.0000238106.10423.00

Cui, L., Jeong, H., Borovecki, F., Parkhurst, C.N., Tanese, N., Krainc, D., 2006. Transcriptional Repression of PGC-1α by Mutant Huntingtin Leads to Mitochondrial Dysfunction and Neurodegeneration. Cell 127, 59–69. https://doi.org/10.1016/j.cell.2006.09.015

Cummings, D.M., Alaghband, Y., Hickey, M.A., Joshi, P.R., Hong, S.C., Zhu, C., Ando, T.K., André, V.M., Cepeda, C., Watson, J.B., Levine, M.S., 2012. A critical window of CAG repeat-length correlates with phenotype severity in the R6/2 mouse model of Huntington's disease. J. Neurophysiol. 107, 677–691. https://doi.org/10.1152/jn.00762.2011

Curran, T., Morgan, J.I., 1995. Fos: An immediate-early transcription factor in neurons. J. Neurobiol. 26, 403–412. https://doi.org/10.1002/neu.480260312

Dalton, S., Treisman, R., 1992. Characterization of SAP-1, a protein recruited by serum response factor to the c-fos serum response element. Cell 68, 597–612. https://doi.org/10.1016/0092-8674(92)90194-H

Damiano, M., Diguet, E., Malgorn, C., D'Aurelio, M., Galvan, L., Petit, F., Benhaim, L., Guillermier, M., Houitte, D., Dufour, N., Hantraye, P., Canals, J.M., Alberch, J., Delzescaux, T., Déglon, N., Beal, M.F., Brouillet, E., 2013. A role of mitochondrial complex II defects in genetic models of Huntington's disease expressing N-terminal fragments of mutant huntingtin. Hum. Mol. Genet. 22, 3869–3882. https://doi.org/10.1093/hmg/ddt242

Damiano, M., Galvan, L., Déglon, N., Brouillet, E., 2010. Mitochondria in Huntington's disease. Biochim. Biophys. Acta - Mol. Basis Dis. 1802, 52–61. https://doi.org/10.1016/j.bbadis.2009.07.012

Dash, P.K., Orsi, S.A., Moore, A.N., 2005. Sequestration of serum response factor in the hippocampus impairs long-term spatial memory. J. Neurochem. 93, 269–278. https://doi.org/10.1111/j.1471-4159.2004.03016.x

Davies, S.W., Turmaine, M., Cozens, B.A., DiFiglia, M., Sharp, A.H., Ross, C.A., Scherzinger, E., Wanker, E.E., Mangiarini, L., Bates, G.P., 1997. Formation of Neuronal Intranuclear Inclusions Underlies the Neurological Dysfunction in Mice Transgenic for the HD Mutation. Cell 90, 537–548. https://doi.org/10.1016/S0092-8674(00)80513-9

Daw, N.D., O'Doherty, J.P., Dayan, P., Seymour, B., Dolan, R.J., 2006. Cortical substrates for exploratory decisions in humans. Nature 441, 876–879. https://doi.org/10.1038/nature04766

De Souza, R.A.G., Islam, S.A., McEwen, L.M., Mathelier, A., Hill, A., Mah, S.M., Wasserman, W.W., Kobor, M.S., Leavitt, B.R., 2016. DNA methylation profiling in human Huntington's disease brain. Hum. Mol. Genet. 25, 2013–2030. https://doi.org/10.1093/hmg/ddw076

Deaton, A.M., Bird, A., 2011. CpG islands and the regulation of transcription. Genes Dev. 25, 1010–1022. https://doi.org/10.1101/gad.2037511

Deckel, A.W., Moran, T.H., Coyle, J.T., Sanberg, P.R., Robinson, R.G., 1986. Anatomical predictors of behavioral recovery following fetal striatal transplants. Brain Res. 365, 249–258. https://doi.org/10.1016/0006-8993(86)91636-7

Deng, P., Torrest, A., Pollock, K., Dahlenburg, H., Annett, G., Nolta, J., Fink, K., 2016. Clinical trial perspective for adult and juvenile Huntington's disease using genetically-engineered mesenchymal stem cells. Neural Regen. Res. 11, 702. https://doi.org/10.4103/1673-5374.182682

Deng, Y.-P., Wong, T., Wan, J.Y., Reiner, A., 2014. Differential loss of thalamostriatal and corticostriatal input to striatal projection neuron types prior to overt motor symptoms in the Q140 knock-in mouse model of Huntington's disease. Front. Syst. Neurosci. 8. https://doi.org/10.3389/fnsys.2014.00198

Desplats, P.A., Kass, K.E., Gilmartin, T., Stanwood, G.D., Woodward, E.L., Head, S.R., Sutcliffe, J.G., Thomas, E.A., 2006. Selective deficits in the expression of striatal-enriched mRNAs in Huntington's disease. J. Neurochem. 96, 743–757. https://doi.org/10.1111/j.1471-4159.2005.03588.x

Devan, B.D., Hong, N.S., McDonald, R.J., 2011. Parallel associative processing in the dorsal striatum: Segregation of stimulus–response and cognitive control subregions. Neurobiol. Learn. Mem. 96, 95–120. https://doi.org/10.1016/j.nlm.2011.06.002

Dey, N.D., Bombard, M.C., Roland, B.P., Davidson, S., Lu, M., Rossignol, J., Sandstrom, M.I., Skeel, R.L., Lescaudron, L., Dunbar, G.L., 2010. Genetically engineered mesenchymal stem cells reduce behavioral deficits in the YAC 128 mouse model of Huntington's disease. Behav. Brain Res. 214, 193–200. https://doi.org/10.1016/j.bbr.2010.05.023

Di Pardo, A., Amico, E., Favellato, M., Castrataro, R., Fucile, S., Squitieri, F., Maglione, V., 2014. FTY720 (fingolimod) is a neuroprotective and disease-modifying agent in cellular and mouse models of Huntington disease. Hum. Mol. Genet. 23, 2251–2265. https://doi.org/10.1093/hmg/ddt615

Di Pardo, A., Maglione, V., Alpaugh, M., Horkey, M., Atwal, R.S., Sassone, J., Ciammola, A., Steffan, J.S., Fouad, K., Truant, R., Sipione, S., 2012. Ganglioside GM1 induces phosphorylation of mutant huntingtin and restores normal motor behavior in Huntington disease mice. Proc. Natl. Acad. Sci. 109, 3528–3533. https://doi.org/10.1073/pnas.1114502109

Dickey, A.S., Pineda, V. V, Tsunemi, T., Liu, P.P., Miranda, H.C., Gilmore-Hall, S.K., Lomas, N., Sampat,

K.R., Buttgereit, A., Torres, M.-J.M., Flores, A.L., Arreola, M., Arbez, N., Akimov, S.S., Gaasterland, T., Lazarowski, E.R., Ross, C.A., Yeo, G.W., Sopher, B.L., Magnuson, G.K., Pinkerton, A.B., Masliah, E., La Spada, A.R., 2016. PPAR-δ is repressed in Huntington's disease, is required for normal neuronal function and can be targeted therapeutically. Nat. Med. 22, 37–45. https://doi.org/10.1038/nm.4003

Dickinson, A., Balleine, B., Watt, A., Gonzalez, F., Boakes, R.A., 1995. Motivational control after extended instrumental training. Anim. Learn. Behav. 23, 197–206. https://doi.org/10.3758/BF03199935

DiFiglia, M., Sapp, E., Chase, K., Schwarz, C., Meloni, A., Young, C., Martin, E., Vonsattel, J.-P., Carraway, R., Reeves, S.A., Boyce, F.M., Aronin, N., 1995. Huntingtin is a cytoplasmic protein associated with vesicles in human and rat brain neurons. Neuron 14, 1075–1081. https://doi.org/10.1016/0896-6273(95)90346-1

DiFiglia, M., Sapp, E., Chase, K.O., Davies, S.W., Bates, G.P., Vonsattel, J.P., Aronin, N., 1997. Aggregation of Huntingtin in Neuronal Intranuclear Inclusions and Dystrophic Neurites in Brain. Science (80-.). 277, 1990–1993. https://doi.org/10.1126/science.277.5334.1990

Ding, W.-X., Yin, X.-M., 2008. Sorting, recognition and activation of the misfolded protein degradation pathways through macroautophagy and the proteasome. Autophagy 4, 141–150. https://doi.org/10.4161/auto.5190

Dompierre, J.P., Godin, J.D., Charrin, B.C., Cordelieres, F.P., King, S.J., Humbert, S., Saudou, F., 2007. Histone Deacetylase 6 Inhibition Compensates for the Transport Deficit in Huntington's Disease by Increasing Tubulin Acetylation. J. Neurosci. 27, 3571–3583. https://doi.org/10.1523/JNEUROSCI.0037-07.2007

Dong, X., Tsuji, J., Labadorf, A., Roussos, P., Chen, J.-F., Myers, R.H., Akbarian, S., Weng, Z., 2015. The Role of H3K4me3 in Transcriptional Regulation Is Altered in Huntington's Disease. PLoS One 10, e0144398. https://doi.org/10.1371/journal.pone.0144398

Dragatsis, I., Goldowitz, D., Del Mar, N., Deng, Y.P., Meade, C.A., Liu, L., Sun, Z., Dietrich, P., Yue, J., Reiner, A., 2009. CAG repeat lengths ≥335 attenuate the phenotype in the R6/2 Huntington's disease transgenic mouse. Neurobiol. Dis. 33, 315–330. https://doi.org/10.1016/j.nbd.2008.10.009

Dragatsis, I., Levine, M.S., Zeitlin, S., 2000. Inactivation of Hdh in the brain and testis results in progressive neurodegeneration and sterility in mice. Nat. Genet. 26, 300–306. https://doi.org/10.1038/81593

Dragileva, E., Hendricks, A., Teed, A., Gillis, T., Lopez, E.T., Friedberg, E.C., Kucherlapati, R., Edelmann, W., Lunetta, K.L., MacDonald, M.E., Wheeler, V.C., 2009. Intergenerational and striatal CAG repeat instability in Huntington's disease knock-in mice involve different DNA repair genes. Neurobiol. Dis. 33, 37–47. https://doi.org/10.1016/j.nbd.2008.09.014

Drewett, V., Devitt, A., Saxton, J., Portman, N., Greaney, P., Cheong, N., Alnemri, T.F., Alnemri, E., Shaw, P.E., 2001. Serum Response Factor Cleavage by Caspases 3 and 7 Linked to Apoptosis in Human BJAB Cells. J. Biol. Chem. 276, 33444–33451. https://doi.org/10.1074/jbc.M103877200

Duennwald, M.L., Lindquist, S., 2008. Impaired ERAD and ER stress are early and specific events in polyglutamine toxicity. Genes Dev. 22, 3308–3319. https://doi.org/10.1101/gad.1673408

Duff, K., Paulsen, J.S., Beglinger, L.J., Langbehn, D.R., Wang, C., Stout, J.C., Ross, C.A., Aylward, E., Carlozzi, N.E., Queller, S., Group, P.-H.I. of the H., 2010. "Frontal" Behaviors Before the Diagnosis of Huntington's Disease and Their Relationship to Markers of Disease Progression: Evidence of Early Lack of Awareness. J. Neuropsychiatry Clin. Neurosci. 22, 196–207. https://doi.org/10.1176/jnp.2010.22.2.196

Duyao, M., Ambrose, C., Myers, R., Novelletto, A., Persichetti, F., Frontali, M., Folstein, S., Ross, C., Franz, M., Abbott, M., Gray, J., Conneally, P., Young, A., Penney, J., Hollingsworth, Z., Shoulson, I., Lazzarini, A., Falek, A., Koroshetz, W., Sax, D., Bird, E., Vonsattel, J., Bonilla, E., Alvir, J., Bickham Conde, J., Cha, J.-H., Dure, L., Gomez, F., Ramos, M., Sanchez-Ramos, J., Snodgrass, S., de Young, M., Wexler, N., Moscowitz, C., Penchaszadeh, G., MacFarlane, H., Anderson, M., Jenkins, B., Srinidhi, J., Barnes, G., Gusella, J., MacDonald, M., 1993. Trinucleotide repeat length instability and age of onset in Huntington's disease. Nat. Genet. 4, 387–392. https://doi.org/10.1038/ng0893-387

Duyao, M., Auerbach, A., Ryan, A., Persichetti, F., Barnes, G., McNeil, S., Ge, P., Vonsattel, J., Gusella, J., Joyner, A., Et, A., 1995. Inactivation of the mouse Huntington's disease gene homolog Hdh. Science (80-.). 269, 407–410. https://doi.org/10.1126/science.7618107

Ehrnhoefer, D.E., Sutton, L., Hayden, M.R., 2011. Small Changes, Big Impact. Neurosci. 17, 475–492. https://doi.org/10.1177/1073858410390378

El-Daher, M., Hangen, E., Bruyère, J., Poizat, G., Al-Ramahi, I., Pardo, R., Bourg, N., Souquere, S., Mayet, C., Pierron, G., Lévêque-Fort, S., Botas, J., Humbert, S., Saudou, F., 2015. Huntingtin proteolysis releases non-polyQ fragments that cause toxicity through dynamin 1 dysregulation. EMBO J. 34, 2255–2271. https://doi.org/10.15252/embj.201490808

Emson, P.C., Arregui, A., Clement-Jones, V., Sandberg, B.E.B., Rossor, M., 1980. Regional distribution of methionine-enkephalin and substance P-like immunoreactivity in normal human brain and in Huntington's disease. Brain Res. 199, 147–160. https://doi.org/10.1016/0006-8993(80)90237-1

Esnault, C., Gualdrini, F., Horswell, S., Kelly, G., Stewart, A., East, P., Matthews, N., Treisman, R., 2017. ERK-Induced Activation of TCF Family of SRF Cofactors Initiates a Chromatin Modification Cascade Associated with Transcription. Mol. Cell 65, 1081-1095.e5. https://doi.org/10.1016/j.molcel.2017.02.005

Estrada-Sánchez, A.M., Rebec, G. V., 2013. Role of cerebral cortex in the neuropathology of Huntington's disease. Front. Neural Circuits 7. https://doi.org/10.3389/fncir.2013.00019

Estrada-Sánchez, A.M., Rebec, G. V., 2012. Corticostriatal dysfunction and glutamate transporter 1 (GLT1) in Huntington's disease: Interactions between neurons and astrocytes. Basal Ganglia 2, 57–66. https://doi.org/10.1016/j.baga.2012.04.029

Etkin, A., Alarcón, J.M., Weisberg, S.P., Touzani, K., Huang, Y.Y., Nordheim, A., Kandel, E.R., 2006. A Role in Learning for SRF: Deletion in the Adult Forebrain Disrupts LTD and the Formation of an Immediate Memory of a Novel Context. Neuron 50, 127–143. https://doi.org/10.1016/j.neuron.2006.03.013

Evers, M.M., Miniarikova, J., Juhas, S., Vallès, A., Bohuslavova, B., Juhasova, J., Skalnikova, H.K., Vodicka, P., Valekova, I., Brouwers, C., Blits, B., Lubelski, J., Kovarova, H., Ellederova, Z., van Deventer, S.J., Petry, H., Motlik, J., Konstantinova, P., 2018. AAV5-miHTT Gene Therapy Demonstrates Broad

Distribution and Strong Human Mutant Huntingtin Lowering in a Huntington's Disease Minipig Model. Mol. Ther. 26, 2163–2177. https://doi.org/10.1016/j.ymthe.2018.06.021

Faideau, M., Kim, J., Cormier, K., Gilmore, R., Welch, M., Auregan, G., Dufour, N., Guillermier, M., Brouillet, E., Hantraye, P., Deglon, N., Ferrante, R.J., Bonvento, G., 2010. In vivo expression of polyglutamine-expanded huntingtin by mouse striatal astrocytes impairs glutamate transport: a correlation with Huntington's disease subjects. Hum. Mol. Genet. 19, 3053–3067. https://doi.org/10.1093/hmg/ddq212

Feng, J., Shao, N., Szulwach, K.E., Vialou, V., Huynh, J., Zhong, C., Le, T., Ferguson, D., Cahill, M.E., Li, Y., Koo, J.W., Ribeiro, E., Labonte, B., Laitman, B.M., Estey, D., Stockman, V., Kennedy, P., Couroussé, T., Mensah, I., Turecki, G., Faull, K.F., Ming, G., Song, H., Fan, G., Casaccia, P., Shen, L., Jin, P., Nestler, E.J., 2015. Role of Tet1 and 5-hydroxymethylcytosine in cocaine action. Nat. Neurosci. 18, 536–544. https://doi.org/10.1038/nn.3976

Feng, J., Zhou, Y., Campbell, S.L., Le, T., Li, E., Sweatt, J.D., Silva, A.J., Fan, G., 2010. Dnmt1 and Dnmt3a maintain DNA methylation and regulate synaptic function in adult forebrain neurons. Nat. Neurosci. 13, 423–430. https://doi.org/10.1038/nn.2514

Fennema-Notestine, C., Archibald, S.L., Jacobson, M.W., Corey-Bloom, J., Paulsen, J.S., Peavy, G.M., Gamst, A.C., Hamilton, J.M., Salmon, D.P., Jernigan, T.L., 2004. In vivo evidence of cerebellar atrophy and cerebral white matter loss in Huntington disease. Neurology 63, 989–995. https://doi.org/10.1212/01.WNL.0000138434.68093.67

Fernandez-Albert, J., Lipinski, M., Lopez-Cascales, M.T., Rowley, M.J., Martin-Gonzalez, A.M., del Blanco, B., Corces, V.G., Barco, A., 2019. Immediate and deferred epigenomic signatures of in vivo neuronal activation in mouse hippocampus. Nat. Neurosci. 22, 1718–1730. https://doi.org/10.1038/s41593-019-0476-2

Ferrante, R., Kowall, N., Beal, M., Richardson, E., Bird, E., Martin, J., 1985. Selective sparing of a class of striatal neurons in Huntington's disease. Science (80-.). 230, 561–563. https://doi.org/10.1126/science.2931802

Ferrante, R.J., Kowall, N.W., Cipolloni, P.B., Storey, E., Beal, M.F., 1993. Excitotoxin Lesions in Primates as a Model for Huntington's Disease: Histopathologic and Neurochemical Characterization. Exp. Neurol. 119, 46–71. https://doi.org/10.1006/exnr.1993.1006

Ferrer, I., Blanco, R., Carmona, M., 2001. Differential expression of active, phosphorylation-dependent MAP kinases, MAPK/ERK, SAPK/JNK and p38, and specific transcription factor substrates following quinolinic acid excitotoxicity in the rat. Mol. Brain Res. 94, 48–58. https://doi.org/10.1016/S0169-328X(01)00198-X

Fink, K.D., Deng, P., Gutierrez, J., Anderson, J.S., Torrest, A., Komarla, A., Kalomoiris, S., Cary, W., Anderson, J.D., Gruenloh, W., Duffy, A., Tempkin, T., Annett, G., Wheelock, V., Segal, D.J., Nolta, J.A., 2016. Allele-Specific Reduction of the Mutant Huntingtin Allele Using Transcription Activator-Like Effectors in Human Huntington's Disease Fibroblasts. Cell Transplant. 25, 677–686. https://doi.org/10.3727/096368916X690863

Finkbeiner, S., 2011. Huntington's Disease. Cold Spring Harb. Perspect. Biol. 3, a007476–a007476. https://doi.org/10.1101/cshperspect.a007476

Finkbeiner, S., Greenberg, M.E., 1998. Ca2+ channel-regulated neuronal gene expression. J. Neurobiol. 37, 171–89.

Finkbeiner, S., Tavazoie, S.F., Maloratsky, A., Jacobs, K.M., Harris, K.M., Greenberg, M.E., 1997. CREB: A Major Mediator of Neuronal Neurotrophin Responses. Neuron 19, 1031–1047. https://doi.org/10.1016/S0896-6273(00)80395-5

Fleige, A., Alberti, S., Groöbe, L., Frischmann, U., Geffers, R., Muöller, W., Nordheim, A., Schippers, A., 2007. Serum Response Factor Contributes Selectively to Lymphocyte Development. J. Biol. Chem. 282, 24320–24328. https://doi.org/10.1074/jbc.M703119200

Floresco, S.B., 2015. The Nucleus Accumbens: An Interface Between Cognition, Emotion, and Action. Annu. Rev. Psychol. 66, 25–52. https://doi.org/10.1146/annurev-psych-010213-115159

Floresco, S.B., 2007. Dopaminergic regulation of limbic-striatal interplay. J. Psychiatry Neurosci. 32, 400–11.

Förstner, P., Knöll, B., 2020. Interference of neuronal activity-mediated gene expression through serum response factor deletion enhances mortality and hyperactivity after traumatic brain injury. FASEB J. 34, 3855–3873. https://doi.org/10.1096/fj.201902257RR

Francelle, L., Galvan, L., Brouillet, E., 2014. Possible involvement of self-defense mechanisms in the preferential vulnerability of the striatum in Huntington's disease. Front. Cell. Neurosci. 8. https://doi.org/10.3389/fncel.2014.00295

Francelle, L., Lotz, C., Outeiro, T., Brouillet, E., Merienne, K., 2017. Contribution of Neuroepigenetics to Huntington's Disease. Front. Hum. Neurosci. 11. https://doi.org/10.3389/fnhum.2017.00017

Frank, D.A., Greenberg, M.E., 1994. CREB: A mediator of long-term memory from mollusks to mammals. Cell 79, 5–8. https://doi.org/10.1016/0092-8674(94)90394-8

Fromm, C., Coso, O.A., Montaner, S., Xu, N., Gutkind, J.S., 1997. The small GTP-binding protein Rho links G protein-coupled receptors and G 12 to the serum response element and to cellular transformation. Proc. Natl. Acad. Sci. 94, 10098–10103. https://doi.org/10.1073/pnas.94.19.10098

Fukui, H., Moraes, C.T., 2007. Extended polyglutamine repeats trigger a feedback loop involving the mitochondrial complex III, the proteasome and huntingtin aggregates. Hum. Mol. Genet. 16, 783–797. https://doi.org/10.1093/hmg/ddm023

Futter, M., Diekmann, H., Schoenmakers, E., Sadiq, O., Chatterjee, K., Rubinsztein, D.C., 2009. Wild-type but not mutant huntingtin modulates the transcriptional activity of liver X receptors. J. Med. Genet. 46, 438–446. https://doi.org/10.1136/jmg.2009.066399

G. Vonsattel, J.P., DiFiglia, M., 1998. Huntington Disease. J. Neuropathol. Exp. Neurol. 57, 369–384. https://doi.org/10.1097/00005072-199805000-00001

Gaj, T., Epstein, B.E., Schaffer, D. V, 2016. Genome Engineering Using Adeno-associated Virus: Basic and Clinical Research Applications. Mol. Ther. 24, 458–464. https://doi.org/10.1038/mt.2015.151

Galmiche, G., Labat, C., Mericskay, M., Aissa, K.A., Blanc, J., Retailleau, K., Bourhim, M., Coletti, D., Loufrani, L., Gao-Li, J., Feil, R., Challande, P., Henrion, D., Decaux, J.-F., Regnault, V., Lacolley, P., Li,

Z., 2013. Inactivation of Serum Response Factor Contributes To Decrease Vascular Muscular Tone and Arterial Stiffness in Mice. Circ. Res. 112, 1035–1045. https://doi.org/10.1161/CIRCRESAHA.113.301076

Galvan, L., Francelle, L., Gaillard, M.-C., de Longprez, L., Carrillo-de Sauvage, M.-A., Liot, G., Cambon, K., Stimmer, L., Luccantoni, S., Flament, J., Valette, J., de Chaldée, M., Auregan, G., Guillermier, M., Joséphine, C., Petit, F., Jan, C., Jarrige, M., Dufour, N., Bonvento, G., Humbert, S., Saudou, F., Hantraye, P., Merienne, K., Bemelmans, A.-P., Perrier, A.L., Déglon, N., Brouillet, E., 2018. The striatal kinase DCLK3 produces neuroprotection against mutant huntingtin. Brain 141, 1434–1454. https://doi.org/10.1093/brain/awy057

Ganai, S.A., Banday, S., Farooq, Z., Altaf, M., 2016. Modulating epigenetic HAT activity for reinstating acetylation homeostasis: A promising therapeutic strategy for neurological disorders. Pharmacol. Ther. 166, 106–122. https://doi.org/10.1016/j.pharmthera.2016.07.001

Gárdián, G., Vécsei, L., 2004. Huntington's disease: pathomechanism and therapeutic perspectives. J. Neural Transm. 111, 1485–94. https://doi.org/10.1007/s00702-004-0201-4

Garriga-Canut, M., Agustin-Pavon, C., Herrmann, F., Sanchez, A., Dierssen, M., Fillat, C., Isalan, M., 2012. Synthetic zinc finger repressors reduce mutant huntingtin expression in the brain of R6/2 mice. Proc. Natl. Acad. Sci. 109, E3136–E3145. https://doi.org/10.1073/pnas.1206506109

Gaskill, B.N., Karas, A.Z., Garner, J.P., Pritchett-Corning, K.R., 2013. Nest Building as an Indicator of Health and Welfare in Laboratory Mice. J. Vis. Exp. https://doi.org/10.3791/51012

Gauthier-Rouvière, C., Qiu-Qiong, C., Lautredou, N., Fernandez, A., Blanchard, J.-M., Lamb, N.J.C., 1993. Expression and Purification of the DNA-Binding Domain of SRF: SRF-DB, a Part of a DNA-Binding Protein Which Can Act as a Dominant Negative Mutant in Vivo. Exp. Cell Res. 209, 208–215. https://doi.org/10.1006/excr.1993.1303

Gauthier-Rouviere, C., Vandromme, M., Tuil, D., Lautredou, N., Morris, M., Soulez, M., Kahn, A., Fernandez, A., Lamb, N., 1996. Expression and activity of serum response factor is required for expression of the muscle-determining factor MyoD in both dividing and differentiating mouse C2C12 myoblasts. Mol. Biol. Cell 7, 719–729. https://doi.org/10.1091/mbc.7.5.719

Gauthier, L.R., Charrin, B.C., Borrell-Pagès, M., Dompierre, J.P., Rangone, H., Cordelières, F.P., De Mey, J., MacDonald, M.E., Leßmann, V., Humbert, S., Saudou, F., 2004. Huntingtin Controls Neurotrophic Support and Survival of Neurons by Enhancing BDNF Vesicular Transport along Microtubules. Cell 118, 127–138. https://doi.org/10.1016/j.cell.2004.06.018

Geater, C., Hernandez, S., Thompson, L., Mattis, V.B., 2018. Cellular Models: HD Patient-Derived Pluripotent Stem Cells. pp. 41–73. https://doi.org/10.1007/978-1-4939-7825-0_4

Genetic Modifiers of Huntington's Disease (GeM-HD) Consortium, 2019. CAG Repeat Not Polyglutamine Length Determines Timing of Huntington's Disease Onset. Cell 178, 887-900.e14. https://doi.org/10.1016/j.cell.2019.06.036

Genetic Modifiers of Huntington's Disease (GeM-HD) Consortium, 2015. Identification of Genetic Factors that Modify Clinical Onset of Huntington's Disease. Cell 162, 516–26. https://doi.org/10.1016/j.cell.2015.07.003

Gerfen, C., Herkenham, M., Thibault, J., 1987. The neostriatal mosaic: II. Patch- and matrix-directed mesostriatal dopaminergic and non-dopaminergic systems. J. Neurosci. 7, 3915–3934. https://doi.org/10.1523/JNEUROSCI.07-12-03915.1987

Gerfen, C.R., 1992. The neostriatal mosaic: multiple levels of compartmental organization. Trends Neurosci. 15, 133–139. https://doi.org/10.1016/0166-2236(92)90355-C

Gerosa, L., Grillo, B., Forastieri, C., Longaretti, A., Toffolo, E., Mallei, A., Bassani, S., Popoli, M., Battaglioli, E., Rusconi, F., 2020. SRF and SRFΔ5 Splicing Isoform Recruit Corepressor LSD1/KDM1A Modifying Structural Neuroplasticity and Environmental Stress Response. Mol. Neurobiol. 57, 393–407. https://doi.org/10.1007/s12035-019-01720-8

Geschwind, M.D., Paras, N., 2016. Deutetrabenazine for Treatment of Chorea in Huntington Disease. JAMA 316, 33. https://doi.org/10.1001/jama.2016.8011

Ghosh, R., Tabrizi, S.J., 2018. Clinical Features of Huntington's Disease. pp. 1–28. https://doi.org/10.1007/978-3-319-71779-1_1

Gil, J.M., Rego, A.C., 2008. Mechanisms of neurodegeneration in Huntington's disease. Eur. J. Neurosci. 27, 2803–2820. https://doi.org/10.1111/j.1460-9568.2008.06310.x

Gineitis, D., Treisman, R., 2001. Differential Usage of Signal Transduction Pathways Defines Two Types of Serum Response Factor Target Gene. J. Biol. Chem. 276, 24531–24539. https://doi.org/10.1074/jbc.M102678200

Giovane, A., Pintzas, A., Maira, S.M., Sobieszczuk, P., Wasylyk, B., 1994. Net, a new ets transcription factor that is activated by Ras. Genes Dev. 8, 1502–1513. https://doi.org/10.1101/gad.8.13.1502

Glajch, K.E., Sadri-Vakili, G., 2015. Epigenetic Mechanisms Involved in Huntington's Disease Pathogenesis. J. Huntingtons. Dis. 4, 1–15. https://doi.org/10.3233/JHD-140134

Gläscher, J., Hampton, A.N., O'Doherty, J.P., 2009. Determining a Role for Ventromedial Prefrontal Cortex in Encoding Action-Based Value Signals During Reward-Related Decision Making. Cereb. Cortex 19, 483–495. https://doi.org/10.1093/cercor/bhn098

Godin, J.D., Poizat, G., Hickey, M.A., Maschat, F., Humbert, S., 2010. Mutant huntingtin-impaired degradation of β-catenin causes neurotoxicity in Huntington's disease. EMBO J. 29, 2433–2445. https://doi.org/10.1038/emboj.2010.117

GOEBEL, H.H., HEIPERTZ, R., SCHOLZ, W., IQBAL, K., TELLEZ-NAGEL, I., 1978. Juvenile Huntington chorea: Clinical, ultrastructural, and biochemical studies. Neurology 28, 23–23. https://doi.org/10.1212/WNL.28.1.23

Gómez-Tortosa, E., MacDonald, M.E., Friend, J.C., Taylor, S.A., Weiler, L.J., Cupples, L.A., Srinidhi, J., Gusella, J.F., Bird, E.D., Vonsattel, J.P., Myers, R.H., 2001. Quantitative neuropathological changes in presymptomatic Huntington's disease. Ann. Neurol. 49, 29–34.

Gonzalez, V., Cif, L., Biolsi, B., Garcia-Ptacek, S., Seychelles, A., Sanrey, E., Descours, I., Coubes, C., de Moura, A.-M.R., Corlobe, A., James, S., Roujeau, T., Coubes, P., 2014. Deep brain stimulation for Huntington's disease: long-term results of a prospective open-label study. J. Neurosurg. 121, 114–122. https://doi.org/10.3171/2014.2.JNS131722

Goodliffe, J.W., Song, H., Rubakovic, A., Chang, W., Medalla, M., Weaver, C.M., Luebke, J.I., 2018. Differential changes to D1 and D2 medium spiny neurons in the 12-month-old Q175+/- mouse model of Huntington's Disease. PLoS One 13, e0200626. https://doi.org/10.1371/journal.pone.0200626

Goold, R., Flower, M., Moss, D.H., Medway, C., Wood-Kaczmar, A., Andre, R., Farshim, P., Bates, G.P., Holmans, P., Jones, L., Tabrizi, S.J., 2019. FAN1 modifies Huntington's disease progression by stabilizing the expanded HTT CAG repeat. Hum. Mol. Genet. 28, 650–661. https://doi.org/10.1093/hmg/ddy375

Goula, A.-V., Merienne, K., 2013. Abnormal Base Excision Repair at Trinucleotide Repeats Associated with Diseases: A Tissue-Selective Mechanism. Genes (Basel). 4, 375–387. https://doi.org/10.3390/genes4030375

Goula, A.-V., Stys, A., Chan, J.P.K., Trottier, Y., Festenstein, R., Merienne, K., 2012. Transcription Elongation and Tissue-Specific Somatic CAG Instability. PLoS Genet. 8, e1003051. https://doi.org/10.1371/journal.pgen.1003051

Gräff, J., Tsai, L.-H., 2013. Histone acetylation: molecular mnemonics on the chromatin. Nat. Rev. Neurosci. 14, 97–111. https://doi.org/10.1038/nrn3427

Grahn, J.A., Parkinson, J.A., Owen, A.M., 2008. The cognitive functions of the caudate nucleus. Prog. Neurobiol. 86, 141–155. https://doi.org/10.1016/j.pneurobio.2008.09.004

Gray, M., Shirasaki, D.I., Cepeda, C., Andre, V.M., Wilburn, B., Lu, X.-H., Tao, J., Yamazaki, I., Li, S.-H., Sun, Y.E., Li, X.-J., Levine, M.S., Yang, X.W., 2008. Full-Length Human Mutant Huntingtin with a Stable Polyglutamine Repeat Can Elicit Progressive and Selective Neuropathogenesis in BACHD Mice. J. Neurosci. 28, 6182–6195. https://doi.org/10.1523/JNEUROSCI.0857-08.2008

Graybiel, A.M., Ragsdale, C.W., 1978. Histochemically distinct compartments in the striatum of human, monkeys, and cat demonstrated by acetylthiocholinesterase staining. Proc. Natl. Acad. Sci. 75, 5723–5726. https://doi.org/10.1073/pnas.75.11.5723

Green and John C. Reed, D.R., 1998. Mitochondria and Apoptosis. Science (80-.). 281, 1309–1312. https://doi.org/10.1126/science.281.5381.1309

GROENEWEGEN, H.J., WRIGHT, C.I., BEIJER, A.V.J., VOORN, P., 1999. Convergence and Segregation of Ventral Striatal Inputs and Outputs. Ann. N. Y. Acad. Sci. 877, 49–63. https://doi.org/10.1111/j.1749-6632.1999.tb09260.x

Gu, M., Gash, M.T., Mann, V.M., Javoy-Agid, F., Cooper, J.M., Schapira, A.H. V., 1996. Mitochondrial defect in Huntington's disease caudate nucleus. Ann. Neurol. 39, 385–389. https://doi.org/10.1002/ana.410390317

Gu, X., Greiner, E.R., Mishra, R., Kodali, R., Osmand, A., Finkbeiner, S., Steffan, J.S., Thompson, L.M., Wetzel, R., Yang, X.W., 2009. Serines 13 and 16 Are Critical Determinants of Full-Length Human Mutant Huntingtin Induced Disease Pathogenesis in HD Mice. Neuron 64, 828–840. https://doi.org/10.1016/j.neuron.2009.11.020

Gualdrini, F., Esnault, C., Horswell, S., Stewart, A., Matthews, N., Treisman, R., 2016. SRF Co-factors Control the Balance between Cell Proliferation and Contractility. Mol. Cell 64, 1048–1061.

https://doi.org/10.1016/j.molcel.2016.10.016

Guettler, S., Vartiainen, M.K., Miralles, F., Larijani, B., Treisman, R., 2008. RPEL Motifs Link the Serum Response Factor Cofactor MAL but Not Myocardin to Rho Signaling via Actin Binding. Mol. Cell. Biol. 28, 732–742. https://doi.org/10.1128/MCB.01623-07

Guiretti, D., Sempere, A., Lopez-Atalaya, J.P., Ferrer-Montiel, A., Barco, A., Valor, L.M., 2016. Specific promoter deacetylation of histone H3 is conserved across mouse models of Huntington's disease in the absence of bulk changes. Neurobiol. Dis. 89, 190–201. https://doi.org/10.1016/j.nbd.2016.02.004

Guo, J.U., Ma, D.K., Mo, H., Ball, M.P., Jang, M.-H., Bonaguidi, M.A., Balazer, J.A., Eaves, H.L., Xie, B., Ford, E., Zhang, K., Ming, G., Gao, Y., Song, H., 2011. Neuronal activity modifies the DNA methylation landscape in the adult brain. Nat. Neurosci. 14, 1345–1351. https://doi.org/10.1038/nn.2900

Gusella, J.F., Wexler, N.S., Conneally, P.M., Naylor, S.L., Anderson, M.A., Tanzi, R.E., Watkins, P.C., Ottina, K., Wallace, M.R., Sakaguchi, A.Y., 2003. A polymorphic DNA marker genetically linked to Huntington's disease. Nature 306, 234–8. https://doi.org/10.1038/306234a0

Gustafson, T.A., Kedes, L., 1989. Identification of multiple proteins that interact with functional regions of the human cardiac alpha-actin promoter. Mol. Cell. Biol. 9, 3269–3283. https://doi.org/10.1128/MCB.9.8.3269

Gutekunst, C.-A., Li, S.-H., Yi, H., Mulroy, J.S., Kuemmerle, S., Jones, R., Rye, D., Ferrante, R.J., Hersch, S.M., Li, X.-J., 1999. Nuclear and Neuropil Aggregates in Huntington's Disease: Relationship to Neuropathology. J. Neurosci. 19, 2522–2534. https://doi.org/10.1523/JNEUROSCI.19-07-02522.1999

Ha, M., Kim, V.N., 2014. Regulation of microRNA biogenesis. Nat. Rev. Mol. Cell Biol. 15, 509–524. https://doi.org/10.1038/nrm3838

Hacein-Bey-Abina, S., von Kalle, C., Schmidt, M., Le Deist, F., Wulffraat, N., McIntyre, E., Radford, I., Villeval, J.-L., Fraser, C.C., Cavazzana-Calvo, M., Fischer, A., 2003. A Serious Adverse Event after Successful Gene Therapy for X-Linked Severe Combined Immunodeficiency. N. Engl. J. Med. 348, 255–256. https://doi.org/10.1056/NEJM200301163480314

Halene, S., Gao, Y., Hahn, K., Massaro, S., Italiano, J.E., Schulz, V., Lin, S., Kupfer, G.M., Krause, D.S., 2010. Serum response factor is an essential transcription factor in megakaryocytic maturation. Blood 116, 1942–1950. https://doi.org/10.1182/blood-2010-01-261743

Halestrap, A.P., 2006. Calcium, mitochondria and reperfusion injury: a pore way to die. Biochem. Soc. Trans. 34, 232. https://doi.org/10.1042/BST20060232

Han, I., You, Y., Kordower, J.H., Brady, S.T., Morfini, G.A., 2010. Differential vulnerability of neurons in Huntington's disease: the role of cell type-specific features. J. Neurochem. https://doi.org/10.1111/j.1471-4159.2010.06672.x

Hansson, O., Guatteo, E., Mercuri, N.B., Bernardi, G., Li, X.-J., Castilho, R.F., Brundin, P., 2001. Resistance to NMDA toxicity correlates with appearance of nuclear inclusions, behavioural deficits and changes in calcium homeostasis in mice transgenic for exon 1 of the huntington gene. Eur. J.

Neurosci. 14, 1492–1504. https://doi.org/10.1046/j.0953-816x.2001.01767.x

Harjes, P., Wanker, E.E., 2003. The hunt for huntingtin function: interaction partners tell many different stories. Trends Biochem. Sci. 28, 425–433. https://doi.org/10.1016/S0968-0004(03)00168-3

Heidenreich, O., Neininger, A., Schratt, G., Zinck, R., Cahill, M.A., Engel, K., Kotlyarov, A., Kraft, R., Kostka, S., Gaestel, M., Nordheim, A., 1999. MAPKAP Kinase 2 Phosphorylates Serum Response Factor in Vitro and in Vivo. J. Biol. Chem. 274, 14434–14443. https://doi.org/10.1074/jbc.274.20.14434

Heintzman, N.D., Stuart, R.K., Hon, G., Fu, Y., Ching, C.W., Hawkins, R.D., Barrera, L.O., Van Calcar, S., Qu, C., Ching, K.A., Wang, W., Weng, Z., Green, R.D., Crawford, G.E., Ren, B., 2007. Distinct and predictive chromatin signatures of transcriptional promoters and enhancers in the human genome. Nat. Genet. 39, 311–318. https://doi.org/10.1038/ng1966

Heng, M.Y., Duong, D.K., Albin, R.L., Tallaksen-Greene, S.J., Hunter, J.M., Lesort, M.J., Osmand, A., Paulson, H.L., Detloff, P.J., 2010. Early autophagic response in a novel knock-in model of Huntington disease. Hum. Mol. Genet. 19, 3702–3720. https://doi.org/10.1093/hmg/ddq285

Herdegen, T., Blume, A., Buschmann, T., Georgakopoulos, E., Winter, C., Schmid, W., Hsieh, T.., Zimmermann, M., Gass, P., 1997. Expression of activating transcription factor-2, serum response factor and cAMP/Ca response element binding protein in the adult rat brain following generalized seizures, nerve fibre lesion and ultraviolet irradiation. Neuroscience 81, 199–212. https://doi.org/10.1016/S0306-4522(97)00170-X

Herman, D., Jenssen, K., Burnett, R., Soragni, E., Perlman, S.L., Gottesfeld, J.M., 2006. Histone deacetylase inhibitors reverse gene silencing in Friedreich's ataxia. Nat. Chem. Biol. 2, 551–558. https://doi.org/10.1038/nchembio815

Hernández, I.H., Torres-Peraza, J., Santos-Galindo, M., Ramos-Morón, E., Fernández-Fernández, M.R., Pérez-Álvarez, M.J., Miranda-Vizuete, A., Lucas, J.J., 2017. The neuroprotective transcription factor ATF5 is decreased and sequestered into polyglutamine inclusions in Huntington's disease. Acta Neuropathol. 134, 839–850. https://doi.org/10.1007/s00401-017-1770-2

Herrera, R.E., Shaw, P.E., Nordheim, A., 1989. Occupation of the c-fos serum response element in vivo by a multi-protein complex is unaltered by growth factor induction. Nature 340, 68–70. https://doi.org/10.1038/340068a0

Hervás-Corpión, I., Guiretti, D., Alcaraz-Iborra, M., Olivares, R., Campos-Caro, A., Barco, Á., Valor, L.M., 2018. Early alteration of epigenetic-related transcription in Huntington's disease mouse models. Sci. Rep. 8, 9925. https://doi.org/10.1038/s41598-018-28185-4

Hetz, C., Papa, F.R., 2018. The Unfolded Protein Response and Cell Fate Control. Mol. Cell 69, 169–181. https://doi.org/10.1016/j.molcel.2017.06.017

HICKEY, M., GALLANT, K., GROSS, G., LEVINE, M., CHESSELET, M., 2005. Early behavioral deficits in R6/2 mice suitable for use in preclinical drug testing. Neurobiol. Dis. 20, 1–11. https://doi.org/10.1016/j.nbd.2005.01.024

Hickey, M.A., Kosmalska, A., Enayati, J., Cohen, R., Zeitlin, S., Levine, M.S., Chesselet, M.-F., 2008. Extensive early motor and non-motor behavioral deficits are followed by striatal neuronal loss in knock-in Huntington's disease mice. Neuroscience 157, 280–295.

https://doi.org/10.1016/j.neuroscience.2008.08.041

Hill, C.S., Wynne, J., Treisman, R., 1995. The Rho family GTPases RhoA, Racl , and CDC42Hsregulate transcriptional activation by SRF. Cell 81, 1159–1170. https://doi.org/10.1016/S0092-8674(05)80020-0

Hodges, A., Strand, A.D., Aragaki, A.K., Kuhn, A., Sengstag, T., Hughes, G., Elliston, L.A., Hartog, C., Goldstein, D.R., Thu, D., Hollingsworth, Z.R., Collin, F., Synek, B., Holmans, P.A., Young, A.B., Wexler, N.S., Delorenzi, M., Kooperberg, C., Augood, S.J., Faull, R.L.M., Olson, J.M., Jones, L., Luthi-Carter, R., 2006. Regional and cellular gene expression changes in human Huntington's disease brain. Hum. Mol. Genet. 15, 965–977. https://doi.org/10.1093/hmg/ddl013

Hodgson, J.G., Agopyan, N., Gutekunst, C.-A., Leavitt, B.R., LePiane, F., Singaraja, R., Smith, D.J., Bissada, N., McCutcheon, K., Nasir, J., Jamot, L., Li, X.-J., Stevens, M.E., Rosemond, E., Roder, J.C., Phillips, A.G., Rubin, E.M., Hersch, S.M., Hayden, M.R., 1999. A YAC Mouse Model for Huntington's Disease with Full-Length Mutant Huntingtin, Cytoplasmic Toxicity, and Selective Striatal Neurodegeneration. Neuron 23, 181–192. https://doi.org/10.1016/S0896-6273(00)80764-3

Holbert, S., 2001. The Gln-Ala repeat transcriptional activator CA150 interacts with huntingtin: Neuropathologic and genetic evidence for a role in Huntington's disease pathogenesis. Proc. Natl. Acad. Sci. 98, 1811–1816. https://doi.org/10.1073/pnas.041566798

Holmberg, C.I., Staniszewski, K.E., Mensah, K.N., Matouschek, A., Morimoto, R.I., 2004. Inefficient degradation of truncated polyglutamine proteins by the proteasome. EMBO J. 23, 4307–4318. https://doi.org/10.1038/sj.emboj.7600426

Holt, D.J., Graybiel, A.M., Saper, C.B., 1997. Neurochemical architecture of the human striatum. J. Comp. Neurol. 384, 1–25. https://doi.org/10.1002/(sici)1096-9861(19970721)384:1<1::aid-cne1>3.0.co;2-5

Holtz, M.L., Misra, R.P., 2008. Endothelial-specific ablation of Serum Response Factor causes hemorrhaging, yolk sac vascular failure, and embryonic lethality. BMC Dev. Biol. 8, 65. https://doi.org/10.1186/1471-213X-8-65

Hombach, D., Schwarz, J.M., Robinson, P.N., Schuelke, M., Seelow, D., 2016. A systematic, large-scale comparison of transcription factor binding site models. BMC Genomics 17, 388. https://doi.org/10.1186/s12864-016-2729-8

Horvath, S., 2013. DNA methylation age of human tissues and cell types. Genome Biol. 14, R115. https://doi.org/10.1186/gb-2013-14-10-r115

Horvath, S., Langfelder, P., Kwak, S., Aaronson, J., Rosinski, J., Vogt, T.F., Eszes, M., Faull, R.L.M., Curtis, M.A., Waldvogel, H.J., Choi, O.-W., Tung, S., Vinters, H. V, Coppola, G., Yang, X.W., 2016. Huntington's disease accelerates epigenetic aging of human brain and disrupts DNA methylation levels. Aging (Albany. NY). 8, 1485–512. https://doi.org/10.18632/aging.101005

Hoss, A.G., Kartha, V.K., Dong, X., Latourelle, J.C., Dumitriu, A., Hadzi, T.C., MacDonald, M.E., Gusella, J.F., Akbarian, S., Chen, J.-F., Weng, Z., Myers, R.H., 2014. MicroRNAs Located in the Hox Gene Clusters Are Implicated in Huntington's Disease Pathogenesis. PLoS Genet. 10, e1004188. https://doi.org/10.1371/journal.pgen.1004188

Hsu, P.D., Lander, E.S., Zhang, F., 2014. Development and Applications of CRISPR-Cas9 for Genome Engineering. Cell 157, 1262–1278. https://doi.org/10.1016/j.cell.2014.05.010

Huang, D.W., Sherman, B.T., Zheng, X., Yang, J., Imamichi, T., Stephens, R., Lempicki, R.A., 2009. Extracting Biological Meaning from Large Gene Lists with DAVID. Curr. Protoc. Bioinforma. 27. https://doi.org/10.1002/0471250953.bi1311s27

Hughes, A.C., Mort, M., Elliston, L., Thomas, R.M., Brooks, S.P., Dunnett, S.B., Jones, L., 2014. Identification of Novel Alternative Splicing Events in the Huntingtin Gene and Assessment of the Functional Consequences Using Structural Protein Homology Modelling. J. Mol. Biol. 426, 1428–1438. https://doi.org/10.1016/j.jmb.2013.12.028

Huntington, G., 2003. On chorea. George Huntington, M.D. J. Neuropsychiatry Clin. Neurosci. 15, 109–12. https://doi.org/10.1176/jnp.15.1.109

Hutvagner, G., Simard, M.J., 2008. Argonaute proteins: key players in RNA silencing. Nat. Rev. Mol. Cell Biol. 9, 22–32. https://doi.org/10.1038/nrm2321

Hyrskyluoto, A., Bruelle, C., Lundh, S.H., Do, H.T., Kivinen, J., Rappou, E., Reijonen, S., Waltimo, T., Petersen, A., Lindholm, D., Korhonen, L., 2014. Ubiquitin-specific protease-14 reduces cellular aggregates and protects against mutant huntingtin-induced cell degeneration: involvement of the proteasome and ER stress-activated kinase IRE1. Hum. Mol. Genet. 23, 5928–5939. https://doi.org/10.1093/hmg/ddu317

Inukai, S., Kock, K.H., Bulyk, M.L., 2017. Transcription factor-DNA binding: beyond binding site motifs. Curr. Opin. Genet. Dev. 43, 110–119. https://doi.org/10.1016/j.gde.2017.02.007

Ito, R., Robbins, T.W., Everitt, B.J., 2004. Differential control over cocaine-seeking behavior by nucleus accumbens core and shell. Nat. Neurosci. 7, 389–397. https://doi.org/10.1038/nn1217

Iyer, D., Belaguli, N., Flück, M., Rowan, B.G., Wei, L., Weigel, N.L., Booth, F.W., Epstein, H.F., Schwartz, R.J., Balasubramanyam, A., 2003. Novel Phosphorylation Target in the Serum Response Factor MADS Box Regulates α-Actin Transcription †. Biochemistry 42, 7477–7486. https://doi.org/10.1021/bi030045n

Iyer, D., Chang, D., Marx, J., Wei, L., Olson, E.N., Parmacek, M.S., Balasubramanyam, A., Schwartz, R.J., 2006. Serum response factor MADS box serine -162 phosphorylation switches proliferation and myogenic gene programs. Proc. Natl. Acad. Sci. 103, 4516–4521. https://doi.org/10.1073/pnas.0505338103

Jacobsen, J.C., Bawden, C.S., Rudiger, S.R., McLaughlan, C.J., Reid, S.J., Waldvogel, H.J., MacDonald, M.E., Gusella, J.F., Walker, S.K., Kelly, J.M., Webb, G.C., Faull, R.L.M., Rees, M.I., Snell, R.G., 2010. An ovine transgenic Huntington's disease model. Hum. Mol. Genet. 19, 1873–1882. https://doi.org/10.1093/hmg/ddq063

Jacquard, C., Trioulier, Y., Cosker, F., Escartin, C., Bizat, N., Hantraye, P., Manuel Cancela, J., Bonvento, G., Brouillet, E., Jacquard, C., Trioulier, Y., Cosker, F., Escartin, C., Bizat, N., Hantraye, P., Manuel Cancela, J., Bonvento, G., Brouillet, E., 2006. Brain mitochondrial defects amplify intracellular [Ca 2+] rise and neurodegeneration but not Ca 2+ entry during NMDA receptor activation. FASEB J. 20, 1021–1023. https://doi.org/10.1096/fj.05-5085fje

Jaeger, B.N., Linker, S.B., Parylak, S.L., Barron, J.J., Gallina, I.S., Saavedra, C.D., Fitzpatrick, C., Lim, C.K., Schafer, S.T., Lacar, B., Jessberger, S., Gage, F.H., 2018. A novel environment-evoked transcriptional signature predicts reactivity in single dentate granule neurons. Nat. Commun. 9, 3084. https://doi.org/10.1038/s41467-018-05418-8

Jaenisch, R., Bird, A., 2003. Epigenetic regulation of gene expression: how the genome integrates intrinsic and environmental signals. Nat. Genet. 33, 245–254. https://doi.org/10.1038/ng1089

Janknecht, R., Ernst, W.H., Pingoud, V., Nordheim, A., 1993. Activation of ternary complex factor Elk-1 by MAP kinases. EMBO J. 12, 5097–104.

Janknecht, R., Nordheim, A., 1992. Elk-1 protein domains required for direct and SRF-assisted DNA-binding. Nucleic Acids Res. 20, 3317–3324. https://doi.org/10.1093/nar/20.13.3317

Jeltsch, A., 2006. Molecular enzymology of mammalian DNA methyltransferases. Curr. Top. Microbiol. Immunol. 301, 203–25. https://doi.org/10.1007/3-540-31390-7_7

Jenkins, B.G., Koroshetz, W.J., Beal, M.F., Rosen, B.R., 1993. Evidence for irnnairment of energy metabofism in vivo in Huntington's disease using localized 1H NMR spectroscopy. Neurology 43, 2689–2689. https://doi.org/10.1212/WNL.43.12.2689

Jenkins, B.G., Rosas, H.D., Chen, Y.-C.I., Makabe, T., Myers, R., MacDonald, M., Rosen, B.R., Beal, M.F., Koroshetz, W.J., 1998. 1H NMR spectroscopy studies of Huntington's disease: Correlations with CAG repeat numbers. Neurology 50, 1357–1365. https://doi.org/10.1212/WNL.50.5.1357

Jenuwein, T., Allis, C.D., 2001. Translating the histone code. Science 293, 1074–80. https://doi.org/10.1126/science.1063127

Jeon, I., Lee, N., Li, J.-Y., Park, I.-H., Park, K.S., Moon, J., Shim, S.H., Choi, C., Chang, D.-J., Kwon, J., Oh, S.-H., Shin, D.A., Kim, H.S., Do, J.T., Lee, D.R., Kim, M., Kang, K.-S., Daley, G.Q., Brundin, P., Song, J., 2012. Neuronal Properties, In Vivo Effects, and Pathology of a Huntington's Disease Patient-Derived Induced Pluripotent Stem Cells. Stem Cells 30, 2054–2062. https://doi.org/10.1002/stem.1135

Jeong, H., Then, F., Melia, T.J., Mazzulli, J.R., Cui, L., Savas, J.N., Voisine, C., Paganetti, P., Tanese, N., Hart, A.C., Yamamoto, A., Krainc, D., 2009. Acetylation Targets Mutant Huntingtin to Autophagosomes for Degradation. Cell 137, 60–72. https://doi.org/10.1016/j.cell.2009.03.018

Jia, H., Pallos, J., Jacques, V., Lau, A., Tang, B., Cooper, A., Syed, A., Purcell, J., Chen, Y., Sharma, S., Sangrey, G.R., Darnell, S.B., Plasterer, H., Sadri-Vakili, G., Gottesfeld, J.M., Thompson, L.M., Rusche, J.R., Marsh, J.L., Thomas, E.A., 2012. Histone deacetylase (HDAC) inhibitors targeting HDAC3 and HDAC1 ameliorate polyglutamine-elicited phenotypes in model systems of Huntington's disease. Neurobiol. Dis. 46, 351–361. https://doi.org/10.1016/j.nbd.2012.01.016

Jia, H., Wang, Y., Morris, C.D., Jacques, V., Gottesfeld, J.M., Rusche, J.R., Thomas, E.A., 2016. The Effects of Pharmacological Inhibition of Histone Deacetylase 3 (HDAC3) in Huntington's Disease Mice. PLoS One 11, e0152498. https://doi.org/10.1371/journal.pone.0152498

Jiang, C., Salton, S., 2013. The role of neurotrophins in major depressive disorder. Transl. Neurosci. 4. https://doi.org/10.2478/s13380-013-0103-8

Jiang, M., Peng, Q., Liu, X., Jin, J., Hou, Z., Zhang, J., Mori, S., Ross, C.A., Ye, K., Duan, W., 2013. Small-molecule TrkB receptor agonists improve motor function and extend survival in a mouse model of Huntington's disease. Hum. Mol. Genet. 22, 2462–2470. https://doi.org/10.1093/hmg/ddt098

Johansen, F.-E., Prywes, R., 1995. Serum response factor: transcriptional regulation of genes induced by growth factors and differentiation. Biochim. Biophys. Acta - Rev. Cancer 1242, 1–10. https://doi.org/10.1016/0304-419X(94)00014-S

Johansen, F.E., Prywes, R., 1993. Identification of transcriptional activation and inhibitory domains in serum response factor (SRF) by using GAL4-SRF constructs. Mol. Cell. Biol. 13, 4640–4647. https://doi.org/10.1128/MCB.13.8.4640

Jones, C., Busse, M., Quinn, L., Dawes, H., Drew, C., Kelson, M., Hood, K., Rosser, A., Edwards, R.T., 2016. The societal cost of Huntington's disease: are we underestimating the burden? Eur. J. Neurol. 23, 1588–1590. https://doi.org/10.1111/ene.13107

Kacher, R., Lamazière, A., Heck, N., Kappes, V., Mounier, C., Despres, G., Dembitskaya, Y., Perrin, E., Christaller, W., Sasidharan Nair, S., Messent, V., Cartier, N., Vanhoutte, P., Venance, L., Saudou, F., Néri, C., Caboche, J., Betuing, S., 2019. CYP46A1 gene therapy deciphers the role of brain cholesterol metabolism in Huntington's disease. Brain 142, 2432–2450. https://doi.org/10.1093/brain/awz174

Kaganovich, D., Kopito, R., Frydman, J., 2008. Misfolded proteins partition between two distinct quality control compartments. Nature 454, 1088–1095. https://doi.org/10.1038/nature07195

Kalita, K., Kharebava, G., Zheng, J.-J., Hetman, M., 2006. Role of Megakaryoblastic Acute Leukemia-1 in ERK1/2-Dependent Stimulation of Serum Response Factor-Driven Transcription by BDNF or Increased Synaptic Activity. J. Neurosci. 26, 10020–10032. https://doi.org/10.1523/JNEUROSCI.2644-06.2006

Kanehisa, M., 2000. KEGG: Kyoto Encyclopedia of Genes and Genomes. Nucleic Acids Res. 28, 27–30. https://doi.org/10.1093/nar/28.1.27

Kanehisa, M., Sato, Y., Furumichi, M., Morishima, K., Tanabe, M., 2019. New approach for understanding genome variations in KEGG. Nucleic Acids Res. 47, D590–D595. https://doi.org/10.1093/nar/gky962

Kassubek, J., Juengling, F.D., Kioschies, T., Henkel, K., Karitzky, J., Kramer, B., Ecker, D., Andrich, J., Saft, C., Kraus, P., Aschoff, A.J., Ludolph, A.C., Landwehrmeyer, G.B., 2004. Topography of cerebral atrophy in early Huntington's disease: a voxel based morphometric MRI study. J. Neurol. Neurosurg. Psychiatry 75, 213–20.

Kawaguchi, Y., Wilson, C.J., Augood, S.J., Emson, P.C., 1995. Striatal interneurones: chemical, physiological and morphological characterization. Trends Neurosci. 18, 527–535. https://doi.org/10.1016/0166-2236(95)98374-8

Kawashima, T., Okuno, H., Nonaka, M., Adachi-Morishima, A., Kyo, N., Okamura, M., Takemoto-Kimura, S., Worley, P.F., Bito, H., 2009. Synaptic activity-responsive element in the Arc/Arg3.1 promoter essential for synapse-to-nucleus signaling in activated neurons. Proc. Natl. Acad. Sci. 106, 316–321. https://doi.org/10.1073/pnas.0806518106

Kazantsev, A., Preisinger, E., Dranovsky, A., Goldgaber, D., Housman, D., 1999. Insoluble detergent-resistant aggregates form between pathological and nonpathological lengths of polyglutamine in mammalian cells. Proc. Natl. Acad. Sci. 96, 11404–11409. https://doi.org/10.1073/pnas.96.20.11404

Kazantsev, A., Walker, H.A., Slepko, N., Bear, J.E., Preisinger, E., Steffan, J.S., Zhu, Y.-Z., Gertler, F.B., Housman, D.E., Marsh, J.L., Thompson, L.M., 2002. A bivalent Huntingtin binding peptide suppresses polyglutamine aggregation and pathogenesis in Drosophila. Nat. Genet. 30, 367–376. https://doi.org/10.1038/ng864

Kee, B.L., Arias, J., Montminy, M.R., 1996. Adaptor-mediated Recruitment of RNA Polymerase II to a Signal-dependent Activator. J. Biol. Chem. 271, 2373–2375. https://doi.org/10.1074/jbc.271.5.2373

Kegel, K.B., Kim, M., Sapp, E., McIntyre, C., Castaño, J.G., Aronin, N., DiFiglia, M., 2000. Huntingtin Expression Stimulates Endosomal–Lysosomal Activity, Endosome Tubulation, and Autophagy. J. Neurosci. 20, 7268–7278. https://doi.org/10.1523/JNEUROSCI.20-19-07268.2000

Kegel, K.B., Schewkunow, V., Sapp, E., Masso, N., Wanker, E.E., DiFiglia, M., Goldmann, W.H., 2009. Polyglutamine expansion in huntingtin increases its insertion into lipid bilayers. Biochem. Biophys. Res. Commun. 387, 472–475. https://doi.org/10.1016/j.bbrc.2009.07.039

Kemp, P.R., Metcalfe, J.C., 2000. Four isoforms of serum response factor that increase or inhibit smooth-muscle-specific promoter activity. Biochem. J. 345 Pt 3, 445–51.

Kendall, A.L., Rayment, F.D., Torres, E.M., Baker, H.F., Ridley, R.M., Dunnett, S.B., 1998. Functional integration of striatal allografts in a primate model of Huntington's disease. Nat. Med. 4, 727–729. https://doi.org/10.1038/nm0698-727

Kennedy, L., 2003. Dramatic tissue-specific mutation length increases are an early molecular event in Huntington disease pathogenesis. Hum. Mol. Genet. 12, 3359–3367. https://doi.org/10.1093/hmg/ddg352

Kennedy, L., 2000. Dramatic mutation instability in HD mouse striatum: does polyglutamine load contribute to cell-specific vulnerability in Huntington's disease? Hum. Mol. Genet. 9, 2539–2544. https://doi.org/10.1093/hmg/9.17.2539

Kerschbamer, E., Biagioli, M., 2016. Huntington's Disease as Neurodevelopmental Disorder: Altered Chromatin Regulation, Coding, and Non-Coding RNA Transcription. Front. Neurosci. 9. https://doi.org/10.3389/fnins.2015.00509

Kim, J., Moody, J.P., Edgerly, C.K., Bordiuk, O.L., Cormier, K., Smith, K., Beal, M.F., Ferrante, R.J., 2010. Mitochondrial loss, dysfunction and altered dynamics in Huntington's disease. Hum. Mol. Genet. 19, 3919–3935. https://doi.org/10.1093/hmg/ddq306

Kim, M., Lee, H.-S., LaForet, G., McIntyre, C., Martin, E.J., Chang, P., Kim, T.W., Williams, M., Reddy, P.H., Tagle, D., Boyce, F.M., Won, L., Heller, A., Aronin, N., DiFiglia, M., 1999. Mutant Huntingtin Expression in Clonal Striatal Cells: Dissociation of Inclusion Formation and Neuronal Survival by Caspase Inhibition. J. Neurosci. 19, 964–973. https://doi.org/10.1523/JNEUROSCI.19-03-00964.1999

Kim, P., Leckman, J.F., Mayes, L.C., Feldman, R., Wang, X., Swain, J.E., 2010. The plasticity of human

maternal brain: Longitudinal changes in brain anatomy during the early postpartum period. Behav. Neurosci. 124, 695–700. https://doi.org/10.1037/a0020884

Kim, T.-K., Hemberg, M., Gray, J.M., Costa, A.M., Bear, D.M., Wu, J., Harmin, D.A., Laptewicz, M., Barbara-Haley, K., Kuersten, S., Markenscoff-Papadimitriou, E., Kuhl, D., Bito, H., Worley, P.F., Kreiman, G., Greenberg, M.E., 2010a. Widespread transcription at neuronal activity-regulated enhancers. Nature 465, 182–7. https://doi.org/10.1038/nature09033

Kim, T.-K., Hemberg, M., Gray, J.M., Costa, A.M., Bear, D.M., Wu, J., Harmin, D.A., Laptewicz, M., Barbara-Haley, K., Kuersten, S., Markenscoff-Papadimitriou, E., Kuhl, D., Bito, H., Worley, P.F., Kreiman, G., Greenberg, M.E., 2010b. Widespread transcription at neuronal activity-regulated enhancers. Nature 465, 182–187. https://doi.org/10.1038/nature09033

Kincaid, A.E., Zheng, T., Wilson, C.J., 1998. Connectivity and Convergence of Single Corticostriatal Axons. J. Neurosci. 18, 4722–4731. https://doi.org/10.1523/JNEUROSCI.18-12-04722.1998

Kirch, R.D., Meyer, P.T., Geisler, S., Braun, F., Gehrig, S., Langen, K.-J., von Hörsten, S., Nikkhah, G., Cassel, J.-C., Döbrössy, M.D., 2013. Early deficits in declarative and procedural memory dependent behavioral function in a transgenic rat model of Huntington's disease. Behav. Brain Res. 239, 15–26. https://doi.org/10.1016/j.bbr.2012.10.048

Klein, A., Lane, E.L., Dunnett, S.B., 2013. Brain Repair in a Unilateral Rat Model of Huntington's Disease: New Insights into Impairment and Restoration of Forelimb Movement Patterns. Cell Transplant. 22, 1735–1751. https://doi.org/10.3727/096368912X657918

Klug, A., 2010. The Discovery of Zinc Fingers and Their Applications in Gene Regulation and Genome Manipulation. Annu. Rev. Biochem. 79, 213–231. https://doi.org/10.1146/annurev-biochem-010909-095056

Knöll, B., Kretz, O., Fiedler, C., Alberti, S., Schütz, G., Frotscher, M., Nordheim, A., 2006. Serum response factor controls neuronal circuit assembly in the hippocampus. Nat. Neurosci. 9, 195–204. https://doi.org/10.1038/nn1627

Knöll, B., Nordheim, A., 2009. Functional versatility of transcription factors in the nervous system: the SRF paradigm. Trends Neurosci. 32, 432–442. https://doi.org/10.1016/j.tins.2009.05.004

Koegel, H., von Tobel, L., Schäfer, M., Alberti, S., Kremmer, E., Mauch, C., Hohl, D., Wang, X.-J., Beer, H.-D., Bloch, W., Nordheim, A., Werner, S., 2009. Loss of serum response factor in keratinocytes results in hyperproliferative skin disease in mice. J. Clin. Invest. 119, 899–910. https://doi.org/10.1172/JCI37771

Kolli, N., Lu, M., Maiti, P., Rossignol, J., Dunbar, G., 2017. CRISPR-Cas9 Mediated Gene-Silencing of the Mutant Huntingtin Gene in an In Vitro Model of Huntington's Disease. Int. J. Mol. Sci. 18, 754. https://doi.org/10.3390/ijms18040754

Kordasiewicz, H.B., Stanek, L.M., Wancewicz, E. V., Mazur, C., McAlonis, M.M., Pytel, K.A., Artates, J.W., Weiss, A., Cheng, S.H., Shihabuddin, L.S., Hung, G., Bennett, C.F., Cleveland, D.W., 2012. Sustained Therapeutic Reversal of Huntington's Disease by Transient Repression of Huntingtin Synthesis. Neuron 74, 1031–1044. https://doi.org/10.1016/j.neuron.2012.05.009

Korzus, E., Rosenfeld, M.G., Mayford, M., 2004. CBP Histone Acetyltransferase Activity Is a Critical

Component of Memory Consolidation. Neuron 42, 961–972. https://doi.org/10.1016/j.neuron.2004.06.002

Kreitzer, A.C., 2009. Physiology and Pharmacology of Striatal Neurons. Annu. Rev. Neurosci. 32, 127–147. https://doi.org/10.1146/annurev.neuro.051508.135422

Krieger, C., Duchen, M.R., 2002. Mitochondria, Ca2+ and neurodegenerative disease. Eur. J. Pharmacol. 447, 177–188. https://doi.org/10.1016/S0014-2999(02)01842-3

Kuhn, A., Goldstein, D.R., Hodges, A., Strand, A.D., Sengstag, T., Kooperberg, C., Becanovic, K., Pouladi, M.A., Sathasivam, K., Cha, J.-H.J., Hannan, A.J., Hayden, M.R., Leavitt, B.R., Dunnett, S.B., Ferrante, R.J., Albin, R., Shelbourne, P., Delorenzi, M., Augood, S.J., Faull, R.L.M., Olson, J.M., Bates, G.P., Jones, L., Luthi-Carter, R., 2007. Mutant huntingtin's effects on striatal gene expression in mice recapitulate changes observed in human Huntington's disease brain and do not differ with mutant huntingtin length or wild-type huntingtin dosage. Hum. Mol. Genet. 16, 1845–61. https://doi.org/10.1093/hmg/ddm133

Kumar, A., Ratan, R.R., 2016. Oxidative Stress and Huntington's Disease: The Good, The Bad, and The Ugly. J. Huntingtons. Dis. 5, 217–237. https://doi.org/10.3233/JHD-160205

Kuras, L., Borggrefe, T., Kornberg, R.D., 2003. Association of the Mediator complex with enhancers of active genes. Proc. Natl. Acad. Sci. 100, 13887–13891. https://doi.org/10.1073/pnas.2036346100

Labadorf, A., Hoss, A.G., Lagomarsino, V., Latourelle, J.C., Hadzi, T.C., Bregu, J., MacDonald, M.E., Gusella, J.F., Chen, J.-F., Akbarian, S., Weng, Z., Myers, R.H., 2016. Correction: RNA Sequence Analysis of Human Huntington Disease Brain Reveals an Extensive Increase in Inflammatory and Developmental Gene Expression. PLoS One 11, e0160295. https://doi.org/10.1371/journal.pone.0160295

Labbadia, J., Novoselov, S.S., Bett, J.S., Weiss, A., Paganetti, P., Bates, G.P., Cheetham, M.E., 2012. Suppression of protein aggregation by chaperone modification of high molecular weight complexes. Brain 135, 1180–1196. https://doi.org/10.1093/brain/aws022

Lamprecht, R., 1999. CREB: a message to remember. Cell. Mol. Life Sci. 55, 554–563. https://doi.org/10.1007/s000180050314

Lan, Z.-J., Lye, R.J., Holic, N., Labus, J.C., Hinton, B.T., 1999. Involvement of Polyomavirus Enhancer Activator 3 in the Regulation of Expression of Gamma-Glutamyl Transpeptidase Messenger Ribonucleic Acid-IV in the Rat Epididymis1. Biol. Reprod. 60, 664–673. https://doi.org/10.1095/biolreprod60.3.664

Lanciego, J.L., Luquin, N., Obeso, J.A., 2012. Functional Neuroanatomy of the Basal Ganglia. Cold Spring Harb. Perspect. Med. 2, a009621–a009621. https://doi.org/10.1101/cshperspect.a009621

Landles, C., Sathasivam, K., Weiss, A., Woodman, B., Moffitt, H., Finkbeiner, S., Sun, B., Gafni, J., Ellerby, L.M., Trottier, Y., Richards, W.G., Osmand, A., Paganetti, P., Bates, G.P., 2010. Proteolysis of Mutant Huntingtin Produces an Exon 1 Fragment That Accumulates as an Aggregated Protein in Neuronal Nuclei in Huntington Disease*. J. Biol. Chem. 285, 8808–8823. https://doi.org/10.1074/jbc.M109.075028

Landwehrmeyer, G.B., Dubois, B., de Yébenes, J.G., Kremer, B., Gaus, W., Kraus, P.H., Przuntek, H., Dib,

M., Doble, A., Fischer, W., Ludolph, A.C., 2007. Riluzole in Huntington's disease: a 3-year, randomized controlled study. Ann. Neurol. 62, 262–272. https://doi.org/10.1002/ana.21181

Langfelder, P., Cantle, J.P., Chatzopoulou, D., Wang, N., Gao, F., Al-Ramahi, I., Lu, X.-H., Ramos, E.M., El-Zein, K., Zhao, Y., Deverasetty, S., Tebbe, A., Schaab, C., Lavery, D.J., Howland, D., Kwak, S., Botas, J., Aaronson, J.S., Rosinski, J., Coppola, G., Horvath, S., Yang, X.W., 2016a. Integrated genomics and proteomics define huntingtin CAG length–dependent networks in mice. Nat. Neurosci. 19, 623–633. https://doi.org/10.1038/nn.4256

Langfelder, P., Cantle, J.P., Chatzopoulou, D., Wang, N., Gao, F., Al-Ramahi, I., Lu, X.-H., Ramos, E.M., El-Zein, K., Zhao, Y., Deverasetty, S., Tebbe, A., Schaab, C., Lavery, D.J., Howland, D., Kwak, S., Botas, J., Aaronson, J.S., Rosinski, J., Coppola, G., Horvath, S., Yang, X.W., 2016b. Integrated genomics and proteomics define huntingtin CAG length-dependent networks in mice. Nat. Neurosci. 19, 623–33. https://doi.org/10.1038/nn.4256

Langfelder, P., Gao, F., Wang, N., Howland, D., Kwak, S., Vogt, T.F., Aaronson, J.S., Rosinski, J., Coppola, G., Horvath, S., Yang, X.W., 2018. MicroRNA signatures of endogenous Huntingtin CAG repeat expansion in mice. PLoS One 13, e0190550. https://doi.org/10.1371/journal.pone.0190550

Larrouy, B., Blonski, C., Boiziau, C., Stuer, M., Moreau, S., Shire, D., Toulmé, J.-J., 1992. RNase H-mediated inhibition of translation by antisense oligodeoxyribo-nucleotides: use of backbone modification to improve specificity. Gene 121, 189–194. https://doi.org/10.1016/0378-1119(92)90121-5

Latchman, D.S., 1997. Transcription factors: An overview. Int. J. Biochem. Cell Biol. 29, 1305–1312. https://doi.org/10.1016/S1357-2725(97)00085-X

Le Gras, S., Keime, C., Anthony, A., Lotz, C., De Longprez, L., Brouillet, E., Cassel, J.-C., Boutillier, A.-L., Merienne, K., 2017. Altered enhancer transcription underlies Huntington's disease striatal transcriptional signature. Sci. Rep. 7, 42875. https://doi.org/10.1038/srep42875

Leavitt, B.R., Raamsdonk, J.M., Shehadeh, J., Fernandes, H., Murphy, Z., Graham, R.K., Wellington, C.L., Hayden, M.R., 2006. Wild-type huntingtin protects neurons from excitotoxicity. J. Neurochem. 96, 1121–1129. https://doi.org/10.1111/j.1471-4159.2005.03605.x

Ledford, H., 2019. Super-precise new CRISPR tool could tackle a plethora of genetic diseases. Nature 574, 464–465. https://doi.org/10.1038/d41586-019-03164-5

Lee, H., Fenster, R.J., Pineda, S.S., Gibbs, W.S., Mohammadi, S., Davila-Velderrain, J., Garcia, F.J., Therrien, M., Novis, H.S., Gao, F., Wilkinson, H., Vogt, T., Kellis, M., LaVoie, M.J., Heiman, M., 2020. Cell Type-Specific Transcriptomics Reveals that Mutant Huntingtin Leads to Mitochondrial RNA Release and Neuronal Innate Immune Activation. Neuron 107, 891-908.e8. https://doi.org/10.1016/j.neuron.2020.06.021

Lee, J.-M., Chao, M.J., Harold, D., Abu Elneel, K., Gillis, T., Holmans, P., Jones, L., Orth, M., Myers, R.H., Kwak, S., Wheeler, V.C., MacDonald, M.E., Gusella, J.F., 2017. A modifier of Huntington's disease onset at the MLH1 locus. Hum. Mol. Genet. 26, 3859–3867. https://doi.org/10.1093/hmg/ddx286

Lee, J.-M., Ramos, E.M., Lee, J.-H., Gillis, T., Mysore, J.S., Hayden, M.R., Warby, S.C., Morrison, P., Nance, M., Ross, C.A., Margolis, R.L., Squitieri, F., Orobello, S., Di Donato, S., Gomez-Tortosa, E., Ayuso, C., Suchowersky, O., Trent, R.J.A., McCusker, E., Novelletto, A., Frontali, M., Jones, R., Ashizawa, T.,

Frank, S., Saint-Hilaire, M.H., Hersch, S.M., Rosas, H.D., Lucente, D., Harrison, M.B., Zanko, A., Abramson, R.K., Marder, K., Sequeiros, J., Paulsen, J.S., Landwehrmeyer, G.B., Myers, R.H., MacDonald, M.E., Gusella, J.F., 2012. CAG repeat expansion in Huntington disease determines age at onset in a fully dominant fashion. Neurology 78, 690–695. https://doi.org/10.1212/WNL.0b013e318249f683

Lee, J., Hwang, Y.J., Kim, K.Y., Kowall, N.W., Ryu, H., 2013. Epigenetic Mechanisms of Neurodegeneration in Huntington's Disease. Neurotherapeutics 10, 664–676. https://doi.org/10.1007/s13311-013-0206-5

Lee, J., Kosaras, B., Del Signore, S.J., Cormier, K., McKee, A., Ratan, R.R., Kowall, N.W., Ryu, H., 2011. Modulation of lipid peroxidation and mitochondrial function improves neuropathology in Huntington's disease mice. Acta Neuropathol. 121, 487–498. https://doi.org/10.1007/s00401-010-0788-5

Lee, S.-T., Chu, K., Jung, K.-H., Im, W.-S., Park, J.-E., Lim, H.-C., Won, C.-H., Shin, S.-H., Lee, S.K., Kim, M., Roh, J.-K., 2009. Slowed progression in models of huntington disease by adipose stem cell transplantation. Ann. Neurol. 66, 671–681. https://doi.org/10.1002/ana.21788

Leitman, J., Ulrich Hartl, F., Lederkremer, G.Z., 2013. Soluble forms of polyQ-expanded huntingtin rather than large aggregates cause endoplasmic reticulum stress. Nat. Commun. 4, 2753. https://doi.org/10.1038/ncomms3753

Leoni, V., Caccia, C., 2015. The impairment of cholesterol metabolism in Huntington disease. Biochim. Biophys. Acta - Mol. Cell Biol. Lipids 1851, 1095–1105. https://doi.org/10.1016/j.bbalip.2014.12.018

Li, S.-H., Cheng, A.L., Zhou, H., Lam, S., Rao, M., Li, H., Li, X.-J., 2002. Interaction of Huntington Disease Protein with Transcriptional Activator Sp1. Mol. Cell. Biol. 22, 1277–1287. https://doi.org/10.1128/MCB.22.5.1277-1287.2002

Li, S., Chang, S., Qi, X., Richardson, J.A., Olson, E.N., 2006. Requirement of a Myocardin-Related Transcription Factor for Development of Mammary Myoepithelial Cells. Mol. Cell. Biol. 26, 5797–5808. https://doi.org/10.1128/MCB.00211-06

Li, X., DiFiglia, M., 2012. The recycling endosome and its role in neurological disorders. Prog. Neurobiol. 97, 127–141. https://doi.org/10.1016/j.pneurobio.2011.10.002

Liljeholm, M., Tricomi, E., O'Doherty, J.P., Balleine, B.W., 2011. Neural Correlates of Instrumental Contingency Learning: Differential Effects of Action-Reward Conjunction and Disjunction. J. Neurosci. 31, 2474–2480. https://doi.org/10.1523/JNEUROSCI.3354-10.2011

Lin, B., Rommens, J.M., Graham, R.K., Kalchman, M., MacDonald, H., Nasir, J., Delaney, A., Goldberg, Y.P., Hayden, M.R., 1993. Differential 3' polyadenylation of the Huntington disease gene results in two mRNA species with variable tissue expression. Hum. Mol. Genet. 2, 1541–1545. https://doi.org/10.1093/hmg/2.10.1541

Lin, C.-H., 2001. Neurological abnormalities in a knock-in mouse model of Huntington's disease. Hum. Mol. Genet. 10, 137–144. https://doi.org/10.1093/hmg/10.2.137

Lindecke, A., Korte, M., Zagrebelsky, M., Horejschi, V., Elvers, M., Widera, D., Prüllage, M., Pfeiffer, J.,

Kaltschmidt, B., Kaltschmidt, C., 2006. Long-term depression activates transcription of immediate early transcription factor genes: involvement of serum response factor/Elk-1. Eur. J. Neurosci. 24, 555–563. https://doi.org/10.1111/j.1460-9568.2006.04909.x

Lione, L.A., Carter, R.J., Hunt, M.J., Bates, G.P., Morton, A.J., Dunnett, S.B., 1999. Selective Discrimination Learning Impairments in Mice Expressing the Human Huntington's Disease Mutation. J. Neurosci. 19, 10428–10437. https://doi.org/10.1523/JNEUROSCI.19-23-10428.1999

Liot, G., Valette, J., Pépin, J., Flament, J., Brouillet, E., 2017. Energy defects in Huntington's disease: Why "in vivo" evidence matters. Biochem. Biophys. Res. Commun. 483, 1084–1095. https://doi.org/10.1016/j.bbrc.2016.09.065

Liot, G., Zala, D., Pla, P., Mottet, G., Piel, M., Saudou, F., 2013. Mutant Huntingtin Alters Retrograde Transport of TrkB Receptors in Striatal Dendrites. J. Neurosci. 33, 6298–6309. https://doi.org/10.1523/JNEUROSCI.2033-12.2013

Llewellyn-Smith, I.J., Arnolda, L.F., Pilowsky, P.M., Chalmers, J.P., Minson, J.B., 1998. GABA- and glutamate-immunoreactive synapses on sympathetic preganglionic neurons projecting to the superior cervical ganglion. J. Auton. Nerv. Syst. 71, 96–110. https://doi.org/10.1016/S0165-1838(98)00069-1

Lonze, B.E., Ginty, D.D., 2002. Function and Regulation of CREB Family Transcription Factors in the Nervous System. Neuron 35, 605–623. https://doi.org/10.1016/S0896-6273(02)00828-0

Lopez-Atalaya, J.P., Barco, A., 2014. Can changes in histone acetylation contribute to memory formation? Trends Genet. 30, 529–39. https://doi.org/10.1016/j.tig.2014.09.003

Love, M.I., Huber, W., Anders, S., 2014. Moderated estimation of fold change and dispersion for RNA-seq data with DESeq2. Genome Biol. 15, 550. https://doi.org/10.1186/s13059-014-0550-8

Lu, X.-H., Yang, X.W., 2012. "Huntingtin Holiday": Progress toward an Antisense Therapy for Huntington's Disease. Neuron 74, 964–966. https://doi.org/10.1016/j.neuron.2012.06.001

Lunkes, A., Lindenberg, K.S., Ben-Haïem, L., Weber, C., Devys, D., Landwehrmeyer, G.B., Mandel, J.-L., Trottier, Y., 2002. Proteases Acting on Mutant Huntingtin Generate Cleaved Products that Differentially Build Up Cytoplasmic and Nuclear Inclusions. Mol. Cell 10, 259–269. https://doi.org/10.1016/S1097-2765(02)00602-0

Luthi-Carter, R., 2002a. Dysregulation of gene expression in the R6/2 model of polyglutamine disease: parallel changes in muscle and brain. Hum. Mol. Genet. 11, 1911–1926. https://doi.org/10.1093/hmg/11.17.1911

Luthi-Carter, R., 2002b. Polyglutamine and transcription: gene expression changes shared by DRPLA and Huntington's disease mouse models reveal context-independent effects. Hum. Mol. Genet. 11, 1927–1937. https://doi.org/10.1093/hmg/11.17.1927

Luthi-Carter, R., Strand, A., Peters, N.L., Solano, S.M., Hollingsworth, Z.R., Menon, A.S., Frey, A.S., Spektor, B.S., Penney, E.B., Schilling, G., Ross, C.A., Borchelt, D.R., Tapscott, S.J., Young, A.B., Cha, J.H., Olson, J.M., 2000. Decreased expression of striatal signaling genes in a mouse model of Huntington's disease. Hum. Mol. Genet. 9, 1259–71. https://doi.org/10.1093/hmg/9.9.1259

Lykken, E.A., Shyng, C., Edwards, R.J., Rozenberg, A., Gray, S.J., 2018. Recent progress and considerations for AAV gene therapies targeting the central nervous system. J. Neurodev. Disord. 10, 16. https://doi.org/10.1186/s11689-018-9234-0

Lynd-Balta, E., Haber, S.N., 1994. Primate striatonigral projections: A comparison of the sensorimotor-related striatum and the ventral striatum. J. Comp. Neurol. 345, 562–578. https://doi.org/10.1002/cne.903450407

Ma, L., Hu, B., Liu, Y., Vermilyea, S.C., Liu, H., Gao, L., Sun, Y., Zhang, X., Zhang, S.-C., 2012. Human Embryonic Stem Cell-Derived GABA Neurons Correct Locomotion Deficits in Quinolinic Acid-Lesioned Mice. Cell Stem Cell 10, 455–464. https://doi.org/10.1016/j.stem.2012.01.021

MACDONALD, M., 1993. A novel gene containing a trinucleotide repeat that is expanded and unstable on Huntington's disease chromosomes. Cell 72, 971–983. https://doi.org/10.1016/0092-8674(93)90585-E

MacDonald, M.E., Barnes, G., Srinidhi, J., Duyao, M.P., Ambrose, C.M., Myers, R.H., Gray, J., Conneally, P.M., Young, A., Penney, J., 1993. Gametic but not somatic instability of CAG repeat length in Huntington's disease. J. Med. Genet. 30, 982–986. https://doi.org/10.1136/jmg.30.12.982

Malankhanova, T.B., Malakhova, A.A., Medvedev, S.P., Zakian, S.M., 2017. Modern Genome Editing Technologies in Huntington's Disease Research. J. Huntingtons. Dis. 6, 19–31. https://doi.org/10.3233/JHD-160222

Malkki, H., 2016. Selective deactivation of Huntington disease mutant allele by CRISPR–Cas9 gene editing. Nat. Rev. Neurol. 12, 614–615. https://doi.org/10.1038/nrneurol.2016.151

Mangiarini, L., Sathasivam, K., Seller, M., Cozens, B., Harper, A., Hetherington, C., Lawton, M., Trottier, Y., Lehrach, H., Davies, S.W., Bates, G.P., 1996. Exon 1 of the HD Gene with an Expanded CAG Repeat Is Sufficient to Cause a Progressive Neurological Phenotype in Transgenic Mice. Cell 87, 493–506. https://doi.org/10.1016/S0092-8674(00)81369-0

Mantamadiotis, T., Lemberger, T., Bleckmann, S.C., Kern, H., Kretz, O., Villalba, A.M., Tronche, F., Kellendonk, C., Gau, D., Kapfhammer, J., Otto, C., Schmid, W., Schütz, G., 2002. Disruption of CREB function in brain leads to neurodegeneration. Nat. Genet. 31, 47–54. https://doi.org/10.1038/ng882

Marco, A., Meharena, H.S., Dileep, V., Raju, R.M., Davila-Velderrain, J., Zhang, A.L., Adaikkan, C., Young, J.Z., Gao, F., Kellis, M., Tsai, L.-H., 2020. Mapping the epigenomic and transcriptomic interplay during memory formation and recall in the hippocampal engram ensemble. Nat. Neurosci. 23, 1606–1617. https://doi.org/10.1038/s41593-020-00717-0

Martí, E., Pantano, L., Bañez-Coronel, M., Llorens, F., Miñones-Moyano, E., Porta, S., Sumoy, L., Ferrer, I., Estivill, X., 2010. A myriad of miRNA variants in control and Huntington's disease brain regions detected by massively parallel sequencing. Nucleic Acids Res. 38, 7219–7235. https://doi.org/10.1093/nar/gkq575

Martin, D.D.O., Ladha, S., Ehrnhoefer, D.E., Hayden, M.R., 2015. Autophagy in Huntington disease and huntingtin in autophagy. Trends Neurosci. 38, 26–35. https://doi.org/10.1016/j.tins.2014.09.003

Martinez-Vicente, M., Talloczy, Z., Wong, E., Tang, G., Koga, H., Kaushik, S., de Vries, R., Arias, E., Harris,

S., Sulzer, D., Cuervo, A.M., 2010. Cargo recognition failure is responsible for inefficient autophagy in Huntington's disease. Nat. Neurosci. 13, 567–576. https://doi.org/10.1038/nn.2528

McBride, J.L., Ramaswamy, S., Gasmi, M., Bartus, R.T., Herzog, C.D., Brandon, E.P., Zhou, L., Pitzer, M.R., Berry-Kravis, E.M., Kordower, J.H., 2006. Viral delivery of glial cell line-derived neurotrophic factor improves behavior and protects striatal neurons in a mouse model of Huntington's disease. Proc. Natl. Acad. Sci. 103, 9345–9350. https://doi.org/10.1073/pnas.0508875103

McColgan, P., Tabrizi, S.J., 2018. Huntington's disease: a clinical review. Eur. J. Neurol. 25, 24–34. https://doi.org/10.1111/ene.13413

McFarland, K.N., Das, S., Sun, T.T., Leyfer, D., Xia, E., Sangrey, G.R., Kuhn, A., Luthi-Carter, R., Clark, T.W., Sadri-Vakili, G., Cha, J.-H.J., 2012. Genome-Wide Histone Acetylation Is Altered in a Transgenic Mouse Model of Huntington's Disease. PLoS One 7, e41423. https://doi.org/10.1371/journal.pone.0041423

McGarry, A., McDermott, M., Kieburtz, K., de Blieck, E.A., Beal, F., Marder, K., Ross, C., Shoulson, I., Gilbert, P., Mallonee, W.M., Guttman, M., Wojcieszek, J., Kumar, R., LeDoux, M.S., Jenkins, M., Rosas, H.D., Nance, M., Biglan, K., Como, P., Dubinsky, R.M., Shannon, K.M., O'Suilleabhain, P., Chou, K., Walker, F., Martin, W., Wheelock, V.L., McCusker, E., Jankovic, J., Singer, C., Sanchez-Ramos, J., Scott, B., Suchowersky, O., Factor, S.A., Higgins, D.S., Molho, E., Revilla, F., Caviness, J.N., Friedman, J.H., Perlmutter, J.S., Feigin, A., Anderson, K., Rodriguez, R., McFarland, N.R., Margolis, R.L., Farbman, E.S., Raymond, L.A., Suski, V., Kostyk, S., Colcher, A., Seeberger, L., Epping, E., Esmail, S., Diaz, N., Fung, W.L.A., Diamond, A., Frank, S., Hanna, P., Hermanowicz, N., Dure, L.S., Cudkowicz, M., 2017. A randomized, double-blind, placebo-controlled trial of coenzyme Q10 in Huntington disease. Neurology 88, 152–159. https://doi.org/10.1212/WNL.0000000000003478

MCGEER, E.G., MCGEER, P.L., 1976. Duplication of biochemical changes of Huntington's chorea by intrastriatal injections of glutamic and kainic acids. Nature 263, 517–519. https://doi.org/10.1038/263517a0

McNeil, S.M., Novelletto, A., Srinidhi, J., Barnes, G., Kornbluth, I., Altherr, M.R., Wasmuth, J.J., Gusella, J.F., MacDonald, M.E., Myers, R.H., 1997. Reduced Penetrance of the Huntington's Disease Mutation. Hum. Mol. Genet. 6, 775–779. https://doi.org/10.1093/hmg/6.5.775

Medjkane, S., Perez-Sanchez, C., Gaggioli, C., Sahai, E., Treisman, R., 2009. Myocardin-related transcription factors and SRF are required for cytoskeletal dynamics and experimental metastasis. Nat. Cell Biol. 11, 257–268. https://doi.org/10.1038/ncb1833

Menalled, L., Brunner, D., 2014. Animal models of Huntington's disease for translation to the clinic: Best practices. Mov. Disord. 29, 1375–1390. https://doi.org/10.1002/mds.26006

Menalled, L., El-Khodor, B.F., Patry, M., Suárez-Fariñas, M., Orenstein, S.J., Zahasky, B., Leahy, C., Wheeler, V., Yang, X.W., MacDonald, M., Morton, A.J., Bates, G., Leeds, J., Park, L., Howland, D., Signer, E., Tobin, A., Brunner, D., 2009. Systematic behavioral evaluation of Huntington's disease transgenic and knock-in mouse models. Neurobiol. Dis. 35, 319–336. https://doi.org/10.1016/j.nbd.2009.05.007

Menalled, L.B., 2005. Knock-in mouse models of Huntington's disease. NeuroRX 2, 465–470. https://doi.org/10.1602/neurorx.2.3.465

Menalled, L.B., Kudwa, A.E., Miller, S., Fitzpatrick, J., Watson-Johnson, J., Keating, N., Ruiz, M., Mushlin, R., Alosio, W., McConnell, K., Connor, D., Murphy, C., Oakeshott, S., Kwan, M., Beltran, J., Ghavami, A., Brunner, D., Park, L.C., Ramboz, S., Howland, D., 2012. Comprehensive Behavioral and Molecular Characterization of a New Knock-In Mouse Model of Huntington's Disease: zQ175. PLoS One 7, e49838. https://doi.org/10.1371/journal.pone.0049838

Menalled, L.B., Kudwa, A.E., Oakeshott, S., Farrar, A., Paterson, N., Filippov, I., Miller, S., Kwan, M., Olsen, M., Beltran, J., Torello, J., Fitzpatrick, J., Mushlin, R., Cox, K., McConnell, K., Mazzella, M., He, D., Osborne, G.F., Al-Nackkash, R., Bates, G.P., Tuunanen, P., Lehtimaki, K., Brunner, D., Ghavami, A., Ramboz, S., Park, L., Macdonald, D., Munoz-Sanjuan, I., Howland, D., 2014. Genetic Deletion of Transglutaminase 2 Does Not Rescue the Phenotypic Deficits Observed in R6/2 and zQ175 Mouse Models of Huntington's Disease. PLoS One 9, e99520. https://doi.org/10.1371/journal.pone.0099520

Menalled, L.B., Sison, J.D., Dragatsis, I., Zeitlin, S., Chesselet, M.-F., 2003. Time course of early motor and neuropathological anomalies in a knock-in mouse model of Huntington's disease with 140 CAG repeats. J. Comp. Neurol. 465, 11–26. https://doi.org/10.1002/cne.10776

Mericskay, M., Blanc, J., Tritsch, E., Moriez, R., Aubert, P., Neunlist, M., Feil, R., Li, Z., 2007. Inducible Mouse Model of Chronic Intestinal Pseudo-Obstruction by Smooth Muscle-Specific Inactivation of the SRF Gene. Gastroenterology 133, 1960–1970. https://doi.org/10.1053/j.gastro.2007.09.010

Merienne, K., Helmlinger, D., Perkin, G.R., Devys, D., Trottier, Y., 2003. Polyglutamine Expansion Induces a Protein-damaging Stress Connecting Heat Shock Protein 70 to the JNK Pathway. J. Biol. Chem. 278, 16957–16967. https://doi.org/10.1074/jbc.M212049200

Merienne, N., Meunier, C., Schneider, A., Seguin, J., Nair, S.S., Rocher, A.B., Le Gras, S., Keime, C., Faull, R., Pellerin, L., Chatton, J.-Y., Neri, C., Merienne, K., Déglon, N., 2019. Cell-Type-Specific Gene Expression Profiling in Adult Mouse Brain Reveals Normal and Disease-State Signatures. Cell Rep. 26, 2477-2493.e9. https://doi.org/10.1016/j.celrep.2019.02.003

Messaoudi, E., Kanhema, T., Soule, J., Tiron, A., Dagyte, G., da Silva, B., Bramham, C.R., 2007. Sustained Arc/Arg3.1 Synthesis Controls Long-Term Potentiation Consolidation through Regulation of Local Actin Polymerization in the Dentate Gyrus In Vivo. J. Neurosci. 27, 10445–10455. https://doi.org/10.1523/JNEUROSCI.2883-07.2007

Mestre, T., Ferreira, J., Coelho, M.M., Rosa, M., Sampaio, C., 2009. Therapeutic interventions for symptomatic treatment in Huntington's disease. Cochrane Database Syst. Rev. https://doi.org/10.1002/14651858.CD006456.pub2

Miano, J.M., Long, X., Fujiwara, K., 2007. Serum response factor: master regulator of the actin cytoskeleton and contractile apparatus. Am. J. Physiol. Physiol. 292, C70–C81. https://doi.org/10.1152/ajpcell.00386.2006

Miano, J.M., Ramanan, N., Georger, M.A., de Mesy Bentley, K.L., Emerson, R.L., Balza, R.O., Xiao, Q., Weiler, H., Ginty, D.D., Misra, R.P., 2004. Restricted inactivation of serum response factor to the cardiovascular system. Proc. Natl. Acad. Sci. 101, 17132–17137. https://doi.org/10.1073/pnas.0406041101

Miller, J.P., Holcomb, J., Al-Ramahi, I., de Haro, M., Gafni, J., Zhang, N., Kim, E., Sanhueza, M., Torcassi,

C., Kwak, S., Botas, J., Hughes, R.E., Ellerby, L.M., 2010. Matrix Metalloproteinases Are Modifiers of Huntingtin Proteolysis and Toxicity in Huntington's Disease. Neuron 67, 199–212. https://doi.org/10.1016/j.neuron.2010.06.021

Milone, M.C., O'Doherty, U., 2018. Clinical use of lentiviral vectors. Leukemia 32, 1529–1541. https://doi.org/10.1038/s41375-018-0106-0

Milunsky, J., Maher, T., Loose, B., Darras, B., Ito, M., 2003. XL PCR for the detection of large trinucleotide expansions in juvenile Huntington's disease. Clin. Genet. 64, 70–73. https://doi.org/10.1034/j.1399-0004.2003.00108.x

Miniarikova, J., Zimmer, V., Martier, R., Brouwers, C.C., Pythoud, C., Richetin, K., Rey, M., Lubelski, J., Evers, M.M., van Deventer, S.J., Petry, H., Déglon, N., Konstantinova, P., 2017. AAV5-miHTT gene therapy demonstrates suppression of mutant huntingtin aggregation and neuronal dysfunction in a rat model of Huntington's disease. Gene Ther. 24, 630–639. https://doi.org/10.1038/gt.2017.71

Miralles, F., Hebrard, S., Lamotte, L., Durel, B., Gilgenkrantz, H., Li, Z., Daegelen, D., Tuil, D., Joshi, R.L., 2006. Conditional inactivation of the murine serum response factor in the pancreas leads to severe pancreatitis. Lab. Investig. 86, 1020–1036. https://doi.org/10.1038/labinvest.3700457

Miralles, F., Posern, G., Zaromytidou, A.-I., Treisman, R., 2003. Actin Dynamics Control SRF Activity by Regulation of Its Coactivator MAL. Cell 113, 329–342. https://doi.org/10.1016/S0092-8674(03)00278-2

Miranti, C.K., Ginty, D.D., Huang, G., Chatila, T., Greenberg, M.E., 1995. Calcium activates serum response factor-dependent transcription by a Ras- and Elk-1-independent mechanism that involves a Ca2+/calmodulin-dependent kinase. Mol. Cell. Biol. 15, 3672–3684. https://doi.org/10.1128/MCB.15.7.3672

Misra, R.P., Bonni, A., Miranti, C.K., Rivera, V.M., Sheng, M., Greenberg, M.E., 1994. L-type voltage-sensitive calcium channel activation stimulates gene expression by a serum response factor-dependent pathway. J. Biol. Chem. 269, 25483–93.

Mitra, S., Tsvetkov, A.S., Finkbeiner, S., 2009. Single Neuron Ubiquitin-Proteasome Dynamics Accompanying Inclusion Body Formation in Huntington Disease. J. Biol. Chem. 284, 4398–4403. https://doi.org/10.1074/jbc.M806269200

Mochel, F., Haller, R.G., 2011. Energy deficit in Huntington disease: why it matters. J. Clin. Invest. 121, 493–499. https://doi.org/10.1172/JCI45691

Moffitt, H., McPhail, G.D., Woodman, B., Hobbs, C., Bates, G.P., 2009. Formation of Polyglutamine Inclusions in a Wide Range of Non-CNS Tissues in the HdhQ150 Knock-In Mouse Model of Huntington's Disease. PLoS One 4, e8025. https://doi.org/10.1371/journal.pone.0008025

MOGENSON, G., JONES, D., YIM, C., 1980. From motivation to action: Functional interface between the limbic system and the motor system. Prog. Neurobiol. 14, 69–97. https://doi.org/10.1016/0301-0082(80)90018-0

Mokalled, M.H., Johnson, A., Kim, Y., Oh, J., Olson, E.N., 2010. Myocardin-related transcription factors regulate the Cdk5/Pctaire1 kinase cascade to control neurite outgrowth, neuronal migration and brain development. Development 137, 2365–2374. https://doi.org/10.1242/dev.047605

Molina-Calavita, M., Barnat, M., Elias, S., Aparicio, E., Piel, M., Humbert, S., 2014. Mutant Huntingtin Affects Cortical Progenitor Cell Division and Development of the Mouse Neocortex. J. Neurosci. 34, 10034–10040. https://doi.org/10.1523/JNEUROSCI.0715-14.2014

Monteys, A.M., Ebanks, S.A., Keiser, M.S., Davidson, B.L., 2017. CRISPR/Cas9 Editing of the Mutant Huntingtin Allele In Vitro and In Vivo. Mol. Ther. 25, 12–23. https://doi.org/10.1016/j.ymthe.2016.11.010

Morris, T.A., Jafari, N., Rice, A.C., Vasconcelos, O., DeLorenzo, R.J., 1999. Persistent Increased DNA-Binding and Expression of Serum Response Factor Occur with Epilepsy-Associated Long-Term Plasticity Changes. J. Neurosci. 19, 8234–8243. https://doi.org/10.1523/JNEUROSCI.19-19-08234.1999

Moumné, L., Betuing, S., Caboche, J., 2013. Multiple Aspects of Gene Dysregulation in Huntington's Disease. Front. Neurol. 4. https://doi.org/10.3389/fneur.2013.00127

Moumné, L., Campbell, K., Howland, D., Ouyang, Y., Bates, G.P., 2012. Genetic Knock-Down of Hdac3 Does Not Modify Disease-Related Phenotypes in a Mouse Model of Huntington's Disease. PLoS One 7, e31080. https://doi.org/10.1371/journal.pone.0031080

Muchowski, P.J., Schaffar, G., Sittler, A., Wanker, E.E., Hayer-Hartl, M.K., Hartl, F.U., 2000. Hsp70 and Hsp40 chaperones can inhibit self-assembly of polyglutamine proteins into amyloid-like fibrils. Proc. Natl. Acad. Sci. 97, 7841–7846. https://doi.org/10.1073/pnas.140202897

Muehlich, S., Cicha, I., Garlichs, C.D., Krueger, B., Posern, G., Goppelt-Struebe, M., 2007. Actin-dependent regulation of connective tissue growth factor. Am. J. Physiol. Physiol. 292, C1732–C1738. https://doi.org/10.1152/ajpcell.00552.2006

Mühlau, M., Winkelmann, J., Rujescu, D., Giegling, I., Koutsouleris, N., Gaser, C., Arsic, M., Weindl, A., Reiser, M., Meisenzahl, E.M., 2012. Variation within the Huntington's Disease Gene Influences Normal Brain Structure. PLoS One 7, e29809. https://doi.org/10.1371/journal.pone.0029809

Naia, L., Ferreira, I.L., Cunha-Oliveira, T., Duarte, A.I., Ribeiro, M., Rosenstock, T.R., Laço, M.N., Ribeiro, M.J., Oliveira, C.R., Saudou, F., Humbert, S., Rego, A.C., 2015. Activation of IGF-1 and Insulin Signaling Pathways Ameliorate Mitochondrial Function and Energy Metabolism in Huntington's Disease Human Lymphoblasts. Mol. Neurobiol. 51, 331–348. https://doi.org/10.1007/s12035-014-8735-4

Nasir, J., Floresco, S.B., O'Kusky, J.R., Diewert, V.M., Richman, J.M., Zeisler, J., Borowski, A., Marth, J.D., Phillips, A.G., Hayden, M.R., 1995. Targeted disruption of the Huntington's disease gene results in embryonic lethality and behavioral and morphological changes in heterozygotes. Cell 81, 811–823. https://doi.org/10.1016/0092-8674(95)90542-1

Nemudryi, A.A., Valetdinova, K.R., Medvedev, S.P., Zakian, S.M., 2014. TALEN and CRISPR/Cas Genome Editing Systems: Tools of Discovery. Acta Naturae 6, 19–40.

Neto, J.L., Lee, J.-M., Afridi, A., Gillis, T., Guide, J.R., Dempsey, S., Lager, B., Alonso, I., Wheeler, V.C., Pinto, R.M., 2017. Genetic Contributors to Intergenerational CAG Repeat Instability in Huntington's Disease Knock-In Mice. Genetics 205, 503–516. https://doi.org/10.1534/genetics.116.195578

Nguyen, G.D., Molero, A.E., Gokhan, S., Mehler, M.F., 2013. Functions of Huntingtin in Germ Layer

Specification and Organogenesis. PLoS One 8, e72698. https://doi.org/10.1371/journal.pone.0072698

Nguyen, H.P., Kobbe, P., Rahne, H., Wörpel, T., Jäger, B., Stephan, M., Pabst, R., Holzmann, C., Riess, O., Korr, H., Kántor, O., Petrasch-Parwez, E., Wetzel, R., Osmand, A., von Hörsten, S., 2006. Behavioral abnormalities precede neuropathological markers in rats transgenic for Huntington's disease. Hum. Mol. Genet. 15, 3177–3194. https://doi.org/10.1093/hmg/ddl394

Nicolas, G., Devys, D., Goldenberg, A., Maltête, D., Hervé, C., Hannequin, D., Guyant-Maréchal, L., 2011. Juvenile Huntington disease in an 18-month-old boy revealed by global developmental delay and reduced cerebellar volume. Am. J. Med. Genet. Part A 155, 815–818. https://doi.org/10.1002/ajmg.a.33911

Nicoleau, C., Viegas, P., Peschanski, M., Perrier, A.L., 2011. Human Pluripotent Stem Cell Therapy for Huntington's Disease: Technical, Immunological, and Safety Challenges. Neurotherapeutics 8, 562–576. https://doi.org/10.1007/s13311-011-0079-4

Nikitin, V.P., Kozyrev, S.A., 2007. Transcription factor serum response factor is selectively involved in the mechanisms of long-term synapse-specific plasticity. Neurosci. Behav. Physiol. 37, 83–88. https://doi.org/10.1007/s11055-007-0153-x

Noh, J.-Y., Lee, H., Song, S., Kim, N.S., Im, W., Kim, M., Seo, H., Chung, C.-W., Chang, J.-W., Ferrante, R.J., Yoo, Y.-J., Ryu, H., Jung, Y.-K., 2009. SCAMP5 Links Endoplasmic Reticulum Stress to the Accumulation of Expanded Polyglutamine Protein Aggregates via Endocytosis Inhibition. J. Biol. Chem. 284, 11318–11325. https://doi.org/10.1074/jbc.M807620200

Nord, A.S., West, A.E., 2020. Neurobiological functions of transcriptional enhancers. Nat. Neurosci. 23, 5–14. https://doi.org/10.1038/s41593-019-0538-5

Norman, C., Runswick, M., Pollock, R., Treisman, R., 1988. Isolation and properties of cDNA clones encoding SRF, a transcription factor that binds to the c-fos serum response element. Cell 55, 989–1003. https://doi.org/10.1016/0092-8674(88)90244-9

Novak, M.J.U., Tabrizi, S.J., 2011. Huntington's Disease: Clinical Presentation and Treatment. pp. 297–323. https://doi.org/10.1016/B978-0-12-381328-2.00013-4

Nucifora, F.C., Sasaki, M., Peters, M.F., Huang, H., Cooper, J.K., Yamada, M., Takahashi, H., Tsuji, S., Troncoso, J., Dawson, V.L., Dawson, T.M., Ross, C.A., 2001. Interference by huntingtin and atrophin-1 with cbp-mediated transcription leading to cellular toxicity. Science 291, 2423–8. https://doi.org/10.1126/science.1056784

Nucifora Jr., F.C., 2001. Interference by Huntingtin and Atrophin-1 with CBP-Mediated Transcription Leading to Cellular Toxicity. Science (80-.). 291, 2423–2428. https://doi.org/10.1126/science.1056784

O'Donnell, P., 2003. Dopamine gating of forebrain neural ensembles. Eur. J. Neurosci. 17, 429–435. https://doi.org/10.1046/j.1460-9568.2003.02463.x

O'Kusky, J.R., Nasir, J., Cicchetti, F., Parent, A., Hayden, M.R., 1999. Neuronal degeneration in the basal ganglia and loss of pallido-subthalamic synapses in mice with targeted disruption of the Huntington's disease gene. Brain Res. 818, 468–479. https://doi.org/10.1016/S0006-

8993(98)01312-2

Oh, J., Richardson, J.A., Olson, E.N., 2005. Requirement of myocardin-related transcription factor-B for remodeling of branchial arch arteries and smooth muscle differentiation. Proc. Natl. Acad. Sci. 102, 15122–15127. https://doi.org/10.1073/pnas.0507346102

Ohrnberger, S., Thavamani, A., Braeuning, A., Lipka, D.B., Kirilov, M., Geffers, R., Authenrieth, S.E., Römer, M., Zell, A., Bonin, M., Schwarz, M., Schütz, G., Schirmacher, P., Plass, C., Longerich, T., Nordheim, A., 2015. Dysregulated serum response factor triggers formation of hepatocellular carcinoma. Hepatology 61, 979–989. https://doi.org/10.1002/hep.27539

OHSAWA, Y., ISAHARA, K., KANAMORI, S., SHIBATA, M., KAMETAKA, S., GOTOW, T., WATANABE, T., KOMINAMI, E., UCHIYAMA, Y., UCHIYAMA, Y., 1998. An Ultrastructural and Immunohistochemical Study of PC12 Cells During Apoptosis Induced by Serum Deprivation with Special Reference to Autophagy and Lysosomal Cathepsins. Arch. Histol. Cytol. 61, 395–403. https://doi.org/10.1679/aohc.61.395

Oliveira, J.M.A., Chen, S., Almeida, S., Riley, R., Goncalves, J., Oliveira, C.R., Hayden, M.R., Nicholls, D.G., Ellerby, L.M., Rego, A.C., 2006. Mitochondrial-Dependent Ca2+ Handling in Huntington's Disease Striatal Cells: Effect of Histone Deacetylase Inhibitors. J. Neurosci. 26, 11174–11186. https://doi.org/10.1523/JNEUROSCI.3004-06.2006

Olson, E.N., Nordheim, A., 2010. Linking actin dynamics and gene transcription to drive cellular motile functions. Nat. Rev. Mol. Cell Biol. 11, 353–365. https://doi.org/10.1038/nrm2890

Ordway, J.M., Tallaksen-Greene, S., Gutekunst, C.-A., Bernstein, E.M., Cearley, J.A., Wiener, H.W., Dure, L.S., Lindsey, R., Hersch, S.M., Jope, R.S., Albin, R.., Detloff, P.J., 1997. Ectopically Expressed CAG Repeats Cause Intranuclear Inclusions and a Progressive Late Onset Neurological Phenotype in the Mouse. Cell 91, 753–763. https://doi.org/10.1016/S0092-8674(00)80464-X

Orr, H.T., 2012a. Polyglutamine neurodegeneration: expanded glutamines enhance native functions. Curr. Opin. Genet. Dev. 22, 251–5. https://doi.org/10.1016/j.gde.2012.01.001

Orr, H.T., 2012b. Polyglutamine neurodegeneration: expanded glutamines enhance native functions. Curr. Opin. Genet. Dev. 22, 251–255. https://doi.org/10.1016/j.gde.2012.01.001

Ortiz, A.N., Osterhaus, G.L., Lauderdale, K., Mahoney, L., Fowler, S.C., von Hörsten, S., Riess, O., Johnson, M.A., 2012. Motor function and dopamine release measurements in transgenic Huntington's disease model rats. Brain Res. 1450, 148–156. https://doi.org/10.1016/j.brainres.2012.02.042

Palidwor, G.A., Shcherbinin, S., Huska, M.R., Rasko, T., Stelzl, U., Arumughan, A., Foulle, R., Porras, P., Sanchez-Pulido, L., Wanker, E.E., Andrade-Navarro, M.A., 2009. Detection of Alpha-Rod Protein Repeats Using a Neural Network and Application to Huntingtin. PLoS Comput. Biol. 5, e1000304. https://doi.org/10.1371/journal.pcbi.1000304

Pandey, U.B., Nie, Z., Batlevi, Y., McCray, B.A., Ritson, G.P., Nedelsky, N.B., Schwartz, S.L., DiProspero, N.A., Knight, M.A., Schuldiner, O., Padmanabhan, R., Hild, M., Berry, D.L., Garza, D., Hubbert, C.C., Yao, T.-P., Baehrecke, E.H., Taylor, J.P., 2007. HDAC6 rescues neurodegeneration and provides an essential link between autophagy and the UPS. Nature 447, 860–864. https://doi.org/10.1038/nature05853

Panov, A. V., Gutekunst, C.-A., Leavitt, B.R., Hayden, M.R., Burke, J.R., Strittmatter, W.J., Greenamyre, J.T., 2002. Early mitochondrial calcium defects in Huntington's disease are a direct effect of polyglutamines. Nat. Neurosci. 5, 731–736. https://doi.org/10.1038/nn884

Papoutsi, M., Labuschagne, I., Tabrizi, S.J., Stout, J.C., 2014. The cognitive burden in Huntington's disease: Pathology, phenotype, and mechanisms of compensation. Mov. Disord. 29, 673–683. https://doi.org/10.1002/mds.25864

Park, I.-H., Arora, N., Huo, H., Maherali, N., Ahfeldt, T., Shimamura, A., Lensch, M.W., Cowan, C., Hochedlinger, K., Daley, G.Q., 2008. Disease-Specific Induced Pluripotent Stem Cells. Cell 134, 877–886. https://doi.org/10.1016/j.cell.2008.07.041

Park, S.-H., Kukushkin, Y., Gupta, R., Chen, T., Konagai, A., Hipp, M.S., Hayer-Hartl, M., Hartl, F.U., 2013. PolyQ Proteins Interfere with Nuclear Degradation of Cytosolic Proteins by Sequestering the Sis1p Chaperone. Cell 154, 134–145. https://doi.org/10.1016/j.cell.2013.06.003

Parkitna, J.R., Bilbao, A., Rieker, C., Engblom, D., Piechota, M., Nordheim, A., Spanagel, R., Schütz, G., 2010a. Loss of the serum response factor in the dopamine system leads to hyperactivity. FASEB J. 24, 2427–2435. https://doi.org/10.1096/fj.09-151423

Parkitna, J.R., Bilbao, A., Rieker, C., Engblom, D., Piechota, M., Nordheim, A., Spanagel, R., Schütz, G., 2010b. Loss of the serum response factor in the dopamine system leads to hyperactivity. FASEB J. 24, 2427–2435. https://doi.org/10.1096/fj.09-151423

Parlakian, A., Charvet, C., Escoubet, B., Mericskay, M., Molkentin, J.D., Gary-Bobo, G., De Windt, L.J., Ludosky, M.-A., Paulin, D., Daegelen, D., Tuil, D., Li, Z., 2005. Temporally Controlled Onset of Dilated Cardiomyopathy Through Disruption of the SRF Gene in Adult Heart. Circulation 112, 2930–2939. https://doi.org/10.1161/CIRCULATIONAHA.105.533778

Parlakian, A., Tuil, D., Hamard, G., Tavernier, G., Hentzen, D., Concordet, J.-P., Paulin, D., Li, Z., Daegelen, D., 2004. Targeted Inactivation of Serum Response Factor in the Developing Heart Results in Myocardial Defects and Embryonic Lethality. Mol. Cell. Biol. 24, 5281–5289. https://doi.org/10.1128/MCB.24.12.5281-5289.2004

Pastor, W.A., Aravind, L., Rao, A., 2013. TETonic shift: biological roles of TET proteins in DNA demethylation and transcription. Nat. Rev. Mol. Cell Biol. 14, 341–356. https://doi.org/10.1038/nrm3589

Peschanski, M., Cesaro, P., Hantraye, P., 1995. Rationale for intrastriatal grafting of striatal neuroblasts in patients with Huntington's disease. Neuroscience 68, 273–285. https://doi.org/10.1016/0306-4522(95)00162-C

Philippar, U., Schratt, G., Dieterich, C., Müller, J.M., Galgóczy, P., Engel, F.B., Keating, M.T., Gertler, F., Schüle, R., Vingron, M., Nordheim, A., 2004. The SRF Target Gene Fhl2 Antagonizes RhoA/MAL-Dependent Activation of SRF. Mol. Cell 16, 867–880. https://doi.org/10.1016/j.molcel.2004.11.039

Pintchovski, S.A., Peebles, C.L., Joo Kim, H., Verdin, E., Finkbeiner, S., 2009. The Serum Response Factor and a Putative Novel Transcription Factor Regulate Expression of the Immediate-Early Gene Arc/Arg3.1 in Neurons. J. Neurosci. 29, 1525–1537. https://doi.org/10.1523/JNEUROSCI.5575-08.2009

Pinto, R.M., Dragileva, E., Kirby, A., Lloret, A., Lopez, E., St. Claire, J., Panigrahi, G.B., Hou, C., Holloway, K., Gillis, T., Guide, J.R., Cohen, P.E., Li, G.-M., Pearson, C.E., Daly, M.J., Wheeler, V.C., 2013. Mismatch Repair Genes Mlh1 and Mlh3 Modify CAG Instability in Huntington's Disease Mice: Genome-Wide and Candidate Approaches. PLoS Genet. 9, e1003930. https://doi.org/10.1371/journal.pgen.1003930

Pittenger, M.F., 1999. Multilineage Potential of Adult Human Mesenchymal Stem Cells. Science (80-.). 284, 143–147. https://doi.org/10.1126/science.284.5411.143

Pla, P., Orvoen, S., Saudou, F., David, D.J., Humbert, S., 2014. Mood disorders in Huntington's disease: from behavior to cellular and molecular mechanisms. Front. Behav. Neurosci. 8. https://doi.org/10.3389/fnbeh.2014.00135

Plank, J.L., Dean, A., 2014. Enhancer Function: Mechanistic and Genome-Wide Insights Come Together. Mol. Cell 55, 5–14. https://doi.org/10.1016/j.molcel.2014.06.015

Plath, N., Ohana, O., Dammermann, B., Errington, M.L., Schmitz, D., Gross, C., Mao, X., Engelsberg, A., Mahlke, C., Welzl, H., Kobalz, U., Stawrakakis, A., Fernandez, E., Waltereit, R., Bick-Sander, A., Therstappen, E., Cooke, S.F., Blanquet, V., Wurst, W., Salmen, B., Bösl, M.R., Lipp, H.-P., Grant, S.G.N., Bliss, T.V.P., Wolfer, D.P., Kuhl, D., 2006. Arc/Arg3.1 Is Essential for the Consolidation of Synaptic Plasticity and Memories. Neuron 52, 437–444. https://doi.org/10.1016/j.neuron.2006.08.024

Plotkin, J.L., Surmeier, D.J., 2015. Corticostriatal synaptic adaptations in Huntington's disease. Curr. Opin. Neurobiol. 33, 53–62. https://doi.org/10.1016/j.conb.2015.01.020

Pol-Bodetto, S., Jeltsch-David, H., Lecourtier, L., Rusnac, N., Mam-Lam-Fook, C., Cosquer, B., Geiger, K., Cassel, J.-C., 2011. The double-H maze test, a novel, simple, water-escape memory task: Acquisition, recall of recent and remote memory, and effects of systemic muscarinic or NMDA receptor blockade during training. Behav. Brain Res. 218, 138–151. https://doi.org/10.1016/j.bbr.2010.11.043

Pollock, K., Dahlenburg, H., Nelson, H., Fink, K.D., Cary, W., Hendrix, K., Annett, G., Torrest, A., Deng, P., Gutierrez, J., Nacey, C., Pepper, K., Kalomoiris, S., Anderson, J.D., McGee, J., Gruenloh, W., Fury, B., Bauer, G., Duffy, A., Tempkin, T., Wheelock, V., Nolta, J.A., 2016. Human Mesenchymal Stem Cells Genetically Engineered to Overexpress Brain-derived Neurotrophic Factor Improve Outcomes in Huntington's Disease Mouse Models. Mol. Ther. 24, 965–977. https://doi.org/10.1038/mt.2016.12

Posern, G., Treisman, R., 2006. Actin' together: serum response factor, its cofactors and the link to signal transduction. Trends Cell Biol. 16, 588–596. https://doi.org/10.1016/j.tcb.2006.09.008

Poudel, G.R., Egan, G.F., Churchyard, A., Chua, P., Stout, J.C., Georgiou-Karistianis, N., 2014. Abnormal synchrony of resting state networks in premanifest and symptomatic Huntington disease: the IMAGE-HD study. J. Psychiatry Neurosci. 39, 87–96. https://doi.org/10.1503/jpn.120226

Pouladi, M.A., Morton, A.J., Hayden, M.R., 2013. Choosing an animal model for the study of Huntington's disease. Nat. Rev. Neurosci. 14, 708–721. https://doi.org/10.1038/nrn3570

Price, M.A., Rogers, A.E., Treisman, R., 1995. Comparative analysis of the ternary complex factors Elk-1, SAP-1a and SAP-2 (ERP/NET). EMBO J. 14, 2589–601.

Qin, Z.-H., 2003. Autophagy regulates the processing of amino terminal huntingtin fragments. Hum. Mol. Genet. 12, 3231–3244. https://doi.org/10.1093/hmg/ddg346

Ramanan, N., Shen, Y., Sarsfield, S., Lemberger, T., Schütz, G., Linden, D.J., Ginty, D.D., 2005. SRF mediates activity-induced gene expression and synaptic plasticity but not neuronal viability. Nat. Neurosci. 8, 759–767. https://doi.org/10.1038/nn1462

Ramaswamy, S., McBride, J.L., Kordower, J.H., 2007. Animal Models of Huntington's Disease. ILAR J. 48, 356–373. https://doi.org/10.1093/ilar.48.4.356

Rasola, A., Sciacovelli, M., Pantic, B., Bernardi, P., 2010. Signal transduction to the permeability transition pore. FEBS Lett. 584, 1989–1996. https://doi.org/10.1016/j.febslet.2010.02.022

Rattray, I., Smith, E.J., Crum, W.R., Walker, T.A., Gale, R., Bates, G.P., Modo, M., 2013. Correlations of Behavioral Deficits with Brain Pathology Assessed through Longitudinal MRI and Histopathology in the R6/1 Mouse Model of Huntington's Disease. PLoS One 8, e84726. https://doi.org/10.1371/journal.pone.0084726

Ravikumar, B., Vacher, C., Berger, Z., Davies, J.E., Luo, S., Oroz, L.G., Scaravilli, F., Easton, D.F., Duden, R., O'Kane, C.J., Rubinsztein, D.C., 2004. Inhibition of mTOR induces autophagy and reduces toxicity of polyglutamine expansions in fly and mouse models of Huntington disease. Nat. Genet. 36, 585–595. https://doi.org/10.1038/ng1362

Rech, J., Barlat, I., Veyrune, J.L., Vie, A., Blanchard, J.M., 1994. Nuclear import of serum response factor (SRF) requires a short amino-terminal nuclear localization sequence and is independent of the casein kinase II phosphorylation site. J. Cell Sci. 107 (Pt 1, 3029–36.

Reilmann, R., Leavitt, B.R., Ross, C.A., 2014. Diagnostic criteria for Huntington's disease based on natural history. Mov. Disord. 29, 1335–1341. https://doi.org/10.1002/mds.26011

Reilmann, R., Schubert, R., 2017. Motor outcome measures in Huntington disease clinical trials. pp. 209–225. https://doi.org/10.1016/B978-0-12-801893-4.00018-3

Reiner, A., Del Mar, N., Meade, C.A., Yang, H., Dragatsis, I., Zeitlin, S., Goldowitz, D., 2001. Neurons Lacking Huntingtin Differentially Colonize Brain and Survive in Chimeric Mice. J. Neurosci. 21, 7608–7619. https://doi.org/10.1523/JNEUROSCI.21-19-07608.2001

Ren, G., Jin, W., Cui, K., Rodrigez, J., Hu, G., Zhang, Z., Larson, D.R., Zhao, K., 2017. CTCF-Mediated Enhancer-Promoter Interaction Is a Critical Regulator of Cell-to-Cell Variation of Gene Expression. Mol. Cell 67, 1049-1058.e6. https://doi.org/10.1016/j.molcel.2017.08.026

Renna, M., Jimenez-Sanchez, M., Sarkar, S., Rubinsztein, D.C., 2010. Chemical Inducers of Autophagy That Enhance the Clearance of Mutant Proteins in Neurodegenerative Diseases. J. Biol. Chem. 285, 11061–11067. https://doi.org/10.1074/jbc.R109.072181

Richard, G.-F., Viterbo, D., Khanna, V., Mosbach, V., Castelain, L., Dujon, B., 2014. Highly Specific Contractions of a Single CAG/CTG Trinucleotide Repeat by TALEN in Yeast. PLoS One 9, e95611. https://doi.org/10.1371/journal.pone.0095611

Rigamonti, D., Bauer, J.H., De-Fraja, C., Conti, L., Sipione, S., Sciorati, C., Clementi, E., Hackam, A., Hayden, M.R., Li, Y., Cooper, J.K., Ross, C.A., Govoni, S., Vincenz, C., Cattaneo, E., 2000. Wild-Type

Huntingtin Protects from Apoptosis Upstream of Caspase-3. J. Neurosci. 20, 3705–3713. https://doi.org/10.1523/JNEUROSCI.20-10-03705.2000

Rigamonti, D., Sipione, S., Goffredo, D., Zuccato, C., Fossale, E., Cattaneo, E., 2001. Huntingtin's Neuroprotective Activity Occurs via Inhibition of Procaspase-9 Processing. J. Biol. Chem. 276, 14545–14548. https://doi.org/10.1074/jbc.C100044200

Rinaldi, C., Wood, M.J.A., 2018. Antisense oligonucleotides: the next frontier for treatment of neurological disorders. Nat. Rev. Neurol. 14, 9–21. https://doi.org/10.1038/nrneurol.2017.148

Ring, K.L., An, M.C., Zhang, N., O'Brien, R.N., Ramos, E.M., Gao, F., Atwood, R., Bailus, B.J., Melov, S., Mooney, S.D., Coppola, G., Ellerby, L.M., 2015. Genomic Analysis Reveals Disruption of Striatal Neuronal Development and Therapeutic Targets in Human Huntington's Disease Neural Stem Cells. Stem Cell Reports 5, 1023–1038. https://doi.org/10.1016/j.stemcr.2015.11.005

Rockabrand, E., Slepko, N., Pantalone, A., Nukala, V.N., Kazantsev, A., Marsh, J.L., Sullivan, P.G., Steffan, J.S., Sensi, S.L., Thompson, L.M., 2007. The first 17 amino acids of Huntingtin modulate its sub-cellular localization, aggregation and effects on calcium homeostasis. Hum. Mol. Genet. 16, 61–77. https://doi.org/10.1093/hmg/ddl440

Rosas, H.D., Doros, G., Gevorkian, S., Malarick, K., Reuter, M., Coutu, J.-P., Triggs, T.D., Wilkens, P.J., Matson, W., Salat, D.H., Hersch, S.M., 2014. PRECREST: A phase II prevention and biomarker trial of creatine in at-risk Huntington disease. Neurology 82, 850–857. https://doi.org/10.1212/WNL.0000000000000187

Rosas, H.D., Koroshetz, W.J., Chen, Y.I., Skeuse, C., Vangel, M., Cudkowicz, M.E., Caplan, K., Marek, K., Seidman, L.J., Makris, N., Jenkins, B.G., Goldstein, J.M., 2003. Evidence for more widespread cerebral pathology in early HD: An MRI-based morphometric analysis. Neurology 60, 1615–1620. https://doi.org/10.1212/01.WNL.0000065888.88988.6E

Rosas, H.D., Tuch, D.S., Hevelone, N.D., Zaleta, A.K., Vangel, M., Hersch, S.M., Salat, D.H., 2006. Diffusion tensor imaging in presymptomatic and early Huntington's disease: Selective white matter pathology and its relationship to clinical measures. Mov. Disord. 21, 1317–1325. https://doi.org/10.1002/mds.20979

Ross, C.A., Poirier, M.A., 2005. What is the role of protein aggregation in neurodegeneration? Nat. Rev. Mol. Cell Biol. 6, 891–898. https://doi.org/10.1038/nrm1742

Ross, C.A., Tabrizi, S.J., 2011. Huntington's disease: from molecular pathogenesis to clinical treatment. Lancet Neurol. 10, 83–98. https://doi.org/10.1016/S1474-4422(10)70245-3

Rowley, M.J., Corces, V.G., 2018. Organizational principles of 3D genome architecture. Nat. Rev. Genet. 19, 789–800. https://doi.org/10.1038/s41576-018-0060-8

Rubinsztein, D.C., Leggo, J., Coles, R., Almqvist, E., Biancalana, V., Cassiman, J.J., Chotai, K., Connarty, M., Crauford, D., Curtis, A., Curtis, D., Davidson, M.J., Differ, A.M., Dode, C., Dodge, A., Frontali, M., Ranen, N.G., Stine, O.C., Sherr, M., Abbott, M.H., Franz, M.L., Graham, C.A., Harper, P.S., Hedreen, J.C., Hayden, M.R., 1996. Phenotypic characterization of individuals with 30-40 CAG repeats in the Huntington disease (HD) gene reveals HD cases with 36 repeats and apparently normal elderly individuals with 36-39 repeats. Am. J. Hum. Genet. 59, 16–22.

Rudolph, D., Tafuri, A., Gass, P., Hammerling, G.J., Arnold, B., Schutz, G., 1998. Impaired fetal T cell development and perinatal lethality in mice lacking the cAMP response element binding protein. Proc. Natl. Acad. Sci. 95, 4481–4486. https://doi.org/10.1073/pnas.95.8.4481

Runne, H., Regulier, E., Kuhn, A., Zala, D., Gokce, O., Perrin, V., Sick, B., Aebischer, P., Deglon, N., Luthi-Carter, R., 2008. Dysregulation of Gene Expression in Primary Neuron Models of Huntington's Disease Shows That Polyglutamine-Related Effects on the Striatal Transcriptome May Not Be Dependent on Brain Circuitry. J. Neurosci. 28, 9723–9731. https://doi.org/10.1523/JNEUROSCI.3044-08.2008

Ruzo, A., Ismailoglu, I., Popowski, M., Haremaki, T., Croft, G.F., Deglincerti, A., Brivanlou, A.H., 2015. Discovery of Novel Isoforms of Huntingtin Reveals a New Hominid-Specific Exon. PLoS One 10, e0127687. https://doi.org/10.1371/journal.pone.0127687

Safety and tolerability of high-dosage coenzyme Q 10 in Huntington's disease and healthy subjects, 2010. . Mov. Disord. 25, 1924–1928. https://doi.org/10.1002/mds.22408

Sandström, J., Heiduschka, P., Beck, S.C., Philippar, U., Seeliger, M.W., Schraermeyer, U., Nordheim, A., 2011. Degeneration of the mouse retina upon dysregulated activity of serum response factor. Mol. Vis. 17, 1110–27.

Sapp, E., Ge, P., Aizawa, H., Bird, E., Penney, J., Young, A.B., Vonsattel, J.-P., Difiglia, M., 1995. Evidence for a preferential loss of enkephalin immunoreactivity in the external globus pallidus in low grade Huntington's disease using high resolution image analysis. Neuroscience 64, 397–404. https://doi.org/10.1016/0306-4522(94)00427-7

Sasakawa, Y., Naoe, Y., Sogo, N., Inoue, T., Sasakawa, T., Matsuo, M., Manda, T., Mutoh, S., 2005. Marker genes to predict sensitivity to FK228, a histone deacetylase inhibitor. Biochem. Pharmacol. 69, 603–616. https://doi.org/10.1016/j.bcp.2004.11.008

Sathasivam, K., Neueder, A., Gipson, T.A., Landles, C., Benjamin, A.C., Bondulich, M.K., Smith, D.L., Faull, R.L.M., Roos, R.A.C., Howland, D., Detloff, P.J., Housman, D.E., Bates, G.P., 2013. Aberrant splicing of HTT generates the pathogenic exon 1 protein in Huntington disease. Proc. Natl. Acad. Sci. 110, 2366–2370. https://doi.org/10.1073/pnas.1221891110

Saudou, F., Finkbeiner, S., Devys, D., Greenberg, M.E., 1998. Huntingtin Acts in the Nucleus to Induce Apoptosis but Death Does Not Correlate with the Formation of Intranuclear Inclusions. Cell 95, 55–66. https://doi.org/10.1016/S0092-8674(00)81782-1

Saudou, F., Humbert, S., 2016a. The Biology of Huntingtin. Neuron 89, 910–26. https://doi.org/10.1016/j.neuron.2016.02.003

Saudou, F., Humbert, S., 2016b. The Biology of Huntingtin. Neuron 89, 910–926. https://doi.org/10.1016/j.neuron.2016.02.003

Saunders, B.T., Robinson, T.E., 2012. The role of dopamine in the accumbens core in the expression of Pavlovian-conditioned responses. Eur. J. Neurosci. 36, 2521–2532. https://doi.org/10.1111/j.1460-9568.2012.08217.x

Savić, N., Schwank, G., 2016. Advances in therapeutic CRISPR/Cas9 genome editing. Transl. Res. 168, 15–21. https://doi.org/10.1016/j.trsl.2015.09.008

Sawa, A., Wiegand, G.W., Cooper, J., Margolis, R.L., Sharp, A.H., Lawler, J.F., Greenamyre, J.T., Snyder, S.H., Ross, C.A., 1999. Increased apoptosis of Huntington disease lymphoblasts associated with repeat length-dependent mitochondrial depolarization. Nat. Med. 5, 1194–1198. https://doi.org/10.1038/13518

Sawiak, S.J., Wood, N.I., Morton, A.J., 2016. Similar Progression of Morphological and Metabolic Phenotype in R6/2 Mice with Different CAG Repeats Revealed by In Vivo Magnetic Resonance Imaging and Spectroscopy. J. Huntingtons. Dis. 5, 271–283. https://doi.org/10.3233/JHD-160208

Schaukowitch, K., Joo, J.-Y., Liu, X., Watts, J.K., Martinez, C., Kim, T.-K., 2014. Enhancer RNA Facilitates NELF Release from Immediate Early Genes. Mol. Cell 56, 29–42. https://doi.org/10.1016/j.molcel.2014.08.023

Schechter, D.C., 1975. St. Vitus' dance and rheumatic disease. N. Y. State J. Med. 75, 1091–102.

Schilling, G., 1999. Intranuclear inclusions and neuritic aggregates in transgenic mice expressing a mutant N-terminal fragment of huntingtin [published erratum appears in Hum Mol Genet 1999 May;8(5):943]. Hum. Mol. Genet. 8, 397–407. https://doi.org/10.1093/hmg/8.3.397

Schipper-Krom, S., Juenemann, K., Jansen, A.H., Wiemhoefer, A., van den Nieuwendijk, R., Smith, D.L., Hink, M.A., Bates, G.P., Overkleeft, H., Ovaa, H., Reits, E., 2014. Dynamic recruitment of active proteasomes into polyglutamine initiated inclusion bodies. FEBS Lett. 588, 151–159. https://doi.org/10.1016/j.febslet.2013.11.023

Schratt, G., 2009. Fine-tuning neural gene expression with microRNAs. Curr. Opin. Neurobiol. 19, 213–219. https://doi.org/10.1016/j.conb.2009.05.015

Schratt, G., Philippar, U., Berger, J., Schwarz, H., Heidenreich, O., Nordheim, A., 2002. Serum response factor is crucial for actin cytoskeletal organization and focal adhesion assembly in embryonic stem cells. J. Cell Biol. 156, 737–750. https://doi.org/10.1083/jcb.200106008

Schratt, G., Philippar, U., Hockemeyer, D., Schwarz, H., Alberti, S., Nordheim, A., 2004. SRF regulates Bcl-2 expression and promotes cell survival during murine embryonic development. EMBO J. 23, 1834–1844. https://doi.org/10.1038/sj.emboj.7600188

Schröter, H., Mueller, C.G., Meese, K., Nordheim, A., 1990. Synergism in ternary complex formation between the dimeric glycoprotein p67SRF, polypeptide p62TCF and the c-fos serum response element. EMBO J. 9, 1123–30.

Schulte, J., Littleton, J.T., 2011. The biological function of the Huntingtin protein and its relevance to Huntington's Disease pathology. Curr. Trends Neurol. 5, 65–78.

Schwarz-Sommer, Z., Huijser, P., Nacken, W., Saedler, H., Sommer, H., 1990. Genetic Control of Flower Development by Homeotic Genes in Antirrhinum majus. Science (80-.). 250, 931–936. https://doi.org/10.1126/science.250.4983.931

Seong, I.S., Woda, J.M., Song, J.-J., Lloret, A., Abeyrathne, P.D., Woo, C.J., Gregory, G., Lee, J.-M., Wheeler, V.C., Walz, T., Kingston, R.E., Gusella, J.F., Conlon, R.A., MacDonald, M.E., 2010. Huntingtin facilitates polycomb repressive complex 2. Hum. Mol. Genet. 19, 573–583. https://doi.org/10.1093/hmg/ddp524

Seredenina, T., Gokce, O., Luthi-Carter, R., 2011. Decreased Striatal RGS2 Expression Is Neuroprotective in Huntington's Disease (HD) and Exemplifies a Compensatory Aspect of HD-Induced Gene Regulation. PLoS One 6, e22231. https://doi.org/10.1371/journal.pone.0022231

Seredenina, T., Luthi-Carter, R., 2012. What have we learned from gene expression profiles in Huntington's disease? Neurobiol. Dis. 45, 83–98. https://doi.org/10.1016/j.nbd.2011.07.001

Setten, R.L., Rossi, J.J., Han, S., 2019. The current state and future directions of RNAi-based therapeutics. Nat. Rev. Drug Discov. 18, 421–446. https://doi.org/10.1038/s41573-019-0017-4

Sgambato, V., Vanhoutte, P., Pagès, C., Rogard, M., Hipskind, R., Besson, M.-J., Caboche, J., 1998. In Vivo Expression and Regulation of Elk-1, a Target of the Extracellular-Regulated Kinase Signaling Pathway, in the Adult Rat Brain. J. Neurosci. 18, 214–226. https://doi.org/10.1523/JNEUROSCI.18-01-00214.1998

Shaid, S., Brandts, C.H., Serve, H., Dikic, I., 2013. Ubiquitination and selective autophagy. Cell Death Differ. 20, 21–30. https://doi.org/10.1038/cdd.2012.72

Sharma, S., Taliyan, R., 2015. Transcriptional dysregulation in Huntington's disease: The role of histone deacetylases. Pharmacol. Res. 100, 157–169. https://doi.org/10.1016/j.phrs.2015.08.002

Shaw, P.E., Schröter, H., Nordheim, A., 1989. The ability of a ternary complex to form over the serum response element correlates with serum inducibility of the human c-fos promoter. Cell 56, 563–572. https://doi.org/10.1016/0092-8674(89)90579-5

Shaywitz, A.J., Greenberg, M.E., 1999. CREB: A Stimulus-Induced Transcription Factor Activated by A Diverse Array of Extracellular Signals. Annu. Rev. Biochem. 68, 821–861. https://doi.org/10.1146/annurev.biochem.68.1.821

Shin, J.W., Kim, K.-H., Chao, M.J., Atwal, R.S., Gillis, T., MacDonald, M.E., Gusella, J.F., Lee, J.-M., 2016. Permanent inactivation of Huntington's disease mutation by personalized allele-specific CRISPR/Cas9. Hum. Mol. Genet. ddw286. https://doi.org/10.1093/hmg/ddw286

Shiota, J., Ishikawa, M., Sakagami, H., Tsuda, M., Baraban, J.M., Tabuchi, A., 2006. Developmental expression of the SRF co-activator MAL in brain: role in regulating dendritic morphology. J. Neurochem. 98, 1778–1788. https://doi.org/10.1111/j.1471-4159.2006.03992.x

Shirendeb, U., Reddy, A.P., Manczak, M., Calkins, M.J., Mao, P., Tagle, D.A., Hemachandra Reddy, P., 2011. Abnormal mitochondrial dynamics, mitochondrial loss and mutant huntingtin oligomers in Huntington's disease: implications for selective neuronal damage. Hum. Mol. Genet. 20, 1438–1455. https://doi.org/10.1093/hmg/ddr024

Shirendeb, U.P., Calkins, M.J., Manczak, M., Anekonda, V., Dufour, B., McBride, J.L., Mao, P., Reddy, P.H., 2012. Mutant huntingtin's interaction with mitochondrial protein Drp1 impairs mitochondrial biogenesis and causes defective axonal transport and synaptic degeneration in Huntington's disease. Hum. Mol. Genet. 21, 406–420. https://doi.org/10.1093/hmg/ddr475

Shore, P., Sharrocks, A.D., 1995. The MADS-Box Family of Transcription Factors. Eur. J. Biochem. 229, 1–13. https://doi.org/10.1111/j.1432-1033.1995.tb20430.x

Sieradzan, K.A., Mechan, A.O., Jones, L., Wanker, E.E., Nukina, N., Mann, D.M.A., 1999. Huntington's

Disease Intranuclear Inclusions Contain Truncated, Ubiquitinated Huntingtin Protein. Exp. Neurol. 156, 92–99. https://doi.org/10.1006/exnr.1998.7005

Silva, A.J., Kogan, J.H., Frankland, P.W., Kida, S., 1998. CREB AND MEMORY. Annu. Rev. Neurosci. 21, 127–148. https://doi.org/10.1146/annurev.neuro.21.1.127

Simmons, D.A., Belichenko, N.P., Yang, T., Condon, C., Monbureau, M., Shamloo, M., Jing, D., Massa, S.M., Longo, F.M., 2013. A Small Molecule TrkB Ligand Reduces Motor Impairment and Neuropathology in R6/2 and BACHD Mouse Models of Huntington's Disease. J. Neurosci. 33, 18712–18727. https://doi.org/10.1523/JNEUROSCI.1310-13.2013

Simpson, S.A., Rae, D., 2012. A standard of care for Huntington's disease: who, what and why. Neurodegener. Dis. Manag. 2, 1–5. https://doi.org/10.2217/nmt.11.85

Singh-Bains, M.K., Waldvogel, H.J., Faull, R.L.M., 2016. The role of the human globus pallidus in Huntington's disease. Brain Pathol. 26, 741–751. https://doi.org/10.1111/bpa.12429

Slow, E.J., 2003. Selective striatal neuronal loss in a YAC128 mouse model of Huntington disease. Hum. Mol. Genet. 12, 1555–1567. https://doi.org/10.1093/hmg/ddg169

Smith, M.R., Syed, A., Lukacsovich, T., Purcell, J., Barbaro, B.A., Worthge, S.A., Wei, S.R., Pollio, G., Magnoni, L., Scali, C., Massai, L., Franceschini, D., Camarri, M., Gianfriddo, M., Diodato, E., Thomas, R., Gokce, O., Tabrizi, S.J., Caricasole, A., Landwehrmeyer, B., Menalled, L., Murphy, C., Ramboz, S., Luthi-Carter, R., Westerberg, G., Marsh, J.L., 2014. A potent and selective Sirtuin 1 inhibitor alleviates pathology in multiple animal and cell models of Huntington's disease. Hum. Mol. Genet. 23, 2995–3007. https://doi.org/10.1093/hmg/ddu010

Smith, Y., Bennett, B.D., Bolam, J.P., Parent, A., Sadikot, A.F., 1994. Synaptic relationships between dopaminergic afferents and cortical or thalamic input in the sensorimotor territory of the striatum in monkey. J. Comp. Neurol. 344, 1–19. https://doi.org/10.1002/cne.903440102

Snell, R.G., MacMillan, J.C., Cheadle, J.P., Fenton, I., Lazarou, L.P., Davies, P., MacDonald, M.E., Gusella, J.F., Harper, P.S., Shaw, D.J., 1993. Relationship between trinucleotide repeat expansion and phenotypic variation in Huntington's disease. Nat. Genet. 4, 393–397. https://doi.org/10.1038/ng0893-393

Song, W., Chen, J., Petrilli, A., Liot, G., Klinglmayr, E., Zhou, Y., Poquiz, P., Tjong, J., Pouladi, M.A., Hayden, M.R., Masliah, E., Ellisman, M., Rouiller, I., Schwarzenbacher, R., Bossy, B., Perkins, G., Bossy-Wetzel, E., 2011. Mutant huntingtin binds the mitochondrial fission GTPase dynamin-related protein-1 and increases its enzymatic activity. Nat. Med. 17, 377–382. https://doi.org/10.1038/nm.2313

Sontag, E.M., Joachimiak, L.A., Tan, Z., Tomlinson, A., Housman, D.E., Glabe, C.G., Potkin, S.G., Frydman, J., Thompson, L.M., 2013. Exogenous delivery of chaperonin subunit fragment ApiCCT1 modulates mutant Huntingtin cellular phenotypes. Proc. Natl. Acad. Sci. 110, 3077–3082. https://doi.org/10.1073/pnas.1222663110

Sorbi, S., Bird, E.D., Blass, J.P., 1983. Decreased pyruvate dehydrogenase complex activity in Huntington and Alzheimer brain. Ann. Neurol. 13, 72–78. https://doi.org/10.1002/ana.410130116

Sorolla, M.A., Reverter-Branchat, G., Tamarit, J., Ferrer, I., Ros, J., Cabiscol, E., 2008. Proteomic and

oxidative stress analysis in human brain samples of Huntington disease. Free Radic. Biol. Med. 45, 667–678. https://doi.org/10.1016/j.freeradbiomed.2008.05.014

Sotiropoulos, A., Gineitis, D., Copeland, J., Treisman, R., 1999. Signal-Regulated Activation of Serum Response Factor Is Mediated by Changes in Actin Dynamics. Cell 98, 159–169. https://doi.org/10.1016/S0092-8674(00)81011-9

Southwell, A.L., Khoshnan, A., Dunn, D.E., Bugg, C.W., Lo, D.C., Patterson, P.H., 2008. Intrabodies Binding the Proline-Rich Domains of Mutant Huntingtin Increase Its Turnover and Reduce Neurotoxicity. J. Neurosci. 28, 9013–9020. https://doi.org/10.1523/JNEUROSCI.2747-08.2008

Spencer, J.A., Misra, R.P., 1996. Expression of the Serum Response Factor Gene Is Regulated by Serum Response Factor Binding Sites. J. Biol. Chem. 271, 16535–16543. https://doi.org/10.1074/jbc.271.28.16535

Squitieri, F., Orobello, S., Cannella, M., Martino, T., Romanelli, P., Giovacchini, G., Frati, L., Mansi, L., Ciarmiello, A., 2009. Riluzole protects Huntington disease patients from brain glucose hypometabolism and grey matter volume loss and increases production of neurotrophins. Eur. J. Nucl. Med. Mol. Imaging 36, 1113–1120. https://doi.org/10.1007/s00259-009-1103-3

Stanek, L.M., Yang, W., Angus, S., Sardi, P.S., Hayden, M.R., Hung, G.H., Bennett, C.F., Cheng, S.H., Shihabuddin, L.S., 2013. Antisense Oligonucleotide-Mediated Correction of Transcriptional Dysregulation is Correlated with Behavioral Benefits in the YAC128 Mouse Model of Huntington's Disease. J. Huntingtons. Dis. 2, 217–228. https://doi.org/10.3233/JHD-130057

Stefanko, D.P., Shah, V.D., Yamasaki, W.K., Petzinger, G.M., Jakowec, M.W., 2017. Treadmill exercise delays the onset of non-motor behaviors and striatal pathology in the CAG140 knock-in mouse model of Huntington's disease. Neurobiol. Dis. 105, 15–32. https://doi.org/10.1016/j.nbd.2017.05.004

Steffan, J.S., Bodai, L., Pallos, J., Poelman, M., McCampbell, A., Apostol, B.L., Kazantsev, A., Schmidt, E., Zhu, Y.-Z., Greenwald, M., Kurokawa, R., Housman, D.E., Jackson, G.R., Marsh, J.L., Thompson, L.M., 2001. Histone deacetylase inhibitors arrest polyglutamine-dependent neurodegeneration in Drosophila. Nature 413, 739–743. https://doi.org/10.1038/35099568

Steffan, J.S., Kazantsev, A., Spasic-Boskovic, O., Greenwald, M., Zhu, Y.-Z., Gohler, H., Wanker, E.E., Bates, G.P., Housman, D.E., Thompson, L.M., 2000. The Huntington's disease protein interacts with p53 and CREB-binding protein and represses transcription. Proc. Natl. Acad. Sci. 97, 6763–6768. https://doi.org/10.1073/pnas.100110097

Stern, S., Sinske, D., Knöll, B., 2012. Serum response factor modulates neuron survival during peripheral axon injury. J. Neuroinflammation 9, 573. https://doi.org/10.1186/1742-2094-9-78

Stine, O.C., Pleasant, N., Franz, M.L., Abbott, M.H., Folstein, S.E., Ross, C.A., 1993. Correlation between the onset age of Huntington's disease and length of the trinucleotide repeat in IT-15. Hum. Mol. Genet. 2, 1547–1549. https://doi.org/10.1093/hmg/2.10.1547

Stopper, C.M., Floresco, S.B., 2011. Contributions of the nucleus accumbens and its subregions to different aspects of risk-based decision making. Cogn. Affect. Behav. Neurosci. 11, 97–112. https://doi.org/10.3758/s13415-010-0015-9

Stout, J.C., Jones, R., Labuschagne, I., O'Regan, A.M., Say, M.J., Dumas, E.M., Queller, S., Justo, D., Santos, R.D., Coleman, A., Hart, E.P., Dürr, A., Leavitt, B.R., Roos, R.A., Langbehn, D.R., Tabrizi, S.J., Frost, C., 2012. Evaluation of longitudinal 12 and 24 month cognitive outcomes in premanifest and early Huntington's disease. J. Neurol. Neurosurg. Psychiatry 83, 687–694. https://doi.org/10.1136/jnnp-2011-301940

Stout, J.C., Paulsen, J.S., Queller, S., Solomon, A.C., Whitlock, K.B., Campbell, J.C., Carlozzi, N., Duff, K., Beglinger, L.J., Langbehn, D.R., Johnson, S.A., Biglan, K.M., Aylward, E.H., 2011. Neurocognitive signs in prodromal Huntington disease. Neuropsychology 25, 1–14. https://doi.org/10.1037/a0020937

Stringer, J.L., Belaguli, N.S., Iyer, D., Schwartz, R.J., Balasubramanyam, A., 2002. Developmental expression of serum response factor in the rat central nervous system. Dev. Brain Res. 138, 81–86. https://doi.org/10.1016/S0165-3806(02)00467-4

Stritt, C., Stern, S., Harting, K., Manke, T., Sinske, D., Schwarz, H., Vingron, M., Nordheim, A., Knöll, B., 2009. Paracrine control of oligodendrocyte differentiation by SRF-directed neuronal gene expression. Nat. Neurosci. 12, 418–427. https://doi.org/10.1038/nn.2280

Sun, K., Battle, M.A., Misra, R.P., Duncan, S.A., 2009. Hepatocyte expression of serum response factor is essential for liver function, hepatocyte proliferation and survival, and postnatal body growth in mice. Hepatology 49, 1645–1654. https://doi.org/10.1002/hep.22834

Sun, Q., Chen, G., Streb, J.W., Long, X., Yang, Y., Stoeckert, C.J., Miano, J.M., 2006. Defining the mammalian CArGome. Genome Res. 16, 197–207. https://doi.org/10.1101/gr.4108706

Sun, Y., Boyd, K., Xu, W., Ma, J., Jackson, C.W., Fu, A., Shillingford, J.M., Robinson, G.W., Hennighausen, L., Hitzler, J.K., Ma, Z., Morris, S.W., 2006. Acute Myeloid Leukemia-Associated Mkl1 (Mrtf-a) Is a Key Regulator of Mammary Gland Function. Mol. Cell. Biol. 26, 5809–5826. https://doi.org/10.1128/MCB.00024-06

Sun, Y., Savanenin, A., Reddy, P.H., Liu, Y.F., 2001. Polyglutamine-expanded Huntingtin Promotes Sensitization of N-Methyl-d-aspartate Receptors via Post-synaptic Density 95. J. Biol. Chem. 276, 24713–24718. https://doi.org/10.1074/jbc.M103501200

Surmeier, D.J., Kitai, S.T., 1997. State-dependent regulation of neuronal excitability by dopamine. Nihon Shinkei Seishin Yakurigaku Zasshi 17, 105–10.

Süssmuth, S.D., Haider, S., Landwehrmeyer, G.B., Farmer, R., Frost, C., Tripepi, G., Andersen, C.A., Di Bacco, M., Lamanna, C., Diodato, E., Massai, L., Diamanti, D., Mori, E., Magnoni, L., Dreyhaupt, J., Schiefele, K., Craufurd, D., Saft, C., Rudzinska, M., Ryglewicz, D., Orth, M., Brzozy, S., Baran, A., Pollio, G., Andre, R., Tabrizi, S.J., Darpo, B., Westerberg, G., 2015. An exploratory double-blind, randomized clinical trial with selisistat, a SirT1 inhibitor, in patients with Huntington's disease. Br. J. Clin. Pharmacol. 79, 465–476. https://doi.org/10.1111/bcp.12512

Suzuki, N., Nakamura, S., Mano, H., Kozasa, T., 2003. G 12 activates Rho GTPase through tyrosine-phosphorylated leukemia-associated RhoGEF. Proc. Natl. Acad. Sci. 100, 733–738. https://doi.org/10.1073/pnas.0234057100

Swami, M., Hendricks, A.E., Gillis, T., Massood, T., Mysore, J., Myers, R.H., Wheeler, V.C., 2009. Somatic expansion of the Huntington's disease CAG repeat in the brain is associated with an earlier age of

disease onset. Hum. Mol. Genet. 18, 3039–3047. https://doi.org/10.1093/hmg/ddp242

Tabrizi, S.J., Cleeter, M.W.J., Xuereb, J., Taanman, J.-W., Cooper, J.M., Schapira, A.H. V., 1999. Biochemical abnormalities and excitotoxicity in Huntington's disease brain. Ann. Neurol. 45, 25–32. https://doi.org/10.1002/1531-8249(199901)45:1<25::AID-ART6>3.0.CO;2-E

Tabrizi, S.J., Flower, M.D., Ross, C.A., Wild, E.J., 2020. Huntington disease: new insights into molecular pathogenesis and therapeutic opportunities. Nat. Rev. Neurol. 16, 529–546. https://doi.org/10.1038/s41582-020-0389-4

Tabrizi, S.J., Ghosh, R., Leavitt, B.R., 2019. Huntingtin Lowering Strategies for Disease Modification in Huntington's Disease. Neuron 101, 801–819. https://doi.org/10.1016/j.neuron.2019.01.039

Tabrizi, S.J., Workman, J., Hart, P.E., Mangiarini, L., Mahal, A., Bates, G., Cooper, J.M., Schapira, A.H. V., 2000. Mitochondrial dysfunction and free radical damage in the Huntington R6/2 transgenic mouse. Ann. Neurol. 47, 80–86. https://doi.org/10.1002/1531-8249(200001)47:1<80::AID-ANA13>3.3.CO;2-B

Takano, H., Gusella, J.F., 2002. The predominantly HEAT-like motif structure of huntingtin and its association and coincident nuclear entry with dorsal, an NF-kB/Rel/dorsal family transcription factor. BMC Neurosci. 3, 15. https://doi.org/10.1186/1471-2202-3-15

Tanaka, S., Hanakawa, T., Honda, M., 2008. [Neural substrates underlying cognitive expertise]. Brain Nerve 60, 257–62.

Telenius, H., Kremer, H.P.H., Thellmann, J., Andrew, S.E., Almqvist, E., Anvret, M., Greenberg, C., Greenberg, J., Lucotte, G., Squltierl, F., Starr, A., Goldberg, Y.P., Hayden, M.R., 1993. Molecular analysis of juvenile Huntington disease: the major influence on (CAG) n repeat length is the sex of the affected parent. Hum. Mol. Genet. 2, 1535–1540. https://doi.org/10.1093/hmg/2.10.1535

Testa, C.M., Jankovic, J., 2019. Huntington disease: A quarter century of progress since the gene discovery. J. Neurol. Sci. 396, 52–68. https://doi.org/10.1016/j.jns.2018.09.022

The HD iPSC Consortium, 2012. Induced Pluripotent Stem Cells from Patients with Huntington's Disease Show CAG-Repeat-Expansion-Associated Phenotypes. Cell Stem Cell 11, 264–278. https://doi.org/10.1016/j.stem.2012.04.027

The U.S.-Venezuela Collaborative, Wexler, N.S., Lorimer, J., Porter, J., Gomez, F., Moskowitz, C., Shackell, E., Marder, K., Penchaszadeh, G., Roberts, S.A., Gayan, J., Brocklebank, D., Cherny, S.S., Cardon, L.R., Gray, J., Dlouhy, S.R., Wiktorski, S., Hodes, M.E., Conneally, P.M., Penney, J.B., Gusella, J., Cha, J.-H., Irizarry, M., Rosas, D., Hersch, S., Hollingsworth, Z., MacDonald, M., Young, A.B., Andresen, J.M., Housman, D.E., de Young, M.M., Bonilla, E., Stillings, T., Negrette, A., Snodgrass, S.R., Martinez-Jaurrieta, M.D., Ramos-Arroyo, M.A., Bickham, J., Ramos, J.S., Marshall, F., Shoulson, I., Rey, G.J., Feigin, A., Arnheim, N., Acevedo-Cruz, A., Acosta, L., Alvir, J., Fischbeck, K., Thompson, L.M., Young, A., Dure, L., O'Brien, C.J., Paulsen, J., Brickman, A., Krch, D., Peery, S., Hogarth, P., Higgins, D.S., Landwehrmeyer, B., 2004. Venezuelan kindreds reveal that genetic and environmental factors modulate Huntington's disease age of onset. Proc. Natl. Acad. Sci. 101, 3498–3503. https://doi.org/10.1073/pnas.0308679101

Thomas, B., Matson, S., Chopra, V., Sun, L., Sharma, S., Hersch, S., Diana Rosas, H., Scherzer, C., Ferrante, R., Matson, W., 2013. A novel method for detecting 7-methyl guanine reveals aberrant methylation

levels in Huntington disease. Anal. Biochem. 436, 112–120. https://doi.org/10.1016/j.ab.2013.01.035

Thomas, E.A., Coppola, G., Desplats, P.A., Tang, B., Soragni, E., Burnett, R., Gao, F., Fitzgerald, K.M., Borok, J.F., Herman, D., Geschwind, D.H., Gottesfeld, J.M., 2008. The HDAC inhibitor 4b ameliorates the disease phenotype and transcriptional abnormalities in Huntington's disease transgenic mice. Proc. Natl. Acad. Sci. U. S. A. 105, 15564–9. https://doi.org/10.1073/pnas.0804249105

Thomas, T., Hitti, E., Kotlyarov, A., Potschka, H., Gaestel, M., 2008. MAP-kinase-activated protein kinase 2 expression and activity is induced after neuronal depolarization. Eur. J. Neurosci. 28, 642–654. https://doi.org/10.1111/j.1460-9568.2008.06382.x

Todd, D., Gowers, I., Dowler, S.J., Wall, M.D., McAllister, G., Fischer, D.F., Dijkstra, S., Fratantoni, S.A., van de Bospoort, R., Veenman-Koepke, J., Flynn, G., Arjomand, J., Dominguez, C., Munoz-Sanjuan, I., Wityak, J., Bard, J.A., 2014. A Monoclonal Antibody TrkB Receptor Agonist as a Potential Therapeutic for Huntington's Disease. PLoS One 9, e87923. https://doi.org/10.1371/journal.pone.0087923

Tong, Y., Ha, T.J., Liu, L., Nishimoto, A., Reiner, A., Goldowitz, D., 2011. Spatial and Temporal Requirements for huntingtin (Htt) in Neuronal Migration and Survival during Brain Development. J. Neurosci. 31, 14794–14799. https://doi.org/10.1523/JNEUROSCI.2774-11.2011

Tousley, A., Kegel-Gleason, K.B., 2016. Induced Pluripotent Stem Cells in Huntington's Disease Research: Progress and Opportunity. J. Huntingtons. Dis. 5, 99–131. https://doi.org/10.3233/JHD-160199

Travessa, A.M., Rodrigues, F.B., Mestre, T.A., Ferreira, J.J., 2017. Fifteen Years of Clinical Trials in Huntington's Disease: A Very Low Clinical Drug Development Success Rate. J. Huntingtons. Dis. 6, 157–163. https://doi.org/10.3233/JHD-170245

Treisman, R., 1995. Inside the MADS box. Nature 376, 468–469. https://doi.org/10.1038/376468a0

Treisman, R., 1994. Ternary complex factors: growth factor regulated transcriptional activators. Curr. Opin. Genet. Dev. 4, 96–101. https://doi.org/10.1016/0959-437X(94)90097-3

Treisman, R., 1987. Identification and purification of a polypeptide that binds to the c-fos serum response element. EMBO J. 6, 2711–7.

Treisman, R., Marais, R., Wynne, J., 1992. Spatial flexibility in ternary complexes between SRF and its accessory proteins. EMBO J. 11, 4631–40.

Tremblay, J.P., 2015. CRISPR, un système qui permet de corriger ou de modifier l'expression de gènes responsables de maladies héréditaires. médecine/sciences 31, 1014–1022. https://doi.org/10.1051/medsci/20153111016

Tricomi, E., Balleine, B.W., O'Doherty, J.P., 2009. A specific role for posterior dorsolateral striatum in human habit learning. Eur. J. Neurosci. 29, 2225–2232. https://doi.org/10.1111/j.1460-9568.2009.06796.x

Trottier, Y., Lutz, Y., Stevanin, G., Imbert, G., Devys, D., Cancel, G., Saudou, F., Weber, C., David, G., Tora, L., Agid, Y., Brice, A., Mandel, J.-L., 1995. Polyglutamine expansion as a pathological epitope in

Huntington's disease and four dominant cerebellar ataxias. Nature 378, 403–406. https://doi.org/10.1038/378403a0

Tsompana, M., Buck, M.J., 2014. Chromatin accessibility: a window into the genome. Epigenetics Chromatin 7, 33. https://doi.org/10.1186/1756-8935-7-33

Tsunemi, T., Ashe, T.D., Morrison, B.E., Soriano, K.R., Au, J., Roque, R.A. V., Lazarowski, E.R., Damian, V.A., Masliah, E., La Spada, A.R., 2012. PGC-1 Rescues Huntington's Disease Proteotoxicity by Preventing Oxidative Stress and Promoting TFEB Function. Sci. Transl. Med. 4, 142ra97-142ra97. https://doi.org/10.1126/scitranslmed.3003799

Turmaine, M., Raza, A., Mahal, A., Mangiarini, L., Bates, G.P., Davies, S.W., 2000. Nonapoptotic neurodegeneration in a transgenic mouse model of Huntington's disease. Proc. Natl. Acad. Sci. 97, 8093–8097. https://doi.org/10.1073/pnas.110078997

Twelvetrees, A.E., Yuen, E.Y., Arancibia-Carcamo, I.L., MacAskill, A.F., Rostaing, P., Lumb, M.J., Humbert, S., Triller, A., Saudou, F., Yan, Z., Kittler, J.T., 2010. Delivery of GABAARs to Synapses Is Mediated by HAP1-KIF5 and Disrupted by Mutant Huntingtin. Neuron 65, 53–65. https://doi.org/10.1016/j.neuron.2009.12.007

Tyan, S.-W., Tsai, M.-C., Lin, C.-L., Ma, Y.-L., Lee, E.H.Y., 2008. Serum- and glucocorticoid-inducible kinase 1 enhances zif268 expression through the mediation of SRF and CREB1 associated with spatial memory formation. J. Neurochem. 105, 820–832. https://doi.org/10.1111/j.1471-4159.2007.05186.x

Unschuld, P.G., Liu, X., Shanahan, M., Margolis, R.L., Bassett, S.S., Brandt, J., Schretlen, D.J., Redgrave, G.W., Hua, J., Hock, C., Reading, S.A., van Zijl, P.C.M., Pekar, J.J., Ross, C.A., 2013. Prefrontal executive function associated coupling relates to Huntington's disease stage. Cortex 49, 2661–2673. https://doi.org/10.1016/j.cortex.2013.05.015

Valor, L.M., 2015. Transcription, Epigenetics and Ameliorative Strategies in Huntington's Disease: a Genome-Wide Perspective. Mol. Neurobiol. 51, 406–423. https://doi.org/10.1007/s12035-014-8715-8

Valor, L.M., Guiretti, D., Lopez-Atalaya, J.P., Barco, A., 2013. Genomic Landscape of Transcriptional and Epigenetic Dysregulation in Early Onset Polyglutamine Disease. J. Neurosci. 33, 10471–10482. https://doi.org/10.1523/JNEUROSCI.0670-13.2013

Valor, L.M., Pulopulos, M.M., Jimenez-Minchan, M., Olivares, R., Lutz, B., Barco, A., 2011. Ablation of CBP in Forebrain Principal Neurons Causes Modest Memory and Transcriptional Defects and a Dramatic Reduction of Histone Acetylation But Does Not Affect Cell Viability. J. Neurosci. 31, 1652–1663. https://doi.org/10.1523/JNEUROSCI.4737-10.2011

van der Burg, J.M., Björkqvist, M., Brundin, P., 2009. Beyond the brain: widespread pathology in Huntington's disease. Lancet Neurol. 8, 765–774. https://doi.org/10.1016/S1474-4422(09)70178-4

van Duijn, E., Kingma, E.M., van der Mast, R.C., 2007. Psychopathology in Verified Huntington's Disease Gene Carriers. J. Neuropsychiatry Clin. Neurosci. 19, 441–448. https://doi.org/10.1176/jnp.2007.19.4.441

Van Raamsdonk, Jeremy M, Pearson, J., Rogers, D.A., Bissada, N., Vogl, A.W., Hayden, M.R., Leavitt, B.R.,

2005. Loss of wild-type huntingtin influences motor dysfunction and survival in the YAC128 mouse model of Huntington disease. Hum. Mol. Genet. 14, 1379–92. https://doi.org/10.1093/hmg/ddi147

Van Raamsdonk, Jeremy M., Pearson, J., Rogers, D.A., Lu, G., Barakauskas, V.E., Barr, A.M., Honer, W.G., Hayden, M.R., Leavitt, B.R., 2005. Ethyl-EPA treatment improves motor dysfunction, but not neurodegeneration in the YAC128 mouse model of Huntington disease. Exp. Neurol. 196, 266–272. https://doi.org/10.1016/j.expneurol.2005.07.021

Vartiainen, M.K., Guettler, S., Larijani, B., Treisman, R., 2007. Nuclear Actin Regulates Dynamic Subcellular Localization and Activity of the SRF Cofactor MAL. Science (80-.). 316, 1749–1752. https://doi.org/10.1126/science.1141084

Vashishtha, M., Ng, C.W., Yildirim, F., Gipson, T.A., Kratter, I.H., Bodai, L., Song, W., Lau, A., Labadorf, A., Vogel-Ciernia, A., Troncosco, J., Ross, C.A., Bates, G.P., Krainc, D., Sadri-Vakili, G., Finkbeiner, S., Marsh, J.L., Housman, D.E., Fraenkel, E., Thompson, L.M., 2013. Targeting H3K4 trimethylation in Huntington disease. Proc. Natl. Acad. Sci. U. S. A. 110, E3027-36. https://doi.org/10.1073/pnas.1311323110

Vidal, R.L., Figueroa, A., Court, F.A., Thielen, P., Molina, C., Wirth, C., Caballero, B., Kiffin, R., Segura-Aguilar, J., Cuervo, A.M., Glimcher, L.H., Hetz, C., 2012. Targeting the UPR transcription factor XBP1 protects against Huntington's disease through the regulation of FoxO1 and autophagy. Hum. Mol. Genet. 21, 2245–2262. https://doi.org/10.1093/hmg/dds040

Vieira, P.A., Korzus, E., 2015. CBP-Dependent memory consolidation in the prefrontal cortex supports object-location learning. Hippocampus 25, 1532–1540. https://doi.org/10.1002/hipo.22473

Vierbuchen, T., Ling, E., Cowley, C.J., Couch, C.H., Wang, X., Harmin, D.A., Roberts, C.W.M., Greenberg, M.E., 2017. AP-1 Transcription Factors and the BAF Complex Mediate Signal-Dependent Enhancer Selection. Mol. Cell 68, 1067-1082.e12. https://doi.org/10.1016/j.molcel.2017.11.026

Visel, A., Blow, M.J., Li, Z., Zhang, T., Akiyama, J.A., Holt, A., Plajzer-Frick, I., Shoukry, M., Wright, C., Chen, F., Afzal, V., Ren, B., Rubin, E.M., Pennacchio, L.A., 2009. ChIP-seq accurately predicts tissue-specific activity of enhancers. Nature 457, 854–858. https://doi.org/10.1038/nature07730

von Horsten, S., Schmitt, I., Nguyen, H.P., Holzmann, C., Schmidt, T., Walther, T., Bader, M., Pabst, R., Kobbe, P., Krotova, J., Stiller, D., Kask, A., Vaarmann, A., Rathke-Hartlieb, S., Schulz, J.B., Grasshoff, U., Bauer, I., Vieira-Saecker, A.M.M., Paul, M., Jones, L., Lindenberg, K.S., Landwehrmeyer, B., Bauer, A., Li, X.-J., Riess, O., 2003. Transgenic rat model of Huntington's disease. Hum. Mol. Genet. 12, 617–624. https://doi.org/10.1093/hmg/ddg075

VONSATTEL, J.-P., MYERS, R.H., STEVENS, T.J., FERRANTE, R.J., BIRD, E.D., RICHARDSON, E.P., 1985. Neuropathological Classification of Huntington's Disease. J. Neuropathol. Exp. Neurol. 44, 559–577. https://doi.org/10.1097/00005072-198511000-00003

Waelter, S., Boeddrich, A., Lurz, R., Scherzinger, E., Lueder, G., Lehrach, H., Wanker, E.E., 2001. Accumulation of Mutant Huntingtin Fragments in Aggresome-like Inclusion Bodies as a Result of Insufficient Protein Degradation. Mol. Biol. Cell 12, 1393–1407. https://doi.org/10.1091/mbc.12.5.1393

Waltereit, R., Dammermann, B., Wulff, P., Scafidi, J., Staubli, U., Kauselmann, G., Bundman, M., Kuhl, D., 2001. Arg3.1/Arc mRNA Induction by Ca 2+ and cAMP Requires Protein Kinase A and Mitogen-

Activated Protein Kinase/Extracellular Regulated Kinase Activation. J. Neurosci. 21, 5484–5493. https://doi.org/10.1523/JNEUROSCI.21-15-05484.2001

Wang, F., Yang, Y., Lin, X., Wang, J.-Q., Wu, Y.-S., Xie, W., Wang, D., Zhu, S., Liao, Y.-Q., Sun, Q., Yang, Y.-G., Luo, H.-R., Guo, C., Han, C., Tang, T.-S., 2013. Genome-wide loss of 5-hmC is a novel epigenetic feature of Huntington's disease. Hum. Mol. Genet. 22, 3641–3653. https://doi.org/10.1093/hmg/ddt214

Wang, L., Schuster, G.U., Hultenby, K., Zhang, Q., Andersson, S., Gustafsson, J.-A., 2002. Liver X receptors in the central nervous system: From lipid homeostasis to neuronal degeneration. Proc. Natl. Acad. Sci. 99, 13878–13883. https://doi.org/10.1073/pnas.172510899

Wang, X., Jin, H., 2010. The epigenetic basis of the Warburg effect. Epigenetics 5, 566–568. https://doi.org/10.4161/epi.5.7.12662

Wellington, C.L., Ellerby, L.M., Gutekunst, C.-A., Rogers, D., Warby, S., Graham, R.K., Loubser, O., van Raamsdonk, J., Singaraja, R., Yang, Y.-Z., Gafni, J., Bredesen, D., Hersch, S.M., Leavitt, B.R., Roy, S., Nicholson, D.W., Hayden, M.R., 2002. Caspase Cleavage of Mutant Huntingtin Precedes Neurodegeneration in Huntington's Disease. J. Neurosci. 22, 7862–7872. https://doi.org/10.1523/JNEUROSCI.22-18-07862.2002

Werth, D., Grassi, G., Konjer, N., Dapas, B., Farra, R., Giansante, C., Kandolf, R., Guarnieri, G., Nordheim, A., Heidenreich, O., 2010. Proliferation of human primary vascular smooth muscle cells depends on serum response factor. Eur. J. Cell Biol. 89, 216–224. https://doi.org/10.1016/j.ejcb.2009.12.002

Wheeler, V., 1999. Length-dependent gametic CAG repeat instability in the Huntington's disease knock-in mouse. Hum. Mol. Genet. 8, 115–122. https://doi.org/10.1093/hmg/8.1.115

Wheeler, V.C., 2003. Mismatch repair gene Msh2 modifies the timing of early disease in HdhQ111 striatum. Hum. Mol. Genet. 12, 273–281. https://doi.org/10.1093/hmg/ddg056

Wheeler, V.C., 2000. Long glutamine tracts cause nuclear localization of a novel form of huntingtin in medium spiny striatal neurons in HdhQ92 and HdhQ111 knock-in mice. Hum. Mol. Genet. 9, 503–513. https://doi.org/10.1093/hmg/9.4.503

Wheeler, V.C., Persichetti, F., McNeil, S.M., Mysore, J.S., Mysore, S.S., MacDonald, M.E., Myers, R.H., Gusella, J.F., Wexler, N.S., 2007. Factors associated with HD CAG repeat instability in Huntington disease. J. Med. Genet. 44, 695–701. https://doi.org/10.1136/jmg.2007.050930

White, J.K., Auerbach, W., Duyao, M.P., Vonsattel, J.-P., Gusella, J.F., Joyner, A.L., MacDonald, M.E., 1997. Huntingtin is required for neurogenesis and is not impaired by the Huntington's disease CAG expansion. Nat. Genet. 17, 404–410. https://doi.org/10.1038/ng1297-404

Whyte, W.A., Orlando, D.A., Hnisz, D., Abraham, B.J., Lin, C.Y., Kagey, M.H., Rahl, P.B., Lee, T.I., Young, R.A., 2013. Master transcription factors and mediator establish super-enhancers at key cell identity genes. Cell 153, 307–19. https://doi.org/10.1016/j.cell.2013.03.035

Wickramasinghe, S.R., Alvania, R.S., Ramanan, N., Wood, J.N., Mandai, K., Ginty, D.D., 2008. Serum Response Factor Mediates NGF-Dependent Target Innervation by Embryonic DRG Sensory Neurons. Neuron 58, 532–545. https://doi.org/10.1016/j.neuron.2008.03.006

Wictorin, K., 1992. Anatomy and connectivity of intrastriatal striatal transplants. Prog. Neurobiol. 38, 611–639. https://doi.org/10.1016/0301-0082(92)90044-F

Wild, E.J., Tabrizi, S.J., 2017. Therapies targeting DNA and RNA in Huntington's disease. Lancet Neurol. 16, 837–847. https://doi.org/10.1016/S1474-4422(17)30280-6

Woldemichael, B.T., Mansuy, I.M., 2016. Micro-RNAs in cognition and cognitive disorders: Potential for novel biomarkers and therapeutics. Biochem. Pharmacol. 104, 1–7. https://doi.org/10.1016/j.bcp.2015.11.021

Wong, Y.C., Holzbaur, E.L.F., 2014. The Regulation of Autophagosome Dynamics by Huntingtin and HAP1 Is Disrupted by Expression of Mutant Huntingtin, Leading to Defective Cargo Degradation. J. Neurosci. 34, 1293–1305. https://doi.org/10.1523/JNEUROSCI.1870-13.2014

Wood, M.A., Attner, M.A., Oliveira, A.M.M., Brindle, P.K., Abel, T., 2006. A transcription factor-binding domain of the coactivator CBP is essential for long-term memory and the expression of specific target genes. Learn. Mem. 13, 609–617. https://doi.org/10.1101/lm.213906

Xia, J., 2003. Huntingtin contains a highly conserved nuclear export signal. Hum. Mol. Genet. 12, 1393–1403. https://doi.org/10.1093/hmg/ddg156

Xia, Z., Dudek, H., Miranti, C.K., Greenberg, M.E., 1996. Calcium Influx via the NMDA Receptor Induces Immediate Early Gene Transcription by a MAP Kinase/ERK-Dependent Mechanism. J. Neurosci. 16, 5425–5436. https://doi.org/10.1523/JNEUROSCI.16-17-05425.1996

Xu, R., Zhang, S., Lei, A., 2014. Chromatin Changes in Reprogramming of Mammalian Somatic Cells. Rejuvenation Res. 17, 3–10. https://doi.org/10.1089/rej.2013.1455

Xu, X., Tay, Y., Sim, B., Yoon, S.-I., Huang, Y., Ooi, J., Utami, K.H., Ziaei, A., Ng, B., Radulescu, C., Low, D., Ng, A.Y.J., Loh, M., Venkatesh, B., Ginhoux, F., Augustine, G.J., Pouladi, M.A., 2017. Reversal of Phenotypic Abnormalities by CRISPR/Cas9-Mediated Gene Correction in Huntington Disease Patient-Derived Induced Pluripotent Stem Cells. Stem cell reports 8, 619–633. https://doi.org/10.1016/j.stemcr.2017.01.022

Yablonska, S., Ganesan, V., Ferrando, L.M., Kim, J., Pyzel, A., Baranova, O. V., Khattar, N.K., Larkin, T.M., Baranov, S. V., Chen, N., Strohlein, C.E., Stevens, D.A., Wang, X., Chang, Y.-F., Schurdak, M.E., Carlisle, D.L., Minden, J.S., Friedlander, R.M., 2019. Mutant huntingtin disrupts mitochondrial proteostasis by interacting with TIM23. Proc. Natl. Acad. Sci. 116, 16593–16602. https://doi.org/10.1073/pnas.1904101116

Yang, H., Patel, D.J., 2017. New CRISPR-Cas systems discovered. Cell Res. 27, 313–314. https://doi.org/10.1038/cr.2017.21

Yang, S.-H., Cheng, P.-H., Banta, H., Piotrowska-Nitsche, K., Yang, J.-J., Cheng, E.C.H., Snyder, B., Larkin, K., Liu, J., Orkin, J., Fang, Z.-H., Smith, Y., Bachevalier, J., Zola, S.M., Li, S.-H., Li, X.-J., Chan, A.W.S., 2008. Towards a transgenic model of Huntington's disease in a non-human primate. Nature 453, 921–924. https://doi.org/10.1038/nature06975

Yano, H., Baranov, S. V, Baranova, O. V, Kim, J., Pan, Y., Yablonska, S., Carlisle, D.L., Ferrante, R.J., Kim, A.H., Friedlander, R.M., 2014. Inhibition of mitochondrial protein import by mutant huntingtin. Nat. Neurosci. 17, 822–831. https://doi.org/10.1038/nn.3721

Yao, Y., Cui, X., Al-Ramahi, I., Sun, X., Li, B., Hou, J., Difiglia, M., Palacino, J., Wu, Z.-Y., Ma, L., Botas, J., Lu, B., 2015. A striatal-enriched intronic GPCR modulates huntingtin levels and toxicity. Elife 4. https://doi.org/10.7554/eLife.05449

Yap, E.-L., Greenberg, M.E., 2018. Activity-Regulated Transcription: Bridging the Gap between Neural Activity and Behavior. Neuron 100, 330–348. https://doi.org/10.1016/j.neuron.2018.10.013

Yin, H.H., 2004. Contributions of Striatal Subregions to Place and Response Learning. Learn. Mem. 11, 459–463. https://doi.org/10.1101/lm.81004

Yin, H.H., Knowlton, B.J., Balleine, B.W., 2005. Blockade of NMDA receptors in the dorsomedial striatum prevents action-outcome learning in instrumental conditioning. Eur. J. Neurosci. 22, 505–512. https://doi.org/10.1111/j.1460-9568.2005.04219.x

Yu-Taeger, L., Bonin, M., Stricker-Shaver, J., Riess, O., Nguyen, H.H.P., 2017. Dysregulation of gene expression in the striatum of BACHD rats expressing full-length mutant huntingtin and associated abnormalities on molecular and protein levels. Neuropharmacology 117, 260–272. https://doi.org/10.1016/j.neuropharm.2017.01.029

Yu-Taeger, L., Petrasch-Parwez, E., Osmand, A.P., Redensek, A., Metzger, S., Clemens, L.E., Park, L., Howland, D., Calaminus, C., Gu, X., Pichler, B., Yang, X.W., Riess, O., Nguyen, H.P., 2012. A Novel BACHD Transgenic Rat Exhibits Characteristic Neuropathological Features of Huntington Disease. J. Neurosci. 32, 15426–15438. https://doi.org/10.1523/JNEUROSCI.1148-12.2012

Zahm, D.S., Heimer, L., 1990. Two transpallidal pathways originating in the rat nucleus accumbens. J. Comp. Neurol. 302, 437–446. https://doi.org/10.1002/cne.903020302

Zala, D., Colin, E., Rangone, H., Liot, G., Humbert, S., Saudou, F., 2008. Phosphorylation of mutant huntingtin at S421 restores anterograde and retrograde transport in neurons. Hum. Mol. Genet. 17, 3837–3846. https://doi.org/10.1093/hmg/ddn281

Zaromytidou, A.-I., Miralles, F., Treisman, R., 2006. MAL and Ternary Complex Factor Use Different Mechanisms To Contact a Common Surface on the Serum Response Factor DNA-Binding Domain. Mol. Cell. Biol. 26, 4134–4148. https://doi.org/10.1128/MCB.01902-05

Zeitler, B., Froelich, S., Marlen, K., Shivak, D.A., Yu, Q., Li, D., Pearl, J.R., Miller, J.C., Zhang, L., Paschon, D.E., Hinkley, S.J., Ankoudinova, I., Lam, S., Guschin, D., Kopan, L., Cherone, J.M., Nguyen, H.-O.B., Qiao, G., Ataei, Y., Mendel, M.C., Amora, R., Surosky, R., Laganiere, J., Vu, B.J., Narayanan, A., Sedaghat, Y., Tillack, K., Thiede, C., Gärtner, A., Kwak, S., Bard, J., Mrzljak, L., Park, L., Heikkinen, T., Lehtimäki, K.K., Svedberg, M.M., Häggkvist, J., Tari, L., Tóth, M., Varrone, A., Halldin, C., Kudwa, A.E., Ramboz, S., Day, M., Kondapalli, J., Surmeier, D.J., Urnov, F.D., Gregory, P.D., Rebar, E.J., Muñoz-Sanjuán, I., Zhang, H.S., 2019. Allele-selective transcriptional repression of mutant HTT for the treatment of Huntington's disease. Nat. Med. 25, 1131–1142. https://doi.org/10.1038/s41591-019-0478-3

Zeitlin, S., Liu, J.-P., Chapman, D.L., Papaioannou, V.E., Efstratiadis, A., 1995. Increased apoptosis and early embryonic lethality in mice nullizygous for the Huntington's disease gene homologue. Nat. Genet. 11, 155–163. https://doi.org/10.1038/ng1095-155

Zhang, H.-M., Li, L., Papadopoulou, N., Hodgson, G., Evans, E., Galbraith, M., Dear, M., Vougier, S., Saxton, J., Shaw, P.E., 2008. Mitogen-induced recruitment of ERK and MSK to SRE promoter

complexes by ternary complex factor Elk-1. Nucleic Acids Res. 36, 2594–2607. https://doi.org/10.1093/nar/gkn099

Zhang, N., An, M.C., Montoro, D., Ellerby, L.M., 2010. Characterization of Human Huntington's Disease Cell Model from Induced Pluripotent Stem Cells. PLoS Curr. 2, RRN1193. https://doi.org/10.1371/currents.RRN1193

Zhang, X., Azhar, G., Helms, S.A., Wei, J.Y., 2011. Regulation of cardiac microRNAs by serum response factor. J. Biomed. Sci. 18, 15. https://doi.org/10.1186/1423-0127-18-15

Zhang, Y., Leavitt, B.R., van Raamsdonk, J.M., Dragatsis, I., Goldowitz, D., MacDonald, M.E., Hayden, M.R., Friedlander, R.M., 2006. Huntingtin inhibits caspase-3 activation. EMBO J. 25, 5896–5906. https://doi.org/10.1038/sj.emboj.7601445

Zheng, G., Dwoskin, L.P., Crooks, P.A., 2006. Vesicular monoamine transporter 2: Role as a novel target for drug development. AAPS J. 8, E682–E692. https://doi.org/10.1208/aapsj080478

Zheng, J., Winderickx, J., Franssens, V., Liu, B., 2018. A Mitochondria-Associated Oxidative Stress Perspective on Huntington's Disease. Front. Mol. Neurosci. 11. https://doi.org/10.3389/fnmol.2018.00329

Zheng, Z., Diamond, M.I., 2012. Huntington Disease and the Huntingtin Protein. pp. 189–214. https://doi.org/10.1016/B978-0-12-385883-2.00010-2

Zuccato, C., 2001. Loss of Huntingtin-Mediated BDNF Gene Transcription in Huntington's Disease. Science (80-.). 293, 493–498. https://doi.org/10.1126/science.1059581

ZUCCATO, C., CATTANEO, E., 2007. Role of brain-derived neurotrophic factor in Huntington's disease. Prog. Neurobiol. 81, 294–330. https://doi.org/10.1016/j.pneurobio.2007.01.003

ZUCCATO, C., CONTI, L., REITANO, E., TARTARI, M., CATTANEO, E., 2005. The Function of the Neuronal Proteins Shc and Huntingtin in Stem Cells and Neurons: Pharmacologic Exploitation for Human Brain Diseases. Ann. N. Y. Acad. Sci. 1049, 39–50. https://doi.org/10.1196/annals.1334.006

Zuccato, C., Tartari, M., Crotti, A., Goffredo, D., Valenza, M., Conti, L., Cataudella, T., Leavitt, B.R., Hayden, M.R., Timmusk, T., Rigamonti, D., Cattaneo, E., 2003. Huntingtin interacts with REST/NRSF to modulate the transcription of NRSE-controlled neuronal genes. Nat. Genet. 35, 76–83. https://doi.org/10.1038/ng1219

Zuccato, C., Valenza, M., Cattaneo, E., 2010. Molecular Mechanisms and Potential Therapeutical Targets in Huntington's Disease. Physiol. Rev. 90, 905–981. https://doi.org/10.1152/physrev.00041.2009

Université de Strasbourg

Ali AWADA

École Doctorale des Sciences de la Vie et de la Santé STRASBOURG

The role of the Serum Response Factor in the pathogenesis of Huntington's disease

Résumé

La maladie de Huntington (MH) est une maladie neurodégénérative progressive. Elle est due à une expansion anormale des répétitions CAG au niveau du gène codant pour la protéine Huntingtine (HTT). Les neurones du striatum sont affectés par la toxicité de la mutation. La MH est caractérisée par des symptômes moteurs, cognitifs et psychiatriques. Des études du laboratoire ont montré que les gènes qui définissent l'identité striatale et les gènes impliqués dans les mécanismes de plasticité neuronale sont sous-régulés chez les patients et les modèles murins de la MH. Le mécanisme de dérégulation transcriptionnelle pourrait impliquer le facteur de transcription Serum Response Factor (SRF), favorisant la plasticité synaptique et les processus de mémoire. L'objectif de mes travaux de thèse a été de caractériser la régulation de SRF dans le contexte de la MH et d'évaluer son rôle dans la pathogenèse. L'analyse de SRF au niveau transcriptionnel et/ou protéique montre en effet qu'il est sous-régulé de façon précoce dans le striatum de souris modèles de la MH. Pour établir un éventuel lien de causalité entre la sous-regulation de SRF dans le striatum et les phénotypes Huntington, nous avons utilisé une approche virale basée sur un AAV pour sur-exprimer SRF dans le striatum des souris transgéniques R6/1, modèles de la MH. En utilisant différents tests comportementaux, nous avons montré que la surexpression de la forme complète de SRF dans le striatum des souris transgéniques entraîne une aggravation des symptômes moteurs. De plus, les analyses histologiques et moléculaires (q-RT-PCR, RNAseq et Western-blot) ne montrent aucun sauvetage des cibles de SRF dans le striatum des souris R6/1, malgré sa surexpression élevée. Nos résultats suggèrent que la régulation striatale de SRF et de ses gènes cibles est altérée par la HTT mutée. Nous avons alors surexprimé une construction consistant en la fusion du domaine de liaison de SRF avec le domaine de transactivation de VP16 (SRF-VP16) dans le striatum des souris R6/1. Nos données indiquent que bien que les gènes de plasticité sont sur-régulés par cette construction, le phénotype comportemental des souris R6/1 n'est pas amélioré, probablement du fait de l'absence d'effet majeur de SRF-VP16 sur les gènes de l'identité striatale. Cela pourrait suggérer que la restauration du niveau de SRF dans la MH n'est pas suffisante pour sauver de manière significative la pathogenèse de la MH.

Mots clés : Maladie de Huntington, Facteur de réponse sérique, Virus adéno-associé, VP16, activité neuronale, fonction motrice, mémoire procédurale.

Abstract

Huntington's Huntington's disease (HD) is a progressive neurodegenerative disease. It is caused by an abnormal expansion of CAG repeats in the gene coding for the Huntingtin protein (HTT). Neurons in the striatum are affected by the toxicity of the mutation. HD is characterized by motor, cognitive and psychiatric symptoms. Studies in the lab have shown that the genes that define striatal identity and the genes involved in the mechanisms of neuronal plasticity are down-regulated in patients and mouse models of HD. The mechanism of transcriptional deregulation could involve the transcription factor Serum Response Factor (SRF), promoting synaptic plasticity and memory processes. The objective of my thesis work was to characterize the regulation of SRF in the context of HD and to evaluate its role in pathogenesis. Indeed, the analysis of SRF at the transcriptional and/or protein level shows that it is down-regulated at an early stage in the striatum of mouse models of HD. To establish a possible causal link between SRF down-regulation in the striatum and Huntington's phenotypes, we used an AAV-based viral approach to over-express SRF in the striatum of R6/1 transgenic mouse, a model of HD. Using different behavioral tests, we showed that overexpression of the full length of SRF in the striatum of transgenic mice leads to an aggravation of motor symptoms. Moreover, histological and molecular analyses (q-RT-PCR, RNAseq and Western-blot) showed no rescue of SRF targets in the striatum of R6/1 mice, despite its high overexpression. Our results suggest that the striatal regulation of SRF and its target genes is altered by mutated HTT. We then overexpressed a construct consisting of the fusion of the SRF binding domain with the VP16 transactivation domain (SRF-VP16) in the striatum of R6/1 mice. Our data indicate that although neuronal plasticity genes are up-regulated by this construct, the behavioral phenotype of R6/1 mice is not improved, probably due to the absence of a major effect of SRF-VP16 on the striatal identity genes. This could suggest that restoring the level of SRF in the HD is not sufficient to significantly rescue HD pathogenesis.

Keywords: Huntington Disease, Serum Response Factor, Adeno Associated virus, VP16, neuronal activity, motor functions, procedural memory.